frontiers | Research Topics

Women in bone research

Edited by
Monica De Mattei, Michaela Tencerova and Katherine A. Staines

Published in
Frontiers in Endocrinology

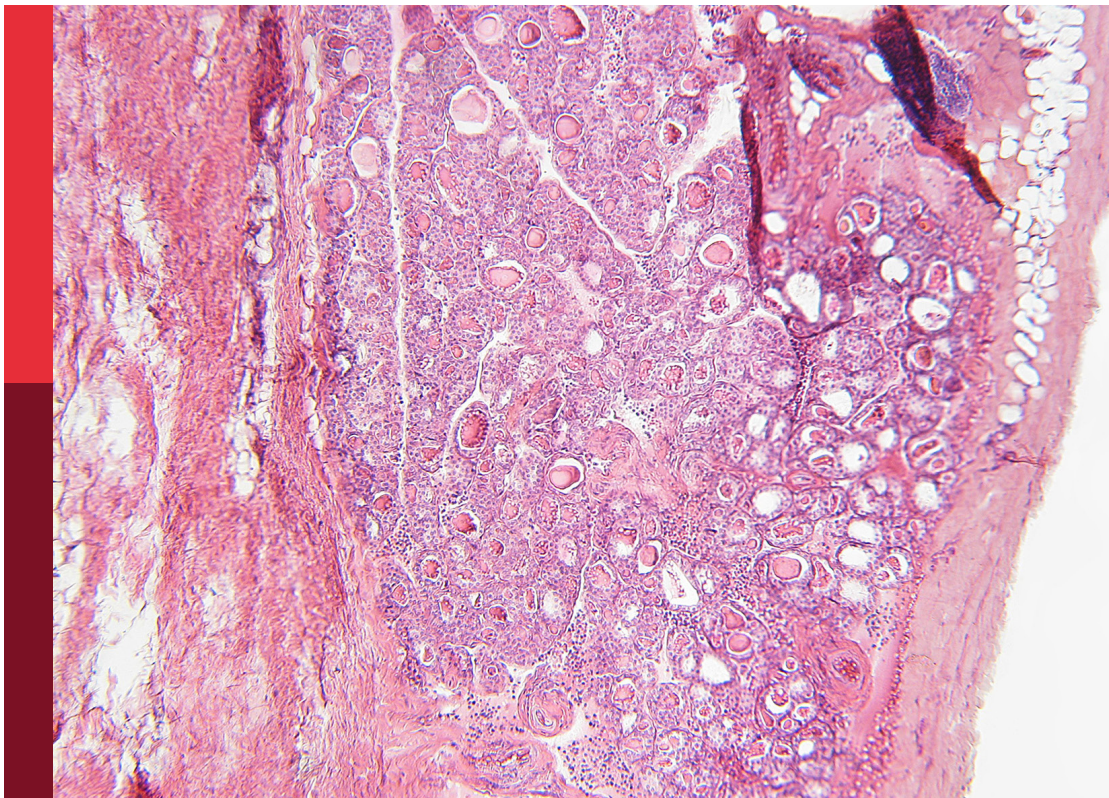

ISSN 1664-8714
ISBN 978-2-8325-6242-0
DOI 10.3389/978-2-8325-6242-0

About Frontiers

Frontiers is more than just an open access publisher of scholarly articles: it is a pioneering approach to the world of academia, radically improving the way scholarly research is managed. The grand vision of Frontiers is a world where all people have an equal opportunity to seek, share and generate knowledge. Frontiers provides immediate and permanent online open access to all its publications, but this alone is not enough to realize our grand goals.

Frontiers journal series

The Frontiers journal series is a multi-tier and interdisciplinary set of open-access, online journals, promising a paradigm shift from the current review, selection and dissemination processes in academic publishing. All Frontiers journals are driven by researchers for researchers; therefore, they constitute a service to the scholarly community. At the same time, the *Frontiers journal series* operates on a revolutionary invention, the tiered publishing system, initially addressing specific communities of scholars, and gradually climbing up to broader public understanding, thus serving the interests of the lay society, too.

Dedication to quality

Each Frontiers article is a landmark of the highest quality, thanks to genuinely collaborative interactions between authors and review editors, who include some of the world's best academicians. Research must be certified by peers before entering a stream of knowledge that may eventually reach the public - and shape society; therefore, Frontiers only applies the most rigorous and unbiased reviews. Frontiers revolutionizes research publishing by freely delivering the most outstanding research, evaluated with no bias from both the academic and social point of view. By applying the most advanced information technologies, Frontiers is catapulting scholarly publishing into a new generation.

What are Frontiers Research Topics?

Frontiers Research Topics are very popular trademarks of the *Frontiers journals series*: they are collections of at least ten articles, all centered on a particular subject. With their unique mix of varied contributions from Original Research to Review Articles, Frontiers Research Topics unify the most influential researchers, the latest key findings and historical advances in a hot research area.

Find out more on how to host your own Frontiers Research Topic or contribute to one as an author by contacting the Frontiers editorial office: frontiersin.org/about/contact

Women in bone research

Topic editors

Monica De Mattei — University of Ferrara, Italy

Michaela Tencerova — Institute of Physiology, Academy of Sciences of the Czech Republic (ASCR), Czechia

Katherine A. Staines — University of Brighton, United Kingdom

Citation

De Mattei, M., Tencerova, M., Staines, K. A., eds. (2025). *Women in bone research*. Lausanne: Frontiers Media SA. doi: 10.3389/978-2-8325-6242-0

Table of contents

frontiers | Frontiers in Endocrinology

TYPE Editorial
PUBLISHED 10 March 2025
DOI 10.3389/fendo.2025.1561904

OPEN ACCESS

EDITED AND REVIEWED BY
Alberto Falchetti,
Grande Ospedale Metropolitano Niguarda, Italy

*CORRESPONDENCE
Michaela Tencerova
drosife@yahoo.com

†These authors have contributed equally to this work

RECEIVED 16 January 2025
ACCEPTED 12 February 2025
PUBLISHED 10 March 2025

CITATION
De Mattei M, Staines KA and Tencerova M (2025) Editorial: Women in bone research. *Front. Endocrinol.* 16:1561904. doi: 10.3389/fendo.2025.1561904

Editorial: Women in bone research

Monica De Mattei[1†], Katherine A. Staines[2†] and Michaela Tencerova[3*†]

[1]Department of Medical Sciences, University of Ferrara, Ferrara, Italy, [2]Centre for Lifelong Health, School of Applied Sciences, University of Brighton, Brighton, United Kingdom, [3]Laboratory of Molecular Physiology of Bone, Institute of Physiology of the Czech Academy of Sciences, Prague, Czechia

KEYWORDS

bone research, women in science, clinical studies, animal models of bone diseases, sex differences

Editorial on the Research Topic
Women in bone research

This Research Topic entitled "*Women in Bone Research*" showcased 15 articles by women scientists, highlighting novel findings in basic and clinical musculoskeletal research.

Among the basic bone research studies, Gilbert et al. used human mesenchymal stem cells (Y201) to develop a 3D *in vitro* model of osteocytes, which highlighted numerous genes implicated in osteoarthritic pain, as well as inflammation and bone remodeling. The findings contribute to a deeper understanding of osteoarthritis pathology and may guide the development of targeted therapies through use of this model. Further work from this group in Jones et al. compared published data sets to reveal a wide array of sex-regulated genes that are also significantly regulated by pathophysiological loading in osteocytes. Their work highlights pain related pathways which may underpin elevated pain susceptibility in females with osteoarthritis and offers potential therapeutic targets. A final study on osteocytes by Yee et al., examined the skeletal effects of glucocorticoids and PTH(1-34), alone and combined on perilacunar canalicular remodeling (PLR). They found sex-dependent differences in responsiveness to glucocorticoids and PTH(1-34) and ultimately no evidence that PTH(1-34) could offset glucocorticoid-dependent effects on PLR, thus highlighting that further studies are required.

Verlinden et al. analyzed the bone phenotype of Klotho deficient mice (kl/kl), an animal model of accelerated aging, in comparison to chronological aged mice. The major differences were in trabecular bone volume, serum calcium and phosphate levels and *Trpv6* expression, which might contribute to better understanding of the mechanism behind the accelerated aging related to the regulation of calcium metabolism. Ali et al. showed that the natural compounds Apigenin and Rutaecarpine, plant-derived antioxidants enhanced osteogenic differentiation of human bone marrow stromal stem cells (hBMSCs) derived from elderly females. Further, these molecules reduced oxidative stress and the accumulation of senescence cells, suggesting the therapeutic potential of

these natural compounds in the age-related bone loss. Prabhakaran et al. explored a novel approach to demonstrate that by guiding the fusion of differentiated rat osteoblast cell spheroids, it is possible to engineer bone macro-tissues that mimic physiological osteogenesis both morphologically and molecularly. This technique holds promise for advancing tissue engineering and regenerative medicine, particularly for bone repair and replacement.

An RNA-seq study by Bourne et al., showed divergent chondrocyte phenotypes in *ex vivo* hip cap articular cartilage and metatarsal growth cartilage cultures. They also revealed that hydrostatic pressure application downregulated biological processes including ossification, connective tissue development, and chondrocyte differentiation. These data therefore provide novel genetic targets for osteoarthritis research.

Finally, Tian et al. summarizes findings from preclinical studies on lactoferrin, a multifunctional protein, which has emerged as a promising therapeutic opportunity for bone diseases. The authors provide a critical discussion on the opportunity to use lactoferrin-derived peptides as potential therapeutic agents for the treatment of orthopedic and metabolic bone diseases and highlight the need to develop strategies for the delivery of lactoferrin or derived peptides to bone.

Several papers of the Research Topic focused on different clinical aspects with the aim to identify risk factors for bone health and potential therapies. A study by Harada et al. found that fat content in vertebral bone marrow (BM) and muscle is associated with increased bone fractions and metabolic complications. Notably, a history of gestational diabetes was significantly associated with a higher proton density fat fraction (PDFF) of the vertebral BM, independent of age and BMI, thus highlighting vertebral BM PDFF as a potential biomarker for the assessment of bone health in premenopausal women as a risk factor of diabetes. An observational study by He et al. investigated the association between the atherogenic index of plasma (AIP) and BMD among adult women using National Health and Nutrition Examination Survey (NHANES). They found a negative correlation between the AIP and total BMD measured by DXA, thus suggesting that high AIP might serve as a good biomarker for a low BMD and contribute to the prevention of the osteoporosis. Aparicio-Bautista et al. analyzed the association between 3 single nucleotide variants MARK3 (rs11623869), PLCB4 (rs6086746) and GEMIN2 (rs2277458), with BMD and vitamin D levels in Mexican women to create genetic risk score (GRS). GRS revealed significant associations between the variants and hip and femur neck BMD and vitamin D. Thus, these findings may contribute to early detection of the pathogenesis of osteoporosis. In the systematic clinical review Liu et al. investigated the efficacy of 5 different Chinese fitness exercises (Baduanjin, Taijiquan, Wuqinxi, Yijinjing, and Liuzijue) both alone and in combination with drug therapy in the treatment of decreased BMD in postmenopausal women. The outcome of the studies confirmed the positive effect of the Chinese fitness trainings, even more effective with drug treatments. However, the small number of studies and participants limits definitive conclusions; further clinical research with larger cohorts is needed.

Chen et al. investigated the causal relationship between hormonal and reproductive factors and low back pain (LBP), by using Mendelian randomization (MR) analysis. Their results showed that early menarche, first birth, last birth, and first sexual intercourse may reduce the risk of LBP. This confirms that reproductive hormones, particularly estrogen, may play a protective role against LBP, possibly by influencing intervertebral disc metabolism and bone health. The paper by Ren et al. analyzed the clinical characteristics and prognostic factors of survival for patients with bone metastases of unknown origin, in a large population-based study including 1224 cases. They found these patients have extremely low 1-year survival rates, only 14.5% for overall survival and 15.9% for cancer-specific survival. In addition, they revealed that radiotherapy and chemotherapy were significantly correlated with prognosis, suggesting that these treatments may be effective in prolonging survival and the need for further research to evaluate the efficacy of treatments. A final clinical aspect explored in this Research Topic was delayed bone healing, reported in the case report by Ryskalin et al. The authors conducted a critical analysis and summary of the present information deriving from basic research and clinical reports concerning the beneficial effects of extracorporeal shockwave therapy (ESWT) on bone healing. Further they showed the promising outcomes of a delayed ulnar fracture treated with focused high-energy ESWT, suggesting EWST as a safe and promising alternative to surgery in the treatment of delayed union and nonunions.

In conclusion, this Research Topic highlights the wide-ranging contributions of women researchers, covering the topics from fundamental scientific investigations to practical clinical applications. Overall, it provides a comprehensive overview of current research in bone biology, and research directions, with particular attention to aging and sex differences, highlighting the complexity of bone homeostasis and the potential for novel therapeutic interventions. By amplifying the voices and relevant research of women scientists, this Research Topic may inspire future generations of women to pursue careers in bone biology and contribute to the advancement of this crucial field.

Author contributions

MT: Writing – original draft, Writing – review & editing. MM: Writing – original draft, Writing – review & editing. KS: Writing – original draft, Writing – review & editing.

Acknowledgments

We appreciate all Authors who submitted their research articles and all Reviewers for their great contributions to this Research Topic.

Conflict of interest

The authors declare that the research was conducted in the absence of any commercial or financial relationships that could be construed as a potential conflict of interest.

The author(s) declared that they were an editorial board member of Frontiers, at the time of submission. This had no impact on the peer review process and the final decision.

Generative AI statement

The author(s) declare that no Generative AI was used in the creation of this manuscript.

Publisher's note

frontiers | Frontiers in Endocrinology

TYPE Review
PUBLISHED 23 August 2023
DOI 10.3389/fendo.2023.1218148

OPEN ACCESS

EDITED BY
Michaela Tencerova,
Academy of Sciences of the Czech Republic (ASCR), Czechia

REVIEWED BY
Naibedya Chattopadhyay,
Central Drug Research Institute (CSIR), India
Anirudha Karvande,
Children's Hospital of Philadelphia, United States

*CORRESPONDENCE
Dan Tian
tdan@mail.jlu.edu.cn

RECEIVED 06 May 2023
ACCEPTED 28 July 2023
PUBLISHED 23 August 2023

CITATION
Tian M, Han Y-b, Yang G-y, Li J-l, Shi C-s and Tian D (2023) The role of lactoferrin in bone remodeling: evaluation of its potential in targeted delivery and treatment of metabolic bone diseases and orthopedic conditions. *Front. Endocrinol.* 14:1218148. doi: 10.3389/fendo.2023.1218148

The role of lactoferrin in bone remodeling: evaluation of its potential in targeted delivery and treatment of metabolic bone diseases and orthopedic conditions

Miao Tian[1], Ying-bo Han[2], Gui-yun Yang[3], Jin-long Li[2], Chang-sai Shi[2] and Dan Tian[4]*

[1]Department of Gynecology and Obstetrics, The Second Hospital of Jilin University, Changchun, China, [2]Department of Gastrointestinal Surgery, The Second Hospital of Jilin University, Changchun, China, [3]Department of Operating Room, The Second Hospital of Jilin University, Changchun, China, [4]Department of Anesthesiology, The Second Hospital of Jilin University, Changchun, China

Lactoferrin (Lf) is a multifunctional protein that is synthesized endogenously and has various biological roles including immunological regulation, antibacterial, antiviral, and anticancer properties. Recently, research has uncovered Lf's critical functions in bone remodeling, where it regulates the function of osteoblasts, chondrocytes, osteoclasts, and mesenchymal stem cells. The signaling pathways involved in Lf's signaling in osteoblasts include (low density lipoprotein receptor-related protein – 1 (LRP-1), transforming growth factor β (TGF-β), and insulin-like growth factor – 1 (IGF-1), which activate downstream pathways such as ERK, PI3K/Akt, and NF-κB. These pathways collectively stimulate osteoblast proliferation, differentiation, and mineralization while inhibiting osteoclast differentiation and activity. Additionally, Lf's inhibitory effect on nuclear factor kappa B (NF-κB) suppresses the formation and activity of osteoclasts directly. Lf also promotes chondroprogenitor proliferation and differentiation to chondrocytes by activating the mitogen-activated protein kinase/extracellular signal-regulated kinase (MAPK/ERK) and phosphoinositide 3-kinase/protein kinase B(PI3K/Akt)signaling pathways while inhibiting the expression of matrix-degrading enzymes through the suppression of the NF-κB pathway. Lf's ability to stimulate osteoblast and chondrocyte activity and inhibit osteoclast function accelerates fracture repair, as demonstrated by its effectiveness in animal models of critical-sized long bone defects. Moreover, studies have indicated that Lf can rescue dysregulated bone remodeling in osteoporotic conditions by stimulating bone formation and suppressing bone resorption. These beneficial effects of Lf on bone health have led to its exploration in nutraceutical and pharmaceutical applications. However, due to the large size of Lf, small bioactive peptides are preferred for pharmaceutical applications. These peptides have been shown to promote bone fracture repair and reverse osteoporosis in animal studies, indicating their potential as therapeutic agents for bone-related diseases. Nonetheless, the active concentration of Lf in serum may not be sufficient at

the site requiring bone regeneration, necessitating the development of various delivery strategies to enhance Lf's bioavailability and target its active concentration to the site requiring bone regeneration. This review provides a critical discussion of the issues mentioned above, providing insight into the roles of Lf in bone remodeling and the potential use of Lf as a therapeutic target for bone disorders.

KEYWORDS

lactoferrin, bone remodeling, signaling pathways, fracture repair, osteoporosis

1 Introduction

Several hormones and cytokines play a crucial role in bone metabolism; some of these have become therapies for osteoporosis. For example, estrogen has been used for many years in hormone replacement therapy to prevent and treat osteoporosis in postmenopausal women (1). Parathyroid hormone (PTH) and calcitonin are also approved for the treatment of osteoporosis and have been shown to increase bone density and reduce fracture risk (2). In addition to hormones, cytokines such as receptor activator of nuclear factor-kappa B ligand (RANKL) and sclerostin have also been identified as potential targets for osteoporosis therapy. Denosumab, a monoclonal antibody that targets RANKL, and romosozumab, a monoclonal antibody that inhibits sclerostin, have both been approved for the treatment of osteoporosis and have demonstrated significant benefits in increasing bone density and reducing fracture risk (3, 4). Endogenous factors naturally occur in the body and therefore have a lower risk of side effects and toxicity. Lactoferrin (Lf) is an endogenous protein in plasma that directly impacts bone cells and modulates bone metabolism (5), making it an attractive candidate for future research for positioning it as a therapeutic target for metabolic bone diseases.

Lf is an iron-binding glycoprotein required for several biological functions, including immune function, antimicrobial activity, and tissue repair. Human serum Lf range from 0.2 to 0.5μg/ml, mostly from neutrophils (6). There is no agreement among researchers on whether there are differences in plasma Lf levels between males and females (6).Lf is remarkably resistant to proteolytic degradation by enzymes such as trypsin, allowing it to be partially resistant to digestion in the gut, likely due to glycan-dependent resistance. The iron-saturated form, holo lactoferrin, is even more resistant to proteolysis than the iron-free form, apo lactoferrin, because the iron ion stabilizes its structure, making it less vulnerable to degradation (7). Resistance to proteolytic degradation enables Lf to be absorbed by the body, making it a significant nutrient for neonatal growth.

In recent years, there has been growing interest in the potential role of Lf in skeletal homeostasis, particularly in maintaining bone health and treating bone-related disorders such as osteoporosis. Studies have shown that Lf is expressed in bone cells, including osteoblasts and osteoclasts, and can modulate bone metabolism by promoting osteoblast differentiation and mineralization, inhibiting osteoclast activity, and regulating bone remodeling (5, 8, 9). The anti-inflammatory (10) and antioxidant (11) effects of Lf could contribute to its salutary effects on bone health. Given the beneficial effects of Lf on bone cells, it has therapeutic potential for treating metabolic bone disorders such as postmenopausal osteoporosis. Lf has also been the subject of extensive research in orthopedics. In recent years, there has been growing interest in using Lf-based therapies to treat various orthopedic conditions, such as fractures, osteoporosis, and implant-associated infections. A promising area of emerging research involves the targeted delivery of Lf to bones through drug delivery methods, in order to leverage its multiple beneficial effects on skeletal health. Expression of Lf receptors on the surface of osteoblasts, which are responsible for bone formation, allows specific targeting of this protein to the bone. Several preclinical and limited clinical research that would be discussed subsequently suggests that Lf has therapeutic promise in metabolic bone disorders and orthopedic applications. The focus of this narrative review is to examine and analyze the interplay between Lf and various cellular and molecular factors involved in maintaining bone health, as well as to assess the potential therapeutic benefits of using Lf-derived molecules for treating metabolic bone diseases and orthopedic conditions.

2 An overview of varied signaling by Lf

Lf has been shown to interact with various receptors and molecules, including CD14 (12), LDL receptor-related protein-1 (LRP-1/CD91) (13, 14), intelectin-1 (omentin-1) (15), Toll-like receptors 2 and 4 (TLR4) (16), cytokine receptor 4, and heparan sulfate proteoglycans (HSPGs) (17). CD14 is a glycosylphosphatidylinositol-anchored protein that acts as a co-receptor for toll-like receptor 4 (TLR4), a receptor recognizing bacterial lipopolysaccharides (LPS) (18). Lf has been shown to bind to CD14 and enhance the recognition of LPS by TLR4, leading to the activation of immune responses (19). LRP-1/CD91 is a multifunctional cell-surface receptor involved in various biological processes, such as endocytosis, cell signaling, and cell migration (20). Lf has been shown to bind to LRP-1/CD91 and regulate the internalization and degradation of the receptor (13). Intelectin-1

(omentin-1) is a lectin-like protein involved in various biological processes, including inflammation, cell adhesion, and angiogenesis. Lf has been shown to bind to intelectin-1 and regulate its biological functions (15). TLR4 is a receptor that recognizes various microbial components, such as LPS, and activates immune responses. Lf has been shown to activate TLR4 to enhance the production of pro-inflammatory cytokines (19). Cytokine receptor 4 (CXCR4) is a G protein-coupled receptor (GPCR) involved in various biological processes, such as cell migration, proliferation, and survival. Lf has been shown to bind to CXCR4 and regulate its signaling pathways (21). HSPGs are cell-surface and extracellular matrix macromolecules involved in various biological processes, such as cell adhesion, migration, and signaling. Lf has been shown to bind to HSPGs and regulate their biological functions, such as cell adhesion and migration (17). These interactions are critical in the innate immune system and other biological processes, such as inflammation, cell adhesion, migration, proliferation, and differentiation.

3 The regulation of bone cells by Lf and its associated signaling mechanisms

3.1 Mesenchymal stem cells (MSC)

In adult mammals, MSCs make up approximately 0.01% to 0.1% of the nucleated cells of bone marrow (22–24). Bone marrow MSCs can differentiate to osteoblasts, adipocytes and chondrocytes. In adult marrow, aging or altered metabolic conditions such as diabetes cause greater adipocyte differentiation over osteoblast differentiation leading to bone loss. Estrogen and PTH are two hormones that support increased osteogenic differentiation of bone marrow MSCs and concomitantly inhibit adipogenic differentiation thus favoring bone formation (25). In human bone marrow-derived MSCs, Lf treatment has been shown to suppress H_2O_2-derived reactive oxygen species (ROS) levels that likely inhibited senescence, and apoptosis of these cells. Moreover, the antiapoptotic effect of Lf in MSC involved inhibition of caspase-3 and activation of AKT activation (26). In MSCs obtained from adipose tissue, Lf showed mitogenic as well as pro-osteogenic effect demonstrated by the upregulation of Runx2 and ALP, and has the potential for bone tissue engineering applications (27). Indeed, incorporating Lf into biodegradable matrices containing hydroxyapatite, can enhance their osteogenic properties when applied to human MSCs (28, 29). However, there are no studies investigating whether Lf inhibits adipogenic differentiation of bone marrow-derived MSC which could have shed light on how Lf regulates the fate of MSCs, particularly their differentiation into osteoblasts and adipocytes.

3.2 Osteoblasts

Lf has been shown to regulate several molecular pathways in osteoblasts responsible for bone formation and remodeling. Several signaling pathways are involved in Lf's actions in osteoblast proliferation, differentiation, and survival. The proximal signaling events identified for these actions include low-density lipoprotein receptor-related protein 1 (LRP1), IGF-1R, and TGFβ receptor pathways. LRP1 is a transmembrane receptor that can promote endocytosis of Lf (13). LRP1 can also produce cytoplasmic membrane-bound vesicles in osteoblasts, essential for the intracellular transport of proteins and other molecules. Lf has been shown to activate the extracellular signal-regulated kinase (ERK) pathway in osteoblasts through LRP1. Activation of the ERK pathway can stimulate osteoblast differentiation and bone formation, and Lf-mediated activation of this pathway may contribute to its osteogenic effects. On the other hand, Lf, through the PI3K/Akt pathway that is independent of LRP-1, inhibits osteoblast apoptosis has been reported (30).

Insulin-like growth factor 1-Insulin-like growth factor 1 receptor (IGF-1-IGF-1R)signaling plays a vital role in regulating bone metabolism, and a decline in IGF-1 has been implicated in age-related bone loss. Lf could address the decline in IGF-1 that occurs with aging by upregulating IGF-1 and IGF-1R in osteoblasts, which improved their viability under apoptotic stimulus (31). In senescent osteoblasts derived from SAMP6 mice (senescence-accelerated mouse-prone 6), an established model of accelerated aging that display several age-related phenotypes, including osteoporosis, sarcopenia, and cognitive decline, Lf enhanced the activity of the IGF1-Akt-mechanistic target of rapamycin (mTOR) signaling pathway. As a consequence of activating the IGF-1R-mediated osteogenic effect, Lf significantly attenuated the progression of osteoporosis due to senility (32). The suppression of senescent proteins, including p16 and p21, and oxidative injury through the upregulation of antioxidant enzyme activity through IGF-1R signaling likely attenuated the senescent-induced bone loss by Lf in SAMP6 model (32). Furthermore, Lf promoted the formation of osteoblasts from adipose tissue-derived stem cells (ADSCs) by activating the PI3K/AKT and IGF-R1 signaling pathways (33). Thus, it appears that to promote Lf's osteogenic function, which includes osteoblast development from stem cells, osteoblast maturation, and osteoblast survival, the IGF-1-IGF-1R signaling is an effector arm. In bone marrow stromal cells (BMSCs), Lf and its digests activated the PI3K/AKT and ERK signaling pathways and promoted the expression of osteoblast-specific genes, such as runt-related transcription factor 2 (Runx2), alkaline phosphatase (ALP), and osteocalcin (OCN), while suppressing the expression of adipocyte-specific genes, such as peroxisome proliferator-activated receptor gamma(PPARγ)and fatty acid-binding protein 4 (FABP4). However, whether, IGF-1-IGF-1R signaling mediated the effect of Lf and its digests has not been studied (34).

Lf also activated the canonical TGF-β signaling pathway involving smad 2 via the TGF-β receptor II (TβRII), as demonstrated by the upregulation of osteogenic genes including Runx2, osterix, and collagen type I (35). Both canonical and noncanonical TGF-β signaling pathways were involved in the Lf-induced osteogenic activity of C3H10T1/2 MSCs. Lf treatment increased the phosphorylation of Smad2/3 and p38 MAP kinase, indicating the activation of canonical TGF-β signaling in the

osteogenic differentiation of C3H10T1/2 cells. Lf also induced the phosphorylation of ERK1/2 in C3H10T1/2 cells, indicating the activation of noncanonical TGF-β signaling in the osteogenic differentiation of the cells (36).

From the preceding discussion, it appears that Lfsignaling through LRP1, IGF-1R, and TGFβ receptor trigger a cascade of events in osteoblasts that result in the activation of several downstream pathways, including ERK1, PI3K, Akt. mTOR and smad2/3 that promote osteoblast growth, survival, and differentiation (for a schematic illustration, refer to Figure 1).

There are reports of additional signaling events elicited by Lf in osteoblasts besides the three receptors described above. For example, Lf stimulates the proliferation of osteoblasts through the upregulation of prostaglandin-endoperoxide synthase 2 (Ptgs2) (the enzyme encoding COX2) and NFATc1 activities. Inhibiting either COX2 or NFATc1 activity blocked the mitogenic effect of Lf in osteoblasts (37). Lf can also regulate gene expression by modulating long non-coding RNAs (lncRNAs). Knockdown of a specific lncRNA (RP11-509I15.3) that was upregulated by Lf treatment impaired osteogenic differentiation of rat BMSCs, suggesting that this lncRNA has roles in mediating the osteogenic effects of Lf (36).

In osteoblasts, Lf can inhibit the NF-κB signaling pathway, which is involved in the regulation of inflammatory responses, and is involved in osteoclast differentiation and bone resorption (38). Activation of NF-κB in osteoblasts results in the increased production of RANKL over OPG, which favors enhanced osteoclastogenesis. E2 negatively regulates RANKL, and its serum levels are increased after menopause (39). Consequently, denosumab, a human antibody against RANKL, is an approved therapy for postmenopausal osteoporosis (3). In the animal model of osteoporosis achieved by OVX, Lf suppressed the OVX-induced increases in RANKL: OPG ratio (38). Lf's anti-oxidant/anti-inflammatory action appears to mediate this effect, although other regulatory mechanisms need to be investigated further.

3.3 Osteoclasts

Bone marrow cells are a heterogeneous population that includes osteoclast precursors, osteoblasts, and other cell types. Lipopolysaccharide (LPS), a component of the outer membrane of gram-negative bacteria, stimulates osteoclastogenesis (the formation of bone-destroying cells) by activating the RANKL signaling pathway in bone marrow cells. In mouse bone marrow cells, Lf inhibited LPS-induced osteoclastogenesis dose-dependently (9). When human peripheral CD14+ monocyte and macrophage cells were induced to differentiate into osteoclasts by a cocktail of macrophage colony-stimulating factor (M-CSF) and RANKL, Lf

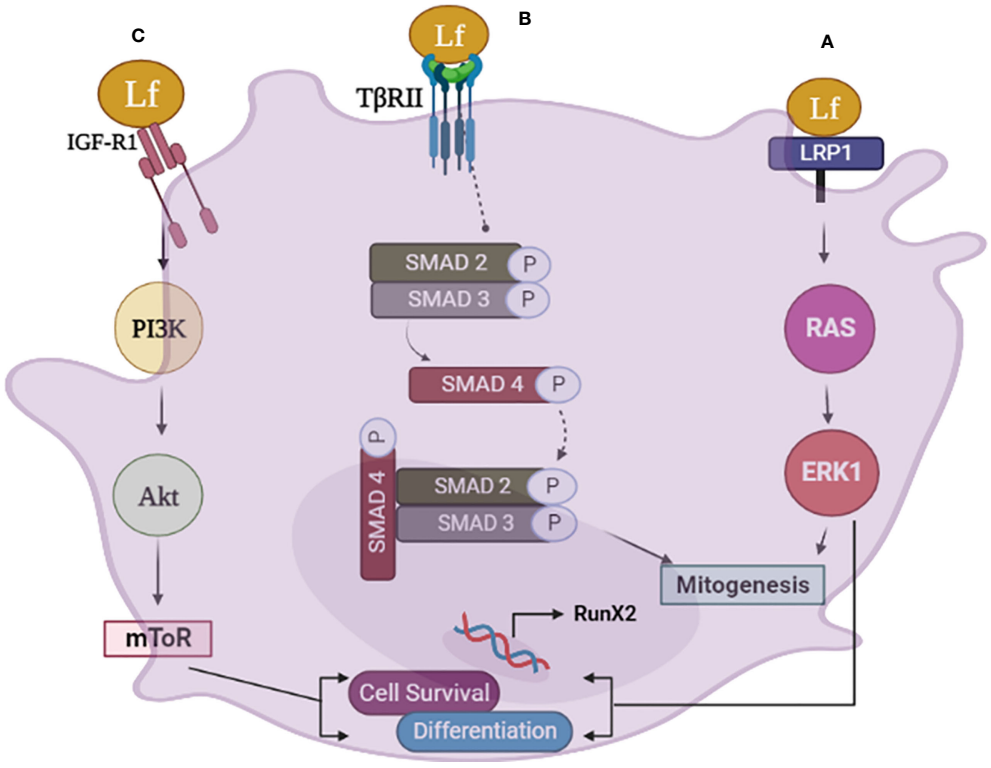

FIGURE 1
The schematic diagram illustrates the various pathways involved in lactoferrin (Lf) signaling in osteoblasts. **(A)** Lfsignaling via LRP1 in osteoblasts leads to mitogenesis and differentiation through the RAS-MAPK pathway. Lf binds to LRP1, triggering the activation of ERK, which promotes osteoblast differentiation and bone formation. The activation of ERK also induces mitogenesis in osteoblasts. **(B)** Lf can also signal through the TGFb receptor II (TβRII) in osteoblasts, activating smad 2, 3. This pathway results in the upregulation of osteogenic genes and promotes osteoblast differentiation. **(C)** Lfsignaling via the IGF-1 receptor in osteoblasts activates the PI3K/Akt and mTOR pathway, promoting osteoblast differentiation and survival independently of LRP1. This pathway promotes the survival of osteoblasts by inhibiting apoptosis. Image is made using the Biorender Software.

suppressed the expression of genes and proteins involved in osteoclast differentiation and activity such as TRAP and cathepsin K.

Overall, Lf regulates osteoclast function via two different mechanisms. Firstly, it lowers the RANKL/OPG ratio by influencing osteoblastic cells (9) and so suppressing osteoclastogenesis. Secondly, through its anti-inflammatory activity, Lf directly reduces osteoclastogenesis by blocking the downstream signaling that occurs when RANKL binds to RANK. Furthermore, by scavenging free radicals, Lf can limit the formation of ROS that are implicated in osteoclastogenesis (for a schematic illustration of osteoclast regulation by Lf, refer to Figure 2). The functional outcome of these suppressive effects was the inhibition of the resorption of bones by Lf ex vivo (40). Inhibition of osteoclastogenesis by Lf may have therapeutic potential for preventing bone loss associated with infectious diseases, periodontitis, and other inflammation-related diseases such as RA besides postmenopausal osteoporosis (41, 42).

3.4 Chondrocyte

Lf has a pro-survival effect in chondrocytes. Lf was found to prevent the programmed cell death of chondrocytes induced by interleukin-1 beta (IL-1β), a cytokine known to contribute to osteoarthritis (OA) development. Lf inhibited chondrocyte apoptosis by activating the protein kinase B (AKT1) pathway, which leads to the activation of the cAMP response element-binding protein 1 (CREB1) transcription factor. CREB1 plays a crucial role in regulating cell survival and has been shown to protect chondrocytes from apoptosis. When OA was induced in mice by destabilization of the medial meniscus (DMM) surgery in the knee joint, Lf significantly reduced cartilage degradation in the knee joints of the mice compared to the control group, as indicated by histological and immunohistochemical analyses (43).

Additionally, the Lf-treated mice showed significantly reduced chondrocyte apoptosis in the cartilage tissues of the knee joints, as indicated by TUNEL staining (43). Lf also protected chondrocytes from dexamethasone (Dex)-induced apoptosis by preventing the Dex-induced down-regulation of ERK1/2 and up-regulation of proteins involved in apoptosis, including FAS, FASL, and caspase 3 (44). By activating ERK1/2, Lf appears to preferentially increase the expression of BMP7, compared to BMP2 or BMP4 in chondrocytes (45). An increase in BMP7 expression in chondrocytes is generally considered beneficial, as it can enhance the ability of these cells to maintain and repair the cartilage matrix by promoting the proliferation, differentiation, and survival of these cells, as well as the synthesis of extracellular matrix proteins, such as collagen and proteoglycans. In the ATDC5 chondroprogenitor cell line, Lf inhibited their hypertrophic differentiation by inhibiting the expression of hypertrophic markers such as collagen X and ALP (46). Hypertrophic differentiation of chondrocytes leads to chondrocyte enlargement during the formation of bone, which is required for bone development. During bone development, chondrocytes undergo hypertrophic differentiation and contribute to the formation of mineralized bone tissue. However, excessive hypertrophic differentiation of chondrocytes can lead to cartilage breakdown and ultimately contribute to the progression of joint diseases such as OA.

4 Conservation of bone mass by Lf

When Lf was given to adult rats, it resulted in a significant increase in the rate at which minerals were deposited on the bone surface (mineral apposition rate), which is an indicator of osteoblast activity, and an increase in the overall amount of bone formed

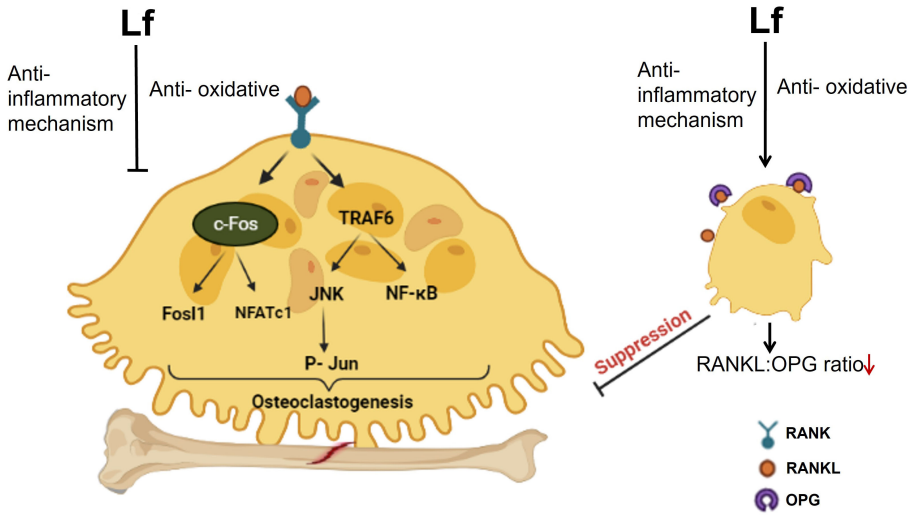

FIGURE 2
The schematic diagram illustrates the regulation of osteoclast function by Lf. Lf inhibits osteoclastogenesis in two ways. Firstly, it lowers the RANKL/OPG ratio by acting on osteoblastic cells. Secondly, it directly inhibits osteoclastogenesis through its anti-inflammatory effect, which prevents downstream signaling following RANKL binding to RANK. Moreover, Lf's ability to scavenge free radicals also inhibits the generation of ROS involved in osteoclastogenesis. Image is made using the Biorender Software.

(cumulative bone formation rate) in skull bone (5). Lf supplementation was found to upregulate vitamin D receptor in both osteoblasts and kidneys, leading to improved BMD in both vitamin D deficient and vitamin D normal mice (47), highlighting its significance in maintaining appropriate vitamin D signaling necessary for optimal bone health. In SAMP6 mice, a model of aging and senescence, which are associated with decreased bone mass and increased risk of osteoporosis, Lf (2 g/kg/day) alleviated the adverse effects of age-related bone loss (32). Dietary supplementation or gavage administration of Lf prevented the loss of bone mass and strength in OVX mice and rats (38, 48–50). Femur is a critical bone for weight-bearing and movement, and the preservation of bone mass and strength in this bone by Lf is important for maintaining overall bone health and reducing the risk of fractures (49, 50). Thus it is conceivable that Lf may find therapeutic application in several disease conditions, including osteoporosis, chronic kidney disease, celiac disease, and vitamin D deficiency, where decreased bone formation rate is one of the reasons for bone loss over time.

Bone turnover markers (BTMs) are molecules released during the process of bone remodeling that include markers of bone resorption (β-CTx and NTx) and markers of bone formation (BALP, P1NP, osteocalcin, etc.) indicating the rate of bone turnover. BTMs are used as biomarkers in clinical trials for osteoporosis and related conditions, as they reflect changes in bone metabolism and can predict the risk of fractures. These markers are typically higher in OVX condition, where estrogen deficiency leads to increased bone resorption and decreased bone formation, resulting in osteoporosis. Higher levels of resorption markers and lower levels of formation markers are associated with bone loss and increased risk of fractures. Lf has been demonstrated to reduce the increases in bone resorption markers, such as CTX and NTx, induced by OVX. In addition, Lf increased markers of bone formation, such as osteocalcin and BSALP, compared to OVx animals (38, 49, 51). BTMs are useful in assessing the efficacy of drugs that aim to modify bone turnover, such as antiresorptive and anabolic agents. Given that Lf has been shown to affect BTMs in preclinical studies, including reducing bone resorption markers and increasing bone formation markers, it is a promising candidate for further investigation in clinical trials.

Consistent with the preclinical studies in OVX animals, where Lf reduced bone resorption markers, and increased bone formation markers, a study in healthy postmenopausal women reported that milk ribonuclease-enriched Lf supplementation resulted in a significant increase in osteocalcin and BSALP, and a decrease in β-CTx compared with the placebo control (52). Monitoring BTMs during clinical trials with Lf could provide insight into its mechanism of action and effectiveness in improving human bone health.

5 Effects of Lf in fracture healing

Fractures of long bones, especially large, comminuted, segmental, transverse, or open, are difficult to heal and have a high risk of non-union (failure to heal), especially in osteoporotic conditions (53).Nonunions require revision surgery that involves removing any hardware (such as screws or plates) used to stabilize the bone during the initial surgery and then using bone grafting to promote proper bone healing. When nonunions are suspected, BMPs (BMP-2/-7) are applied locally to the fracture site to stimulate the growth of new bone tissue and promote healing. However, BMPs (BMP-2/-7) are typically reserved for more complex or difficult-to-heal fractures and are not considered a first-line treatment for most fractures (54). Moreover, a high amount of BMP-2 in the graft can stimulate the local production of noggin, a protein that inhibits BMP-2 activity (55). This can lead to a negative feedback loop in which the efficacy of BMP-2 in promoting bone healing is diminished. As a result, bone growth promoters such as Lf could be evaluated for systemic delivery to reduce the rate of nonunions in large fractures.

The primary process involved in fracture healing is endochondral ossification. In this process, MSCs differentiate into chondrocytes that form a cartilage template, which is then mineralized. Blood vessels invade the calcified cartilage and bring osteoblasts that deposit new bone tissue, while osteoclasts break down and remodel the newly formed bone (56). Osteoporotic conditions can delay fracture healing by promoting excessive bone resorption and delaying the formation of nascent bone. This can lead to weaker callus formation and reduced bone strength at the fracture site, making it more prone to re-injury. Our preceding discussion described that Lf has salutary effects in osteoblasts, chondrocytes, and osteoclasts that support its use in nonunions by acting as a systemic bone growth promoter.

In the laboratory setting, the rabbit tibia is a commonly used model for studying long bone defects and fracture healing. The rabbit tibia offers several advantages as a model for studying bone healing, including its similar size and anatomy to human long bones and its weight-bearing. The unilateral tibial osteodistraction model is an animal model for studying bone regeneration and is often used to evaluate potential therapies for bone defects and fractures (57). In the osteodistraction model, a small cut (osteotomy) is made in the tibia, and an external fixator device is attached to the bone on either side of the osteotomy. The device is then slowly adjusted over time, causing the bone ends to gradually separate and new bone tissue to form in the gap between them. The osteodistraction technique can be used to study the effects of mechanical loading and other factors on bone formation and healing. Oral Lf was found to promote bone regeneration during distraction osteogenesis in rabbit tibia by increasing OPG to RANKL ratio, inhibiting the bone resorption rate (58). Another large bone defect model that is difficult to heal is a surgically created critical-sized defect. This defect is too large to heal on its own and is used in research to mimic open tibial fractures in humans that require orthopedic reconstructive procedures (59). By creating a critical-sized bone defect in the rabbit tibia, it is possible to study various interventions, such as bone grafting, growth factors, and tissue engineering, to promote bone regeneration and healing and to develop new treatments for orthopedic injuries and disorders in humans. An 18 amino acid peptide (RKVRGPPVSCIKRDSPIQ) from the N-terminus of the N-lobe of human Lf called LP2 stimulated bone regeneration in the critical-sized defect in rabbits by increasing the production of BMP-

2 in osteoblasts. Additionally, the LP2 peptide had an anti-osteoclastogenic effect by enhancing the ratio of OPG to RANKL in osteoblasts (60). These data suggest that the upregulation of OPG is the critical mechanism underlying the healing of long bone fracture by Lf.

6 Designing therapeutic peptides from Lf FOR treating bone diseases

Lf is a large and multifunctional protein. Hence, small peptides made from Lf are useful for therapeutic purposes because they allow for more efficient delivery and targeting of specific biological functions. Furthermore, smaller peptides are less immunogenic than bigger proteins, lowering the risk of unfavorable immune responses and adverse effects. Smaller peptides are also more likely to penetrate tissues and reach their target cells or molecules, increasing their bioavailability and efficacy (61).

Positively charged amino acid segments, such as those containing arginine, lysine, and histidine, are often preferred for the design of bioactive peptides because they can interact with negatively charged molecules in biological systems. These positively charged amino acids, in particular, can generate electrostatic interactions with negatively charged cell membranes and other macromolecules, resulting in various biological effects. Moreover, positively charged amino acid segments can facilitate the uptake of peptides into cells, as some cellular uptake mechanisms are known to be selective for peptides with positively charged residues. This enhanced cellular uptake can increase the bioavailability and efficacy of peptides. Thus, the N-terminal region of Lf has become a focal point for designing peptides with potential therapeutic applications. Lactoferricin (62–64) and lactoferrampin (65, 66) deserve special mention because these have undergone extensive research for their anti-microbial effect. Both are cationic and α-helical peptides with a hydrophobic N-terminus and a hydrophilic C-terminus that are stable over a wide pH and temperature range (67).Lactoferricin has potent antimicrobial activity against a broad range of bacteria, fungi, and viruses, and lactoferrampin has broad-spectrum activity against bacteria, fungi, and protozoa (62–66). Given the anti-microbial property of Lf may be considered in the treatment of osteomyelitis, a bone infection commonly caused by Staphylococcus aureus. In this regard, a human Lf-derived peptide in both prophylactic and therapeutic modes significantly reduced severity of osteomyelitis in a rabbit model evident from improved microbiological, radiological and histological scores compared to the placebo group. Strikingly, the effect of the peptide was on a par with gentamicin (68, 69). The rabbit model of osteomyelitis mimics the progression of human disease because the long bones of rabbits are physiologically similar to humans - both species having Haversian remodeling. Hence, the findings of the reports showing the mitigation of osteomyelitis by Lf-derived peptide in the rabbit model of the disease holds potential translational value for human applications.

The anti-microbial mechanism of Lf-derived peptides could also be useful in affording protection against cartilage degradation. For example, lactoferricin inhibits the effects of IL-1 and fibroblast growth factor 2, which are known to cause cartilage degradation (70). Lactoferricin also induces the production of interleukin-11 (IL-11), an anti-inflammatory cytokine, which then activates the STAT3 signaling pathway to up-regulate the expression of TIMP-1 in human adult articular chondrocytes. The up-regulation of TIMP-1 expression by IL-11 may be a secondary cellular response after IL-11 induction by lactoferricin via the ERK-AP-1 axis (71). Together, these reports suggest that lactoferricin may have a dual mechanism of action in reducing inflammation in human articular cartilage by both inducing the production of anti-inflammatory cytokines and inhibiting the production of pro-inflammatory cytokines. These reports also underscore the potential of lactoferricin as a therapeutic agent for the treatment of inflammatory joint diseases such as OA. However, the effect of lactoferricin on metabolic bone diseases such as postmenopausal osteoporosis has not been investigated. As discussed in the preceding section, by suppressing inflammatory mediators including TNFα, IL-1β and IL-6, Lf/Lf-derived peptides also inhibit osteoclast formation and activity. In this regard, the effect of lactoferricin and other Lf-derived peptides on osteoclast formation and function, and inhibition of bone resorption *in vivo* has not been investigated.

Two Lf-derived peptides have been shown to have potential effects on osteoblast function. LFP-C, a 9-amino acid peptide was isolated from Lf hydrolysates by pepsin digestion enhanced osteoblast differentiation and mineralization and increased the expression of genes involved in bone formation (72). LP2 is another osteogenic peptide derived from human Lf. This synthetic peptide has a self-assembling property and assumes nanoglobular structures owing to which it spontaneously aggregate and form stable, spherical structures, without the need for external assembly factors or scaffolds. LP2, when systemically administered, demonstrated osteogenic and anti-resorptive effects in maintaining bone mass and strength in OVX rats by activating p38 MAPK and BMP-2 production and increasing OPG production, and in rabbits with a critical-sized defect in the tibia, it led to faster healing of the defect than control (60). For various Lf-derived peptides and their functions, refer to Table 1. Taken together, it appears that Lf-derived peptides hold great promise as potential therapeutic agents for the treatment of orthopedic and metabolic bone diseases.

7 Delivery of Lf to the bone

Although Lf is present in serum, its active concentration may not be present at the site requiring bone regeneration. Bone regeneration is a complex process that requires the presence of various growth factors and biomolecules at the site of injury, and the levels of these factors can vary depending on the location and extent of the injury. Delivering Lf to the site of bone regeneration can ensure that it is present in sufficient quantities to promote bone growth and regeneration. Additionally, Lf delivery strategies can protect it from degradation and provide sustained release over time, further enhancing its effectiveness. Biocompatibility of Lf, i.e. non-toxicity to cells and tissue makes it an attractive target for delivery to the bone to promote bone growth, reduce inflammation, and

TABLE 1 Lf-derived peptides with their activities.

Name	Sequence	Activity	Reference
Lactoferrin			
b-lactoferrin	FKSETKNLL	osteogenesis	(72)
h-lactoferrin	RKVRGPPVSCIKRDSPIQ	Osteogenesis	(60)
h-lactoferrin	GRRRRSVQWCA	Osteomyelitis	(68, 69)
Lactoferricin			
b-lactoferricin	FKCRR WQWRMKKLGAPSITCVRRAF	Anti-microbial	(63, 64)
b-lactoferricin	FKCRRWQWRMKKLG	Anti-microbial and antibiofilm	(73)
b-lactoferricin	FKCRRWQWRMKKLGAPSITCVRRAF	Anti-cancer	(74)
Lactoferrampin			
h-lactoferrampin	WNLLRQAQEKFGKDKSPK	Anti-viral	(65)
h-lactoferrampin	WNLLRQAQEKFGKDKSP	Anti-microbial	(66, 75)
d-lactoferrampin	WKLLSKAQEKFGKMKSR	Antimicrobial, candidacidal and anti-bacterial	(76, 77)

b, bovine; h, human; d, deer.

prevent infections. Effective delivery of Lf to the site of bone regeneration has been achieved mostly through hydrogels, which protect it from degradation and enable sustained release over time.

Hydrogels are cross-linked polymer networks that can absorb large amounts of water while maintaining their three-dimensional structure and have a similar mechanical strength and elasticity to natural tissues (78). Lf can be added to the hydrogel during the synthesis process or can be incorporated after the hydrogel is formed. Once implanted at the site of bone regeneration, the hydrogel can slowly release Lf, providing sustained delivery over time. Additionally, the hydrogel can provide a matrix for cell attachment and proliferation, promoting bone growth and regeneration. Hydrogels can also be functionalized with specific chemical groups to enhance the delivery of Lf with other growth factors.

Gelatin hydrogels are hydrophilic and biodegradable, and they are commonly used in biomedical applications due to their biocompatibility and ability to mimic the extracellular matrix of natural tissues. When the release of Lf from a gelatin hydrogel was sustained for 28 days, it promoted the proliferation and differentiation of osteoblasts. In a rat femoral defect model, the Lf-releasing gelatin hydrogel resulted in bone regeneration. The newly formed bone showed good integration with the surrounding bone tissue and no signs of inflammation or necrosis (79).

Poloxamer hydrogels are a class of hydrogels made up of a triblock copolymer of poly(ethylene oxide)-poly(propylene oxide)-poly(ethylene oxide) that can exist as a liquid at low temperatures but form a gel at body temperature (80). However, poloxamer hydrogels are non-biodegradable and have a relatively low mechanical strength compared to gelatin hydrogels. Besides thermal reversibility, poloxamer hydrogels have good biocompatibility and low toxicity, making them suitable for various biomedical applications as injectable gel formulations. Poloxamer hydrogels loaded with Lf can sustain the release of Lf for up to 21 days, which promotes bone regeneration. This sustained release formulation of Lf enhanced the osteogenic differentiation of rat MSCs and improved mechanical strength compared to the non-loaded hydrogels. In a rat calvarial defect model, this formulation promoted bone regeneration and new bone formation, and the newly formed bone tissue showed no signs of inflammation or necrosis (81).

Chitin/PLGA-$CaSO_4$ hydrogel has distinct advantages over other hydrogels, such as osteogenic and angiogenic activity, a porous structure, good biocompatibility, sol-gel transition at body temperature, and controlled release of bioactive molecules. The chitin/PLGA-$CaSO_4$ hydrogel loaded with Lf and substance P significantly promoted bone regeneration and new bone formation in the calvarial bone defect model compared to the hydrogel alone or hydrogel loaded with Lf or substance P alone. As substance P has bone regenerative action and improves bone healing, it was included with Lf, which resulted in synergistic effects on bone regeneration and improved the therapeutic efficacy of the hydrogel. The combination of Lf and substance P enhanced the osteogenic and angiogenic activity of the hydrogel, as evidenced by increased expression of osteogenic and angiogenic markers *in vitro* and *in vivo* (82). The findings of this study suggest that combining Lf with other osteogenic agents, such as teriparatide, could potentially enhance the overall bone regeneration response. Figure 3 describes various strategies to improve the delivery of Lf or Lf-derived peptides to the bone to accelerate critical-sized bone defects that are observed in comminuted fractures in humans.

8 Summary & future research

This review covered the roles of Lf bone remodeling and resorption, bone healing, and regeneration. LRP1, IGF-1R, and TGFβ receptor pathways have been identified as the proximal

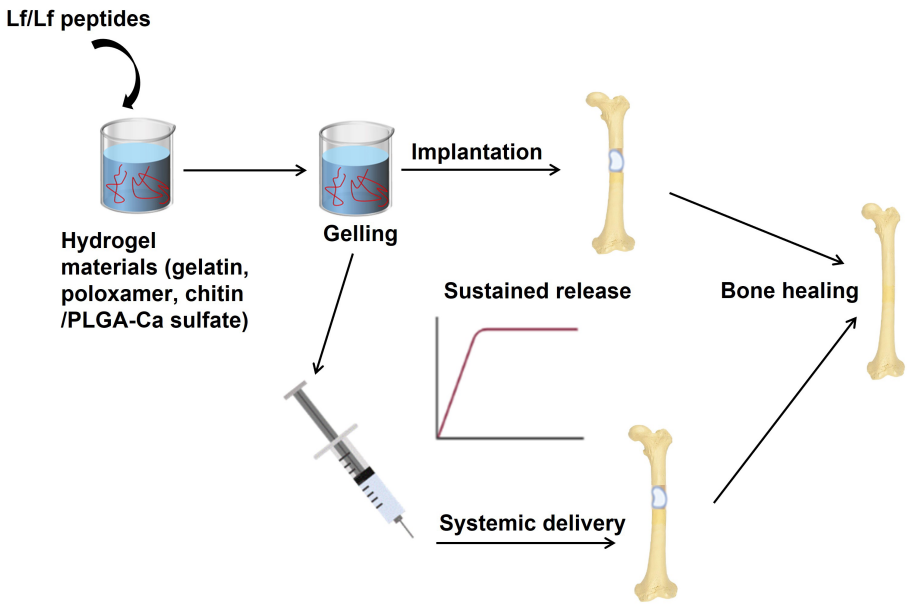

FIGURE 3
Strategies to improve the delivery of Lf or Lf-derived peptides to the bone. Hydrogels have been used in preclinical models of critical-sized bone defects (mimicking non-unions) as sustained-release formulations to deliver high amounts of Lf to bones. In these models, Lf has been used for local delivery of Lf as implants at the site of the bone defect. This approach ensures Lf's sustained release, which can stimulate bone regeneration and repair. In addition, systemic delivery of Lf through hydrogels has also been explored. In this case, hydrogels containing Lf are injected into the bloodstream, allowing for the controlled release of Lf over time. These approaches have shown promising results in promoting bone regeneration in critical-sized bone defects. Image is made using the Biorender Software.

signaling events involved in the actions of Lf in osteoblasts. The downstream events of these proximal signaling pathways lead to the activation of ERK1/2, Akt, PI3K/Akt, MAPK, and SMAD pathways. These signaling pathways promote proliferation, migration, survival, differentiation, and extracellular matrix formation in osteoblasts, which are important for tissue repair and regeneration. Lf inhibits osteoclast differentiation and activity by suppressing NF-κB signaling, inducing OPG expression, and downregulating RANKL expression, thereby modulating key regulatory pathways involved in osteoclastogenesis and bone resorption. Lf also modulates matrix metalloproteinase activity, which is involved in bone remodeling. Lf's actions on chondrocytes involve activating multiple signaling pathways, including Akt, CREB, ERK, and BMP7, which promote chondrogenesis, cell survival, and cartilage formation. Regulation of these signaling events in bone cells by Lf contributes to tissue repair and regeneration and inhibits bone loss in osteoporosis. By improving bone mineral density and reducing the risk of bone loss, Lf may help prevent fractures and other osteoporosis-related complications. In addition, further investigation is needed to elucidate the exact mechanisms of action of Lf on bone metabolism, including the role of Lf receptors in bone cells.

The limitations of current osteoporosis therapies are that they tend to have a one-sided approach that either inhibits bone resorption or stimulates bone formation. For example, bisphosphonates, which are one of the most commonly used osteoporosis drugs, inhibit bone resorption but do not stimulate bone formation. On the other hand, anabolic agents such as teriparatide and abaloparatide stimulate bone formation but have no effect on bone resorption. Therefore, there is a need for a therapy that can inhibit bone resorption as well as stimulate bone formation, providing a dual benefit for osteoporosis patients. Estrogen was once the only therapy that could inhibit bone resorption and stimulate bone formation. However, significant cancer and cardiovascular risks associated with estrogen use in postmenopausal women have resulted in its discontinuation. Therefore, there is currently no therapy that can provide the dual benefit of estrogen without the associated risks (for additional details, refer to Figure 4). Lf has the potential to fill the void left by estrogen as a therapy that can inhibit bone resorption and stimulate bone formation in osteoporosis patients. As an endogenously produced protein that has a good safety profile, low toxicity, and availability make it an attractive candidate for further investigation as a therapeutic agent for osteoporosis. However, further research is needed to fully understand its mechanisms of action and to determine its optimal dose and delivery route for therapeutic use.

Since osteogenic and chondrogenic peptides from Lf have already been found, a rational design strategy may be appropriate for developing more such peptides from Lf with improved function. By analyzing the amino acid sequences and structural features of existing osteogenic/chondrogenic peptides, key amino acid residues implicated in their biological activities can be identified and included in the design of novel osteogenic/chondrogenic peptides. Additionally, alanine scanning can be used to confirm the importance of specific amino acid residues identified through rational design and ensure that they are essential for the osteogenic/chondrogenic activity of the peptide. Combining these techniques can provide a more thorough understanding of the structure-function correlations of Lf-derived peptides and aid in

10.3389/fendo.2023.1218148

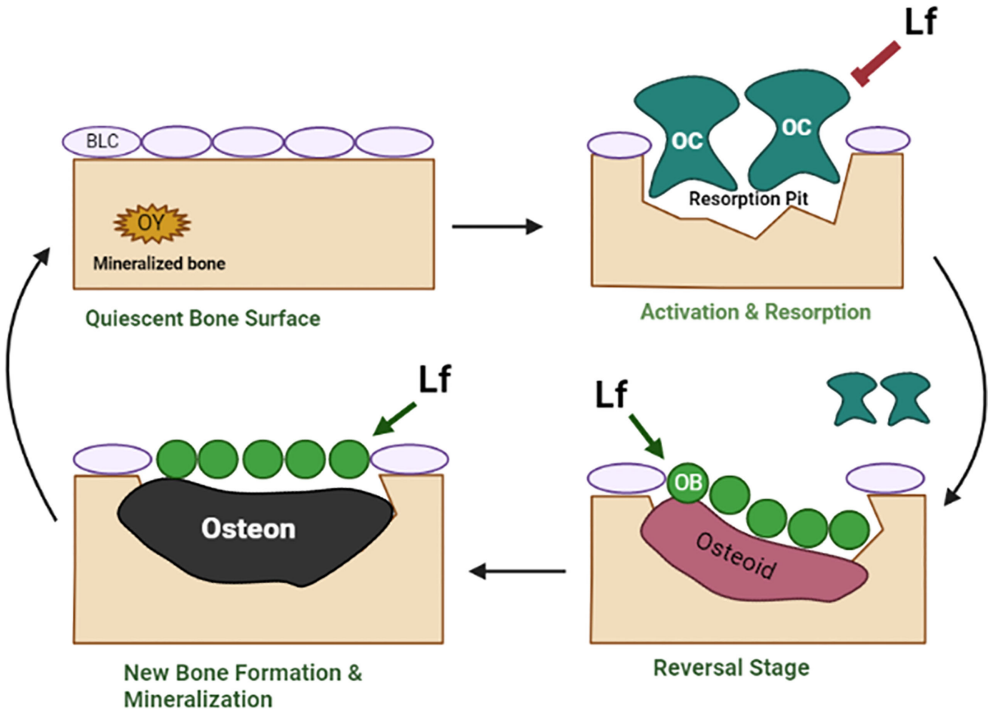

FIGURE 4
The schematic diagram shows the effects of Lf in bone remodeling. The bone remodeling cycle comprises several stages, including quiescence, activation & resorption, reversal, and formation. In the activation & resorption stage, osteoclasts are recruited to the bone surface and resorb the old bone. In the reversal stage, osteoblasts are recruited to the bone surface to begin the process of new bone formation. The final stage involves the production of new bone matrix by osteoblasts, which undergoes mineralization. In the normal bone remodeling cycle, there is a balance between bone resorption and bone formation such that the amount of bone that is resorbed is replaced by an equal amount of new bone formation, resulting in the maintenance of a constant bone mass. In osteoporosis, there is an imbalance between bone resorption and formation because osteoclast activity is increased. In contrast, osteoblast activity is decreased, resulting in decreased bone mass and an increased risk of fractures. Lf acts at the activation & resorption phases by the mechanisms described in Figure 2 to inhibit bone resorption. Lf also acts at the reversal and formation stages to stimulate bone formation by the mechanisms described in Figure 1. By these mechanisms, Lf corrects the remodeling cycle and restores bone mass. Osteioid, unmineralized bone matrix; osteon, mineralized bone matrix. Image is made using the Biorender Software.

generating novel osteogenic/chondrogenic peptides with increased potency and selectivity.

Hydrogels may enhance their therapeutic potential in bone-related applications by protecting Lf from degradation and enabling sustained release. Hence, hydrogels have been utilized as a drug delivery system and discussed here. However, further studies are needed to investigate the potential synergistic effects of combining Lf with other osteogenic agents in these hydrogels. There is also a need to develop hydrogels that mimic the complex mechanical properties of natural bone tissue and that can degrade over time and be replaced by new bone tissue. pH is an important factor during bone remodeling and the formulation of hydrogels because it can affect the solubility, stability, and bioactivity of biomolecules such as Lf. In bone regeneration, the pH of the local environment can affect the activity of bone cells. For example, a slightly acidic environment (pH 6.8-7.2) is beneficial for osteoclast activity required for initiating remodeling, while a slightly alkaline environment (pH 7.4-7.8) is beneficial for osteoblast activity. Therefore, enhancing the efficiency of Lf administration for bone regeneration may require regulating the pH of the local environment and the hydrogel formulation. This can be accomplished by using pH-sensitive hydrogels or by incorporating pH-modulating agents into the hydrogel formulation. Other approaches to more efficiently targeting Lf to bones may include encapsulating it in liposomes or polymeric nanoparticles and functionalizing the nanoparticles with bone-targeting molecules such as bisphosphonates, or conjugating Lf with bone-targeting peptides derived from osteocalcin or bone sialoprotein.

Future research areas for Lf and bone include determining its optimal dose and delivery routes for bone regeneration and osteoporosis. In addition, further investigation is needed to elucidate the exact mechanisms of action of Lf on bone metabolism, including the role of Lf receptors in bone cells. Clinical trials are also necessary to evaluate the safety and efficacy of Lf as an osteoporosis therapy in humans and to investigate its long-term effects on bone density and fracture risk. Additionally, considering its osteogenic and anti-resorptive effects, there is potential use for Lf in combination with osteogenic anti-osteoporosis drugs including teriparatide, abaloparatide or romosozumab, whether in the form of intact Lf, enzymatically digested Lf or a bioactive peptide such as LP2. Combining Lf or suitable Lf-derived peptide with any of the osteogenic drugs could potentially have a synergistic effect in the treatment of osteoporosis. Because Lf or the proteolytic digests have neutraceutical use, it could be conveniently assessed in clinical trials via oral administration. For Lf-derived peptides, however, given their parenteral route of administration, regulatory studies to assess safety, efficacy and optimal dosage are required before their use in humans. Finally, Lf may have therapeutic

applications in other bone diseases, such as OA and periodontitis, and further research is needed to explore its potential in these conditions.

Overall, the research on Lf has shown its potential in various aspects of bone remodeling, signaling, fracture healing, peptide synthesis, and Lf delivery to bones. Further research in this area may lead to the development of new treatments for bone-related disorders.

Author contributions

MT, Y-BH, G-YY, J-LL, and C-SH conducted literature search and wrote the manuscript. DT conceptualized the theme of the review and finalized the manuscript. DT takes responsibility for the integrity of the substance described in the review as a whole as 'guarantor'. All authors contributed to the article and approved the submitted version.

Conflict of interest

The authors declare that the research was conducted in the absence of any commercial or financial relationships that could be construed as a potential conflict of interest.

Publisher's note

References

1. Gosset A, Pouilles JM, Tremollieres F. Menopausal hormone therapy for the management of osteoporosis. *Best Pract Res Clin Endocrinol Metab* (2021) 35 (6):101551. doi: 10.1016/j.beem.2021.101551

2. Tella SH, Gallagher JC. Prevention and treatment of postmenopausal osteoporosis. *J Steroid Biochem Mol Biol* (2014) 142:155–70. doi: 10.1016/j.jsbmb.2013.09.008

3. Cummings SR, San Martin J, McClung MR, Siris ES, Eastell R, Reid IR, et al. Denosumab for prevention of fractures in postmenopausal women with osteoporosis. *N Engl J Med* (2009) 361(8):756–65. doi: 10.1056/NEJMoa0809493

4. Bhattacharyya S, Pal S, Chattopadhyay N. Targeted inhibition of sclerostin for post-menopausal osteoporosis therapy: A critical assessment of the mechanism of action. *Eur J Pharmacol* (2018) 826:39–47. doi: 10.1016/j.ejphar.2018.02.028

5. Cornish J, Callon KE, Naot D, Palmano KP, Banovic T, Bava U, et al. Lactoferrin is a potent regulator of bone cell activity and increases bone formation *in vivo*. *Endocrinology* (2004) 145(9):4366–74. doi: 10.1210/en.2003-1307

6. Levay PF, Viljoen M. Lactoferrin: A general review. *Haematologica* (1995) 80 (3):252–67.

7. Brines RD, Brock JH. The effect of trypsin and chymotrypsin on the *in vitro* antimicrobial and iron-binding properties of lactoferrin in human milk and bovine colostrum. Unusual resistance of human apolactoferrin to proteolytic digestion. *Biochim Biophys Acta* (1983) 759(3):229–35. doi: 10.1016/0304-4165(83)90317-3

8. Inubushi T, Kosai A, Yanagisawa S, Chanbora C, Miyauchi M, Yamasaki S, et al. Bovine lactoferrin enhances osteogenesis through smad2/3 and P38 mapk activation. *J Oral Biosci* (2020) 62(2):147–54. doi: 10.1016/j.job.2020.05.001

9. Inubushi T, Kawazoe A, Miyauchi M, Yanagisawa S, Subarnbhesaj A, Chanbora C, et al. Lactoferrin inhibits infection-related osteoclastogenesis without interrupting compressive force-related osteoclastogenesis. *Arch Oral Biol* (2014) 59(2):226–32. doi: 10.1016/j.archoralbio.2013.11.002

10. Conneely OM. Antiinflammatory activities of lactoferrin. *J Am Coll Nutr* (2001) 20(5 Suppl):389S–95S. doi: 10.1080/07315724.2001.10719173. discussion 96S-97S.

11. Mulder AM, Connellan PA, Oliver CJ, Morris CA, Stevenson LM. Bovine lactoferrin supplementation supports immune and antioxidant status in healthy human males. *Nutr Res* (2008) 28(9):583–9. doi: 10.1016/j.nutres.2008.05.007

12. Rawat P, Kumar S, Sheokand N, Raje CI, Raje M. The multifunctional glycolytic protein glyceraldehyde-3-phosphate dehydrogenase (Gapdh) is a novel macrophage lactoferrin receptor. *Biochem Cell Biol* (2012) 90(3):329–38. doi: 10.1139/o11-058

13. Grey A, Banovic T, Zhu Q, Watson M, Callon K, Palmano K, et al. The low-density lipoprotein receptor-related protein 1 is a mitogenic receptor for lactoferrin in osteoblastic cells. *Mol Endocrinol* (2004) 18(9):2268–78. doi: 10.1210/me.2003-0456

14. Ikoma-Seki K, Nakamura K, Morishita S, Ono T, Sugiyama K, Nishino H, et al. Role of lrp1 and erk and camp signaling pathways in lactoferrin-induced lipolysis in mature rat adipocytes. *PloS One* (2015) 10(10):e0141378. doi: 10.1371/journal.pone.0141378

15. Shin K, Wakabayashi H, Yamauchi K, Yaeshima T, Iwatsuki K. Recombinant human intelectin binds bovine lactoferrin and its peptides. *Biol Pharm Bull* (2008) 31 (8):1605–8. doi: 10.1248/bpb.31.1605

16. Gao CH, Dong HL, Tai L, Gao XM. Lactoferrin-containing immunocomplexes drive the conversion of human macrophages from M2- into M1-like phenotype. *Front Immunol* (2018) 9:37. doi: 10.3389/fimmu.2018.00037

17. Ji ZS, Mahley RW. Lactoferrin binding to heparan sulfate proteoglycans and the ldl receptor-related protein. Further evidence supporting the importance of direct binding of remnant lipoproteins to hspg. *Arterioscler Thromb* (1994) 14(12):2025–31. doi: 10.1161/01.atv.14.12.2025

18. Ciesielska A, Matyjek M, Kwiatkowska K. Tlr4 and cd14 trafficking and its influence on lps-induced pro-inflammatory signaling. *Cell Mol Life Sci* (2021) 78 (4):1233–61. doi: 10.1007/s00018-020-03656-y

19. Curran CS, Demick KP, Mansfield JM. Lactoferrin activates macrophages via tlr4-dependent and -independent signaling pathways. *Cell Immunol* (2006) 242(1):23–30. doi: 10.1016/j.cellimm.2006.08.006

20. Gonias SL, Campana WM. Ldl receptor-related protein-1: A regulator of inflammation in atherosclerosis, cancer, and injury to the nervous system. *Am J Pathol* (2014) 184(1):18–27. doi: 10.1016/j.ajpath.2013.08.029

21. Takayama Y, Aoki R, Uchida R, Tajima A, Aoki-Yoshida A. Role of cxc chemokine receptor type 4 as a lactoferrin receptor. *Biochem Cell Biol* (2017) 95 (1):57–63. doi: 10.1139/bcb-2016-0039

22. Tewari D, Khan MP, Sagar N, China SP, Singh AK, Kheruka SC, et al. Ovariectomized rats with established osteopenia have diminished mesenchymal stem cells in the bone marrow and impaired homing, osteoinduction and bone regeneration at the fracture site. *Stem Cell Rev Rep* (2015) 11(2):309–21. doi: 10.1007/s12015-014-9573-5

23. Rebolj K, Veber M, Drobnic M, Malicev E. Hematopoietic stem cell and mesenchymal stem cell population size in bone marrow samples depends on patient's age and harvesting technique. *Cytotechnology* (2018) 70(6):1575–83. doi: 10.1007/s10616-018-0250-4

24. Li H, Ghazanfari R, Zacharaki D, Lim HC, Scheding S. Isolation and characterization of primary bone marrow mesenchymal stromal cells. *Ann N Y Acad Sci* (2016) 1370(1):109–18. doi: 10.1111/nyas.13102

25. Wang LT, Chen LR, Chen KH. Hormone-related and drug-induced osteoporosis: A cellular and molecular overview. *Int J Mol Sci* (2023) 24(6). doi: 10.3390/ijms24065814

26. Park SY, Jeong AJ, Kim GY, Jo A, Lee JE, Leem SH, et al. Lactoferrin protects human mesenchymal stem cells from oxidative stress-induced senescence and apoptosis. *J Microbiol Biotechnol* (2017) 27(10):1877–84. doi: 10.4014/jmb.1707.07040

27. Ying X, Cheng S, Wang W, Lin Z, Chen Q, Zhang W, et al. Effect of lactoferrin on osteogenic differentiation of human adipose stem cells. *Int Orthop* (2012) 36(3):647–53. doi: 10.1007/s00264-011-1303-x

28. Montesi M, Panseri S, Iafisco M, Adamiano A, Tampieri A. Effect of hydroxyapatite nanocrystals functionalized with lactoferrin in osteogenic differentiation of mesenchymal stem cells. *J BioMed Mater Res A* (2015) 103(1):224–34. doi: 10.1002/jbm.a.35170

29. Icriverzi M, Bonciu A, Rusen L, Sima LE, Brajnicov S, Cimpean A, et al. Human mesenchymal stem cell response to lactoferrin-based composite coatings. *Mater (Basel)* (2019) 12(20). doi: 10.3390/ma12203414

30. Grey A, Zhu Q, Watson M, Callon K, Cornish J. Lactoferrin potently inhibits osteoblast apoptosis, via an lrp1-independent pathway. *Mol Cell Endocrinol* (2006) 251 (1-2):96–102. doi: 10.1016/j.mce.2006.03.002

31. Hou JM, Chen EY, Wei SC, Lin F, Lin QM, Lan XH, et al. Lactoferrin inhibits apoptosis through insulin-like growth factor I in primary rat osteoblasts. *Acta Pharmacol Sin* (2014) 35(4):523–30. doi: 10.1038/aps.2013.173

32. Chen XW, Li YH, Zhang MJ, Chen Z, Ke DS, Xue Y, et al. Lactoferrin ameliorates aging-suppressed osteogenesis via igf1 signaling. *J Mol Endocrinol* (2019) 63(1):63–75. doi: 10.1530/JME-19-0003

33. Chang Y, Ping A, Chang C, Betz VM, Cai L, Ren B. Lactoferrin mediates enhanced osteogenesis of adipose-derived stem cells: innovative molecular and cellular therapy for bone repair. *Int J Mol Sci* (2023) 24(2). doi: 10.3390/ijms24021749

34. Hou JM, Chen EY, Lin F, Lin QM, Xue Y, Lan XH, et al. Lactoferrin induces osteoblast growth through igf-1r. *Int J Endocrinol* (2015) 2015:282806. doi: 10.1155/2015/282806

35. Li Y, Wang J, Ren F, Zhang W, Zhang H, Zhao L, et al. Lactoferrin promotes osteogenesis through tgf-beta receptor ii binding in osteoblasts and activation of canonical tgf-beta signaling in mc3t3-E1 cells and C57bl/6j mice. *J Nutr* (2018) 148 (8):1285–92. doi: 10.1093/jn/nxy097

36. Xu Y, An JJ, Tabys D, Xie YD, Zhao TY, Ren HW, et al. Effect of lactoferrin on the expression profiles of long non-coding rna during osteogenic differentiation of bone marrow mesenchymal stem cells. *Int J Mol Sci* (2019) 20(19). doi: 10.3390/ijms20194834

37. Naot D, Chhana A, Matthews BG, Callon KE, Tong PC, Lin JM, et al. Molecular mechanisms involved in the mitogenic effect of lactoferrin in osteoblasts. *Bone* (2011) 49(2):217–24. doi: 10.1016/j.bone.2011.04.002

38. Hou JM, Xue Y, Lin QM. Bovine lactoferrin improves bone mass and microstructure in ovariectomized rats via opg/rankl/rank pathway. *Acta Pharmacol Sin* (2012) 33(10):1277–84. doi: 10.1038/aps.2012.83

39. Bord S, Ireland DC, Beavan SR, Compston JE. The effects of estrogen on osteoprotegerin, rankl, and estrogen receptor expression in human osteoblasts. *Bone* (2003) 32(2):136–41. doi: 10.1016/s8756-3282(02)00953-5

40. Lorget F, Clough J, Oliveira M, Daury MC, Sabokbar A, Offord E. Lactoferrin reduces *in vitro* osteoclast differentiation and resorbing activity. *Biochem Biophys Res Commun* (2002) 296(2):261–6. doi: 10.1016/s0006-291x(02)00849-5

41. Yanagisawa S, Nagasaki K, Chea C, Ando T, Ayuningtyas NF, Inubushi T, et al. Oral administration of bovine lactoferrin suppresses the progression of rheumatoid arthritis in an skg mouse model. *PloS One* (2022) 17(2):e0263254. doi: 10.1371/journal.pone.0263254

42. Kawazoe A, Inubushi T, Miyauchi M, Ishikado A, Tanaka E, Tanne K, et al. Orally administered liposomal lactoferrin inhibits inflammation-related bone breakdown without interrupting orthodontic tooth movement. *J Periodontol* (2013) 84(10):1454–62. doi: 10.1902/jop.2012.120508

43. Xue H, Tu Y, Ma T, Liu X, Wen T, Cai M, et al. Lactoferrin inhibits il-1beta-induced chondrocyte apoptosis through akt1-induced creb1 activation. *Cell Physiol Biochem* (2015) 36(6):2456–65. doi: 10.1159/000430206

44. Tu Y, Xue H, Francis W, Davies AP, Pallister I, Kanamarlapudi V, et al. Lactoferrin Inhibits Dexamethasone-Induced Chondrocyte Impairment from Osteoarthritic Cartilage through up-Regulation of Extracellular Signal-Regulated Kinase 1/2 and Suppression of Fasl, Fas, and Caspase 3. *Biochem Biophys Res Commun* (2013) 441(1):249–55. doi: 10.1016/j.bbrc.2013.10.047

45. Zhang C, Li Y, Tang W, Kamiya N, Kim H. Lactoferrin activates bmp7 gene expression through the mitogen-activated protein kinase erk pathway in articular cartilage. *Biochem Biophys Res Commun* (2013) 431(1):31–5. doi: 10.1016/j.bbrc.2012.12.111

46. Takayama Y, Mizumachi K. Inhibitory effect of lactoferrin on hypertrophic differentiation of atdc5 mouse chondroprogenitor cells. *Biometals* (2010) 23(3):477–84. doi: 10.1007/s10534-010-9291-7

47. Li Y, Huang J, Wang J, Ma M, Lu Y, Wang R, et al. Lactoferrin is a potential activator of the vitamin D receptor in its regulation of osteogenic activities in C57bl/6j mice and mc3t3-E1 cells. *J Nutr* (2021) 151(8):2105–13. doi: 10.1093/jn/nxab105

48. Blais A, Malet A, Mikogami T, Martin-Rouas C, Tome D. Oral bovine lactoferrin improves bone status of ovariectomized mice. *Am J Physiol Endocrinol Metab* (2009) 296(6):E1281–8. doi: 10.1152/ajpendo.90938.2008

49. Guo HY, Jiang L, Ibrahim SA, Zhang L, Zhang H, Zhang M, et al. Orally administered lactoferrin preserves bone mass and microarchitecture in ovariectomized rats. *J Nutr* (2009) 139(5):958–64. doi: 10.3945/jn.108.100586

50. Fan F, Shi P, Liu M, Chen H, Tu M, Lu W, et al. Lactoferrin preserves bone homeostasis by regulating the rankl/rank/opg pathway of osteoimmunology. *Food Funct* (2018) 9(5):2653–60. doi: 10.1039/c8fo00303c

51. Li W, Hu J, Ji P, Zhu S, Zhu Y. Oral administration of bovine lactoferrin accelerates the healing of fracture in ovariectomized rats. *J Bone Miner Metab* (2020) 38 (5):648–57. doi: 10.1007/s00774-020-01105-1

52. Bharadwaj S, Naidu AG, Betageri GV, Prasadarao NV, Naidu AS. Milk ribonuclease-enriched lactoferrin induces positive effects on bone turnover markers in postmenopausal women. *Osteoporos Int* (2009) 20(9):1603–11. doi: 10.1007/s00198-009-0839-8

53. Giannoudis P, Tzioupis C, Almalki T, Buckley R. Fracture healing in osteoporotic fractures: is it really different? A basic science perspective. *Injury* (2007) 38(Suppl 1):S90–9. doi: 10.1016/j.injury.2007.02.014

54. Conway JD, Shabtai L, Bauernschub A, Specht SC. Bmp-7 versus bmp-2 for the treatment of long bone nonunion. *Orthopedics* (2014) 37(12):e1049–57. doi: 10.3928/01477447-20141124-50

55. Gazzerro E, Gangji V, Canalis E. Bone morphogenetic proteins induce the expression of noggin, which limits their activity in cultured rat osteoblasts. *J Clin Invest* (1998) 102(12):2106–14. doi: 10.1172/JCI3459

56. Einhorn TA, Gerstenfeld LC. Fracture healing: mechanisms and interventions. *Nat Rev Rheumatol* (2015) 11(1):45–54. doi: 10.1038/nrrheum.2014.164

57. Li Y, Chen SK, Li L, Qin L, Wang XL, Lai YX. Bone defect animal models for testing efficacy of bone substitute biomaterials. *J Orthop Translat* (2015) 3(3):95–104. doi: 10.1016/j.jot.2015.05.002

58. Li W, Zhu S, Hu J. Bone regeneration is promoted by orally administered bovine lactoferrin in a rabbit tibial distraction osteogenesis model. *Clin Orthop Relat Res* (2015) 473(7):2383–93. doi: 10.1007/s11999-015-4270-5

59. Sagar N, Pandey AK, Gurbani D, Khan K, Singh D, Chaudhari BP, et al. In-vivo efficacy of compliant 3d nano-composite in critical-size bone defect repair: A six month preclinical study in rabbit. *PloS One* (2013) 8(10):e77578. doi: 10.1371/journal.pone.0077578

60. Pal S, Sayeed M, Kumar A, Verma DP, Harioudh MK, Verma NK, et al. Self-assembling nano-globular peptide from human lactoferrin acts as a systemic enhancer of bone regeneration: A novel peptide for orthopedic application. *ACS Appl Mater Interf* (2021) 13(15):17300–15. doi: 10.1021/acsami.1c01513

61. Gray T, Storz G, Papenfort K. Small proteins; big questions. *J Bacteriol* (2022) 204(1):e0034121. doi: 10.1128/JB.00341-21

62. Bruni N, Capucchio MT, Biasibetti E, Pessione E, Cirrincione S, Giraudo L, et al. Antimicrobial activity of lactoferrin-related peptides and applications in human and veterinary medicine. *Molecules* (2016) 21(6). doi: 10.3390/molecules21060752

63. Hwang PM, Zhou N, Shan X, Arrowsmith CH, Vogel HJ. Three-dimensional solution structure of lactoferricin B, an antimicrobial peptide derived from bovine lactoferrin. *Biochemistry* (1998) 37(12):4288–98. doi: 10.1021/bi972323m

64. Ulvatne H, Samuelsen O, Haukland HH, Kramer M, Vorland LH. Lactoferricin B inhibits bacterial macromolecular synthesis in escherichia coli and bacillus subtilis. *FEMS Microbiol Lett* (2004) 237(2):377–84. doi: 10.1016/j.femsle.2004.07.001

65. Wang WY, Wong JH, Ip DT, Wan DC, Cheung RC, Ng TB. Bovine lactoferrampin, human lactoferricin, and lactoferrin 1-11 inhibit nuclear translocation of hiv integrase. *Appl Biochem Biotechnol* (2016) 179(7):1202–12. doi: 10.1007/s12010-016-2059-y

66. Haney EF, Nazmi K, Lau F, Bolscher JG, Vogel HJ. Novel lactoferrampin antimicrobial peptides derived from human lactoferrin. *Biochimie* (2009) 91(1):141–54. doi: 10.1016/j.biochi.2008.04.013

67. Adao R, Nazmi K, Bolscher JG, Bastos M. C- and N-truncated antimicrobial peptides from lfampin 265 - 284: biophysical versus microbiology results. *J Pharm Bioallied Sci* (2011) 3(1):60–9. doi: 10.4103/0975-7406.76467

68. Stallmann HP, Faber C, Bronckers AL, Nieuw Amerongen AV, Wuisman PI. Osteomyelitis prevention in rabbits using antimicrobial peptide hlf1-11- or gentamicin-containing calcium phosphate cement. *J Antimicrob Chemother* (2004) 54(2):472–6. doi: 10.1093/jac/dkh346

69. Faber C, Stallmann HP, Lyaruu DM, Joosten U, von Eiff C, van Nieuw Amerongen A, et al. Comparable efficacies of the antimicrobial peptide human lactoferrin 1-11 and gentamicin in a chronic methicillin-resistant staphylococcus aureus osteomyelitis model. *Antimicrob Agents Chemother* (2005) 49(6):2438–44. doi: 10.1128/AAC.49.6.2438-2444.2005

70. Yan D, Chen D, Shen J, Xiao G, van Wijnen AJ, Im HJ. Bovine lactoferricin is anti-inflammatory and anti-catabolic in human articular cartilage and synovium. *J Cell Physiol* (2013) 228(2):447–56. doi: 10.1002/jcp.24151

71. Yan D, Kc R, Chen D, Xiao G, Im HJ. Bovine lactoferricin-induced anti-inflammation is, in part, via up-regulation of interleukin-11 by secondary activation of stat3 in human articular cartilage. *J Biol Chem* (2013) 288(44):31655–69. doi: 10.1074/jbc.M112.440420

72. Shi P, Fan F, Chen H, Xu Z, Cheng S, Lu W, et al. A bovine lactoferrin-derived peptide induced osteogenesis via regulation of osteoblast proliferation and differentiation. *J Dairy Sci* (2020) 103(5):3950–60. doi: 10.3168/jds.2019-17425

73. Vergis J, Malik SS, Pathak R, Kumar M, Ramanjaneya S, Kurkure NV, et al. Exploiting lactoferricin (17-30) as a potential antimicrobial and antibiofilm candidate against multi-drug-resistant enteroaggregative escherichia coli. *Front Microbiol* (2020) 11:575917. doi: 10.3389/fmicb.2020.575917

74. Rahman R, Fonseka AD, Sua SC, Ahmad M, Rajendran R, Ambu S, et al. Inhibition of breast cancer xenografts in a mouse model and the induction of apoptosis in multiple breast cancer cell lines by lactoferricin B peptide. *J Cell Mol Med* (2021) 25 (15):7181–9. doi: 10.1111/jcmm.16748

75. van der Kraan MI, Nazmi K, Teeken A, Groenink J, van 't Hof W, Veerman EC, et al. Lactoferrampin, an antimicrobial peptide of bovine lactoferrin, exerts its candidacidal activity by a cluster of positively charged residues at the C-terminus in combination with a helix-facilitating N-terminal part. *Biol Chem* (2005) 386(2):137–42. doi: 10.1515/BC.2005.017

76. Wang Y, Morton JD, Bekhit AEA, Carne A, Mason SL. Amino acid sequences of lactoferrin from red deer (Cervus elaphus) milk and antimicrobial activity of its derived peptides lactoferricin and lactoferrampin. *Foods* (2021) 10(6). doi: 10.3390/foods10061305

77. van der Kraan MI, Groenink J, Nazmi K, Veerman EC, Bolscher JG, Nieuw Amerongen AV. Lactoferrampin: A novel antimicrobial peptide in the N1-domain of bovine lactoferrin. *Peptides* (2004) 25(2):177–83. doi: 10.1016/j.peptides.2003.12.006

78. Vigata M, Meinert C, Hutmacher DW, Bock N. Hydrogels as drug delivery systems: A review of current characterization and evaluation techniques. *Pharmaceutics* (2020) 12(12). doi: 10.3390/pharmaceutics12121188

79. Takaoka R, Hikasa Y, Hayashi K, Tabata Y. Bone regeneration by lactoferrin released from a gelatin hydrogel. *J Biomater Sci Polym Ed* (2011) 22(12):1581–9. doi: 10.1163/092050610X517095

80. Russo E, Villa C. Poloxamer hydrogels for biomedical applications. *Pharmaceutics* (2019) 11(12). doi: 10.3390/pharmaceutics11120671

81. Park YE, Chandramouli K, Watson M, Zhu M, Callon KE, Tuari D, et al. Sustained delivery of lactoferrin using poloxamer gels for local bone regeneration in a rat calvarial defect model. *Mater (Basel)* (2021) 15(1). doi: 10.3390/ma15010212

82. Amirthalingam S, Lee SS, Rajendran AK, Kim I, Hwang NS, Rangasamy J. Addition of lactoferrin and substance P in a chitin/plga-caso(4) hydrogel for regeneration of calvarial bone defects. *Mater Sci Eng C Mater Biol Appl* (2021) 126:112172. doi: 10.1016/j.msec.2021.112172

frontiers | Frontiers in Endocrinology

TYPE Original Research
PUBLISHED 06 November 2023
DOI 10.3389/fendo.2023.1193318

OPEN ACCESS

EDITED BY
Guanwu Li,
Shanghai University of Traditional Chinese Medicine, China

REVIEWED BY
Brandon Peter Lucke-Wold,
University of Florida, United States
Chuan Hu,
Qingdao University Medical College, China

*CORRESPONDENCE
Zhan Wang
wangzhanhz@zju.edu.cn
Ning Zhang
zhangning@zju.edu.cn

†These authors have contributed equally to this work

RECEIVED 24 March 2023
ACCEPTED 19 October 2023
PUBLISHED 06 November 2023

CITATION
Ren Y, Qian S, Xu G, Cai Z, Zhang N and Wang Z (2023) Predicting survival of patients with bone metastasis of unknown origin. *Front. Endocrinol.* 14:1193318. doi: 10.3389/fendo.2023.1193318

Predicting survival of patients with bone metastasis of unknown origin

Ying Ren[1,2,3,4,5,6†], Shengjun Qian[2,3,4,5,6†], Guoping Xu[1,2,3,4,5,6†], Zhenhai Cai[7], Ning Zhang[2,3,4,5,6*] and Zhan Wang[2,3,4,5,6*]

[1]Department of Nursing, The Second Affiliated Hospital of Zhejiang University School of Medicine, Hangzhou, China, [2]Department of Orthopedic Surgery, The Second Affiliated Hospital, Zhejiang University School of Medicine, Hangzhou, China, [3]Orthopedics Research Institute of Zhejiang University, Hangzhou, China, [4]Key Laboratory of Motor System Disease Research and Precision Therapy of Zhejiang Province, Hangzhou, China, [5]Zhejiang Provincial Clinical Medical Research Center for Motor System Diseases, Hangzhou, China, [6]International Chinese Musculoskeletal Research Society, Hangzhou, China, [7]Department of Orthopedics Surgery, The Second Affiliated Hospital of Jiaxing University, Jiaxing, China

Purpose: Bone metastasis of unknown origin is a rare and challenging situation, which is infrequently reported. Therefore, the current study was performed to analyze the clinicopathologic features and risk factors of survival among patients with bone metastasis of unknown origin.

Patients and methods: We retrospectively analyzed the clinical data for patients with bone metastasis of unknown origin between 2010 and 2016 based on the Surveillance, Epidemiology, and End Results (SEER) database. Overall survival (OS) and cancer-specific survival (CSS) were first analyzed by applying univariable Cox regression analysis. Then, we performed multivariable analysis to confirm independent survival predictors.

Results: In total, we identified 1224 patients with bone metastasis of unknown origin for survival analysis, of which 704 males (57.5%) and 520 females (42.5%). Patients with bone metastasis of unknown origin had a 1-year OS rate of 14.50% and CSS rate of 15.90%, respectively. Race, brain metastasis, liver metastasis, radiotherapy, and chemotherapy were significant risk factors of OS on both univariable and multivariable analyses ($p < 0.05$). As for CSS, both univariable and multivariable analyses revealed that no brain metastasis, no liver metastasis, radiotherapy, and chemotherapy were associated with increased survival ($p < 0.05$).

Conclusion: Patients with bone metastasis of unknown origin experienced an extremely poor prognosis. Radiotherapy and chemotherapy were beneficial for prolonging the survival of those patients.

KEYWORDS

bone metastasis, unknown origin, clinical characteristics, survival, risk factor

Introduction

Bone is one of the most common organs in cancer metastasis, especially in lung, breast, and prostate cancer (1, 2). Once bone metastasis is developed, patients' survival and quality of life will be significantly declined (3). The prognosis of bone metastases from different tumor types varies greatly. Therefore, to identify the primary pathologic type of bone metastasis is the key to the treatment of such patients. However, up to 30% of patients present with bone metastasis of unknown origin after detailed investigations (4). The spine is reported to be the most common site of bone metastasis of unknown origin, followed by the pelvis and long bones (5). Some studies showed that patients with bone metastasis of unknown origin had a poor outcome with a mean survival ranging from 3 to 12 months from diagnosis (6–9). The characteristics and survival of patients with bone metastasis of a certain known origin have been widely reported. However, few studies have been reported on the characteristics and risk factors affecting the prognosis in patients with bone metastasis of unknown origin. Additionally, effective treatments for such patients remain unknown.

To date, there was no large-sample studies to analyze the prognosis of patients with bone metastasis of unknown origin. The different characteristics and survival of patients with bone metastasis of unknown origin still need to be elucidated. In order to provide an insight into the bone metastasis of unknown origin, we used the Surveillance, Epidemiology, and End Results (SEER) database to reveal the clinicopathologic features and prognostic factors. Our findings may provide timely interventions for those patients to improve their survival.

Materials and methods

Patient population

Patients with bone metastasis of unknown origin were retrieved between 2010 and 2016 from the SEER database. This study used the case-listing session on the SEER*Stat version 8.3.9 software to extract the clinical data. We selected patients with unknown origin by using the Primary Site - labeled "C80.9-Unknown primary site". Meanwhile, we set the SEER Combined Mets at DX-bone (2010+) to be YES. Patients without pathological diagnosis were excluded. Medical ethics review was not required in this study because clinical data in the present study were extracted from a public database.

Race, gender, age at diagnosis, histopathological type, brain metastasis, liver metastasis, lung metastasis, radiotherapy, chemotherapy, marital status, vital status, survival time, and cause of death were included for analysis. Overall survival (OS) and cancer-specific survival (CSS) were defined as the time from diagnosis till death due to any cause and due to the cancer, respectively.

Statistical analysis

All statistical and descriptive analysis were performed by using the SPSS 22.0 software. Univariable Cox regression models were used to investigate the potential risk factors for prognosis. Significant risk factors from univariable analysis were incorporated for multivariable Cox regression analysis. Meanwhile, hazard ratio (HR) and its 95% confidence interval (95% CI) were recorded in univariable and multivariable analyses. The Kaplan-Meier method was applied to draw survival curves, and the Log-rank test was performed to compare the survival difference. The difference was statistically significant with bilateral p value less than 0.05.

Results

Baseline characteristics

The detailed patient clinical characteristics are summarized in Table 1. In total, 1224 cases who met the eligibility criteria were included in this study.

There were 704 males (57.5%) and 520 females (42.5%). Their mean age was 68 years (range, 3-100 years). We divided the age into two groups: ≤60 years (26.1%), and >60 years (73.9%). About four fifths (82.8%) of patients were white race. Adenomas and adenocarcinomas type was the main histological type, accounting for 48.4% of all cases, followed by epithelial neoplasms, NOS type. In terms of other organ metastasis, 144 (11.8%) cases had brain metastasis, 568(46.4%) had liver metastasis, and 439(35.9%) had lung metastasis. Overall, 34.1% of patients underwent radiotherapy, and 28.6% of patients had chemotherapy. There were 615(50.2%) patients with married status, 548(44.8%) patients with other marital status, and 61(5.0%) patients with unknown marital status. The 1-year OS and CSS rates of patients were 14.5% and 15.9%, respectively.

Univariable Cox regression analysis

The detailed univariable analysis results of patients with bone metastasis of unknown origin were showed in Table 2. No significance on both OS and CSS were observed in terms of gender, histological type, and marital status. Patients with other races were significantly associated with better OS but not CSS. Age >60 years was independently associated with worse survival. Other distant metastases significantly decreased OS and CSS. Patients underwent radiotherapy and chemotherapy had better OS and CSS.

Multivariable Cox regression analysis

The detailed multivariable analysis results of patients with bone metastasis of unknown origin were showed in Table 3. Age at diagnosis and lung metastasis were no longer significant risk factors for prognosis. On multivariable analysis of OS, white race, brain metastasis, liver metastasis, no radiotherapy, and no chemotherapy were significantly associated with decreased survival. On multivariable analysis of CSS, brain metastasis, liver metastasis, no radiotherapy, and no chemotherapy were significantly associated

10.3389/fendo.2023.1193318

TABLE 1 Baseline characteristics of 1224 patients with bone metastasis of unknown origin.

Variable	Value
Race	
White	1014 (82.8%)
Black	135 (11.0%)
Others	75 (6.1%)
Gender	
Female	520 (42.5%)
Male	704 (57.5%)
Age at diagnosis	
≤60	319 (26.1%)
>60	905 (73.9%)
Histology group	
Epithelial neoplasms, NOS	373 (30.5%)
Squamous cell neoplasms	114 (9.3%)
Adenomas and adenocarcinomas	593 (48.4%)
Others	144 (11.8%)
Brain metastasis	
No	889 (72.6%)
Yes	144 (11.8%)
Unknown	191 (15.6%)
Liver metastasis	
No	512 (41.8%)
Yes	568 (46.4%)
Unknown	144 (11.8%)
Lung metastasis	
No	606 (49.5%)
Yes	439 (35.9%)
Unknown	179 (14.6%)
Radiotherapy	
Yes	417 (34.1%)
No	807 (65.9%)
Chemotherapy	
Yes	350 (28.6%)
No	874 (71.4%)
Marital status	
Married	615 (50.2%)
Others	548 (44.8%)
Unknown	61 (5.0%)
Dead	
Yes	1034 (84.5%)
No	190 (15.5%)
1-year OS rate	14.50%
1-year CSS rate	15.90%

OS, overall survival; CSS, cancer-specific survival.

with decreased survival. Kaplan-Meier survival analysis stratified by radiotherapy and chemotherapy were shown in Figures 1, 2, respectively.

Discussion

Bone is the third most common metastatic site following the liver and lung (10). Cancer of unknown origin refers to malignancies, where metastases are histologically confirmed, but where no primary site can be identified on the basis of a comprehensive clinical and imaging evaluation (11–13). To our knowledge, the current study is the largest population-based study to explore the clinical features and survival predictors for patients with bone metastasis of unknown origin. With the progress of diagnosis and treatment technology, the proportion of unknown primary tumors in metastatic tumors has steadily declined (13). However, those patients experienced extremely poor prognosis. In the present study, we first defined the clinicopathological features and prognosis of this special population. Our study found that the 1-year OS and CSS rates for patients with bone metastasis of unknown origin were 14.5% and 15.9%, respectively. Therefore, accurate assessment of patients' prognostic risk factors is helpful to improve their prognosis and assist clinicians to make reasonable treatment decisions. More importantly, this study provides evidence for future treatment guidelines for such patients.

It is worth mentioning that our analysis found that gender and age were not independent risk factors for survival. However, many previous studies on bone metastasis have found that they indeed correlated with the patient's prognosis (14, 15). This may be due to the diverse pathologic types of the primary lesion. In terms of race, significant difference was observed in OS but not in CSS, which was not in line with other studies on bone metastasis (16, 17). Further researches are needed to clarify this risk factor. Regarding the tumor histopathology, adenomas and adenocarcinomas type accounted for almost half of all cases, but it was not an independent predictor of survival. It seems that the histopathologic type of the tumor has little effect on prognosis in patients with bone metastasis of unknown origin.

Generally, once a tumor develops distant metastasis in one organ, it may accelerate metastasis in other organs. Interestingly, bone metastasis combined with lung metastasis do not result in a worse prognosis in these patients, whereas bone metastasis combined with brain or liver metastases do. Ya Qin et al. (18) also reported the similar results among esophageal cancer patients with bone metastasis. It seems that there is a homologous

10.3389/fendo.2023.1193318

TABLE 2 Univariate Cox analysis of variables in patients with bone metastasis of unknown origin.

Variable	OS		CSS	
	HR (95% CI)	*P*	HR (95% CI)	*P*
Race				
White	1		1	
Black	0.888 (0.732-1.078)	0.23	0.901 (0.716-1.134)	0.377
Others	0.746 (0.565-0.985)	0.039	0.758 (0.548-1.048)	0.093
Gender				
Female	1		1	
Male	1.029 (0.909-1.165)	0.648	0.966 (0.834-1.118)	0.642
Age at diagnosis				
≤60	1		1	
>60	1.203 (1.045-1.384)	0.01	1.196 (1.016-1.407)	0.032
Histology group				
Epithelial neoplasms, NOS	1		1	
Squamous cell neoplasms	0.898(0.715-1.129)	0.357	0.882(0.661-1.175)	0.39
Adenomas and adenocarcinomas	1.043 (0.906-1.202)	0.554	1.050(0.888-1.242)	0.566
Others	0.991 (0.805-1.220)	0.93	0.926 (0.714-1.200)	0.56
Brain metastasis				
No	1		1	
Yes	1.218(1.009-1.470)	0.04	1.259(1.015-1.562)	0.036
Liver metastasis				
No	1		1	
Yes	1.306(1.145-1.489)	<0.001	1.387(1.185-1.624)	<0.001
Lung metastasis				
No	1		1	
Yes	1.204(1.052-1.378)	0.007	1.213(1.033-1.424)	0.019
Radiotherapy				
Yes	1		1	
No	1.434(1.259-1.634)	<0.001	1.500(1.281-1.756)	<0.001
Chemotherapy				
Yes	1		1	
No	2.048(1.778-2.358)	<0.001	2.058(1.738-2.438)	<0.001
Marital status				
Married	1		1	
Others	1.041 (0.919-1.180)	0.526	1.031 (0.887-1.198)	0.691

relationship between bone metastasis and lung metastasis. Most studies have found that lung, liver and brain metastases are closely related to the prognosis of patients (19–21). Our study revealed that marital status was not associated with survival. However, some researches demonstrated that marital status was an independent prognostic factor for survival among patients with bone metastasis of known origin (19, 22).

A standard treatment for patients with bone metastasis of unknown origin has not yet been developed. Treatments for vertebral lesions include surgical excision and non-surgical

10.3389/fendo.2023.1193318

TABLE 3 Multivariate Cox analysis of variables in patients with bone metastasis of unknown origin.

Variable	OS		CSS	
	HR (95% CI)	*P*	HR (95% CI)	*P*
Race				
White	1		-	
Black	0.860(0.708-1.046)	0.132	-	-
Others	0.656 (0.496-0.868)	0.003	-	-
Age at diagnosis				
≤60	1		1	
>60	1.108 (0.960-1.280)	0.161	1.082 (0.915-1.280)	0.357
Brain metastasis				
No	1		1	
Yes	1.292(1.063-1.570)	0.01	1.336(1.070-1.669)	0.011
Liver metastasis				
No	1		1	
Yes	1.267(1.096-1.463)	0.001	1.336(1.125-1.587)	0.001
Lung metastasis				
No	1		1	
Yes	1.115(0.965-1.289)	0.14	1.094(0.922-1.299)	0.301
Radiotherapy				
Yes	1		1	
No	1.316(1.147-1.509)	<0.001	1.327(1.124-1.567)	0.001
Chemotherapy				
Yes	1		1	
No	2.133(1.843-2.469)	<0.001	2.088(1.751-2.489)	<0.001

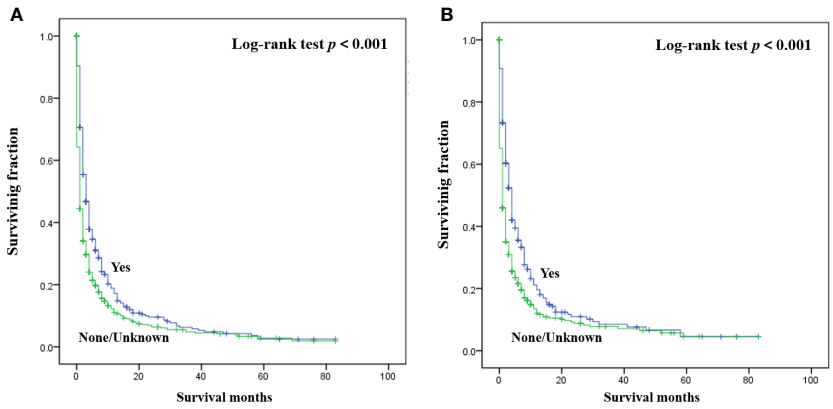

FIGURE 1
Kaplan-Meier method estimated OS **(A)** and CSS **(B)** in patients with bone metastasis of unknown origin stratified by radiotherapy. (OS, overall survival; CSS, cancer-specific survival).

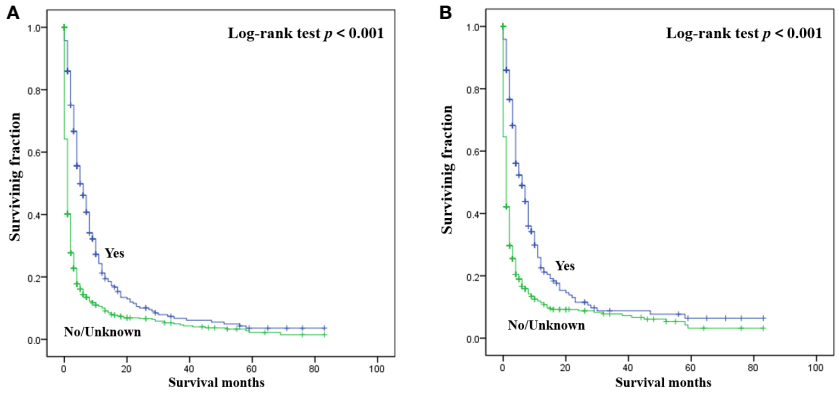

FIGURE 2
Kaplan-Meier method estimated OS **(A)** and CSS **(B)** in patients with bone metastasis of unknown origin stratified by chemotherapy. (OS, overall survival; CSS, cancer-specific survival).

management (10, 23). Our multivariable analyses revealed that radiotherapy and chemotherapy were significantly correlated with prognosis, which provides an optimal strategy for treating them. Chemotherapy was also an independent survival predictor for primary bone tumors, such as osteosarcoma (24). Various chemotherapeutic regimens are reported in the treatment of malignant primary bone tumors of the spine. However, rare studies reported the chemotherapeutic regimens for treating bone metastasis. This may be an important research direction for bone metastases in the future. Recently, some novel treatments including molecular targeting, immunotherapy and stem cell therapy provide hope for the treatment of spinal tumors (10). Further studies are warranted to determine the novel treatment methods for those patients.

The current study still has certain limitations. First, this is a retrospective study with inherent bias. Second, detailed data regarding the radiotherapy and chemotherapy were unavailable. Third, the SEER database does not provide any information regarding local recurrence or distant metastasis during follow-up. Therefore, clinical randomized trials are urgently needed to verify our findings and improve the survival.

Conclusion

Survival predictors for patients with bone metastasis of unknown origin included race, brain metastasis, liver metastasis, radiotherapy, and chemotherapy. Therefore, large range screening of the above independent risk factors can effectively improve the prognosis to a certain extent. Additionally, this study provides valuable reference information for clinicians and patients to make treatment decisions.

Data availability statement

The raw data supporting the conclusions of this article will be made available by the authors, without undue reservation.

Ethics statement

The studies involving humans were approved by Ethics Committee of the Second Affiliated Hospital, Zhejiang University School of Medicine. The studies were conducted in accordance with the local legislation and institutional requirements. The ethics committee/institutional review board waived the requirement of written informed consent for participation from the participants or the participants' legal guardians/next of kin because clinical data in the present study were extracted from a public database with no patient identification info.

Author contributions

ZW and NZ conceived and designed the study. YR, SQ, and GX collected the data. YR, SQ, GX, and ZC performed the statistical analysis. YR wrote the manuscript. ZW revised it. All authors contributed to the article and approved the submitted version.

Funding

This work was supported by National Natural Science Foundation of China (No.81972514, 81603126), China Postdoctoral Science Foundation (2021M692792), Zhejiang Provincial Natural Science Foundation (LQ22H160040), and Jiaxing Science and Technology Plan Project (2022AD30016).

Conflict of interest

The authors declare that the research was conducted in the absence of any commercial or financial relationships that could be construed as a potential conflict of interest.

Publisher's note

References

1. Fang C, Kang Y. Cellular plasticity in bone metastasis. *Bone* (2022) 158:115693. doi: 10.1016/j.bone.2020.115693

2. Ryan C, Stoltzfus KC, Horn S, Chen H, Louie AV, Lehrer EJ, et al. Epidemiology of bone metastases. *Bone* (2022) 158:115783. doi: 10.1016/j.bone.2020.115783

3. Shao H, Varamini P. Breast cancer bone metastasis: a narrative review of emerging targeted drug delivery systems. *Cells* (2022) 11(3):388. doi: 10.3390/cells11030388

4. Piccioli A, Maccauro G, Spinelli MS, Biagini R, Rossi B. Bone metastases of unknown origin: epidemiology and principles of management. *J Orthopaedics Traumatol* (2015) 16(2):81–6. doi: 10.1007/s10195-015-0344-0

5. Ugras N, Yalcinkaya U, Akesen B, Kanat O. Solitary bone metastases of unknown origin. *Acta Orthopaedica Belgica* (2014) 80(1):139–43.

6. Nottebaert M, Exner GU, von Hochstetter AR, Schreiber A. Metastatic bone disease from occult carcinoma: a profile. *Int orthopaedics* (1989) 13(2):119–23. doi: 10.1007/bf00266372

7. Shih LY, Chen TH, Lo WH. Skeletal metastasis from occult carcinoma. *J Surg Oncol* (1992) 51(2):109–13. doi: 10.1002/jso.2930510209

8. Jacobsen S, Stephensen SL, Paaske BP, Lie PG, Lausten GS. Skeletal metastases of unknown origin: a retrospective analysis of 29 cases. *Acta Orthopaedica Belgica* (1997) 63 (1):15–22.

9. Ettinger DS, Handorf CR, Agulnik M, Bowles DW, Cates JM, Cristea M, et al. Occult primary, version 3.2014. *J Natl Compr Canc Netw* (2014) 12(7):969–74. doi: 10.6004/jnccn.2014.0093

10. Amadasu E, Panther E, Lucke-Wold B. Characterization and treatment of spinal tumors. *Intensive Care Res* (2022) 2(3-4):76–95. doi: 10.1007/s44231-022-00014-3

11. Lee MS, Sanoff HK. Cancer of unknown primary. *BMJ (Clinical Res ed)* (2020) 371:m4050. doi: 10.1136/bmj.m4050

12. Bochtler T, Löffler H, Krämer A. Diagnosis and management of metastatic neoplasms with unknown primary. *Semin Diagn Pathol* (2018) 35(3):199–206. doi: 10.1053/j.semdp.2017.11.013

13. Bytnar JA, Lin J, Moncur JT, Shriver CD, Zhu K. Cancers of unknown primary: A descriptive study in the U.S. Military health system. *Military Med* (2021) 188(3–4): e516–e523. doi: 10.1093/milmed/usab291

14. Dong Q, Deng J, Mok TN, Chen J, Zha Z. Construction and validation of two novel nomograms for predicting the overall survival and cancer-specific survival of NSCLC patients with bone metastasis. *Int J Gen Med* (2021) 14:9261–72. doi: 10.2147/ijgm.S342596

15. Zhang W, Ji L, Wang X, Zhu S, Luo J, Zhang Y, et al. Nomogram predicts risk and prognostic factors for bone metastasis of pancreatic cancer: a population-based analysis. *Front Endocrinol* (2021) 12:752176. doi: 10.3389/fendo.2021.752176

16. Hu H, Wang Z, Zhang M, Niu F, Yu Q, Ren Y, et al. Clinicopathological characteristics and prognosis in endometrial cancer with bone metastasis: a SEER-based study of 584 women. *Front Oncol* (2021) 11:694718. doi: 10.3389/fonc.2021.694718

17. Wang Z, Shao H, Xu Q, Wang Y, Ma Y, Diaty DM, et al. Establishment and verification of prognostic nomograms for young women with breast cancer bone metastasis. *Front Med* (2022) 9:840024. doi: 10.3389/fmed.2022.840024

18. Qin Y, Mao J, Liang X, Wang N, Yuan M, Zhu J, et al. Bone metastasis in esophageal adenocarcinoma and squamous cell carcinoma: a SEER-based study. *Gen Thorac Cardiovasc Surg* (2022) 70(5):479–90. doi: 10.1007/s11748-021-01765-4

19. Huang Z, Hu C, Liu K, Yuan L, Li Y, Zhao C, et al. Risk factors, prognostic factors, and nomograms for bone metastasis in patients with newly diagnosed infiltrating duct carcinoma of the breast: a population-based study. *BMC Cancer* (2020) 20(1):1145. doi: 10.1186/s12885-020-07635-1

20. Dong S, Yang H, Tang ZR, Ke Y, Wang H, Li W, et al. Development and validation of a predictive model to evaluate the risk of bone metastasis in kidney cancer. *Front Oncol* (2021) 11:731905. doi: 10.3389/fonc.2021.731905

21. Lyu X, Luo B. Prognostic factors and survival prediction in HER2-positive breast cancer with bone metastases: A retrospective cohort study. *Cancer Med* (2021) 10 (22):8114–26. doi: 10.1002/cam4.4326

22. Liu D, Kuai Y, Zhu R, Zhou C, Tao Y, Han W, et al. Prognosis of prostate cancer and bone metastasis pattern of patients: a SEER-based study and a local hospital based study from China. *Sci Rep* (2020) 10(1):9104. doi: 10.1038/s41598-020-64073-6

23. Chalamgari A, Valle D, Palau Villarreal X, Foreman M, Liu A, Patel A, et al. Vertebral primary bone lesions: review of management options. *Curr Oncol* (2023) 30 (3):3064–78. doi: 10.3390/curroncol30030232

24. Wang Z, Wu B, Zhou Y, Huang X, Pan W, Liu M, et al. Predictors of the survival of primary and secondary older osteosarcoma patients. *J Cancer* (2019) 10(19):4614–22. doi: 10.7150/jca.32627

frontiers | Frontiers in Endocrinology

TYPE Case Report
PUBLISHED 15 November 2023
DOI 10.3389/fendo.2023.1286480

OPEN ACCESS

EDITED BY
Jonathan H. Tobias,
University of Bristol, United Kingdom

REVIEWED BY
Fiona Limanaqi,
University of Milan, Italy
Stefano Ratti,
University of Bologna, Italy

*CORRESPONDENCE
Larisa Ryskalin
larisa.ryskalin@unipi.it

†These authors have contributed equally to this work and share first authorship

RECEIVED 31 August 2023
ACCEPTED 25 October 2023
PUBLISHED 15 November 2023

CITATION
Ryskalin L, Fulceri F, Morucci G, Dell'Agli S, Soldani P and Gesi M (2023) Treatment of delayed union of the forearm with extracorporeal shockwave therapy: a case report and literature review.
Front. Endocrinol. 14:1286480.
doi: 10.3389/fendo.2023.1286480

Treatment of delayed union of the forearm with extracorporeal shockwave therapy: a case report and literature review

Larisa Ryskalin[1,2*†], Federica Fulceri[3†], Gabriele Morucci[1,2], Stefania Dell'Agli[2], Paola Soldani[1,2] and Marco Gesi[1,2]

[1]Department of Translational Research and New Technologies in Medicine and Surgery, University of Pisa, Pisa, Italy, [2]Center for Rehabilitative Medicine "Sport and Anatomy", University of Pisa, Pisa, Italy, [3]Independent Researcher, Livorno, Italy

Compared to other long bones, forearm fractures are particularly challenging due to the high rate of complications. These include malunion, delayed/nonunion, wrist and elbow movement reduction, and pain. Surgical procedure is considered the gold standard for managing delayed union and nonunion of the long bones. However, in the last decades, extracorporeal shockwave therapy (ESWT) has emerged as an effective and less invasive approach to enhance bone regeneration and fracture healing, avoiding major complications of surgical procedures. In contrast to the broad literature reporting good clinical results of ESWT in the treatment of nonunions, there is currently limited evidence regarding the clinical application of shock waves on long bone delayed fractures, particularly those of the forearm. In the present paper, we report a case of delayed bone healing of the diaphyseal region of the ulna treated with focused ESWT. The successful case experienced bone healing at the fracture site in less than 3 months after initial ESWT treatment. Acknowledging the limitation of reporting a case report, however, the remarkable clinical results and the absence of side effects contribute valuable information in support of the use of ESWT as an effective alternative to standard surgery for forearm fractures.

KEYWORDS

extracorporeal shockwave therapy, delayed union fracture, bone healing, long bone fracture, forearm

1 Introduction

Physiological fracture healing occurs within 3 months after bone injury hrough an intricate and highly coordinated regenerative process (1). However, several local and/or systemic factors can contribute to retardation or failure of bone consolidation (2). As a result, up to 10% of patients with long bone fractures suffer from healing complications, which include both delayed and nonunion (1, 3). In particular, a delayed union is defined as the absence of radiological progression of healing 3 months after the initial injury, whereas

nonunion is considered when the fracture fails to unite over 6 months (4, 5). This, in turn, has several clinical complications that can lead to patients' reduced mobility in daily activities and working capacities, reduced quality of life, and increased healthcare costs (6).

Albeit conventional surgery intervention represents the gold standard for treating delayed unions and nonunions, in the last decades less invasive approaches have been implemented to enhance bone regeneration and fracture healing while avoiding hazards and complications of surgical interventions (2, 7). In this regard, delayed unions require careful evaluation, as this can change their clinical course and management. In fact, delayed unions may result in further surgery with subsequent prolonged or repeat hospitalization. This, in turn, may prolong patient's disability, and delay his return to the workforce, while adversely impacting his quality of life (4). Thus, if a delayed union is suspected, less invasive treatments may be tried at first, before pursuing major surgery. These include electromagnetic stimulation (8), electrical capacitive coupling (9), low-intensity pulsed ultrasound (10), or other biological stimulation methods such as bone autograft and cell-based therapies (11).

Within this frame, the use of ESWT has gathered increasing attention due to its biological potential in enhancing osteogenesis (12, 13) and thus promoting fracture healing (5, 7, 14).

Increasing evidence in basic research demonstrates that shock wave stimulation generates its effect in tissue via mechanotransduction which triggers several endogenous bone regeneration processes via cell proliferation, differentiation, and migration (15–17). Furthermore, there are several clinical observational studies on the beneficial effects of ESWT on bone healing (7, 13, 14, 18, 19). For instance, a very recent systematic review of the literature conducted on three main databases (i.e., PubMed, Scopus, and Web of Science) showed that out of 1200 total long bone nonunions, 876 (73%) healed after being treated with ESWT, with hypertrophic cases achieving 3-fold higher healing rates when compared to oligotrophic or atrophic cases (14). Again, another recent retrospective study reported positive outcomes, defined by radiographic bone consolidation 6-month follow-up and absence of both pain and functional limitations during normal weight loading, in 16 out of 22 (73%) patients treated with rESWT for fracture nonunions that failed to heal despite initial surgical fixation (13). Although the healing rates achieved with surgery are sometimes comparable to those of ESWT treatments, however these latter do not carry any risk of possible complications.

Compared to the substantial body of current literature supporting the use of shock waves in the treatment of long bone nonunions, there is little evidence concerning the efficacy of high-energy ESWT for the treatment of delayed fractures. Furthermore, most of these studies concern the delayed union of the long bones of the lower limbs, as well as metatarsal and scaphoid fractures (20).

To our knowledge, there is currently little evidence of the treatment of the ulnar delayed unions of the diaphyseal region with ESWT. Among forearm fractures, isolated diaphyseal fractures of the ulna, without an accompanying radius injury, are fairly rare. Moreover, forearm fractures show a high complication rate including malunion, nonunion, reduction in the range of wrist and elbow movements, and pain (21). Indeed, the management of forearm bone fractures is particularly challenging because the two bones (i.e., the ulna and the radius) act in a particular way in the prono-supination phenomenon and several key muscles assisting prono-supination may exert deforming forces leading to long-term forearm disability if neglected (22). Therefore, timely and accurate management of these patients is pivotal in gaining optimal functional outcomes, preserving upper limb function, as well as minimizing complications.

Here, we report the promising outcomes of a delayed ulnar fracture treated with focused high-energy ESWT.

2 Case presentation

A 28-year-old, right-dominant handed man, involved in a road traffic accident has sustained an injury to his left forearm resulting in an isolated distal-third fracture of the ulna (Figures 1A, B). Due to the occurrence of a concomitant contused lacerated wound at the level of the volar aspect of the ulna, within the next 24h, the fracture was fixed and stabilized with percutaneous intramedullary Kirschner wire (K-wire), inserted through the olecranon in a proximal-distal direction (Figures 1C, D). The post-operative X-ray was satisfactory, with no sign of immediate surgical complications.

The patient was discharged from the hospital after 72 h of observation with no sign of peripheral neuro-vascular injury associated with the bone fracture. The patient was advised by the orthopedic surgeon to keep the forearm immobilized with a splint, to keep unloaded the arm, and to avoid straining and weightlifting with his left hand. Radiological assessment was the primary outcome, and it was performed at different time points (i.e., monthly) to monitor fracture healing. However, over 3 months after surgery, X-ray imaging showed no osteogenesis and absence of bone union at the fracture site. Thus, a delayed bone union was diagnosed (Figure 2).

At that time, the patient presented himself at the Center for Rehabilitative Medicine "Sport and Anatomy" of the University of Pisa and a series of shock wave sessions was started. In detail, high-energy focused ESWT (f-ESWT) was performed at the fracture site using a DUOLITH® SD1 ultra (Storz Medical AG., Tägerwilen, Switzerland); no local anesthesia was applied. The patient underwent two cycles of treatments, at 3 weeks intervals, each one consisting of 5 and 4 sessions per cycle, respectively. Each f-ESWT session was performed once a week, with an average of 3,500 pulses at a 4.5 Hz frequency. The average energy flux density (EFD) was 0.25 mJ/mm^2, depending on the patient's pain tolerance limit. Total energy was 25.000 mJ per session on average (Supplementary Table 1). Treatment success was monitored with radiographs and clinical examinations. During both cycles of f-ESWT, no side effects (i.e., bruising or swelling at the treatment site, slight reddening of the skin, or transient local hematoma) were observed.

Eleven weeks after f-ESWT, x-ray examination showed callus formation at the fracture site (Figure 3), as well as evidence of full bony healing in the further follow-up controls. Functional improvements in the affected limb were also observed after the

10.3389/fendo.2023.1286480

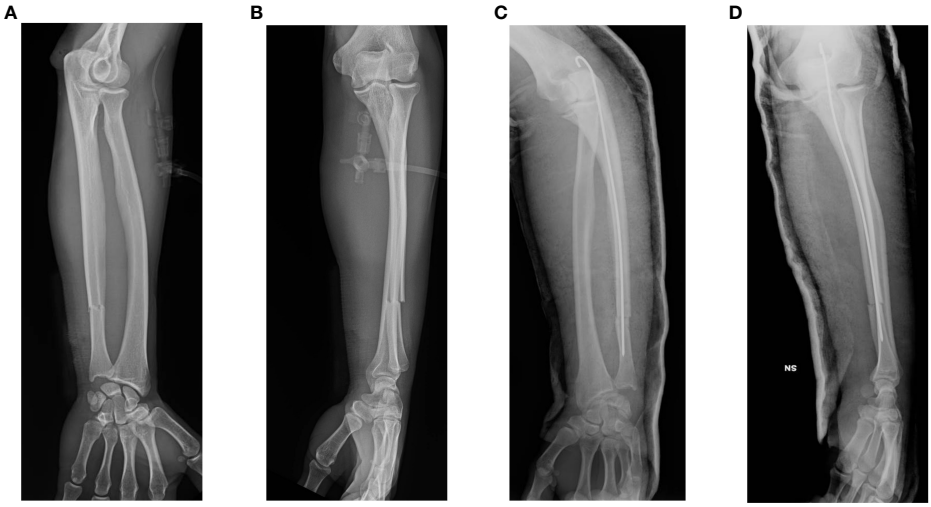

FIGURE 1
Pre- and post-operative imaging of the patient's left forearm fracture. Preoperative anterior–posterior **(A)** and lateral **(B)** radiographs show the complete fracture of the left distal ulna. Postoperative anterior-posterior **(C)** and lateral **(D)** X-rays the day after internal fixation surgery.

FIGURE 2
Radiographs at 3 months after surgery. Fracture consolidation is still not achieved as shown by anterior–posterior **(A)** and lateral **(B)** X-rays of the left ulna.

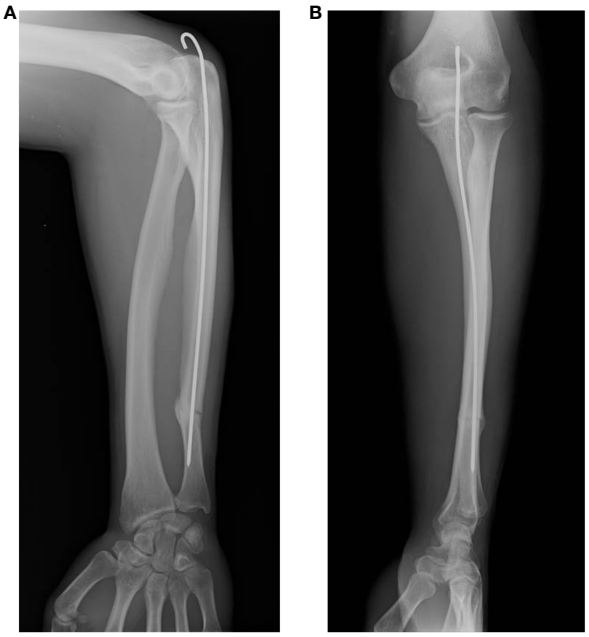

FIGURE 3
Radiographic consolidation at the fracture site after ESWT treatment. The presence of callus is visible on anterior–posterior **(A)** and lateral **(B)** X-rays of the left ulna.

second ESWT treatment. In addition, no pain or limited range of motion was observed, and the patient was able to return to daily life and work activities at full capacity.

3 Discussion

Diaphyseal fractures of the long bones of the forearm are commonly encountered in orthopedics and traumatological clinical practice and their management is still challenging (23, 24). Compared to other long bone fractures, those of the forearm are relatively complex, and proper treatment intervention is crucial to completely restore upper limb functions (25). Furthermore, several key muscles that assist forearm pronation/supination (i.e., pronator teres and pronator quadratus/biceps brachii and supinator, respectively) may exert deforming forces upon fracture fragments leading to forearm deformities (22), and thus significant disability.

To date, surgical approaches remain the gold standard to achieve anatomic fracture reduction, stable fixation, and

functional preservation, thereby enabling patients to return to daily life activities as early as possible. However, the invasiveness of these approaches can negatively interfere with the clinical outcomes often leading to serious complications such as infections, peripheral nerve injury, persistent pain, malunion, and nonunion (24).

In an effort to achieve bony union more rapidly and in a non-invasive way, over the last decade, EWST has emerged as a promising alternative to surgery. Pioneer studies on dog and rabbit nonunion models showed the effectiveness of ESWT in promoting callous formation (18, 26, 27), enhancing recovery of the mechanical properties of the bone (28, 29), as well as increasing union rates (30, 31). In line with this, a recent paper showed that ESWT might accelerate endochondral ossification and bone formation in a rat femur delayed-union model (32). Since then, the beneficial effect of ESWT for nonunion fractures of long bones has been reported in several experimental and clinical studies (7, 13, 14, 28–33). According to some reports, ESWT is also recommended as a first treatment choice for delayed bone healing (16, 34–37) or pseudarthrosis (20, 38–40). Nevertheless, when analyzing more in-depth the current literature, it appears less supportive of the ESWT-induced bone healing process for delayed unions. Indeed, contrary to the broad experience of ESWT treatment for nonunion fractures, there is a lack of sufficient amount of data regarding delayed unions.

Despite preliminary clinical data reported studies demonstrating good clinical results for ESWT in delayed union fractures, the results (though all positive) greatly varied among the studies with ratings of success ranging from 50% up to 80% (41). For instance, in 2010, Zelle et al. reviewed 10 clinical studies and found that the overall union rate in patients with delayed union/nonunion was 76% (95% confidence interval 73%-79%), ranging from 41% to 85% (42). In another recent literature review on delayed fracture healings, Willems et al. found an average union rate after ESWT of 86% (5). This, in turn, may be due to the variability of treatment protocols and/or the limited methodological quality of these studies. Some authors argued about deficiencies in the study design of most previously published studies (5, 42–44).

Therefore, we carefully revised the current literature in order to provide evidence for the effectiveness of ESWT in the treatment of delayed long-bone fractures of the forearm, and especially those of the ulna (Table 1). When analyzing the literature, it emerges that the anatomic fracture localization of delayed unions is quite heterogeneous within studies, with the long bones of the lower extremity (i.e., femur and tibia) being the most affected ones. With reference to the upper limb, the scaphoid bone is the most frequently fractured one. However, most of the studies do not separate the results for delayed unions from those of nonunions (14, 36, 43, 45, 46). At the same time, in some previous publications, the precise localization of delayed fracture is not always described. For instance, Schaden et al. (35) reported the successful use of ESWT in the treatment of over 3,500 delayed healing fractures and pseudarthroses with an average success rate of almost 80% after six months of follow-up, without indicating the different fracture locations. In the paper by Biederman et al. (43), patients with delayed bone healing showed a higher and earlier rate of union (93%; mean time to union, 3.4 months; range, 0.2–4.9 months) compared with patients with nonunion. However, the study does not specify the site of delayed unions, rather it reports "long bones and others" in a quite general way. Similarly, in another paper, it is not indicated whether the 349 specific bones treated with ESWT were associated with a delayed or fracture nonunion (45).

Another key point is that there is a high variability in the definition of "delayed union" which is not homogeneous among the studies. For instance, some Authors defined delayed unions as fractures that do not show radiological union 3 months after fracture (5). In the paper by Schaden et al. (36), the delay from the initial injury or the last operation was 3 to 6 months (delayed healing). Otherwise, in other papers, the

TABLE 1 Evidence for ESWT application for delayed unions of the forearm.

Refs.	DU (no.)	Localization	Time from injury/ diagnosis and ESWT	Time to union (mo.)	ESWT device	No. of shocks per session	EFD (mJ/ mm^2)	Healing results (success rate %)
(2)	9	Long bones and others	≤181 days	3 to 6 mo.	LithoSpaceOrtho	3000	0.36	8/9 (88.8%)
(37)	42	Long bones *	NR	3 to 6 mo.	Econolith 2000 lithotripter	1500-3000 (20 kV)	NR	40/42 (95%)
(36)	35	Long bones and others *	3 to 6 mo.	NR	NR	1000-12000^	0.25-0.4	26/35 (74.3%)
(43)	16[#]	Long bones (n=13)[§] Others (n=1)	5±3 mo.	3.4±1.4	Electrohydraulic MFL 5000 Lithotriptor	2900 (23 kV)	0.7	12/13 (93%)
(45)	120	Long bones and others *	≤181 days	NR	Orthowave 280	4000-12000 (26-28 kV)	0.38-0.40	102/120 (85.0%)
(46)	9	Long bones and others *	71.33 weeks (for successful DU)	NR[‡]	Electrohydraulic lithotripter Econolith 2000	3000 (20-21 kV)	NR	4/9 (44.4%)

DU (no.), number of delayed union; mo., months; EFD, Energy flux density; NR, Not reported; * The anatomic localization of delayed union is not specified; ^ Shock wave intensity and number of shock waves were selected according to the area of the fracture gap and the cross section of the bone to be treated (Scaphoid: 0.25 to 0.35 mJ/mm2 (20–24 kV), 1000–2500 shock waves; tibias and femurs: 0.4 mJ/mm2 (28 kV), 12,000 shock waves); # Two patients with delayed metatarsal stress fractures refused radiographic controls, as they were free of complaint 6 weeks after therapy; § The Authors do not specify whether delayed union occurred in upper or lower limbs; ‡ follow-up at 24 weeks.

Authors included those fractures that showed no progressive callus formation as well as the absence of radiographic progression of healing upon clinical examination by six months after injury (2, 4, 43, 45, 47). However, this may be due to the fact that there is no clear consensus among orthopedic surgeons in the assessment of fracture healing based on clinical evaluation and radiological examinations (47–49).

Again, there is a lot of heterogeneity in the treatment protocols for delayed unions between the studies, both in terms of ESWT devices, number of sessions, number of shock waves per session, total energy flux density, and so on. This, in turn, might be another explanation for those divergent healing rates.

Despite all the limitations reported above regarding previous literature, in any case, it is important to underline that no adverse severe effects (i.e., neuromuscular, systemic, or device-related local complications) have been reported, which strongly suggests that ESWT is a safer alternative option to surgical treatment of delayed union and nonunions (5, 19, 37, 50). Remarkably, in a very recent paper, Dahm et al. reported that older age and fracture localization in the diaphysis or distal metaphysis of the humerus represent negative predictive factors for a successful ESWT outcome (47). In fact, the largest late healing effects between the 3- and 6-month follow-up were found for humeral diaphysis compared to other anatomical regions, such as the proximal metaphyseal localization of the lesion. Data reported in the present case report are encouraging since with our treatment protocol we achieved bony consolidation of the diaphyseal region of the ulna in less than 3 months after the first ESWT treatment. Besides anatomic fracture location, the time to the shockwave therapy following the injury may negatively impact healing outcomes (45). In particular, concerning the ulnar bone, the estimated probability of a positive fracture-healing at < 181 days between injury and ESWT therapy is 80.0%, whereas it significantly deteriorates down to 64.9% when more than eleven months (339 days) elapsed between the injury and first ESWT treatment exceeds (45).

4 Conclusions

The good clinical results and the absence of side effects reported in the present study suggest that ESWT should be considered a valid noninvasive treatment option for stimulating bone healing for delayed fractures of the ulnar bone.

Acknowledging the limitation of a case report, however, this paper contributes valuable information. In fact, according to our data, it emerges how the timeliness of an adequate diagnosis and early ESWT therapeutic approach is pivotal in avoiding unfavorable evolution of the delayed fracture unions, which are configured with functional limitations and patient disability.

Further randomized, prospective clinical trials are needed to standardize both the healthcare decision-making as well as the optimal site-specific ESWT protocol for the treatment of delayed and non-healing fractures.

Data availability statement

The raw data supporting the conclusions of this article will be made available by the authors, without undue reservation.

Ethics statement

Ethical review and approval were waived for this treatment since it was part of ordinary clinical activity. The studies were conducted in accordance with the local legislation and institutional requirements. The participants provided their written informed consent to participate in this study. Written informed consent was obtained from the individual(s) for the publication of any potentially identifiable images or data included in this article.

Author contributions

LR: Conceptualization, Data curation, Formal analysis, Methodology, Writing – original draft, Writing – review & editing. FF: Conceptualization, Formal analysis, Methodology, Writing – original draft, Writing – review & editing. GM: Writing – review & editing. SD: Formal analysis, Writing – review & editing. PS: Supervision, Writing – review & editing. MG: Conceptualization, Funding acquisition, Methodology, Supervision, Writing – review & editing.

Funding

The author(s) declare financial support was received for the research, authorship, and/or publication of this article. This research was funded by the University of Pisa (Fondi di Ateneo) and by the Center for Rehabilitative Medicine “Sport and Anatomy”, University of Pisa.

Conflict of interest

The authors declare that the research was conducted in the absence of any commercial or financial relationships that could be construed as a potential conflict of interest.

Publisher’s note

Supplementary material

The Supplementary Material for this article can be found online at: https://www.frontiersin.org/articles/10.3389/fendo.2023.1286480/full#supplementary-material

References

1. Einhorn TA, Gerstenfeld LC. Fracture healing: mechanisms and interventions. *Nat Rev Rheumatol* (2015) 11:45–54. doi: 10.1038/nrrheum.2014.164

2. Everding J, Roßlenbroich S, Raschke MJ. Ultraschall und Stoßwelle in der Pseudarthrosentherapie: Sinnvoll oder nicht und wann? *Trauma Berufskrankh* (2017) 19:260–6. doi: 10.1007/s10039-017-0310-6

3. ElHawary H, Baradaran A, Abi-Rafeh J, Vorstenbosch J, Xu L, Efanov JI. Bone healing and inflammation: principles of fracture and repair. *Semin Plast Surg* (2021) 35:198–203. doi: 10.1055/s-0041-1732334

4. Volpin G, Shtarker H. Management of delayed union, non-union and mal-union of long bone fractures. In: Bentley G, editor. *European Surgical Orthopaedics and Traumatology*. Berlin, Heidelberg: Springer Berlin Heidelberg (2014). p. 241–66. doi: 10.1007/978-3-642-34746-7_10

5. Willems A, van der Jagt OP, Meuffels DE. Extracorporeal shock wave treatment for delayed union and nonunion fractures: A systematic review. *J Orthopaedic Trauma* (2019) 33:97–103. doi: 10.1097/BOT.0000000000001361

6. Tay W-H, De Steiger R, Richardson M, Gruen R, Balogh ZJ. Health outcomes of delayed union and nonunion of femoral and tibial shaft fractures. *Injury* (2014) 45:1653–8. doi: 10.1016/j.injury.2014.06.025

7. Vulpiani MC, Vetrano M, Conforti F, Minutolo L, Trischitta D, Furia JP, et al. Effects of extracorporeal shock wave therapy on fracture nonunions. *Am J Orthop (Belle Mead NJ)* (2012) 41:E122–7.

8. Schemitsch E, Kuzyk P. The science of electrical stimulation therapy for fracture healing. *Indian J Orthop* (2009) 43:127. doi: 10.4103/0019-5413.50846

9. Griffin XL, Costa ML, Parsons N, Smith N. Electromagnetic field stimulation for treating delayed union or non-union of long bone fractures in adults. *Cochrane Database Sys Rev* (2011). doi: 10.1002/14651858.CD008471.pub2

10. Bhan K, Patel R, Hasan K, Pimplé M, Sharma S, Nandwana V, et al. Fracture nonunions and delayed unions treated with low-intensity pulsed ultrasound therapy: A clinical series. *Cureus* (2021) 13(8):1–12. doi: 10.7759/cureus.17067

11. Gómez-Barrena E, Rosset P, Lozano D, Stanovici J, Ermthaller C, Gerbhard F. Bone fracture healing: Cell therapy in delayed unions and nonunions. *Bone* (2015) 70:93–101. doi: 10.1016/j.bone.2014.07.033

12. Petrisor B, Lisson S, Sprague S. Extracorporeal shockwave therapy: A systematic review of its use in fracture management. *Indian J Orthop* (2009) 43:161. doi: 10.4103/0019-5413.50851

13. Kertzman P, Császár NBM, Furia JP, Schmitz C. Radial extracorporeal shock wave therapy is efficient and safe in the treatment of fracture nonunions of superficial bones: a retrospective case series. *J Orthop Surg Res* (2017) 12:164. doi: 10.1186/s13018-017-0667-z

14. Sansone V, Ravier D, Pascale V, Applefield R, Del Fabbro M, Martinelli N. Extracorporeal shockwave therapy in the treatment of nonunion in long bones: A systematic review and meta-analysis. *JCM* (2022) 11:1977. doi: 10.3390/jcm11071977

15. d'Agostino MC, Craig K, Tibalt E, Respizzi S. Shock wave as biological therapeutic tool: From mechanical stimulation to recovery and healing, through mechanotransduction. *Int J Surg* (2015) 24:147–53. doi: 10.1016/j.ijsu.2015.11.030

16. Mittermayr R, Haffner N, Feichtinger X, SChaden W. The role of shockwaves in the enhancement of bone repair - from basic principles to clinical application. *Injury* (2021) 52:S84–90. doi: 10.1016/j.injury.2021.02.081

17. Ryskalin L, Morucci G, Natale G, Soldani P, Gesi M. Molecular mechanisms underlying the pain-relieving effects of extracorporeal shock wave therapy: A focus on fascia nociceptors. *Life (Basel)* (2022) 12:743. doi: 10.3390/life12050743

18. Wang C-J, Huang H-Y, Chen H-H, Pai C-H, Yang KD. Effect of shock wave therapy on acute fractures of the tibia: A study in a dog model. *Clin Orthopaedics Related Res* (2001) 387:112–8. doi: 10.1097/00003086-200106000-00015

19. Cacchio A, Giordano L, Colafarina O, Rompe JD, Tavernese E, Ioppolo F, et al. Extracorporeal shock-wave therapy compared with surgery for hypertrophic long-bone nonunions. *J Bone Joint Surg* (2009) 91:2589–97. doi: 10.2106/JBJS.H.00841

20. Fallnhauser T, Wilhelm P, Priol A, Windhofer C. Hochenergetische extrakorporale Stoßwellentherapie bei verzögerter Heilung von Kahnbeinfrakturen und Pseudarthrosen: eine retrospektive Analyse der Konsolidierungsrate und therapieentscheidungsrelevanter Faktoren. *Handchir Mikrochir Plast Chir* (2019) 51:164–70. doi: 10.1055/a-0914-2963

21. Handoll HH, Pearce P. Interventions for treating isolated diaphyseal fractures of the ulna in adults. *Cochrane Database Sys Rev* (2012) 2012(6):1–27. doi: 10.1002/14651858.CD000523.pub4

22. Jayakumar P, Jupiter JB. Reconstruction of malunited diaphyseal fractures of the forearm. *Handb (New York N,Y)* (2014) 9:265–73. doi: 10.1007/s11552-014-9635-9

23. Bartoníček J, Kozánek M, Jupiter JB. History of operative treatment of forearm diaphyseal fractures. *J Handb Surg* (2014) 39:335–42. doi: 10.1016/j.jhsa.2013.06.020

24. Kostenuik P, Mirza FM. Fracture healing physiology and the quest for therapies for delayed healing and nonunion: THERAPIES FOR DELAYED/NON-UNION FRACTURES. *J Orthop Res* (2017) 35:213–23. doi: 10.1002/jor.23460

25. Al-Sadek TA, Niklev D, Al-Sadek A. Diaphyseal fractures of the forearm in adults, plating or intramedullary nailing is a better option for the treatment? *Open Access Maced J Med Sci* (2016) 4:670–3. doi: 10.3889/oamjms.2016.138

26. Ikeda K, Tomita K, Takayama K. Application of extracorporeal shock wave on bone: preliminary report. *J Trauma: Injury Infection Crit Care* (1999) 47:946. doi: 10.1097/00005373-199911000-00024

27. Bulut O, Eroglu M, Ozturk H, Tezeren G, Bulut S, Koptagel E. Extracorporeal shock wave treatment for defective nonunion of the radius: A rabbit model. *J Orthop Surg (Hong Kong)* (2006) 14:133–7. doi: 10.1177/230949900601400205

28. Wang C-J, Wang F-S, Yang KD. Biological effects of extracorporeal shockwave in bone healing: a study in rabbits. *Arch Orthop Trauma Surg* (2008) 128:879–84. doi: 10.1007/s00402-008-0663-1

29. Hsu RW-W, Tai C-L, Chen CY-C, Hsu W-H, Hsueh S. Enhancing mechanical strength during early fracture healing *via* shockwave treatment: an animal study. *Clin Biomech* (2003) 18:S33–9. doi: 10.1016/S0268-0033(03)00082-2

30. Maier M, Milz S, Tischer T, Münzing W, Manthey N, Stäbler A, et al. Influence of extracorporeal shock-wave application on normal bone in an animal model in *vivo*: SCINTIGRAPHY, MRI AND HISTOPATHOLOGY. *J Bone Joint Surg Br* (2002) 84-B:592–9. doi: 10.1302/0301-620X.84B4.0840592

31. Johannes EJ, Kaulesar DMKS, Matura E. High-energy shock waves for the treatment of nonunions: an experiment on dogs. *J Surg Res* (1994) 57:246–52. doi: 10.1006/jsre.1994.1139

32. Kobayashi M, Chijimatsu R, Yoshikawa H, Yoshida K. Extracorporeal shock wave therapy accelerates endochondral ossification and fracture healing in a rat femur delayed-union model. *Biochem Biophys Res Commun* (2020) 530:632–7. doi: 10.1016/j.bbrc.2020.07.084

33. Wang C-J, Chen H-S, Chen C-E, Yang KD. Treatment of nonunions of long bone fractures with shock waves. *Clin Orthopaedics Related Res* (2001) 387:95–101. doi: 10.1097/00003086-200106000-00013

34. Valchanou VD, Michailov P. High energy shock waves in the treatment of delayed and nonunion of fractures. *Int Orthopaedics* (1991) 15:181–4. doi: 10.1007/BF00192289

35. SChaden W, Mittermayr R, Haffner N, Smolen D, Gerdesmeyer L, Wang C-J. Extracorporeal shockwave therapy (ESWT) – First choice treatment of fracture non-unions? *Int J Surg* (2015) 24:179–83. doi: 10.1016/j.ijsu.2015.10.003

36. SChaden W, Fischer A, Sailler A. Extracorporeal shock wave therapy of nonunion or delayed osseous union. *Clin Orthopaedics Related Res* (2001) 387:90–4. doi: 10.1097/00003086-200106000-00012

37. Bara T, Synder M. Nine-years experience with the use of shock waves for treatment of bone union disturbances. *Ortop Traumatol Rehabil* (2007) 9:254–8.

38. Notarnicola A, Moretti L, Tafuri S, Gigliotti S, Russo S, Musci L, et al. Extracorporeal shockwaves versus surgery in the treatment of pseudoarthrosis of the carpal scaphoid. *Ultrasound Med Biol* (2010) 36:1306–13. doi: 10.1016/j.ultrasmedbio.2010.05.004

39. Vogel J, Hopf C, Eysel P, Rompe J-D. Application of extracorporeal shock-waves in the treatment of pseudarthrosis of the lower extremity: Preliminary results. *Arch Orthop Trauma Surg* (1997) 116:480–3. doi: 10.1007/BF00387581

40. Schatz KD, Nehrer S, Dorotka R, Kotz R. 3D-navigierte hochenergetische Stoßwellentherapie und Achskorrektur nach fehlgeschlagener Distraktionsbehandlung bei kongenitaler Tibiapseudarthrose. *Orthopäde* (2002) 31:663–6. doi: 10.1007/s00132-002-0327-8

41. Alkhawashki HMI. Shock wave therapy of fracture nonunion. *Injury* (2015) 46:2248–52. doi: 10.1016/j.injury.2015.06.035

42. Zelle BA, Gollwitzer H, Zlowodzki M, Bühren V. Extracorporeal shock wave therapy: current evidence. *J Orthopaedic Trauma* (2010) 24:S66–70. doi: 10.1097/BOT.0b013e3181cad510

43. Biedermann R, Martin A, Handle G, Auckenthaler T, Bach C, Krismer M. Extracorporeal shock waves in the treatment of nonunions. *J Trauma: Injury Infection Crit Care* (2003) 54:936–42. doi: 10.1097/01.TA.0000042155.26936.03

44. Heller K-D, Niethard F. Der Einsatz der extrakorporalen Stoßwellentherapie in der Orthopädie - eine Metaanalyse. *Z Orthop Ihre Grenzgeb* (2008) 136:390–401. doi: 10.1055/s-2008-1053674

45. Stojadinovic A, Kyle Potter B, Eberhardt J, Shawen SB, Andersen RC, Forsberg JA, et al. Development of a prognostic naïve bayesian classifier for successful treatment of nonunions. *J Bone Joint Surg-Am Vol* (2011) 93:187–94. doi: 10.2106/JBJS.I.01649

46. Czarnowska-Cubała M, Gwoździewicz K, Studniarek M, Lasek J. Predictive role of scintigraphy (BS) in bone union induction using extracorporeal shock wave treatment (ESWT). *J Orthopaedics* (2013) 10:70–3. doi: 10.1016/j.jor.2013.04.005

47. Dahm F, Feichtinger X, Vallant S-M, Haffner N, SChaden W, Fialka C, et al. High-energy extracorporeal shockwave therapy in humeral delayed and non-unions. *Eur J Trauma Emerg Surg* (2022) 48:3043–9. doi: 10.1007/s00068-021-01782-1

48. Bhandari M, Guyatt GH, Swiontkowski MF, Tornetta P, Sprague S, Schemitsch EH. A lack of consensus in the assessment of fracture healing among orthopaedic surgeons. *J Orthopaedic Trauma* (2002) 16:562–6. doi: 10.1097/00005131-200209000-00004

49. Oulianski M, Avraham D, Lubovsky O. Radiographic evaluation of distal radius fracture healing by time: orthopedist versus qualitative assessment of image processing. *Trauma Care* (2022) 2:481–6. doi: 10.3390/traumacare2030040

50. Elster EA, Stojadinovic A, Forsberg J, Shawen S, Andersen RC, SChaden W. Extracorporeal shock wave therapy for nonunion of the tibia. *J Orthopaedic Trauma* (2010) 24:133–41. doi: 10.1097/BOT.0b013e3181b26470

frontiers | Frontiers in Endocrinology

TYPE Original Research
PUBLISHED 07 December 2023
DOI 10.3389/fendo.2023.1278596

OPEN ACCESS

EDITED BY
Kyung-Hyun Park-Min,
Hospital for Special Surgery, United States

REVIEWED BY
Alice Berardo,
University of Padua, Italy
Elisa Belluzzi,
University of Padua, Italy

*CORRESPONDENCE
Katherine A. Staines
k.staines@brighton.ac.uk

RECEIVED 16 August 2023
ACCEPTED 20 November 2023
PUBLISHED 07 December 2023

CITATION
Bourne LE, Hesketh A, Sharma A, Bucca G, Bush PG and Staines KA (2023) The effects of physiological and injurious hydrostatic pressure on murine *ex vivo* articular and growth plate cartilage explants: an RNAseq study. *Front. Endocrinol.* 14:1278596. doi: 10.3389/fendo.2023.1278596

The effects of physiological and injurious hydrostatic pressure on murine *ex vivo* articular and growth plate cartilage explants: an RNAseq study

Lucie E. Bourne[1], Andrew Hesketh[1], Aikta Sharma[2], Giselda Bucca[1], Peter G. Bush[1] and Katherine A. Staines[1]*

[1]Centre for Lifelong Health, School of Applied Sciences, University of Brighton, Brighton, United Kingdom, [2]Department of Mechanical Engineering, University College London, London, United Kingdom

Introduction: Chondrocytes are continuously exposed to loads placed upon them. Physiological loads are pivotal to the maintenance of articular cartilage health, while abnormal loads contribute to pathological joint degradation. Similarly, the growth plate cartilage is subject to various loads during growth and development. Due to the high-water content of cartilage, hydrostatic pressure is considered one of the main biomechanical influencers on chondrocytes and has been shown to play an important role in the mechano-regulation of cartilage.

Methods: Herein, we conducted RNAseq analysis of ex vivo hip cap (articular), and metatarsal (growth plate) cartilage cultures subjected to physiological (5 MPa) and injurious (50 MPa) hydrostatic pressure, using the Illumina platform (n = 4 replicates).

Results: Several hundreds of genes were shown to be differentially modulated by hydrostatic pressure, with the majority of these changes evidenced in hip cap cartilage cultures (375 significantly upregulated and 322 downregulated in 5 MPa versus control; 1022 upregulated and 724 downregulated in 50 MPa versus control). Conversely, fewer genes were differentially affected by hydrostatic pressure in the metatarsal cultures (5 significantly upregulated and 23 downregulated in 5 MPa versus control; 7 significantly upregulated and 19 downregulated in 50 MPa versus control). Using Gene Ontology annotations for Biological Processes, in the hip cap data we identified a number of pathways that were modulated by both physiological and injurious hydrostatic pressure. Pathways upregulated in response to 50 MPa versus control, included those involved in the generation of precursor metabolites and cellular respiration. Biological processes that were downregulated in this tissue included ossification, connective tissue development, and chondrocyte differentiation.

Discussion: Collectively our data highlights the divergent chondrocyte phenotypes in articular and growth plate cartilage. Further, we show that the magnitude of hydrostatic pressure application has distinct effects on gene

expression and biological processes in hip cap cartilage explants. Finally, we identified differential expression of a number of genes that have previously been identified as osteoarthritis risk genes, including Ctsk, and Chadl. Together these data may provide potential genetic targets for future investigations in osteoarthritis research and novel therapeutics.

KEYWORDS

cartilage, osteoarthritis, hydrostatic pressure, chondrocytes, endochondral ossification, RNAseq

1 Introduction

Articular cartilage is a specialized connective tissue that covers the ends of bones in synovial joints and facilitates joint movement. It is load bearing and therefore protects underlying subchondral bone from excessive forces. The articular cartilage consists of chondrocytes which retain a stable phenotype to ensure the longevity of the tissue (1, 2). This is in contrast to the chondrocytes of the growth plate cartilage which undergo defined stages of maturation and differentiation to enable longitudinal bone growth (3).

Structurally, the articular cartilage can be divided into superficial, intermediate, and deep zones which are distinct in their organization of both the chondrocytes, surrounded by their individual pericellular matrix, and the collagen type-II and aggrecan-rich matrix (3). The articular cartilage functions to withstand physiological loading over the life-course. However, in the degenerative joint disease osteoarthritis, pathology is characterized by progressive articular cartilage degradation (4). Whilst osteoarthritis is well established to affect all tissues of the joint, the cellular and molecular mechanisms are incompletely understood (5–7). Various forms of mechanical stimuli are involved in the maintenance of the articular cartilage and thus the mechanoresponse of the chondrocyte plays an important role in the development of osteoarthritis (8–10). Compression, tensile and shear stress result in deformative loading, whereas osmotic and hydrostatic pressure induce stress without tissue or cellular deformation (8, 9, 11, 12). As a highly hydrated tissue, interstitial fluid pressurization within the articular cartilage is considered one of the main biomechanical influencers on chondrocytes (13–15). Throughout the cartilage zones, chondrocytes are subjected and respond to a hydrostatic pressure gradient, ranging from 0.1-10 MPa, to direct matrix remodeling, chondrogenesis and chondrocyte metabolism (13, 14). However, excessive hydrostatic pressure (≥20 MPa) outside the physiological range has been shown to induce apoptosis, alter cell morphology and metabolism, reduce extracellular matrix (ECM) synthesis, induce inflammatory cytokine production, and modulate oxidative stress (16–19).

In vitro, hydrostatic pressure can be applied experimentally to cells and tissues derived from both animals and humans to investigate mechanotransduction, for example in monolayer cultures (20–23), micromass or pellet cultures (24, 25), 3D cell scaffolds (26–29), and explant cultures (17, 22, 30, 31). The ability to provide either dynamic or continuous hydrostatic pressure, alter the magnitude and/or the duration of pressure provides an alternative approach to study the effects of mechanical stimulation (13, 32). Whilst there is little consensus within the field on the duration and pressure magnitudes in cultures, our previous meta-analysis has indicated that in human and animal- derived cells, low pressure (5 MPa) leads to anabolic responses, including elevated aggrecan expression and proteoglycan release, whereas a higher pressure (50 MPa) has a negative effect on proteoglycan production (33). Therefore, it is possible to investigate the effects of hydrostatic pressure at both physiological and pathophysiological levels.

To determine the effects of hydrostatic pressure on the molecular pathways involved in the regulation of chondrocyte physiology, transcriptomic analyses are often employed to identify responsive genes. Several studies in animal cells have utilized these approaches in the study of chondrocyte progenitor cells, immortalized chondrocytes, and primary chondrocytes within a hydrogel; however, transcriptome sequencing on *ex vivo* models has not yet been performed (21, 29, 34). Phenotypic changes are often observed in cells cultured in a monolayer, with cells de-differentiating or altering morphology, whereas *ex vivo* models allow examination of cells within their native environment (35). Herein, the aim of this study was to perform RNAseq analysis on two murine *ex vivo* cartilage models (hip cap and metatarsal) after exposure to physiological and injurious hydrostatic pressure, to examine the effects of hydrostatic pressure on gene expression in two different chondrocyte phenotypes.

2 Methods

2.1 Isolation and culture of ex vivo cartilage models

All mice utilized in these studies were kept in controlled conditions at the University of Brighton and all tissue isolation procedures were performed in accordance with the UK Animals (Scientific Procedures) Act of 1986 and regulations set by the UK Home Office and local institutional guidelines (PPL: PP3310437). Analyses were conducted blindly where possible to minimize the

effects of subjective bias. Animal studies were conducted in line with the ARRIVE guidelines.

Femoral heads were isolated from 4-week-old male C57/BL6J mice (Charles River), as previously described (Figure 1) (36). In brief, the hip joint was dislocated by applying slight pressure at the joint, and the femoral cap was avulsed using forceps. At this developmental stage, the predominant component of this tissue is the articular cartilage, therefore underlying subchondral bone was not included. Both hip caps were pooled from each individual mouse (n=4 mice/experimental group). Hip caps were cultured in Dulbecco's Modified Eagle Medium with GlutaMAX, substituted with 100 U/ml penicillin, 100µg/ml streptomycin (Thermo Fisher Scientific) in a humidified atmosphere (37°C, 5% CO_2).

Embryonic metatarsal organ cultures provide a well-established model of endochondral bone growth (Figure 1) (37). Metatarsals were isolated from E15 embryos of C57/BL6J (Charles River) mice as previously described (36). Six metatarsal bones were pooled per sample (n=4 samples/experimental group). Metatarsal bones were cultured in α-Minimum Essential Medium supplemented with 0.2% BSA Fraction V; 1 mmol/l β-glycerophosphate (βGP); 0.05 mg/ml L-ascorbic acid phosphate; 0.05 mg/ml gentamicin and 1.25 µg/ml fungizone (Thermo Fisher Scientific) in a humidified atmosphere (37°C, 5% CO_2).

2.2 Application of hydrostatic pressure

After 24 hours of culture, hips caps and metatarsals were placed into 5 ml sterile plastic syringes fitted with Luer lock end caps, taking care to eliminate all air bubbles (Suppl. Figure 1). Movement of the syringe plunger allowed for equilibration of pressure between syringe contents and the pressure vessel water (17). The syringes were placed in a water-filled pressure vessel at room temperature. Syringes were pressurized to 0 MPa (control), 5 MPa (physiological) or 50 MPa (injurious) hydrostatic pressure for 1 hour (Figure 1; Suppl. Figure 1). Following exposure to hydrostatic pressure, tissues were placed back into the incubator and cultured for a further 24 hours in the respective media, then flash frozen at -80°C until RNA extraction.

2.3 RNA extraction and sequencing

Tissue (<100 mg) were defrosted on ice and 1 ml Trizol (Qiagen) was added to each sample; tissues were homogenised using a mechanical disruptor, making sure to keep them cool by putting on ice every 15 seconds. Samples were incubated at room temperature for a minimum of 10 minutes to allow for cell lysis and centrifuged at 12,000 x *g* for 15 minutes at 4°C to pellet the excess tissue, whilst retaining RNA in solution. The supernatant was transferred to a clean tube and 200 µL of chloroform (Sigma) added. After vigorous shaking for 20 seconds, the samples were incubated at room temperature for 3 minutes and then centrifuged at 12,000 x *g* for 15 minutes at 4°C to enable phase separation. The upper, aqueous phase was transferred to a new tube, avoiding the interface. Following the addition of an equal volume of 70% ethanol, the samples were mixed thoroughly by vortexing and total RNA purified using RNeasy Mini spin columns (Qiagen), according to the manufacturer's recommendations. Purified RNA was eluted in 30 µl of RNase-free water, repeating the elution twice by reapplying the elute. The concentration and purity of the RNA samples were assessed using a Nanodrop One C spectrophotometer (Labtech) and the quality of the RNA was assessed on a TapeStation 4200 (Agilent Technologies).

All samples passed purity quality control checks but exhibited RNA Integrity Number (RIN) equivalent values below the ideal minimum of 7 (average value 2.8). The low RIN values obtained are considered typical for these explant tissue samples and suggest some partial degradation of the total RNA. DV200 analysis using the Agilent TapeStation 4200 software showed a percentage of

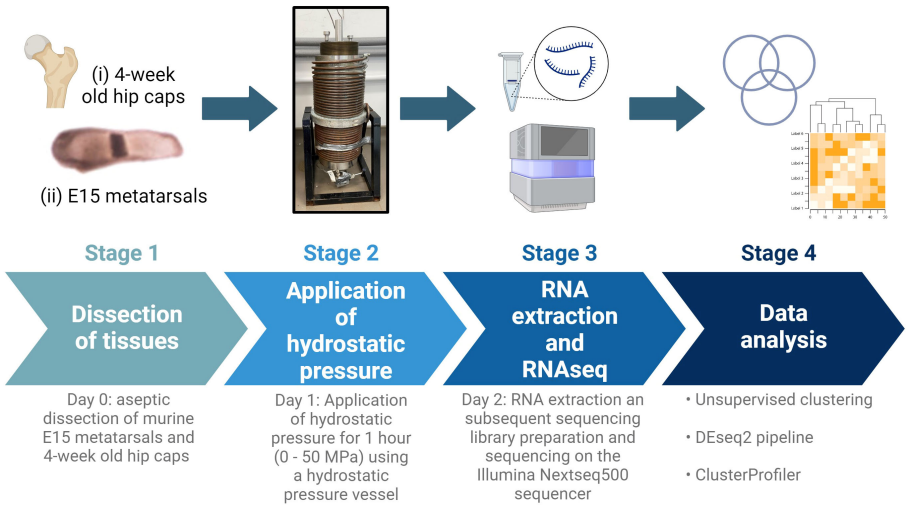

FIGURE 1
Schematic of experimental design. E15 metatarsal bones and 4-week-old hip cap cartilage explants were subjected to hydrostatic pressure (0-50 MPa) for 1 hour. After 24 hours, RNA was extracted and RNAseq and downstream analyses conducted. Created with BioRender.com.

fragments between 200 and 10000 bp ranging between 53.51-87.4% in all RNA samples. Sequencing libraries were prepared using the Universal Plus™ Total RNASeq with NuQuant kit and a mouse rRNA depletion module (Tecan Genomics), required for partially degraded RNA samples. Library construction strategy was pair end and strand specific. Libraries were checked for quality using the TapeStation 4200, quantified, normalized and sequenced on the Illumina NextSeq500 sequencer using a high-output kit (17 libraries) and a mid-output kit (7 libraries).

2.4 Data analysis

Initial sequencing read quality control was conducted using fastqc (version 0.11.9) (38) and multiqc (version 1.8) (39). Trimming was performed using TrimGalore using a minimum quality threshold of 20, discarding any trimmed reads shorter than 20 nucleotides. Trimmed reads were quantified using kallisto quant and transcript quantifications were converted to gene level by tximport. The transcriptome mapping data for all samples was imported into R for data summarization at the gene level. The data was normalized and analyzed using the DESeq2 pipeline (40). Unsupervised clustering of the sample data was performed using the R packages pheatmap and pcaMethods. Significant genes were identified by analysis using a model design that considered the sequencing run and strandedness of the library as possible batch effects (design= ~SeqRun + Library + Condition) and applying a 5% significance threshold to p-values adjusted using the Benjamini and Hochberg procedure (a significance threshold referred to elsewhere in the text as padj<=0.05, or 5% FDR). For functional analysis of the groups of differentially expressed genes, clusterProfiler was utilized to identify significantly over-represented functional categories using a significance threshold of 5% on the Benjamini and Hochberg corrected p-values (41). Annotations for the Gene Ontology (GO) Biological Process (BP), from the R package org.Mm.eg.db (version 3.11.4) were used (42). Genes that were significantly differentially expressed between our samples were compared to recent genome-wide association studies of osteoarthritis that have identified a number of osteoarthritis risk genes (43, 44).

3 Results

Herein, we conducted RNAseq analysis of murine *ex vivo* hip cap (articular), and metatarsal (growth plate) cartilage cultures (n=4 replicates) subjected to physiological (5 MPa) and injurious (50 MPa) hydrostatic pressure. Unsupervised clustering of the gene expression data indicated a clear distinction between the hip cap and metatarsal sample data, but two of the hip cap cartilage samples (*H502* [exposed to 50 MPa hydrostatic pressure] and *HC4* [control, 0 MPa hydrostatic pressure]) appeared to be outliers, thus were excluded from all downstream statistical analyses (Figures 2A, B; Suppl. Figures 2, 3).

3.1 Gene expression profiles of articular and growth plate cartilage

Prior to differential gene expression analyses focusing on the effects of hydrostatic pressure, the gene expression profiles of the two different cartilage explants were investigated to assess the genes and pathways that may be differentially expressed between a transient (growth plate) and an inherently stable (articular) cartilage phenotype (Suppl. Data 1). There were 2775 genes upregulated and 3368 genes downregulated in hip cap cartilage in comparison to metatarsal cartilage (Figure 3A). Upregulated genes with the greatest $\log_2$ fold change included ribosomal protein L9 (*Rpl9-ps4*, 39.4-fold), collagen type X (*Col10a1*, 7.7-fold), and frizzled-related protein (*Frzb*, 7.2-fold) (Table 1). Downregulated genes with the greatest $\log_2$ fold change included microfibrillar-associated protein 4 (*Mfap4*, 8.6-fold), insulin-like growth factor binding protein 2 (*Igfbp2*, 7.3-fold) and fibroblastic growth factor 10 (*Fgf10*, 7.2-fold) (Table 1).

Next, we sought to examine whether these differentially expressed genes were enriched in particular biological processes. Using annotations for GO BP, the data revealed a number of significantly enriched processes, which include ossification (GO:0001503; 124 genes), bone development (GO:0060348; 81 genes), cartilage development (GO:0051216; 83 genes), connective tissue development (GO:0061448; 98 genes), and extracellular matrix organization (GO:0030198; 84 genes), in hip cap cultures in comparison to metatarsals (Suppl. Table 1). Conversely, those that were downregulated included muscle tissue development (GO:0060537; 140 genes) and muscle cell differentiation (GO:0042692; 127 genes), as well as synapse organization (GO:0050808; 142 genes) (Suppl. Table 1).

When comparing the two datasets, the hip cap data yielded many more significant changes than the metatarsal data, and the greater spread of $\log_2$ fold changes taking place in the hip cap samples suggests that the hip cap cartilage explants are more responsive to changes in pressure than the metatarsal explants (Figure 3). Therefore, subsequent analyses focused on the data from the hip cap explants, with the highest up- and down-regulated genes, either commonly or uniquely expressed between each group, in the metatarsal data sets detailed in Suppl. Tables 2, 3.

3.2 Effects of physiological and injurious hydrostatic pressure on gene expression in hip cap cartilage explants

Compared to control, there were 375 genes significantly upregulated with 5 MPa hydrostatic pressure and 322 significantly downregulated in hip cap cultures (Figure 3A; Suppl. Data 1). With injurious hydrostatic pressure (50 MPa), there were 1022 significantly upregulated and 724 significantly downregulated genes (Figure 3A; Suppl. Data 1). Whilst some of the genes were consistently up- or down-regulated across the two hydrostatic pressures in both the hip cap and the metatarsal datasets, most of these significant genes were uniquely expressed by the hip cap datasets at 5 or 50 MPa (Figure 3B).

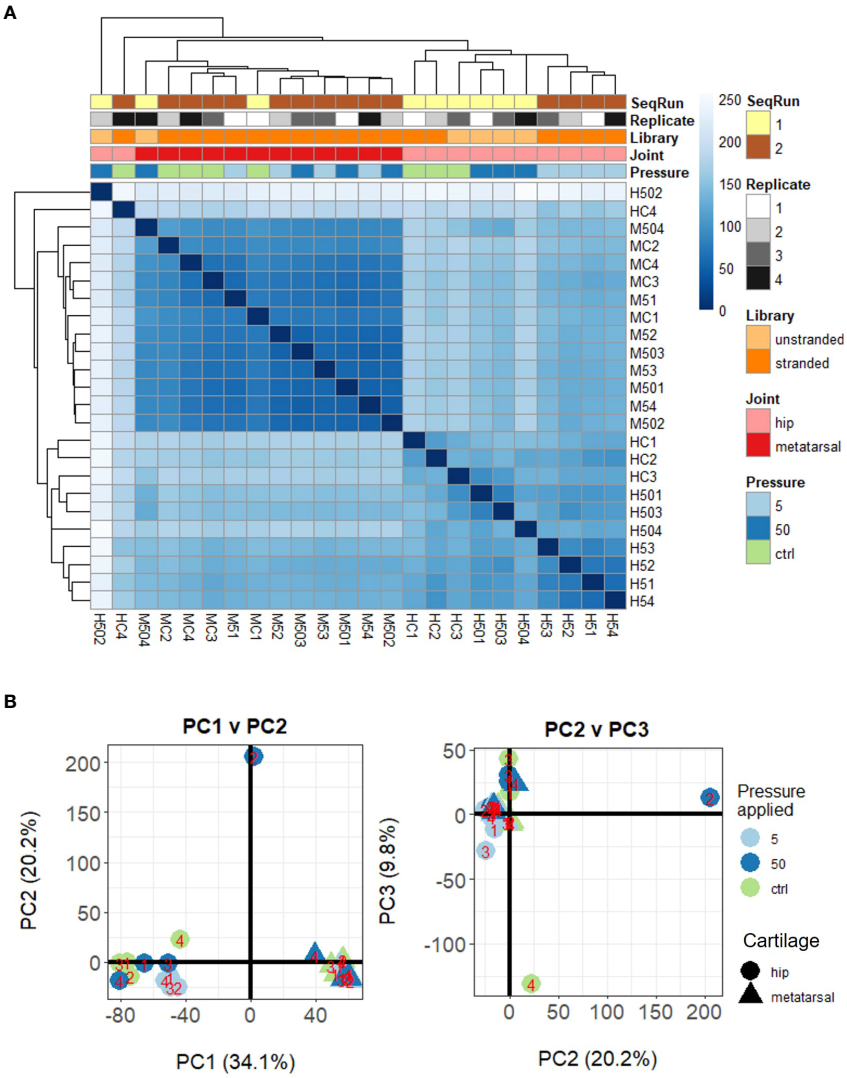

FIGURE 2
Unsupervised clustering of samples based on their DESeq2 normalized gene-level counts. **(A)** Heat map of inter-sample Euclidean distances, where darker blue colors indicate closer similarity. **(B)** Principal components analysis. Samples are labelled as M (metatarsal) and H (hip cap), followed by C (control – 0 MPa), 5 (5 MPa) or 50 (50 MPa) and replicate number (1–4).

Genes commonly modulated by hydrostatic pressure in these cultures with the greatest $\log_2$ fold changes are detailed in Suppl. Table 4. The genes uniquely expressed in response to hydrostatic pressure magnitudes include *Car2* (upregulated in 5 MPa versus control, 1.5-fold), *Mlip* (upregulated in 50 MPa vs control, 2.6-fold), *Tg* (downregulated in 5 MPa versus control, 2.2-fold) and *Ryr3* (downregulated in 50 MPa versus control, 2.6-fold) (Table 2).

3.3 GO BP enrichment analysis of differentially expressed genes

Using annotations for GO BP, the data revealed significantly enriched processes including regulation of cytokine production (GO:001819; 21 genes), Ras protein signal transduction (GO:007265; 20 genes) and ATP metabolic processes (GO0046034; 18 genes) with 5 MPa hydrostatic pressure application (Table 3; Suppl. Data 2). Conversely, process including cellular component disassembly (GO:0022411; 16 genes) and nuclear transport (GO0051169; 15 genes) were downregulated (Table 3; Suppl. Data 2). With injurious hydrostatic pressure (50 MPa), enriched pathways included generation of precursor metabolites and energy (GO:0006091; 39 genes), and cellular respiration (GO:0045333, 31 genes) (Figure 4; Table 3; Suppl. Data 2). Other upregulated GO BP relevant to the known functions of chondrocytes included regulation of developmental growth (GO0048638; 33 genes), and regulation of cell size (GO0008361; 21 genes) (Suppl. Data 2). Whereas those downregulated included ossification (GO:0001503; 25 genes), cartilage development (GO:0051216; 18 genes), connective tissue development (GO:0061448; 21 genes), and chondrocyte differentiation (GO:0002062; 17 genes) (Table 3; Suppl. Data 2). Further analysis of these enriched pathways in injurious hydrostatic pressure highlighted differential expression of several genes known

A

Comparison	Sig. Up	Sig. Down	Not Sig.
Control: Hip cap vs Metatarsal	2775	3368	36552
Metatarsal: 5 MPa vs Control	5	23	42667
Metatarsal: 50 MPa vs Control	7	19	42669
Hip cap: 5 MPa vs Control	375	322	41998
Hip cap: 50 MPa vs Control	1022	724	40949

B

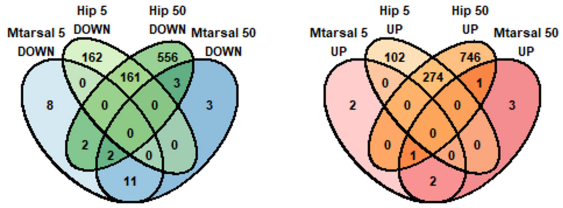

FIGURE 3
Summary of genes identified as significantly differently expressed between the main sample conditions of interest (DESeq2 padj<=0.05 (5% FDR)). **(A)** Numbers of significant genes (padj<=0.05) in each comparison. Sig. Down indicates genes down-regulated in the first condition listed in the comparison column relative to the second, while Sig. Up indicates those up-regulated in the first condition. **(B)** Overlap between the significant genes identified in each hip cap (Hip) and metatarsal (Mtarsal) cartilage explant group.

to be involved in osteoarthritis, such as *Fgf2, Ep300, Ngf, Adam9, Igfbp3, Sox9, Comp, Col6a1, Col6a2* and *Col11a1*.

3.4 Differential expression of previously identified osteoarthritis risk genes

Recent genome-wide association studies of osteoarthritis have identified a number of osteoarthritis risk genes (43, 44).

TABLE 1 Top 10 genes with highest upregulation and top 10 genes with highest downregulation in the hip cap versus metatarsal RNAseq datasets.

	Gene Name	Log_2 Fold Change	Adjusted *p* value
Top 10 genes with highest upregulation	*Rpl9-ps4*	39.41761815	6.53953E-15
	Gm10925	23.98054338	1.87468E-05
	Gm22969	21.45491466	5.33958E-06
	Mif-ps4	14.34623609	1.37344E-05
	Col10a1	7.736184458	3.71322E-08
	Serpina1d	7.646536307	5.54893E-13
	Frzb	7.219881296	2.58347E-50
	Cytl1	7.218161967	2.07064E-45
	Gpx3	7.055584365	1.53747E-28
	Clec3a	7.031246207	4.9778E-14
Top 10 genes with highest downregulation	*Mfap4*	-8.564081588	4.07328E-34
	Xist	-8.407700367	5.36182E-12
	Actc1	-8.087469882	1.48585E-10
	Hoxd13	-7.737458742	1.44143E-30
	Myh3	-7.539165841	9.66177E-24
	Kera	-7.465016823	2.52732E-12
	Igfbp2	-7.34202703	1.197E-12
	Crabp1	-7.311799886	8.05824E-13
	Fgf10	-7.176158119	4.15686E-11
	Ptn	-7.059869481	1.53489E-97

We therefore sought to compare whether these genes were differentially expressed in response to hydrostatic pressure in our datasets (Table 4). Only one of these genes was differentially expressed in our 5 MPa versus control datasets (*Wscd2*, 0.6-fold downregulation; data not shown). However, with injurious (50 MPa) hydrostatic pressure application, there were 12 genes differentially expressed (Table 4). These included cathepsin K (*Ctsk*, 0.9-fold upregulation), and chondroadherin-like (*Chadl*, 0.9-fold downregulation) (Table 4; Suppl. Figure 4).

4 Discussion

In this study we conducted RNAseq analysis of two different *ex vivo* cartilage explants (metatarsal and hip cap), to examine the effects of two magnitudes of hydrostatic pressure on gene expression. We observed clear differences between the cartilage types, including the upregulation of key genes such as *Frzb* and *Col10a1* in the hip cap explants. Extensive changes in gene expression were observed with hydrostatic pressure in the hip cap cartilage groups, however this was to a weaker extent in the metatarsal explants. Within the hip cap data set, enriched GO BP in the genes that were significantly downregulated in response to injurious hydrostatic pressure (50 MPa) versus control, included those involved in cartilage, bone and connective tissue development. Interestingly, these pathways were also increased when comparing the hip cap to the metatarsal data, suggesting that injurious hydrostatic pressure may promote a more transient-like phenotype in the hip cap cultures. This is further supported by our observed enrichment of the GO BPs for developmental growth and cell size in hip caps exposed to 50 MPa hydrostatic pressure. Indeed, it is well established that in osteoarthritis, the inherently stable articular cartilage undergoes changes that reflect a more developmental cartilage phenotype, such as that in the growth plate (3, 7). Therefore, lessons can be learnt from a better understanding of these two phenotypes, and their similarities and differences in our pursuit of maintaining articular cartilage health in ageing. This is of particular importance given the lack of regenerative capability of the articular cartilage, thus meaning therapies for osteoarthritis remain limited (4, 7).

TABLE 2 Top 10 genes with highest upregulation and greatest downregulation that are uniquely expressed in 5 MPa versus control and 50 MPa versus control in the hip cap RNAseq datasets.

	5 MPa vs Control			50 MPa vs Control		
	Gene Name	Log_2 Fold Change	Adjusted *p* value	Gene Name	Log_2 Fold Change	Adjusted *p* value
Top 10 genes with highest upregulation	*Abhd15*	3.22895414	0.000519	*Gm2451*	18.04382867	1.98582E-05
	Car2	1.466531813	0.008049	*H2ac23*	15.91830736	0.000179818
	Gm45665	1.436157039	0.00787	*Gm9973*	3.311225437	5.25837E-08
	Olfr1380	1.18544216	0.033261	*Gm48942*	3.201576037	3.37509E-06
	Mpp5	1.14918265	0.000377	*Gm29408*	3.061996469	4.83774E-06
	Gm9962	1.142757676	0.013066	*Mlip*	2.567534817	0.000385784
	Fpr1	1.061193105	0.016204	*Mmp12*	2.501682447	3.10048E-05
	Atp5g2	1.039789631	0.00418	*Abcd2*	2.312011543	0.001575342
	Fam81a	1.004756565	0.011008	*Ywhaq-ps3*	2.243694849	0.046074893
	Alg8	0.977342633	0.001856	*mt-Nd6*	2.195320542	0.001507966
Top 10 genes with highest downregulation	*Rps18-ps6*	-3.33818292	0.005493	*Gm44732*	-4.24186258	0.000124443
	Gm23680	-3.158700551	0.000322	*Gm16479*	-3.327634912	0.000538299
	Gm9968	-3.054024647	0.000146	*Ryr3*	-2.596299426	0.002870783
	Gm24514	-2.45810073	1.17E-06	*Gm3625*	-2.176518378	1.83627E-05
	Tg	-2.18679795	0.001011	*Pla2g2c*	-2.166700674	0.046074893
	Gm25682	-1.92383803	0.003421	*Gm8249*	-1.940743018	0.002267981
	Gm42715	-1.658526363	0.000376	*Serpina1a*	-1.854010245	0.014092563
	Adgrb1	-1.380005988	0.005428	*H2-M5*	-1.718905493	0.003710939
	Gm26822	-1.305512292	0.001159	*Gm15807*	-1.69503207	0.003989171
	Rap1gap2	-1.246295417	0.012053	*Serpina1d*	-1.649670074	0.000777013

Articular cartilage covers the ends of the bones in synovial joints, and the chondrocytes within maintain a stable phenotype to ensure joint health and longevity. This is in contrast to the growth plate cartilage, which is more transient in nature, with chondrocytes undergoing differentiation processes which drive endochondral ossification and longitudinal bone growth (3). The chondrocytes of these two cartilaginous structures express different programs, further defined by our RNAseq analysis in hip cap (articular) and metatarsal (growth plate) cartilage. Amongst the most differentially expressed genes in our studies were *Frzb*, and *Col10a1* (both upregulated) and *Igfbp2*, and *Fgf10* (both downregulated). *Col10a1* is a key determinant of chondrocyte hypertrophy, with mutant or abnormal human *Col10a1* expression associated with abnormalities in this process (45–47). The increase in *Col10a1* in our hip cap explants therefore suggests a greater degree of hypertrophy than in our metatarsal explants. Abnormal *Col10a1* expression is a well-established feature in osteoarthritis (48–50). Similarly, two SNPs in *Frzb*, an antagonist of the canonical WNT pathway, have been associated with osteoarthritis (51–53). Further, in pre-clinical models, osteoarthritis severity scores are significantly higher in the joints with deletion of *Frzb* compared to littermates (54). Together, our data are consistent with previous studies considering the different phenotypes of these cells, thus suggesting diverging phenotypes of these cell populations (55–57).

The high-water content of cartilage (approx. 70-80% water per wet mass) is maintained by an abundance of proteoglycans in the matrix. Chondrocytes in both the growth plate and the articular cartilage are subjected to a number of mechanical forces, including compressive and shear stresses, during loading (9, 13). These mechanical signals then modulate biochemical activity and changes in chondrocyte behavior (22). The majority of research to date has focused on understanding compressive forces on the health of the articular cartilage, however most of this force transforms to hydrostatic pressure due to the interstitial fluid content of joints (14, 58). As such, it can be assumed that hydrostatic pressure is the more prevalent stress to which chondrocytes are exposed. Chondrocytes demonstrate an improved cartilaginous physiology when exposed to hydrostatic pressure, as indicated by their increased ECM production (13). This therefore suggests that understanding the complexities of hydrostatic pressure could be a potential avenue for tissue regeneration in osteoarthritis.

Despite the application of hydrostatic pressure being experimentally controllable, studies have varied in their

magnitude, style and duration of hydrostatic pressure application. Our previous meta-analysis informed these factors in the experimental set up for our RNAseq study herein (33). In articular cartilage during normal movement, typical hydrostatic pressure loading of 0.5–10 MPa have been measured (13, 59). Our meta-analysis in 3D cultured chondrocytes confirmed that, based on aggrecan gene expression data, 4–5 MPa can significantly enhance proteoglycan production (33). Conversely, our meta-analysis detailed that the hydrostatic pressure magnitude of 50 MPa had a negative effect on proteoglycans (33). As such, we deemed the magnitudes of physiological (5 MPa) and injurious (50 MPa) hydrostatic pressure to be applicable in our pursuit of understanding gene changes in our explants.

In an RNAseq study performed on monolayer cultures, Zhu et al. used human articular chondrocytes to compare hydrostatic pressure (0.1 MPa) and perfusion methods on the chondrocyte phenotype, with the aim of understanding methods for reducing chondrocyte dedifferentiation in culture (60). Their RNAseq analysis revealed upregulation of well-known chondrocyte genes with hydrostatic pressure and conclude that a low hydrostatic pressure can be beneficial to chondrocytes (60). Further, a previous microarray study examined the effects of continuous hydrostatic pressure (25 MPa) on the chondrogenic ATDC5 cell line, again cultured in monolayer (21). Similarities can be observed between the genes they observe to be modulated by hydrostatic pressure and ours described herein, including differential expression of apoptosis-related and cartilage matrix genes (21). However, Montagne et al. applied a continuous hydrostatic pressure for 24 hours, which is in comparison to our study whereby we applied a single load for 1 hour and is akin to a single injurious event. Further, our examination of two different magnitudes of hydrostatic pressure and in physiologically-relevant cartilage explants adds further strength to our study. In addition, several genes known to play a key role in progression of osteoarthritis (e.g., *Fgf2, Ep300, Ngf, Adam9, Igfbp3, Sox9, Comp, Col6a1, Col6a2* and *Col11a1*) were modulated in our injurious hydrostatic pressure hip cap datasets, thereby validating this approach.

Overall, our results seem to indicate osteoarthritic-like effects of injurious hydrostatic pressure on our hip cap cartilage explants. Among the modulated genes identified in our study, several genes which have been identified as osteoarthritis risk genes from recent GWAS studies were differentially expressed, however verification of

TABLE 3 Annotations for the Gene Ontology (GO) Biological Process (BP) for genes that are differentially expressed in 5 MPa versus control and 50 MPa versus control in the hip cap RNAseq datasets.

5 MPa vs Control				
	ID	Description	No. genes	Adjusted *p* value
Top 10 upregulated GOBP	GO:0001819	positive regulation of cytokine production	21	1.38E-06
	GO:0007265	Ras protein signal transduction	20	1.50E-06
	GO:0046034	ATP metabolic process	18	1.05E-08
	GO:0045333	cellular respiration	17	1.39E-10
	GO:0015980	energy derivation by oxidation of organic compounds	17	1.11E-07
	GO:0022904	respiratory electron transport chain	13	8.59E-11
	GO:0022900	electron transport chain	13	1.61E-10
	GO:0042773	ATP synthesis coupled electron transport	12	3.79E-11
	GO:0006119	oxidative phosphorylation	12	9.95E-09
	GO:0042775	mitochondrial ATP synthesis coupled electron transport	9	8.31E-08
Top 10 downregulated GOBP	GO:0022411	cellular component disassembly	16	3.92E-06
	GO:0006913	nucleocytoplasmic transport	15	1.31E-06
	GO:0051169	nuclear transport	15	1.31E-06
	GO:0033157	regulation of intracellular protein transport	11	3.94E-05
	GO:0051168	nuclear export	10	3.58E-06
	GO:0015931	nucleobase-containing compound transport	10	4.64E-05
	GO:0006611	protein export from nucleus	9	1.07E-05
	GO:0034453	microtubule anchoring	5	1.01E-05
	GO:0018023	peptidyl-lysine trimethylation	5	0.000157
	GO:0034454	microtubule anchoring at centrosome	3	0.000166

(Continued)

TABLE 3 Continued

	50 MPa vs Control			
	ID	Description	No. genes	Adjusted *p* value
Top 10 upregulated GOBP	GO:0006091	generation of precursor metabolites and energy	39	5.16E-09
	GO:0015980	energy derivation by oxidation of organic compounds	34	2.82E-11
	GO:0045333	cellular respiration	31	1.64E-14
	GO:0046034	ATP metabolic process	29	1.28E-08
	GO:0022904	respiratory electron transport chain	22	4.28E-14
	GO:0022900	electron transport chain	22	1.27E-13
	GO:0006119	oxidative phosphorylation	20	1.47E-10
	GO:0042773	ATP synthesis coupled electron transport	19	1.49E-13
	GO:0042775	mitochondrial ATP synthesis coupled electron transport	16	7.34E-11
	GO:0009060	aerobic respiration	14	2.61E-07
Top 10 downregulated GOBP	GO:0001503	ossification	25	5.11E-05
	GO:0032386	regulation of intracellular transport	23	6.10E-05
	GO:0061448	connective tissue development	21	3.88E-05
	GO:0006913	nucleocytoplasmic transport	21	4.75E-05
	GO:0051169	nuclear transport	21	4.75E-05
	GO:0048193	Golgi vesicle transport	20	3.78E-05
	GO:0051216	cartilage development	18	2.02E-05
	GO:0002062	chondrocyte differentiation	17	2.76E-08
	GO:0051168	nuclear export	13	8.25E-05
	GO:1903909	regulation of receptor clustering	5	9.33E-05

these by *in situ* hybridization or RT-qPCR would be beneficial (43, 44). There was only one gene (*Wscd2*, WSC Domain-Containing Protein 2) modulated in the 5 MPa versus control dataset, with the majority being in the 50 MPa comparison. Interestingly, *Wscd2* has previously been identified as an osteocyte transcriptome signature gene and downregulated in murine bone with ageing, although its role in cartilage has, to our knowledge, not yet fully been defined (61, 62).

Of these risk genes modulated by 50 MPa hydrostatic pressure, the gene that underwent the highest fold upregulation was cathepsin K (*Ctsk*), a protein expressed by osteoclasts used for collagen degradation (63). This finding is consistent with the previous microarray study by Montague et al. in which *Ctsk* was found to be strongly induced following the exposure of hydrostatic pressure for 4 hours (21). Indeed, *Ctsk* has been shown to be overexpressed in the articular cartilage and subchondral bone in osteoarthritis (64, 65). Further, *Ctsk* deletion in a murine surgical osteoarthritis model (destabilization of the medial meniscus) protected against disease progression (66), as did pharmacological treatment with a cathepsin K inhibitor (SB-553484) in a canine model (67). Pre-clinical findings have been translated to clinical trials with the selective cathepsin K inhibitor MIV-711 reducing bone and cartilage disease progression in individuals with symptomatic, radiographic knee osteoarthritis (68).

Chadl, which encodes for chondroadherin-like protein, plays a role in collagen binding and in the negative regulation of chondrocyte (69). In our studies, its expression underwent the highest fold downregulation with 50 MPa hydrostatic pressure. This is consistent with a previous RNAseq study which examined the subchondral bone of patients who underwent total joint replacement due to osteoarthritis (70). In this study both *Chadl* and *Il11*, also identified in our studies, were identified as the most consistently differentially expressed genes and thus have the potential to be targeted for clinical therapies.

Whilst several ion channels known to be involved in chondrocyte mechanotransduction (e.g., *Piezo1*, *Trpv4*, *Trpv5*) (9) were unchanged in our datasets, upregulation of *Piezo2* and downregulation of *Trpm4* was observed in hip caps exposed to both magnitudes of hydrostatic pressure (Suppl. Data 1). Interestingly, reliable detection of *Piezo2* transcripts in primary murine chondrocytes appears to be conflicting in the literature (71, 72). *Trpm4* has been identified in cartilage samples from osteoarthritic patients (73), however its role in cartilage mechanotransduction is unclear. Downregulation of *Trpm5* and

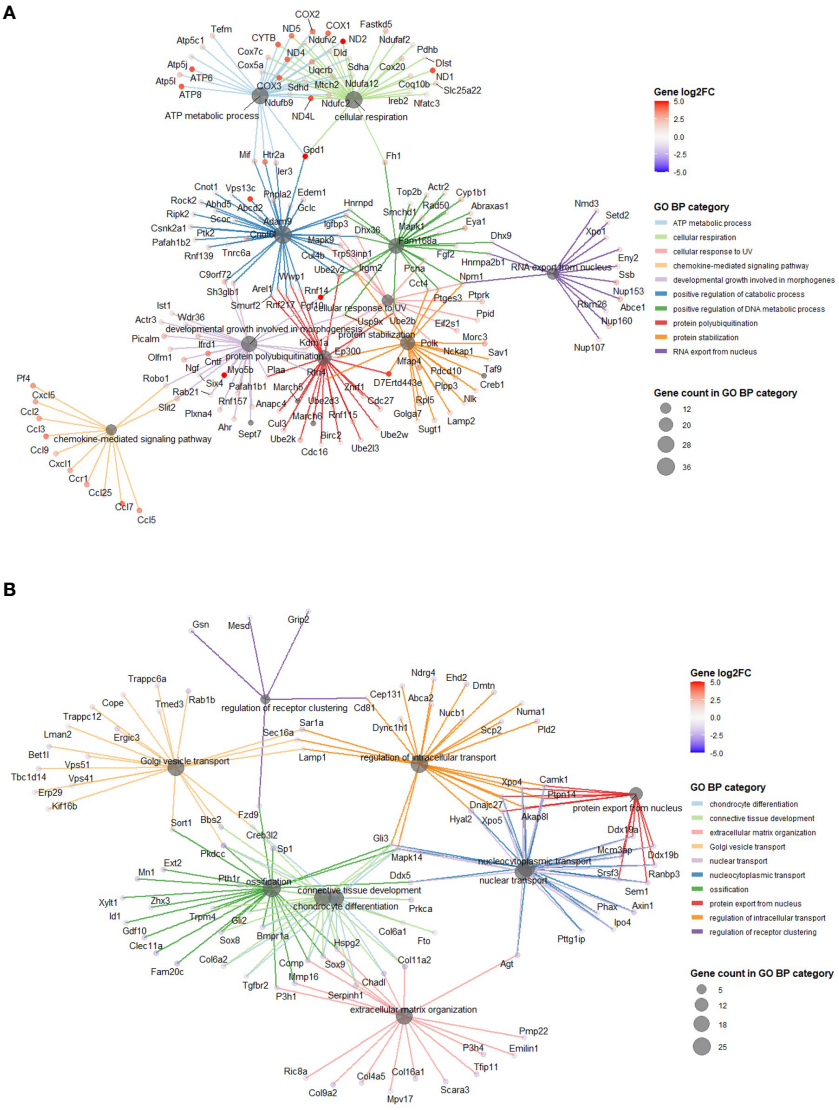

FIGURE 4
GO BP categories in 50 MPa versus control hip cap datasets. **(A)** Pathways enriched in the genes significantly up in the 50 MPa versus control comparisons. **(B)** Pathways enriched in the genes significantly down in the 50 MPa versus control comparisons.

P2rx7 was only observed in hip caps exposed to 5 MPa compared to control (Suppl. Data 1). This suggests that whilst our *ex vivo* models are sensitive to some changes in ion channel expression with hydrostatic pressure, other mechanisms may exist.

Our study is unique in using two different cartilage explants, both of which offer a physiological model system. We have also applied hydrostatic pressure at magnitudes based on findings from our previous meta-analysis to ensure these are representative of both physiological and injurious load (33). However, we do recognize the limitation in our sample size presented herein. Therefore, the biological interpretation of our findings should be considered appropriately, with the need for a more detailed consideration of the differences observed. For example, it would be pertinent to use a temporal approach to the application of hydrostatic pressure as in this study we applied a single load for 1 hour and is akin to a single injurious event, rather than the continual degradation seen in osteoarthritis. It would also be of further interest to utilize cartilage from an osteoarthritis model (e.g., STR/ort mouse), or ultimately from human samples, to both validate our results here, and also examine the effects of hydrostatic pressure on gene expression in disease pathology. Despite these limitations, the current study was able to statistically differentiate the effects of hydrostatic pressure on chondrocytes.

In conclusion, we identified distinct differential gene expression signatures in hip cap and metatarsal cartilage explants, indicative of the divergent phenotypes of their residing chondrocytes. Our RNAseq studies examining the cartilage response to hydrostatic pressure provided evidence for injurious hydrostatic pressure to be associated with decreases in processes including cartilage development and chondrocyte differentiation. Together this informs on the potential benefits of hydrostatic pressure in

TABLE 4 Differential expression of osteoarthritis risk genes identified in recent genome-wide association studies in response to injurious hydrostatic pressure (50 MPa) versus control in our hip cap datasets.

	Gene Name	Log_2 Fold Change	Adjusted *p* value
Upregulated genes	*Ctsk*	0.852667719	0.016121811
	Il11	0.750247415	0.036698304
	Sbno1	0.740095825	0.005159578
	Aldh1a2	0.648544373	0.037375403
Downregulated genes	*Chadl*	-0.904205798	0.009053645
	Apoe	-0.899057162	0.001558965
	Mn1	-0.790048116	0.020283481
	Pfkm	-0.736351338	0.017447093
	Megf8	-0.647300732	0.001249084
	Fto	-0.492563212	0.035580843
	Vgll4	-0.490894811	0.049748082
	Smg6	-0.47338466	0.043509481

cartilage tissue engineering strategies, which need to carefully consider the magnitude of application and the effects on gene expression. Further, we identified the differential expression of a number of genes that have previously been identified as osteoarthritis risk genes, including *Ctsk* and *Chadl*, further highlighting their potential as therapeutic targets. These data will therefore contribute to a better understanding of the role of hydrostatic pressure and the chondrocyte phenotype in health and osteoarthritis.

Data availability statement

The RNA sequencing data are available from NCBI Gene Expression Omnibus (https://www.ncbi.nlm.nih.gov/geo) under accession number GSE234112.

Ethics statement

The animal study was approved by University of Brighton institutional review board. The study was conducted in accordance with the local legislation and institutional requirements.

Author contributions

LB: Formal analysis, Writing – original draft, Writing – review & editing, Data curation, Investigation, Methodology. AH: Data curation, Formal analysis, Investigation, Methodology, Writing – review & editing. AS: Data curation, Formal analysis, Writing – original draft, Writing – review & editing. GB: Conceptualization, Data curation, Formal analysis, Investigation, Methodology, Writing – review & editing. PB: Conceptualization, Funding acquisition, Investigation, Methodology, Resources, Writing – review & editing. KS: Conceptualization, Formal analysis, Funding acquisition, Investigation, Methodology, Project administration, Resources, Supervision, Writing – original draft, Writing – review & editing.

Funding

The author(s) declare financial support was received for the research, authorship, and/or publication of this article. We are grateful to Medical Research Council (to KS; MR/R022240/2 & MR/V033506/1) for funding. We are also grateful to the University of Brighton for a Rising Stars Award to KS.

Acknowledgments

The authors would like to thank the Bioresources Unit at the University of Brighton for the assistance with the care of animal models in this study.

Conflict of interest

The authors declare that the research was conducted in the absence of any commercial or financial relationships that could be construed as a potential conflict of interest.

The author(s) declared that they were an editorial board member of Frontiers, at the time of submission. This had no impact on the peer review process and the final decision.

Publisher's note

Supplementary material

The Supplementary Material for this article can be found online at: https://www.frontiersin.org/articles/10.3389/fendo.2023.1278596/full#supplementary-material

References

1. Archer CW, Francis-West P. The chondrocyte. *Int J Biochem Cell Biol* (2003) 35 (4):401–4. doi: 10.1016/S1357-2725(02)00301-1

2. Pap T, Korb-Pap A. Cartilage damage in osteoarthritis and rheumatoid arthritis–two unequal siblings. *Nat Rev Rheumatol* (2015) 11(10):606–15. doi: 10.1038/nrrheum.2015.95

3. Staines KA, Pollard AS, McGonnell IM, Farquharson C, Pitsillides AA. Cartilage to bone transitions in health and disease. *J Endocrinol* (2013) 219(1):R1–R12. doi: 10.1530/JOE-13-0276

4. Goldring MB. Articular cartilage degradation in osteoarthritis. *HSS J* (2012) 8 (1):7–9. doi: 10.1007/s11420-011-9250-z

5. Poole AR. Osteoarthritis as a whole joint disease. *HSS J* (2012) 8(1):4–6. doi: 10.1007/s11420-011-9248-6

6. Sandell LJ, Aigner T. Articular cartilage and changes in arthritis. An introduction: cell biology of osteoarthritis. *Arthritis Res* (2001) 3(2):107–13. doi: 10.1186/ar148

7. Pitsillides AA, Beier F. Cartilage biology in osteoarthritis–lessons from developmental biology. *Nat Rev Rheumatol* (2011) 7(11):654–63. doi: 10.1038/nrrheum.2011.129

8. Hodgkinson T, Kelly DC, Curtin CM, O'Brien FJ. Mechanosignalling in cartilage: an emerging target for the treatment of osteoarthritis. *Nat Rev Rheumatol* (2022) 18 (2):67–84. doi: 10.1038/s41584-021-00724-w

9. Pettenuzzo S, Arduino A, Belluzzi E, Pozzuoli A, Fontanella CG, Ruggieri P, et al. Biomechanics of chondrocytes and chondrons in healthy conditions and osteoarthritis: A review of the mechanical characterisations at the microscale. *Biomedicines* (2023) 11 (7):1942. doi: 10.3390/biomedicines11071942

10. Belluzzi E, Todros S, Pozzuoli A, Ruggieri P, Carniel EL, Berardo A. Human cartilage biomechanics: experimental and theoretical approaches towards the identification of mechanical properties in healthy and osteoarthritic conditions. *Processes* (2023) 11(4):1014. doi: 10.3390/pr11041014

11. Bachrach NM, Mow VC, Guilak F. Incompressibility of the solid matrix of articular cartilage under high hydrostatic pressures. *J Biomech* (1998) 31(5):445–51. doi: 10.1016/S0021-9290(98)00035-9

12. O'Conor CJ, Case N, Guilak F. Mechanical regulation of chondrogenesis. *Stem Cell Res Ther* (2013) 4(4):61. doi: 10.1186/scrt211

13. Elder BD, Athanasiou KA. Hydrostatic pressure in articular cartilage tissue engineering: from chondrocytes to tissue regeneration. *Tissue Eng Part B Rev* (2009) 15 (1):43–53. doi: 10.1089/ten.teb.2008.0435

14. Pattappa G, Zellner J, Johnstone B, Docheva D, Angele P. Cells under pressure - the relationship between hydrostatic pressure and mesenchymal stem cell chondrogenesis. *Eur Cell Mater* (2019) 37:360–81. doi: 10.22203/eCM.v037a22

15. Mizuno S, Ogawa R. Using changes in hydrostatic and osmotic pressure to manipulate metabolic function in chondrocytes. *Am J Physiol Cell Physiol* (2011) 300 (6):C1234–45. doi: 10.1152/ajpcell.00309.2010

16. Cheleschi S, Tenti S, Barbarino M, Giannotti S, Bellisai F, Frati E, et al. Exploring the crosstalk between hydrostatic pressure and adipokines: an in vitro study on human osteoarthritic chondrocytes. *Int J Mol Sci* (2021) 22(5):2745. doi: 10.3390/ijms22052745

17. Hall AC, Urban JP, Gehl KA. The effects of hydrostatic pressure on matrix synthesis in articular cartilage. *J Orthop Res* (1991) 9(1):1–10. doi: 10.1002/jor.1100090102

18. Nakamura S, Arai Y, Takahashi KA, Terauchi R, Ohashi S, Mazda O, et al. Hydrostatic pressure induces apoptosis of chondrocytes cultured in alginate beads. *J Orthop Res* (2006) 24(4):733–9. doi: 10.1002/jor.20077

19. Takahashi K, Kubo T, Arai Y, Kitajima I, Takigawa M, Imanishi J, et al. Hydrostatic pressure induces expression of interleukin 6 and tumour necrosis factor alpha mRNAs in a chondrocyte-like cell line. *Ann Rheum Dis* (1998) 57(4):231–6. doi: 10.1136/ard.57.4.231

20. Inoue H, Arai Y, Kishida T, Terauchi R, Honjo K, Nakagawa S, et al. Hydrostatic pressure influences HIF-2 alpha expression in chondrocytes. *Int J Mol Sci* (2015) 16 (1):1043–50. doi: 10.3390/ijms16011043

21. Montagne K, Onuma Y, Ito Y, Aiki Y, Furukawa KS, Ushida T. High hydrostatic pressure induces pro-osteoarthritic changes in cartilage precursor cells: A transcriptome analysis. *PloS One* (2017) 12(8):e0183226. doi: 10.1371/journal.pone.0183226

22. Parkkinen JJ, Ikonen J, Lammi MJ, Laakkonen J, Tammi M, Helminen HJ. Effects of cyclic hydrostatic pressure on proteoglycan synthesis in cultured chondrocytes and articular cartilage explants. *Arch Biochem Biophys* (1993) 300 (1):458–65. doi: 10.1006/abbi.1993.1062

23. Montagne K, Furukawa KS, Taninaka Y, Ngao B, Ushida T. Modulation of the long non-coding RNA Mir155hg by high, but not moderate, hydrostatic pressure in cartilage precursor cells. *PloS One* (2022) 17(12):e0275682. doi: 10.1371/journal.pone.0275682

24. Kawanishi M, Oura A, Furukawa K, Fukubayashi T, Nakamura K, Tateishi T, et al. Redifferentiation of dedifferentiated bovine articular chondrocytes enhanced by cyclic hydrostatic pressure under a gas-controlled system. *Tissue Eng* (2007) 13(5):957–64. doi: 10.1089/ten.2006.0176

25. Rieder B, Weihs AM, Weidinger A, Szwarc D, Nurnberger S, Redl H, et al. Hydrostatic pressure-generated reactive oxygen species induce osteoarthritic conditions in cartilage pellet cultures. *Sci Rep* (2018) 8(1):17010. doi: 10.1038/s41598-018-34718-8

26. Kunitomo T, Takahashi KA, Arai Y, Sakao K, Honjo K, Saito M, et al. Influence of extracellular matrix on the expression of inflammatory cytokines, proteases, and apoptosis-related genes induced by hydrostatic pressure in three-dimensionally cultured chondrocytes. *J Orthop Sci* (2009) 14(6):776–83. doi: 10.1007/s00776-009-1393-0

27. Toyoda T, Seedhom BB, Yao JQ, Kirkham J, Brookes S, Bonass WA. Hydrostatic pressure modulates proteoglycan metabolism in chondrocytes seeded in agarose. *Arthritis Rheumatol* (2003) 48(10):2865–72. doi: 10.1002/art.11250

28. Wenger R, Hans MG, Welter JF, Solchaga LA, Sheu YR, Malemud CJ. Hydrostatic pressure increases apoptosis in cartilage-constructs produced from human osteoarthritic chondrocytes. *Front Biosci* (2006) 11:1690–5. doi: 10.2741/1914

29. Zhao X, Hua Y, Wang T, Ci Z, Zhang Y, Wang X, et al. *In vitro* cartilage regeneration regulated by a hydrostatic pressure bioreactor based on hybrid photocrosslinkable hydrogels. *Front Bioeng Biotechnol* (2022) 10:916146. doi: 10.3389/fbioe.2022.916146

30. Chang SH, Mori D, Kobayashi H, Mori Y, Nakamoto H, Okada K, et al. Excessive mechanical loading promotes osteoarthritis through the gremlin-1-NF-kappaB pathway. *Nat Commun* (2019) 10(1):1442. doi: 10.1038/s41467-019-09491-5

31. Henstock JR, Rotherham M, Rose JB, El Haj AJ. Cyclic hydrostatic pressure stimulates enhanced bone development in the foetal chick femur in vitro. *Bone* (2013) 53(2):468–77. doi: 10.1016/j.bone.2013.01.010

32. Dehghan-Baniani D, Mehrjou B, Chu PK, Lee WYW, Wu H. Recent advances in "Functional engineering of articular cartilage zones by polymeric biomaterials mediated with physical, mechanical, and biological/chemical cues". *Adv Healthc Mater* (2023) 12 (10):e2202581. doi: 10.1002/adhm.202202581

33. Hodder E, Guppy F, Covill D, Bush P. The effect of hydrostatic pressure on proteoglycan production in articular cartilage in *vitro*: a meta-analysis. *Osteoarthritis Cartilage* (2020) 28(8):1007–19. doi: 10.1016/j.joca.2020.03.021

34. Sironen R, Elo M, Kaarniranta K, Helminen HJ, Lammi MJ. Transcriptional activation in chondrocytes submitted to hydrostatic pressure. *Biorheology* (2000) 37(1-2):85–93.

35. Samvelyan HJ, Hughes D, Stevens C, Staines KA. Models of osteoarthritis: relevance and new insights. *Calcif Tissue Int* (2021) 109(3):243–56. doi: 10.1007/s00223-020-00670-x

36. Staines KA, Brown G, Farquharson C. The ex vivo organ culture of bone. *Methods Mol Biol* (2019) 1914:199–215. doi: 10.1007/978-1-4939-8997-3_10

37. Houston DA, Staines KA, MacRae VE, Farquharson C. Culture of murine embryonic metatarsals: A physiological model of endochondral ossification. *J Vis Exp* (2016) 118. doi: 10.3791/54978-v

38. Andrews SK,F, Segonds-Pichon A, Biggins L, Krueger C, Wingett S. *FastQC*. Babraham, UK: Babraham Institute (2012).

39. Ewels P, Magnusson M, Lundin S, Kaller M. MultiQC: summarize analysis results for multiple tools and samples in a single report. *Bioinformatics* (2016) 32 (19):3047–8. doi: 10.1093/bioinformatics/btw354

40. Love MI, Huber W, Anders S. Moderated estimation of fold change and dispersion for RNA-seq data with DESeq2. *Genome Biol* (2014) 15(12):550. doi: 10.1186/s13059-014-0550-8

41. Yu G, Wang LG, Han Y, He QY. clusterProfiler: an R package for comparing biological themes among gene clusters. *OMICS* (2012) 16(5):284–7. doi: 10.1089/omi.2011.0118

42. Carlson M. org.Mm.eg.db: Genome wide annotation for Mouse. R package version 3.8.2. *Bioconductor* (2019). doi: 10.18129/B9.bioc.org.Mm.eg.db

43. Boer CG, Hatzikotoulas K, Southam L, Stefansdottir L, Zhang Y, Coutinho de Almeida R, et al. Deciphering osteoarthritis genetics across 826,690 individuals from 9 populations. *Cell* (2021) 184(18):4784–818 e17. doi: 10.1016/j.cell.2021.07.038

44. Tachmazidou I, Hatzikotoulas K, Southam L, Esparza-Gordillo J, Haberland V, Zheng J, et al. Identification of new therapeutic targets for osteoarthritis through genome-wide analyses of UK Biobank data. *Nat Genet* (2019) 51(2):230–6. doi: 10.1038/s41588-018-0327-1

45. Ain NU, Makitie O, Naz S. Autosomal recessive chondrodysplasia with severe short stature caused by a biallelic COL10A1 variant. *J Med Genet* (2018) 55(6):403–7. doi: 10.1136/jmedgenet-2017-104885

46. Ikegawa S, Nishimura G, Nagai T, Hasegawa T, Ohashi H, Nakamura Y. Mutation of the type X collagen gene (COL10A1) causes spondylometaphyseal dysplasia. *Am J Hum Genet* (1998) 63(6):1659–62. doi: 10.1086/302158

47. Warman ML, Abbott M, Apte SS, Hefferon T, McIntosh I, Cohn DH, et al. A type X collagen mutation causes Schmid metaphyseal chondrodysplasia. *Nat Genet* (1993) 5(1):79–82. doi: 10.1038/ng0993-79

48. Gratal P, Mediero A, Sanchez-Pernaute O, Prieto-Potin I, Lamuedra A, Herrero-Beaumont G, et al. Chondrocyte enlargement is a marker of osteoarthritis severity. *Osteoarthritis Cartilage* (2019) 27(8):1229–34. doi: 10.1016/j.joca.2019.04.013

49. He Y, Manon-Jensen T, Arendt-Nielsen L, Petersen KK, Christiansen T, Samuels J, et al. Potential diagnostic value of a type X collagen neo-epitope biomarker for knee osteoarthritis. *Osteoarthritis Cartilage* (2019) 27(4):611–20. doi: 10.1016/j.joca.2019.01.001

50. von der Mark K, Frischholz S, Aigner T, Beier F, Belke J, Erdmann S, et al. Upregulation of type X collagen expression in osteoarthritic cartilage. *Acta Orthop Scand Suppl* (1995) 266:125–9. doi: 10.3109/17453679509157667

51. Lories RJ, Boonen S, Peeters J, de Vlam K, Luyten FP. Evidence for a differential association of the Arg200Trp single-nucleotide polymorphism in FRZB with hip osteoarthritis and osteoporosis. *Rheumatol (Oxford)* (2006) 45(1):113–4. doi: 10.1093/rheumatology/kei148

52. Loughlin J, Dowling B, Chapman K, Marcelline L, Mustafa Z, Southam L, et al. Functional variants within the secreted frizzled-related protein 3 gene are associated with hip osteoarthritis in females. *Proc Natl Acad Sci USA* (2004) 101(26):9757–62. doi: 10.1073/pnas.0403456101

53. Min JL, Meulenbelt I, Riyazi N, Kloppenburg M, Houwing-Duistermaat JJ, Seymour AB, et al. Association of the Frizzled-related protein gene with symptomatic osteoarthritis at multiple sites. *Arthritis Rheumatol* (2005) 52(4):1077–80. doi: 10.1002/art.20993

54. Thysen S, Luyten FP, Lories RJ. Loss of Frzb and Sfrp1 differentially affects joint homeostasis in instability-induced osteoarthritis. *Osteoarthritis Cartilage* (2015) 23 (2):275–9. doi: 10.1016/j.joca.2014.10.010

55. Chau M, Lui JC, Landman EB, Spath SS, Vortkamp A, Baron J, et al. Gene expression profiling reveals similarities between the spatial architectures of postnatal articular and growth plate cartilage. *PloS One* (2014) 9(7):e103061. doi: 10.1371/journal.pone.0103061

56. Haseeb A, Kc R, Angelozzi M, de Charleroy C, Rux D, Tower RJ, et al. SOX9 keeps growth plates and articular cartilage healthy by inhibiting chondrocyte dedifferentiation/osteoblastic redifferentiation. *Proc Natl Acad Sci USA* (2021) 118(8): e2019152118. doi: 10.1073/pnas.2019152118

57. Lui JC, Chau M, Chen W, Cheung CS, Hanson J, Rodriguez-Canales J, et al. Spatial regulation of gene expression during growth of articular cartilage in juvenile mice. *Pediatr Res* (2015) 77(3):406–15. doi: 10.1038/pr.2014.208

58. Mow VC, Wang CC, Hung CT. The extracellular matrix, interstitial fluid and ions as a mechanical signal transducer in articular cartilage. *Osteoarthritis Cartilage* (1999) 7(1):41–58. doi: 10.1053/joca.1998.0161

59. Hodge WA, Fijan RS, Carlson KL, Burgess RG, Harris WH, Mann RW. Contact pressures in the human hip joint measured in vivo. *Proc Natl Acad Sci USA* (1986) 83 (9):2879–83. doi: 10.1073/pnas.83.9.2879

60. Zhu G, Mayer-Wagner S, Schroder C, Woiczinski M, Blum H, Lavagi I, et al. Comparing effects of perfusion and hydrostatic pressure on gene profiles of human chondrocyte. *J Biotechnol* (2015) 210:59–65. doi: 10.1016/j.jbiotec.2015.06.409

61. Kaya S, Bailey KN, Schurman CA, Evans DS, Alliston T. Bone-cartilage crosstalk informed by aging mouse bone transcriptomics and human osteoarthritis genome-wide association studies. *Bone Rep* (2023) 18:101647. doi: 10.1016/j.bonr.2022.101647

62. Youlten SE, Kemp JP, Logan JG, Ghirardello EJ, Sergio CM, Dack MRG, et al. Osteocyte transcriptome mapping identifies a molecular landscape controlling skeletal homeostasis and susceptibility to skeletal disease. *Nat Commun* (2021) 12(1):2444. doi: 10.1038/s41467-021-22517-1

63. Costa AG, Cusano NE, Silva BC, Cremers S, Bilezikian JP. Cathepsin K: its skeletal actions and role as a therapeutic target in osteoporosis. *Nat Rev Rheumatol* (2011) 7(8):447–56. doi: 10.1038/nrrheum.2011.77

64. Konttinen YT, Mandelin J, Li TF, Salo J, Lassus J, Liljestrom M, et al. Acidic cysteine endoproteinase cathepsin K in the degeneration of the superficial articular hyaline cartilage in osteoarthritis. *Arthritis Rheumatol* (2002) 46(4):953–60. doi: 10.1002/art.10185

65. Morko JP, Soderstrom M, Saamanen AM, Salminen HJ, Vuorio EI. Up regulation of cathepsin K expression in articular chondrocytes in a transgenic mouse model for osteoarthritis. *Ann Rheum Dis* (2004) 63(6):649–55. doi: 10.1136/ard.2002.004671

66. Soki FN, Yoshida R, Paglia DN, Duong LT, Hansen MF, Drissi H. Articular cartilage protection in Ctsk(-/-) mice is associated with cellular and molecular changes in subchondral bone and cartilage matrix. *J Cell Physiol* (2018) 233(11):8666–76. doi: 10.1002/jcp.26745

67. Connor JR, LePage C, Swift BA, Yamashita D, Bendele AM, Maul D, et al. Protective effects of a cathepsin K inhibitor, SB-553484, in the canine partial medial meniscectomy model of osteoarthritis. *Osteoarthritis Cartilage* (2009) 17(9):1236–43. doi: 10.1016/j.joca.2009.03.015

68. Conaghan PG, Bowes MA, Kingsbury SR, Brett A, Guillard G, Rizoska B, et al. Disease-modifying effects of a novel cathepsin K inhibitor in osteoarthritis: A randomized controlled trial. *Ann Intern Med* (2020) 172(2):86–95. doi: 10.7326/M19-0675

69. Tillgren V, Ho JC, Onnerfjord P, Kalamajski S. The novel small leucine-rich protein chondroadherin-like (CHADL) is expressed in cartilage and modulates chondrocyte differentiation. *J Biol Chem* (2015) 290(2):918–25. doi: 10.1074/jbc.M114.593541

70. Tuerlings M, van Hoolwerff M, Houtman E, Suchiman E, Lakenberg N, Mei H, et al. RNA sequencing reveals interacting key determinants of osteoarthritis acting in subchondral bone and articular cartilage: identification of IL11 and CHADL as attractive treatment targets. *Arthritis Rheumatol* (2021) 73(5):789–99. doi: 10.1002/art.41600

71. Lee W, Leddy HA, Chen Y, Lee SH, Zelenski NA, McNulty AL, et al. Synergy between Piezo1 and Piezo2 channels confers high-strain mechanosensitivity to articular cartilage. *Proc Natl Acad Sci USA* (2014) 111(47):E5114–22. doi: 10.1073/pnas.1414298111

72. Servin-Vences MR, Moroni M, Lewin GR, Poole K. Direct measurement of TRPV4 and PIEZO1 activity reveals multiple mechanotransduction pathways in chondrocytes. *Elife* (2017) 6:e21074. doi: 10.7554/eLife.21074

73. Halonen L, Pemmari A, Nummenmaa E, Hamalainen M, Moilanen T, Vuolteenaho K, et al. Human osteoarthritic chondrocytes express nineteen different TRP-genes-TRPA1 and TRPM8 as potential drug targets. *Int J Mol Sci* (2023) 24 (12):10057. doi: 10.3390/ijms241210057

frontiers | Frontiers in Endocrinology

TYPE Original Research
PUBLISHED 19 December 2023
DOI 10.3389/fendo.2023.1308604

OPEN ACCESS

EDITED BY
Katherine A. Staines,
University of Brighton, United Kingdom

REVIEWED BY
Larisa Ryskalin,
University of Pisa, Italy
Yi-Zhou Huang,
Sichuan University, China

*CORRESPONDENCE
Jennifer Z. Paxton
j.z.paxton@ed.ac.uk

RECEIVED 06 October 2023
ACCEPTED 27 November 2023
PUBLISHED 19 December 2023

CITATION
Prabhakaran V, Melchels FPW, Murray LM and Paxton JZ (2023) Engineering three-dimensional bone macro-tissues by guided fusion of cell spheroids.
Front. Endocrinol. 14:1308604.
doi: 10.3389/fendo.2023.1308604

Engineering three-dimensional bone macro-tissues by guided fusion of cell spheroids

Vinothini Prabhakaran[1,2], Ferry P.W. Melchels[3,4], Lyndsay M. Murray[1,2,5] and Jennifer Z. Paxton[1,2*]

[1]Anatomy@Edinburgh, Edinburgh Medical School, Biomedical Sciences, University of Edinburgh, Edinburgh, United Kingdom, [2]Centre for Discovery Brain Sciences, College of Medicine and Veterinary Medicine, University of Edinburgh, Edinburgh, United Kingdom, [3]School of Engineering and Physical Sciences, Institute of Biological Chemistry, Biophysics and Bioengineering, Heriot-Watt University, Edinburgh, United Kingdom, [4]Future Industries Institute, University of South Australia, Adelaide, SA, Australia, [5]Euan McDonald Centre for Motor Neuron Disease Research, University of Edinburgh, Edinburgh, United Kingdom

Introduction: Bioassembly techniques for the application of scaffold-free tissue engineering approaches have evolved in recent years toward producing larger tissue equivalents that structurally and functionally mimic native tissues. This study aims to upscale a 3-dimensional bone *in-vitro* model through bioassembly of differentiated rat osteoblast (dROb) spheroids with the potential to develop and mature into a bone macrotissue.

Methods: dROb spheroids in control and mineralization media at different seeding densities (1×10^4, 5×10^4, and 1×10^5 cells) were assessed for cell proliferation and viability by trypan blue staining, for necrotic core by hematoxylin and eosin staining, and for extracellular calcium by Alizarin red and Von Kossa staining. Then, a novel approach was developed to bioassemble dROb spheroids in pillar array supports using a customized bioassembly system. Pillar array supports were custom-designed and printed using Formlabs Clear Resin® by Formlabs Form2 printer. These supports were used as temporary frameworks for spheroid bioassembly until fusion occurred. Supports were then removed to allow scaffold-free growth and maturation of fused spheroids. Morphological and molecular analyses were performed to understand their structural and functional aspects.

Results: Spheroids of all seeding densities proliferated till day 14, and mineralization began with the cessation of proliferation. Necrotic core size increased over time with increased spheroid size. After the bioassembly of spheroids, the morphological assessment revealed the fusion of spheroids over time into a single macrotissue of more than 2.5 mm in size with mineral formation. Molecular assessment at different time points revealed osteogenic maturation based on the presence of osteocalcin, downregulation of Runx2 ($p < 0.001$), and upregulated alkaline phosphatase ($p < 0.01$).

Discussion: With the novel bioassembly approach used here, 3D bone macrotissues were successfully fabricated which mimicked physiological

osteogenesis both morphologically and molecularly. This biofabrication approach has potential applications in bone tissue engineering, contributing to research related to osteoporosis and other recurrent bone ailments.

KEYWORDS

bone, scaffold-free, bioassembly, spheroid, macrotissue, tissue engineering

1 Introduction

Bone defects and diseases are prevalent worldwide with high morbidity rates and significant clinical challenges in repair and regeneration. Metabolic, metastatic, and genetic bone diseases cause severe pain, reduced mobility, and increased socioeconomic costs and can also lead to secondary defects like fractures (1). Pharmacological drugs such as antiresorptive agents and osteoanabolics were developed for treating these debilitating diseases, and surgical grafts are also common in orthopedic practice to repair and rebuild damaged bones (2). However, clinical drug trials have limitations such as insufficient trial patients and a greater risk of unpredicted side effects (3, 4). Also, surgical auto- and allografts are in short supply along with other limitations such as donor site morbidity, graft rejection, and infection (5). To minimize these limitations, bone tissue engineering plays a crucial role in developing *in-vitro* biomimetic models for preclinical drug tests (6) and as replacement for bone grafts (7).

Osteoblast monolayer cell cultures are common *in-vitro* models used to investigate physiopathological and pharmacological mechanisms in bone diseases as well as toxicity tests of investigative drugs. However, cellular and extracellular matrix (ECM) interactions in monolayer cell cultures are not biomimetic due to their two-dimensional nature (8). Alternatively, three-dimensional (3D) cultures recapitulate the complex cellular microenvironment more closely related to natural bone tissues (8). Different scaffold materials have been used for 3D cultures which either act like native ECM allowing growth and differentiation of cells, e.g., decellularized ECM (9), or provide an environment for cells to produce their own ECM, e.g., functional hydrogels (8). Despite the interest in scaffolding materials for bone tissue engineering, there are significant limitations, specifically the high costs, complex fabricating procedures, limited cell density, hindrance to mechanotransduction between cells, and fate of the foreign material after implantation for applications in regenerative medicine (10). Thus, scaffold-free tissue engineering is gaining importance in developing clinically useful tissue constructs by excluding the use of exogenous scaffolds (11).

Scaffold-free 3D models, especially spheroids, have great potential in fabricating biomimetic tissues due to their self-assembling and self-organizing properties which better reflect natural tissues. This approach has varied applications as drug screening models, developmental and disease models, and large-scale biofabricated tissue to replace irreversibly damaged tissues (12). In recent years, spheroids (i.e., microtissues) have been considered as building blocks to fabricate macrotissues and organs through guided assembly and fusion (13–15).

Three-dimensional spheroid-based bioassembly approaches are emerging to manufacture large-scale tissues. An automated bioassembly system has been developed by the Woodfield group to produce scaffold-based chondrocyte tissue constructs using a PEGT/PBT copolymer (13). Alternatively, in order to develop a "scaffold-free" osteogenic macrotissue, Heo et al. (16) employed sacrificial materials, i.e., sodium alginate cross-linked with calcium chloride which was removed by citrate after spheroid fusion, making the construct scaffold-free. However, the effect of citrate chelation on calcium of osteogenic tissue was not addressed. Another research group has developed the Kenzan method to form scaffold-free tissues by inserting microneedles into spheroids (17). Although this method has been effective, there is a high possibility of tissue disintegration during the removal process (18). These drawbacks demand an alternative approach to bioassemble osteoblast spheroids into macrotissues without any destructive effects.

Our study aims to fabricate a biomimetic rat osteoblast macrotissue using a customized bioassembly system. To achieve this aim, osteogenic induction using mineralization media was first studied to observe cell proliferation, cellular arrangement, and extracellular matrix synthesis in osteoblast spheroids. Spheroids were then bioassembled and assessed to demonstrate the biomimetic nature of the fabricated macrotissue construct by morphological and molecular analyses.

2 Materials and methods

2.1 Cells

Rat osteoblasts (RObs) were procured from Cell Applications, Inc. (USA) and cultured according to the manufacturer's protocol for expansion and differentiation, resulting in a population of

differentiated rat osteoblasts (dRObs) that were cryopreserved and thawed when required. dRObs passage numbers 5 to 12 were used in this study.

2.2 Culture media

2.2.1 Growth media

Dulbecco's modified Eagle's medium (DMEM) containing high glucose with sodium pyruvate and L-glutamine (Product #41966052, Gibco™, Fisher Scientific, UK) was supplemented with 10% fetal bovine serum (FBS; Product #FB-1001, LabTech Inc., UK) and 1% antibiotic–antimycotic solution (ABAM; Product #A5955, Sigma-Aldrich, UK). This supplemented DMEM was used as a standard growth medium (GM) for cell culture.

2.2.2 Mineralization media

Mineralization media (MM) was prepared by further supplementing GM with 10 nM of dexamethasone (Product #D4902, Sigma-Aldrich, Germany), 10 mM of β-glycerophosphate disodium salt (Product #G9422, Sigma-Aldrich, USA), and 10 ng/ml of recombinant human BMP-4 (Product #AF-120-05ET, Peprotech®, UK). L-Ascorbic acid 2-phosphate sesquimagnesium salt hydrate (50 µg/ml) (Product #A8960, Sigma-Aldrich, USA) was freshly added on the day of media usage. The prepared media was filter-sterilized (0.22 µm pore size) before use.

2.3 Spheroids' growth and mineralization

The dRObs were plated in triplicates for spheroid formation in 96-well "U" bottom cell-repellent plates (Product #650970, CELLSTAR®, Greiner Bio-One, UK) at three different cell seeding densities, i.e., 1×10^4, 5×10^4, and 1×10^5 cells/150 µl of GM per well, and incubated at 37°C and 5% CO_2. After 48 h, the GM was replaced with MM, while control spheroids were maintained in GM. The spheroids were assessed for cell proliferation and viability, presence of a necrotic core, and ECM calcium deposits on days 7, 14, 21, and 28.

2.3.1 Cell proliferation and viability

The dROb spheroids were dissociated by placing them in 100 µl of accutase (Product #00-4555-56, Invitrogen™ Thermo Scientific, CA, USA) and incubating for 40 min at 37°C and 5% CO_2. Cell count and viability were assessed by a trypan blue staining method (Product #15250-061, Thermo Fisher, USA) according to the manufacturer's protocol. One-way ANOVA and *post-hoc* Tukey test were performed to compare cell proliferation and viability among different seeding densities ($N = 3$). The spheroid diameter was measured by Fiji/ImageJ software using images taken on Leica DMi1 phase contrast inverted microscope.

2.3.2 Necrotic core assessment

Spheroids were washed with phosphate buffered saline (PBS 1×) twice and fixed with 4% paraformaldehyde (Product #J19943-K2, Thermo Scientific, Belgium) for 1 h at room temperature. As each of the spheroids is of an extremely small size, they were embedded in agarose blocks before wax processing. In brief, a drop of 2% agarose (Product #15510-027, Invitrogen, UK) was placed on a glass slide onto which a spheroid was deposited and covered with another drop of 2% agarose. After trimming the agarose blocks into a cubic shape, they were wax-processed using a Leica ASP300S tissue processor and embedded in paraffin wax blocks. Paraffin-embedded spheroids were sliced into 10 µm sections using a rotary microtome (Leica Biosystems, UK) and placed onto SuperFrost Plus™ glass slides. Harris hematoxylin and eosin staining (H&E) was performed on spheroid sections according to the manufacturer's protocol. In brief, the sections were dewaxed in xylene, hydrated with alcohol series (100%, 90%, 70%, and running water), followed by hematoxylin (Product #RBA-4205-00A, CellPath, UK) for 3 min which was differentiated by acid alcohol and eosin staining (Product #6766008, Shandon™, Fisher Scientific, UK) for 2 min which was differentiated by potassium alum and final dehydration by alcohol series, cleared by xylene, and mounted with DPX using coverslips.

2.3.3 Extracellular matrix production (calcium deposits)

Fixed spheroids were subjected to Alizarin red staining for assessing calcium deposits. First, the spheroids were washed twice with distilled water, and 100 µl of Alizarin red stain (Product #2003999, EMD Millipore, USA) was added and incubated at room temperature and protected from light for 10 min. Then, spheroids were thoroughly washed four times with distilled water and observed for calcium deposits under Leica DMi1 inverted microscope (bright field).

2.4 Bioassembly of spheroids

2.4.1 Three-dimensional modeling and printing

The pillar array support used in this study was designed with an online 3D computer-aided design (CAD) program (https://www.tinkercad.com/) with 0.5 mm pillar-to-pillar distance, 0.5 mm pillar diameter, 3 mm pillar height, and 1 mm base thickness (15 mm L × 10 mm W) (Figure 1A). The designs were printed (Figure 1B) with "Formlabs Clear Resin®" (Product #RS-F2-GPCL-04) using a Formlabs Form2 3D printer and postprocessed by rinsing in isopropyl alcohol (IPA) followed by postcuring for 60 min within a UV cabinet (UVP CL-1000L, 365 nm, 3 mW/cm^2). Prints were then extracted in IPA within a Soxhlet apparatus overnight. Before use, the printed materials were sterilized by 70% alcohol for 30 min followed by a PBS (1×) wash. Based on preliminary studies (data not included), the postprocessed resin material used in this study has been confirmed as non-cytotoxic.

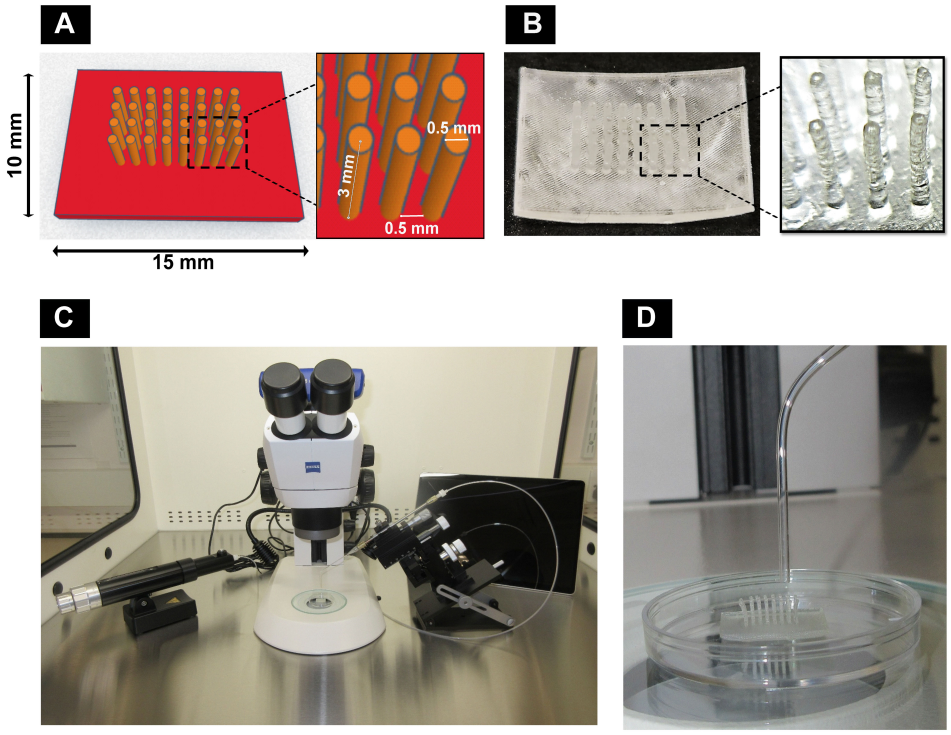

FIGURE 1
Components of the customized bioassembly system: **(A)** computer-aided design with dimensions using Tinkercad and **(B)** 3D-printed pillar array supports using Formlabs Clear Resin® with Formlabs Form2 3D printer. **(C)** Customized spheroid bioassembly system with CellTram®4r Air, micromanipulator, stereomicroscope, and Microsoft Surface Pro 9 installed with Zeiss Labscope. **(D)** Pillar array support along with bent capillary to deposit spheroids.

2.4.2 Customized 3D bioassembly system

A customized setup (Figure 1C) was developed by assembling a stereomicroscope (Stemi305, Zeiss, UK) with a camera connected to a Zeiss Labscope software in Microsoft Surface Pro 9 (Product #QCH-00003, XMA Ltd., UK) and a manual micromanipulator (Product #M3301-M3-R, World Precision Instruments, UK) to fix a capillary holder connected to CellTram®4r Air (Product #5196000013, Eppendorf, UK), inside a vertical laminar flow hood (Product #VLF-36, Purair®, UK). Borosilicate capillaries (Product #PG52151-4, WPI, UK) of the size 1.5 mm OD were heat bent slightly (Figure 1D) and inserted into the capillary holder.

2.4.3 Three-dimensional bioassembly of bone cell spheroids

Fifteen-day-old GM and MM cultured dROb spheroids were aspirated into the capillary and transferred to the sterile pillar array supports under microscopic guidance. Six spheroids were deposited in between pillars in a single-layered fashion and incubated at 37°C and 5% CO_2 in GM and MM, respectively ($N = 3$). Spheroids were removed from supports on days 2, 4, and 6 to determine the extent of fusion. In brief, pillars were cut using a surgical blade (size 22), and spheroids were carefully manipulated to detach from the base using a 22G needle and by inverse tapping into media. The removed spheroids were cultured (*vide infra*) or fixed with 4% paraformaldehyde for 2 h. H&E staining was performed on wax-embedded sections (10 µm).

2.4.4 Scaffold-free culture of bioassembled 3D macrotissues

After the successful removal from the pillar array supports, the fused spheroids (macrotissue) were cultured in a 24-well cell-repellent plate (Product #662970, CELLSTAR®, Greiner Bio-One, UK) at 37°C and 5% CO_2 ($N = 3$) in 1 ml of mineralization media to observe further fusion changes in scaffold-free conditions on days 2, 4, and 8 after removal (depicted as dAR2, dAR4, and dAR8, where dAR is "day after removal"). Media was changed every 2–3 days.

2.5 Morphological assessment

2.5.1 Histological staining

Scaffold-free cultured macrotissues over time from dAR2 to dAR8 were fixed with 4% paraformaldehyde for 2 h and sectioned at 10 µm thickness after wax embedding. H&E, Alizarin red, and Von Kossa staining were performed according to the manufacturer's protocol.

Alizarin red staining: After dewaxing and hydrating, the sections were covered with Alizarin red solution (product #2003999, EMD Millipore) for 5–15 min followed by blotting with filter paper and dehydrating by acetone and acetone–xylene mix (1:1), cleared by xylene, and mounted with DPX.

Von Kossa staining (Product #ab150687, Abcam, UK): After dewaxing and hydrating, the sections were incubated with 5% silver

nitrate under UV light for 1 h, followed by 5% sodium thiosulfate for 2–3 min at room temperature and nuclear fast red for 5 min. The sections were thoroughly washed with distilled water between each step, then dehydrated with absolute alcohol, cleared with xylene, and mounted with DPX.

2.5.2 Scanning electron microscopy

Scanning electron microscopic imaging was performed on dAR8 fused spheroid macrotissue (i.e., day 25 from the initial seeding date) cultured in mineralization media and compared with approximately similar-aged spheroid in growth media (day 28). They were fixed with 4% paraformaldehyde and stored in PBS 1× at 4°C until SEM sample preparation. In brief, the samples were fixed in a solution of 3% glutaraldehyde in 0.1 M of sodium cacodylate buffer (pH 7.3) for 2 h. They were then washed in 3 × 10-min changes of 0.1 M sodium cacodylate buffer. Samples were then postfixed in 1% osmium tetroxide in 0.1 M of sodium cacodylate buffer for 45 min. A further 3 × 10-min washes were performed in 0.1 M of sodium cacodylate buffer. Dehydration in graded concentrations of acetone (50%, 70%, 90%, and 3 × 100%) for 10 min each was followed by critical point drying using liquid carbon dioxide. After mounting on aluminum stubs with carbon tabs attached, the specimens were coated with 9 nm palladium using a Safematic CCU-010 HV sputter coater. The samples were imaged using a Zeiss Crossbeam 550 at 2 and 7 kV using a probe current of 100 pA. An In-lens detector was used to image surface topography.

2.6 Molecular assessment

2.6.1 Gene expression by qRT-PCR

RNA from dAR2 and dAR8 macrotissue was extracted using RNeasy® minikit (Product #74104, Qiagen, USA). RNA from the dROb monolayer in GM on day 7 was used as a control/calibrator. The concentration and purity of RNA samples were evaluated using a NanoDrop spectrophotometer. After quality checking, cDNA synthesis was performed using an RT^2 first-strand kit (Product #330404, #79254, Qiagen, USA). KAPA SYBR® Fast qPCR universal kit (Product #KK4601, KAPA Biosystems Inc., USA) was used to evaluate gene expression in the samples at an annealing temperature of 58.6°C for 40 cycles in Bio-Rad CFX Connect Real-Time PCR Detection System. Target genes were alkaline phosphatase (ALP) [forward primer (f): 5`-GACCCTGCCTTACCAACTC-3`, reverse primer (r): 5`-CCCATACCATCTCCCAGGAA-3`] and Runx2 (f: 5`-GCTTCTCCAACCCACGAATG-3`, r: 5`-GAACTGATAGGACGCTGACGA-3`), and the reference genes were GAPDH (f: 5`-TGTTCTAGAGACAGCCGCAT-3`, r: 5`-GTAACCAGGCGTCCGATACG-3`) and β-actin (f: 5`-TCTGTGTGGATTGGTGGCTCTA-3`, r: 5`-AGGGTGTAAAACGCAGCTCA-3`) (forward and reverse primers from Sigma Aldrich, UK). The amplification was performed in triplicates, and data were analyzed for relative expression using the $2^{-\Delta\Delta Ct}$ method (19).

2.6.2 Osteocalcin immunostaining

Osteocalcin immunostaining was performed on paraffin-embedded bone macrotissues (dAR2, 4, and 8) and control dROb spheroid (day 7 in growth media). Antigen retrieval was performed using citrate buffer (pH 6.0) for 20 min. Sections were blocked using 10% bovine serum albumin (Product #A4503, Sigma Aldrich, USA) and incubated overnight at 4°C with rabbit anti-rat osteocalcin polyclonal antibody (product #PA5-78871, Invitrogen) with a dilution of 1 µg/ml, followed by Alexa Fluor™ 488 donkey anti-rabbit IgG (1:500 dilution) (Product #A21206, Invitrogen, USA) incubation in the dark for 2 h. DAPI-counterstained sections (1:1,000) were imaged using a fluorescent microscope (Leica THUNDER).

2.7 Statistical analysis

Data were graphically presented as mean ± standard error in spheroid diameter, cell proliferation and viability, and mean ± standard deviation in relative gene expression analysis. One-way ANOVA and *post-hoc* Tukey test were performed to compare between groups using Past 4.13 software (20).

3 Results

3.1 Cell proliferation and viability

dRObs at three seeding densities (1×10^4, 5×10^4, 1×10^5 cells) compactly aggregated at 24 h, 36 h, and 48 h, respectively (Figure 2A), and spheroid growth commenced thereafter. In GM, the cell number of all spheroids increased gradually from day 7 to day 28 (Figure 2B). In MM, the cell number drastically increased up to day 14 and declined thereafter (Figure 2C). Among the three seeding densities, 1×10^5 cell spheroids had a greater reduction in cell number after day 14 in MM. In both GM and MM, cell viability declined with increasing culture time point from day 7 to day 28 in all seeding densities (Figure 2D). There was no significant difference ($p > 0.05$) in cell viability between seeding densities at any time point (one-way ANOVA, Tukey *post-hoc* test, $N = 3$).

3.2 Spheroid diameter

In all three seeding densities, the diameter of the spheroids increased from day 1 to day 28 in both GM and MM with a significant difference between each time point on days 7, 14, 21, and 28 (Figures 3A–C). Spheroids in MM have significantly larger diameters than GM ($p \leq 0.01$) at all time points and seeding densities except on day 7 in 5×10^4 and 1×10^5 seeded spheroids. Comparing spheroids among the seeding densities, spheroid size was significantly different on days 7 and 14 in GM ($p \leq 0.01$) and on day 7 only in MM ($p \leq 0.01$). They reached an approximately similar diameter range (~1.2 to 1.3 mm) on day 21 in GM and on day 14 in MM (no significant difference $p > 0.05$) and increased at a similar rate over time till day 28. Using a low seeding density (1×10^4), a faster increase in spheroid size was observed, and upon reaching a critical size (1.2–1.3 mm), they increased at an equal rate as that of higher seeding densities (Figure 3D).

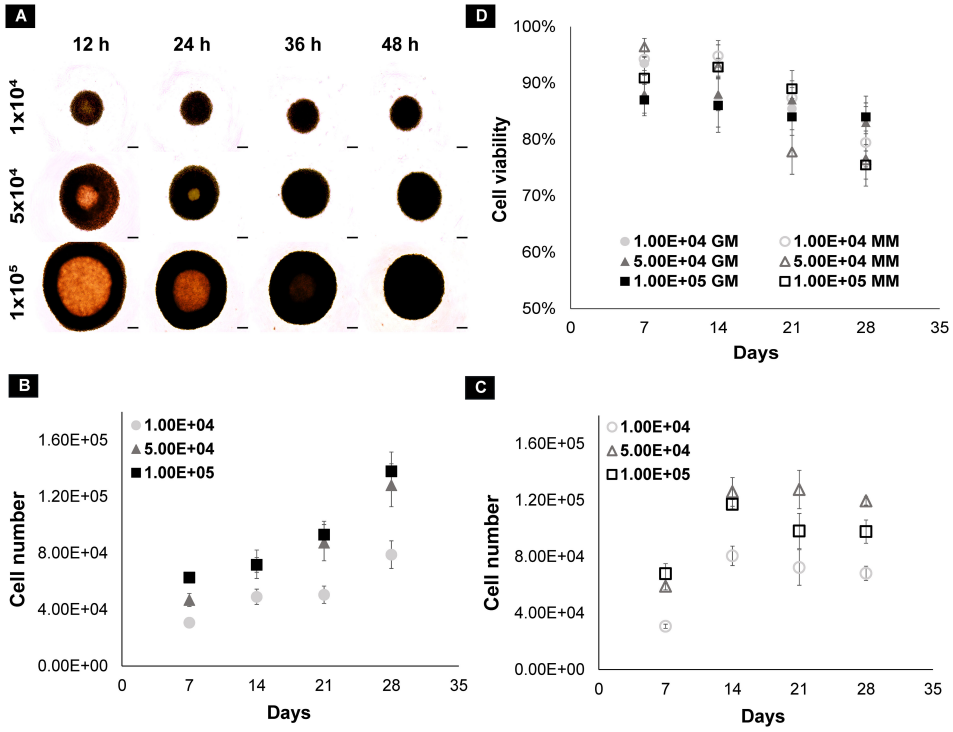

FIGURE 2
(A) Spheroid formation of dROb cells up to 48 h; scale bar: 200 µm. Graphs representing the cell count of dROb spheroids in **(B)** growth media and **(C)** mineralization media and **(D)** cell viability at 1 × 10^4, 5 × 10^4, and 1 × 10^5 seeding densities from day 7 to day 28 (*N* = 3). Legends: "GM" denotes growth media and "MM" denotes mineralization media. Error bars: standard error; *N*: experimental replicates.

3.3 Necrotic core observation

Cellular arrangement and necrotic cores were observed by H&E staining on spheroid sections (10 µm). The dROb cells were evenly distributed in all spheroids with three typical zones: proliferative, quiescent, and necrotic (Figure 4A). The presence of a pink core region with pyknotic, karyorrhectic, and karyolyzed nuclei indicates necrosis (21). The necrotic core size was dependent on the size of the spheroid, i.e., the larger the spheroid size, the greater the necrosis. Any dROb spheroid of more than 1,300 µm demonstrated a necrotic core that continued to widen over time (Figure 4B) regardless of the seeding density and media conditions. The presence of a necrotic core was corroborated by cell viability analyses which demonstrated a decline in cell viability over time from day 7 to day 28 (Figure 2D).

3.4 Extracellular matrix calcium deposits

Alizarin red staining demonstrated the presence of red calcium deposits in spheroids cultured in MM from day 14 in all three seeding densities (Figure 4C). Spheroids sectioned after staining revealed brick red-colored calcium deposits (Figure 4D). Spheroids in GM do not show the presence of calcium deposits. This suggests that MM induces dROb spheroids to produce an extracellular matrix containing calcium phosphate deposits between day 7 and day 14.

3.5 Three-dimensional bioassembly of spheroids

The 3D-printed pillar array supports had upright pillars to hold the spheroids during the bioassembly process and subsequent culture period until fusion of the spheroids occurred (Figure 5A). Removal of spheroids from the pillar array supports on different days (days 2, 4, and 6) revealed that spheroids fused together in MM but not in GM (Figure 5B). On day 2 in MM, the spheroids removed from the pillar array supports were clearly fused in regions other than the pillar area (Figure 5C). Over time (on days 4 and 6), spheroids were closely connected to each other (Figure 5C). However, the removal process was difficult in tightly fused spheroids, as in some cases the pillars remained attached to the spheroids. Considering the difficulty of removal, day 2 after deposition was deduced as the ideal time for spheroid removal from the pillar array supports. H&E staining revealed that the edges of the spheroids were fused compactly (Figure 5D). Necrotic core regions were noted to increase over time but did not appear to affect the fusion.

3.6 Scaffold-free culture of 3D macrotissue

3.6.1 Fusion and mineralization of macrotissue cultures

The removed spheroids cultured in a 24-well cell-repellent plate fused together into macrotissues over time (Figure 6A), i.e., 2.64 ±

10.3389/fendo.2023.1308604

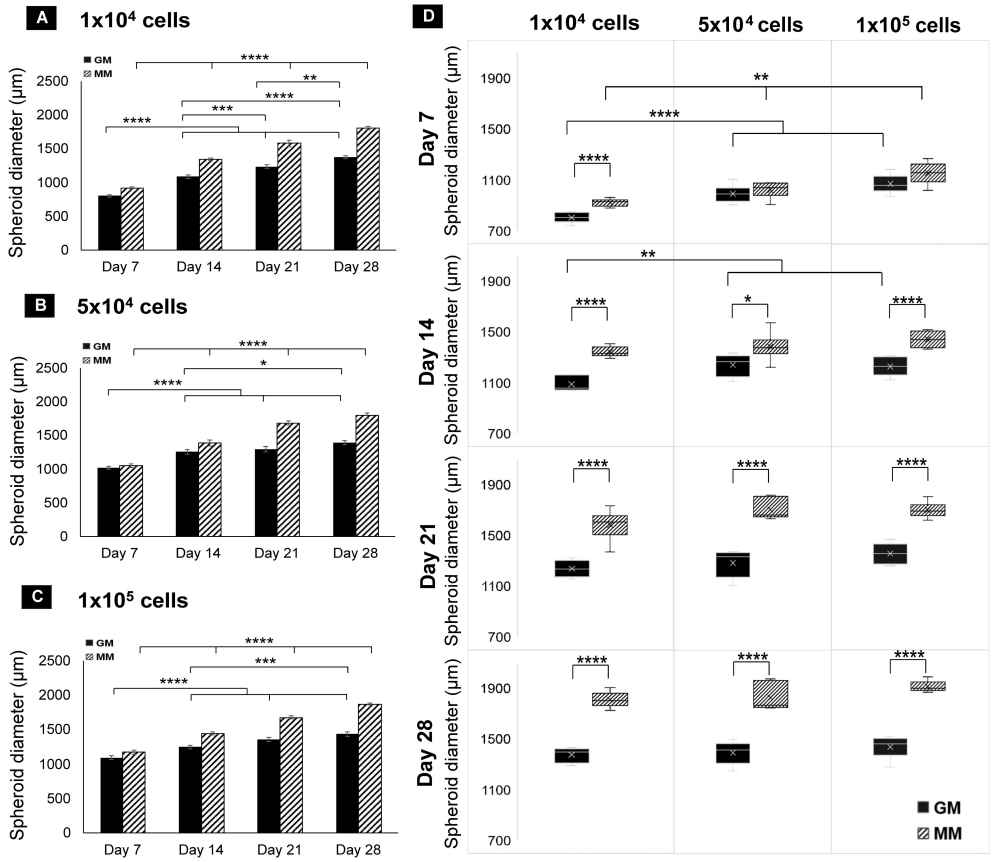

FIGURE 3
Bar charts of dROb spheroid diameters showing significant differences "between days" at 1 × 10^4 **(A)**, 5 × 10^4 **(B)**, and 1 × 10^5 **(C)** seeding densities (*N* = 3). **(D)** Box plots of spheroid diameter showing significant differences "between media" and "between seeding densities" from day 7 to day 28 (*N* = 3). Legends: "GM" denotes growth media and "MM" denotes mineralization media. Error bars: standard error; significant differences calculated by one-way ANOVA and Tukey *post-hoc* test; *$p \leq 0.05$, **$p \leq 0.01$, ***$p \leq 0.001$, ****$p \leq 0.0001$. *N:* experimental replicates.

0.23 mm diameter on dAR8. H&E staining showed the merging of spheroids into one another with an even distribution of cells. Spheroids can be individually identified with a fusion line present in between each until dAR4. On dAR8, the fusion lines disappeared and merged into a single macrotissue with a minimal necrotic core (Figure 6A). Alizarin red and Von Kossa staining showed red- and black-stained calcium deposits, respectively, in macrotissues at all time points (Figure 6B).

3.6.1.1 Bone-specific hydroxyapatite mineralization in macrotissues

In control samples (dROb spheroids cultured in GM), the cells were round-shaped and loosely located with no compact cell–cell attachment (Figures 7A–C). Lamellipodia (flat ruffled structures) and filopodia (thin filamentous structures) were observed on the surface of each cell; however, the filaments showed minimal contact with adjacent cells (Figures 7D, E).

In contrast, in macrotissues cultured in MM, the cells were flattened and elongated with close contact with each other through visible lamellipodia and filopodia (Figures 8A–D). A fibrous collagenous network was observed inside the macrotissue with closely packed cells (Figure 8E). Rod-shaped crystal structures indicative of hydroxyapatite were observed on the surface of the macrotissue (Figure 8F).

3.6.2 Osteogenic differentiation of macrotissues

3.6.2.1 Gene expression

Runx2 is a transcription factor of early osteoblast differentiation. In osteoblastogenesis, the expression of Runx2 peaks in immature osteoblasts and decreases in mature osteoblasts. The expression of Runx2 on dAR2 and dAR8 significantly downregulated ($p < 0.001$) than the control samples (dRObs monolayer in GM on day 7) (Figure 9A). ALP expression continues to increase during bone maturation and mineralization and reduces during terminal osteocyte formation. ALP expression was significantly higher ($p < 0.01$) on dAR2 compared with control, while it was decreased on dAR8, but no statistically significant difference was observed (Figure 9B).

3.6.2.2 Osteocalcin immunofluorescence

Osteocalcin is a late differentiation marker expressed by mature osteoblasts and early osteocytes. Immunofluorescence staining

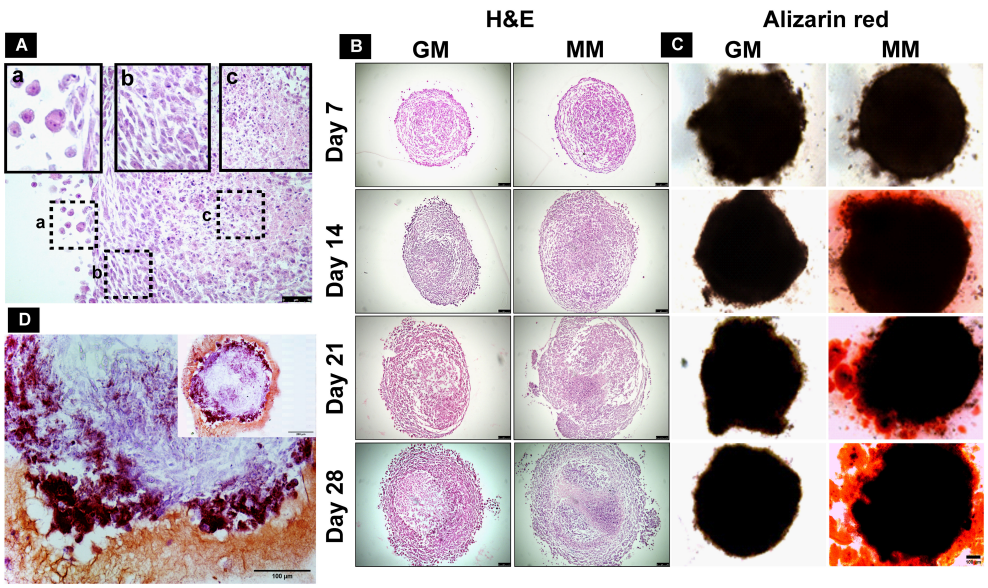

FIGURE 4
(A) H&E-stained section of mineralized dROb spheroid demonstrating different zones: (a) proliferating zone, (b) quiescent zone, and (c) necrotic zone (scale bar: 50 µm). Representative microscopic images of **(B)** H&E-stained spheroid sections (scale bar: 100 µm) and **(C)** Alizarin red-stained spheroids (scale bar: 100 µm) in control (GM) and mineralization media (MM) from day 7 to day 28 (seeding density: 1 × 10^5cells). **(D)** Section of Alizarin red-stained spheroid (cultured in mineralization media) showing brick red-colored calcium deposits (scale bar: 100 µm); inset image: spheroid section at lower magnification (scale bar: 200 µm).

confirmed the presence of an osteocalcin marker on dAR2, 4, and 8, whereas the control spheroid lacked the osteocalcin marker (Figure 9C). This suggests that fused dROb spheroids in mineralization media are capable of advancing toward bone maturation.

4 Discussion

In this project, osteogenic 3D macrotissues (2.64 ± 0.23 mm diameter) were engineered by guided fusion of dROb spheroids

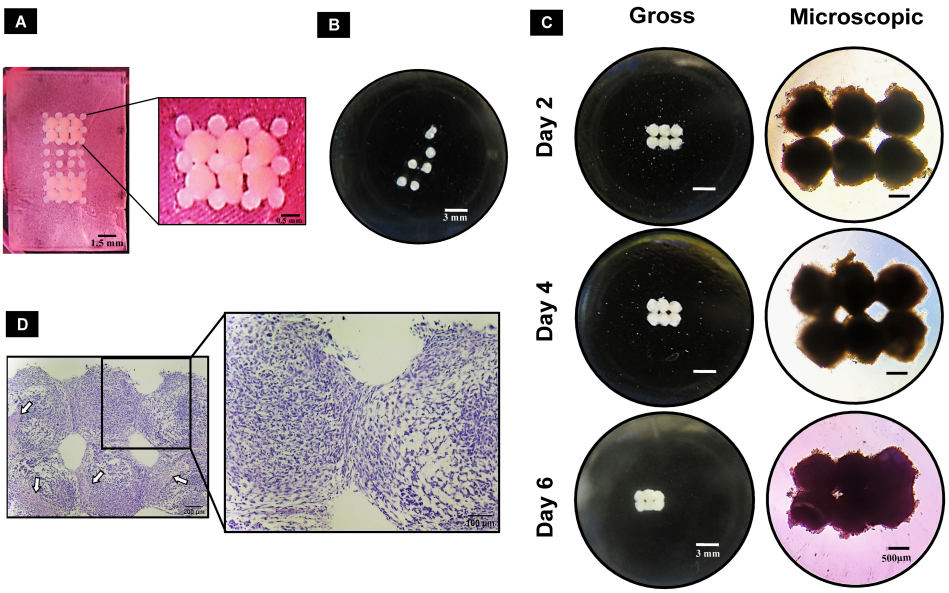

FIGURE 5
Guided fusion of dROb spheroids: **(A)** dROb spheroids directly after deposition in pillar array support using the customized bioassembly system. **(B)** Gross image of dROb spheroids in growth media (GM) showing no fusion after removal from the pillar array support (scale bar: 3 mm). **(C)** Gross (scale bar: 3 mm) and microscopic images (scale bar: 500 µm) of fused spheroids in mineralization media (MM) removed from the pillar array supports on day 2, day 4, and day 6. **(D)** H&E-stained fused spheroids (removed on day 2) showing tight aggregation between spheroids (scale bar: 200 µm; zoomed image: 100 µm); white arrows indicate necrotic regions.

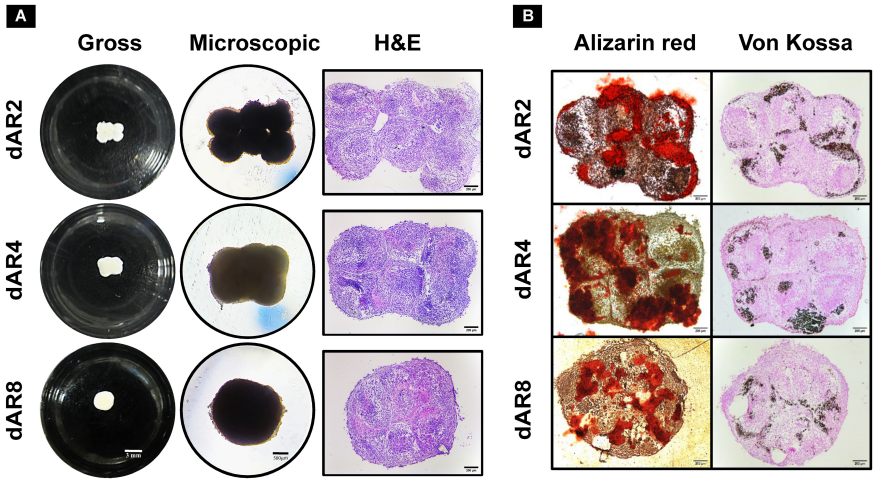

FIGURE 6
Scaffold-free culture of fused spheroids in mineralization media (MM) on day 2, day 4, and day 8 after removal (depicted as dAR2, dAR4, and dAR8, respectively) from the pillar array supports (N = 3). **(A)** Gross (scale bar: 3 mm), microscopic (scale bar: 500 μm), and H&E-stained images (scale bar: 200 μm) of fused spheroids. **(B)** Calcium deposits in Alizarin red and Von Kossa-stained sections of fused spheroids (scale bar: 200 μm).

using the customized 3D bioassembly system. Modular tissue engineering is a bottom-up approach aimed at recreating biomimetic tissues at a macroscale level. Modular or microscale tissues such as spheroids, cell sheets, and cell-laden hydrogels can be used as building blocks to bioassemble into a macroscale tissue (22). In this study, spheroids were used as building blocks due to their close mimicry of natural tissue formation by self-assembly and self-organization. Despite recent developments in bioassembling techniques to produce larger tissues (13, 18, 23, 24), non-invasive and non-destructive bioassembly remains a challenge. Our study involved developing a simple bioassembly system (Figure 1C) using a novel non-invasive temporary pillar array support (Figure 1B) to fabricate bone macrotissues.

4.1 Characterization of dROb spheroids

Prior to the investigation into macrotissue formation, dRObs were assessed for their spheroid-forming ability and the effect of different seeding densities on cell proliferation and viability, cellular arrangement, and ECM production. dRObs at three seeding densities (1×10^4, 5×10^4, 1×10^5 cells) required 12 h, 36 h, and 48 h, respectively, to form compactly aggregated spheroids (Figure 2A). This suggests that complete cell aggregation time is dependent on the seeding density; the lower the seeding density, the faster the spheroid formation. This is in agreement with other cell types such as 3×10^4 iPSCs completely aggregating in 24 h (25) and 2.5×10^5 MC3T3 cells aggregating in 2 days (26).

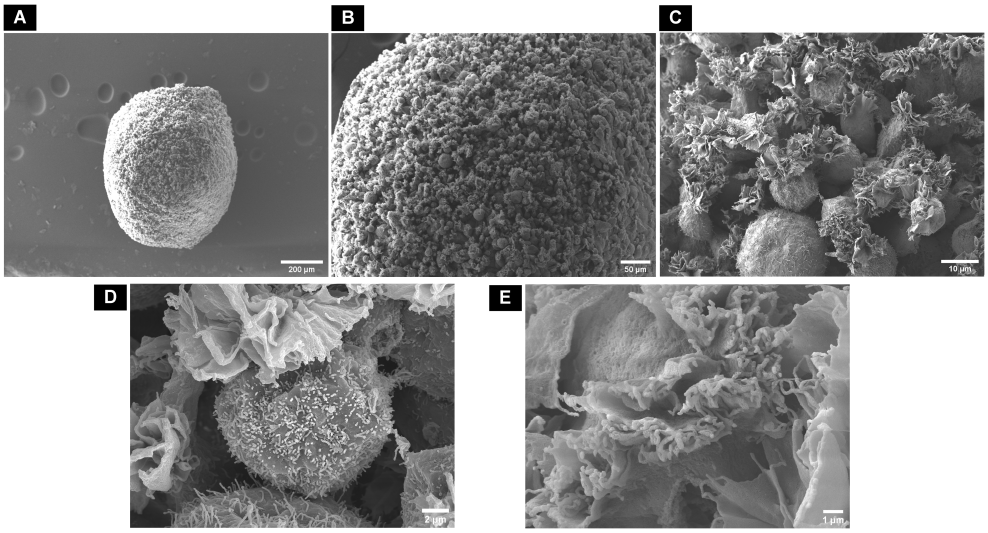

FIGURE 7
Scanning electron microscopic surface morphology of **(A)** control dROb spheroid on day 28 showing **(B, C)** loosely attached round-shaped cells with **(D, E)** lamellipodia and filopodia.

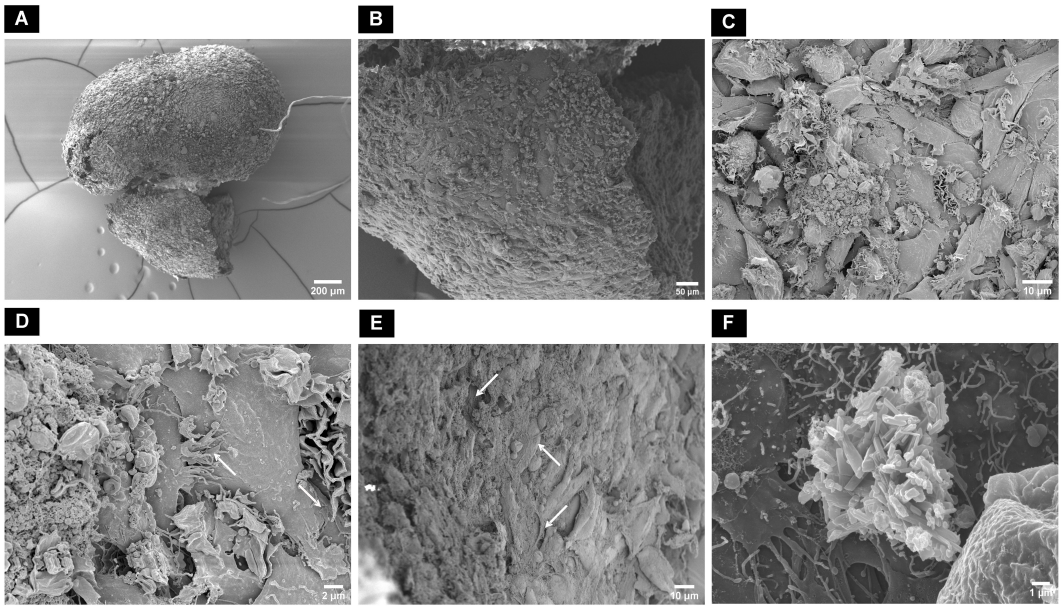

FIGURE 8
Scanning electron microscopic surface morphology of **(A)** dAR8 macrotissue showing **(B, C)** compactly attached flattened and elongated cells. **(D)** Lamellipodia and filopodia closely attached to adjacent cells (white arrows). **(E)** Fibrous mesh network indicative of collagen fibers (white arrows) with tightly arranged cells in the internal regions of the macrotissue. **(F)** Rod-shaped hydroxyapatite crystals on the surface of macrotissue.

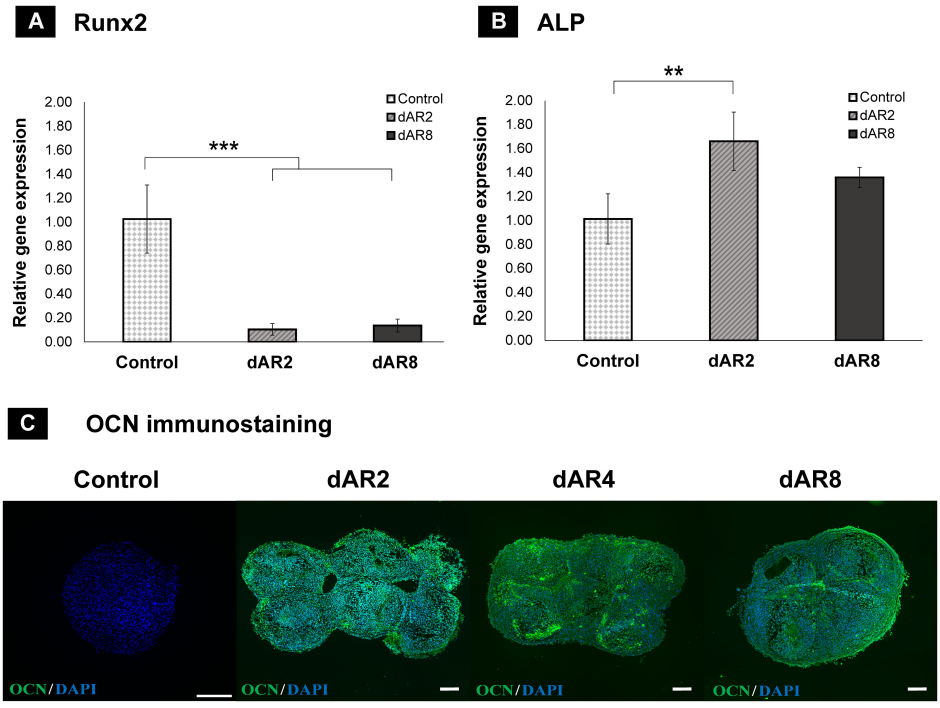

FIGURE 9
Relative gene expression of **(A)** Runx2 and **(B)** ALP by the $2^{-\Delta\Delta Ct}$ method; Control: day 7 dROb monolayer; dAR2 and dAR8: day 2 and day 8 scaffold-free macrotissue; error bars: standard deviation; significant difference calculated by one-way ANOVA and Tukey *post-hoc* test; $^{**}p < 0.01$, $^{***}p < 0.001$. **(C)** Osteocalcin (OCN) immunostaining (green) on control, day 2, day 4, and day 8 scaffold-free macrotissue with DAPI counterstain (cell nuclei in blue); scale bar: 200 µm.

Under the influence of mineralization media, dROb spheroids went through a cell proliferation phase till day 14 which then ceased (Figure 2C). Calcium deposits observed from day 14 onwards confirmed that dRObs have entered the mineralization phase (Figure 4C). This is an interesting finding that cell proliferation ceased when mineralization began. Similar observations were reported in other studies during osteogenic differentiation of osteoblast-like cells (27) and human adipose mesenchymal stem cells (haMSCs) (28). Moreover, despite arrested cell proliferation, the spheroid diameter increased over time which is suggestive of increased extracellular calcium production (26). These observations demonstrate that dRObs undergo osteogenesis when cultured in mineralization media in all three seeding densities.

The necrotic core size increased over time with increasing spheroid size, regardless of seeding density (Figure 4B). This is associated with a reduction in cell viability over time confirming cell death in the core region (Figure 2D). The presence of a necrotic core has not been reported in other osteogenic spheroids (26, 29, 30) which may be due to cell type and size differences. These studies produced spheroids of approximately 600 μm; however, dRObs formed spheroids of >1 mm. Despite the presence of a necrotic core, dROb spheroids continued to grow and mineralize. Studies showed high levels of hypoxia-inducible factor 1-alpha (HIF-1α) during endochondral ossification, which suggests that a hypoxic microenvironment can support bone formation, i.e., promotes differentiation of osteoblasts to osteocytes (31, 32). Therefore, the necrosis observed in dROb spheroids might be beneficial for osteocytogenesis. This lays the ground for future investigation of osteocyte formation and characterization in dROb spheroids.

Based on the interest of using dROb spheroids that reach a larger size (~1.5 mm) relatively sooner (day 14), 1×10^5 seeding density was considered ideal and used for depositing the spheroids in pillar array supports of current printed size (Figure 1B). However, a future study with lower seeding densities in downsized pillar array supports might be advantageous in reducing the necrotic core.

4.2 Three-dimensional macrotissue fabrication

Pillar arrays manufactured from Clear Resin® (Formlabs) were used as temporary supports to hold spheroids in place (Figure 5A). Subsequent physical removal of the pillar array support would leave the tissue construct scaffold-free for maturation. With pillar array supports, we successfully demonstrated the fusion of mineralized dROb spheroids within 2 days of bioassembly (Figure 5C). In the literature, the Ozbolat research group bioassembled osteogenic spheroids using the sacrificial material made of alginate and calcium chloride which was sacrificed by citrate chelation (16, 24, 33, 34). Considering the possible detrimental effects of citrate on extracellular calcium, our pillar array scaffold method would be beneficial. Other approaches such as PEGT/PBT copolymer (13), PCL microwell arrays (35), Kenzan needle arrays (18), and self-healing support hydrogels (36) have also been used for the bioassembly of spheroids. However, there are some limitations in these approaches compared with the pillar array support method. For example, the permanent presence of scaffold materials PEGT/PBT and PCL (13, 35) might hinder mechanical signal transduction between cells (10). The Kenzan method is an invasive method involving needle insertion into spheroids which could be detrimental to cells (18). Support hydrogels take a longer time (4 days) for spheroid fusion (36) than pillar array supports (2 days) as well as there is a possibility of dilution and disturbance to the support hydrogels during media changes leading to loss of mechanical strength to hold spheroids. In addition, the inability to exchange media would affect the viability of metabolically demanding cells. Thus, pillar array supports are beneficial for rapid fusion of dROb spheroids without detrimental effects on spheroid integrity and extracellular calcium as well as for holding spheroids even under excessive manipulation. The method could be further enhanced by improving the ease of separation of macrotissues from the pillar following fusion, for example by using a non-fouling material such as poly(ethylene glycol) that cells would adhere less to or a sacrificial material that could be removed by a method less detrimental to mineralized tissues than citrate chelation.

After removal of the pillar array supports, the fusion between spheroids extended from the mere edges (on dAR2) to the close contact reorganization encompassing all spheroids together (on dAR4 and dAR8) making it a macrotissue of approximately 2.6 mm diameter (Figure 6A). Calcium deposits detected by staining (Figure 6B) and bone-like hydroxyapatite mineral structures in SEM imaging (Figure 8F) demonstrate that dROb macrotissues are capable of producing appropriate bone extracellular matrix. Additionally, the presence of collagen networks and compactly arranged cells through lamellipodia and filopodia shows cell–cell and cell–ECM interactions. This proves that our bioassembly approach is effective in maintaining the functionality of dROb cells to produce bone-specific mineralization in large-scaled tissues. Energy-dispersive X-ray analysis to quantify bone-specific hydroxyapatite mineral content was attempted which was not successful in quantifying phosphorus due to masking of phosphate peaks by osmium used during sample preparation. Further analysis is required after modifying the sample preparation procedure.

Relative Alizarin red quantification assay would provide information on macrotissues' ability to continually increase ECM mineral synthesis during and after fusion. However, this assay is commonly used for 2D culture (37) and needs modification to extract minerals from core regions of tightly packed 3D macrotissues.

Runx2 gene downregulation and the presence of osteocalcin (late osteogenic marker) in dROb macrotissues (Figures 9A, C) reveal that the cells are in late osteogenic phase, i.e., mature osteoblasts and early osteocytes in association with hydroxyapatite deposition (38–40). Furthermore, upregulated ALP expression on dAR2 shows that the cells are undergoing matrix maturation. Although there is no significant difference, the decline of ALP expression on dAR8 might suggest its progress toward osteocyte predominance over osteoblasts (41, 42). These findings provide a base for future investigation to confirm the presence of osteocytes by extending the culture period of macrotissues. Osteocyte-specific immuno-markers like podoplanin (43) and significantly reduced ALP expression over time (41) would confirm the presence of osteocytes.

Based on these findings from single-layered bioassembly, multilayered bioassembly of dROb spheroids can be investigated for

further scaling up of bone tissue constructs. A potential limitation of the multilayered bioassembly approach is that the spheroids were transferred individually which would be time-consuming during further upscaling of tissue. Also, the necrotic core in multilayered bioassembly is important to be considered as larger tissue areas in the core would be deprived of oxygen and nutrients.

Overall, dROb macrotissue developed by our novel bioassembly system can be a viable 3D *in-vitro* model of bone tissue. Rat-originated osteoblast cells were used in this study due to their easy availability and close biological resemblance to human cells (44). We predict that this bioassembly setup could be used as a novel methodology to engineer a variety of other types of macrotissues such as tendon, muscle, or multitissue constructs using cells of human origin.

5 Conclusion

In this study, we fabricated a 3D *in-vitro* bone macrotissue model using differentiated rat osteoblasts which recapitulate the mineralization of native bone tissue. The bioassembly approach using a temporary pillar array support is simple and effective in manufacturing a scaffold-free macrotissue product without any physical and/or chemical damage. This fabricated model and bioassembly system can be widely used in tissue engineering and pharmacological research to understand bone-related diseases and their treatment strategies.

Data availability statement

The original contributions presented in the study are included in the article/supplementary materials, further inquiries can be directed to the corresponding author/s.

Author contributions

VP: Conceptualization, Data curation, Formal analysis, Funding acquisition, Investigation, Methodology, Validation, Visualization, Writing – original draft, Writing – review & editing. FM: Conceptualization, Funding acquisition, Methodology, Resources, Supervision, Writing – review & editing. LM: Methodology, Resources, Supervision, Writing – review & editing. JP: Conceptualization, Funding acquisition, Methodology, Project administration, Resources, Supervision, Writing – review & editing.

Funding

The author(s) declare financial support was received for the research, authorship, and/or publication of this article. This research work was supported by Tenovus Scotland (grant no. E22-05BG). VP's PhD was funded by Principal's career development scholarship and Edinburgh global research scholarship, University of Edinburgh.

Acknowledgments

The authors thank Rosie Hawkswell and Anya Sobrattee for their contributions. We acknowledge the use of the Zeiss Crossbeam Cryo FIB/SEM bought with the EPSRC grant EP/P030564/1 and Fraser Laidlaw for the help with image acquisition and Steve Mitchell for the help with SEM sample preparation.

Conflict of interest

The authors declare that the research was conducted in the absence of any commercial or financial relationships that could be construed as a potential conflict of interest.

Publisher's note

References

1. el Demellawy D, Davila J, Shaw A, Nasr Y. Brief review on metabolic bone disease. *Acad Forensic Pathol* (2018) 8:611–40. doi: 10.1177/1925362118797737

2. Drake MT, Cremers S, Russell RG, Bilezikian JP. Drugs for the treatment of metabolic bone diseases. *Br J Clin Pharmacol* (2019) 85:1049–51. doi: 10.1111/bcp.13857

3. Skjødt MK, Frost M, Abrahamsen B. Side effects of drugs for osteoporosis and metastatic bone disease. *Br J Clin Pharmacol* (2019) 85:1063–71. doi: 10.1111/bcp.13759

4. Stubenrouch FE, Cohen ES, Bossuyt PMM, Koelemay MJW, van der Vet PCR, Ubbink DT. Systematic review of reporting benefits and harms of surgical interventions in randomized clinical trials. *BJS Open* (2020) 4:171–81. doi: 10.1002/bjs5.50240

5. Amini AR, Laurencin CT, Nukavarapu SP. Bone tissue engineering: recent advances and challenges. *Crit Rev BioMed Eng* (2012) 40:363–408. doi: 10.1615/CritRevBiomedEng.v40.i5.10

6. de Wildt BWM, Ansari S, Sommerdijk NAJM, Ito K, Akiva A, Hofmann S. From bone regeneration to three-dimensional in *vitro* models: tissue engineering of organized bone extracellular matrix. *Curr Opin BioMed Eng* (2019) 10:107–15. doi: 10.1016/j.cobme.2019.05.005

7. Laurencin CT, Ambrosio AM, Borden MD, Cooper JA. Tissue engineering: orthopedic applications. *Annu Rev BioMed Eng* (1999) 1:19–46. doi: 10.1146/annurev.bioeng.1.1.19

8. Yuste I, Luciano FC, González-Burgos E, Lalatsa A, Serrano DR. Mimicking bone microenvironment: 2D and 3D in *vitro* models of human osteoblasts. *Pharmacol Res* (2021) 169:105626. doi: 10.1016/j.phrs.2021.105626

9. Lin X, Patil S, Gao Y-G, Qian A. The bone extracellular matrix in bone formation and regeneration. *Front Pharmacol* (2020) 11:757. doi: 10.3389/fphar.2020.00757

10. Athanasiou KA, Eswaramoorthy R, Hadidi P, Hu JC. Self-organization and the self-assembling process in tissue engineering. *Annu Rev BioMed Eng* (2013) 15:115–36. doi: 10.1146/annurev-bioeng-071812-152423

11. DuRaine GD, Brown WE, Hu JC, Athanasiou KA. Emergence of scaffold-free approaches for tissue engineering musculoskeletal cartilages. *Ann BioMed Eng* (2015) 43:543–54. doi: 10.1007/s10439-014-1161-y

12. Decarli MC, Amaral R, dos Santos DP, Tofani LB, Katayama E, Rezende RA, et al. Cell spheroids as a versatile research platform: formation mechanisms, high throughput production, characterization and applications. *Biofabrication* (2021) 13:032002. doi: 10.1088/1758-5090/abe6f2

13. Mekhileri NV, Lim KS, Brown GCJ, Mutreja I, Schon BS, Hooper GJ, et al. Automated 3D bioassembly of micro-tissues for biofabrication of hybrid tissue engineered constructs. *Biofabrication* (2018) 10:024103. doi: 10.1088/1758-5090/aa9ef1

14. Mironov V, Visconti RP, Kasyanov V, Forgacs G, Drake CJ, Markwald RR. Organ printing: tissue spheroids as building blocks. *Biomaterials* (2009) 30:2164–74. doi: 10.1016/j.biomaterials.2008.12.084

15. Tripathi S, Mandal SS, Bauri S, Maiti P. 3D bioprinting and its innovative approach for biomedical applications. *MedComm* (2023) 4(1):e194. doi: 10.1002/mco2.194

16. Heo DN, Ayan B, Dey M, Banerjee D, Wee H, Lewis GS, et al. Aspiration-assisted bioprinting of co-cultured osteogenic spheroids for bone tissue engineering. *Biofabrication* (2021) 13:015013. doi: 10.1088/1758-5090/abc1bf

17. Itoh M, Nakayama K, Noguchi R, Kamohara K, Furukawa K, Uchihashi K, et al. Scaffold-free tubular tissues created by a bio-3D printer undergo remodeling and endothelialization when implanted in rat aortae. *PloS One* (2015) 10:e0136681. doi: 10.1371/journal.pone.0136681

18. Aguilar IN, Smith LJ, Olivos DJ, Chu T-MG, Kacena MA, Wagner DR. Scaffold-free bioprinting of mesenchymal stem cells with the regenova printer: optimization of printing parameters. *Bioprinting (Amsterdam Netherlands)* (2019) 15:e00048. doi: 10.1016/j.bprint.2019.e00048

19. Livak KJ, Schmittgen TD. Analysis of relative gene expression data using real-time quantitative PCR and the 2(-Delta Delta C(T)) Method. *Methods* (2001) 25:402–8. doi: 10.1006/meth.2001.1262

20. Hammer Ø, Harper DAT, Ryan PD. Past: Paleontological statistics software package for education and data analysis. *Palaeontol Electron* (2001) 4:178.

21. Elmore S. Apoptosis: a review of programmed cell death. *Toxicol Pathol* (2007) 35:495–516. doi: 10.1080/01926230701320337

22. Nichol JW, Khademhosseini A. Modular tissue engineering: engineering biological tissues from the bottom up. *Soft Matter* (2009) 5:1312–9. doi: 10.1039/b814285h

23. Lindberg GCJ, Cui X, Durham M, Veenendaal L, Schon BS, Hooper GJ, et al. Probing multicellular tissue fusion of cocultured spheroids-A 3D-bioassembly model. *Adv Sci (Weinheim Baden-Wurttemberg Ger* (2021) 8:e2103320. doi: 10.1002/advs.202103320

24. Kim MH, Banerjee D, Celik N, Ozbolat IT. Aspiration-assisted freeform bioprinting of mesenchymal stem cell spheroids within alginate microgels. *Biofabrication* (2022) 14:024103. doi: 10.1088/1758-5090/ac4dd8

25. Zhang M, Shi J, Xie M, Wen J, Niibe K, Zhang X, et al. Recapitulation of cartilage/bone formation using iPSCs via biomimetic 3D rotary culture approach for developmental engineering. *Biomaterials* (2020) 260:120334. doi: 10.1016/j.biomaterials.2020.120334

26. Koblenzer M, Weiler M, Fragoulis A, Rütten S, Pufe T, Jahr H. Physiological mineralization during *in vitro* osteogenesis in a biomimetic spheroid culture model. *Cells* (2022) 11:2702. doi: 10.3390/cells11172702

27. Gentili C, Bianco P, Neri M, Malpeli M, Campanile G, Castagnola P, et al. Cell proliferation, extracellular matrix mineralization, and ovotransferrin transient expression during in *vitro* differentiation of chick hypertrophic chondrocytes into osteoblast-like cells. *J Cell Biol* (1993) 122:703–12. doi: 10.1083/jcb.122.3.703

28. Hanna H, Mir LM, Andre FM. *In vitro* osteoblastic differentiation of mesenchymal stem cells generates cell layers with distinct properties. *Stem Cell Res Ther* (2018) 9:203. doi: 10.1186/s13287-018-0942-x

29. Ayan B, Wu Y, Karuppagounder V, Kamal F, Ozbolat IT. Aspiration-assisted bioprinting of the osteochondral interface. *Sci Rep* (2020) 10:13148. doi: 10.1038/s41598-020-69960-6

30. Wolff A, Frank M, Staehlke S, Springer A, Hahn O, Meyer J, et al. 3D spheroid cultivation alters the extent and progression of osteogenic differentiation of mesenchymal stem/stromal cells compared to 2D cultivation. *Biomedicines* (2023) 11:1049. doi: 10.3390/biomedicines11041049

31. Amarilio R, Viukov SV, Sharir A, Eshkar-Oren I, Johnson RS, Zelzer E. HIF1alpha regulation of Sox9 is necessary to maintain differentiation of hypoxic prechondrogenic cells during early skeletogenesis. *Development* (2007) 134:3917–28. doi: 10.1242/dev.008441

32. Kim J, Adachi T. Cell condensation triggers the differentiation of osteoblast precursor cells to osteocyte-like cells. *Front Bioeng Biotechnol* (2019) 7:288. doi: 10.3389/fbioe.2019.00288

33. Ayan B, Celik N, Zhang Z, Zhou K, Kim MH, Banerjee D, et al. Aspiration-assisted freeform bioprinting of prefabricated tissue spheroids in a yield-stress gel. *Commun Phys* (2020) 3:183. doi: 10.1038/s42005-020-00449-4

34. Akkouch A, Yu Y, Ozbolat IT. Microfabrication of scaffold-free tissue strands for three-dimensional tissue engineering. *Biofabrication* (2015) 7:31002. doi: 10.1088/1758-5090/7/3/031002

35. Burdis R, Chariyev-Prinz F, Kelly DJ. Bioprinting of biomimetic self-organised cartilage with a supporting joint fixation device. *Biofabrication* (2021) 14:015008. doi: 10.1088/1758-5090/ac36be

36. Daly AC, Davidson MD, Burdick JA. 3D bioprinting of high cell-density heterogeneous tissue models through spheroid fusion within self-healing hydrogels. *Nat Commun* (2021) 12:753. doi: 10.1038/s41467-021-21029-2

37. Gregory CA, Gunn WG, Peister A, Prockop DJ. An Alizarin red-based assay of mineralization by adherent cells in culture: comparison with cetylpyridinium chloride extraction. *Anal Biochem* (2004) 329:77–84. doi: 10.1016/J.AB.2004.02.002

38. Owen TA, Aronow M, Shalhoub V, Barone LM, Wilming L, Tassinari MS, et al. Progressive development of the rat osteoblast phenotype in *vitro*: reciprocal relationships in expression of genes associated with osteoblast proliferation and differentiation during formation of the bone extracellular matrix. *J Cell Physiol* (1990) 143:420–30. doi: 10.1002/jcp.1041430304

39. Mukherjee S, Sharma S, Soni V, Joshi A, Gaikwad A, Bellare J, et al. Improved osteoblast function on titanium implant surfaces coated with nanocomposite Apatite-Wollastonite-Chitosan- an experimental *in-vitro* study. *J Mater Sci Mater Med* (2022) 33:25. doi: 10.1007/s10856-022-06651-w

40. Komori T. Regulation of proliferation, differentiation and functions of osteoblasts by runx2. *Int J Mol Sci* (2019) 20:1694. doi: 10.3390/ijms20071694

41. Kato Y, Windle JJ, Koop BA, Mundy GR, Bonewald LF. Establishment of an osteocyte-like cell line, MLO-Y4. *J Bone Miner Res* (1997) 12:2014–23. doi: 10.1359/jbmr.1997.12.12.2014

42. Amarasekara DS, Kim S, Rho J. Regulation of osteoblast differentiation by cytokine networks. *Int J Mol Sci* (2021) 22:2851. doi: 10.3390/ijms22062851

43. Kaur K, Das S, Ghosh S. Regulation of human osteoblast-to-osteocyte differentiation by direct-write 3D microperiodic hydroxyapatite scaffolds. *ACS Omega* (2019) 4:1504–15. doi: 10.1021/acsomega.8b03272

44. Czekanska EM, Stoddart MJ, Richards RG, Hayes JS. In search of an osteoblast cell model for in *vitro* research. *Eur Cells Mater* (2012) 24:1–17. doi: 10.22203/ECM.V024A01

frontiers | Frontiers in Endocrinology

TYPE Original Research
PUBLISHED 16 January 2024
DOI 10.3389/fendo.2023.1303126

OPEN ACCESS

EDITED BY
Michaela Tencerova,
Academy of Sciences of the Czech Republic (ASCR), Czechia

REVIEWED BY
Andrei Tica,
University of Craiova, Romania
Loïc Treffel,
Institut Toulousain d'Ostéopathie, France

*CORRESPONDENCE
Saori Harada
sah003@mail.harvard.edu

†These authors have contributed equally to this work and share first authorship

RECEIVED 27 September 2023
ACCEPTED 19 December 2023
PUBLISHED 16 January 2024

CITATION
Harada S, Gersing AS, Stohldreier Y, Dietrich O, Lechner A, Seissler J, Ferrari U, Pappa E and Hesse N (2024) Associations of gestational diabetes and proton density fat fraction of vertebral bone marrow and paraspinal musculature in premenopausal women. *Front. Endocrinol.* 14:1303126. doi: 10.3389/fendo.2023.1303126

Associations of gestational diabetes and proton density fat fraction of vertebral bone marrow and paraspinal musculature in premenopausal women

Saori Harada[1,2*†], Alexandra S. Gersing[3†], Yannick Stohldreier[3], Olaf Dietrich[4], Andreas Lechner[1,5], Jochen Seissler[1,5], Uta Ferrari[1,5], Eleni Pappa[1,5] and Nina Hesse[4]

[1]Medizinische Klinik und Poliklinik IV, Diabetes Zentrum - Campus Innenstadt, LMU Klinikum, Ludwig-Maximilians-Universität München, Munich, Germany, [2]Institute for Medical Information Processing, Biometry and Epidemiology (IBE), Faculty of Medicine, LMU Munich, Pettenkofer School of Public Health, Munich, Germany, [3]Department of Neuroradiology, LMU University Hospital, LMU Munich, Munich, Germany, [4]Department of Radiology, LMU University Hospital, LMU Munich, Munich, Germany, [5]German Center for Diabetes Research (DZD), Neuherberg, Germany

Background and objective: Fat content in bones and muscles, quantified by magnetic resonance imaging (MRI) as a proton density fat fraction (PDFF) value, is an emerging non-invasive biomarker. PDFF has been proposed to indicate bone and metabolic health among postmenopausal women. Premenopausal women with a history of gestational diabetes (GDM) carry an increased risk of developing type 2 diabetes and an increased risk of fractures. However, no studies have investigated the associations between a history of GDM and PDFF of bone or of paraspinal musculature (PSM), composed of autochthonous muscle (AM) and psoas muscle, which are responsible for moving and stabilizing the spine. This study aims to investigate whether PDFF of vertebral bone marrow and of PSM are associated with a history of GDM in premenopausal women.

Methods: A total of 37 women (mean age 36.3 ± 3.8 years) who were 6 to 15 months postpartum with (n=19) and without (n=18) a history of GDM underwent whole-body 3T MRI, including a chemical shift encoding-based water-fat separation. The PDFF maps were calculated for the vertebral bodies and PSM. The cross-sectional area (CSA) of PSM was obtained. Associations between a history of GDM and PDFF were assessed using multivariable linear and logistic regression models.

Results: The PDFF of the vertebral bodies was significantly higher in women with a history of GDM (GDM group) than in women without (thoracic: median 41.55 (interquartile range 32.21-49.48)% vs. 31.75 (30.03-34.97)%; p=0.02, lumbar: 47.84 (39.19-57.58)% vs. 36.93 (33.36-41.31)%; p=0.02). The results remained significant after adjustment for age and body mass index (BMI) (p=0.01-0.02). The receiver operating characteristic curves showed optimal thoracic and lumbar vertebral PDFF cutoffs at 38.10% and 44.18%, respectively, to differentiate GDM (AUC 0.72 and 0.73, respectively, sensitivity 0.58,

specificity 0.89). The PDFF of the AM was significantly higher in the GDM group (12.99 (12.18-15.90)% vs. 10.83 (9.39-14.71)%; p=0.04) without adjustments, while the CSA was similar between the groups (p=0.34).

Conclusion: A history of GDM is significantly associated with a higher PDFF of the vertebral bone marrow, independent of age and BMI. This statistical association between GDM and increased PDFF highlights vertebral bone marrow PDFF as a potential biomarker for the assessment of bone health in premenopausal women at risk of diabetes.

KEYWORDS

bone marrow, spine, paraspinal musculature, gestational diabetes mellitus, magnetic resonance imaging, proton density fat fraction, women in bone research

1 Introduction

Chemical shift encoding-based water-fat MRI (CSE-MRI), determining the proton density fat fraction (PDFF), is an emerging non-invasive quantification method for bone marrow composition (1–6). In previous studies, bone mineral density (BMD) was inversely correlated with increased vertebral bone marrow fat (7–9). Bone marrow adipocytes are considered insulin-sensitive, by expressing insulin receptors. Under metabolic disturbances, such as obesity and type 2 diabetes (T2D), bone marrow adiposity is induced with impaired bone health (10). The link between elevated bone marrow PDFF and systemic insulin resistance was reported in postmenopausal women with newly diagnosed T2D (11). Systemic insulin resistance is another potential cause of bone fragility via the impairment of osteoblast functions and other pathophysiological mechanisms (12). In postmenopausal women, T2D was associated with an increased fracture risk (13). Paradoxically, patients with T2D often show normal or increased BMD (13). The quantitative computed tomography (QCT)-based assessment of the BMD showed no significant changes within 1 year prior to the occurrence of a vertebral compression fracture (14). On the other hand, a further study demonstrated that over 1 year prior to the occurrence of an incidental vertebral compression fracture, the PDFF had significantly increased in the respective vertebral bodies compared to the PDFF of the vertebral bodies of the controls without vertebral compression fracture (14). Several other studies have indicated that bone marrow PDFF may be predictive for vertebral compression fractures and a potential biomarker for bone health (15, 16).

Furthermore, T2D has been demonstrated to have an impact on other compartments of the body containing fat including the paraspinal musculature (PSM) (17). T2D is known to cause changes in muscle architecture, composed of a shift in myocyte composition, increased myosteatosis (fatty infiltration of skeletal muscle), and a decreased capacity for muscle regeneration (18, 19). These changes are associated with impaired skeletal muscle mass function and degeneration of the skeletal muscles (20) Numerous studies proposed that an intricate cellular and molecular mechanism was responsible, involving insulin, sex hormones, myokines, lipid metabolites, a subset of fibro-adipogenic progenitors, and other factors (18, 20, 21). These pathologic cascades ultimately culminate in increased morbidity and disability (21). Lipid accumulation in muscles of the lower limbs was found to be associated with increased fracture risk in an older population (22). Increased intramyocellular lipids in lower leg muscles, measured with 1H nuclear magnetic resonance spectroscopy, were observed in women with a history of gestational diabetes mellitus (GDM) (23). However, no studies have looked at the associations between a history of GDM and the PDFF of bone marrow or of the PSM.

GDM, a transient disturbance of glucose tolerance, is one of the most common medical complications during pregnancy, with a prevalence of 1.1% to 24.3% (24). Women with a recent history of GDM show characteristics associated with T2D and are at risk of developing T2D (25, 26). A previous study reported an association between a history of GDM and an increased fracture risk (27).

This study aims to investigate whether MRI-based PDFF measurements of vertebral bone marrow and PSM are associated with a history of GDM in premenopausal women.

Abbreviations: MRI, magnetic resonance imaging; PDFF, proton density fat fraction; GDM, gestational diabetes mellitus; CSA, cross-sectional area; PSM, paraspinal musculature (psoas and autochthonous muscles); AM, autochthonous muscles; PM, psoas muscles; L1 – L4, lumbar vertebrae 1 to 4; Th9 – Th12, thoracic vertebrae 9 to 12; BMI, body mass index; QCT, quantitative computed tomography; BMD, bone mineral density; CSE-MRI, chemical shift encoding-based water-fat MRI; T2D, type 2 diabetes mellitus; OGTT, oral glucose tolerance test; FPG, fasting plasma glucose; ROI, region of interest; ROC, receiver operating characteristic; AUC, area under the curve.

2 Materials and methods

2.1 Study participant selection

The study was approved by the local institutional review board (Ethics Commission of the Medical Faculty, Ludwig-Maximilians-Universität München) and all study participants provided written informed consent prior to their participation in the study, which was conducted in accordance with the declaration of Helsinki. Cross-sectional analyses were performed at baseline visits after delivery within a monocentric prospective observational cohort study, as reported previously (25). Women with a history of GDM as well as women following normoglycemic pregnancy (controls) were included in the study, from 6 to 15 months after delivery, between April 2013 and September 2015. The diagnosis of GDM was based on a 75 g oral glucose tolerance test (OGTT) after the 23rd week of gestation following the criteria of the International Association of the Diabetes and Pregnancy Study (IADPSG) recommendations (28). Study participants who underwent MRI after the baseline visit, using the same MRI protocol and MR system, were selected for this study.

2.2 Anthropometric data, steps per day, and oral glucose tolerance test

Body weight in kilogram (kg) was assessed using a bioelectrical impedance analysis scale (Tanita BC-418, Tanita Corporation, Tokyo, Japan). For clothing, 0.5 kg was subtracted. Height and waist circumference were measured with an accuracy of 0.5 cm, using a tape measure. BMI was calculated as weight divided by the square of height (kg/m^2).

As an indicator of daily physical activity, steps per day were tracked among the study participants, using an accelerometer (Aiper Motion 440, v3.2.4.0, Aipermon GmbH). The participants carried the accelerometer for at least 10-14 days except for holidays. The average steps per day were calculated based on the number of days when they were able to carry the device.

A 5-point 75 g OGTT was performed at the baseline visit. Definitions of the American Diabetes Association were used to distinguish between normal vs. pathologic glucose metabolism (impaired fasting glucose 100-125 mg/dl [5.6-6.9 mmol/L]), impaired glucose tolerance (120 minutes of OGTT 140-199 mg/dl [7.8-11.0 mmol/L]), or newly diagnosed T2D (fasting plasma glucose (FPG) ≥ 126 mg/dl [7.0 mmol/L] or 120 minutes of OGTT ≥ 200 mg/dl [11.1 mmol/L])) (29).

For the criteria of metabolic syndrome, we used the International Diabetes Federation (IDF) Worldwide Definition of Metabolic Syndrome for women (1. Waist circumference > 88 cm, 2. Triglycerides ≥ 150 mg/dl, 3. High-density lipoprotein cholesterol < 50 mg/dl, 4. Hypertension as systolic blood pressure ≥ 130 mmHg or diastolic blood pressure ≥ 85 mmHg, 5. FPG ≥ 100 mg/dl) (30). Each required examination was performed at the baseline visit.

2.3 Magnetic resonance imaging

MRI scans were scheduled after the baseline visit. Whole-body magnetic resonance examinations were performed with a 3-tesla system (Ingenia, Philips Healthcare, Best, Netherlands) using an anterior body coil and a posterior coil. The latter was integrated into the MR table. Subjects were placed in the scanner in a supine position with arms extended above their head. A slab-selective three-point-echo 3D gradient-echo sequence (Dixon) was used to acquire all echoes in a single TR, using bipolar gradients (repetition time 4.1 ms, first echo time 1.45 ms, second echo time 2.19 ms, third eco 2.93 ms, flip angle 10°, slice thickness 10 mm, gap 0 mm, 400 × 400 matrix, 520×520 mm^2 field of view). Water and fat images were calculated by the MRI software (Philips Healthcare). The PDFF maps were determined by pixelwise evaluating the ratio of the fat (F) signal over the sum of fat and water (W) signals, F/(F + W) * 100%. The same approach for the fat fraction calculation that we used is described and confirmed to be reproducible in previous literature (31, 32).

2.4 Quantitative vertebral body and paraspinal muscle analysis

All MR images were checked for vertebral fractures or vertebral deformities, yet, there were no fractures detected in any of the study participants. Segmentations of the thoracic and lumbar vertebrae and the paraspinal muscles were performed by a trained researcher (Y.S.) and reviewed by two board-certified radiologists (N.H., A.S.G. with 9 and 12 years of experience in musculoskeletal imaging, respectively), primarily to confirm the adequacy of the selected areas of interest excluding other unintended areas such as vertebral discs, on the PDFF maps using Visage PACS (Visage Imaging, Inc., San Diego, CA, United States). The region of interest (ROI) was placed in the center of the vertebral body from Th9 to Th12 and from L1 to L4. The mean value and standard deviation for thoracic or lumbar vertebral bodies were calculated. Beginning at the level of L1, the cross-sectional area (CSA) of the paraspinal musculature (autochthonous muscle (AM) and psoas muscle (PM) on both sides) in cm² was semiautomatically segmented bilaterally on three slices 5 cm apart of the thickest part of the muscle, and then it was averaged. A representative PDFF map with an assessment of CSA and PDFF ROI measurement at the level of L4 is shown in Figure 1. All measurements were performed blinded to the clinical data and demographics of the participants. A random sample of 10 subjects was independently analyzed by N.H. after a 6-month interval following the mentioned review process, in order to assess the inter-reader reproducibility. A random sample of 10 subjects was reanalyzed 4 weeks later in order to assess the intra-reader reproducibility.

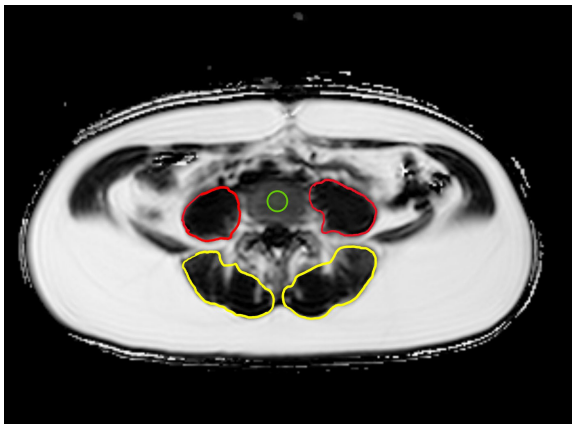

FIGURE 1
Example PDFF map at the level of L4: Region of interest (ROI) placement in the center of L4 (green) as well as representative segmentations of the autochthonous muscles (AM, yellow) and psoas muscles (PM, red) on both sides.

2.5 Statistical analysis

All statistical analyses were performed using RStudio Build 492 "Mountain Hydrangea" (R Foundation for Statistical Computing, Vienna, Austria). The statistical analysis was performed by S.H. (8 years of experience with statistical analysis). All statistical tests performed were two-sided with a level of significance (α) of 0.05. Normally distributed metric variables are expressed as mean ± standard deviation. Non-normally distributed metric variables are reported as median (interquartile range of the first quartile to the third quartile). Pearson correlation was used to assess correlations between normally distributed variables, and Spearman's rank correlation was used for non-normally distributed variables. To compare groups without adjustments, a two-sample t-test (for normal distributions) and Wilcoxon rank sum test/Mann-Whitney U test (for non-normal distributions) were used for variables with equal variances. Welch t-test (for normal distributions) and Mood's median test (for non-normal distributions) were used for variables with unequal variances. For categorical variables, the Fisher exact test (if the sample size in one group was less than 5) and the Chi-squared test were conducted. Multivariable linear and logistic regression models were performed to evaluate the associations between measured mean PDFF of the vertebral bodies or PSM and history of GDM, adjusting for age and BMI at the baseline visit. A history of GDM was defined as an independent variable in linear regression models and as a dependent variable in logistic regression models. ROC curves were drawn in order to assess the PDFF cutoff values from the sensitivity and specificity, differentiating between women with and without a history of GDM. The optimal cutoff values were selected to maximize the sum of sensitivity and specificity. The area under the ROC curve (AUC) was computed with a 95% confidence interval. Inter-reader and intra-reader reproducibility for PDFF values were assessed by calculating the intraclass correlation coefficient and the root mean square coefficient of variation (RMSCV) of the differences between the respective measurements.

3 Results

3.1 Study participant characteristics

A total of 37 women (mean age at delivery was 35.4 ± 3.8 years) with (n=19) and without (n=18) history of GDM were included in this study. No significant differences in age at delivery, in time from delivery to baseline visit, from delivery to MR imaging, and from baseline visit to MR imaging were found between the women with a history of GDM (GDM group) and the women without a history of GDM (control group). The GDM group and the control group did not differ significantly in terms of BMI (GDM group 24.35 (21.14 to 26.92) kg/m^2 vs. control group 21.91 (20.53 to 25.01) kg/m^2; p = 0.23).

Out of the 37 women, 13 were categorized as overweight, having a BMI ≥ 25 kg/m^2 (GDM group, n=8; control group, n=5), and 9 women of the GDM group and none of the control group presented a pathologic glucose metabolism. Out of the 37 individuals, 15 met at least one diagnostic criterion for the metabolic syndrome (GDM group, n=9; control group, n=6) and 2 women of the GDM group fulfilled at least three diagnostic criteria for the metabolic syndrome.

Steps per day were counted among 32 women with (n=17) and without (n=15) history of GDM. Three women showed 10,000 or more steps per day (GDM group, n=1; control group, n=2). The steps per day did not differ significantly between the groups (GDM group 7543 ± 1705 steps vs. control group 7962 ± 1643 steps, p=0.49). Study participant characteristics are displayed in Table 1.

3.2 PDFF of the vertebral bone marrow

By the group comparisons without adjustments, PDFF values of the thoracic (Th9-Th12) and lumbar (L1-L4) vertebral bodies were significantly higher in the GDM group than in the control group (thoracic: 41.55 (32.21 to 49.48)% vs. 31.75 (30.03 to 34.97)%; p=0.02 and lumbar: 45.93 ± 12.22% vs. 38.22 ± 7.79%; p=0.03; Table 2, Figure 2). After adjusting the analysis for age and BMI using multivariable linear regression analyses, these effects remained significant. History of GDM was significantly associated with the mean PDFF of thoracic vertebral bodies (beta coefficient (β) of history of GDM = 8.94% (95% confidence interval (CI): 2.09 to 15.79%); p=0.01), and with that of lumbar vertebral bodies (β = 9.26% (95% CI 1.93 to 16.59%; p=0.02; Table 3).

In the multivariable logistic regression analyses adjusted for age and BMI, the odds of having a history of GDM were significantly greater in individuals with higher mean PDFF values of the thoracic or lumbar vertebral bodies (both odds ratios 1.10, 95% CI 1.02 to 1.2: p=0.02; Table 4).

For the differentiation between women with and without a history of GDM based on the mean PDFF of thoracic and lumbar vertebral bodies, the areas under the ROC curves (AUCs) were 0.72 and 0.73, respectively (Figure 3). The optimal thoracic and lumbar vertebral PDFF cutoff values were 38.10% and 44.18%, respectively (sensitivity 0.58 and specificity 0.89 for both).

10.3389/fendo.2023.1303126

TABLE 1 Characteristics of women, differentiated by women with a history of gestational diabetes mellitus (GDM group) and women without a history of GDM (control group).

		GDM group	Control group	p-value
Study participants (n)		19	18	
Age at time of delivery (years)				
	Mean ± SD	36.16 ± 4.07	34.56 ± 3.40	p=0.20 [a]
	Median (IQR)	36.00 (32.50-39.50)	35.00 (32.00-36.00)	
	Range	29 – 42	28 – 40	
Age at time of baseline visit (years)				
	Mean ± SD	37.11 ± 4.01	35.44 ± 3.57	p=0.19 [a]
	Median (IQR)	37.00 (33.00-40.50)	36.00 (33.00-37.00)	
	Range	30 – 43	28 – 41	
BMI at time of baseline visit (kg/m^2)				
	Mean ± SD	25.46 ± 6.45	22.84 ± 3.95	p=0.23 [b]
	Median (IQR)	24.35 (21.14-26.92)	21.91 (20.53-25.01)	
	Range	18.56 – 44.12	17.47 – 30.56	
Overweight (BMI ≥ 25 kg/m^2; n)		8	5	p=0.57 [c]
Pathologic glucose metabolism (n)		9	0	p ≤ 0.01 [d]
At least one diagnostic criterion for metabolic syndrome (n)		9	6	p=0.59 [c]
Three or more diagnostic criteria for metabolic syndrome (n)		2	0	p=0.49 [d]
Steps per day at time of baseline visit (steps)		(n=17)	(n=15)	
	Mean ± SD	7543 ± 1705	7962 ± 1643	p=0.49 [a]
	Median (IQR)	7783 (6519-8230)	7811 (7212-8866)	
	Range	4595 – 11200	3682 – 10600	
Time between delivery and baseline visit (months)				
	Mean ± SD	9.46 ± 2.68	9.38 ± 2.04	p=0.82 [b]
	Median (IQR)	8.77 (7.05-12.17)	9.25 (7.63-11.16)	
	Range	6.13 – 14.53	6.40 – 12.83	
Time between delivery and MRI (months)				
	Mean ± SD	11.05 ± 2.74	11.50 ± 2.05	p=0.57 [a]
	Median (IQR)	11.27 (9.03-13.03)	12.07 (10.01-13.05)	
	Range	7.23 – 16.60	7.77 – 14.30	
Time between baseline visit and MRI (days)				
	Mean ± SD	47.84 ± 41.84	63.61 ± 40.92	p=0.15 [b]
	Median (IQR)	33.00 (15.00-74.50)	48.00 (32.25-91.00)	
	Range	5 – 138	16 – 150	

[a]Two-sample t-test.
[b]Wilcoxon rank sum test/Mann-Whitney U test.
[c]Chi-squared test.
[d]Fisher exact test.
GDM, gestational diabetes mellitus; SD, standard deviation; IQR, interquartile range (the first quartile-the third quartile); BMI, body mass index; MRI, magnetic resonance imaging.

10.3389/fendo.2023.1303126

TABLE 2 PDFF and CSA analyses, differentiated by women with a history of gestational diabetes mellitus (GDM group) and women without a history of GDM (control group).

		GDM group	Control group	p-value
PDFF of thoracic vertebrae from 9 to 12 (percentage)				
	Mean ± SD	40.37 ± 11.60	33.11 ± 7.00	**p=0.022** [a]
	Median (IQR)	41.55 (32.21-49.48)	31.75 (30.03-34.97)	
	Range	14.95 – 56.09	19.97 – 49.46	
PDFF of lumbar vertebrae from 1 to 4 (percentage)				
	Mean ± SD	45.93 ± 12.22	38.22 ± 7.79	**p=0.029** [b]
	Median (IQR)	47.84 (39.19-57.58)	36.93 (33.36-41.31)	
	Range	18.11 – 61.47	26.63 – 55.52	
PDFF of the right and left psoas muscles (percentage)				
	Mean ± SD	9.65 ± 2.08	8.31 ± 2.35	p=0.07 [b]
	Median (IQR)	9.68 (8.06-11.27)	8.29 (6.60-9.92)	
	Range	6.47 – 13.36	4.18 – 13.33	
PDFF of the right and left autochthonous muscles (percentage)				
	Mean ± SD	14.28 ± 3.81	11.67 ± 3.55	**p=0.036** [c]
	Median (IQR)	12.99 (12.18-15.90)	10.83 (9.39-14.71)	
	Range	10.22 – 27.03	6.03 – 18.11	
CSA of the right and left psoas muscles (cm^2)				
	Mean ± SD	7.75 ± 1.70	7.88 ± 0.96	p=0.79 [d]
	Median (IQR)	7.52 (6.81-8.87)	7.75 (7.21-8.71)	
	Range	4.83 – 11.1	6.33 – 9.45	
CSA of the right and left autochthonous muscles (cm^2)				
	Mean ± SD	14.88 ± 3.14	15.70 ± 1.84	p=0.34 [d]
	Median (IQR)	15.74 (12.68-17.41)	15.24 (14.71-17.02)	
	Range	9.04 – 19.31	12.66 – 18.99	

[a]Mood's median test.
[b]Two-sample t-test.
[c]Wilcoxon rank sum test/Mann-Whitney U test.
[d]Welch t-test.
PDFF, proton density fat fraction; CSA, cross-sectional area; GDM, gestational diabetes mellitus; SD, standard deviation; IQR, interquartile range (the first quartile-the third quartile).
The bold values are considered statistically significant.

As examples, the PDFF maps at the level of lumbar (L4) vertebral bone marrow are shown: one in a woman after normoglycemic pregnancy and the other in a woman with a history of GDM (Figure 4).

3.3 PDFF and CSA of the paraspinal musculature

When analyzing the group comparisons without adjustments, the PDFF values of the autochthonous muscles (AM) were significantly higher in the GDM group than in the control group (12.99 (12.18 to 15.90)% vs. 10.83 (9.39 to 14.71)%; p=0.04; Table 2, Figure 2). Only in the unadjusted univariable linear regression model, the history of GDM was significantly associated with the mean PDFF value of AM (β = 2.61% (95% CI 0.15 to 5.07%; p=0.04; Table 3). No significant differences between the GDM group and the control group were detected in PDFF values of the PM (GDM group 9.65 ± 2.08% vs. control group 8.31 ± 2.35%; p=0.07), in CSA of the AM (GDM group 14.88 ± 3.14 cm^2 vs. control group 15.70 ± 1.84 cm^2; p=0.34) or in CSA of the PM (GDM group 7.75 ± 1.70 cm^2 vs. control group 7.88 ± 0.96 cm^2; p= 0.79). These analyses continued to show no significant associations with the history of GDM after adjusting for age and BMI (p ≥ 0.05; Tables 3, 4).

Neither was there a significant correlation found between CSA and PDFF of the PSM (PM: GDM group r=-0.08, p=0.75; control

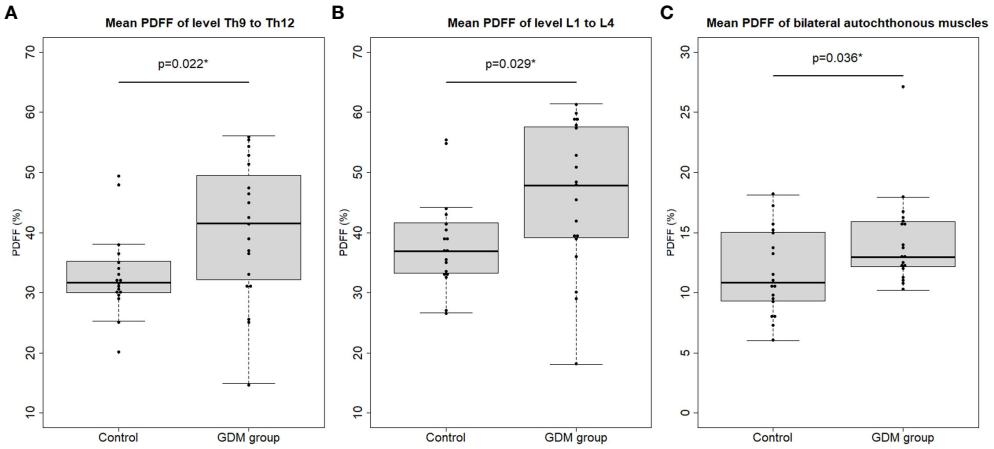

FIGURE 2
Mean proton density fat fraction (PDFF) of the **(A)** thoracic (level Th9 to Th12) and **(B)** lumbar (level L1 to L4) vertebral bone marrow and **(C)** mean PDFF of the bilateral autochthonous muscles (AM) in the control vs. the women with a history of gestational diabetes mellitus (GDM group). Dots represent the mean PDFF value of each study participant. Asterisks indicate $p < 0.05$.

group r=-0.24, p=0.34; AM: GDM group r=-0.14, p=0.58; control group r=-0.15, p=0.55) nor was there a significant correlation found between the PDFF of the PSM and the PDFF of vertebral bodies (PM and Th9-Th12: GDM group r=0.02, p=0.93; control group r=0.28, p=0.26; PM and L1-L4: GDM group r=-0.02, p=0.93; control group r=0.31, p=0.21; AM and Th9-Th12: GDM group r=-0.27, p=0.26; control group r=0.06, p=0.82; AM and L1-L4: GDM group r=-0.32, p=0.19; control group r=0.10, p=0.70) in any of the groups.

3.4 Inter-reader and intra-reader reproducibility

Inter-reader agreement for mean PDFF within the thoracic and lumbar vertebral bodies (Th9 – L4) and the PSM was excellent (ICC, 0.98 [95% CI, 0.96-0.99] and 0.97 [95% CI, 0.96-0.99] for these mean PDFF analyses, respectively).

Inter-reader reproducibility, calculated by the RMSCV, was excellent with < 1.0% (0.95% and 0.97% for these mean PDFF analyses, respectively).

Intra-reader agreement for the corresponding PDFF was excellent (ICC, 0.98 [95% CI, 0.96–0.99] for both mean PDFF analyses).

Intra-reader reproducibility, calculated by the RMSCV, was excellent with < 1.0% (0.91% and 0.93% for these mean PDFF analyses, respectively).

4 Discussion

In this study, the vertebral bone PDFF and the paraspinal muscle PDFF and CSA of premenopausal women, with and without a history of gestational diabetes, were investigated. Our study demonstrates that women with a history of GDM (GDM group) show significantly higher PDFF values of the thoracic or

TABLE 3 Linear regression models, for the association of PDFF or CSA with a history of gestational diabetes mellitus (GDM).

	Unadjusted univariable model		Adjusted multivariable model*	
Dependent variable	βcoefficient of GDM (95% CI of β)	p-value	βcoefficient of GDM (95% CI of β)	p-value
Mean PDFF of thoracic vertebrae from 9 to 12 (percentage)	7.26 (0.82, 13.70)	**0.028**	8.94 (2.09, 15.79)	**0.012**
Mean PDFF of lumbar vertebrae from 1 to 4 (percentage)	7.71 (0.83, 14.59)	**0.029**	9.26 (1.93, 16.59)	**0.015**
Mean PDFF of the right and left psoas muscles (percentage)	1.34 (-0.14, 2.82)	0.07	0.87 (-0.69, 2.43)	0.27
Mean PDFF of the right and left autochthonous muscles (percentage)	2.61 (0.15, 5.07)	**0.038**	1.95 (-0.58, 4.49)	0.13
Mean CSA of the right and left psoas muscles (cm^2)	-0.12 (-1.05, 0.81)	0.79	-0.31 (-1.25, 0.63)	0.51
Mean CSA of the right and left autochthonous muscles (cm^2)	-0.82 (-2.55, 0.91)	0.34	-1.66 (-3.31, -0.01)	0.049

*Adjusted multivariable models are adjusted for age and body mass index at baseline visit.
PDFF, proton density fat fraction; CSA, cross-sectional area; GDM, gestational diabetes mellitus; CI, confidence interval.
The bold values are considered statistically significant.

10.3389/fendo.2023.1303126

TABLE 4 Logistic regression models, for the association of PDFF or CSA with a history of gestational diabetes mellitus (GDM).

:	Unadjusted univariable model		Adjusted multivariable model*	
Independent variable	Odds ratio (OR) for GDM (95% CI of OR)	p-value	Odds ratio (OR) for GDM (95% CI of OR)	p-value
Mean PDFF of thoracic vertebrae from 9 to 12 (percentage)	1.08 (1.01, 1.18)	**0.039**	1.10 (1.02, 1.21)	**0.019**
Mean PDFF of lumbar vertebrae from 1 to 4 (percentage)	1.08 (1.01, 1.17)	**0.039**	1.10 (1.02, 1.20)	**0.021**
Mean PDFF of the right and left psoas muscles (percentage)	1.33 (0.98, 1.89)	0.08	1.22 (0.87, 1.77)	0.25
Mean PDFF of the right and left autochthonous muscles (percentage)	1.26 (1.02, 1.63)	0.052	1.21 (0.97, 1.58)	0.13
Mean CSA of the right and left psoas muscles (cm^2)	0.94 (0.57, 1.52)	0.78	0.81 (0.43, 1.43)	0.48
Mean CSA of the right and left autochthonous muscles (cm^2)	0.88 (0.66, 1.14)	0.34	0.72 (0.48, 0.99)	0.07

*Adjusted multivariable models are adjusted for age and body mass index at baseline visit.
PDFF, proton density fat fraction; CSA, cross-sectional area; GDM, gestational diabetes mellitus; CI, confidence interval.
The bold values are considered statistically significant.

lumbar vertebral bodies than women without a history of GDM (control group), independent of age and BMI. Without adjusting for age and BMI, the PDFF of the autochthonous musculature was significantly higher in the GDM group than in the control group, while the CSA was similar between the groups. These statistical findings do not prove any causality in our study.

A previous study reported that the mean lumbar vertebral PDFF was significantly higher in osteoporotic/osteopenic patients than in non-osteoporotic/non-osteopenic patients among an older population (15). A further study identified a significantly higher mean vertebral PDFF increase over 12 months before the occurrence of an incidental vertebral compression fracture compared to the longitudinally measured mean vertebral PDFF in patients without incidental vertebral compression fractures (14). Again, this previous study was performed in an older study population.

Diabetes presents with a wide heterogeneity when looking closely at the diagnosed population (33). This may be the reason for the contradictory results of previous studies regarding marrow fat content in patients with T2D compared to healthy individuals. Some studies showed higher bone marrow fat in healthy individuals (11, 34) or no significant difference in bone marrow fat content between patients with T2D and healthy controls (35–37). One specific diabetic disease subtype is GDM. The diagnosis is being held at lower glucose measures during the oral glucose tolerance test than for T2D during pregnancy. Women with a history of GDM

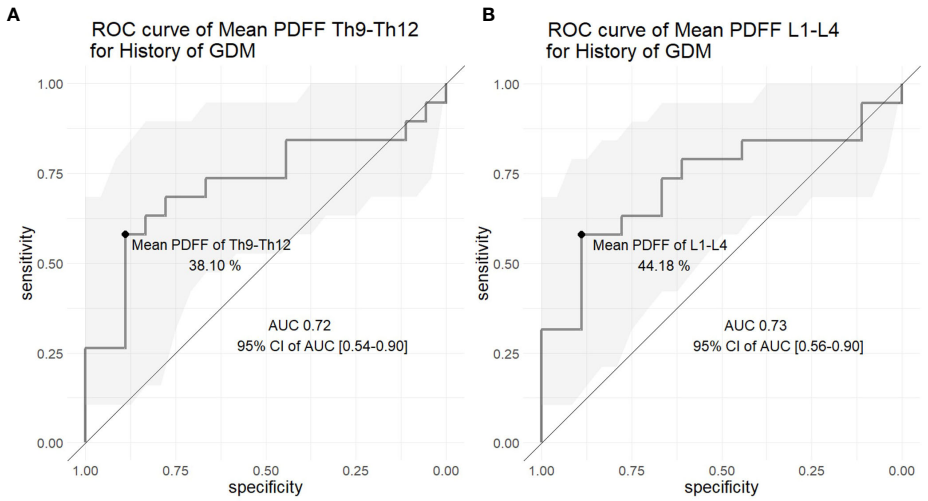

FIGURE 3
Receiver operating characteristic (ROC) curves of the mean proton density fat fraction (PDFF) of the **(A)** thoracic (level Th9 to Th12) and **(B)** lumbar (level L1 to L4) vertebral bone marrow to differentiate between the control and the women with a history of gestational diabetes mellitus (GDM). The gray area represents the 95% confidence interval (CI) of the area under the curve (AUC).

10.3389/fendo.2023.1303126

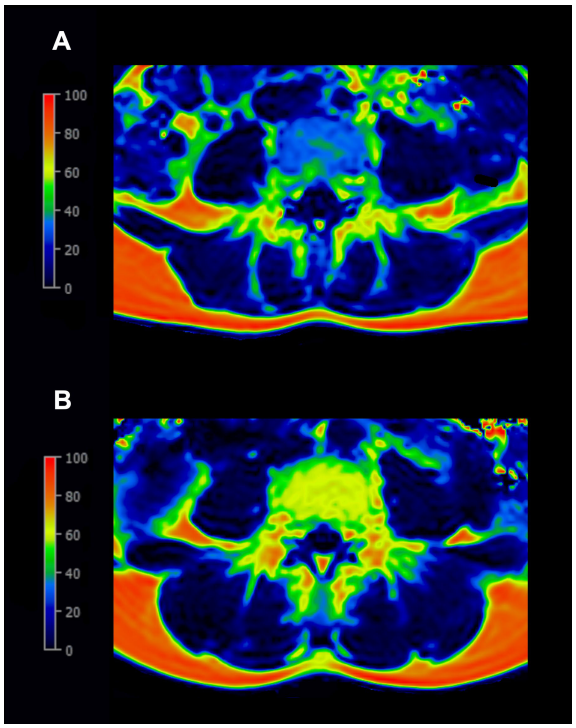

FIGURE 4
Examples of the color-coded proton-density-fat-fraction (PDFF) map at the level L4: **(A)** A 33-year-old woman after normoglycemic pregnancy (BMI 19.15 kg/m^2, PDFF of L4 32.13%) with blue indicating lower PDFF values. **(B)** A 37-year-old woman with a history of gestational diabetes mellitus (BMI 18.56 kg/m^2, PDFF of L4 62.96%) with yellow indicating higher PDFF values.

show lower insulin sensitivity and the risk of developing type 2 diabetes is significantly increased compared to women without a history of GDM (25, 26). The pathophysiological pathways in GDM are considered to be less heterogeneous than those in T2D. In terms of bone health, similar to T2D, it has been reported that women with a history of GDM have an increased fracture risk (27). Therefore, in this study we focused on premenopausal women with and without a history of GDM, to investigate PDFF biomarkers in relation to possible early bone changes under the risk of diabetes progression.

Our result is in line with a previous study, reporting that premenopausal women with metabolic syndrome showed significantly higher PDFF values of the lumbar spine than controls (38). In our study cohort, 9 out of 19 women in the GDM group showed a pathologic glucose metabolism, and 2 women in the GDM group fulfilled more than three criteria for the diagnosis of a metabolic syndrome.

Aside from bone marrow fat, metabolic diseases have previously been shown to affect the musculature. A previous study has reported significantly higher PSM PDFF in osteoporotic patients compared to normal controls and found an inverse correlation between paraspinal muscle PDFF and BMD (39). Additionally, higher vertebral PDFF and PSM PDFF were associated with more severe bone fragility (14). In our study, the GDM group showed significantly higher AM PDFF compared to the control group, while there was no significant difference in PS PDFF and PSM CSA between the groups. We found no correlation between AM PDFF and vertebral PDFF in our premenopausal cohort. This result is consistent with a previous study, reporting an association between AM PDFF and vertebral PDFF only in postmenopausal women, but not in premenopausal women (40). It needs to be noted that PSM PDFF in postmenopausal women was significantly higher compared to premenopausal women (40).

Both bone marrow and muscle adiposity have been acknowledged to be associated with physical activity or exercise (41, 42). Several pathophysiological mechanisms are presented, such that physical activity promotes bone marrow fat lipolysis, and that physical inactivity increases intramuscular fat content, while decreasing muscle mass and muscle cross-sectional area (41, 43). We employed steps per day as a measure of daily physical activity. A previous study revealed that young healthy adults could reduce their step count from ~10,000 steps per day to ~1,300 steps per day simply by taking the elevator instead of stairs and by driving instead of walking. Following 21 days of these step reductions, their insulin sensitivity and postprandial lipid metabolism were decreased, and intra-abdominal fat mass increased (44). Our study participants did not show significant discrepancies in steps per day between the GDM group and the control group, however, excluding the impact of physical activity is difficult. We suggest that steps per day can be both the cause and the consequence of the changes in bone and muscle tissue, because the fat-infiltrated bones and muscles can alter the microenvironment, compromising function and performance (21, 22, 45, 46). In this regard, physical activity levels can be influenced both by a history of GDM and by fat infiltrations in bones and muscles, as reflected in higher PDFFs. In this relationship, steps per day would be a collider in the context of directed acyclic graphs (DAG), and adjusting the analysis for this factor may introduce a collider bias. Furthermore, considering our sample size, we decided not to add steps per day as one of the covariates in our linear and logistic regression models.

Our study has several limitations. First, the sample size is limited because only MRI study participants with the identical protocol and system were selected since we prioritized minimizing a potential measurement bias due to different measurement methods. Moreover, given that only those participants who granted consent and were able to complete MRI scans were included in this study, a selection bias cannot be ruled out. Future studies in larger study cohorts are needed to confirm the external validity of our findings. Second, the hormonal status of these women was unidentifiable, which may have had effects on the bone marrow composition. Third, the cohort did not have quantitative information available regarding the BMD (e.g. QCT).

In conclusion, our data suggests that a history of GDM is associated with a higher mean PDFF of the thoracic and lumbar vertebral bone marrow, regardless of age and BMI adjustments, and is associated with a higher mean PDFF of the AM without adjustments in premenopausal women. These findings indicate that PDFF may be a useful biomarker for the assessment of musculoskeletal health in premenopausal women at risk of diabetes. We note that no causality is verified by our findings.

Data availability statement

The raw data supporting the conclusions of this article will be made available by the authors, upon the further scientific inquiries without undue reservation.

Ethics statement

The studies involving humans were approved by Ethics Commission of the Medical Faculty, Ludwig-Maximilians-Universität München. The studies were conducted in accordance with the local legislation and institutional requirements. The participants provided their written informed consent to participate in this study.

Author contributions

SH: Validation, Visualization, Writing – original draft, Writing – review & editing, Data curation, Formal analysis, Investigation, Methodology, Resources, Software, Supervision. ASG: Conceptualization, Data curation, Formal analysis, Funding acquisition, Investigation, Methodology, Project administration, Resources, Software, Supervision, Validation, Visualization, Writing – original draft, Writing – review & editing. YS: Data curation, Formal analysis, Investigation, Methodology, Resources, Software, Validation, Visualization, Writing – original draft, Writing – review & editing. OD: Data curation, Investigation, Methodology, Resources, Software, Supervision, Validation, Visualization, Writing – original draft, Writing – review & editing. AL: Funding acquisition, Resources, Supervision, Writing – review & editing. JS: Conceptualization, Funding acquisition, Investigation, Project administration, Supervision, Writing – original draft, Writing – review & editing. UF: Conceptualization, Investigation, Project administration, Resources, Supervision, Writing – original draft. EP: Resources, Writing – review & editing. NH: Conceptualization, Data curation, Formal analysis, Funding acquisition, Investigation, Project administration, Resources, Software, Supervision, Validation, Visualization, Writing – original draft, Writing – review & editing.

Funding

The author(s) declare financial support was received for the research, authorship, and/or publication of this article. This work was funded by the Munich Clinician Scientist Program (MCSP) of the University of Munich (LMU; grant number ACS-10), LMU Klinikum, the German Center for Diabetes Research (DZD), and the Helmholtz Zentrum München. SH is supported by research overseas grants from the Nakatani Foundation (Japan) and Deutscher Akademischer Austauschdienst (DAAD, Germany).

Acknowledgments

Professor Ulrich Mansmann (Institute for Medical Information Processing, Biometry and Epidemiology (IBE), Faculty of Medicine, LMU Munich, Munich, Germany) kindly provided statistical advice for this research work.

Conflict of interest

The authors declare that the research was conducted in the absence of any commercial or financial relationships that could be construed as a potential conflict of interest.

Publisher's note

References

1. Reeder SB, Hu HH, Sirlin CB. Proton density fat-fraction: a standardized MR-based biomarker of tissue fat concentration. *J Magn Reson Imaging.* (2012) 36(5):1011–4. doi: 10.1002/jmri.23741

2. Hu HH, Kan HE. Quantitative proton MR techniques for measuring fat. *NMR Biomed* (2013) 26(12):1609–29. doi: 10.1002/nbm.3025

3. Sollmann N, Löffler MT, Kronthaler S, Böhm C, Dieckmeyer M, Ruschke S, et al. MRI-based quantitative osteoporosis imaging at the spine and femur. *J Magn Reson Imaging.* (2021) 54(1):12–35. doi: 10.1002/jmri.27260

4. Baum T, Yap SP, Dieckmeyer M, Ruschke S, Eggers H, Kooijman H, et al. Assessment of whole spine vertebral bone marrow fat using chemical shift-encoding based water-fat MRI. *J Magn Reson Imaging.* (2015) 42(4):1018–23. doi: 10.1002/jmri.24854

5. Karampinos DC, Ruschke S, Dieckmeyer M, Diefenbach M, Franz D, Gersing AS, et al. Quantitative MRI and spectroscopy of bone marrow. *J Magn Reson Imaging.* (2018) 47(2):332–53. doi: 10.1002/jmri.25769

6. Schmeel FC, Vomweg T, Träber F, Gerhards A, Enkirch SJ, Faron A, et al. Proton density fat fraction MRI of vertebral bone marrow: Accuracy, repeatability, and reproducibility among readers, field strengths, and imaging platforms. *J Magn Reson Imaging.* (2019) 50(6):1762–72. doi: 10.1002/jmri.26748

7. Li GW, Xu Z, Chen QW, Tian YN, Wang XY, Zhou L, et al. Quantitative evaluation of vertebral marrow adipose tissue in postmenopausal female using MRI chemical shift-based water-fat separation. *Clin Radiol* (2014) 69(3):254–62. doi: 10.1016/j.crad.2013.10.005

8. Kühn JP, Hernando D, Meffert PJ, Reeder S, Hosten N, Laqua R, et al. Proton-density fat fraction and simultaneous R2* estimation as an MRI tool for assessment of osteoporosis. *Eur Radiol* (20132013) 23(12):3432–9. doi: 10.1007/s00330-013-2950-7

9. Justesen J, Stenderup K, Ebbesen EN, Mosekilde L, Steiniche T, Kassem M, et al. Adipocyte tissue volume in bone marrow is increased with aging and in patients with osteoporosis. *Biogerontology* (2001) 2(3):165–71. doi: 10.1023/a:1011513223894

10. Tencerova M, Okla M, Kassem M. Insulin signaling in bone marrow adipocytes. *Curr Osteoporos Rep* (2019) 17(6):446–54. doi: 10.1007/s11914-019-00552-8

11. Zhu L, Xu Z, Li G, Wang Y, Li X, Shi X, et al. Marrow adiposity as an indicator for insulin resistance in postmenopausal women with newly diagnosed type 2 diabetes - an investigation by chemical shift-encoded water-fat MRI. *Eur J Radiol* (2019) 113:158–64. doi: 10.1016/j.ejrad.2019.02.020

12. Palermo A, D'Onofrio L, Buzzetti R, Manfrini S, Napoli N. Pathophysiology of bone fragility in patients with diabetes. *Calcif Tissue Int* (2017) 100(2):122–32. doi: 10.1007/s00223-016-0226-3

13. Vestergaard P. Discrepancies in bone mineral density and fracture risk in patients with type 1 and type 2 diabetes–a meta-analysis. *Osteoporos Int* (2007) 18 (4):427–44. doi: 10.1007/s00198-006-0253-4

14. Leonhardt Y, Ketschau J, Ruschke S, Gassert FT, Glanz L, Feuerriegel GC, et al. Associations of incidental vertebral fractures and longitudinal changes of MR-based proton density fat fraction and T2* measurements of vertebral bone marrow. *Front Endocrinol (Lausanne)* (2022) 13:1046547. doi: 10.3389/fendo.2022.1046547

15. Gassert FT, Glanz L, Boehm C, Stelter J, Gassert FG, Leonhardt Y, et al. Associations between bone mineral density and longitudinal changes of vertebral bone marrow and paraspinal muscle composition assessed using MR-based proton density fat fraction and T2* Maps in patients with and without osteoporosis. *Diagnostics (Basel)* (2022) 12(10):2467. doi: 10.3390/diagnostics12102467

16. Gassert FT, Kufner A, Gassert FG, Leonhardt Y, Kronthaler S, Schwaiger BJ, et al. MR-based proton density fat fraction (PDFF) of the vertebral bone marrow differentiates between patients with and without osteoporotic vertebral fractures. *Osteoporos Int* (2022) 33(2):487–96. doi: 10.1007/s00198-021-06147-3

17. Karampinos DC, Baum T, Nardo L, Alizai H, Yu H, Carballido-Gamio J, et al. Characterization of the regional distribution of skeletal muscle adipose tissue in type 2 diabetes using chemical shift-based water/fat separation. *J Magn Reson Imaging.* (2012) 35(4):899–907. doi: 10.1002/jmri.23512

18. Tack W, De Cock AM, Dirinck EL, Bastijns S, Ariën F, Perkisas S. Pathophysiological interactions between sarcopenia and type 2 diabetes: A two-way street influencing diagnosis and therapeutic options. *Diabetes Obes Metab* (2023). doi: 10.1111/dom.15321

19. Hamrick MW, McGee-Lawrence ME, Frechette DM. Fatty infiltration of skeletal muscle: mechanisms and comparisons with bone marrow adiposity. *Front Endocrinol (Lausanne)* (2016) 20:69. doi: 10.3389/fendo.2016.00069

20. Farup J, Just J, de Paoli F, Lin L, Jensen JB, Billeskov T, et al. Human skeletal muscle CD90+ fibro-adipogenic progenitors are associated with muscle degeneration in type 2 diabetic patients. *Cell Metab* (2021) 33(11):2201–14.e11. doi: 10.1016/j.cmet.2021.10.001

21. Collao N, Farup J, De Lisio M. Role of metabolic stress and exercise in regulating fibro/adipogenic progenitors. *Front Cell Dev Biol* (2020) 8:9. doi: 10.3389/fcell.2020.00009

22. Lang T, Cauley JA, Tylavsky F, Bauer D, Cummings S, Harris TB, et al. Computed tomographic measurements of thigh muscle cross-sectional area and attenuation coefficient predict hip fracture: the health, aging, and body composition study. *J Bone Miner Res* (2010) 25(3):513–9. doi: 10.1359/jbmr.090807

23. Kautzky-Willer A, Krssak M, Winzer C, Pacini G, Tura A, Farhan S, et al. Increased intramyocellular lipid concentration identifies impaired glucose metabolism in women with previous gestational diabetes. *Diabetes* (2003) 52(2):244–51. doi: 10.2337/diabetes.52.2.244

24. Farrar D. Hyperglycemia in pregnancy: prevalence, impact, and management challenges. *Int J Womens Health* (2016) 8:519–27. doi: 10.2147/IJWH.S102117

25. Rottenkolber M, Ferrari U, Holland L, Aertsen S, Kammer NN, Hetterich H, et al. The diabetes risk phenotype of young women with recent gestational diabetes. *J Clin Endocrinol Metab* (2015) 100(6):E910–918. doi: 10.1210/jc.2014-3898

26. Bellamy L, Casas JP, Hingorani AD, Williams D. Type 2 diabetes mellitus after gestational diabetes: a systematic review and meta-analysis. *Lancet* (2009) 373 (9677):1773–9. doi: 10.1016/S0140-6736(09)60731-5

27. Ahmeidat A, Bhattacharya S, Luben RN, Khaw KT, Myint PK. Long-term effects of gestational diabetes on bone mineral density and fracture risk: Analysis of the Norfolk cohort of the European Prospective Investigation into Cancer (EPIC-Norfolk) population-based study. *Maturitas* (2021) 144:68–73. doi: 10.1016/j.maturitas.2020.11.005

28. International Association of Diabetes and Pregnancy Study Groups Consensus Panel, Metzger BE, Gabbe SG, Persson B, Buchanan TA, Catalano PA, et al. International association of diabetes and pregnancy study groups recommendations on the diagnosis and classification of hyperglycemia in pregnancy. *Diabetes Care* (2010) 33(3):676–82. doi: 10.2337/dc09-1848

29. American Diabetes Association. Standards of medical care in diabetes–2014. *Diabetes Care* (2014) 37 Suppl 1:S14–80. doi: 10.2337/dc14-S014

30. Alberti KG, Zimmet P, Shaw J. Metabolic syndrome–a new world-wide definition. A Consensus Statement from the International Diabetes Federation. *Diabetes Med* (2006) 23(5):469–80. doi: 10.1111/j.1464-5491.2006.01858.x

31. Brix G, Heiland S, Bellemann ME, Koch T, Lorenz WJ. MR imaging of fat-containing tissues: valuation of two quantitative imaging techniques in comparison with localized proton spectroscopy. *Magn Reson Imaging.* (1993) 11(7):977–91. doi: 10.1016/0730-725x(93)90217-2

32. Kang GH, Cruite I, Shiehmorteza M, Wolfson T, Gamst AC, Hamilton G, et al. Reproducibility of MRI-determined proton density fat fraction across two different MR scanner platforms. *J Magn Reson Imaging.* (2011) 34(4):928–34. doi: 10.1002/jmri.22701

33. Del Prato S. Heterogeneity of diabetes: heralding the era of precision medicine. *Lancet Diabetes Endocrinol* (2019) 7(9):659–61. doi: 10.1016/S2213-8587(19)30218-9

34. Sheu Y, Amati F, Schwartz AV, Danielson ME, Li X, Boudreau R, et al. Vertebral bone marrow fat, bone mineral density and diabetes: The Osteoporotic Fractures in Men (MrOS) study. *Bone* (2017) 97:299–305. doi: 10.1016/j.bone.2017.02.001

35. Baum T, Yap SP, Karampinos DC, Nardo L, Kuo D, Burghardt AJ, et al. Does vertebral bone marrow fat content correlate with abdominal adipose tissue, lumbar spine bone mineral density, and blood biomarkers in women with type 2 diabetes mellitus? *J Magn Reson Imaging* (2012) 35(1):117–24. doi: 10.1002/jmri.22757

36. Patsch JM, Li X, Baum T, Yap SP, Karampinos DC, Schwartz AV, et al. Bone marrow fat composition as a novel imaging biomarker in postmenopausal women with prevalent fragility fractures. *J Bone Miner Res* (2013) 28(8):1721–8. doi: 10.1002/jbmr.1950

37. de Araújo IM, Salmon CE, Nahas AK, Nogueira-Barbosa MH, Elias JJr., de Paula FJ. Marrow adipose tissue spectrum in obesity and type 2 diabetes mellitus. *Eur J Endocrinol* (2017) 176(1):21–30. doi: 10.1530/EJE-16-0448

38. Ma Q, Cheng X, Hou X, Yang Z, Ma D, Wang Z. Bone marrow fat measured by a chemical shift-encoded sequence (IDEAL-IQ) in patients with and without metabolic syndrome. *J Magn Reson Imaging.* (2021) 54(1):146–53. doi: 10.1002/jmri.27548

39. Zhao Y, Huang M, Serrano Sosa M, Cattell R, Fan W, Li M, et al. Fatty infiltration of paraspinal muscles is associated with bone mineral density of the lumbar spine. *Arch Osteoporos* (2019) 14(1):99. doi: 10.1007/s11657-019-0639-5

40. Sollmann N, Dieckmeyer M, Schlaeger S, Rohrmeier A, Syvaeri J, Diefenbach MN, et al. Associations between lumbar vertebral bone marrow and paraspinal muscle fat compositions-an investigation by chemical shift encoding-based water-fat MRI. *Front Endocrinol (Lausanne)* (2018) 9:563. doi: 10.3389/fendo.2018.00563

41. Peng H, Hu B, Xie LQ, Su T, Li CJ, Liu Y, et al. A mechanosensitive lipolytic factor in the bone marrow promotes osteogenesis and lymphopoiesis. *Cell Metab* (2022) 34(8):1168–82.e6. doi: 10.1016/j.cmet.2022.05.009

42. Oikawa SY, Holloway TM, Phillips SM. The impact of step reduction on muscle health in aging: protein and exercise as countermeasures. *Front Nutr* (2019) 6:75. doi: 10.3389/fnut.2019.00075

43. Atherton PJ, Greenhaff PL, Phillips SM, Bodine SC, Adams CM, Lang CH. Control of skeletal muscle atrophy in response to disuse: clinical/preclinical contentions and fallacies of evidence. *Am J Physiol Endocrinol Metab* (2016) 311: E594–604. doi: 10.1152/ajpendo.00257.2016

44. Olsen RH, Krogh-Madsen R, Thomsen C, Booth FW, Pedersen BK. Metabolic responses to reduced daily steps in healthy nonexercising men. *J Am Med Assoc* (2008) 299:1261–3. doi: 10.1001/jama.299.11.1259

45. Tencerova M, Duque G, Beekman KM, Corsi A, Geurts J, Bisschop PH, et al. The impact of interventional weight loss on bone marrow adipose tissue in people living with obesity and its connection to bone metabolism. *Nutrients* (2023) 15(21):4601. doi: 10.3390/nu15214601

46. Al Saedi A, Debruin DA, Hayes A, Hamrick M. Lipid metabolism in sarcopenia. *Bone* (2022) 164:116539. doi: 10.1016/j.bone.2022.116539

frontiers | Frontiers in Endocrinology

TYPE Original Research
PUBLISHED 30 January 2024
DOI 10.3389/fendo.2024.1310466

OPEN ACCESS

EDITED BY
Michaela Tencerova,
Academy of Sciences of the Czech Republic (ASCR), Czechia

REVIEWED BY
Mark B. Meyer,
University of Wisconsin-Madison, United States
Sarah E. Little-Letsinger,
Duke University, United States

*CORRESPONDENCE
Sylvia Christakos
christak@njms.rutgers.edu

†These authors have contributed equally to this work

RECEIVED 09 October 2023
ACCEPTED 09 January 2024
PUBLISHED 30 January 2024

CITATION
Verlinden L, Li S, Veldurthy V, Carmeliet G and Christakos S (2024) Relationship of the bone phenotype of the Klotho mutant mouse model of accelerated aging to changes in skeletal architecture that occur with chronological aging. *Front. Endocrinol.* 15:1310466. doi: 10.3389/fendo.2024.1310466

Relationship of the bone phenotype of the Klotho mutant mouse model of accelerated aging to changes in skeletal architecture that occur with chronological aging

Lieve Verlinden[1†], Shanshan Li[2†], Vaishali Veldurthy[2], Geert Carmeliet[1] and Sylvia Christakos[2*]

[1]Clinical and Experimental Endocrinology, KU Leuven, Leuven, Belgium, [2]Department of Microbiology, Biochemistry and Molecular Genetics, New Jersey Medical School, Rutgers, the State University of New Jersey, Newark, NJ, United States

Introduction: Due to the relatively long life span of rodent models, in order to expediate the identification of novel therapeutics of age related diseases, mouse models of accelerated aging have been developed. In this study we examined skeletal changes in the male and female *Klotho* mutant (*kl/kl*) mice and in male and female chronically aged mice to determine whether the accelerated aging bone phenotype of the *kl/kl* mouse reflects changes in skeletal architecture that occur with chronological aging.

Methods: 2, 6 and 20-23 month old C57BL/6 mice were obtained from the National Institute of Aging aged rodent colony and wildtype and *kl/kl* mice were generated as previously described by M. Kuro-o. Microcomputed tomography analysis was performed *ex vivo* to examine trabecular and cortical parameters from the proximal metaphyseal and mid-diaphyseal areas, respectively. Serum calcium and phosphate were analyzed using a colorimetric assay. The expression of duodenal *Trpv6*, which codes for TRPV6, a vitamin D regulated epithelial calcium channel whose expression reflects intestinal calcium absorptive efficiency, was analyzed by quantitative real-time PCR.

Results and discussion: Trabecular bone volume (BV/TV) and trabecular number decreased continuously with age in males and females. In contrast to aging mice, an increase in trabecular bone volume and trabecular number was observed in both male and female *kl/kl* mice. Cortical thickness decreased with advancing age and also decreased in male and female *kl/kl* mice. Serum calcium and phosphate levels were significantly increased in *kl/kl* mice but did not change with age. Aging resulted in a decline in *Trpv6* expression. In the *kl/kl* mice duodenal *Trpv6* was significantly increased. Our findings reflect differences in bone architecture as well as differences in calcium and phosphate homeostasis and expression of *Trpv6* between the *kl/kl* mutant mouse model of accelerated aging and chronological aging. Although the *Klotho* deficient mouse has provided a new understanding of the regulation of mineral homeostasis and

bone metabolism, our findings suggest that changes in bone architecture in the *kl/kl* mouse reflect in part systemic disturbances that differ from pathophysiological changes that occur with age including dysregulation of calcium homeostasis that contributes to age related bone loss.

KEYWORDS

aging, Klotho, calcium phosphate, TRPV6, skeletal architecture

1 Introduction

Aging is a complex process that occurs as physiological changes in body functions and changes at the cellular and molecular level contribute to gradual deterioration of function (1). Changes in bone structure and strength are associated with the aging process. Intestinal calcium absorption is dysregulated with age and can result in hyperparathyroidism and significant bone loss (2). Low fractional calcium absorption is associated with increased risk of fracture in the elderly (2). Calcium absorption is primarily regulated by 1,25-dihydroxyvitamin D_3 [$1,25(OH)_2D_3$], the hormonally active form of vitamin D_3, which is produced by two sequential hydroxylations of vitamin D_3 (at C-25 by CYP2R1 in the liver and at C-1 in the kidney by CYP27B1) (3–5). It has been suggested that the age related decrease in intestinal calcium absorption is due in part to resistance to $1,25(OH)_2D_3$ (2, 6, 7). In addition to vitamin D, klotho, a coreceptor for FGF23 involved in phosphate and calcium homeostasis, is also important for the maintenance of certain physiological functions with age and for the regulation of mineral metabolism (8). A deficiency in *Klotho* is associated with a state of accelerated aging and it has been characterized, in part, by shortened life span, infertility, skin atrophy, osteoporosis and vascular calcification (9). Klotho is expressed highly in the kidney, parathyroid gland and in the choroid plexus (9, 10). Klotho was found to be an obligate coreceptor for fibroblast growth factor (FGF) 23 after reports indicated that *Fgf23*$^{-/-}$ mice showed a similar aging phenotype as the *Klotho* deficient mouse (11–13). Similar phenotypes were reported compared to both the *kl/kl* mouse (which has a hypomorphic mutation for α klotho which was used in this study) as well as the *Klotho*$^{-/-}$ mouse (which lacks the sequence for the klotho protein) (11–13). FGF23 is a bone derived hormone that promotes phosphate diuresis by reducing phosphate reabsorption via suppression of the activity of type II Na dependent phosphate co-transporters in the proximal tubules in a klotho dependent manner (14–16). Klotho decreases transporter activity by promoting NaPi2a proteolytic degradation (17). Elevated $1,25(OH)_2D_3$ stimulates production of FGF23 and klotho (3, 14, 15). In a negative feedback mechanism secreted FGF23 activates the FGF receptor bound by klotho in renal tubular cells resulting in the suppression of CYP27B1 and increased expression of CYP24A1, an enzyme involved in the catabolism of $1,25(OH)_2D_3$ (3, 12, 18). In both the *Klotho* deficient mouse and the *Fgf23*$^{-/-}$ mouse increased levels of $1,25(OH)_2D_3$ and phosphate and reduced levels of PTH have been reported (13, 19). Thus $1,25(OH)_2D_3$, PTH and FGF23/klotho act together to regulate calcium and phosphate homeostasis. Understanding the regulation of mineral metabolism and its dysregulation with aging is important to provide insight into mechanisms involved in skeletal aging and to define causes of age related skeletal disease.

Due to the relatively long life span of rodent models, in order to expediate the identification of novel therapeutics of age related diseases, mouse models of accelerated aging have been developed. Since a bone phenotype has been reported in the *Klotho* deficient mouse models of accelerated aging (19–22), in this study we examined skeletal changes in male and female *Klotho* mutant *kl/kl* mice and in male and female chronically aged mice (whose changes in skeletal structure have been reported to be similar to human aging) (23, 24) in order to understand mechanisms involved in bone metabolism and to determine the relationship of the bone phenotype of the *Klotho* deficient mouse to changes in skeletal architecture that occur with age.

2 Materials and methods

2.1 Animals

C57BL/6 mice (2, 6 and 20 - 23 months old) were obtained from the National Institutes of Aging (NIA) aged rodent colony. *kl/kl* mice were generated by M. Kuro-o by backcrossing the original *kl/+* mice (9) (a hybrid of C3H and B6) with 129S1svlmJ mice for more than 12 generations. Thus the WT (+/+) mice are 129S1SvlmJ and the *kl/kl* mice are on the 129 genetic background and compared to WT (+/+) controls. The mice were analyzed at 6 – 7.5 weeks of age (*kl/kl* mice die prematurely at 8 -9 weeks of age). Mice were maintained in a virus and parasite-free barrier facility, given standard rodent chow diet (Rodent Laboratory Chow 5001; Ralston Purina co., St. Louis, Mo) and water *ad libitum* and exposed to a 12h-light, 12h-dark cycle. Both male and female mice were used. All the animal procedures were approved by the Institutional Animal Care and Use Committee (IACUC) at Rutgers,

New Jersey Medical School. Sample sizes of the different experimental groups are indicated in Supplementary Tables 1, 2.

2.2 Tissue harvest and serum analysis

Mouse duodenum was rinsed in ice-cold phosphate buffered saline, flash frozen in liquid nitrogen and stored at -80°C. Blood was collected and serum was prepared for analysis of calcium and phosphate using a colorimetric assay (Pointe Scientific, Inc., Canton MI) determined by Heartland Laboratories, Ames, IA. Tibiae were fixed in 2% paraformaldehyde for 24h. Micro-computed tomography (μCT) analysis of the left tibiae was performed as described below.

2.3 Bone analysis

μCT analysis was performed *ex vivo* using a high-resolution SkyScan 1172 (50 kV, 200 μA, 0.5-mm aluminum filter, 0.6° rotation step, 5 μm pixel size) to examine trabecular and cortical bone parameters (25). Serial tomographs, reconstructed from raw data using the cone-beam reconstruction software (NRecon, v.1.4.4.0; Skyscan with following settings: smoothing:0; ring artifact reduction: 7; beam hardening: 30%) with global thresholding. The thresholds set to detect trabecular bone were 80-255 and for cortical bone 90-255. Volumes of interest for 3D morphometric analysis were between 0.85 and 2.35 mm distal to the growth plate for trabecular analysis and between 3 and 3.5 mm distal to the growth plate for cortical analysis. Analysis was performed according to the guidelines of the American Society for Bone and Mineral Research (26).

2.4 RNA isolation and expression analysis

Total RNA was isolated from mouse duodenum using Ribozol RNA extraction reagent (Amresco, Solon, OH) or TRizol reagent (Invitrogen, Carlsbad, CA) according to the manufacturer's instructions and subsequently purified with an RNeasy Plus universal kit (Qiagen, Hilden, Germany) using on-column DNase digestion (Qiagen). RNA concentration was measured with a NanoDrop spectrophotometer (ND-1000; Isogen, Life Science, Utrecht, The Netherlands), RNA integrity was assessed using a denaturing agarose gel stained with ethidium bromide or by a bioanalyzer nanochip (Agilent Technologies, Santa Clara, CA). For quantitative real-time PCR (qRT-PCR), 2 μg of total RNA was used to synthesize cDNA using a Superscript III first-strand synthesis system (Invitrogen) according to the manufacturer's instructions. Relative quantification of target gene expression was performed using TaqMan analyses. Mm00499069-m1 TaqMan gene expression probe (Applied Biosystems, Foster City, CA) was used for qRT-PCR analysis of *Trpv6*. The cycle steps were as follows: an initial 2-min incubation at 50°C, and 10 min at 95°C followed by 40 cycles of 95°C for 15 s; 60°C for 60 s. Expression levels of *Trpv6* were normalized to *Gapdh* (Mm999999-g1). The comparative threshold cycle ($2^{-\Delta\Delta CT}$) method was used to calculate relative gene expression.

2.5 Statistical analysis

Results are displayed in the figures as means ± standard deviations of the means (SD). Additional information on the experimental groups [sample size, 95% confidence intervals (CI), effect sizes are summarized in Supplementary Table 1 for the aging mice and Supplementary Table 2 for the *kl/kl* mice and their wildtype littermates]. To consider significant difference between groups, data were analyzed using Student's t test, with Welch's correction in case of unequal variances, or analysis of variance (ANOVA) followed by Tukey's multiple comparisons tests.

3 Results

3.1 Relationship of the bone phenotype of the *kl/kl* mouse to changes in skeletal architecture that occur with chronological aging

To investigate whether the accelerated aging bone phenotype of the *Klotho* deficient mouse reflects changes in skeletal architecture that occur with chronological aging, changes in bone architecture in the tibia with age (2 months, 6 months and 20-23 months) and in wildtype (+/+) and *Klotho* mutant (*kl/kl*) mice were assessed by μCT analysis. Cross-sectional 3D-analysis of the tibia indicated a progressive decline in bone mass with chronological aging in both males and females and indicated cortical thinning with age, whereas increased cortical porosity was observed in the *kl/kl* mice in both males and females compared to wildtype (+/+) controls (Figures 1). Trabecular BV/TV decreased continuously with age in both males and females (Figures 2A, B, upper left panels). BV/TV in males decreased 37% between 2 and 6 months and 65% between 2 and 20-23 months. The change in BV/TV between 6 and 20- 23 months was not significant in males (Figure 2A, upper left panel). In females significant decreases in BV/TV were observed between 2 and 20-23 months (70%) and between 6 and 20-23 months of age (65%) (Figure 2B, upper left panel). Changes with chronological age in trabecular number followed a similar pattern as BV/TV in both males and females (Figures 2A, B middle left panels). Significantly lower BV/TV and trabecular number was observed in females compared to males at 2 months of age (Supplementary Figure 1). In contrast to chronological aging, trabecular volume and trabecular number were increased in both male and female *kl/kl* mice compared to wildtype (+/+) mice [Figures 2A, B upper right panel: BV/TV (169% and 268% increase in males and females, respectively) and Figures 2A, B, middle right panel: Trab N (135% and 215% increase in males and females, respectively)]. No significant differences between males and females were detected for wildtype (+/+) and *Klotho* deficient (*kl/kl*) mice (Supplementary Figure 1). Trabecular thickness increased in males between 2 and 6 months of age but with increasing age remained constant in both

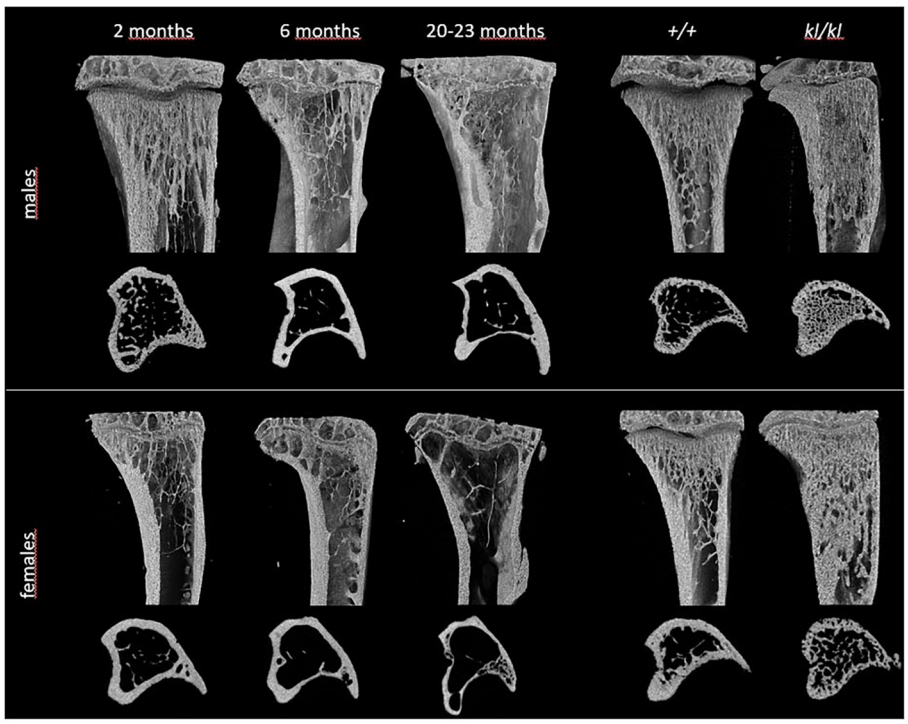

FIGURE 1
Representative 3D models of tibial epiphyses and metaphyses and cross-sections of the tibial mid-diaphysis from aging (left panels) and *klotho* wildtype (*+/+*) and deficient (*kl/kl*) mice (right panels).

males and females (Figures 2A, B lower left panels). There were no significant changes in trabecular thickness in male or female *kl/kl* mice compared to wildtype mice (+/+) (Figures 2A, B, lower right panels). With regard to cortical bone, there were no changes in total cross-sectional tissue area with advancing age in males and females and in male and female *kl/kl* mice compared to +/+ mice (Figures 3A, B upper panel). Cortical thickness increased significantly between 2 and 6 months in males and then decreased with advancing age in both males and females (Figures 3A, B middle left panels). A decrease in the thickness of cortical bone was also observed in both male and female *kl/kl* mice (Figures 3A, B middle right panels). Cortical porosity decreased with age in males, was unchanged in females and was significantly increased in male and female *Klotho* deficient (*kl/kl*) mice (192% and 340% respectively, Figures 3A, B, lower panels).

3.2 Serum data and duodenal *Trpv6* expression

There were no significant differences with age in serum calcium and phosphate levels (Figures 4A, B, left panels). Serum calcium and phosphate levels were significantly increased in the *kl/kl* mice (Figures 4A, B, right panels). Low bone density with age has been associated with intestinal calcium malabsorption, which has been suggested to be due in part to resistance to $1,25(OH)_2D_3$ (2, 6, 7). Therefore, we examined the expression of duodenal *Trpv6*, which codes for TRPV6 an epithelial calcium channel whose expression reflects calcium absorptive efficiency and is considered a rate limiting step in the process of vitamin D dependent intestinal calcium absorption (4, 27, 28). Aging resulted in a decline in *Trpv6* expression (Figure 4C, left panel). However, in *Klotho* deficient (*kl/kl*) mice duodenal *Trpv6* was significantly increased compared to wildtype mice (+/+) (Figure 4C, right panel).

4 Discussion

The *kl/kl* mouse discovered by Kuro-o in 1997 (9) was the first animal model caused by a single mutation that displayed many features of age associated disease. A major contribution to the discovery of α klotho and its function as a coreceptor for FGF23 is that it resulted in new insights that have changed the concepts related to mechanisms involved in the regulation of mineral homeostasis. Elevations in FGF23 in order to maintain phosphate excretion and a decline in klotho, which can cause a compensatory increase in FGF23, have been reported to be early events in CKD (29–31). These findings have led to a new understanding of mechanisms involved in the pathophysiology of CKD. In addition, the potential for klotho together with other known treatments to attenuate age associated pathologies and as a biomarker for certain diseases including renal, cardiovascular and neurodegenerative diseases has been suggested (32, 33). In this study in order to understand mechanisms involved in skeletal aging we examined the bone architecture of the *Klotho* deficient mouse and its relationship to changes in skeletal architecture that occur

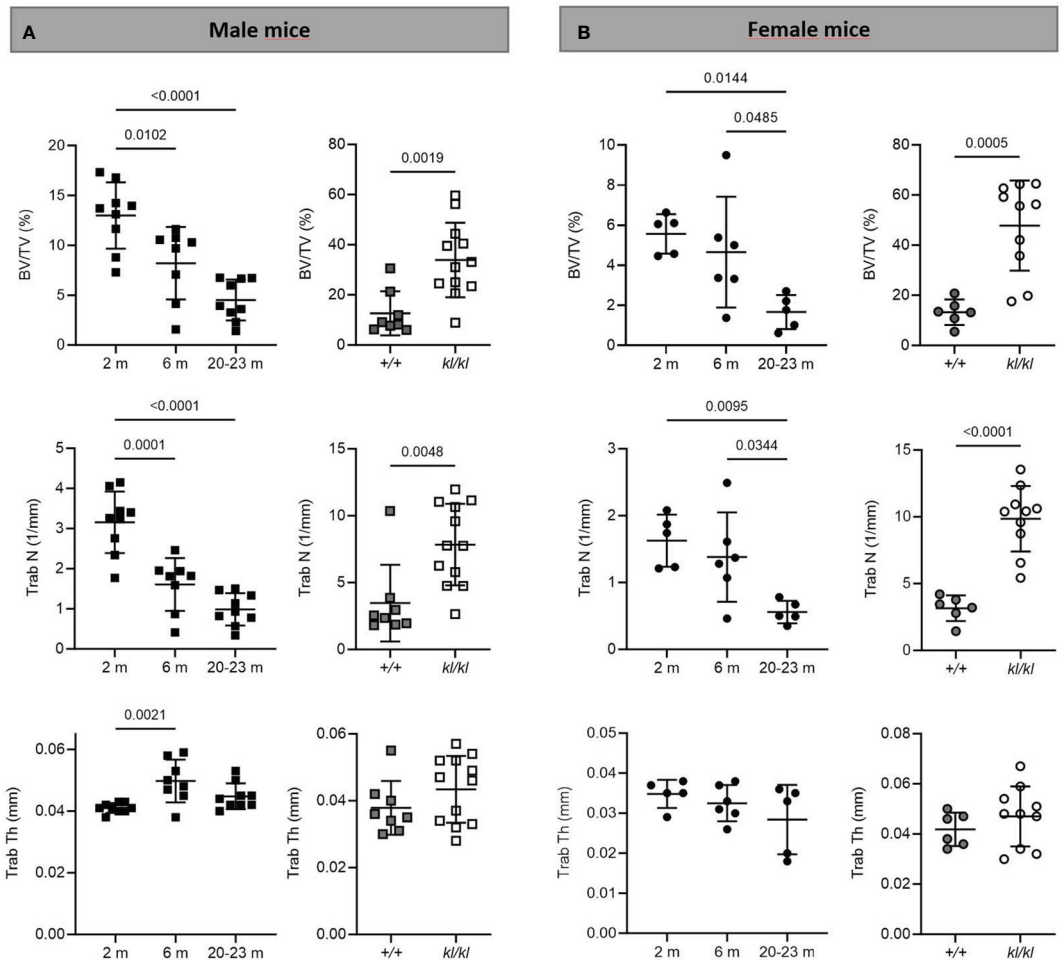

FIGURE 2
Trabecular analysis in aging and in *klotho* wildtype and deficient mice. Trabecular bone volume (BV/TV), trabecular number (Trab N), and trabecular thickness (Trab Th) were determined by μCT analysis in tibia of male **(A)** and female **(B)** aging and *klotho* wildtype (*+/+*) and deficient (*kl/kl*) mice (n = 5-12). Data are expressed as mean and SD. One-way ANOVA analysis, followed by Tukey's multiple comparisons test, was applied to detect significant effects between the different age groups and student's t-tests were performed to identify significant differences between *klotho* wildtype (*+/+*) and deficient (*kl/kl*) mice.

with chronological age. Our findings reflect differences in bone architecture as well as differences in calcium and phosphate homeostasis and expression of *Trpv6* involved in intestinal calcium absorption between the *Klotho* deficient (*kl/kl*) model of accelerated aging and the chronologically aged mouse. Although the *kl/kl* mouse has provided a new understanding of the regulation of mineral homeostasis and bone metabolism and a model of premature aging that includes atherosclerosis and infertility, our findings suggest that changes in bone architecture in the *kl/kl* mouse reflect in part systemic disturbances that differ from pathophysiological changes that occur with age including dysregulation of calcium homeostasis that contribute to age related bone loss.

Our results showed marked changes in bone architecture with age as well as in the *kl/kl* mouse. Micro CT analysis of tibia in aging mice showed that trabecular bone volume and trabecular number decreased with age in both sexes. A significant decrease in females compared to males in BV/TV and trabecular thickness was observed at 2 months. Cortical thickness decreased with advancing age in both sexes. Trabecular thickness remained relatively constant in mice with age which may be due to a compensatory mechanism. In human aging in both sexes, similar to our studies in mice, elderly individuals have been reported to have lower BV/TV accompanied by a reduction in cortical thickness and in most studies in a reduction in trabecular number (34–36). However, unlike findings observed in the elderly. an age-related reduction in trabecular thickness was not observed in mice. The changes we observed in bone architecture in aging mice as well as relatively constant trabecular thickness are similar to what has been reported by Halloran and Glatt (23, 24). Although collectively our data are similar to changes in skeletal architecture observed in the elderly, differences observed may be due in part to different mechanisms of bone loss. In the *kl/kl* mouse, although decreased cortical thickness and increased cortical porosity were observed,

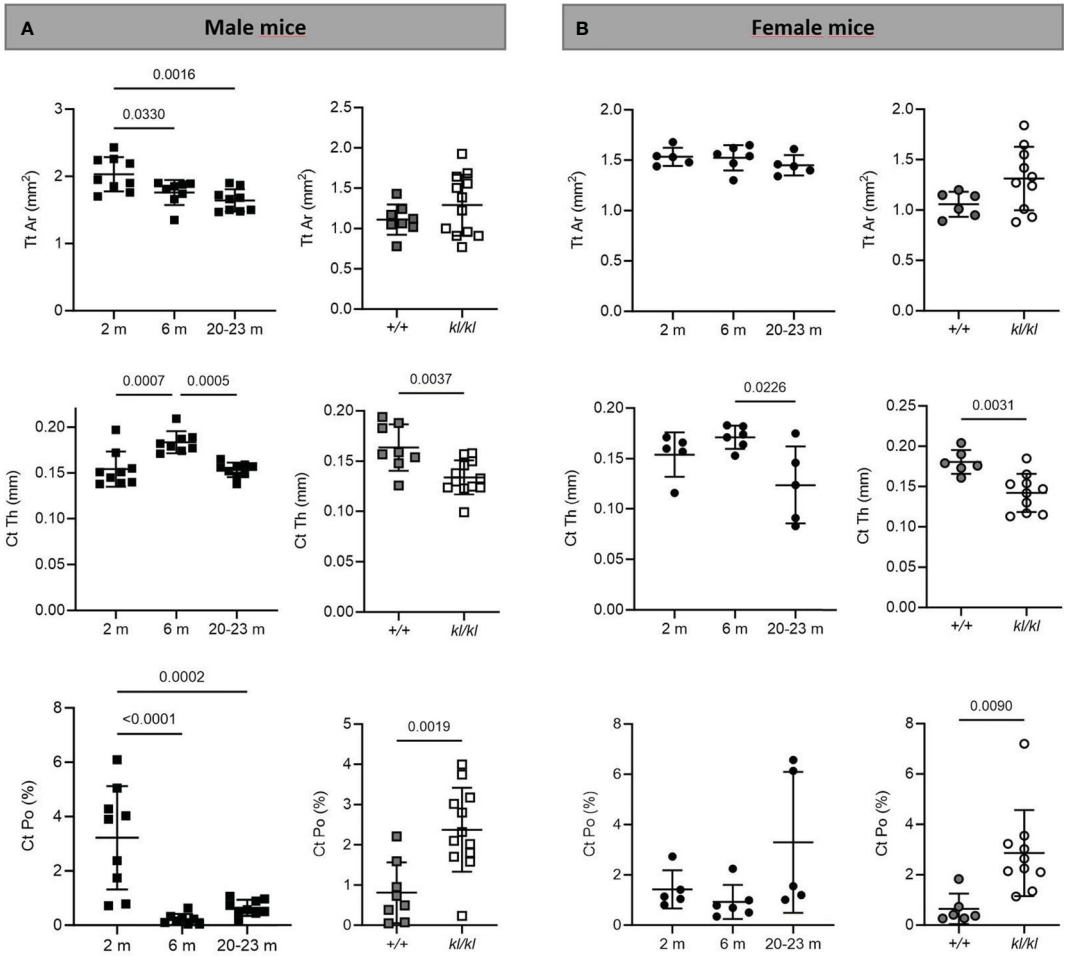

FIGURE 3
Cortical analysis in aging and in *klotho* wildtype and deficient mice. Mean total cross-sectional tissue area (Tt Ar), cortical thickness (Ct Th), and cortical porosity (Ct Po) were determined by µCT analysis in tibia of male **(A)** and female **(B)** aging and *klotho* wildtype (*+/+*) and deficient (*kl/kl*) mice (n = 5-12). Data are expressed as mean and SD. One-way ANOVA analysis, followed by Tukey's multiple comparisons test, was applied to detect significant effects between the different age groups and student's t-tests were performed to identify significant differences between *klotho* wildtype (*+/+*) and deficient (*kl/kl*) mice.

trabecular volume and number were increased which is in contrast to the pattern of bone impairment in mouse and human aging. Intestinal *Trpv6* declined with age which is consistent with the decrease in *Trpv6* reported in the 12 month old mouse and the decline in intestinal calcium transport as a function of age previously reported (37, 38). The decline in *Trpv6* with age suggests that the decrease in *Trpv6* may be one factor involved in intestinal malabsorption with age that contributes to age related bone loss. However intestinal *Trpv6* was increased in the *kl/kl* mouse. The increase in *Trpv6* may be due in part to the increase in $1,25(OH)_2D_3$ levels that have been observed in the *kl/kl* mouse (19). An increase in *Trpv6* may reflect metabolic dysfunction in the *kl/kl* mice arising in part from excess intestinal calcium absorption compared to chronological aging and reflected by an increase in serum calcium (Figure 4).

In order to understand the mechanisms that result in the bone defects observed in the *kl/kl* mouse, Yamashita et al. (39) used a bone marrow ablation model. They noted a site-specific reduction in the number and size of osteoclasts as well as high expression of osteoprotegerin (OPG), an inhibitor of osteoclastogenesis and osteoclast function. They concluded that the abnormal trabecular bone structure is due to part to a defect in bone resorption and that the *kl/kl* mice exhibit an osteopetrotic as well as an osteopenic phenotype. An earlier study by Kawaguchi et al. suggested that the phenotype of the *kl/kl* mouse is due to independent impairment of osteoblast as well as osteoclast differentiation (40).

Different bone phenotypes have been reported for the *Klotho* deficient mice. Kaludjerovic and Lanske reviewed the findings from several research groups that have independently investigated the bone phenotype of *Klotho* deficient mice (20). They concluded that although it had been reported that *Klotho* deficient mice have osteoporotic bones, the common observation across these studies was that the *kl/kl* mouse as well as the *Klotho*$^{-/-}$ mouse have high trabecular bone volume, similar to our findings. The authors

10.3389/fendo.2024.1310466

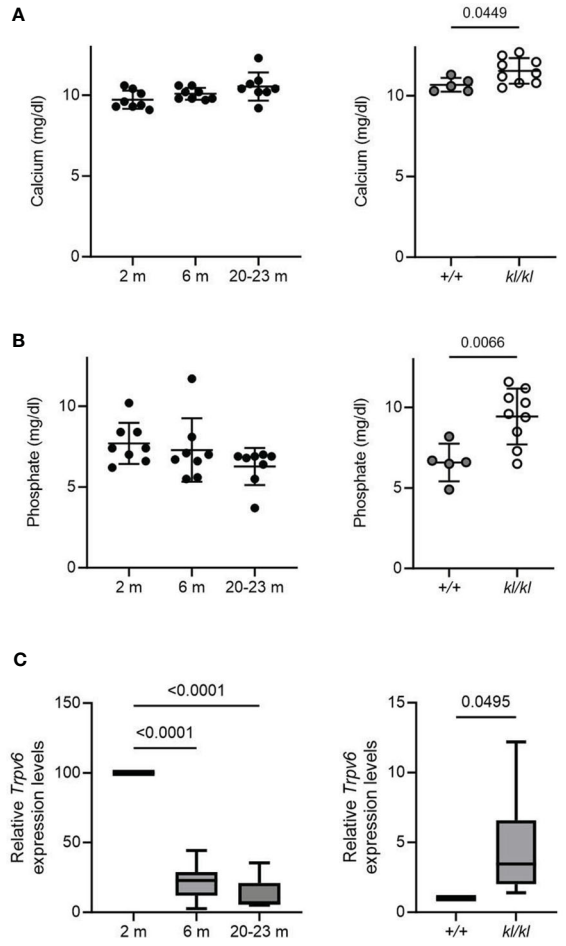

FIGURE 4
Serum calcium and phosphate and duodenal *Trpv6* expression in aging and in *klotho* wildtype and deficient mice. Serum calcium **(A)** and phosphate **(B)** concentrations were determined in aging and in *klotho* wildtype (*+/+*) and deficient (*kl/kl*) mice. Data from male and female mice were pooled (n = 5-9). **(C)** *Trpv6* transcript levels in duodenum were determined by qPCR analysis in aging and in *klotho* wildtype (*+/+*) and deficient (*kl/kl*) mice. Data from male and female mice were pooled (n = 6-8). All data are expressed as mean and SD. One-way ANOVA analysis, followed by Tukey's multiple comparisons test, or student's t-tests were performed to identify significant differences.

suggested that the different bone phenotypes reported for the *Klotho* deficient mice may be due in part to analysis of different bone regions and site-specific changes in the bones of the *Klotho* deficient mice. Mature osteocyte specific knock down of *Klotho* was shown to result in significantly higher trabecular volume and connectivity in 5-week-old animals compared to healthy controls (41, 42). This finding indicates a role for klotho in the bone independent of the endocrine effects on bone due to global *Klotho* deficiency and that klotho is a negative regulator of bone formation.

With regard to further mechanisms involved in the *kl/kl* accelerated aging model, it was noted that the aging symptoms of the *kl/kl* mice were alleviated when the mice were fed a vitamin D-deficient or low phosphate diet indicating an underlying metabolic dysfunction arising from excess phosphate or $1,25(OH)_2D_3$ (43, 44). Whether excess phosphate or $1,25(OH)_2D_3$ is responsible for the aging phenotype had been a matter of debate (44, 45). Studies showing that ablation of the Napi2a gene from *Klotho*$^{-/-}$ mice result in reduction or elimination of soft tissue calcification even in the presence of high $1,25(OH)_2D_3$ and calcium levels suggested that retention of phosphate may be one key factor involved in accelerated aging in the *Klotho*$^{-/-}$ deficient mouse model (46). It was also suggested that the metabolic dysfunction in *kl/kl* mice may be due to both increased calcium and phosphate resulting in calcium phosphate precipitates and calciprotein particles that can induce cell damage and inflammation (8).

Since the discovery of the *Klotho* deficient models additional murine models of accelerated aging have been developed which may provide new insight into mechanisms involved in age related diseases including age related skeletal disease (47–50). One model that has been found to reflect natural aging is the *Ercc1*$^{-/\Delta}$ model which carries mutations in the ERCC-XPF exonuclease, important for multiple DNA repair pathways (48). The *Ercc1*$^{-/\Delta}$ mice develop many age-related diseases including severe and progressive osteoporosis, premature senescence of osteoblastic progenitors and enhanced osteoclastogenesis (48). At 22 weeks of age the mice had > 60% reduction in BV/TV, reduced trabecular thickness and an increase in trabecular space compared to WT controls demonstrating the importance of ERCC1-XPF dependent DNA repair for maintaining normal bone homeostasis (48). Another marker of aging is telomerase dysfunction, a cause of cellular senescence. The accelerated aging mouse model of telomere dysfunction (*Terc*$^{-/-}$ mice; deletion of telomerase reverse transcriptase) was suggested as a model for human bone aging since at three months of age *Terc*$^{-/-}$ mice had significant decreases in BV/TV, trabecular number, trabecular thickness, increased trabecular spacing as well as decreased cortical thickness and increased porosity. These skeletal changes became more pronounced with age. Osteoblast dysfunction was noted as the primary mechanism for osteoporosis in these mice (47). Although further studies are needed these findings suggest that mice with defects in telomerase maintenance may be an additional useful model for studying age related osteoporosis.

In summary, studying mouse models of accelerated aging has provided new insight into mechanisms involved in multiple pathologies including age related skeletal disease. The *Klotho* deficient mouse model provided a new understanding of the regulation of mineral homeostasis and bone metabolism. There is a strong rationale for the use of additional mouse models of accelerated aging which mimic changes observed with human aging. It should be noted that each mouse model may reflect different traits related to skeletal changes that occur with human aging. Future studies are needed to determine which factors, identified using models of accelerated aging, can be potential targets for therapeutic approaches to delay skeletal aging.

Data availability statement

The original contributions presented in the study are included in the article/Supplementary Material. Further inquiries can be directed to the corresponding author.

Ethics statement

The animal study was approved by Institutional Animal Care and Use committee Rutgers, New Jersey Medical School. The study was conducted in accordance with the local legislation and institutional requirements.

Author contributions

LV: Conceptualization, Data curation, Formal Analysis, Investigation, Writing – original draft, Writing – review & editing. SL: Conceptualization, Data curation, Formal Analysis, Investigation, Writing – original draft, Writing – review & editing. VV: Conceptualization, Data curation, Formal Analysis, Investigation, Writing – original draft, Writing – review & editing. GC: Conceptualization, Funding acquisition, Supervision, Writing – review & editing. SC: Conceptualization, Data curation, Formal Analysis, Funding acquisition, Investigation, Supervision, Writing – original draft, Writing – review & editing.

Funding

The author(s) declare financial support was received for the research, authorship, and/or publication of this article. This was supported by the National Institutes of Health grant AG-04452 and DK112365 to SC and Fonds voor Wetenschappelijk Onderzoek-Flanders: Hercules-I013518N to GC.

Acknowledgments

We would like to thank P. Dhawan, C. Hsaio, M. Aburadi and J. De La Cruz for their assistance in certain aspects of this investigation We are grateful to Dr. M. Kuro-o for providing us with the *kl/kl* mice.

Conflict of interest

The authors declare that the research was conducted in the absence of any commercial or financial relationships that could be construed as a potential conflict of interest.

Publisher's note

Supplementary material

The Supplementary Material for this article can be found online at: https://www.frontiersin.org/articles/10.3389/fendo.2024.1310466/full#supplementary-material

SUPPLEMENTARY FIGURE 1
Comparison of trabecular bone volume and number between male and female mice. Direct comparison of tibial μCT analysis of trabecular bone volume **(A)** and trabecular number **(B)** between male (black bars) and female (grey bars) aging and *klotho* wildtype (*+/+*) and deficient (*kl/kl*) mice (n = 5-12). Data are expressed as mean and SD. Two-way ANOVA analysis followed by Tukey's multiple comparisons test. $^{\#}p < 0.05$ vs. 2 and 6 months; $^{+}p < 0.05$ vs. 2 months; $^{*}p < 0.05$ compared to +/+ (WT) mice in that same sex, $ vs male mice of the same age.

References

1. Lopez-Otin C, Blasco MA, Partridge L, Serrano M, Kroemer G. Hallmarks of aging: An expanding universe. *Cell* (2023) 186(2):243–78. doi: 10.1016/j.cell.2022.11.001

2. Pattanaungkul S, Riggs BL, Yergey AL, Vieira NE, O'Fallon WM, Khosla S. Relationship of intestinal calcium absorption to 1,25-dihydroxyvitamin D [1,25(OH)2D] levels in young versus elderly women: evidence for age-related intestinal resistance to 1,25(OH)2D action. *J Clin Endocrinol Metab* (2000) 85(11):4023–7. doi: 10.1210/jc.85.11.4023

3. Christakos S, Ajibade DV, Dhawan P, Fechner AJ, Mady LJ. Vitamin D: metabolism. *Rheum Dis Clin North Am* (2012) 38(1):1–11, vii. doi: 10.1016/j.rdc.2012.03.003

4. Christakos S, Veldurthy V, Patel N, Wei R. Intestinal regulation of calcium: vitamin D and bone physiology. *Adv Exp Med Biol* (2017) 1033:3–12. doi: 10.1007/978-3-319-66653-2_1

5. Fleet JC. The role of vitamin D in the endocrinology controlling calcium homeostasis. *Mol Cell Endocrinol* (2017) 453:36–45. doi: 10.1016/j.mce.2017.04.008

6. Scopacasa F, Wishart JM, Horowitz M, Morris HA, Need AG. Relation between calcium absorption and serum calcitriol in normal men: evidence for age-related intestinal resistance to calcitriol. *Eur J Clin Nutr* (2004) 58(2):264–9. doi: 10.1038/sj.ejcn.1601777

7. Wood RJ, Fleet JC, Cashman K, Bruns ME, Deluca HF. Intestinal calcium absorption in the aged rat: evidence of intestinal resistance to 1,25(OH)2 vitamin D. *Endocrinol* (1998) 139(9):3843–8. doi: 10.1210/endo.139.9.6176

8. Kuro OM. Aging and FGF23-klotho system. *Vitam Horm* (2021) 115:317–32. doi: 10.1016/bs.vh.2020.12.013

9. Kuro-o M, Matsumura Y, Aizawa H, Kawaguchi H, Suga T, Utsugi T, et al. Mutation of the mouse klotho gene leads to a syndrome resembling ageing. *Nature* (1997) 390(6655):45–51. doi: 10.1038/36285

10. Nabeshima Y, Imura H. alpha-Klotho: a regulator that integrates calcium homeostasis. *Am J Nephrol* (2008) 28(3):455–64. doi: 10.1159/000112824

11. Kurosu H, Ogawa Y, Miyoshi M, Yamamoto M, Nandi A, Rosenblatt KP, et al. Regulation of fibroblast growth factor-23 signaling by klotho. *J Biol Chem* (2006) 281(10):6120–3. doi: 10.1074/jbc.C500457200

12. Nakatani T, Sarraj B, Ohnishi M, Densmore MJ, Taguchi T, Goetz R, et al. *In vivo* genetic evidence for klotho-dependent, fibroblast growth factor 23 (Fgf23)-mediated regulation of systemic phosphate homeostasis. *FASEB J* (2009) 23(2):433–41. doi: 10.1096/fj.08-114397

13. Shimada T, Kakitani M, Yamazaki Y, Hasegawa H, Takeuchi Y, Fujita T, et al. Targeted ablation of Fgf23 demonstrates an essential physiological role of FGF23 in phosphate and vitamin D metabolism. *J Clin Invest* (2004) 113(4):561–8. doi: 10.1172/JCI200419081

14. Agoro R, White KE. Regulation of FGF23 production and phosphate metabolism by bone-kidney interactions. *Nat Rev Nephrol* (2023) 19(3):185–93. doi: 10.1038/s41581-022-00665-x

15. Erben RG, Andrukhova O. FGF23-Klotho signaling axis in the kidney. *Bone* (2017) 100:62–8. doi: 10.1016/j.bone.2016.09.010

16. Hu MC, Shi M, Moe OW. Role of alphaKlotho and FGF23 in regulation of type II Na-dependent phosphate co-transporters. *Pflugers Arch* (2019) 471(1):99–108. doi: 10.1007/s00424-018-2238-5

17. Hu MC, Shi M, Zhang J, Pastor J, Nakatani T, Lanske B, et al. Klotho: a novel phosphaturic substance acting as an autocrine enzyme in the renal proximal tubule. *FASEB J* (2010) 24(9):3438–50. doi: 10.1096/fj.10-154765

18. Urakawa I, Yamazaki Y, Shimada T, Iijima K, Hasegawa H, Okawa K, et al. Klotho converts canonical FGF receptor into a specific receptor for FGF23. *Nature* (2006) 444(7120):770–4. doi: 10.1038/nature05315

19. Yoshida T, Fujimori T, Nabeshima Y. Mediation of unusually high concentrations of 1,25-dihydroxyvitamin D in homozygous klotho mutant mice by increased expression of renal 1alpha-hydroxylase gene. *Endocrinol* (2002) 143(2):683–9. doi: 10.1210/endo.143.2.8657

20. Kaludjerovic J, Komaba H, Lanske B. Effects of klotho deletion from bone during chronic kidney disease. *Bone* (2017) 100:50–5. doi: 10.1016/j.bone.2017.02.006

21. Yamashita T, Nabeshima Y, Noda M. High-resolution micro-computed tomography analyses of the abnormal trabecular bone structures in klotho gene mutant mice. *J Endocrinol* (2000) 164(2):239–45. doi: 10.1677/joe.0.1640239

22. Yamashita T, Nifuji A, Furuya K, Nabeshima Y, Noda M. Elongation of the epiphyseal trabecular bone in transgenic mice carrying a klotho gene locus mutation that leads to a syndrome resembling aging. *J Endocrinol* (1998) 159(1):1–8. doi: 10.1677/joe.0.1590001

23. Glatt V, Canalis E, Stadmeyer L, Bouxsein ML. Age-related changes in trabecular architecture differ in female and male C57BL/6J mice. *J Bone Miner Res* (2007) 22 (8):1197–207. doi: 10.1359/jbmr.070507

24. Halloran BP, Ferguson VL, Simske SJ, Burghardt A, Venton LL, Majumdar S. Changes in bone structure and mass with advancing age in the male C57BL/6J mouse. *J Bone Miner Res* (2002) 17(6):1044–50. doi: 10.1359/jbmr.2002.17.6.1044

25. Verlinden L, Doms S, Janssens I, Meyer MB, Pike JW, Carmeliet G, et al. Neuropilin 2 in osteoblasts regulates trabecular bone mass in male mice. *Front Endocrinol (Lausanne)* (2023) 14:1223021. doi: 10.3389/fendo.2023.1223021

26. Bouxsein ML, Boyd SK, Christiansen BA, Guldberg RE, Jepsen KJ, Muller R. Guidelines for assessment of bone microstructure in rodents using micro-computed tomography. *J Bone Miner Res* (2010) 25(7):1468–86. doi: 10.1002/jbmr.141

27. Song Y, Peng X, Porta A, Takanaga H, Peng JB, Hediger MA, et al. Calcium transporter 1 and epithelial calcium channel messenger ribonucleic acid are differentially regulated by 1,25 dihydroxyvitamin D3 in the intestine and kidney of mice. *Endocrinol* (2003) 144(9):3885–94. doi: 10.1210/en.2003-0314

28. Van Cromphaut SJ, Dewerchin M, Hoenderop JG, Stockmans I, Van Herck E, Kato S, et al. Duodenal calcium absorption in vitamin D receptor-knockout mice: functional and molecular aspects. *Proc Natl Acad Sci U S A* (2001) 98(23):13324–9. doi: 10.1073/pnas.231474698

29. Christakos S, Li S, de la Cruz J, Bikle DD. New developments in our understanding of vitamin metabolism, action and treatment. *Metabolism* (2019) 98:112–20. doi: 10.1016/j.metabol.2019.06.010

30. Kuro OM, Moe OW. FGF23-alphaKlotho as a paradigm for a kidney-bone network. *Bone* (2017) 100:4–18. doi: 10.1016/j.bone.2016.11.013

31. Quarles LD. Role of FGF23 in vitamin D and phosphate metabolism: implications in chronic kidney disease. *Exp Cell Res* (2012) 318(9):1040–8. doi: 10.1016/j.yexcr.2012.02.027

32. Abraham CR, Li A. Aging-suppressor Klotho: Prospects in diagnostics and therapeutics. *Ageing Res Rev* (2022) 82:101766. doi: 10.1016/j.arr.2022.101766

33. Prud'homme GJ, Kurt M, Wang Q. Pathobiology of the Klotho antiaging protein and therapeutic considerations. *Front Aging* (2022) 3:931331. doi: 10.3389/fragi.2022.931331

34. Khosla S, Riggs BL, Atkinson EJ, Oberg AL, McDaniel LJ, Holets M, et al. Effects of sex and age on bone microstructure at the ultradistal radius: a population-based noninvasive *in vivo* assessment. *J Bone Miner Res* (2006) 21(1):124–31. doi: 10.1359/JBMR.050916

35. Macdonald HM, Nishiyama KK, Kang J, Hanley DA, Boyd SK. Age-related patterns of trabecular and cortical bone loss differ between sexes and skeletal sites: a population-based HR-pQCT study. *J Bone Miner Res* (2011) 26(1):50–62. doi: 10.1002/jbmr.171

36. van den Bergh JP, Szulc P, Cheung AM, Bouxsein M, Engelke K, Chapurlat R. The clinical application of high-resolution peripheral computed tomography (HR-pQCT) in adults: state of the art and future directions. *Osteoporos Int* (2021) 32 (8):1465–85. doi: 10.1007/s00198-021-05999-z

37. van Abel M, Huybers S, Hoenderop JG, van der Kemp AW, van Leeuwen JP, Bindels RJ. Age-dependent alterations in Ca2+ homeostasis: role of TRPV5 and TRPV6. *Am J Physiol Renal Physiol* (2006) 291(6):F1177–83. doi: 10.1152/ajprenal.00038.2006

38. Armbrecht HJ, Zenser TV, Bruns ME, Davis BB. Effect of age on intestinal calcium absorption and adaptation to dietary calcium. *Am J Physiol* (1979) 236(6): E769–74. doi: 10.1152/ajpendo.1979.236.6.E769

39. Yamashita T, Yoshitake H, Tsuji K, Kawaguchi N, Nabeshima Y, Noda M. Retardation in bone resorption after bone marrow ablation in klotho mutant mice. *Endocrinol* (2000) 141(1):438–45. doi: 10.1210/endo.141.1.7252

40. Kawaguchi H, Manabe N, Miyaura C, Chikuda H, Nakamura K, Kuro-o M. Independent impairment of osteoblast and osteoclast differentiation in klotho mouse exhibiting low-turnover osteopenia. *J Clin Invest* (1999) 104(3):229–37. doi: 10.1172/JCI5705

41. Komaba H, Kaludjerovic J, Hu DZ, Nagano K, Amano K, Ide N, et al. Klotho expression in osteocytes regulates bone metabolism and controls bone formation. *Kidney Int* (2017) 92(3):599–611. doi: 10.1016/j.kint.2017.02.014

42. Komaba H, Lanske B. Role of Klotho in bone and implication for CKD. *Curr Opin Nephrol Hypertens* (2018) 27(4):298–304. doi: 10.1097/MNH.0000000000000423

43. Morishita K, Shirai A, Kubota M, Katakura Y, Nabeshima Y, Takeshige K, et al. The progression of aging in klotho mutant mice can be modified by dietary phosphorus and zinc. *J Nutr* (2001) 131(12):3182–8. doi: 10.1093/jn/131.12.3182

44. Tsujikawa H, Kurotaki Y, Fujimori T, Fukuda K, Nabeshima Y. Klotho, a gene related to a syndrome resembling human premature aging, functions in a negative regulatory circuit of vitamin D endocrine system. *Mol Endocrinol* (2003) 17(12):2393–403. doi: 10.1210/me.2003-0048

45. Kuro OM. A phosphate-centric paradigm for pathophysiology and therapy of chronic kidney disease. *Kidney Int Suppl (2011)* (2013) 3(5):420–6. doi: 10.1038/kisup.2013.88

46. Ohnishi M, Nakatani T, Lanske B, Razzaque MS. Reversal of mineral ion homeostasis and soft-tissue calcification of klotho knockout mice by deletion of vitamin D 1alpha-hydroxylase. *Kidney Int* (2009) 75(11):1166–72. doi: 10.1038/ki.2009.24

47. Brennan TA, Egan KP, Lindborg CM, Chen Q, Sweetwyne MT, Hankenson KD, et al. Mouse models of telomere dysfunction phenocopy skeletal changes found in human age-related osteoporosis. *Dis Model Mech* (2014) 7(5):583–92. doi: 10.1242/dmm.014928

48. Chen Q, Liu K, Robinson AR, Clauson CL, Blair HC, Robbins PD, et al. DNA damage drives accelerated bone aging via an NF-kappaB-dependent mechanism. *J Bone Miner Res* (2013) 28(5):1214–28. doi: 10.1002/jbmr.1851

49. Farr JN, Khosla S. Cellular senescence in bone. *Bone* (2019) 121:121–33. doi: 10.1016/j.bone.2019.01.015

50. Hambright WS, Niedernhofer LJ, Huard J, Robbins PD. Murine models of accelerated aging and musculoskeletal disease. *Bone* (2019) 125:122–7. doi: 10.1016/j.bone.2019.03.002

frontiers | Frontiers in Endocrinology

TYPE Systematic Review
PUBLISHED 06 February 2024
DOI 10.3389/fendo.2024.1323595

OPEN ACCESS

EDITED BY
Katherine A. Staines,
University of Brighton, United Kingdom

REVIEWED BY
Lifei Liu,
The People's Hospital of Liaoning Province, China
Blair Hamilton,
University of Brighton, United States

*CORRESPONDENCE
Lin Wang
wanglin123@126.com

RECEIVED 18 October 2023
ACCEPTED 15 January 2024
PUBLISHED 06 February 2024

CITATION
Liu S, Wu S, Qi J and Wang L (2024) Effect of traditional Chinese fitness exercises on bone mineral density in postmenopausal women: a network meta-analysis of randomized controlled trials.
Front. Endocrinol. 15:1323595.
doi: 10.3389/fendo.2024.1323595

Effect of traditional Chinese fitness exercises on bone mineral density in postmenopausal women: a network meta-analysis of randomized controlled trials

Shijie Liu, Sijun Wu, Juancai Qi and Lin Wang*

School of Physical Education, Wuhan University of Technology, Wuhan, China

We aimed to evaluate the clinical efficacy of five traditional Chinese fitness exercises (Baduanjin, Taijiquan, Wuqinxi, Yijinjing, and Liuzijue), as well as their efficacy when combined with drug therapy, in the treatment of decreased bone mineral density in postmenopausal women

Methods: This study strictly followed the evaluation guidelines of PRISMA and followed the "PICOS" principle outlined in the Cochrane Handbook. We performed a systematic search on Web of Science, Springer Link, Scopus, EMBASE, EBSCO, PubMed, the Cochrane Library, CNKI, Wanfang, CBMdisc, and the VIP Database, and we targeted RCTs studying the effect of TCE on BMD in postmenopausal women published prior to September 2023. The quality of the literature and the risk of bias of the included studies were assessed according to ROB2 and GRADE criteria, and data analysis was performed using Stata 14.

Results: A total of 33 RCTs (3658 post-menopausal women) were included. Network meta-analysis showed that Taiji (SMD=0.72, 95% CI: 0.22, 1.21, P<0.01) and Yijinjing (SMD=0.51, 95% CI: 0.03, 0.99, P<0.05) were significantly superior to conventional rehabilitation in lumbar BMD. In terms of improvement of femoral neck BMD, Baduanjin (SMD=1.63, 95% CI: -3.58, 6.85, P<0.001) and Taiji (SMD=0.46, 95% CI: 0.14, 0.79, P<0.05) had statistically different outcomes to conventional rehabilitation. Regarding Ward's triangle BMD, Taiji (SMD= 0.32, 95% CI: 0.14, 0.50, P< 0.05) had statistically different outcomes to conventional rehabilitation. The results of the SUCRA probability ranking showed that Baduanjin + drug interventions achieved the most significant improvement in lumbar BMD (SUCRA=83.6%) and femoral neck BMD (SUCRA=90.2%). Taiji + drug interventions most effectively improved Ward's triangle BMD (SUCRA=86.0%). In terms of traditional Chinese fitness exercises alone, Taiji was the most effective in improving lumbar BMD (SUCRA=64.4%) and Ward's triangle BMD (SUCRA=46.8%), and Baduanjin was the most effective in treating femoral neck BMD (SUCRA=89.9%).

Conclusion: Traditional Chinese fitness exercises can significantly improve the BMD levels of postmenopausal women. Taiji, Yijinjing, and Baduanjin combined

with medication showed better intervention effects overall. However, due to the limitations of the number of studies and sample sizes of individual interventions, definitive conclusions need to be verified by more high-quality studies.

KEYWORDS

traditional Chinese fitness exercises, BMD, network meta-analysis, postmenopausal, women

Introduction

As women age, they experience degeneration of ovarian function. A lack of estrogen leads to reduced bone mass, decreased bone density, and structural changes in bone tissue, which increases bone fragility and fracture susceptibility (1–4). In an observational study, lack of estrogen increased osteoporosis-related fractures by about 50% (5). An estimated 32 million people in Europe had osteoporosis in 2019, with around 80% of cases involving postmenopausal women (6), where the residual lifetime risk of a hip fracture at the age of 50 years ranged from 7.0% (Romania) to 25.1% (Sweden) (7). As human life expectancy increases and the global aging process accelerates, the prevalence of postmenopausal osteoporosis will increase in the coming decades (8, 9). The data show that the rate of bone loss in older women is significantly accelerated 1–10 years after menopause, with an annual loss rate of 1.5–2.5% and a reduction in BMD, which increases the risk of fracture by 2.6 times (10). Recently, European data showed that menopausal women are 40% more likely to experience fractures (11). In summary, postmenopausal osteoporosis and the accompanying loss of bone density have become a severe public health problem and a threat to older women's health.

Given the prevalence of postmenopausal osteoporosis and the many disadvantages of pharmacological treatment, such as long cycle times, high costs, adverse effects, and poor compliance, exercise therapy is gaining increasing attention as a complementary therapy to pharmacological treatment, due to its advantages of being economical and having few side effects (12). In recently years, traditional Chinese exercise (TCE), including Taiji, Yijinjing, Baduanjin, Wuqinxi, and Liuzijue, has played a significant role in the treatment of osteoporosis, and has been widely and flexibly used in clinical practice (13–15). Compared to other exercises, TCEs are easy to learn and are not restricted by exercise venues. They impact personal health and disease prevention by improving body balance (16), strengthening lower limb muscles (17, 18), and preventing postmenopausal osteoporosis (19).

Despite differences in the design of experiments testing this, TCE is a safe option for the prevention and treatment of primary osteoporosis or bone loss. Recent meta-analyses have shown that Taiji interventions prevent further osteoporotic BMD decline in elderly female patients with osteopenia or osteoporosis (20). Another meta-analysis showed that, of a range of exercises, Baduanjin was most effective in inhibiting or even reversing BMD in older adults with osteoporosis (21). However, there has been a lack of systematic reviews of TCE's effects on BMD in older postmenopausal adults, other than Taiji. Furthermore, a recent meta-analysis suggested that different exercise patterns may affect BMD in older adults (10). Therefore, it is crucial to systematically determine the pathways of BMD influence of TCE in postmenopausal women.

Therefore, we aimed to integrate the relevant clinical evidence of the direct and indirect comparative relationships between different TCEs using a network analysis. The effect of different TCEs on BMD at different sites was assessed using a network analysis, based on a probability ranking of the superiority of the index efficacy in postmenopausal women.

Methods

Search strategy

This study followed the international guidelines for writing meta-analyses (PRISMA) (22). The registration number for our study is INPLASY2022110030 (DOI number 10.37766/inplasy2022.11.0030). The literature was obtained from Web of Science, Springer link, Scopus EMBASE, Cochrane Library, EBSCO, PubMed, CNKI, Wanfang, CBMdisc, and VIPdatabases. Our study aimed to identify published RCTs on the effects of TCE on BMD in postmenopausal women, with a deadline of 30 September 2023. The words used in the search of databases included "Taiji (Tai Chi or Tai Ji Quan or Taijiquan, etc.) or Health Qigong or Qigong or Qi Gong or Chi Kung or Baduanjin or Wuqinxi or Yijinjing or Liuzijue or traditional Chinese exercise AND bone density or bone mass or osteoporosis AND menopause or postmenopausal or women or female. Taking PubMed, Embase, and China Knowledge as examples, Appendix I outlines the specific search strategies.

Two researchers (S.J.L. and W.L.) independently determined the relevant research data. The degree of agreement between the two researchers was quantified using Cohen's Kappa; the Cohen's

Kappa value of the two researchers was 0.679, indicating good agreement (23).

Inclusion criteria and study selection

Two independent reviewers (S.J.L. and W.L.) examined the titles and abstracts of the retrieved articles and performed the primary screening based on inclusion and exclusion criteria. After obtaining the full text of the RCTs, the full text of the first selected studies was rechecked, and the studies to be analyzed were finalized. A Cohen's Kappa value of 0.655 was obtained between the researchers, indicating moderate agreement. The studies were further reviewed by the two independent researchers until a consensus was reached. The third reviewer's opinion (S.J.W.) was adopted without a contract.

Eligibility criteria for inclusion in the study were as follows: (1) RCTs; (2) the participants were diagnosed as postmenopausal women with osteopenia, or with normal bone mass, and had no serious complications or other diseases; (3) the experimental group included traditional Chinese fitness exercises (e.g., Taiji, Baduanjin, Wuqinxi, Yijinjing, and Liuzijue), and was compared with control groups (e.g., drugs, usual care, and exercise training); (4) outcome indicators included BMD in the lumbar spine or femoral neck, or Ward's triangle BMD, as one of the outcome indicators; (5) before the test, each group of indicators showed a consistent baseline among subjects; (6) the study data were in the form of mean ± standard deviation or could be transformed into M ± SD (if the data in the literature were presented as the standard error (*SE*), then SD=SE× $\sqrt{N}$ (*N* is the sample size) was used for transformation); and (7) the studies were published in Chinese or English.

The exclusion criteria were: (1) duplicated studies; (2) no major TCE interventions; (3) abstract-only articles and non-RCT studies; (4) conference emails not able to be contacted; and (5) no data or data not clearly reported for analysis.

Data extraction and quality assessment

We followed the PICO model in the reporting, design, and descriptive data extraction, including the following: first author, country, and year of publication, sample size (attrition rate), mean age or age range, years of menopause, bone mass of participant, intervention design (intervention, time, frequency), and main outcome indicators. Detailed information for inclusion in the study is shown in Table 1.

This study assessed the methodological quality of the randomized controlled trials included in the survey using RoB2, which considered the following domains: bias during randomization, inclination to deviate from established interventions (including the effect of intervention allocation and the impact of intervention adherence), bias related to missing outcome data, bias related to measurement of outcomes, and prejudice related to reporting the results selectively. Under each domain, there are multiple "signaling questions", each of which provides five answers: Yes, Probably Yes, Probably No, No, and No Information, and based on the answers to the signaling questions, RoB2 generates a recommended risk assessment outcome.

Two independent reviewers (S.J.L. and W.L.) performed a quality assessment of the literature, and based on the RoB2 risk assessment, the included randomized controlled trials were classified as "high risk of bias", "some concerns", and "low risk of bias".

In addition, we invited the first two independent reviewers to review the literature in which there was inconsistency in opinion until a consensus was reached. In the absence of agreement, the third reviewer's opinion (S.J.W.) was adopted.

Statistical analysis

A traditional meta-analysis was performed by applying the MetaXL program (version 5.3). Given the small sample size of the screened and suitable literature and the slight differences in evaluation tools and units used in individual studies, the standardized mean difference (SMD) and its 95% confidence interval (CI) calculated by the Hedges'g method were used to estimate the relative effect of each intervention. For each direct comparison, effect sizes were aggregated using an inverse heterogeneity (IVhet) model, which corrects for heterogeneity and generates more robust results relative to traditional fixed- and random-effects models.

Both the Q-test and I^2 results determined heterogeneity in the literature. The meta-analysis was performed using a fixed-effects model when $P \geq 0.1$ for the Q-test and $I^2 < 50\%$ indicated that inter-study heterogeneity was within acceptable limits, and vice versa using the random-effects model. The outcomes were categorized as either very low (<25%), low 25–50%), moderate (50–75%), or significant (>75%) (56). Furthermore, publication bias was measured using Doi plots with the LFK index, which has been shown to have higher accuracy than traditional funnel plots with the egger test, especially when the number of studies is small. Finally, sources of heterogeneity were sought through sensitivity analyses (rejected one by one) and subgroup analyses.

A network meta-analysis was performed using Stata 14.0 in a frequency-based framework. A grid relationship diagram was drawn by network meta-analysis (in the diagram, each node indicates the intervention, the size of the area of the node indicates the number of samples corresponding to the intervention, and the thickness of the line connecting the nodes indicates the number of studies included for the intervention) (57). When there was a closed-loop structure between interventions, inconsistency tests were required, and the model type was selected accordingly. If the lower limit of the 95% CI of the inconsistency factor's (IF) value was zero (or close to zero), this indicated that the direct evidence and indirect evidence were consistent (58). Finally, the area under the cumulative ranked probability curve (surface under the cumulative, SUCRA) showed the magnitude of the likelihood of each intervention being the best intervention (56).

Evidence certainty assessment

The Grading Recommendations to Assess Development and Evaluation system (GRADE) is an evidence evaluation system,

TABLE 1 Summary table of the studies.

Reference	Location (Language)	Participant Characteristics				Intervention Program	Intervention Characteristics			Outcome Measured	Adverse Event; Follow-Up
		Sample Size (Attrition Rate)	Mean Age or Age Range	Duration of Menopause (years)	Bone Mass of Participants		Frequency (weekly)	Time (min)	Duration (week)		
Cai. et al.(2018) (24)	Guangdong, China (Chinese)	60(0%)	EG: 51.4 ± 4.9 CG: 52.1 ± 4.2	>2	(-2.5SD<BMD≤ -1SD)	EG: Baduanjin (DT) CG: Drug group	5	60	48	①	No;No
Chen (2016) (25)	Kunming, China (Chinese)	100 (11.43%)	EG:61.2 ± 4.9 CG:60.8 ± 5.8	EG: 7.2 ± 1.5 CG: 7.5 ± 1.2	(BMD>-1SD)	EG: Baduanjin (DT) CG: Drug group	7	NR	48	① ②	No;No
Su (2018) (26)	Gansu, China (Chinese)	80(6.25%)	EG:58.93 ± 4.01 CG:59.12 ± 3.88	EG: 7.2 ± 1.5 CG: 7.5 ± 1.2	(≤2.5SD)	EG: Baduanjin (DT) CG: Drug group	5	45-60	24	①	No;No
Cheng, et al.(2017) (27),	Nanjing, China (Chinese)	65(0%)	EG: 59.4 + 6.3 CG: 58.7 + 7.9	NR	(≤2.5SD)	EG: Taiji (DT) CG: Drug group	2-3	15-20	12	① ②	No;No
Peng (2019) (28)	Gansu, China (Chinese)	72(9.72%)	EG:60.88 ± 4.59 CG:62.31 ± 4.96	EG:11.20 ± 3.16 CG:12.11 ± 3.55	(≤2.5SD)	EG: Baduanjin (DT) CG: Drug group	5	45-60	24	①	No;No
Zhou (2014) (29)	Xian, China (Chinese)	60(0%)	55.94 ± 2.83	6.58 ± 1.53	(BMD>-1SD)	EG: Taiji CG1: Exercise training CG2: Usual care	5-7	45-60	40	①	No;No
Dan (2015) (30)	Beijing, China (Chinese)	120(8.4%)	EG:60.52 ± 6.25 CG:61. 12 ± 5.87	EG:11.64 ± 5.23 CG:12.15 ± 4.67	(≤2.5SD)	EG: Taiji (DT) CG: Drug group	7	45-60	24	①	No;Yes
Liu et al. (2015) (31)	Guangzhou, China (English)	98(3.06%)	EG:61.45 ± 5.89 EG:63.23 ± 7.5 CG:62.29 ± 6.47 CG:61.87 ± 8.29	EG:11.21 ± 5.29 EG:13.79 ± 6.27 CG:12.53 ± 5.69 CG:13.24 ± 6.77	(≤2.5SD)	EG1: Baduanjin (DT) EG2: Baduanjin CG1: Drug group CG2: Usual care	3	60	48	① ②	No;Yes
Chen et al., (2018) (32)	Jinhua, China (Chinese)	120(14%)	EG:54.80 ± 4.50 CG:55.40 ± 5.70	>1	(≤2.5SD)	EG: Wuqinxi (DT) CG: Drug group	7	20-30	48	①	No;No
Wang et al. (2018) (33)	Chaohu, China (Chinese)	86(13.4%)	EG:65.60 ± 3.80 CG:66.0 ± 4.40	10~15	NR	EG: Wuqinxi CG: Usual care	4	70	24	① ②③	No;No

(Continued)

10.3389/fendo.2024.1323595

TABLE 1 Continued

Reference	Location (Language)	Participant Characteristics				Intervention Program	Intervention Characteristics			Outcome Measured	Adverse Event; Follow-Up
		Sample Size (Attrition Rate)	Mean Age or Age Range	Duration of Menopause (years)	Bone Mass of Participants		Frequency (weekly)	Time (min)	Duration (week)		
Li et al. (2014) (34)	Hangzhou, China (Chinese)	60(6.67%)	EG:55.10 ± 6.52 CG:55.03 ± 5.71	EG: 8.70 ± 6.70 CG: 8.63 ± 5.60	(≤2.5SD)	EG: Wuqinxi (DT) CG: Drug group	6-7	30-60	24	①	No;Yes
Shen (2012) (35)	Guangxi, China (Chinese)	60(0%)	EG:60.44 ± 6.11 CG:60.07 ± 5.08	10.07 ± 5.39	(BMD>-1SD)	EG: Wuqinxi CG: Usual care	6	45	24	①	No;No
Gu (2021) (36)	Changsha, China (Chinese)	145(13.18%)	EG:66.36 ± 9.13 CG:65.72 ± 8.84	EG: 14.54 ± 7.54 CG: 14.87 ± 6.78	(≤2.5SD)	EG: Wuqinxi CG: Usual care	4	70	24	①②③	No;No
Shi (2017) (37)	Hangzhou, China (Chinese)	800(18.62%)	EG:58.42 ± 4.20 CG:60.07 ± 5.08	>1	(-2.5SD<BMD≤ -1SD)	EG: Wuqinxi (DT) CG: Usual care	7	20-30	48	①②	No;Yes
Li (2019) (38)	Chengdu, China (Chinese)	114(15.8%)	EG1:66.2 ± 3.5 EG2:65.7 ± 3.0 EG3: 65.7 ± 3.0 EG3: 65.7 ± 3.0	NR	(BMD>-1SD)	EG1: Yijingjin EG2:Wuqinxi EG3:Baduanjin CG: Usual care	5	70	48	①②③	No;Yes
Miao (2012) (39)	Dalian, China (Chinese)	60(0%)	56.12 ± 2.96	NR	(BMD>-1SD)	EG1: Yijingjin EG2:Wuqinxi EG3:Baduanjin EG4:Liuzijue CG: Usual care	6	60	24	①	No;No
Kuo et al. (2014) (40)	Taiwan, China (English)	75(18.7%)	>50	NR	(BMD<-1SD)	EG: Taiji (DT) CG: Drug group	4-5	60	12	②	No;No
Liu, Huang (2019) (41)	Fuzhou, China (Chinese)	100(12%)	EG:55.68 ± 3.37 CG:56.92 ± 2.38	NR	正常(BMD>-1SD)	EG: Taiji CG: Usual care	3	90	16	①②	No;Yes
Liu, Liu (2014) (42)	Xian, China (Chinese)	82(0%)	55-69	NR	正常(BMD>-1SD)	EG: Taiji CG1: Exercise training CG2: Usual care	>3	30-45	96	①	No;No
Mao et al.(2009) (43)	Xian, China (Chinese)	80(0%)	56.78 ± 2.91	6.78 ± 3.04	骨量减少 (-2.5SD<BMD≤ -1SD)	EG1: Taiji (DT) EG2: Taiji CG1: Drug group CG2: Usual care	7	30	20	①	No;No

(Continued)

10.3389/fendo.2024.1323595

TABLE 1 Continued

Reference	Location (Language)	Participant Characteristics				Intervention Program	Intervention Characteristics			Outcome Measured	Adverse Event; Follow-Up
		Sample Size (Attrition Rate)	Mean Age or Age Range	Duration of Menopause (years)	Bone Mass of Participants		Frequency (weekly)	Time (min)	Duration (week)		
Song et al.(2018) (44)	Dazhou, China (Chinese)	146(17.8%)	EG:64. 3 ± 3. 2 CG:64. 7 ± 4. 1 CG:64. 8 ± 2. 9	NR	正常(BMD>-1SD)	EG: Taiji CG: Exercise training CG: Usual care	5	70	48	① ②③	No;Yes
Xu et al.(2017) (45)	Zhejiang, China (Chinese)	86(0%)	EG:56.2 ± 5.6 CG:57.1 ± 6.0	EG: 7.4 ± 2.7 CG: 7.6 ± 2.9	(BMD>-1SD)	EG: Taiji CG: Usual care	6	40	48	① ②③	No;No
Ye et al.(2016) (46)	Beijing, China (Chinese)	50(15%)	EG:55.38 ± 6.08 CG:57.02 ± 8.47	>2	(BMD>-1SD)	EG: Taiji CG: Usual care	3	60	24	① ②③	No;No
Yu et al.(2014) (47)	Shanghai, China (Chinese)	117(0%)	EG:55.38 ± 6.08 CG:57.02 ± 8.47	NR	(-2.5SD<BMD≤ -1SD)	EG: Taiji CG: Usual care	4	60	48	① ②③	No;No
Zhao,Cheng (2020) (48)	Chengdu, China (Chinese)	250(0%)	EG:66. 0 ± 2. 6 CG:65. 8 ± 5. 0 CG:65. 7 ± 3. 2	NR	(-2.5SD<BMD≤ -1SD)	EG: Taiji CG1: Exercise training CG2: Usual care	5-7	50-60	12	① ②③	No;No
Zhao et al. (2015) (49)	Xian, China (Chinese)	60(0%)	EG:58.8 ± 3.2	EG: 8.83 ± 0.78 CG: 8.91 ± 0.81	NR	EG: Taiji CG: Usual care	6	55	24	① ②③	No;No
Zhou et al. (2015) (50)	Xian, China (Chinese)	64(0%)	57.21 ± 3.41	6.58 ± 1.53	(-2.5SD<BMD≤ -1SD)	EG1: Taiji (DT) EG2: Taiji CG1: Drug group CG2: Usual care	5	45-60	24	①	No;No
Chan et al., (2004) (51)	Hongkong, China (English)	132(16.9%)	EG:54.4 ± 3.3 CG:53.6 ± 3.2	EG: 4.9 ± 2.5 CG: 4.5 ± 2.4	(BMD>-1SD)	EG: Taiji CG: Usual care	5	50	48	①	No;Yes
Wayne et al., (2012) (52)	Boston, USA (English)	86(0%)	EG:58.8 ± 5.6 CG:53.6 ± 3.2	>1	(≤2.5SD)	EG: Taiji (DT) CG: Drug group	3-5	60	36	① ② ③	No;Yes
Wang et al.(2015) (53)	Shanghai, China (Chinese)	79(0%)	EG:58.54 ± 3.37 CG:58.54 ± 3.37	>0.5	(-2.5SD<BMD≤ -1SD)	EG: Taiji CG: Usual care	4	60	48	① ② ③	No;Yes
Liu, Liu (2021) (54)	Wuhan, China (Chinese)	52(1.9%)	56.48 ± 3.41	5~8	(BMD>-1SD)	EG: Taiji CG: Usual care	3	60	48	① ② ③	No;No

(Continued)

10.3389/fendo.2024.1323595

10.3389/fendo.2024.1323595

TABLE 1 Continued

Reference	Location (Language)	Participant Characteristics				Intervention Program	Intervention Characteristics			Outcome Measured	Adverse Event; Follow-Up
		Sample Size (Attrition Rate)	Mean Age or Age Range	Duration of Menopause (years)	Bone Mass of Participants		Frequency (weekly)	Time (min)	Duration (week)		
Li et al.(2022) (55)	Gdan´sk, Poland (English)	32(6.5%)	EG: 57.31 ± 1.48 CG: 56.41 ± 1.68	EG: 6.23 ± 2.21 CG: 6.44 ± 1.81	(≤-2.5SD)	EG: Baduanjin (DT) CG: Drug group	5	45	16	① ②	No;No
Cheng (2020) (55)	Chengdu, China (English)	52(23.5%)	EG: 61.5 ± 3.0 CG: 61.9 ± 2.5	NR	(BMD>-2.5SD)	EG: Taiji CG: Usual care	5	60	48	① ② ③	No;No

NR, not reported; EG, experimental group; CG, control group; osteopenia = (-2.5SD<BMD≤ -1SD; osteoporosis = (≤-2.5SD); normal = (BMD>-1SD); ① lumbar bone mineral density; ② femoral neck bone mineral density; ③ Ward's triangle bone density.

and is one of the international standards for evidence quality and the classification of recommendation strength (13). We evaluated the quality of the evidence for each outcome using the GRADE classification with four possible levels: I (high), where the real effect is similar to a credible estimate; II (moderate), where the true effect is closest to the estimated effect; III (low), where the actual effect may be significantly different from the estimated effect; and IV (very low), where the actual effect is likely to be significantly different from the estimated effect. Five factors can cause the quality of the evidence to decrease: (1) risk of bias; (2) imprecision; (3) inconsistency; (4) indirectness; and (5) publication bias (59).

Results

Literature search

A total of 585 articles were found from 11 databases (Figure 1), and 490 were removed by title and abstract. The remaining 95 articles were further screened by reading the complete text, and 62 records were excluded as they were non-RCTs (n=21), they had no reported data for analysis (n = 14), they were reviews (n = 6), they had no major TCE interventions (n = 13), and conference emails were not provided (n = 8). Finally, 33 studies were included in our network analysis.

Study characteristics

In total, there were 3658 participants [the smallest sample was 30 (60) and the largest sample was 800 (37)]. The ages of the participants ranged from 50 to 70 years old. Three studies had an intervention period of 12 weeks (27, 40, 48), and 13 studies had an intervention period of 48 weeks, in addition to one study with an intervention period of 96 weeks (42). The experimental group involved 62 cases of traditional Chinese fitness exercises in a single treatment protocol, of which 15, 3, 5, 2, and 1 group used Taiji, Baduanjin, Wuqinxi, Yijinjing, and Liuzijue techniques as interventions, respectively. The protocols using Taiji, Baduanjin, and Wuqinxi in combination with medication included 5, 6, and 3 groups, respectively. The control groups were treated with usual care or drug therapy. Furthermore, 32 articles metrics measured lumbar spine BMD, 20 articles measured femoral neck BMD, and 13 articles measured Ward's triangle BMD. During the intervention period, 11 articles (30, 31, 34, 37, 38, 41, 44, 51–53, 61) reported the follow-up status.

Study quality assessment

The results of the risk of bias evaluation of the RCTs are shown in Figure 2. Thirty-three articles in our study reported the random allocation method as a random number table method/computer randomized generation, sixteen articles reported deviation from the intended intervention, one paper was missing outcome data, and no selective outcomes were reported in any article.

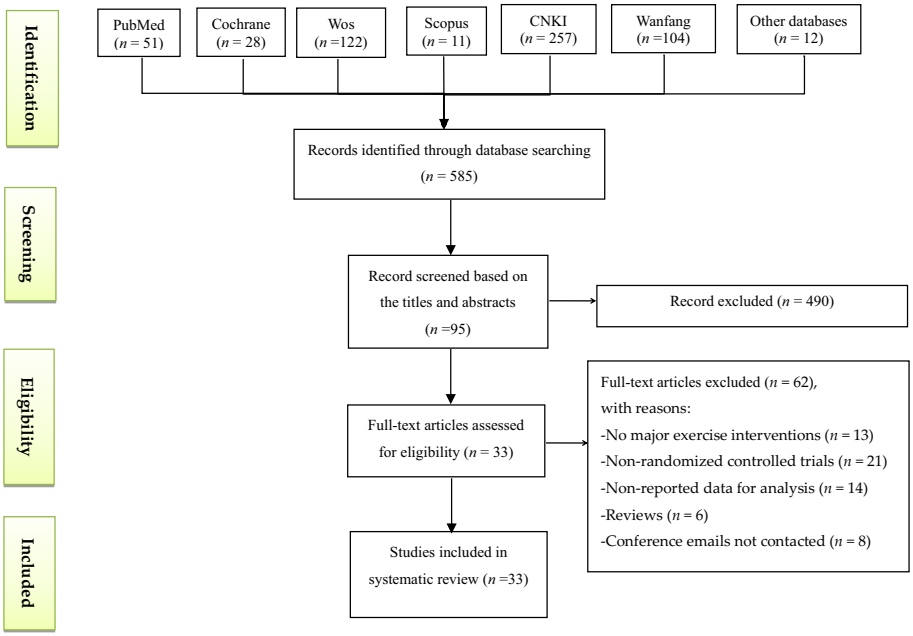

FIGURE 1
Flow of study selection.

GRADE quality evaluation

Based on the criteria of GRADE, the assessment of the certainty of the evidence regarding the significant impact of traditional Chinese fitness exercises on bone mineral density in postmenopausal women was carried out separately (Table 2). Specifically, traditional Chinese fitness exercises has medium-high quality evidence for the lumbar spine, femoral neck, and Ward's triangle BMD of postmenopausal women, indicating that the quality assessment of this study had a high degree of credibility.

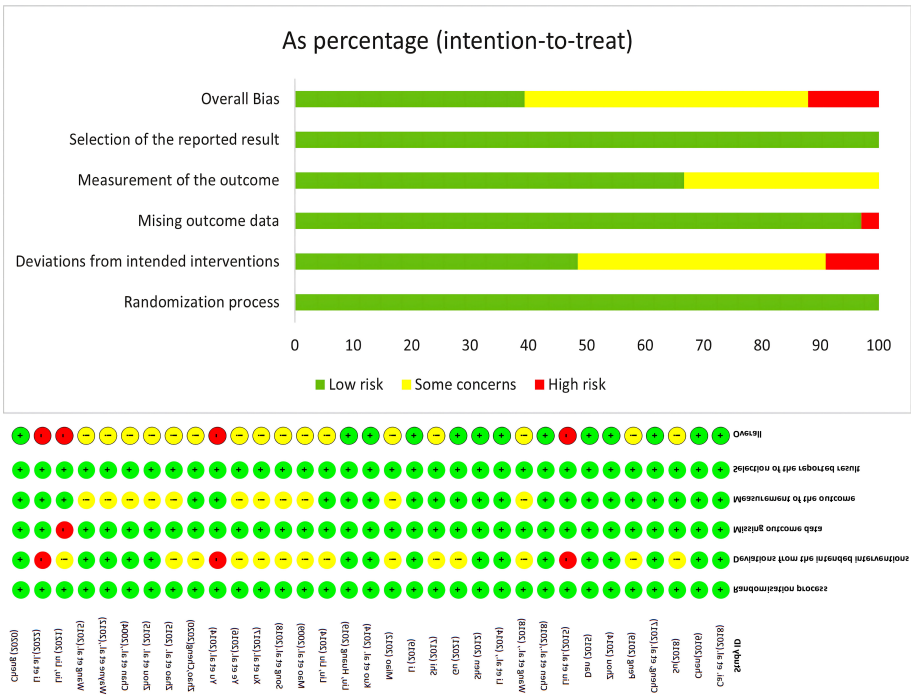

FIGURE 2
Graph of Cochrane Risk Bias Assessment.

TABLE 2 Grading Recommendations to Assess Development and Evaluation system (GRADE) assessment of the evidence of certainty for traditional Chinese fitness exercises.

Outcomes	Presence of downgrading item of GRADE					Level of certainty of evidence
	Risk of bias	Inconsistency	Indirectness	Imprecision	Publication bias	
lumbar spine BMD	No	No	No	Yes	No	II (Moderate) (4)
femoral neck BMD	No	No	No	No	No	I (High)
Ward's triangle BMD	No	No	No	Yes	No	II (Moderate) (4)

(1) Risk of bias: if the risk of bias of the included studies is present in the meta-analysis, e.g., randomization, concealed allocation, or blinding of assessors/subjects; (2) Inconsistency: point estimates are concentrated, confidence intervals can overlap, and the results of the heterogeneity tests are not statistically significant; (3) Indirectness: present if the intervention studied in the meta-analysis is not directly relevant to the outcome; (4) Imprecision: present if the sum of sample sizes of all individual studies included in meta-analysis is less than 500, and if the effect size's 95% Cl is comparatively large; (5) Publication bias: present if the author only searched the Chinese database, or only one database.

Traditional meta-analysis

Heterogeneity test

A total of 33 articles were included in the traditional meta-analysis, which used Doi plots and the LFK index. The LFK index in the ±1 interval suggests that there may have been minimal publication bias, in the ±2 interval suggests that there may have been a slight publication bias, and outside the ±2 interval suggests that there may have been a significant publication bias (62). Specifically, as shown in Table 3, in the Lumbar Spine BMD and Femoral Neck BMD indexes, the publication bias of the interventions involving Baduanjin was more significant, and in general, the studies on the effects of Baduanjin on each index of BMD in postmenopausal women had a significant bias. In contrast, the bias of studies of other Chinese traditional fitness exercises was negligible. Further heterogeneity analysis revealed that the heterogeneity of Lumbar Spine BMD and Femoral Neck BMD was significant (I^2 > 50%, P< 0.1), and the heterogeneity of Ward's triangle BMD was weak (I^2< 50%, P > 0.1). Based on the data in this study, subgroup analyses were conducted by classifying different exercise forms, and sensitivity analyses (article-by-article elimination) were performed to find the source of heterogeneity (Table 4), which showed that except for the subgroups of Taiji and Baduanjin, which were still heterogeneous, the rest of the groups were homogeneous. A random effects model was used for the analysis to ensure the study's accuracy.

TABLE 3 LFK index.

Indicator	Subgroup	LFK index
Lumbar Spine BMD	BDJ(DG)-Drug Group	3.16
	WQX(DG)-Drug Group	1.24
	TC(DG)-Drug Group	0.62
	BDJ-Usual Care	2.28
	WQX-Usual Care	1.41
	TC-Usual Care	1.44
	YJJ-Usual Care	NR
	LZJ-Usual Care	NR
	Exercise Training-Usual Care	-1.47
	Drug Group-Usual Care	1.74
Femoral Neck BMD	TC(DG)-Drug Group	0.56
	BDJ(DG)-Drug Group	5.42
	WQX(DG)-Drug Group	NR
	TC-Usual Care	-0.68
	BDJ-Usual Care	NR
	WQX-Usual Care	1.80
Ward's Triangle BMD	TC-Usual Care	-0.59
	WQX-Usual Care	0.56
	YJJ-Usual Care	NR
	BDJ-Usual Care	NR

NR, not reported.

Traditional meta-analysis results

Traditional Chinese fitness exercises significantly improved L-BMD (SMD = 0.58, 95% CI -0.34 to 0.82, p< 0.01) and Femoral Neck BMD (SMD = 0.63, 95% CI 0.28 to 0.98, p< 0.01) in postmenopausal women, with some statistically significant improvement in Ward's triangle BMD (SMD=0.26, 95% CI 0.15 to 0.36, p< 0.05) (Table 5). Subgroup analyses based on different exercise modalities showed that Taiji had a high effect size for improvement in L-BMD (SMD=0.72, 95% CI 0.22 to 1.21, p< 0.01) and a medium effect size for improvement in Femoral Neck BMD (SMD=0.46, 95% CI 0.14 to 0.79, p< 0.01) and Ward's triangle BMD (SMD = 0.32, 95% CI 0.14 to 0.50, p< 0.01). Baduanjin had a high effect size for the improvement effect on Femoral Neck BMD (SMD = 1.63, 95% CI -3.58 to 6.85, p< 0.01) in postmenopausal women, and small effect sizes for both Ward's triangle BMD (SMD = 0.19, 95% CI - 0.39 to 0.78, p< 0.05), and L-BMD (SMD = 0.03, 95% CI - 1.05 to 1.10, p > 0.05), which were not statistically different. Wuqinxi had a slight effect size for improvement on all BMD indicators in postmenopausal women (p< 0.05). Yijinjing had a significant improvement effect in L-BMD (SMD = 0.51, 95% CI 0.03 to 0.99, p< 0.01) and a minor improvement effect in Femoral Neck BMD (SMD=0.23, 95% CI 0.35 to 0.80, p< 0.05).

TABLE 4 Heterogeneity test.

Indicator	Subgroup	Culling before		After culling	
		I^2/%	*P*	I^2/%	P
Lumbar Spine BMD	BDJ(DG)-Drug Group	96.63	0.000	96.63	0.000
	WQX(DG)-Drug Group	37.78	0.201	0	0.670
	TC(DG)-Drug Group	0	0.691	0	0.691
	Summary	94.10	0.000	94.10	0.000
	BDJ-Usual Care	98.53	0.000	77.91	0.033
	WQX-Usual Care	0	0.857	0	0.857
	TC-Usual Care	90.04	0.000	77.63	0.000
	YJJ-Usual Care	0	0.970	0	0.970
	LZJ-Usual Care	NR	NR	NR	NR
	Exercise Training-Usual Care	17.49	0.303	0	0.433
	Drug Group-Usual Care	96.75	0.000	97.98	0.000
	Summary	90	0.000	86.48	0.000
Femoral Neck BMD	TC(DG)-Drug Group	51.74	0.125	0	0.636
	BDJ(DG)-Drug Group	98.09	0.000	94.08	0.000
	WQX(DG)-Drug Group	NR	NR	NR	NR
	Exercise Training-Drug Group	NR	NR	NR	NR
	Summary	91.50	0.000	53.15	0.014
	TC-Usual Care	68.59	0.001	64.63	0.001
	BDJ-Usual Care	98.86	0.000	97.51	0.000
	WQX-Usual Care	0	0.960	0	0.960
	Exercise Training-Usual Care	0	0.986	0	0.986
	YJJ-Usual Care	NR	NR	NR	NR
	Drug Group-Usual Care	NR	NR	NR	NR
	Summary	90.30	0.000	86.12	0.000
Ward's Triangle BMD	TC-Usual Care	29.26	0.175	4.85	0.394
	WQX-Usual Care	0	0.756	0	0.756
	YJJ-Usual Care	NR	NR	NR	NR
	BDJ-Usual Care	NR	NR	NR	NR
	Exercise Training-Usual Care	0	0.372	0	0.372
	Summary	5.40	0.391	5.40	0.391

NR, not reported.

Network meta-analysis

Effect of TCE on L-BMD in postmenopausal women

The overall inconsistency test showed that the L-BMD outcome indicator $P > 0.05$, which indicated that the overall consistency was good. Further tests of the consistency of each closed loop showed that the value of the inconsistency factor (IF) ranged from 0.06 to 0.14, and the lower limit of the 95% CI all contained 0, which indicated that the consistency of each closed loop was better, so the consistency model was used for analysis.

In total, 32 RCT studies reported changes in L-BMD pretest-posttest intervention in 2771 subjects; 14 studies included drug therapy as the control group and 18 studies had usual care as the control group, with three studies reporting both drug therapy and usual care, incorporating a web of relationships between studies (Figure 3). The pairwise comparison between the two found that Taiji was superior to exercise training (SMD=-0.05, 95% CI -0.10

TABLE 5 Results of Traditional Meta-Analysis.

Indicator	Subgroup	Amount	SM D(95%CO	Forest Plot	Q	*P*	*I-sugare*
Lumbar Spine BMD	BDJ(DG)-Drug group	5	1.73(0.20,3.26)	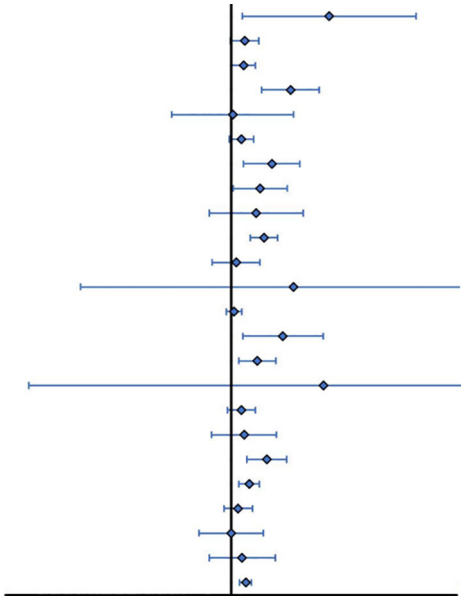	81.33	0.000	96.63
	WQX(DG)-Drug gro up	3	0.24(-0.02,0.49		3.22	0.200	37.78
	TC(DG)-Drug group	5	0.22(0.00,0.43)		2.24	0.692	0.00
	Summary	13	1.05(0.54,1.55)		120.4	0.000	94.10
	BDJ-Usual Care	3	0.03(-1.05,1.10)		4.528	0.033	77.91
	WQX-Usual Care	5	0.18(-0.04,0.4)		1.322	0.858	0.00
	TC-Usual Care	15	0.72(0.22,1.21)		58.12	0.000	90.04
	YJJ-Usual Care	2	0.51(0.03,0.99)		0.00	0.970	0.00
	LZJ-Usual Care	1	0.44(-0.39,1.27)		/	/	/
	Summary	26	0.58(0.34,0.82)		246.35	0.000	89.9
femoral neck BMD	TC(DG)-Drug group	3	0.09(-0.34,0.51)		4.14	0.126	51.74
	BDJ(DG)-Drug gro up	3	1.1(-2.66,4.86)		104.74	0.000	98.09
	WQX(DG)-Drug group	1	0.05(-0.09,0.19		/	/	/
	Summary	7	1.09(0.30,1.88)		142.83	0.000	95.8
	TC-Usual Care	9	0.46(0.14,0.79)		5.47	0.103	68.59
	BDJ-Usual Care	2	1.63(-3.58,6.85		88.25	0.000	98.86
	WQX-Usual Care	3	0.18(-0.07,0.43)		0.08	0.960	0.00
	YJJ-Usual Care	1	0.23(-0.35,0.8)		/	/	/
	Summary	15	0.63(0.28,0.98)		174.56	0.000	90.30
Ward's triangle BMD	TC-Usual Care	10	0.32(0.14,0.50)		12.72	0.176	29.26
	WQX-Usual Care	3	0.12(-0.13,0.38)		0.56	0.757	0.00
	YJJ-Usual Care	1	0(-0.57,0.57)		/	/	/
	BDJ-Usual Care	1	0.19(-0.39,0.78)		/	/	/
	Summary	5	0.26(0.15,0.36)		17.97	0.39	5.40

Meaning of the symbol "/" stands for NR (not reported).

10.3389/fendo.2024.1323595

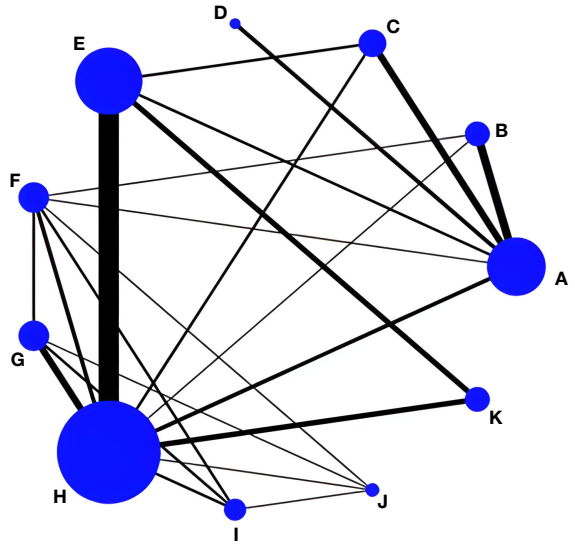

FIGURE 3
Network evidence for L-BMD. **(A)** Drug group; **(B)** Baduanjin+Drug group; **(C)** Taiji+Drug group; **(D)** Wuqinxi+Drug group; **(E)** Taiji; **(F)** Baduanjin; **(G)** Wuqinxi; **(H)** Usual care; **(I)** Yujinjin; **(J)** Liuzijue; **(K)** Exercise training.

to -0.02, p<0.05) and Wuqinxi (SMD=-0.05, 95% CI -0.13 to -0.01, p<0.05) and Baduanjin (SMD=-0.06, 95% CI -0.16 to -0.02, p<0.05). It is worth noting that the Baduanjin+drug group was better than Baduanjin (SMD=-0.11, 95% CI -0.24 to -0.04, p<0.05), and the drug group (SMD=-0.08, 95% CI -0.14 to -0.02, p<0.05) (Table 6).

In addition, the final ranking of the five single modulation interventions, the three-drug combination interventions, and the three control groups was performed using SUCRA, with percentages indicating that the more significant the portion of the area under the SUCRA curve, the better the treatment effect (Figure 4). The final ranking was as follows: Baduanjin+drug (83.6%) > Taiji+drug (78.7%) > Taiji (64.4%) > drug (59.3%) > Yijinjin (49.7%) > Liuzijue (48.2%) > exercise training (47.1%) > Wuqinxi+drug (46.9%) > Wuqinxi (35%) > Baduanjin (32%) > usual care (5.2%).

Effect of TCE on femoral neck BMD in postmenopausal women

Twenty RCT studies reported changes in femoral neck BMD before and after the intervention, amounting to 2593 subjects; six included drug therapy as the control group and 13 included usual care, of which one study reported both drug therapy and usual care, and the reticulation between the included studies was performed as in Figure 5. Subsequently, the overall inconsistency test showed the femoral neck BMD outcome indicator P<0.05 and the overall consistency was poor, so the inconsistency model was used for analysis.

An indirect comparison between the two found that Taiji was superior to Yinjin (SMD= -0.07, 95% CI -0.12 to -0.05, p<0.05) and Wuqinxi (SMD= -0.07, 95% CI -0.13 to -0.04, p<0.05), but compared with Baduanjin and Baduanjin+drug, the Taiji+drug intervention effect was slightly worse. In addition, Baduanjin was superior to Taiji (SMD= 0.12, 95% CI 0.08 to 0.16, p<0.05) and Wuqinxi (SMD= -0.02, 95% CI -0.09 to -0.05, p<0.05), and the difference was statistically significant. Moreover, the Baduanjin+drug group (SMD= -0.14, 95%CI -0.23 to -0.05, p<0.01) was superior to the Baduanjin and the Taiji+drug group (SMD= -0.10, 95%CI -0.18 to -0.01, p<0.05), which was superior to Taiji (Table 7).

The final ranking using SUCRA was as follows (Figure 6): Baduanjin+drug (90.2%) > Baduanjin (89.9%) > Taiji+drug (84.5%) > drug (66.7%) > Taiji (51.3%) > Yijinjin (42.4%) > Wuqinxi+drug (39.4%) > exercise training (19%) > Wuqinxi (14.8%) > usual care (1.9%).

Effect of TCE on Ward's triangle BMD in postmenopausal women

LI tests and a net meta-analysis of the included data showed IF values ranging from 0.01 to 0.10 and a lower 95% CI of 0, indicating no significant inconsistency across the closed loop analyses using the consistency model. Thirteen RCT studies reported changes in Ward's triangle bone density before and after the intervention, amounting to 1324 subjects; one included drug therapy as the control group, and 12 had usual care as the control group, with a mesh relationship between the included studies (Figure 7).

Of the six pairwise comparisons produced in the reticulated network analysis (Table 8), they were not statistically significantly different from the Taiji+drug group (SMD= -0.01,95%CI -0.06 to 0.04, p >0.05), Taiji (SMD= 0.02, 95%CI -0.01 to 0.05, p>0.05), and Wuqinxi (SMD= 0.03, 95%CI -0.04 to 0.09, p>0.05), but the drug group was superior to Baduanjin (SMD= 0.03, 95%CI 0.02 to 0.05, p<0.05). In addition, Taiji was superior to usual care (SMD= -0.06, 95%CI -0.13 to -0.03, p<0.05). In an indirect comparison, only Taiji was superior to Baduanjin (SMD= -0.02, 95% CI -0.04 to -0.01, p<0.05). The final SUCRA ranking was as follows (Figure 8): Taiji +drug (86%) > drug (68.7%) > Taiji (46.8%) > Baduanjin (41.2%) > Wuqinxi (39.8%) > usual care (15.5%).

Discussion

To our knowledge, this article is the first to compare the effects of TCE (including drug treatment, usual care, exercise training, Taiji, Baduanjin, Wuqinxi, Yijinjin, and their combinations) on BMD in postmenopausal women by network analysis, using direct and indirect evidence to compare the effect of L-BMD, femoral neck BMD, and Ward's triangle BMD in 33 randomized controlled trials (3658 postmenopausal women). The results showed that, compared with drug treatment, routine nursing, and exercise training, Taiji, Baduanjin, and Yijinjin can effectively prevent bone loss, and the effect of Wuqinxi needs to be further explored. Further, we distinguished between TCE and drug interventions to prevent the combined intervention from potentially exaggerating the impact of the intervention and causing bias in the experimental design.

In this study, all the traditional Chinese fitness exercise interventions improved the L-BMD status of postmenopausal women. Baduanjin+drug, Taiji+drug, Taiji, drug, and Yijinjin had better intervention effects. From the point of view of Chinese traditional fitness exercise alone (without combining their use with drugs), Taiji and Yijinjin achieved a more significant improvement in L-BMD and femoral neck BMD.

10.3389/fendo.2024.1323595

TABLE 6 Results of the network meta-analysis for L-BMD.

	Drug group	Exercise training	Liuzijue	Yijinjin	Usual care	Wuqinxi	Baduanjin	Taiji	Wuqinxi+ drug group	Taiji +drug group
Drug group										
Exercise training	-0.02 (-0.12,0.08)									
Liuzijue	-0.01 (-0.18,0.15)	0 (-0.17,0.17)								
Yijinjin	-0.04 (-0.16,0.09)	-0.02 (-0.15,0.11)	-0.02 (-0.19,0.14)							
Usual care	0.06 (-0.01,0.13)	0.08 (0.00,0.15) *	0.07 (-0.08,0.23)	0.20 (0.01,0.51) *						
Wuqinxi	0.01 (-0.09,0.11)	0.03 (-0.08,0.13)	0.02 (-0.13,0.18)	0.04 (-0.07,0.16)	-0.05 (-0.13,0.03)					
Baduanjin	0.02 (-0.10,0.13)	0.05 (-0.06,0.16)	0.03 (-0.18,0.23)	0.04 (-0.04,0.08)	-0.03 (-0.11, 0.03)	0.08 (-0.08,0.12)				
Taiji	-0.04 (-0.24,0.03)	-0.05 (-0.10, -0.02) *	-0.09 (-0.21, -0.04) *	0 (-0.12,0.11)	-0.29 (-0.44, -0.06) *	-0.05 (-0.13, -0.01) *	-0.06 (-0.16,-0.02) *			
Wuqinxi + drug group	-0.02 (-0.11,0.07)	0 (-0.14,0.13)	-0.01 (-0.20,0.18)	0.02 (-0.14,0.17)	-0.08 (-0.20,0.04)	-0.03 (-0.17,0.11)	-0.05 (-0.19,0.08)	0.02 (-0.10,0.14)		
Taiji+ drug group	-0.02 (-0.08,0.05)	0 (-0.10,0.11)	0 (-0.17,0.17)	0.02 (-0.11,0.15)	-0.07 (-0.15, -0.02) *	-0.02 (-0.13,0.08)	-0.05 (-0.15,0.06)	0.02 (-0.06,0.11)	0 (-0.11,0.12)	
Baduanjin + drug group	-0.08 (-0.14, -0.02) *	-0.06 (-0.17,0.05)	-0.06 (-0.23,0.11)	-0.04 (-0.17,0.09)	-0.14 (-0.22, -0.05) *	-0.03 (-0.19,0.03)	-0.11 (-0.24,-0.04) *	-0.01 (-0.13,0.02)	-0.06 (-0.17,0.05)	-0.06 (-0.15,0.03)

shows that the data differ. *p< 0.05.

Many of the movements in Taiji required the subjects to adopt a semi-squatting posture, such as the Wild Horse Splitting Mane, Knee-Wrapping Reversing Stance, and Left and Right Ranging Sparrow's Tail, etc. During the practice process, the subjects are required to adjust the stability of their body postures continuously. Moreover, when practicing, the subjects are required to sink their qi into the dantian and adopt abdominal breathing, which plays a role in exercising the core muscles of the torso, and long-term practice produces stress changes and increases bone mass of the lumbar spine (63), which in turn has a positive effect on L-BMD and femoral neck BMD. In Ward's triangle BMD, Taiji+drug, drug, and Taiji were the optimal approaches for improving BMD symptoms in postmenopausal women, and this intervention was better than the control group, suggesting that Taiji has some muscle-strengthening effects. This finding was similar to previous studies by Zou, which showed that Taiji could improve L- BMD, femoral neck BMD, and Ward's triangle BMD (18).

The effect of Yijinjing intervention was consistent with previous studies that concluded that Yijinjing was the best method for improving lumbar spine and femoral bone density via TCE (64). A previous study also showed that Yijinjing may be more beneficial for bone formation to improve BMD (65). A recent meta-analysis on osteoporosis in older people showed that, for femoral neck BMD and L-BMD, Yijinjing was better than Baduanjin and Wuqinxi, which yielded results of 0.02-0.05 g/cm^2 and 0.07-0.08 g/cm^2 (15). This was because the practice of Yijinjing uses the torso to drive the limbs to complete stretching, spreading, retracting, and rotating movements, which leads to the bones, muscles, ligaments, and joints moving from multiple angles, increasing the stimulation of the bones and improving their metabolic capacity (64). Through static stretching of the muscles and synergistic movement of the joints, we can stretch the tendons and bones, improve microcirculation and muscle mobility, and increase the body's potential for change, thus strengthening the spleen, kidneys, and blood, as well as the tendons and bones. Furthermore, studies have shown that the estradiol level in older women increases significantly after Yijinjing, which positively affects bone density (66). However, considering the small number of studies focused on Yijinjing, its effectiveness in improving BMD in postmenopausal women has yet to be confirmed. Therefore, future high-quality original studies or systematic evaluations of the above interventions are needed.

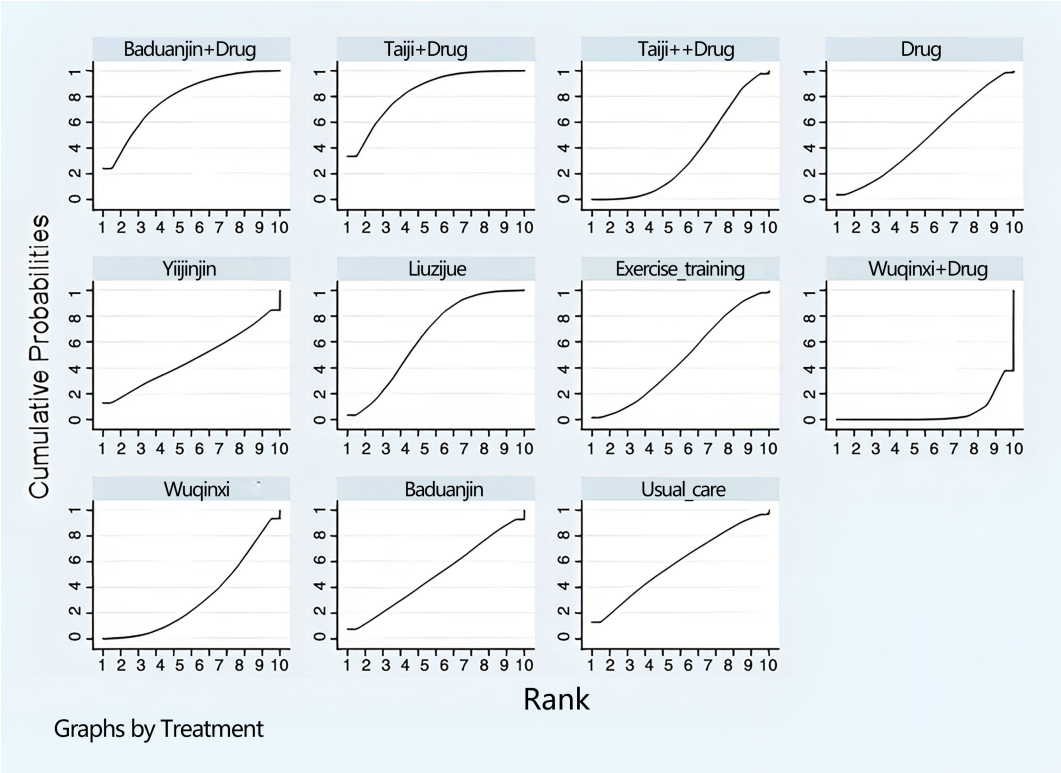

FIGURE 4
Ranking diagram of each intervention (L-BMD).

In this study we identified a novel phenomenon: the effect of Baduanjin combined with medication on postmenopausal women's L-BMD and femoral neck BMD was highly effective. Previous meta-analyses did not identify this, and we believe that this is because postmenopausal women were considered in this study. Related research confirms our other view that long-term regular Baduanjin exercises combined with medication can alleviate the lower back pain caused by osteoporosis in postmenopausal women and improve bone density. This is because the loss of bone density in postmenopausal women occurs mainly due to a decrease in the level of hormones synthesized by the ovaries, which disrupts the equilibrium of bone metabolism in the patient's body, with more bone resorption than bone formation, thus accelerating the rate of bone loss in the patient. Pharmacological treatment supplements the hormones or may utilize osteoclast-inhibiting drugs (e.g., calcitonin, vitamin D, aluminophosphates, and calcium supplements) (14, 67). For this reason, postmenopausal women who choose Baduanjin+drug as an intervention should follow it long-term to treat L-BMD and femoral neck BMD. However, Taiji is relatively backward in overall alignment in L-BMD and femoral neck BMD. Some studies have pointed out that Taiji's foot movements are variable in direction, slower, and lighter, similar to "stirring the feet" and "pointing the ground with a false toe step", and that the ground reaction force on the soles of the feet is low during Taijiquan practice (68). However, previous studies have pointed to a positive correlation between the load applied to the bone and bone density, with the maximum force significantly increasing bone density. Therefore, compared to the Baduanjin interventions, Taiji is slightly less effective in decreasing BMD loss in postmenopausal women.

However, it is worth noting that this study found no improvement effect of Baduanjin on L-BMD in direct and indirect comparisons. As a traditional Chinese medicine fitness qigong, Baduanjin has slow and

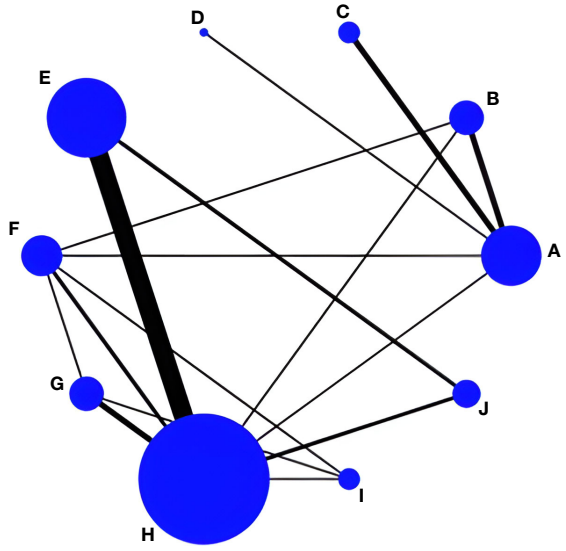

FIGURE 5
Network evidence for femoral neck BMD. **(A)** Drug group; **(B)** Baduanjin+Drug group; **(C)** Taiji+Drug group; **(D)** Wuqinxi+Drug group; **(E)** Taiji; **(F)** Baduanjin; **(G)** Wuqinxi; **(H)** Usual care; **(I)** Yujinjin; **(J)** Exercise training.

10.3389/fendo.2024.1323595

TABLE 7 Results of the network meta-analysis for femoral neck BMD.

	Drug group	Exercise training	Yijinjin	Usual care	Wuqinxi	Baduanjin	Taiji	Wuqinxi + drug group	Taiji +drug group
Drug group									
Exercise training	-0.16 (-0.27,-0.06)								
Yijinjin	0.25 (0.14,0.37)*	-0.25 (-0.37,-0.12)*							
Usual care	-0.14 (-0.21,0.08)	0.03 (-0.03,0.08)	0.07 (0.01,0.19) *						
Wuqinxi	0.07 (-0.00,0.15)	-0.25 (-0.36,-0.13)*	0 (-0.09,0.09)	-0.04 (-0.07,-0.01)*					
Baduanjin	-0.03 (-0.10,0.03)	-0.23 (-0.31,-0.14)*	0.02 (-0.07,0.11)	-0.18 (-0.32,-0.19)*	-0.02 (-0.09,-0.01)*				
Taiji	0 (-0.07,0.06)	-0.10 (-0.17,0.05)	-0.07 (-0.12,0.05) *	-0.11 (-0.23,-0.07)*	-0.07 (-0.13,-0.04)*	0.12 (0.08,0.16)*			
Wuqinxi+ drug group	-0.02 (-0.07,0.02)	-0.10 (-0.19,0.02)	0.16 (0.03,0.29) *	-0.12 (-0.21,-0.02)*	-0.09 (-0.14,-0.05)*	0.11 (0.05,0.13)*	-0.08 (-0.17,0.02)		
Taiji+ drug group	-0.07 (-0.12,-0.02)*	-0.11 (-0.20,-0.01)*	0.14 (0.02,0.26) *	-0.14 (-0.22,-0.06)*	0.04 (-0.13,0.25)	0.12 (0.04,0.26)*	-0.1 (-0.18,-0.01)*	0.02 (-0.07,0.09)	
Baduanjin+ drug group	-0.08 (-0.16,-0.01)*	-0.15 (-0.25,-0.05)*	-0.02 (-0.23,0.11)	-0.27 (-0.32,-0.19)*	-0.09 (-0.21,-0.03)*	0.07 (-0.01,0.16)	-0.14 (-0.23,-0.05)*	-0.07 (-0.14,0.01)	-0.04 (-0.11,0.02)

shows that the data differ. *p< 0.05.

gentle movements, mainly used to regulate qi and blood, dredge meridians and channels, and then restrict the body's internal organs and meridians. The movement of the joints needs to combine qi regulation and static force to play a role in strengthening the bones (69). Our findings may have been related to the differences in the trial subjects, the duration of the trial intervention, and the frequency of practice of Baduanjin. From the three articles included, it was found that the length and frequency of the intervention were short, which may have contributed to the poor results for the Baduanjin intervention in L-BMD in postmenopausal women. In contrast to the L-BMD results, the Baduanjin intervention alone significantly affected femoral neck BMD. The reasons for this phenomenon may be that the intervention used was a modified version of Baduanjin, the eighth stance of which in traditional Baduanjin is known as the toe posture, which can stimulate the immune system and enhance osteogenesis through the vertical pressure generated by the body's gravity. However, the modified eighth stance of Baduanjin adds two training movements, such as tiptoeing and clapping. When the heel is suddenly put down, combined with the palm clapping action, the ankle, knee, and femur joints will increase the body's gravity, hitting the ground and creating a reaction force, which will lead to vibration. Secondly, fewer studies were included, and it is possible that further research will confirm its effectiveness in improving femoral neck BMD in postmenopausal women. Therefore, future high-quality original studies or systematic evaluations of the above interventions based are needed.

Wuqinxi had a particular mitigating effect on BMD in postmenopausal women, and this finding was similar to the findings in previous studies (38, 70). Some studies have concluded that in elderly patients, Wuqinxi significantly improves BMD and prevents POP fractures compared with control groups, as it can enhance the bone formation index, reduce the rate of bone resorption, and achieve a dynamic and positive balance between osteogenesis and osteoblast genesis (35).

Some scholars have also shown that when older women practiced Wuqinxi for 24 weeks, lumbar spine L2-4, greater trochanter, Ward's triangle, and femoral neck BMD improved to varying degrees. While not statistically significant, the static and dynamic balance in the left and right directions were improved, and the risk of falling was reduced (33). The reasons for these findings may be related to the duration, frequency, and intensity of Wuqinxi practice and the small sample size. A previous study showed that the protective BMD effect was difficult to observe in a 12-week intervention trial, as the bone remodeling cycle usually takes at least 24 weeks (71). However, there has yet to be a longitudinal study to demonstrate the effect of long-term exercise on changes in

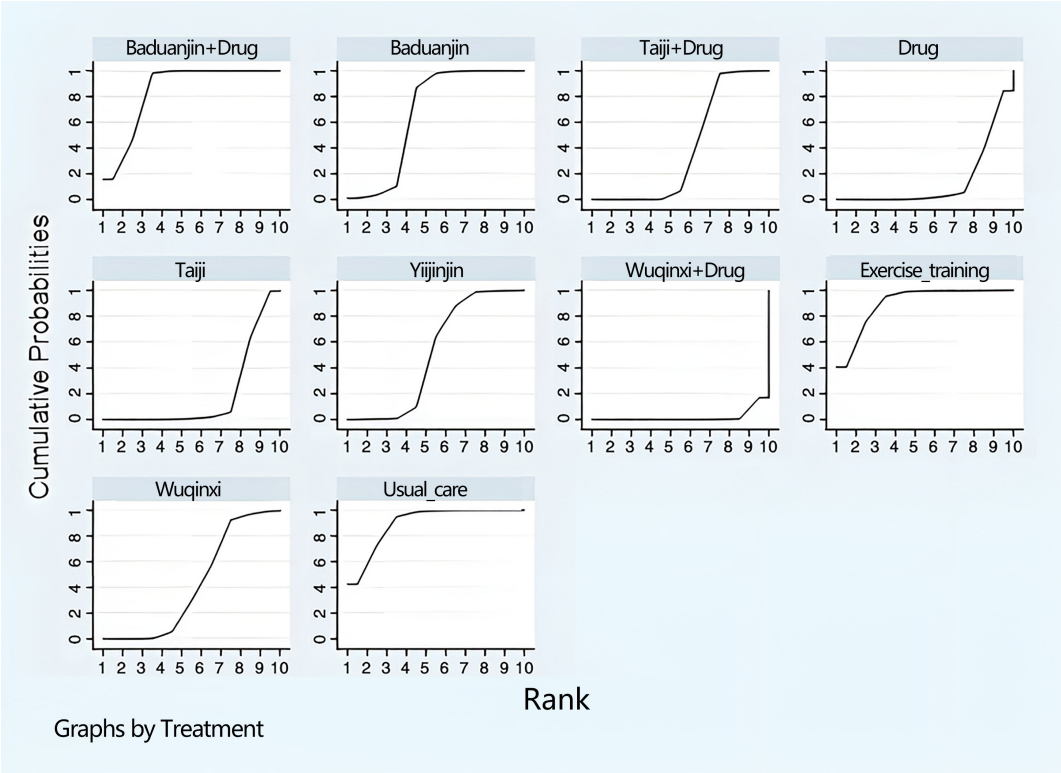

FIGURE 6
Ranking diagram of each intervention (femoral neck BMD).

bone mineral density in older adults over time. Therefore, the comparison between different durations suggests interesting future directions for exploring protective bone density loss, and further research is needed.

This study has several limitations: (1) although we used 11 electronic databases, they were limited to Chinese and English articles, which may have led to a specific language bias; (2) we did not include VAS and serum ALP, as the number of studies on VAS and serum ALP were insufficient for network analysis, which may have weakened the strength of the evidence; (3) most of the studies were assigned inappropriately and non-double-blinded to exaggerate the effects of the treatment; (4) most studies lacked follow-up information, resulting in incomplete data on the effectiveness and safety of treatment regimens; and (5) this study focused on TCE interventions and discussed mainly single exercise interventions, distinguishing between combined TCE and drug interventions to avoid exaggerating or reducing the degree of effect of these interventions, but it remains unclear by which mechanism the combination of TCE and different medications affects BMD. Given the limitations of this study, there is a need to objectify and standardize the study design in this field to support the development of more high-quality literature, such as large-scale, prospective, double-blind RCTs.

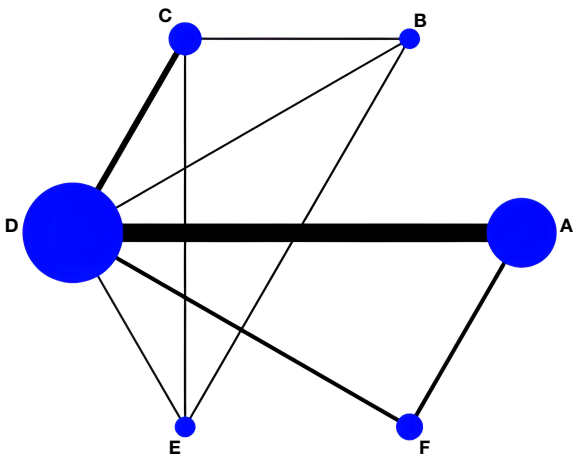

FIGURE 7
Network evidence for Ward's triangle BMD. **(A)** Drug group; **(B)** Taiji +Drug group; **(C)** Taiji; **(D)** Baduanjin; **(E)** Wuqinxi; **(F)** Usual care.

Conclusions

The results of the reticulated network analysis showed that all five traditional gong methods (Wuqinxi, Taiji, Baduanjin, Yijinjin, and Liuzijue) were effective in addressing BMD in postmenopausal women. The probability ranking showed that Taiji and Yijinjing alone have significant advantages, while Baduanjin still needs more studies to testify that it has substantial benefits if combined with medication. Therefore, Taiji or Baduanjin combined with medication

TABLE 8 Results of the network meta-analysis for Ward's triangle BMD.

	Drug group	Usual care	Wuqinxi	Baduanjin	Taiji
Drug group					
Usual care	0.02 (0.01,0.03)*				
Wuqinxi	0.03 (-0.04,0.09)	-0.01 (-0.07,0.01)			
Baduanjin	0.03 (0.02,0.05) *	-0.01 (-0.03,0.01)	0.01 (-0.06,0.07)		
Taiji	0.02 (-0.01,0.05)	-0.06 (-0.13,-0.03) *	0 (-0.07,0.06)	-0.02 (-0.04,-0.01) *	
Taiji+ drug group	0.01 (-0.04,0.06)	-0.07 (-0.10,-0.04) *	-0.02 (-0.09,0.05)	-0.03 (-0.08,0.02)	-0.02 (-0.06,0.03)

shows that the data differ. *p< 0.05.

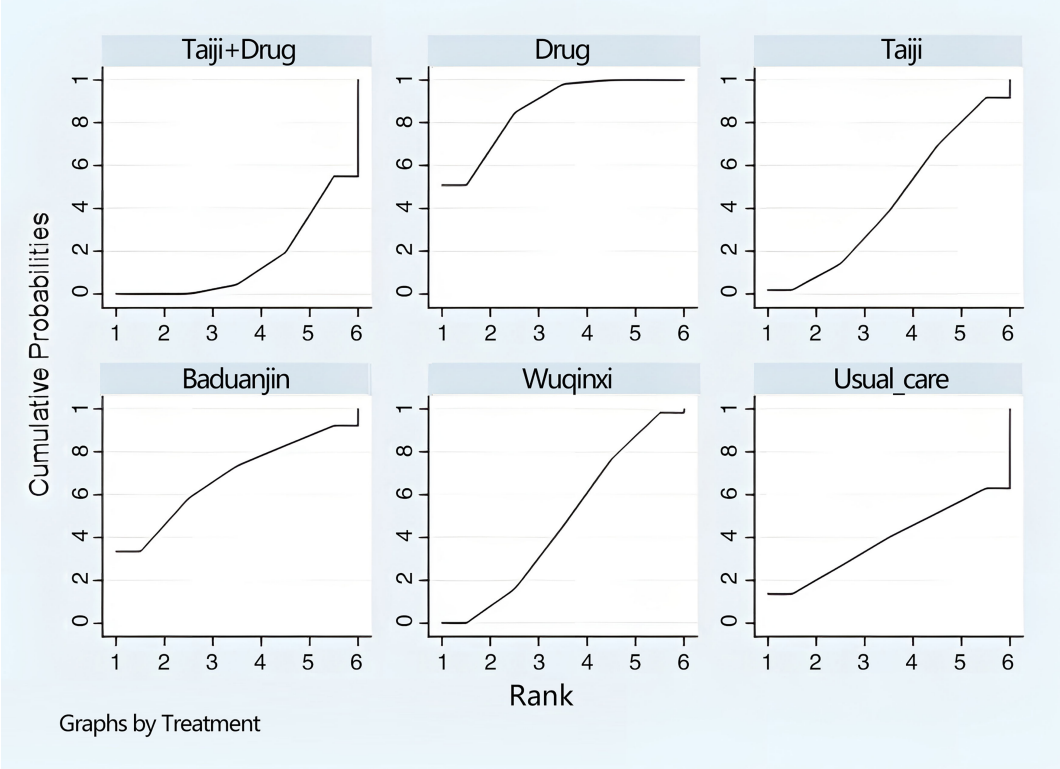

FIGURE 8
Ranking diagram of each intervention (Ward's triangle BMD).

may be preferred to effectively prevent and treat osteoporosis in postmenopausal women in clinical practice at this stage. However, the specific disease should be considered, along with the patient's actual situation, to choose the patient's recommended fitness qigong rationally and discriminatively.

Date availability statement

The original contributions presented in the study are included in the article/Supplementary Material. Further inquiries can be directed to the corresponding author.

Author contributions

SL: Conceptualization, Data curation, Resources, Visualization, Writing – original draft. SW: Data curation, Formal analysis, Methodology, Software, Writing – review & editing. JQ: Data curation, Software, Supervision, Validation, Writing – review & editing. LW: Data curation, Funding acquisition, Supervision, Writing – review & editing.

Funding

The author(s) declare financial support was received for the research, authorship, and/or publication of this article. This study was supported by Fundamental Research Funds for the Central Universities (WUT: 2021VI034), the 2023 Undergraduate Teaching Reform Research Project of Wuhan University of Technology (W2023048), and the Fundamental Research Funds for the Central Universities (WUT: 2024IVA084).

Conflict of interest

The authors declare that the research was conducted in the absence of any commercial or financial relationships that could be construed as a potential conflict of interest.

Publisher's note

Supplementary material

The Supplementary Material for this article can be found online at: https://www.frontiersin.org/articles/10.3389/fendo.2024.1323595/full#supplementary-material

References

1. Tella SH, Gallagher JC. Prevention and treatment of postmenopausal osteoporosis. *J Steroid Biochem Mol Biol* (2014) 6(142):155–70. doi: 10.1016/j.jsbmb.2013.09.008

2. Panel NI. Osteoporosis prevention, diagnosis, and therapy. *JAMA* (2001) 285 (6):785–95. doi: 10.1001/jama.285.6.785

3. Silva I, Branco JC. Denosumab: recent update in postmenopausal osteoporosis. *Acta Reumatolgica Portuguesa* (2012) 37(4):302–13.

4. Sanchez-Rodriguez D, Bergmann P, Body JJ, Cavalier E, Gielen E, Goemaere S, et al. The Belgian bone club 2020 guidelines for the management of osteoporosis in postmenopausal women. *Maturitas* (2020) 139:69–89. doi: 10.1016/j.maturitas.2020.05.006

5. Dalal PK, Agarwal M. Postmenopausal syndrome. *Indian J Psychiat* (2015) 57: S222–32. doi: 10.4103/0019-5545.161483

6. Mornar M, Novak A, Bozic J. Quality of life in postmenopausal women with osteoporosis and osteopenia: associations with bone microarchitecture and nutritional status. *Qual Life Res* (2023) 32(2):1–20. doi: 10.1007/s11136-023-03542-7

7. Kanis JA, Norton N, Harvey NC. Scope 2021: A new scorecard for osteoporosis in Europe. *Arch Osteoporos* (2021) 16:82–9. doi: 10.1007/s11657-020-00871-9

8. David L, Nichols E. Bone health and osteoporosis. *Clinics Sports Med* (2000) 23 (1):466–70. doi: 10.1016/S0278-5919(05)70201-5

9. Zolfaroli I, Ortiz E, Garcia-Perez M-A, Jose Hidalgo-Mora J, Tarin JJ, Cano A. Positive association of high-density lipoprotein cholesterol with lumbar and femoral neck bone mineral density in postmenopausal women. *Maturitas* (2021) 147:41–6. doi: 10.1016/j.maturitas.2021.03.001

10. Zhang SF, Huang XX, Zhao XR. Effect of exercise on bone mineral density among patients with osteoporosis and osteopenia: A systematic review and network meta-analysis. *J Clin Nurs* (2021) 31(15):2100–11. doi: 10.1111/jocn.16101

11. Kanis JA, Cooper C, Rizzoli R, R JY. European guidance for the diagnosis and management of osteoporosis in postmenopausal women. *Osteoporos Int* (2019) 30 (1):3–44. doi: 10.1007/s00198-018-4704-5

12. Center JR, Bliuc D, Nguyen ND, Nguyen TV, Eisman JA. Osteoporosis medication and reduced mortality risk in elderly women and men. *J Clin Endocrinol Metab* (2011) 96(4):1006–14. doi: 10.1210/jc.2010-2730

13. Zhang YJ, Loprinzi PD, Yang L. The beneficial effects of traditional Chinese exercises for adults with low back pain: A meta-analysis of randomized controlled trials. *Medicina* (2019) 55(5):118. doi: 10.3390/medicina55050118

14. Liu J, Wu WZ, Xu DM. Clinical research progress of traditional exercises in the treatment of primary osteoporosis. *Chin J Osteoporosis* (2019) 25(12):1817–20. doi: 10.3969/j.issn.1006–7108

15. Li YJ, Niu XR, Hu S. Efficacy evaluation of different forms of traditional Chinese health-preservation exercises for osteoporosis: A network meta-analysis. *J Acupunct Tuina Sci* (2021) 19(4):258–70. doi: 10.1007/s11726-021-1256-6

16. Zou LY, Wang CY. Baduanjin exercise for stroke rehabilitation: A systematic review with meta-analysis of randomized controlled trials. *Int J Environ Res Public Health* (2018) 15(1):322–42. doi: 10.3390/ijerph15040600

17. Zou L, Zhang Y, Liu Y, Tian X, Xiao T, Liu X, et al. The effects of Tai Chi Chuan versus core stability training on lower-limb neuromuscular function in aging individuals with non-specific chronic lower back pain. *Medicina* (2019) 55(3):345–75. doi: 10.3390/medicina55030060

18. Zou L, Han J, Li C, Yeung AS, Hui SC, Tsang WWN, et al. The effects of tai chi on lower limb proprioception in adults aged over 55: A systematic review and meta-analysis article type: systematic/meta-analytic reviews. *Arch Phys Med Rehabil* (2018) 16(7):168–83. doi: 10.1016/j.apmr.2018.07.425

19. Wei X, Xu A, Yin Y, Zhang R. The potential effect of Wuqinxi exercise for primary osteoporosis: A systematic review and meta-analysis. *Maturitas* (2015) 82 (4):346–54. doi: 10.1016/j.maturitas.2015.08.013

20. Pan YR, Wang MD. The influence of Taijiquan on bone mineral density of natural menopausal women. *Sichuan Sports Sci* (2021) 40(6):26–30+61. doi: 10.13932/j.cnki.sctykx

21. Varahra I. Exercise to improve functional outcomes in persons with osteoporosis: A systematic review and meta-analysis. *Osteoporosis Int* (2018) 29 (2):265–86. doi: 10.1007/s00198-017-4339-y

22. Shamseer L, Moher D, Clarke M, Ghersi D, Liberati A, Petticrew M. Preferred reporting items for systematic review and meta-analysis protocols (Prisma-P) 2015: elaboration and explanation. *Bmj-British Med J* (2015) 349(21):489–99. doi: 10.1136/bmj.g7647

23. Bangshi X, Jinhua W. Kappa consistency test in test medicine research. *Chin J Lab Med* (2006) 1(1):83–4. doi: 10.3760/j:issn:1009-9158.2006.01.030

24. Cai YX, Li XL, Zhao JJ. A clinical observation on prevention of postmenopausal osteoporosis in 30 cases with Baduanjin combined with Calcine D. *Chin Ethnic Folk Med* (2018) 27(23):130–2. doi: 10.19664/j.cnki.1002-2392.180090

25. Chen C. Effects of exercise therapy on bone density, lean body weight and fat content in postmenopausal osteoporosis. *Nanjing Univ Chin Med* (2016) 32:42–8.

26. Su JH, Deng Q. Clinical study of baduanjin combined with anti osteoporosis drugs in the treatment of postmenopausal osteoporosis. *J Traditional Chin Med* (2018) 46(3):84–8. doi: 10.19664/j.cnki.1002-2392.180090

27. Cheng L, Lei Y, Hu Y, Kang KL, Wang XY. Effect of Baduan Jin exercise on bone mineral density in community perimenopausal women. *Chin foreign Med Res* (2017) 15 (1):135–7. doi: 10.14033/j.cnki.cfmr.2017.1.076

28. Peng RD, Deng Q. The effect of Baduanjin on glucose and bone metabolism indicators in postmenopausal type 2 diabetes patients with osteoporosis. *J Traditional Chin Med* (2019) 25(23):53–6. doi: 10.13862/j.cnki.cn43-1446/r.2019.23.013

29. Zhou Y. Effect of traditional sports on bone mineral density of menopausal women. *J Beijing Sport Univ* (2014) 3(1):354–5+60. doi: 10.19582/j.cnki.11-3785/g8.2014.03.024

30. Dan X, Kang JW. Effects of Taijiquan in the adjuvant therapy of postmenopausal osteoporosis. *Chin J modern Nurs* (2015) 21(31):3729–31. doi: 10.3760/cma.j.issn.1674-2907.2015.31.003

31. Liu BX, Chen SP, Li YD, Wang J, Zhang B, Lin Y, et al. The effect of the modified eighth section of eight-section brocade on osteoporosis in postmenopausal women: A prospective randomized trial. *Medicine* (2015) 94(25):e991. doi: 10.1097/MD.0000000000000991

32. Chen WL, Mao YF, Zhang JF, Liu Z, Xiao WL. Observation on the clinical efficacy of Yiqi Wenjing prescription in combination with the newly compiled Wuqinxi on postmenopausal patients with bone loss. *Chin J Osteoporosis* (2018) 24(7):954–8. doi: 10.3969/j.issn.1006-7108

33. Wang FH, Zhang JM, Xu HX. The influence of the newly compiled Wuqinxi exercise on the balance ability and bone density of elderly women. *China J Osteoporosis* (2018) 24(12):1577–81. doi: 10.3969/j.issn.1006-7108

34. Li JW, Pan DQ, He KH, Shi XL. Improved Wuqinxi I Prevention and treatment of primary osteoporosis clinical application experience. *Chin J osteoporosis* (2014) 20 (8):920–3. doi: 10.3969/j.issn.1006-7108

35. Shen MR, Feng YJ, Wang T. Effect of Wuqin exercise on lumbar vertebra density in postmenopausal women. *J integrated traditional Chin western Med* (2012) 22 (8):804–5+20. doi: 10.3969/j.issn.1006-7108

36. Gu L, Liu Y. The effect of the new Wuqinxi on bone mineral density of elderly women. *Chin J Gerontology* (2021) 41(1):79–82. doi: 10.3969/j.issn.1005-9202

37. Shi ZY, Liu Z, Chen WL. Multi-center clinical study on the prevention and treatment of postmenopausal bone mass reduction by integrated therapy of traditional Chinese medicine. *Chin Bone setting* (2017) 29(4):1–7. doi: 10.3969/j.issn.1006-7108.2017.07.017

38. Li J. Effects of three exercises on bone density in elderly women. *Chin J osteoporosis* (2019) 25(3):339–42+50. doi: 10.3969/j.issn.1006-7108

39. Miao FS, Wang M. Effect of fitness qigong on bone density and bone metabolism in postmenopausal women. *J jilin Phys Educ Univ* (2012) 28(3):107–9. doi: 10.21203/rs.2.23049/v1

40. Kuo LT, Hsu RWW, Hsu WH, R. LZ. The comparison of impact of circuit exercise training and Tai-Chi exercise on multiple fracture-related risk factors in postmenopausal osteopenic women. *J Clin Densitometry* (2014) 17(1):427–8. doi: 10.1016/j.jocd.2014.04.102

41. Liu SF, Huang SY. An analysis of the effect of Taijiquan combined with resistance training on bone mineral density in women aged 55-60 years. *J Anyang Normal Univ* (2019) 23(3):82–6. doi: 10.16140/j.cnki.1671-5330.2019.05.021

42. Liu CJ, Liu G. Effects of regular taijiquan exercise on serum lipids, leptin levels and bone mineral density in retired women. *Liaoning sports Sci Technol* (2014) 36 (3):55–8. doi: 10.13940/j.cnki.lntykj.2014.03.019

43. Mao HN. Effect of Taijiquan combined with calcium supplement on bone mineral density in postmenopausal women. *Chin J Rehabil Med* (2009) 24(9):814–6.

44. Song JL, Cheng L, Chang SW. Effects of 48-week shadowboxing, brisk walking and square dancing on bone density in elderly women. *J Shandong Institute Phys Educ* (2018) 34(6):105–8. doi: 10.14104/j.cnki.1006-2076.2018.06.018

45. Xu F. Effect of 24 style simplified Taijiquan on bone mineral density in postmenopausal women. *J Pract Chin Med* (2017) 33(12):1428–9.

46. Ye CQ, Wang CW, Wang GY. The influence of Taijiquan on the health status of middle-aged and old women. *Chin J Health Med* (2016) 18(6):494–5. doi: 10.3969/.issn.1674-3245.2016.06.022

47. Yu DH, Wang HR, Xie YL. Effects of Tai Chi calisthenics on bone mineral density in postmenopausal women. *J Shanghai institute Phys Educ* (2014) 38(6):100–4. doi: 10.16099/j.cnki.jsus.2014.06.019

48. Zhao J, Cheng L. Effects of different types of long-term exercise on bone mineral density in elderly women. *Chin J osteoporosis* (2020) 26(1):50–3. doi: 10.3969/j.issn.1006-7108

49. Zhao MY, Li N, Fan C, Yuan SH. Influence of Tai Chi push-hand exercise combined with nutritional intervention on rehabilitation of patients with primary osteoporosis. *Liaoning sports Sci Technol* (2015) 37(3):44–6. doi: 10.13940/j.cnki.lntykj.2015.03.013

50. Zhou Y. LIJ, Chen YB, Jia JY. Effects of Tai Chi push-hand exercise and calcium supplementation on bone mineral density in postmenopausal women. *Chin J Sports Med* (2015) 2(1):106–8. doi: 10.13940/j.cnki.lntykj.2015.03.013

51. Chan KM, Qin L, Lau MC, Woo J, Au S, Choy WY, et al. A randomized, prospective study of the effects of Tai Chi Chun exercise on bone mineral density in postmenopausal women. *Arch Phys Med Rehabil* (2004) 85(5):717–22. doi: 10.1016/j.apmr.2003.08.091

52. Wayne PM, Kiel DP, Buring JE, Connors EM, Davis RB. Impact of Tai Chi exercise on multiple fracture-related risk factors in post-menopausal osteopenic women: A pilot pragmatic, randomized trial. *BMC Complementary Altern Med* (2012) 12(1):7. doi: 10.1186/1472-6882-12-7

53. Wang HR, Yu B, Chen WH. Simplified Tai Chi resistance training versus traditional Tai Chi in slowing bone loss in postmenopausal women. *Evidence-Based Complementray Altern Med* (2015) 2015(2):1–6. doi: 10.1155/2015/379451

54. Liu GL, Liu XQ. The influence of Taijiquan exercise on bone mineral density and bone metabolism indicators of postmenopausal women. *Contemp Sports Sci Technol* (2021) 11(24):19–21. doi: 10.16655/j.cnki.2095-2813.2012-1579-1245

55. Li KQ, Yu HG, Lin XJ. The effects of Er Xian decoction combined with Baduanjin exercise on bone mineral density, lower limb balance function, and mental health in women with postmenopausal osteoporosis: A randomized controlled trial. *Evidence-Based Complementary Altern Med* (2022) 2022(1):13. doi: 10.1155/2022/8602753

56. Salanti G, Ades AE. Graphical methods and numerical summaries for presenting results from multiple-treatment meta-analysis: an overview and tutorial. *J Clin Epidemiol* (2011) 64(2):163. doi: 10.1016/j.jclinepi.2010.03.016

57. Hutton B, Salanti G, Caldwell DM. The prisma extension statement for reporting of systematic reviews inCorporating network meta-analyses of health care interventions: checklist and explanations. *Ann Internal Med* (2015) 162(11):777. doi: 10.7326/M14-2385

58. Zhang C, Yan JZ, Sun F. Methods for identification and treatment of consistency of reticular meta-analysis. *Chin J Evidence Based Med* (2014) 14(7):884. doi: 10.7507/1672-2531.20140146

59. Liu SJ, Yu Q, Li ZM, Cunha PM, Zhang Y, Kong ZW, et al. Effects of acute and chronic exercises on executive function in children and adolescents: A systemic review and meta-analysis. *Front Psychol* (2020) 11:554915. doi: 10.3389/fpsyg.2020.554915

60. Du XL, Zhao XH. Clinical observation on the improvement of osteoporosis symptoms in postmenopausal women with traditional Chinese medicine combined with Eight Duan Jingong. *Chin Health standards Manage* (2014) 5(5):65–8. doi: 10.3969/J.ISSN.1674-9316.2014.05.038

61. Sun W, Wang JN, Yang CR. A follow-up study on the effects of Taijiquan and fast walking exercise on bone density and bone metabolism in elderly women. *Chin J osteoporosis* (2017) 23(8):1034–40. doi: 10.3969/j.issn.1006-7108

62. Furuya-Kanamori L, Barendregt JJ, Doi SA. A new improved graphical and quantitative method for detecting bias in meta-analysis. *J Int J Evid Based Healthc* (2018) 53:1–23. doi: 10.1097/XEB.0000000000000141

63. Li JY, Cheng L. Effects of tai chi exercise with different frequencies on bone mineral density in elderly women for 48 weeks. *Chin J Osteoporosis* (2017) 23 (10):1309–12. doi: 10.3969/j.issn.1006-7108.2017.10.010

64. Yu Y. Net meta-analysis of four traditional Chinese fitness exercise therapy on osteoporosis in middle-aged and elderly people. *China sports Sci Technol* (2020) 56 (9):37–44. doi: 10.16470/j.csst.2020115

65. Jing FJ, Z J. Effect of tendon changing exercise on bone mineral density of patients with primary osteoporosis. *China Sports Sci Technol* (2008) 1(2):88–90+102. doi: 10.16470/j.csst.2008.02.002

66. Robinson JA, Riggs BL, Spelsberg TC. Osteoclasts and transforming growth factor-beta: estrogen-mediated inform-specific regulation of production. *Endocrinology* (1996) 137(2):615–21. doi: 10.1210/ENDO.137.2.8593810

67. Chen J. Clinical observation on the improvement of postmenopausal women's osteoporosis symptoms with traditional Chinese medicine diet and Baduanjingong. *Asia Pacific Traditional Med* (2015) 11(7):104–5. doi: 10.1089/jwh.2017.6706

68. Mao DW, Li JX, Hong Y. The duration and plantar pressure distribution during one-leg stance in Tai Chi exercise. *Clin biomechanics (Bristol Avon)* (2008) 21(6):640–5. doi: 10.1016/J.CLINBIOMECH.2006.01.008

69. Li H, Ge D, Liu S, Zhang W, Wang J, Si J, et al. Baduanjin exercise for low back pain: A systematic review and meta-analysis. *Complementary Therapies Med* (2019) 43:109–16. doi: 10.1016/j.ctim.2019.01.021

70. Wang XW, Chen GQ. Research progress of traditional health and modern sports in prevention and treatment of primary osteoporosis. *Int J Geriatr* (2022) 43 (6):755–8.

71. Zou L, Wang C, Chen K, Sh Y, Chen X, Luo L, et al. The effect of Taichi practice on attenuating bone mineral density loss: A systematic review and meta-analysis of randomized controlled trials. *Int J Environ Res Public Health* (2017) 15(14):156–79. doi: 10.3390/ijerph14091000

frontiers | Frontiers in Endocrinology

TYPE Original Research
PUBLISHED 04 April 2024
DOI 10.3389/fendo.2024.1360054

OPEN ACCESS

EDITED BY
Katherine A. Staines,
University of Brighton, United Kingdom

REVIEWED BY
Farasat Zaman,
Karolinska University Hospital, Sweden
Anirudha Sanjay Karvande,
Children's Hospital of Philadelphia,
United States

*CORRESPONDENCE
Dalia Ali
dayesh@health.sdu.dk
Meshail Okla
meokla@ksu.edu.sa

†These authors contributed equally to this work and share first authorship

RECEIVED 22 December 2023
ACCEPTED 15 March 2024
PUBLISHED 04 April 2024

CITATION
Ali D, Okla M, Abuelreich S, Vishnubalaji R, Ditzel N, Hamam R, Kowal JM, Sayed A, Aldahmash A, Alajez NM and Kassem M (2024) Apigenin and Rutaecarpine reduce the burden of cellular senescence in bone marrow stromal stem cells.
Front. Endocrinol. 15:1360054.
doi: 10.3389/fendo.2024.1360054

Apigenin and Rutaecarpine reduce the burden of cellular senescence in bone marrow stromal stem cells

Dalia Ali[1*†], Meshail Okla[2,3*†], Sarah Abuelreich[3], Radhakrishnan Vishnubalaji[3], Nicholas Ditzel[1], Rimi Hamam[3], Justyna M. Kowal[1], Ahmed Sayed[1], Abdullah Aldahmash[4], Nehad M. Alajez[3] and Moustapha Kassem[1,5]

[1]Department of Endocrinology and Metabolism, Molecular Endocrinology & Stem Cell Research Unit (KMEB), Odense University Hospital, University of Southern Denmark, Odense, Denmark, [2]Department of Community Health Sciences, College of Applied Medical Sciences, King Saud University, Riyadh, Saudi Arabia, [3]Stem Cell Unit, Department of Anatomy, College of Medicine, King Saud University, Riyadh, Saudi Arabia, [4]Department of Medical Basic Sciences, College of Medicine, Vision College, Riyadh, Saudi Arabia, [5]Institute for Cellular and Molecular Medicine (ICMM), Faculty of Health Sciences, University of Copenhagen, Copenhagen, Denmark

Introduction: Osteoporosis is a systemic age-related disease characterized by reduced bone mass and microstructure deterioration, leading to increased risk of bone fragility fractures. Osteoporosis is a worldwide major health care problem and there is a need for preventive approaches.

Methods and results: Apigenin and Rutaecarpine are plant-derived antioxidants identified through functional screen of a natural product library (143 compounds) as enhancers of osteoblastic differentiation of human bone marrow stromal stem cells (hBMSCs). Global gene expression profiling and Western blot analysis revealed activation of several intra-cellular signaling pathways including focal adhesion kinase (FAK) and TGFβ. Pharmacological inhibition of FAK using PF-573228 (5 μM) and TGFβ using SB505124 (1μM), diminished Apigenin- and Rutaecarpine-induced osteoblast differentiation. *In vitro* treatment with Apigenin and Rutaecarpine, of primary hBMSCs obtained from elderly female patients enhanced osteoblast differentiation compared with primary hBMSCs obtained from young female donors. *Ex-vivo* treatment with Apigenin and Rutaecarpine of organotypic embryonic chick-femur culture significantly increased bone volume and cortical thickness compared to control as estimated by μCT-scanning.

Discussion: Our data revealed that Apigenin and Rutaecarpine enhance osteoblastic differentiation, bone formation, and reduce the age-related effects of hBMSCs. Therefore, Apigenin and Rutaecarpine cellular treatment represent a potential strategy for maintaining hBMSCs health during aging and osteoporosis.

KEYWORDS

bone marrow stromal stem cells, osteoblasts, senescence, aging, antioxidants, osteoporosis

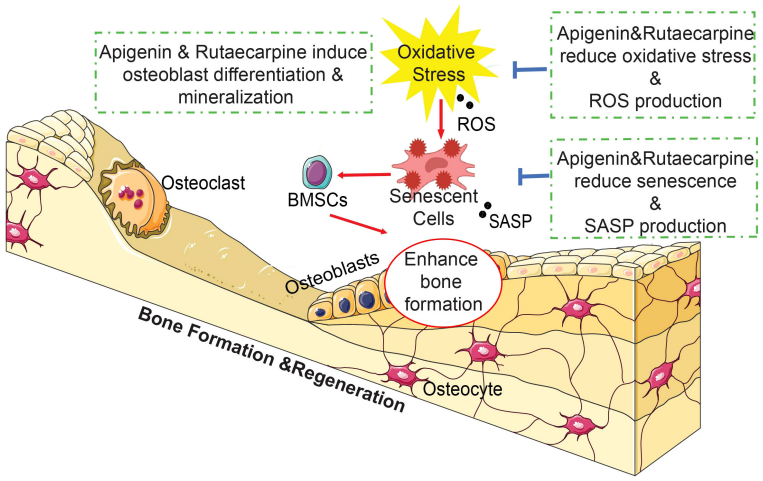

GRAPHICAL ABSTRACT
In brief, the natural compounds Apigenin and Rutaecarpine enhanced osteoblastic differentiation of hBMSCs and reduced the burden of cellular senescence and inflammation. Our results suggest a possible role for Apigenin and Rutaecarpine as small molecule antioxidant agents that can be used to prevent impaired osteoblastic functions and bone loss associated with aging and osteoporosis.

1 Introduction

Osteoporosis is a systemic skeletal disease characterized by decreased bone mass and micro-architectural deterioration of bone tissue, leading to bone fragility and increased fracture risk (1). Osteoporosis is caused by imbalance between bone formation and bone resorption during bone remodeling (2). The mechanisms underlying the age-related osteoporosis are either intrinsic cellular mechanisms leading to cellular senescence and affecting osteoblastic functions e.g. telomere shortening, impaired mitochondrial function and increased oxidative stress, or extrinsic factors associated with endocrine aging (3) e.g. menopause or age-related decreased in levels of male sex steroids, GH-IGF system. Both mechanisms affect the cellular and molecular signaling in BMSCs leading to impaired cell proliferation, differentiation, and function (2, 4).

There are currently few drugs that are being used to treat osteoporosis such as Bisphosphonates and Denosumab (5). These medications come with side effects ranging from gastroesophageal irritation to serious problems of increased risk for osteonecrosis of the jaw (6). Preventive strategies include adequate daily intake of calcium, vitamin D supplementation, maintaining optimal body weight, regular physical activity and cessation of smoking and alcohol intake (7). There is an increasing interest in identifying herbal supplements that are affordable and have minimal side effects (8). For example, a Chinese herbal formula (ZD-1) was found to inhibit mineralization and downregulation of several osteogenic markers such as osteocalcin, BMP-2, and osteopontin of hBMSCs (9, 10). Another study reported that Naringin enhanced the osteogenic differentiation via activating the β-catenin pathway (11). Giacomo et al, demonstrated that Tithonia diversifolia inhibited adipogenesis and promoted osteogenesis of hBMSCs via acting as a potent antioxidant (12). Moreover, Resveratrol, a plant derived natural antioxidant and SIRT1 activator, enhances osteogenic differentiation, inhibits adipogenic differentiation, and reduces the senescence-associated phenotype and oxidative stress in aged hBMSCs (13). Apigenin is a major polyphenol in olives and parsley, that was found to inhibit osteoclastogenesis and suppress trabecular bone loss in OVX mice (14). In cultured hBMSCs, Apigenin induced osteogenesis via activating JNK and p38 MAPK signaling pathways (15). Rutaecarpine is derived from the plant *Evodia rutaecarpa* (a dried fruit called 'Wu-Chu-Yu' in China) and has been employed in the treatment of cardiovascular diseases (16), obesity (17), gastrointestinal disorders, headache, amenorrhea, and postpartum hemorrhage (18, 19). Additionally, Rutaecarpine inhibits osteoclastogenesis and bone resorption of bone marrow-derived osteoclasts (20).

In the current study, to identify plant-derived natural compounds with significant effects on osteoblast differentiation and bone formation, we conducted a functional osteogenic screening of a natural product library. We identified Apigenin and Rutaecarpine as significant positive regulators of osteoblasts differentiation in hBMSCs and examined their possible underlying molecular mechanisms in the context of aging.

2 Materials and methods

2.1 Screening natural compounds

Screening Natural compounds library (Supplementary Table 1) was purchased from Selleckchem (Selleckchem Inc., Houston, TX, USA, Catalog No. L1400), compounds were dissolved in DMSO at stock concentration of 10mM. Considering previous investigations, which have utilized these compounds within a range of 100nM to 10μM (13, 21, 22), the screening test was conducted with a mid-range concentration of 500nM. For all subsequent experiments, Apigenin and Rutaecarpine were used at a final concentration of 1μM.

2.2 Cell culture and osteogenic differentiation

Human Bone Marrow stromal stem cells (hBMSCs) was created by the overexpression of the human telomerase reverse transcriptase gene (hTERT) (23). hBMSCs cell line expresses known markers of primary hBMSCs, exhibits stemness characteristics, and is able to form bone and bone marrow microenvironment when implanted *in vivo* (24). BMSCs were cultured in Minimum Essential Medium (MEM) supplemented with D-glucose 4,500 mg/L, 4 mM l-glutamine, 110 mg/L sodium pyruvate, 10% fetal bovine serum, 1% penicillin–streptomycin (Pen-Strep), and 1% nonessential amino acids. All reagents were purchased from Gibco-Invitrogen (Carlsbad, CA, USA). Cells were incubated in 5.5% CO_2 incubators at 37°C, hBMSCs were cultured to reach 80%–90% confluence before exposing the cells to osteogenic differentiation induction media supplemented with Apigenin or Rutaecarpine at 1μM. Control cells were treated with basal medium containing dimethyl sulfoxide (DMSO) as vehicle. Primary hBMSCs that were used for compounds validation were purchased from Thermo Fisher Scientific. hBMSCs or primary hBMSCs were cultured as noted in the previous section and exposed to osteogenic induction medium (MEM containing 10% FBS, 1% penicillin-streptomycin, 50 mg/ml L-ascorbic acid (Wako-chemicals), 10mM β glycerophosphatase (Sigma-Aldrich), 10 nM calcitriol (1a,25-dihydroxyvitamin D3; Sigma Aldrich), and 100 nM dexamethasone (Sigma-Aldrich) supplemented with the compounds Apigenin or Rutaecarpine at 1μM, media was changed every two days for 10 days. To evaluate the involvement of FAK and TGFβ signaling, hBMSCs were cultured in 96-well plates under osteogenic induction media supplemented with Apigenin, Rutaecarpine or vehicle control and were additionally supplemented with FAK inhibitor (PF-573228, at 5 μM) (Sigma-Aldrich) or transforming growth factor β (TGFβ) signaling inhibitor (SB505124, at 1 μM) (Sigma-Aldrich), media was replaced every 2 days. ALP quantification for osteogenesis was performed on day10.

2.3 Primary hBMSCs

Bone marrow samples were collected from female femur of two healthy young donors (Age 25 and 26 years old) and two aged osteoporotic patients (Age 91 and 86 years old) undergoing routine orthopaedic surgeries at the Department of Orthopaedic and Traumatology, Odense University Hospital. The subjects received oral and written project information and signed written consent. The study was approved by the Scientific Ethics Committee of Southern Denmark (project ID: S-20160084). Our selection of the aged patients for this study was based on their BMSCs' low osteogenic differentiation capacity, as identified in previously published studies (25, 26), as we aim to explore the efficacy of Apigenin and Rutaecarpine in enhancing osteogenic differentiation capacity. Primary hBMSCs were obtained from mononuclear cell population isolated from bone marrow samples following gradient centrifugation in lymphoprep, through plastic adherence. The cells were cultured in MEM media supplemented with 10% foetal bovine serum (FBS) and 1% penicillin/streptomycin (P/S). When the first adherent cells were observed, the media was changed to MEM media supplemented with 10% FBS, 1% P/S, 1% GlutaMAX, 1% sodium pyruvate and 1% non-essential amino acids (S-MEM growing medium). These primary hBMSCs were cultured in 37°C in humidified 5% CO_2 incubator. Cells from each participant were cultured separately, and only cells from passage two were utilized in the experiments conducted in this study. In primary culture experiments, "n=2" corresponds to the number of subjects per experimental group. In ALP test, each subject contributed 6 technical replicates, resulting in a total of 12 observations. In qPCR, each subject contributed 4 technical replicates, resulting in a total of 8 observations.

2.4 Evaluation of osteoblast differentiation

To quantify alkaline phosphatase (ALP) activity in control and osteoblast-differentiated hBMSCs the BioVision ALP activity colorimetric assay kit (BioVision, Inc., Milpitas, CA, http://www.biovision.com/) was used with some modifications. Cells were cultured in 96-well plates under normal or osteogenic induction conditions supplemented with Apigenin or Rutaecarpine at 1μM. On day 10, wells were rinsed once with PBS and were fixed using 3.7% formaldehyde in 90% ethanol for 30 seconds at room temperature. Then the fixative reagent was removed and 50 μl of p-nitrophenyl phosphate solution was added to each well and incubated for 20–30 minutes in the dark at room temperature until a clear yellow color is developed. Reaction was subsequently stopped by adding 20 μl of stop solution. Optical density was then measured at 405nm using a SpectraMax/M5 fluorescence spectrophotometer plate reader. Cell viability was measured using alamarBlue assay according to the manufacturer's recommendations (Thermo Fisher Scientific). Cell viability was taken in consideration when performing ALP quantification activity on osteogenic differentiated cells. In brief, AlamarBlue was added at ratio of 10% from the volume of the media added on cultured cells in 96-well plates of osteogenic differentiated cells. Plates were incubated in the dark at 37°C for 1h. Reading was subsequently taken using fluorescent mode (Ex 530 nm/Em 590 nm) using BioTek Synergy II microplate reader (BioTek Inc., Winooski, VT, USA).

For ALP staining, cells were washed in PBS, fixed in acetone/citrate buffer and incubated with ALP substrate solution (naphthol AS-TR phosphate 0.1M Tris buffer, pH 9.0) for 1 h at room temperature and subsequently images were taken using an EVOS Cell Imaging System (Thermo Fisher Scientific).

Alzarin Red S staining (ALZR) (ScienCell Research Laboratories, Cat No 0223, San Diego, CA, USA) was used to stain for calcium deposits, which are indicators of mature osteocytes, on day 14 of osteogenic differentiation and upon exposure to Apigenin or Rutaecarpine and according to manufacturer's protocol. Cells were washed twice with PBS then were fixed with 4% Paraformaldehyde in PBS for 15 min at room temperature, then washed three times with distilled water then

added 1ml of 2% ALZR stain to each well for 30 mints then final wash with distilled water at least 3 times before taking images. Images were captured using an EVOS Cell Imaging System (Thermo Fisher Scientific).

2.5 Quantitative real-time qPCR

Total RNA was isolated from cell pellets after 10 days of osteogenic differentiation using the Total RNA Purification Kit (Norgen Biotek Corp., Thorold, ON, Canada, https://norgenbiotek.com/) according to the manufacturer's protocol. The concentrations of total RNA were measured using NanoDrop 2000 (Thermo Fisher Scientific). cDNA was synthesized using 500 ng of total RNA. The Thermo Fisher Scientific High-Capacity cDNA Transcription Kit was used according to manufacturer's protocol. Expression levels of osteoblast-related genes (Supplementary Table 2) were quantified using the ViiA 7 Real-Time PCR device (Thermo Fisher Scientific). Expression was quantified using Fast SYBR Green Master Mix and a ViiA 7 Real-Time PCR device (Thermo Fisher Scientific). The 2DCT value method was used to calculate relative expression, and analysis was performed as previously described (27).

2.6 DNA microarray gene expression profiling

A total of 150 ng RNA was labelled using low input Quick Amp Labeling Kit (Agilent Technologies, Santa Carla, CA, USA) and then hybridized to the Agilent Human SurePrint G3 Human GE 8x60k microarray chip (Agilent Technologies, Santa Carla, CA, USA). All microarray experiments were performed at the Microarray Core Facility (Stem Cell Unit, King Saud University College of Medicine, Riyadh, Saudi Arabia). The extracted data were normalized and analyzed using GeneSpring 13.0 software (Agilent Technologies, Santa Carla, CA, USA). Pathway analysis was performed using the Single Experiment Pathway analysis feature in GeneSpring 13.0 (Agilent Technologies Agilent Technologies, Santa Carla, CA, USA). Two-fold cut-off and a $p< 0.05$ were used to enrich for significantly changed transcripts.

2.7 Western blot analysis

hBMSCs were seeded until reaching 60-80% confluence before incubation in serum reduced medium (0.2% FBS), low glucose MEM medium for 6 hours prior to treatment with 1μM of Apigenin, Rutaecarpine or DMSO-vehicle control in osteogenic induction media. Protein samples were harvested at 0, 30, 60, 120 & 240 minutes after treatment. Briefly, cells were washed in PBS and were lysed in RIPA buffer (Invitrogen) supplemented with protease inhibitors (Roche). After 30 min incubation at 4°C, samples were centrifuged for 10 min at 12,000 rpm, 4°C. Protein concentration was determined using Pierce Coomassie Plus Bradford assay (Thermo Fisher Scientific), and equal amounts of proteins were loaded on a 10% polyacrylamide gel (Invitrogen). Blotted nitrocellulose membranes were incubated overnight with antibodies against p-FAK, FAK, p-ERK, ERK2, p-SMAD2, SMAD2 & Actin (Cell Signaling) at 4°C. Membranes were incubated with HRP conjugated anti-mouse or anti-rabbit secondary antibody (Santa Cruz Biotechnology) for 45 min at room temperature, and protein bands were visualized with Amersham ECL chemiluminescence detection system (GE Healthcare Bio-Sciences Corp).

2.8 Senescence-associated β-galactosidase (β-gal) staining

To investigate the possible protective role of Apigenin or Rutaecarpine treatmement on senescent cells, we used a commercial kit for β-gal staining (Cell Signaling TechnologyNetherlands, Cat# 9860). BMSCs were cultured in black 96-well clear bottom plate and were treated with Apigenin or Rutaecarpine at 1μM for 2 days. After that cells were differentiated using osteogenic induction media for one week with vehicle control DMSO or Apigenin or Rutaecarpine with or without 50μM TBHP. Cells were washed with PBS, and then were fixed for 10 minutes at room temperature. After fixation the cells were rinsed with PBS and incubated with β-gal staining solution (pH = 6.0) at 37°C in dry incubator (none-CO_2) overnight. The blue color as a reaction result of senescence was monitored after 10-12h. Images of cells were captured with inverted microscope under bright field.

2.9 Cellular reactive oxygen species (ROS) detection

A commercial kit of DCFDA (2,7-dichloro-dihydro-fluorescein diacetate; Abcam, Cambridge, MA) was used to measure the intracellular ROS level. hBMSCs were seeded at $2.5x10^4$ cells/well into a black 96 well plate with a clear bottom and were allowed to adhere. First, cells were treated with Apigenin or Rutaecarpine at 1μM for 2 days and then exposed to tert-butyl hydrogen peroxide (TBHP) at 55μM for 2 hours. Next, cells were loaded with DCFDA according to the manufacturer's protocol and incubated for 45 minutes at 37 °C. After that, DCFDA was removed, and experimental conditions were added again to the cells for 15 minutes. Then, the fluorescent intensity was measured at Excitation 485nm and Emission 535 nm using SpectraMax M5 (Molecular Devices).

2.10 Chick femur and micro-computed tomography scanning (μCT)

Ex vivo cultures of embryonic, day 11 (E11) and 13 (E13), chick femurs were performed as described previously (28). In brief, control non-induced femurs were cultured in the basal culture media with ascorbic acid 2-phosphate (100 mM), while other femurs were cultured in osteogenic induction medium along with either DMSO or Apigenin or Rutaecarpine at 1μM. All the femurs placed onto Millicell inserts

(0.4-mm pore size, 30-mm diameter; Millipore) in six-well tissue culture plates containing 1mL media per well at the liquid/gas interface. Femurs were cultured for 10 days at 37°C, 5% CO_2, with media changed every 24 h. Femurs were then fixed in 4% paraformaldehyde (PFA) for 24hr. The chick femurs were micro-CT imaged in air using a vivaCT40-scanner (SCANCO Medical AG, Brüttisellen, Switzerland). Samples were scanned with 70kV, 114μA, and a sampling time of 300ms. Three-dimensional images were reconstructed and analyzed at a resolution of 10.5 μm isotropic voxels using the software supplied by the manufacturer of the scanner.

2.11 Statistical analysis

Statistical analyses were performed on Prism 9 (GraphPad Software). Bar graphs are shown as mean % ± *SEM*, and statistical significance between groups was determined by at least 2 independent experiments. The statistical significance was determined by unpaired t-test and one-way ANOVA. All results are compared to DMSO-control unless otherwise stated by the line arrow. *P* value < 0.05 was considered statistically significant.

3 Results

3.1 Effect of Natural Compounds on Osteogenic Differentiation of hBMSCs

Initially, a library of 143 natural compounds (Supplementary Table 1) were screened for thier effect on osteoblastic differentiation of hBMSCs at a dose of 500nM. Cells were continuously exposed to compounds during osteoblastic differentiation media and were assessed by (ALP activity) (Figure 1A). Eleven of the most potent significant compounds were chosen and assessed their effects on ALP activity as shown in (Figure 1B). Two compounds were chosen, Apigenin and Rutaecarpine as they exerted pronounced effects (Figure 1C) and conducted a dose response effect of the compounds on osteoblast differentiation as estimated by ALP activity (Figure 1D) that revealed 1μM is the optimum dose to induce osteoblast differentiation of cultured hBMSCs. Apigenin and Rutaecarpine were chosen to be further investigated and at dose of 1μM, results were validated in primary hBMSCs (Figure 1E). Similarly, the intensity of ALP staining was higher in Apigenin and Rutaecarpine-treated hBMSCs compared to vehicle-treated control cells (Figure1F, upper panel). In addition, *in vitro* mineralization as evidenced by ALZR staining, was more intense in Apigenin and Rutaecarpine-treated hBMSCs compared to vehicle-treated control cells (Figure 1F, lower panel). To identify molecular mechanism mediating enhanced osteoblast differentiation in Apigenin and Rutaecarpine treated cells, we evaluated mRNA levels of selected osteoblastic genes panel using mRNA from hBMSCs post osteogenic differentiation with Apigenin (Figure 1G) and Rutaecarpine (Figure 1H). Employing osteogenesis-related Apigenin treatment revealed significant up-regulation in: (SPP1, FOS, SMAD2, SMAD4, LEF1, NOG, MAPK9, TGFβR2, BMP4, LAMA3, COMP, BLK, RUNX2, ALP, OC and ON). Rutaecarpine treatment significantly revealed up regulation of osteoblastic markers of: COMP, LAMA3, THBS2, JUN, RUNX2, TGFβR2, OC, ON and ALP.

3.2 Genes and pathways differentially regulated in osteoblasts by Apigenin and Rutaecarpine treatments

3.2.1 Apigenin

Microarray-based gene expression profiling was conducted on hBMSCs following exposure to Apigenin along with osteoblastic induction for 21 days and compared to that of vehicle-treated control cells. Hierarchical clustering based on differentially expressed transcripts showed clear separation between the Apigenin-treated and control cells (Figure 2A). We identified 687 upregulated and 913 downregulated transcripts (> 2.0 FC, P (corr) < 0.05; Supplementary Table 3). Analysis of the differentially expressed upregulated genes revealed strong enrichment for several cellular processes involved in osteoblastic differentiation, including focal adhesion, endochondral ossification, osteoblast signaling, TGFβ pathway, oxidative stress, and selenium pathway (Figure 2B). Heatmap for the up-regulated genes, upon Apigenin treatment, that are involved in skeletal system development and regulation of osteoblast differentiation pathways are shown (Figure 2C). The activation of several intracellular signaling pathways: focal adhesion kinase (FAK), extracellular signal regulated kinase (ERK) and (SMAD2) were observed upon Apigenin treatment as indicated by western blotting of p-FAK, p-ERK, and p-SMAD2 (Figure 2D). To identify the relevant contribution of FAK and TGFβ in Apigenin-induced osteogenesis, we tested the effects of inhibition of these pathways using FAK inhibitor (FAKi) (using PF-573228) or TGFβ inhibitor (TGFβi) (using SB505124). The results showed that Apigenin-mediated increase in ALP activity was significantly reduced by FAKi, and TGFβi (Supplementary Figure 1A).

3.2.2 Rutaecarpine

Microarray-based gene expression profiling was conducted on hBMSCs following exposure to Rutaecarpine along with osteoblastic induction for 21 days and compared to that of vehicle-treated control cells. Hierarchical clustering based on differentially expressed transcripts showed clear separation between the Rutaecarpine-treated and control cells (Figure 3A). We identified 348 upregulated and 533 downregulated transcripts (> 2.0 FC, P (corr) < 0.05; Supplementary Table 4). Analysis of the differentially expressed upregulated revealed strong enrichment for several cellular processes involved in osteoblastic differentiation, including focal adhesion, endochondral ossification, TGFβ pathway, Toll-like receptor pathway, oxidative stress, and selenium pathway (Figure 3B). Heatmap for up-regulated genes,upon Rutaecarpine treatment, that are involved in skeletal system and bone development pathways are shown (Figure 3C). The activation of several intracellular signaling pathways: focal adhesion kinase (FAK), extracellular signal regulated kinase (ERK) and SMAD2 was observed

10.3389/fendo.2024.1360054

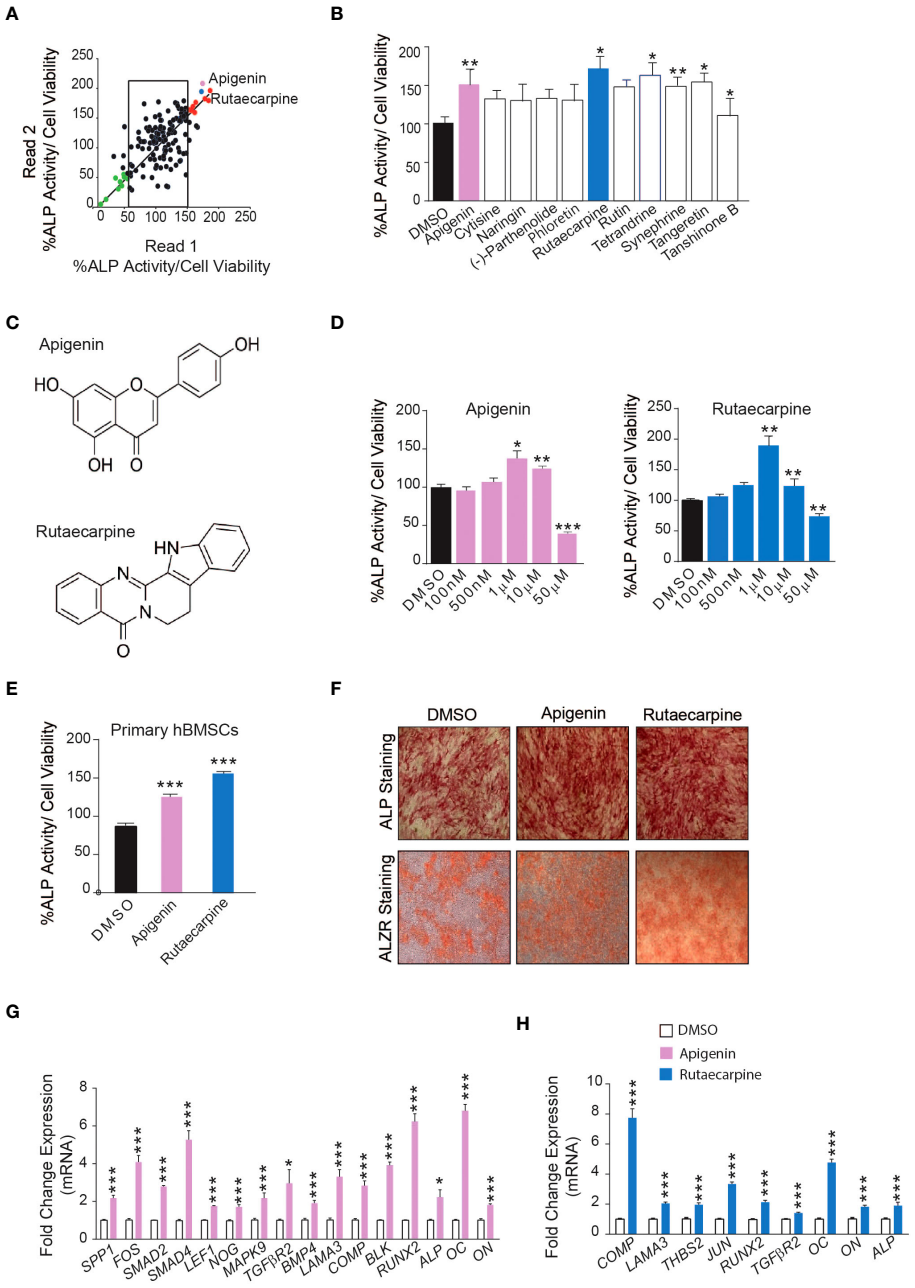

FIGURE 1
Screening of 143 natural compounds library on osteoblast differentiation revealed significant impact of Apigenin and Rutaecarpine on osteogenesis **(A)** Quantification of Alkaline phosphatase (ALP) activity in 144 compounds treated hBMSCs vs control-treated cells at a dose of 500nM. **(B)** Quantification of Alkaline phosphatase (ALP) activity in 11 compounds at 500nM **(C)** Chemical structure of Apigenin and Rutaecarpine **(D)** Dose response effect of Apigenin, Rutaecarpine on osteogenic differentiation of hBMSCs via quantification of ALP activity at concentrations of 100nM, 500nM, 1μM, 10μM & 50μM, (n=6) from two independent experiments **(E)** Quantification of Alkaline phosphatase (ALP) activity in primary hBMSCs treated with Apigenin or Rutaecarpine or Vehicle control cells at 1μM, (n=12) from two independent experiments **(F)** ALP staining, upper panel (4x magnification) and alizarin red staining for mineralized matrix formation, lower-panel (4x magnification). **(G)** qRT-PCR of a panel of osteoblast-related genes in the presence of Apigenin compared to vehicle control, normalized to β-actin. Data are presented as mean fold changes ± SEM compared with vehicle-treated controls; n = 6 from two independent experiments **(H)** qRT-PCR of a panel of osteoblast-related genes in the presence of Rutaecarpine compared to vehicle control, normalized to β-actin. Data are presented as mean fold changes ± SEM compared with vehicle-treated controls; n = 6 from two independent experiments. Data are presented as mean ± SEM, from two independent experiments, using two-tailed unpaired Student's t test. (*P< 0.05, **P< 0.005, ***P< 0.0005). All results are compared to DMSO-control unless otherwise stated by the line arrow. Data without the line arrow indicates no statistical significance.

upon Rutaecarpine treatment as indicated by western blotting of p-FAK, p-ERK, and p-SMAD2 (Figure 3D). To identify the relevant contribution of FAK and TGFβ in Rutaecarpine-induced osteogenesis, we tested the effects of inhibition of these pathways using FAK inhibitor (FAKi) (using PF-573228) or TGFβ inhibitor (TGFβi) (using SB505124). The results showed that Rutaecarpine-mediated increase in ALP activity was significantly reduced by FAKi, and TGFβI (Supplementary Figure 1B).

10.3389/fendo.2024.1360054

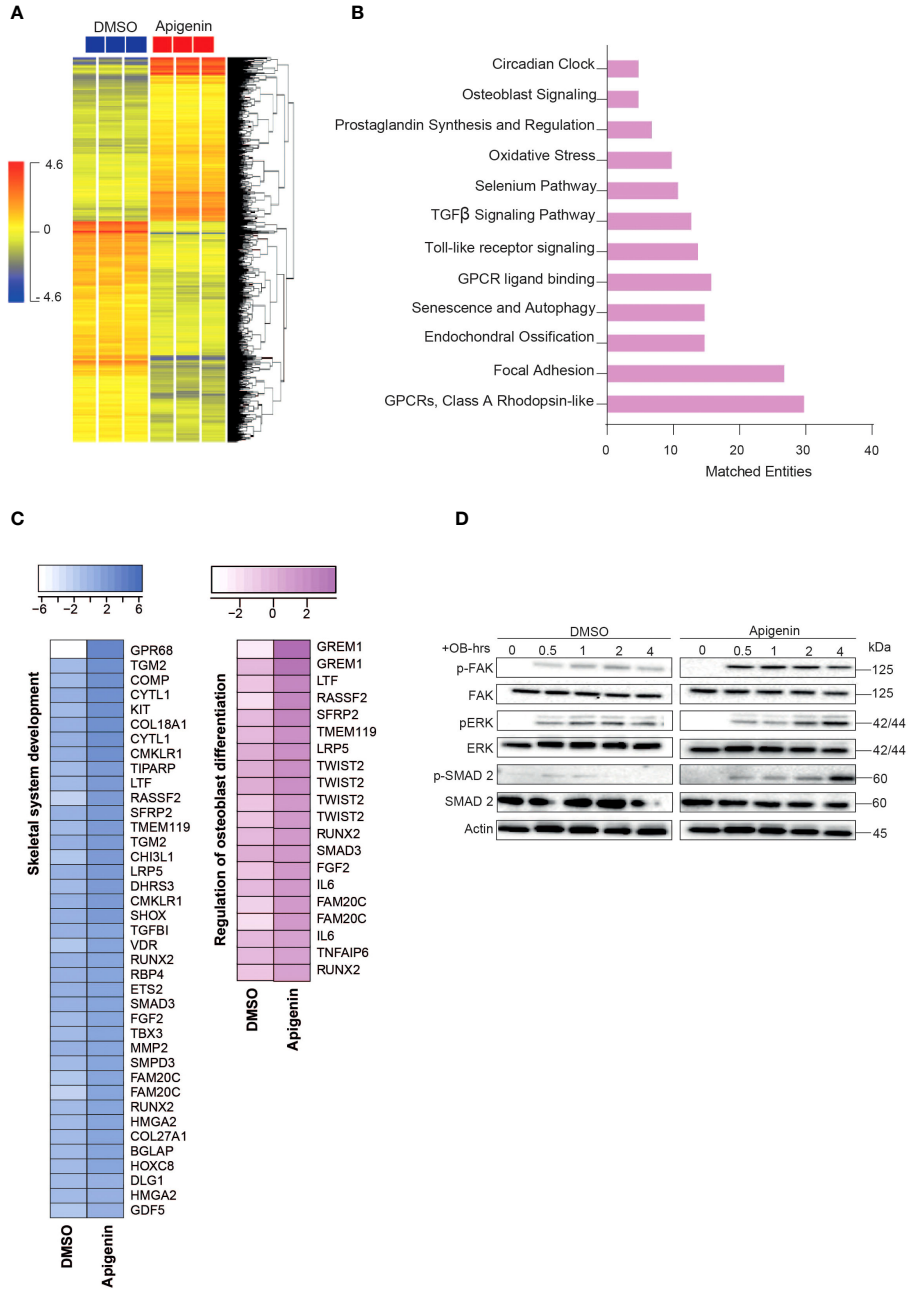

FIGURE 2
Microarray gene expression profiling of human bone marrow stromal cells (hBMSCs)-derived osteoblasts following Apigenin treatment. **(A)** Unsupervised hierarchical clustering on differentially expressed genes induced by Apigenin compared to vehicle-treated controls at day 21 following osteoblastic differentiations. **(B)** Graph illustrating the distribution of the top enriched pathways in Apigenin vs control-treated upregulated after osteoblastic differentiation of hBMSCs, where the size of the bar corresponds to the number of the matched entities. **(C)** Heat maps showing the up-regulated genes induced by Apigenin that are involved in skeletal system development, and regulation of osteoblast differentiation. **(D)** Representative western blot of hBMSCs cultures treated by Apigenin under osteogenic induction conditions on a time range from (0-4 hours), Actin was used as normal control. All results are compared to DMSO-control unless otherwise stated by the line arrow. Data without the line arrow indicates no statistical significance.

3.3 Apigenin and Rutaecarpine reduce senescence and oxidative stress of hBMSCs

Pathway analysis on the differentially expressed upregulated genes in Apigenin or Rutaecarpine vs control-treated cells revealed enrichment in the oxidative stress and Selenium pathway, suggesting a possible role for Apigenin and Rutaecarpine in regulating hBMSCs biology through their antioxidant effect (29, 30). To test this hypothesis, hBMSCs were pretreated with 1μM of Apigenin or Rutaecarpine for 48 hours, followed by osteoblast differentiation. During differentiation, cells were continuously exposed to Apigenin or Rutaecarpine in the presence or absence of 50 μM of the oxidative stress inducer, Tert-butyl hydroperoxide (TBHP) (31). ALP

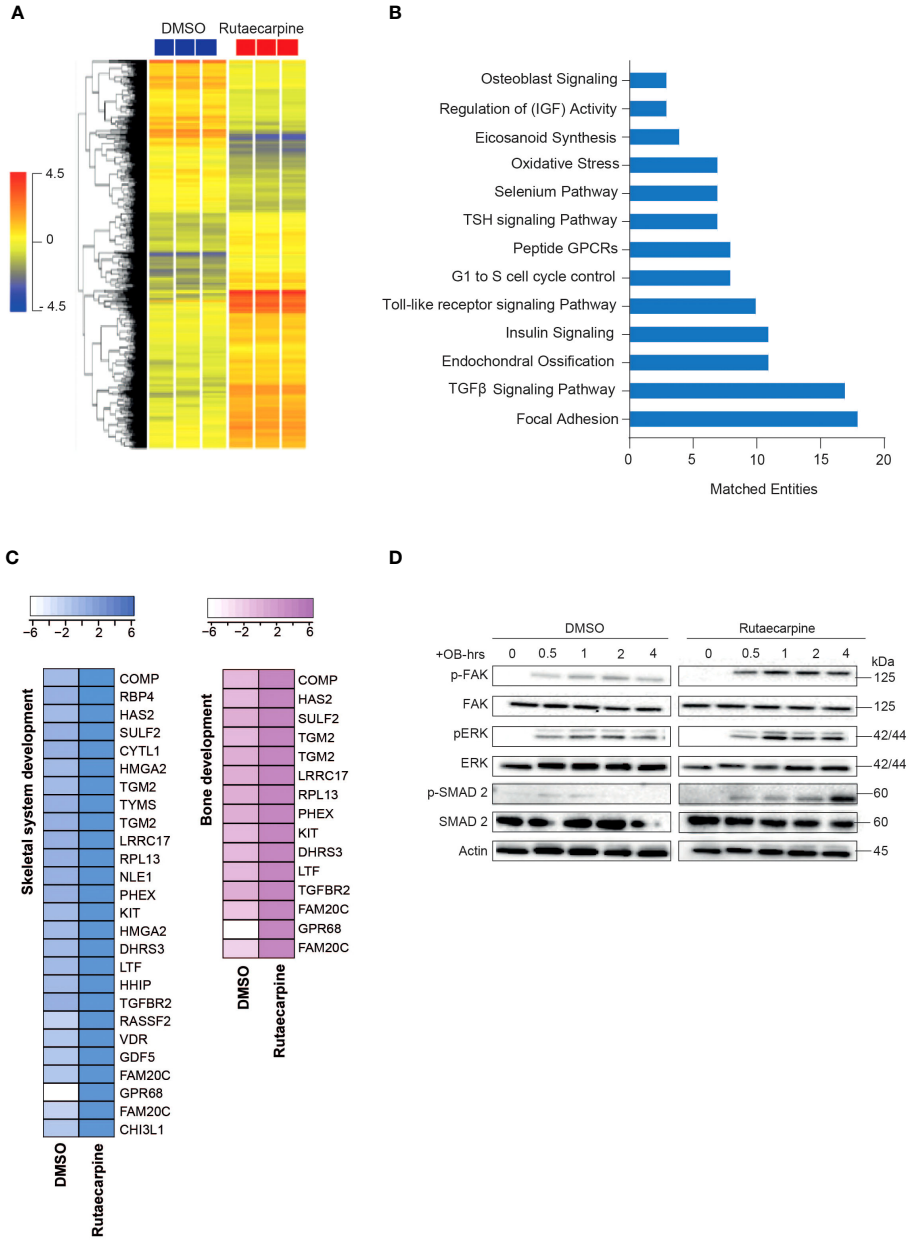

FIGURE 3
Microarray gene expression profiling of human bone marrow stromal cells (hBMSCs)-derived osteoblasts following Rutaecarpine treatment. **(A)** Unsupervised hierarchical clustering on differentially expressed genes induced by Rutaecarpine compared to vehicle-treated controls at day 21 following osteoblastic differentiations. **(B)** Graph illustrating the distribution of the top enriched pathways in Rutaecarpine vs control-treated after osteoblastic differentiation of hBMSCs where the size of the bar corresponds to the number of the matched entities. **(C)** Heat maps showing the up-regulated genes by Rutaecarpine treatment in skeletal system and bone development pathways. **(D)** Representative western blot of hBMSCs cultures treated by Rutaecarpine under osteogenic induction conditions on a time range from (0-4 hours), Actin was used as normal control. All results are compared to DMSO-control unless otherwise stated by the line arrow. Data without the line arrow indicates no statistical significance.

activity (Figure 4A) of hBMSCs exposed to TBHP during osteogenesis revealed negative impacts of oxidative stress on the differentiation potentials of hBMSCs that was partially rescued by the treatment with Apigenin or Rutaecarpine. Apigenin or Rutaecarpine treatment reduced senescence as visualized by β-gal staining (Figure 4B-right-panel) and enhanced osteogenic differentiation as shown by ALP staining (Figure 4B-left-panel) regardless of TBHP treatment. The mRNA levels of senescence-associated markers (P53, P21, P16) (Figure 4C) and senescence-associated secretory phenotype markers (SASP) (Figure 4D), that reflect senescence microenvironment (32), were all induced in presence of TBHP but significantly suppressed when TBHP is combined with Apigenin or Rutaecarpine. The reduced senescence in Apigenin and Rutaecarpine-treated cells was accompanied by significant reduction in the levels of reactive oxygen species (ROS) (Figure 4E), while the expression levels of the antioxidant enzymes (HMOX1 and SOD2) were significantly induced upon Apigenin or Rutaecarpine treatments (Figure 4F).

10.3389/fendo.2024.1360054

3.4 Apigenin and Rutaecarpine rescue osteoblast differentiation capacity in aged-primary hBMSCs

To determine the possible therapeutic relevance of Apigenin and Rutaecarpine, we investigated the effects of Apigenin and Rutaecarpine on differentiation potentials of primary hBMSCs obtained from two young female donors and two female elderly patients. The elderly primary hBMSCs exhibited low levels of osteoblast differentiation potentials. The cells were induced to osteoblast differentiation supplementing the media with Apigenin or Rutaecarpine or vehicle control for 10 days. Apigenin or Rutaecarpine pretreatment enhanced osteoblast differentiation of the aged hBMSCs as revealed in the increase of ALP staining intensity (Figure 5A-lower

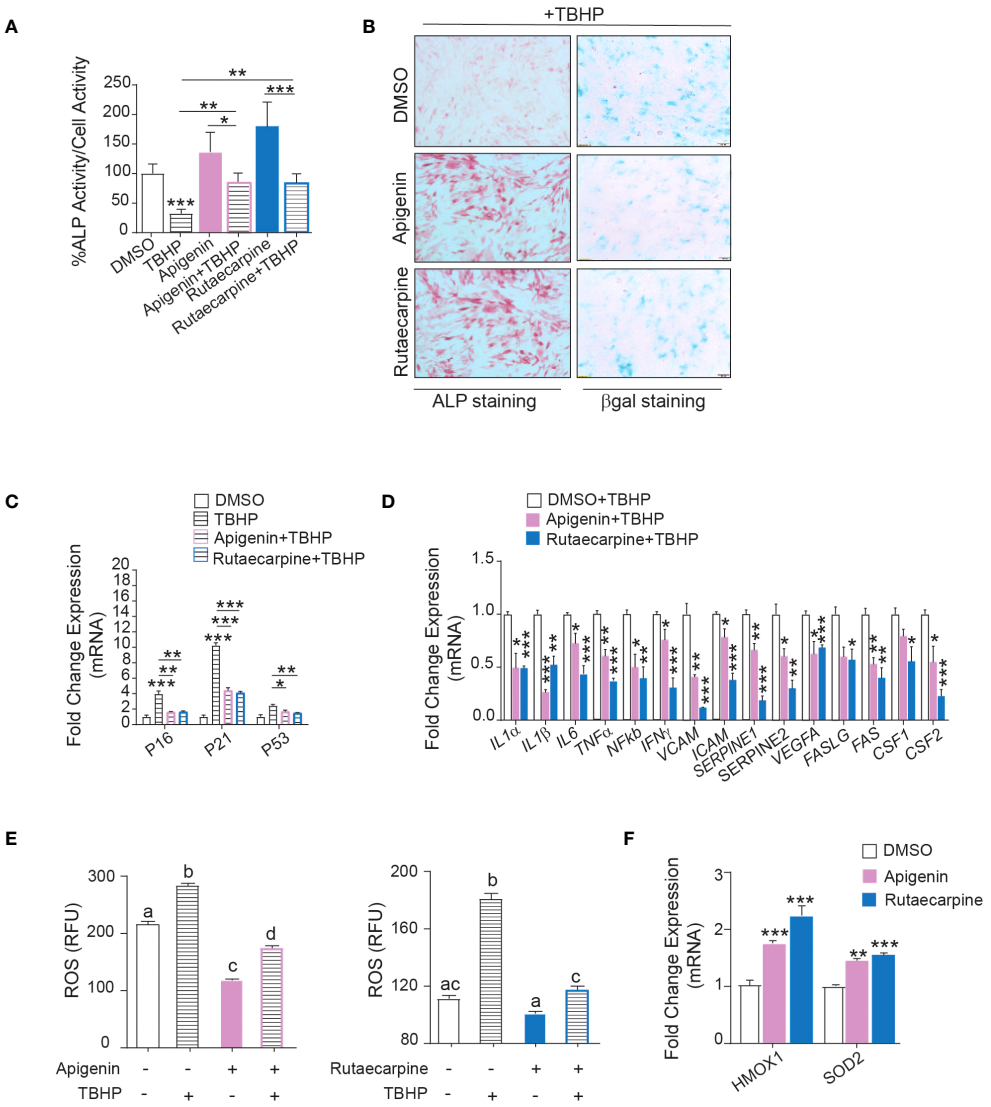

FIGURE 4
Apigenin and Rutaecarpine promote osteogenesis through downregulation of senescence and oxidative stress. Human bone marrow stromal cells (hBMSCs) were pretreated with 1μM of Apigenin or Rutaecarpine for 48 hours, followed by osteoblast differentiation. During differentiation, cells were continuously exposed to Apigenin or Rutaecarpine in the presence or absence of 50 μM of TBHP. **(A)** Quantification of ALP activity (n= 8 from two independent experiments). **(B)** ALP staining hBMSCs post treatment with vehicle control, Apigenin or Rutaecarpine, with TBHP (left panel) (4x magnification). Representative β-gal staining (right panel) in hBMSCs post treatment with vehicle control, Apigenin, or Rutaecarpine in presence of TBHP, blue cells are senescent cells (10x magnification). Gene expression was performed at day 10 and data were normalized to βactin and presented as fold change ± SEM compared with vehicle-treated controls, n=6 from 2 independent experiments. **(C)** Gene expression of senescence-associated markers (P53, P16&P21). **(D)** Gene expression of senescence associated secretory phenotype (SASP). **(E)** ROS production in Apigenin (left graph) and Rutaecarpine (right graph) as determined by DCF fluorescence. **(F)** Gene expression of antioxidant enzymes, n= 6 from 2 independent experiments. Data are presented as mean ± SEM; **(A, C, D, F)** two-tailed unpaired Student's t test compared to control; **(E)** one-way ANOVA on which values not sharing a common letter differ significantly (*P< 0.05, **P< 0.005, ***P< 0.0005). All results are compared to DMSO-control unless otherwise stated by the line arrow. Data without the line arrow indicates no statistical significance.

10.3389/fendo.2024.1360054

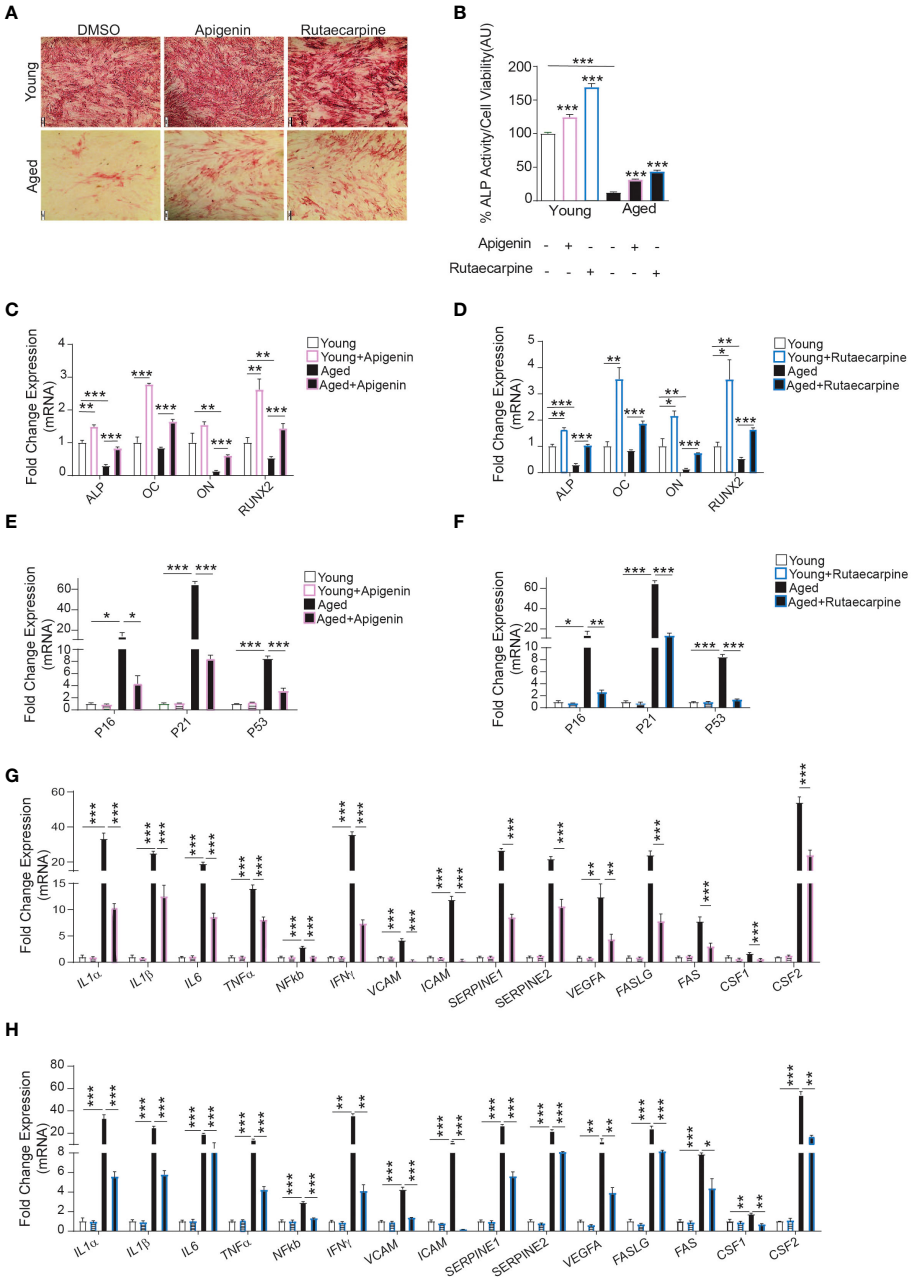

FIGURE 5
Apigenin and Rutaecarpine rescued the osteogenic differentiation phenotype of aged primary hBMSCs compared to young primary hBMSCs. Human primary bone marrow stromal cells (hBMSCs) obtained from young female donors (n=2) and aged female patients (n=2) were cultured under osteogenic differentiation supplemented with Apigenin, Rutaecarpine (1μM) or vehicle control. Cells from each participant were cultured separately, and only cells from passage two were utilized in the experiments conducted in this study. **(A)** ALP staining (4x magnification) of hBMSCs obtained from young donors (upper-panel) and old patients (lower-panel). **(B)** Quantification of ALP activity. **(C)** Gene expression of osteoblastic-specific genes post treatment with Apigenin. **(D)** Gene expression of osteoblastic-specific genes post treatment with Rutaecarpine. **(E)** Gene expression of senescence associated markers (P53, P21 &P16) post treatment with Apigenin. **(F)** Gene expression of senescence associated markers (P53, P21 &P16) post treatment with Rutaecarpine. **(G)** Gene expression of senescence-associated secretory phenotype (SASP) post treatment with Apigenin. **(H)** Gene expression of senescence-associated secretory phenotype (SASP) post treatment with Rutaecarpine. Data are presented as mean ± SEM; two-tailed unpaired Student's t test. (*P< 0.05, **P< 0.005, ***P< 0.0005). All results are compared to young-control or aged-control unless otherwise stated by the line arrow. Data without the line arrow indicates no statistical significance. In ALP test, each subject contributed 6 technical replicates, resulting in a total of 12 observations. In qPCR, each subject contributed 4 technical replicates, resulting in a total of 8 observations.

panel) and significant increase in ALP activity (Figure 5B), as well as up-regulation of osteoblast differentiation marker genes in Apigenin-treated (Figure 5C) and Rutaecarpine-treated cells (Figure 5D). Interestingly, we observed significant down-regulation in gene expression of senescence-associated markers in cells treated with Apigenin (Figure 5E) or Rutaecarpine (Figure 5F) and SASP gene markers (Figures 5G, H). The expression levels of the antioxidant enzymes (HMOX1, SOD2 and SOD3) were induced upon Apigenin

or Rutaecarpine treatments in both young and aged BMSCs-derived osteoblasts (Supplementary Figure 2AB).

3.5 Effects of Apigenin and Rutaecarpine on bone-formation in organ culture of chick femur

Ex vivo organotypic cultures of embryonic chick femurs were used to test the impact of Apigenin and Rutaecarpine on bone formation and were scanned by µCT. Changes in bone mass were determined post 14 days of treatment of femurs with Apigenin or Rutaecarpine and compared with vehicle control DMSO (Figure 6A). Apigenin increased average bone volume (by ~+26% BV/TV), cortical thickness (by ~+4.8% Cort-Th) and bone density (by ~+4.8% B-Den) when compared to control (Figure 6B). While in Rutaecarpine, it increased the average bone volume (by ~+13.4% BV/TV), and cortical thickness (by ~+9.8% Cort-Th), but not bone density when compared to the control (Figure 6C).

4 Discussion

In the present study, we have performed a small molecule screening of a library of 143 natural compounds and identified Apigenin and Rutaecarpine for their effects on enhancing osteoblast differentiation in hBMSCs. Furthermore, we identified the possible molecular mechanisms and changes in several intracellular signaling pathways as well as their antioxidant effect against reactive oxygen species (ROS) and oxidative stress.

Several molecular pathways may explain the enhanced effects of Apigenin and Rutaecarpine on osteoblastic differentiation in hBMSCs. Apigenin and Rutaecarpine activated osteogenesis-related genes such as ALP, OC, ON and RUNX2. These genes play important roles in osteogenic maturation, matrix mineralization, and the regulation of transcription factors important for osteogenesis and bone formation (33–36). COMP is another osteogenic gene marker that was upregulated in our results with Apigenin and Rutaecarpine treatments. COMP has been shown to enhance osteogenesis via activating BMP2 and ALP activity in an ectopic bone formation rat model (37).

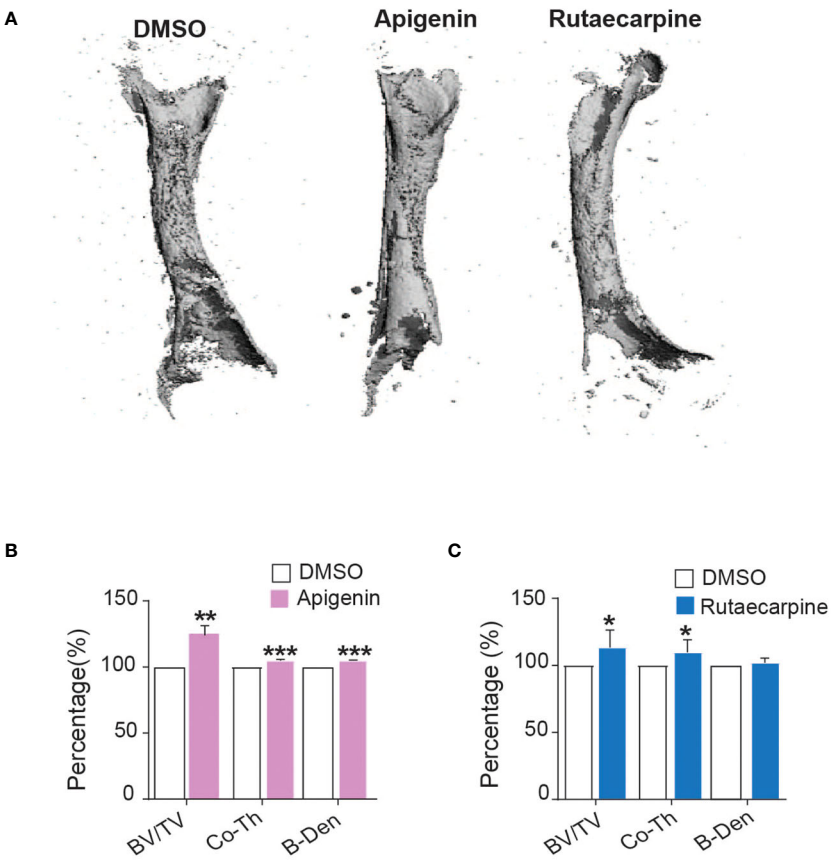

FIGURE 6
Apigenin and Rutaecarpine promoted bone-formation in chick femur model. **(A)** Representative images for µCT 3D reconstruction of bone formation in chick femur post pretreatment in Apigenin or Rutaecarpine or vehicle control in osteogenic differentiation media for 14 days, Images were analyzed at a resolution of 10.5 µm. Bone parameters were analyzed post treatment with Apigenin as bone volume per total volume (BV/TV), cortical thickness (Co.Th) and bone volume density (B.Dens). **(B)** Bone parameters were analyzed post treatment with Apigenin **(C)** Bone parameters were analyzed post treatment with Rutaecarpine. data are presented as mean fold changes ± SEM compared with vehicle-treated controls; n = 6, (*P< 0.05, **P< 0.005, ***P< 0.0005). All results are compared to DMSO-control unless otherwise stated by the line arrow. Data without the line arrow indicates no statistical significance.

Microarray pathway analysis revealed enrichment and upregulation of genes involved in skeletal development, osteoblast differentiation, and bone development in cells treated with Apigenin and Rutaecarpine compared to control cells. Apigenin and Rutaecarpine activated FAK pathway which is crucial for the induction of osteogenesis and bone generation. Deficiency in this pathway has been shown to delay bone healing and interrupt mechanical stimuli in an *in vivo* tibial injury model (38, 39). Additionally, FAK inhibition blocked osterix transcriptional activity and the osteogenic differentiation of hBMSCs (40). Hu et al, reported that extracorporeal shockwave stimulation enhanced osteogenesis of hBMSCs via activation of FAK that led to activation of ERK1/2 and RUNX2. This indicates the significance of the FAK pathway in initiating the cross talk needed for osteogenesis (41). In our study, pharmacological inhibition of the FAK pathway inhibited the osteogenic induction effect of Apigenin and Rutaecarpine.

TGFβ is another upregulated pathway upon exposure of hBMSCs to Apigenin and Rutaecarpine. TGFβ regulates the postnatal bone and cartilage maintenance and recruits stromal stem cells to the bone resorption through the SMAD signaling pathway. TGFβ has been involved in coupling bone construction by osteoblasts and inducing bone destruction by osteoclastogenesis (42, 43). TGFβ isoforms and their receptors as TGFβR2 play an important signaling role in bone formation. TGFβ2 knockout mice showed lack of distal parts of the ribs (44) and transgenic mice with negative form of TGFβ2 developed hypoplastic cartilage (45). Inhibition of TGFβ pathway in our study resulted in the downregulation of the osteogenic induction effects of Apigenin and Rutaecarpine. Toll-like receptor signaling pathway was also upregulated in the presence of Apigenin and Rutaecarpine. TLRs, which are type I single-pass transmembrane proteins, have been shown to be involved in inducing osteocyte differentiation in hBMSCs. Also, activation of TLR4 promoted osteoblastic differentiation of murine MSCs through activation of WNT signaling (46).

Oxidative stress and selenium pathways are also activated in hBMSCs post treatments with Apigenin and Rutaecarpine, indicating their protective antioxidant role against age-associated bone loss. Accumulation of senescent cells and chronic up-regulation in the pro-inflammatory cytokines and SASP markers in the bone marrow microenvironment play a crucial role in age-related bone loss (47–49). Oxidative stress reduced osteogenesis of murine pre-osteoblastic (MC3T3-E1) and bone marrow-derived stromal (M2-10B4) cell lines, whereas treatments with antioxidant compounds restored the osteogenic differentiation (50). We observed that addition of exogenous H_2O_2 to hBMSCs downregulated osteogenesis and upregulated senescent cell accumulation, senescence-associated markers, SASP-related genes, and ROS production. These effects were all reversed by the pretreatment of cells with Apigenin and Rutaecarpine.

Primary hBMSCs from two elderly female patients exhibited low osteogenesis and higher expression of both senescence and SASP markers when compared to hBMSCs from young donors. However, treatments with Apigenin and Rutaecarpine reduced the burden of age-associated impaired osteoblast differentiation. These results indicate a potential therapeutic role of Apigenin and Rutaecarpine in reducing senescent cells and protecting against age-related bone loss.

In addition, ex vivo organotypic cultures of embryonic chick femurs with Apigenin and Rutaecarpine indicated a positive role of these compounds on bone parameters, including both BV/TV and cortical thickness. In the OVX mouse model, administration of Apigenin at 10 mg/kg at 3-day intervals for 28 days revealed a protective impact against OVX-induced trabecular bone loss, and inhibited osteoclast differentiation in mouse splenic cells (14). Rutaecarpine was also investigated for its protective role against OVX-induced bone loss in rats. Tretaments of OVX rats for 3 months with either 5 or 45 mg/kg/day of Rutaecarpine incresaed bone density, possibily due to mechansims related to osteoprotegerin induction (51).

Cardiovascular diseases are major public health problems that are positively associated with osteoporosis. Men and women with cardiovascular diseases tend to have lower bone mass density (52) and that the use of anti-osteoporotic drugs may increase the risk of cardiovascular diseases, myocardial Infarction and a stroke (53). Apigenin and Rutaecarpine were investigated earlier for their positive effect in reducing the risk of cardiac diseases, as modulators of inflammation and antioxidants (16, 54). In our investigation both compounds exhibited positive upregulation of bone formation which makes them potentially beneficial for patients with osteoporosis and cardiovascular diseases.

In summary, our findings indicate protective roles of Apigenin and Rutaecarpine in enhancing bone formation via increasing the osteoblast differeniation potential of hBMSCs and reducing the levels of oxidative stress and the burden of senescent cells. Our study suggests the need for more intervention studies to investigate the impact of small-molecule natural compounds and their potential therapeutic targeting of hBMSCs differentiation and bone formation.

Data availability statement

The datasets presented in this study can be found in online repositories. The names of the repository/repositories and accession number(s) can be found below: https://www.ncbi.nlm.nih.gov/geo/, GSE252845.

Ethics statement

The studies involving humans were approved by the Scientific Ethics Committee of Southern Denmark (project ID: S-20160084). The studies were conducted in accordance with the local legislation and institutional requirements. The participants provided their written informed consent to participate in this study. The animal study was approved by the Institution Review Board of King Saud University Medical College and Hospital (10-2815-IRB). The study

was conducted in accordance with the local legislation and institutional requirements.

Author contributions

DA: Writing – review & editing, Writing – original draft, Visualization, Validation, Supervision, Software, Resources, Project administration, Methodology, Investigation, Formal analysis, Data curation, Conceptualization. MO: Writing – review & editing, Writing – original draft, Visualization, Validation, Supervision, Software, Resources, Project administration, Methodology, Investigation, Formal analysis, Data curation, Conceptualization. SA: Writing – review & editing, Methodology. RV: Writing – review & editing, Methodology. ND: Writing – review & editing, Methodology. RH: Writing – review & editing, Methodology. JK: Writing – review & editing, Methodology. AS: Writing – review & editing, Methodology. AA: Writing – review & editing, Funding acquisition. NA: Writing – review & editing, Visualization, Validation, Supervision, Software, Resources, Project administration, Investigation, Funding acquisition, Formal analysis, Data curation, Conceptualization. MK: Funding acquisition, Writing – review & editing, Visualization, Validation, Supervision, Software, Resources, Project administration, Investigation, Formal analysis, Data curation, Conceptualization.

Funding

The author(s) declare financial support was received for the research, authorship, and/or publication of this article. This work was supported by the Deanship of Scientific Research at King Saud University Research Group No. RG-1438-033. We thank Department of Endocrinology and Metabolism, Molecular Endocrinology & Stem Cell Research Unit (KMEB), Odense University Hospital, University of Southern Denmark, Odense, Denmark for providing experimental and financial support to publish this investigation.

Conflict of interest

The authors declare that the research was conducted in the absence of any commercial or financial relationships that could be construed as a potential conflict of interest.

Publisher's note

Supplementary material

The Supplementary Material for this article can be found online at: https://www.frontiersin.org/articles/10.3389/fendo.2024.1360054/full#supplementary-material

SUPPLEMENTARY FIGURE 1
Effects of Apigenin and Rutaecarpine on FAK and TGFβ signaling pathways during osteogenic differentiation of human bone marrow stromal cells hBMSCs. Quantification of ALP activity in hBMSCs pretreated with **(A)** Apigenin and **(B)** Rutaecarpine in the presence or absence of FAK inhibitor (FAKi, PF-573228, 5.0μM) or TGFβ inhibitor (TGFβi, SB505124, 5.0μM). Data are presented as mean± SEM compared with vehicle-treated controls; n = 16 from two independent experiments; (*P< 0.05, **P< 0.005, ***P< 0.0005); two-tailed unpaired Student's t test. All results are compared to DMSO-control unless otherwise stated by the line arrow. Data without the line arrow indicates no statistical significance.

SUPPLEMENTARY FIGURE 2
Effects of Apigenin and Rutaecarpine on antioxidant enzyme gene expressions in primary hBMSCs obtained from young and aged participants. Gene expression analysis of HMOX1, SOD2, and SOD3 post treatment with **(A)** Apigenin and **(B)** Rutaecarpine. Data are presented as mean ± SEM; two-tailed unpaired Student's t test. (*P< 0.05, **P< 0.005). All results are compared to young-control or aged-control unless otherwise stated by the line arrow. Data without the line arrow indicates no statistical significance.

References

1. Hendrickx G, Boudin E, Van Hul W. A look behind the scenes: the risk and pathogenesis of primary osteoporosis. *Nat Rev Rheumatol.* (2015) 11:462–74. doi: 10.1038/nrrheum.2015.48

2. Kassem M, Marie PJ. Senescence-associated intrinsic mechanisms of osteoblast dysfunctions. *Aging Cell.* (2011) 10:191–7. doi: 10.1111/j.1474-9726.2011.00669.x

3. Ali D, Figeac F, Caci A, Ditzel N, Schmal C, Kerckhofs G, et al. High-fat diet-induced obesity augments the deleterious effects of estrogen deficiency on bone: Evidence from ovariectomized mice. *Aging Cell.* (2022) 21:e13726. doi: 10.1111/acel.13726

4. Marie PJ, Kassem M. Extrinsic mechanisms involved in age-related defective bone formation. *J Clin Endocrinol Metab.* (2011) 96:600–9. doi: 10.1210/jc.2010-2113

5. Wu J, Zhang Q, Yan G, Jin X. Denosumab compared to bisphosphonates to treat postmenopausal osteoporosis: a meta-analysis. *J orthopaedic Surg Res.* (2018) 13:194. doi: 10.1186/s13018-018-0865-3

6. Kennel KA, Drake MT. Adverse effects of bisphosphonates: implications for osteoporosis management. *Mayo Clin Proc.* (2009) 84:632–7; quiz 8. doi: 10.1016/S0025-6196(11)60752-0

7. Reid IR. Short-term and long-term effects of osteoporosis therapies. *Nat Rev Endocrinol.* (2015) 11:418–28. doi: 10.1038/nrendo.2015.71

8. Zhao H, Zhao N, Zheng P, Xu X, Liu M, Luo D, et al. Prevention and treatment of osteoporosis using chinese medicinal plants: special emphasis on mechanisms of immune modulation. *J Immunol Res.* (2018) 2018:6345857. doi: 10.1155/2018/6345857

9. Chen M, Feng W, Cao H, Zou L, Chen C, Baatrup A, et al. A traditional Chinese medicine formula extracts stimulate proliferation and inhibit mineralization of human mesenchymal stem cells in vitro. *J Ethnopharmacol.* (2009) 125:75–82. doi: 10.1016/j.jep.2009.06.013

10. Udalamaththa VL, Jayasinghe CD, Udagama PV. Potential role of herbal remedies in stem cell therapy: proliferation and differentiation of human mesenchymal stromal cells. *Stem Cell Res Ther.* (2016) 7:110. doi: 10.1186/s13287-016-0366-4

11. Zhang P, Dai KR, Yan SG, Yan WQ, Zhang C, Chen DQ, et al. Effects of naringin on the proliferation and osteogenic differentiation of human bone mesenchymal stem cell. *Eur J Pharmacol*. (2009) 607:1–5. doi: 10.1016/j.ejphar.2009.01.035

12. Di Giacomo C, Vanella L, Sorrenti V, Santangelo R, Barbagallo I, Calabrese G, et al. Effects of Tithonia diversifolia (Hemsl.) A. Gray extract on adipocyte differentiation of human mesenchymal stem cells. *PloS One*. (2015) 10:e0122320. doi: 10.1371/journal.pone.0122320

13. Ali D, Chen L, Kowal JM, Okla M, Manikandan M, AlShehri M, et al. Resveratrol inhibits adipocyte differentiation and cellular senescence of human bone marrow stromal stem cells. *Bone*. (2020) 133:115252. doi: 10.1016/j.bone.2020.115252

14. Goto T, Hagiwara K, Shirai N, Yoshida K, Hagiwara H. Apigenin inhibits osteoblastogenesis and osteoclastogenesis and prevents bone loss in ovariectomized mice. *Cytotechnology*. (2015) 67:357–65. doi: 10.1007/s10616-014-9694-3

15. Zhang X, Zhou C, Zha X, Xu Z, Li L, Liu Y, et al. Apigenin promotes osteogenic differentiation of human mesenchymal stem cells through JNK and p38 MAPK pathways. *Mol Cell Biochem*. (2015) 407:41–50. doi: 10.1007/s11010-015-2452-9

16. Jia S, Hu C. Pharmacological effects of rutaecarpine as a cardiovascular protective agent. *Molecules*. (2010) 15:1873–81. doi: 10.3390/molecules15031873

17. Zhang WL, Zhu L, Jiang JG. Active ingredients from natural botanicals in the treatment of obesity. *Obes Rev*. (2014) 15:957–67. doi: 10.1111/obr.12228

18. Lee SH, Son JK, Jeong BS, Jeong TC, Chang HW, Lee ES, et al. Progress in the studies on rutaecarpine. *Molecules*. (2008) 13:272–300. doi: 10.3390/molecules13020272

19. Wang L, Hu CP, Deng PY, Shen SS, Zhu HQ, Ding JS, et al. The protective effects of rutaecarpine on gastric mucosa injury in rats. *Planta Med*. (2005) 71:416–9. doi: 10.1055/s-2005-864135

20. Fukuma Y, Sakai E, Komaki S, Nishishita K, Okamoto K, Tsukuba T. Rutaecarpine attenuates osteoclastogenesis by impairing M-CSF and RANKL-stimulated signaling pathways. *Clin Exp Pharmacol Physiol*. (2018) 45(8):863–865. doi: 10.1111/1440-1681.12941

21. Attari F, Zahmatkesh M, Aligholi H, Mehr SE, Sharifzadeh M, Gorji A, et al. Curcumin as a double-edged sword for stem cells: dose, time and cell type-specific responses to curcumin. *Daru*. (2015) 23:33. doi: 10.1186/s40199-015-0115-8

22. Wu Y, Liu Y, Xu Y, Zheng A, Du J, Cao L, et al. Bioactive natural compounds as potential medications for osteogenic effects in a molecular docking approach. *Front Pharmacol*. (2022) 13:955983. doi: 10.3389/fphar.2022.955983

23. Simonsen JL, Rosada C, Serakinci N, Justesen J, Stenderup K, Rattan SIS, et al. Telomerase expression extends the proliferative life-span and maintains the osteogenic potential of human bone marrow stromal cells. *Nat Biotechnol*. (2002) 20:592–6. doi: 10.1038/nbt0602-592

24. Abdallah BM, Haack-Sorensen M, Burns JS, Elsnab B, Jakob F, Hokland P, et al. Maintenance of differentiation potential of human bone marrow mesenchymal stem cells immortalized by human telomerase reverse transcriptase gene despite [corrected] extensive proliferation. *Biochem Biophys Res Commun*. (2005) 326:527–38. doi: 10.1016/j.bbrc.2004.11.059

25. Kowal JM, Schmal H, Halekoh U, Hjelmborg JB, Kassem M. Single-cell high-content imaging parameters predict functional phenotype of cultured human bone marrow stromal stem cells. *Stem Cells Transl Med*. (2020) 9:189–202. doi: 10.1002/sctm.19-0171

26. Kowal JM, Möller S, Ali D, Figeac F, Barington T, Schmal H, et al. Identification of a clinical signature predictive of differentiation fate of human bone marrow stromal cells. *Stem Cell Res Ther*. (2021) 12:265. doi: 10.1186/s13287-021-02338-1

27. Livak KJ, Schmittgen TD. Analysis of relative gene expression data using real-time quantitative PCR and the 2(-Delta Delta C(T)) Method. *Methods*. (2001) 25:402–8. doi: 10.1006/meth.2001.1262

28. Aldahmash A, Vishnubalaji R. Transplantation of human neonatal foreskin stromal cells in ex vivo organotypic cultures of embryonic chick femurs. *Saudi J Biol Sci*. (2017) 24:857–63. doi: 10.1016/j.sjbs.2016.04.006

29. Lee SJ, Ahn H, Nam KW, Kim KH, Mar W. Effects of rutaecarpine on hydrogen peroxide-induced apoptosis in murine hepa-1c1c7 cells. *Biomolecules Ther*. (2012) 20:487–91. doi: 10.4062/biomolther.2012.20.5.487

30. Kim M, Jung J, Jeong NY, Chung HJ. The natural plant flavonoid apigenin is a strong antioxidant that effectively delays peripheral neurodegenerative processes. *Anatomical Sci Int*. (2019) 94:285–94. doi: 10.1007/s12565-019-00486-2

31. Bhattacharya S, Gachhui R, Sil PC. Hepatoprotective properties of kombucha tea against TBHP-induced oxidative stress via suppression of mitochondria dependent apoptosis. *Pathophysiology*. (2011) 18:221–34. doi: 10.1016/j.pathophys.2011.02.001

32. Khosla S, Farr JN, Tchkonia T, Kirkland JL. The role of cellular senescence in ageing and endocrine disease. *Nat Rev Endocrinol*. (2020) 16:263–75. doi: 10.1038/s41574-020-0335-y

33. Nakamura A, Dohi Y, Akahane M, Ohgushi H, Nakajima H, Funaoka H, et al. Osteocalcin secretion as an early marker of in *vitro* osteogenic differentiation of rat mesenchymal stem cells. *Tissue Eng Part C Methods*. (2009) 15:169–80. doi: 10.1089/ten.tec.2007.0334

34. Chen G, Deng C, Li YP. TGF-β and BMP signaling in osteoblast differentiation and bone formation. *Int J Biol Sci*. (2012) 8:272–88. doi: 10.7150/ijbs.2929

35. Chen Q, Shou P, Zheng C, Jiang M, Cao G, Yang Q, et al. Fate decision of mesenchymal stem cells: adipocytes or osteoblasts? *Cell Death Differ*. (2016) 23:1128–39. doi: 10.1038/cdd.2015.168

36. Shapiro JR, Lewiecki EM. Hypophosphatasia in adults: clinical assessment and treatment considerations. *J Bone Miner Res*. (2017) 32:1977–80. doi: 10.1002/jbmr.3226

37. Ishida K, Acharya C, Christiansen BA, Yik JH, DiCesare PE, Haudenschild DR. Cartilage oligomeric matrix protein enhances osteogenesis by directly binding and activating bone morphogenetic protein-2. *Bone*. (2013) 55:23–35. doi: 10.1016/j.bone.2013.03.007

38. Leucht P, Kim JB, Currey JA, Brunski J, Helms JA. FAK-Mediated mechanotransduction in skeletal regeneration. *PloS One*. (2007) 2:e390. doi: 10.1371/journal.pone.0000390

39. Kim JB, Leucht P, Luppen CA, Park YJ, Beggs HE, Damsky CH, et al. Reconciling the roles of FAK in osteoblast differentiation, osteoclast remodeling, and bone regeneration. *Bone*. (2007) 41:39–51. doi: 10.1016/j.bone.2007.01.024

40. Salasznyk RM, Klees RF, Williams WA, Boskey A, Plopper GE. Focal adhesion kinase signaling pathways regulate the osteogenic differentiation of human mesenchymal stem cells. *Exp Cell Res*. (2007) 313:22–37. doi: 10.1016/j.yexcr.2006.09.013

41. Hu J, Liao H, Ma Z, Chen H, Huang Z, Zhang Y, et al. Focal adhesion kinase signaling mediated the enhancement of osteogenesis of human mesenchymal stem cells induced by extracorporeal shockwave. *Sci Rep*. (2016) 6:20875. doi: 10.1038/srep20875

42. Crane JL, Xian L, Cao X. Role of TGF-beta signaling in coupling bone remodeling. *Methods Mol Biol*. (2016) 1344:287–300. doi: 10.1007/978-1-4939-2966-5_18

43. Tang Y, Wu X, Lei W, Pang L, Wan C, Shi Z, et al. TGF-beta1-induced migration of bone mesenchymal stem cells couples bone resorption with formation. *Nat Med*. (2009) 15:757–65. doi: 10.1038/nm.1979

44. Dunker N, Krieglstein K. Tgfbeta2 -/- Tgfbeta3 -/- double knockout mice display severe midline fusion defects and early embryonic lethality. *Anat Embryol (Berl)*. (2002) 206:73–83. doi: 10.1007/s00429-002-0273-6

45. Hiramatsu K, Iwai T, Yoshikawa H, Tsumaki N. Expression of dominant negative TGF-beta receptors inhibits cartilage formation in conditional transgenic mice. *J Bone Miner Metab*. (2011) 29:493–500. doi: 10.1007/s00774-010-0248-2

46. Shirjang S, Mansoori B, Solali S, Hagh MF, Shamsasenjan K. Toll-like receptors as a key regulator of mesenchymal stem cell function: An up-to-date review. *Cell Immunol*. (2017) 315:1–10. doi: 10.1016/j.cellimm.2016.12.005

47. Farr JN, Khosla S. Cellular senescence in bone. *Bone*. (2019) 121:121–33. doi: 10.1016/j.bone.2019.01.015

48. Coppé JP, Patil CK, Rodier F, Sun Y, Muñoz DP, Goldstein J, et al. Senescence-associated secretory phenotypes reveal cell-nonautonomous functions of oncogenic RAS and the p53 tumor suppressor. *PloS Biol*. (2008) 6:2853–68. doi: 10.1371/journal.pbio.0060301

49. Coppé JP, Desprez PY, Krtolica A, Campisi J. The senescence-associated secretory phenotype: the dark side of tumor suppression. *Annu Rev Pathol*. (2010) 5:99–118. doi: 10.1146/annurev-pathol-121808-102144

50. Mody N, Parhami F, Sarafian TA, Demer LL. Oxidative stress modulates osteoblastic differentiation of vascular and bone cells. *Free Radic Biol Med*. (2001) 31:509–19. doi: 10.1016/S0891-5849(01)00610-4

51. Li Y-N, Han X-W, Wang W-Z, Jiang X-H, Han J-X, Zhang J, et al. Rutaecarpine exerted anti-osteroporosis. *Acta Pharm Sin*. (2021) 12:511–9.

52. Szulc P. Association between cardiovascular diseases and osteoporosis-reappraisal. *Bonekey Rep*. (2012) 1:144. doi: 10.1038/bonekey.2012.144

53. Sing CW, Wong AY, Kiel DP, Cheung EY, Lam JK, Cheung TT, et al. Association of alendronate and risk of cardiovascular events in patients with hip fracture. *J Bone Miner Res*. (2018) 33(8):1422–1434. doi: 10.1002/jbmr.3448

54. Li F, Lang F, Zhang H, Xu L, Wang Y, Zhai C, et al. Apigenin alleviates endotoxin-induced myocardial toxicity by modulating inflammation, oxidative stress, and autophagy. *Oxid Med Cell Longev*. (2017) 2017:2302896. doi: 10.1155/2017/2302896

frontiers | Frontiers in Endocrinology

TYPE Original Research
PUBLISHED 23 April 2024
DOI 10.3389/fendo.2024.1392063

OPEN ACCESS

EDITED BY
Katherine A. Staines,
University of Brighton, United Kingdom

REVIEWED BY
Melanie Haffner-Luntzer,
University of Ulm, Germany
Dina Keumala Sari,
Universitas Sumatera Utara, Indonesia

*CORRESPONDENCE
Rafael Velázquez-Cruz
rvelazquez@inmegen.gob.mx

†These authors have contributed equally to this work

RECEIVED 26 February 2024
ACCEPTED 03 April 2024
PUBLISHED 23 April 2024

CITATION
Aparicio-Bautista DI, Jiménez-Ortega RF, Becerra-Cervera A, Aquino-Gálvez A, de León-Suárez VP, Casas-Ávila L, Salmerón J, Hidalgo-Bravo A, Rivera-Paredez B and Velázquez-Cruz R (2024) Interaction between MARK3 (rs11623869), PLCB4 (rs6086746) and GEMIN2 (rs2277458) variants with bone mineral density and serum 25-hidroxivitamin D levels in Mexican Mestizo women. *Front. Endocrinol.* 15:1392063. doi: 10.3389/fendo.2024.1392063

Interaction between MARK3 (rs11623869), PLCB4 (rs6086746) and GEMIN2 (rs2277458) variants with bone mineral density and serum 25-hidroxivitamin D levels in Mexican Mestizo women

Diana I. Aparicio-Bautista[1†], Rogelio F. Jiménez-Ortega[1,2†], Adriana Becerra-Cervera[1,3], Arnoldo Aquino-Gálvez[4], Valeria Ponce de León-Suárez[5], Leonora Casas-Ávila[5], Jorge Salmerón[6], Alberto Hidalgo-Bravo[5], Berenice Rivera-Paredez[6] and Rafael Velázquez-Cruz[1*]

[1]Laboratorio de Genómica del Metabolismo Óseo, Instituto Nacional de Medicina Genómica (INMEGEN), Mexico City, Mexico, [2]Departamento de Ciencias de la Acupuntura. Universidad Estatal del Valle de Ecatepec. Ecatepec de Morelos, Estado de Mexico, Mexico, [3]Consejo Nacional de Humanidades, Ciencias y Tecnologías (CONAHCYT), Mexico City, Mexico, [4]Laboratorio de Biología Molecular, Departamento de Fibrosis Pulmonar, Instituto Nacional de Enfermedades Respiratorias "Ismael Cosío Villegas", Mexico City, Mexico, [5]Departamento de Medicina Genómica, Instituto Nacional de Rehabilitación, Mexico City, Mexico, [6]Centro de Investigación en Políticas, Población y Salud, Facultad de Medicina, Universidad Nacional Autónoma de México, Mexico City, Mexico

Introduction: Understanding the genetic factors contributing to variations in bone mineral density (BMD) and vitamin D could provide valuable insights into the pathogenesis of osteoporosis. This study aimed to evaluate the association of single nucleotide variants in *MARK3* (rs11623869), *PLCB4* (rs6086746), and *GEMIN2* (rs2277458) with BMD in Mexican women.

Methods: The gene-gene interaction was evaluated in these variants in serum 25 (OH)D levels and BMD. A genetic risk score (GRS) was created on the basis of the three genetic variants. Genotyping was performed using predesigned TaqMan assays.

Results: A significant association was found between the rs6086746-A variant and BMD at the total hip, femoral neck, and lumbar spine, in women aged 45 years or older. However, no association was observed between the variants rs11623869 and rs2277458. The rs11623869 × rs2277458 interaction was associated with total hip (p=0.002) and femoral neck BMD (p=0.013). Similarly, for vitamin D levels, we observed an interaction between the variants rs6086746 × rs2277458 (p=0.021). GRS revealed a significant association with total hip BMD (p trend=0.003) and femoral neck BMD (p trend=0.006), as well as increased vitamin D levels (p trend=0.0003). These findings provide evidence of the individual and joint effect of the *MARK3*, *PLCB4*, and *GEMIN2* variants on BMD and serum vitamin D levels in Mexican women.

Discussion: This knowledge could help to elucidate the interaction mechanism between BMD-related genetic variants and 25OHD, contributing to the determination of the pathogenesis of osteoporosis and its potential implications during early interventions.

KEYWORDS

osteoporosis, bone mineral density, vitamin D, genetic risk score, genetic association, postmenopausal

1 Introduction

Osteoporosis (OP) is a skeletal disease characterized by decreased bone mass and impaired microarchitecture leading to decreased mechanical strength and increased fracture risk (1). It has become a significant global public health concern due to the increasing number of fractures and the negative impact on the quality of life of affected individuals (2). Recent reports indicate that about 75 million people in Europe, the United States, and Japan are affected by OP, of which about 8.9 million have suffered fragility fractures. In Mexico, according to data from the 2020 population and housing census, the current population is around 126 million inhabitants, from which 17.4% correspond to individuals the subpopulation aged 50 years or older. It is estimated that about 10 million people in Mexico are living with OP (3, 4).

This disease is characterized by being multifactorial and complex where the predisposition, pathogenesis, or response to treatments are modulated by the interaction between genetic and environmental factors (5). The heritability of OP has been reported as high 50–85% (6, 7). The most effective approach for detecting the Single Nucleotide Variants (SNVs) associated to a multifactorial condition is through genome-wide association studies (GWAS). Therefore, several studies have aimed to link SNVs across the genome with the occurrence of OP, with the goal of identifying individuals at higher risk (8).

Microtubule affinity-regulating kinase 3 (*MARK3*) gene encodes a serine/threonine kinase, which is activated by the hepatic tumor suppressor kinase B1 (LKB1) and antagonizes oncogenic pathways, including the cell cycle pathway through phosphorylation of CDC25C (9). Regarding bone metabolism, a GWAS identified a locus containing multiple genes, including *MARK3*, *TRMT61*, and *CKB*. The main SNV associated was rs11623869, which lies in the second intron of *MARK3*. This locus was associated with femoral neck (FN) and lumbar spine (LS) BMD, and consistently replicated in Chinese and European populations (10, 11). A recent study implicates this kinase as an important signaling molecule in osteoblasts influencing bone mass (12).

Another study carried out in Taiwanese population identified the SNV rs6086746 upstream the Phosphoinositide Phospholipase C-Beta-4 (*PLCB4*) gene associated with low BMD in postmenopausal women. *PLCB4* encodes a phospholipase C which participates in the phosphoinositide cycle signaling pathway, transmitting information from the extracellular environment into the cell, influencing several cellular processes. It has been reported that rs6086746 may affect the binding of the transcription factor *RUNX2* to the promoter region of *PLCB4*, this might be part of the mechanisms contributing to the development of OP (13). *RUNX2* is a key transcription regulatory factor in osteoblast differentiation, it plays an important role in regulating osteoblast maturation and balance (14). Several studies reported that polymorphisms on the promoter of *RUNX2* are associated with BMD, in Korean and European populations (15–17).

The Gemin protein associated with the nuclear organelle 2 (GEMIN2) is part of a complex composed by the survival motor neuron protein (SMN) and seven additional Gemin proteins (*GEMIN2–8*). This complex is mainly involved in the assembly of the small nuclear ribonucleoprotein (snRNP) machinery, which regulates mRNA splicing in the cytoplasm (18). In particular, the SMN complex functions as a molecular chaperone whose phosphorylation regulates the biogenesis and function of snRNPs involved in mRNA splicing (19). Additionally, the SNV rs2277458 of the *GEMIN2* gene has been reported to be associated with the variation in plasma concentrations of 25-hydroxyvitamin D in the Danish population. In this population, low plasma concentration of 25-hydroxyvitamin D has been associated with a higher risk of osteoporotic fractures (20). Based on current evidence, this study aimed to investigate the effect of three recently identified SNVs (*MARK3*-rs11623869, *PLCB4*-rs6086746, and *GEMIN2*-rs2277458) on BMD, in a cohort of Mexican women. Additionally, we explored the effect of the interaction between these genetic variants with serum 25(OH)D levels and BMD.

2 Materials and methods

2.1 Study population

The study population included women born in Mexico whose parents and grandparents identified themselves as Mexican-mestizo. The population sample was composed of 1,300 middle-aged, unrelated women participating in the Health Workers Cohort Study (HWCS). The HWCS is a prospective study including

workers from the Mexican Social Security Institute (IMSS) in Cuernavaca Morelos (central area of Mexico), focused on lifestyle and chronic diseases. Information on demographic characteristics, smoking status, menopausal status, medical history, and medication use was collected from each participant through a structured questionnaire (21). All study's procedures were approved by the Ethics and Research Committee of the IMSS and all participants signed an informed consent form.

2.2 Bone mineral density measurement

Lumbar spine (L2-L4), femoral neck (FN), and total hip BMD were assessed using a Lunar DPX NT dual x-ray absorptiometry (DXA) instrument (Lunar Radiation Corp., Madison WI). Standard calibration of the instrument was performed daily using a phantom provided by the manufacturer for the femoral spine and neck. Technicians ensured that the daily coefficient of variation (CV) remained within normal operating standards and that the *in vivo* CV was less than 1.5%. BMD was calculated from bone mineral content (g) and bone area (cm^2) to express it in g/cm^2 and these data were used to analyze variations in BMD.

2.3 Single nucleotide variants genotyping and selection

A peripheral blood sample was taken from each patient and stored at 4°C until later use. Genomic DNA was extracted using a commercial isolation kit (QIAGEN System Inc., Valencia, CA), according to the manufacturer's instructions. SNVs were selected from previous genome-wide association studies in the NCBI (www.ncbi.nlh.nih.gov/snp/) and Ensembl (http://asia.ensembl.org/) databases. Homo_sapiens/Info/Index). Genotyping of the rs11623869, rs6086746 and rs2277458 SNVs was performed using predesigned commercial TaqMan probes (Applied Biosystems, Foster City, CA, USA.) using a QuantStudio 7 Flex PCR system (Applied Biosystems, New Jersey, USA). Data were analyzed using Sequence Detection System (SDS) software, version 2.2.1.

2.4 Statistical analysis

Data from the study population are shown as median for quantitative variables and absolute and relative frequencies for qualitative variables. Hardy-Weinberg equilibrium was conducted for each SNV using the standard χ^2 test, which is a fundamental analysis in population genetics to assess whether a population is evolving at a neutral state. This test helps ensure the reliability of genetic association studies by evaluating the expected and observed genotype frequencies within a population. Linear and logistic regression analysis were used to test the association between BMD, serum 25(OH)D levels, and genotype. Both continuous and categorical measurements of BMD and serum 25(OH)D levels were considered in the analysis, as appropriate. Codominant, additive, recessive, and dominant genetic models were used. The BMD models were adjusted for age (years), BMI categories, energy intake, calcium intake (tertiles), vitamin D intake (tertiles), calcium supplementation, alcohol consumption (g/day), smoking status (never, current and past), physical activity, and hormone replacement therapy (HRT). The vitamin D models were adjusted for age (years), BMI categories, energy intake, vitamin D intake (tertiles), alcohol consumption (g/day), smoking status (never, current and past), physical activity, blood collection season, and HRT. To explore potential gene-gene interactions, we incorporated a term for gene-gene interaction into the statistical models. This allowed us to assess how the effects of one gene may modify or influence the effects of another gene within the studied population. By examining these interactions, we aimed to gain deeper insights into the complex interplay between genetic factors and their combined impact on the outcome of interest. We estimated the genetic risk score by summing the risk alleles of the three genetic variants. We collapsed women with 4 and 5 risk alleles into the category of 3 alleles due to their low frequency. For all statistical tests, we used Statistical Software for Data Science version 18 (STATA v18.0, TX, USA.). Values of $p< 0.05$ were considered statistically significant.

3 Results

3.1 Population characteristics- HWCS

For the present study, a total of 1,300 females were included. The median age of the study sample was 54 years (P25-P75, 43-63). According to the body mass index, 39.9% were overweight and 26.2% were obese. The median total hip BMD was 0.964 g/cm^2 (0.871-1.072), and 27.9% had low total hip BMD. The median femoral neck BMD was 0.932 g/cm^2 (0.830-1.027), and 42.1% had low femoral neck BMD. The median lumbar spine BMD was 1.068 g/cm^2 (0.950-1.174), and 53.1% had low lumbar spine BMD (Supplementary Table 1).

3.2 Minor allele frequency of SNVs

The distributions of the alleles of the three SNVs were analyzed by Hardy–Weinberg equilibrium in the HWCS. The variants demonstrated Hardy-Weinberg equilibrium, with *p*-values of 0.36 for rs1050450, 0.38 for rs6086746, and 0.72 for rs11623869. The MAFs of the three SNVs differ from the reported for CEU population. However, were similar to data reported for the Mexican Ancestry population living in Los Angeles, CA, USA (MXL) (Data not shown).

3.3 Association analyses between the SNVs and bone mineral density (g/cm^2), and low-BMD

Anthropometric and biochemical characteristics of the study population based on rs11623869, rs6086746, and rs2277458

genotypes are presented in Supplementary Tables 2–4, respectively. Women carrying at least one copy of the T allele of rs11623869 had a higher median of LDL levels, and a higher prevalence of elevated LDL. In addition, these women also had a higher prevalence of low BMD at the total hip and femoral neck. No other statistically significant differences were observed (Supplementary Table 2). On the other hand, women carrying at least one copy of the A allele of rs6086746 had a lower median fasting glucose level, lower triglyceride levels, and lower prevalence of elevated triglycerides compared to women homozygous for the ancestral allele. Furthermore, women carrying at least one copy of the A allele had a lower prevalence of low BMD, at the femoral neck, total hip and lumbar spine (Supplementary Table 3). We did not observe statistically significant differences for the genotypes of the SNV rs2277458 variant (Supplementary Table 4).

Afterwards, we looked for association of the SNVs with BMD and levels of 25-hydroxivitamin D. Association analysis was conducted through adjusted logistic regression models. The adjusted models revealed that rs11623869 and rs2277458 were not associated with BMD at the analyzed sited. In contrast, the rs6086746 variant, under different inheritance models, showed that the A allele was associated with higher values of BMD at the total hip, femoral neck, and lumbar spine compared to the G allele (Table 1). Consistent associations were observed in women aged 45 years or older, where the A allele of variant rs6086746 showed a significant association with higher BMD at the total hip, femoral neck, and lumbar spine, compared to the G allele (Table 2). In contrast, no significant associations were observed in women younger than 45 years old (Data not shown).

In the adjusted additive, codominant, and dominant models, only the A allele of the rs6086746 variant showed a protective effect for low BMD at various sites (Table 3, Supplementary Table 5). These associations showed a reduction of the odds of having low BMD of approximately 33-55% at the sites analyzed.

3.4 Association analyses between the SNVs and serum 25-hydroxyvitamin D levels

The variants rs11623869 and rs2277458 were associated with higher levels of vitamin D. Under the dominant model, having at least one copy of the T allele of variant rs11623869 and at least one copy of the A allele of variant rs2277458 was associated with higher serum vitamin D levels compared to women carrying the wild-type allele (β= 0.94, 95% CI 0.19-1.68 and β = 0.86, 95% CI 0.16-1.57, respectively). However, variant rs6086746 did not show a statistically significant association (Table 1). Stratified analysis by age groups revealed a similar association only in women aged 45 years or older (Supplementary Table 5, Table 2). The associations for vitamin D deficiency were not statistically significant in either the total women or the age-stratified analysis (Table 3, Supplementary Table 5).

3.5 Interaction between SNVs with bone mineral density

We observed an interaction between the variants rs11623869 × rs2277458 with total hip (p interaction=0.002) and femoral neck BMD (p interaction=0.013). In carriers with at least one copy of the G allele of variant rs11623869 and at least one copy of the A allele of variant rs2277458, lower BMD was observed in the total hip (β= -0.030, 95%CI -0.052, -0.008, p=0.007) and femoral neck (β= -0.026, 95%CI -0.048, -0.006, p=0.013), compared to carriers of the wild-type allele of variant rs2277458. While carriers of the wild-type allele of variant rs11623869 showed no significant differences, carriers with at least one copy of the A allele of variant rs2277458 demonstrated lower BMD at the total hip (β=0.012, 95%CI -0.004, 0.028, p=0.128) and femoral neck (β=0.012, 95%CI -0.003, 0.028, p=0.115) (Figures 1A, B). These patterns were observed in women aged ≥45 years (Figures 2A, B) but not in women aged <45 years (p interaction total hip=0.623 and p interaction femoral neck=0.827). No significant interactions were observed with lumbar spine BMD.

3.6 Interaction between SNVs with serum 25-hydroxivitamin D levels

Similarly, for vitamin D levels, we found a distinct interaction between the variants rs6086746 × rs2277458 (p interaction=0.021). Carriers with at least one copy of the A allele of variant rs6086746 and at least one copy of the A allele of variant rs2277458 exhibited higher vitamin D levels (β=1.83, 95%CI 0.78, 2.88, p=0.001). However, this is not significant with respect to individuals carrying the wild-type allele of the rs2277458 variant. Conversely, in carriers of at least one copy of the G allele of variant rs2277458 association was not statistically significant (β= 0.14, 95%CI -0.83, 1.11, p=0.776), when rs6086746 was of the wild-type (Figure 1C). These patterns were consistently observed in women aged ≥45 years (p=0.030) (Figure 2C) but not in women aged <45 years (p interaction=0.672).

3.7 Genetic risk score

We created a risk score based on the number of risk alleles across the three genetic variants. Since rs11623869 and rs2277458 were statistically associated with higher vitamin D levels, and rs6086746 showed a borderline association, we clustered together the categories of 3, 4, and 5 risk alleles due to their low frequency. Among women aged ≥45 years, those carrying ≥3 risk alleles had, on average, higher total hip (p trend=0.003) and femoral neck BMD (p trend=0.006), as well as elevated serum 25(OH) D levels (p trend=0.00003), compared to those carrying 0 risk alleles (Figures 3A, B, D). However, this association was not statistically significant for lumbar spine BMD (Figure 3C). Notably, we observed an association solely between the risk score and vitamin D levels for the overall cohort of women, but not for BMD. Furthermore, in women aged <45 years, no significant associations were identified.

10.3389/fendo.2024.1392063

TABLE 1 Association between the SNVs, BMD at different sites, and 25-hydroxivitamin D levels in total women.

		Total hip BMD		Femoral neck BMD		Lumbar spine BMD		25-hydroxivitamin D	
rs11623869		β (95%CI)	*p*-value	β (95%CI)	*p*-value	β (95%CI)	*p*-value	β (95%CI)*	*p*-value
Additive		-0.0001 (-0.012,0.012)	0.982	0.003 (-0.009,0.014)	0.662	0.002 (-0.013,0.016)	0.834	0.76 (0.12,1.40)	0.021
Codominant	GG	0.0		0.0		0.0		0.0	
	GT	0.004 (-0.010,0.018)	0.577	0.004 (-0.010,0.017)	0.579	0.008 (-0.010,0.025)	0.382	0.95 (0.18,1.72)	0.016
	TT	-0.015 (-0.051,0.021)	0.412	-0.001 (-0.034,0.035)	0.983	-0.019 (-0.064,0.026)	0.398	0.84 (-1.16,2.84)	0.411
Dominant	GG	0.0		0.0		0.0		0.0	
	GT+TT	0.002 (-0.011,0.016)	0.752	0.003 (-0.010,0.016)	0.600	0.005 (-0.012,0.022)	0.543	0.94 (0.19,1.68)	0.013
Recessive	GG+GT	0.0		0.0		0.0		0.0	
	TT	-0.005 (-0.052,0.019)	0.366	-0.0009 (-0.035,0.034)	0.958	-0.022 (-0.067,0.023)	0.332	0.51 (-1.47,2.50)	0.611
rs6086746									
Additive		0.020 (0.010,0.031)	0.0002	0.019 (0.008,0.029)	0.0004	0.028 (0.015,0.042)	0.00003	0.37 (-0.22,0.96)	0.224
Codominant	GG	0.0		0.0		0.0		0.0	
	GA	0.020 (0.007,0.033)	0.004	0.018 (0.005,0.031)	0.007	0.034 (0.017,0.051)	0.00006	0.68 (-0.06,1.42)	0.072
	AA	0.042 (0.014,0.070)	0.003	0.039 (0.012,0.066)	0.005	0.043 (0.008,0.078)	0.016	0.04 (-1.50,1.58)	0.963
Dominant	GG	0.0		0.0		0.0		0.0	
	GA+AA	0.023 (0.010,0.034)	0.001	0.021 (0.008,0.033)	0.001	0.035 (0.019,0.051)	0.00002	0.60 (-0.12,1.32)	0.101
Recessive	GG+GA	0.0		0.0		0.0		0.0	
	AA	0.033 (0.006,0.060)	0.017	0.031 (0.004,0.057)	0.023	0.028 (-0.006,0.063)	0.110	-0.26 (-1.77,1.24)	0.731
rs2277458									
Additive		-0.003 (-0.013,0.009)	0.631	-0.0003 (-0.010,0.010)	0.946	-0.004 (-0.017,0.009)	0.591	0.78 (0.21,1.35)	0.008
Codominant	GG	0.0		0.0		0.0		0.0	
	GA	-0.003 (-0.016,0.011)	0.702	-0.003 (-0.016,0.010)	0.694	-0.008 (-0.024,0.009)	0.374	0.74 (0.001,1.47)	0.050
	AA	-0.005 (-0.032,0.022)	0.716	0.004 (-0.022,0.030)	0.775	0.0009 (-0.033,0.034)	0.959	1.63 (0.16,3.10)	0.029
Dominant	GG	0.0		0.0		0.0		0.0	
	GA+AA	-0.003 (-0.016,0.010)	0.653	-0.002 (-0.014,0.011)	0.788	-0.006 (-0.022,0.010)	0.434	0.86 (0.16,1.57)	0.017
Recessive	GG+GA	0.0		0.0		0.0		0.0	
	AA	-0.004 (-0.030,0.022)	0.772	0.005 (-0.020,0.030)	0.706	0.004 (-0.029,0.037)	0.807	1.32 (-0.11,2.76)	0.071

Model adjusted for age (years), BMI categories, energy intake, calcium intake (tertiles), vitamin D intake (tertiles), calcium supplementation, alcohol consumption (g/day), smoking status (never, current and past), physical activity, and hormone replacement therapy (HRT). *Model adjusted for age (years), BMI categories, energy intake, vitamin D intake (tertiles), alcohol consumption (g/day), smoking status (never, current and past), physical activity, blood collection season, and hormone replacement therapy (HRT).

10.3389/fendo.2024.1392063

TABLE 2 Association between the SNVs and BMD at different sites and 25-hydroxivitamin D levels among women aged 45 years and older.

		Total hip BMD		Femoral neck BMD		Lumbar spine BMD		25-hydroxivitamin D	
rs11623869		β (95%CI)	*p*-value	β (95%CI)	*p*-value	β (95%CI)	*p*-value	β (95%CI)*	*p*-value
Additive		0.004 (-0.009,0.018)	0.556	0.005 (-0.008,0.018)		0.003 (-0.015,0.021)	0.741	0.78 (0.03,1.54)	0.041
Codominant	GG	0.0		0.0		0.0		0.0	
	GT	0.007 (-0.009,0.023)	0.400	0.007 (-0.008,0.023)	0.352	0.007 (-0.014,0.028)	0.524	0.91 (0.02,1.80)	0.045
	TT	-0.003 (-0.045,0.040)	0.906	0.001 (-0.039,0.042)	0.945	-0.009 (-0.064,0.047)	0.762	1.09 (-1.25,3.44)	0.361
Dominant	GG	0.0		0.0		0.0		0.0	
	GT+TT	0.006 (-0.010,0.022)	0.446	0.007 (-0.008,0.022)	0.373	0.005 (-0.015,0.026)	0.600	0.93 (0.06,1.79)	0.036
Recessive	GG+GT	0.0		0.0		0.0		0.0	
	TT	-0.005 (-0.047,0.037)	0.817	-0.001 (-0.041,0.039)	0.957	-0.011 (-0.066,0.044)	0.696	0.78 (-1.55,3.11)	0.510
rs6086746									
Additive		0.023 (0.011,0.036)	0.00002	0.020 (0.008,0.031)	0.001	0.034 (0.018,0.051)	0.00004	0.69 (-0.006,1.39)	0.052
Codominant	GG	0.0		0.0		0.0		0.0	
	GA	0.025 (0.009,0.041)	0.002	0.022 (0.007,0.037)	0.005	0.044 (0.023,0.064)	0.00003	1.17 (0.29,2.05)	0.009
	AA	0.042 (0.010,0.075)	0.011	0.034 (0.003,0.066)	0.031	0.048 (0.005,0.091)	0.028	0.34 (-1.48,2.17)	0.713
Dominant	GG	0.0		0.0		0.0		0.0	
	GA+AA	0.027 (0.012,0.042)	0.0004	0.023 (0.009,0.038)	0.002	0.044 (0.024,0.064)	0.00001	1.06 (0.22,1.91)	0.014
Recessive	GG+GA	0.0		0.0		0.0		0.0	
	AA	0.031(-0.0005,0.063)	0.054	0.025(-0.006,0.056)	0.109	0.029 (-0.013,0.072)	0.173	-0.17 (-1.96,1.62)	0.851
rs2277458									
Additive		0.001 (-0.011,0.013)	0.862	0.002 (-0.010,0.013)	0.768	-0.003 (-0.019,0.013)	0.727	0.96 (0.29,1.64)	0.005
Codominant	GG	0.0		0.0		0.0		0.0	
	GA	-0.0002 (-0.016,0.015)	0.977	-0.003 (-0.018,0.012)	0.678	-0.006 (-0.026,0.014)	0.563	0.87 (0.01,1.74)	0.048
	AA	0.005 (-0.026,0.036)	0.765	0.013 (-0.017,0.043)	0.382	0.0007 (-0.040,0.041)	0.972	2.11 (0.38,3.85)	0.017
Dominant	GG	0.0		0.0		0.0		0.0	
	GA+AA	0.0005 (-0.014,0.015)	0.951	-0.0009 (-0.015,0.013)	0.906	-0.005 (-0.025,0.014)	0.611	1.04 (0.21,1.87)	0.014
Recessive	GG+GA	0.0		0.0		0.0		0.0	
	AA	0.005 (-0.026,0.035)	0.755	0.015 (-0.015,0.044)	0.325	0.003 (-0.037,0.043)	0.873	1.73 (0.05,3.46)	0.044

Model adjusted for age (years), BMI categories, energy intake, calcium intake (tertiles), vitamin D intake (tertiles), calcium supplementation, alcohol consumption (g/day), smoking status (never, current and past), physical activity, and hormone replacement therapy (HRT). *Model adjusted for age (years), BMI categories, energy intake, vitamin D intake (tertiles), alcohol consumption (g/day), smoking status (never, current and past), physical activity, blood collection season, and hormone replacement therapy (HRT).

TABLE 3 Association between the variants of interest and low-BMD at different sites and VD deficiency in total women.

		Total hip BMD		Femoral neck BMD		Lumbar spine BMD		VD Deficiency*	
rs11623869		OR (95%CI)	*p*-value	OR (95%CI)	*p*-value	OR (95%CI)	*p*-value	OR (95%CI)	*p*-value
Additive		1.18 (0.91-1.54)	0.220	1.13 (0.89-1.45)	0.321	0.96 (0.76-1.21)	0.731	0.84 (0.68-1.04)	0.118
Codominant	GG	1.0		1.0		1.0		1.0	
	GT	1.39 (1.01-1.90)	0.042	1.21 (0.90-1.62)	0.212	0.88 (0.67-1.15)	0.346	0.79 (0.61-1.02)	0.069
	TT	0.77 (0.32-1.82)	0.547	1.03 (0.48-2.20)	0.936	1.29 (0.63-2.63)	0.491	0.91 (0.47-1.75)	0.766
Dominant	GG	1.0		1.0		1.0		1.0	
	GT+TT	1.31 (0.97-1.79)	0.080	1.19 (0.89-1.58)	0.236	0.91 (0.70-1.18)	0.478	0.80 (0.63-1.02)	0.076
Recessive	GG+GT	1.0		1.0		1.0		1.0	
	TT	0.68 (0.29-1.61)	0.383	0.97 (0.46-2.04)	0.928	1.35 (0.66-2.73)	0.411	0.98 (0.51-1.88)	0.951
rs6086746									
Additive		0.74 (0.57-0.95)	0.020	0.68 (0.54-0.86)	0.001	0.71 (0.57-0.86)	0.001	0.91 (0.75-1.10)	0.329
Codominant	GG	1.0		1.0		1.0		1.0	
	GA	0.69 (0.50-0.95)	0.021	0.68 (0.50-0.91)	0.009	0.65 (0.50-0.86)	0.002	0.85 (0.67-1.09)	0.198
	AA	0.65 (0.33-1.29)	0.217	0.47 (0.25-0.88)	0.018	0.60 (0.34-1.04)	0.070	0.95 (0.57-1.57)	0.843
Dominant	GG	1.0		1.0		1.0		1.0	
	GA+AA	0.69 (0.51-0.93)	0.015	0.65 (0.49-0.86)	0.002	0.65 (0.50-0.84)	0.001	0.86 (0.68-1.09)	0.222
Recessive	GG+GA	1.0		1.0		1.0		1.0	
	AA	0.76 (0.39-1.48)	0.419	0.55 (0.30-1.02)	0.060	0.72 (0.42-1.24)	0.236	1.02 (0.62-1.66)	0.940
rs2277458									
Additive		1.11 (0.87-1.41)	0.409	1.08 (0.87-1.32)	0.494	0.87 (0.69-1.09)	0.219	0.90 (0.74-1.08)	0.253
Codominant	GG	1.0		1.0		1.0		1.0	
	GA	1.06 (0.78-1.46)	0.695	1.06 (0.81-1.38)	0.674	0.95 (0.71-1.26)	0.708	0.90 (0.71-1.14)	0.385
	AA	1.32 (0.72-2.42)	0.372	1.19 (0.70-2.04)	0.519	0.63 (0.35-1.14)	0.126	0.80 (0.49-1.30)	0.365
Dominant	GG	1.0		1.0		1.0		1.0	
	GA+AA	1.12 (0.83-1.50)	0.472	1.08 (0.83-1.39)	0.573	0.90 (0.68-1.18)	0.437	0.88 (0.70-1.11)	0.296
Recessive	GG+GA	1.0		1.0		1.0		1.0	
	AA	1.38 (0.77-2.46)	0.277	1.16 (0.69-1.97)	0.570	0.65 (0.36-1.15)	0.138	0.83 (0.51-1.35)	0.457

Model adjusted for age (years), BMI categories, energy intake, calcium intake (tertiles), vitamin D intake (tertiles), calcium supplementation, alcohol consumption (g/day), smoking status (never, current and past), physical activity, and hormone replacement therapy (HRT). Low-BMD as a T-score below -1 at the total hip, and lumbar spine. *Model adjusted for age (years), BMI categories, energy intake, vitamin D intake (tertiles), alcohol consumption (g/day), smoking status (never, current and past), physical activity, blood collection season, and hormone replacement therapy (HRT).

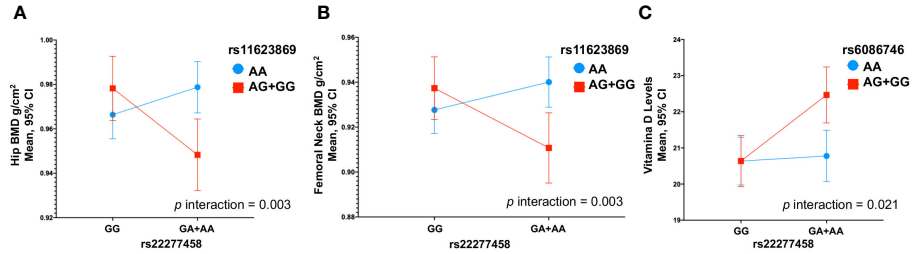

FIGURE 1
Gene-Gene Interactions Impacting BMD and 25(OH)D Levels in Total Women. **(A)** rs11623869 × rs2277458 interaction with total hip, **(B)** rs11623869 × rs2277458 interaction with femoral neck, and **(C)** rs6086746 × rs2277458 interaction with vitamin D levels. Model **(A, B)** adjusted for age (years), BMI categories, energy intake, calcium intake (tertiles), vitamin D intake (tertiles), calcium supplementation, alcohol consumption (g/day), smoking status (never, current, and past), physical activity, and hormone replacement therapy (HRT). Low-BMD as a T-score below -1 at the total hip, and lumbar spine. Model **(C)** adjusted for age (years), BMI categories, energy intake, vitamin D intake (tertiles), alcohol consumption (g/day), smoking status (never, current, and past), physical activity, blood collection season, and hormone replacement therapy (HRT).

4 Discussion

Our study confirmed previous evidence indicating associations between the genetic variants *MARK3* (rs11623869), *PLCB4* (rs6086746), and *GEMIN2* (rs2277458) with osteoporosis and serum 25OHD levels in a European-descent population and a southern Chinese cohort also associated with an admixed population such as the Mexican-Mestizo. These findings suggest that the genetic factors influencing osteoporosis and vitamin D levels may transcend ethnic boundaries, emphasizing their relevance across diverse population groups.

In recent years, it has been reported that circulating factors such as calcium, phosphate, 25(OH)D, PTH and ALP, have been related to the variation of DMO. They can act directly or indirectly on skeletal cells, regulating bone remodeling and metabolism. Vitamin D is essential for efficient calcium absorption. An adequate amount of vitamin D is required to maintain bone strength and prevent fragility fractures (22) Vitamin D deficiency (25OHD <20 ng/mL) is common in Mexican older adults and linked with factors such as sex, age, genetics, diet and obesity (23, 24). In addition, the lower intake of vitamin D and calcium reported in the Mexican population (25) can cause inefficient absorption of calcium, which in turn can stimulate the release of calcium from the bones to maintain a normal concentration of calcium in the blood and consequently cause bone loss. Decreasing serum calcium levels can stimulate PTH secretion, and PTH in turn can improve serum calcium concentration by releasing calcium from bone by increasing bone resorption. However, several studies have reported the negative impact of elevated serum PTH levels on BMD (26). Calcium and phosphate are co-dependent for bone development, a sufficient amount of phosphate in the blood has a positive effect on calcium use and adequate bone growth (27), while ALP plays an important role in the formation and mineralization of osteoid and is used as a biomarker to evaluate bone turnover. The high rate of bone turnover in elderly people can lead to rapid bone loss and reduced bone mass. Interactions between genetic, dietary, hormonal, metabolic, and lifestyle factors have been suggested to play an important role in susceptibility to low BMD. In this sense, the risk caused by genetic variants may vary between individual's due to differential modifications of the different concentrations of circulating factors involved in bone remodeling and metabolism. While a study by Xiao SM, et al. in 2013 reported an association between the SNV rs11623869 of the MARK3 gene and BMD, particularly strengthened in the presence of high serum levels of ALP (22), no association studies have been conducted for the SNVs rs6086746 in PLCB4 and rs2277458 in GEMIN2 with serum

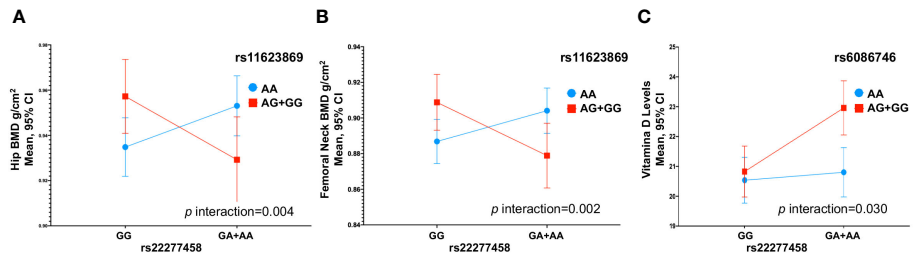

FIGURE 2
Gene-Gene Interactions Affecting BMD and 25(OH)D Levels in Women Aged > 45 Years. **(A)** rs11623869 × rs2277458 interaction with total hip, **(B)** rs11623869 × rs2277458 interaction with femoral neck, and **(C)** rs6086746 × rs2277458 interaction with vitamin D levels. Model **(A, B)** adjusted for age (years), BMI categories, energy intake, calcium intake (tertiles), vitamin D intake (tertiles), calcium supplementation, alcohol consumption (g/day), smoking status (never, current, and past), physical activity, and hormone replacement therapy (HRT). Low-BMD as a T-score below -1 at the total hip, and lumbar spine. Model **(C)** adjusted for age (years), BMI categories, energy intake, vitamin D intake (tertiles), alcohol consumption (g/day), smoking status (never, current, and past), physical activity, blood collection season, and hormone replacement therapy (HRT).

10.3389/fendo.2024.1392063

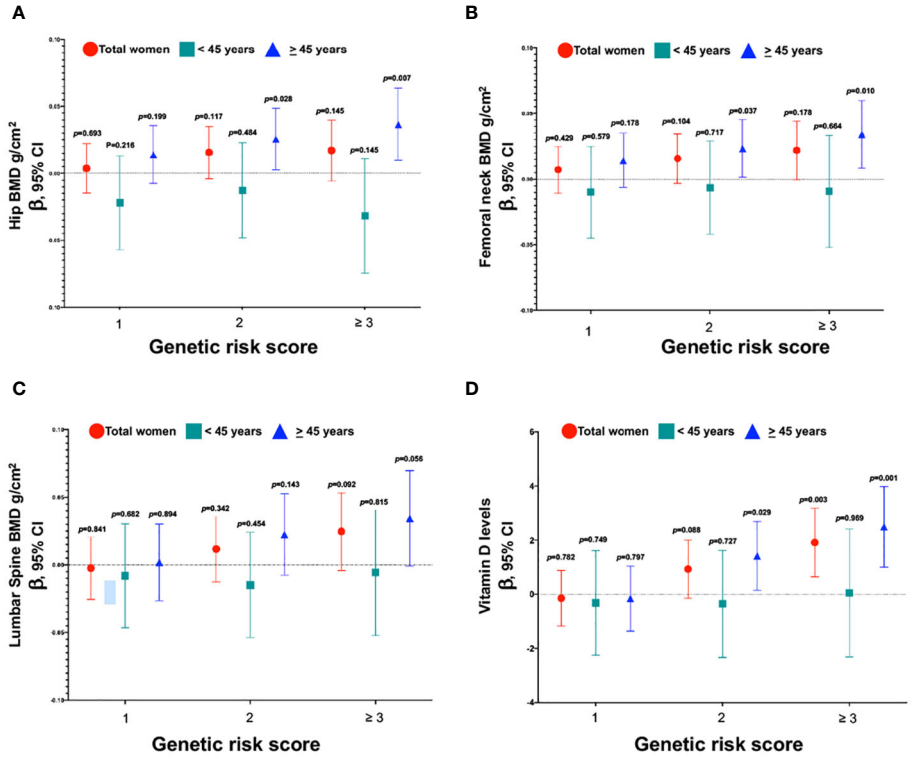

FIGURE 3
Association between the genetic risk score of variants with BMD and vitamin D levels. **(A)** Genetic risk score and total hip, **(B)** Genetic risk score and femoral neck, **(C)** Genetic risk score and lumbar spine, and **(D)** Genetic risk score and vitamin D levels. Model **(A–C)** were adjusted for age (years), BMI categories, energy intake, calcium intake (tertiles), vitamin D intake (tertiles), calcium supplementation, alcohol consumption (g/day), smoking status (never, current, and past), physical activity, and hormone replacement therapy (HRT). Low-BMD as a T-score below -1 at the total hip, and lumbar spine. Model **(D)** was adjusted for age (years), BMI categories, energy intake, vitamin D intake (tertiles), alcohol consumption (g/day), smoking status (never, current, and past), physical activity, blood collection season, and hormone replacement therapy (HRT).

variables such as vitamin D, calcium or ALP, and their potential effects on BMD variation.

It has been reported that the *MARK3* gene is involved in different biological processes such as cell cycle, ciliated cell differentiation, and osteoclast differentiation (28). So far, the role of *MARK3* has been studied in several pathological conditions (9, 29–31). In osteoporosis, the variant rs11623869 in *MARK3* has been associated with bone mineral density and low-trauma fractures (32, 33). Our results showed that the rs11623869-T variant is associated with low BMD at the total hip. These data are consistent with previous reports where the T allele was associated with a decreased BMD at femoral neck accompanied by an increased expression of *MARK3* (32). The authors showed that *Mark3*-deficient osteoblasts exhibited an increase of bone mass, through reduced *Jag1/Hes1* expression and decreased downstream JNK signaling stimulating osteoblast activity. On the other hand, in Chinese population, it was observed that the effect of the SNV rs11623869 on BMD was greater in the presence of high serum levels of ALP, a biomarker for osteoblast activity, and considered a predictor of BMD in postmenopausal females (33). Together these data suggest that genetic variation of *MARK3* influences bone mineral density. However, current data also suggest that circulating factors in serum may also affect bone turnover and metabolism modifying the association of *MARK3* with BMD. Further research is necessary to clarify the role of these circulatory factors in Mexican postmenopausal women.

Another gene of interest is *PLCB4*, its product catalyzes the formation of inositol 1,4,5-trisphosphate and diacylglycerol from phosphatidylinositol 4,5-bisphosphate, using calcium as a cofactor. *PLCB4* plays an essential role in signal transduction (34). Genetic variants in *PLCB4* have been identified as cause of the Auriculocondylar syndrome 2 (ARCND2), a disease characterized by craniofacial malformations (13), *PLCB4* acts as a direct signaling effector of the endothelin receptor type A (EDNRA)-Gq/11 pathway. Kanai et al, 2022 demonstrated that variants in *PLCB4* gene interfere with the EDNRA signaling pathway, leading to the development of ARCND2 (35). However, the role of genetic variants in *PLCB4* on BMD has been explored only to a limited extent. Only one study in the Chinese population reported that carriers of the A alleles of the rs6086746 variant in *PLCB4*, showed a decrease in BMD and an increased risk of developing osteoporosis. Furthermore, they found that the rs6086746 variant was significantly associated with osteoporosis, by participating on the binding of *RUNX2*, a master transcription factor involved in the osteoblast maturation. Through luciferase assays, they showed increased to that *PLCB4* activity in individuals carrying the rs6086746-A allele, proposing a functional explanation for the observed association (13). In contrast, our results shown that

variant rs6086746 was associated with higher BMD and protective effect against low-BMD in women aged 45 years or older. These results are consistent with an independent group of OP patients from the National Institute of Rehabilitation (INR) in Mexico City (36). Although the frequencies were similar in both cohorts, we did not observe statistical differences (OR = 0.74, 95%CI 0.47-1.16), perhaps due to the small sample size (n=384).

Recently, three genotypes associated to plasma 25-hydroxyvitamin D levels were identified through genome-wide association studies; among which is the variant rs2277458 in *GEMIN2* (37). GEMIN2 encodes a protein of the SMN complex, this complex includes several Gemin proteins and the SMN protein. The SMN complex is located at a subnuclear compartment called gems (Gemin of coiled bodies) and is necessary for the assembly of spliceosomal snRNPs and for pre-mRNA splicing. Although there is no evidence implicating *GEMIN2* in vitamin-D-related physiological pathways.

More recently, in a study in the Danish population, the rs2277458-A allele of *GEMIN2* was associated with lower serum 25-hydroxyvitamin D concentrations in a dose-dependent manner (20). These data are consistent with our results where the rs2277458-G allele of *GEMIN2* was associated with lower serum 25-hydroxyvitamin D levels, in women aged 45 years or older. Low vitamin D concentrations are believed to affect bone metabolism by decreasing dietary calcium and phosphorus absorption and increasing the production of parathyroid hormone (38). In addition, vitamin D activates osteoblasts and osteoclasts to dissolve the mineralized collagen in bones, causing osteopenia and osteoporosis, thus increasing the risk of fractures. Together these data suggest that genetic variants in *GEMIN2* influences serum 25-hydroxyvitamin D concentrations, in different populations (39).

Vitamin D has been shown to play a fundamental role in calcium and phosphate homeostasis, furthermore, serum levels of vitamin D are positively correlated with BMD values (40). In contrast, vitamin D deficiency causes a reduction of BMD, increasing the risk of bone fractures in the elderly (41). In our study, the genetic risk score constructed using the three variants (equivalent to 3 risk alleles) was significantly associated with higher BMD at the hip and femoral neck, as well as elevated serum 25OHD levels. These associations were particularly pronounced among postmenopausal women aged 45 years and older. This suggests that the cumulative genetic risk, as represented by the GRS, may contribute to improved bone health and vitamin D status in this population. These results are consistent with those reported by Mithal, et al., 2009, who analyzed a population from Latin America including Mexico that was composed of postmenopausal women and in which they observed that vitamin D levels are below of the average values, due to geographical and population characteristics (23, 42).

A possible explanation for these findings is that vitamin D consumption could improve BMD levels in women over 45 years of age with higher genetic risk, given that the associated genetic variants are linked to vitamin D levels in the body. Additionally, the SNVs included in the genetic risk score may influence vitamin D metabolism, thereby strengthening the response. Therefore, these data may generate a new focus on the possible role of these SNVs on vitamin D metabolism. Nevertheless, these data should be taken with caution, as a larger and more diverse population is needed for confirming or discarding these findings.

The literature regarding the interaction between genes related to vitamin D levels and BMD, in Mexican Mestizo population is scarce (43). This study provides evidence suggesting that this phenomenon could be participating in the high prevalence of vitamin D deficiency in the Mexican population. Furthermore, interactions between genes are proposed to serve as a key factor involved in the variance of BMD. We have identified an effect of the interaction between SNV rs11623869 in the *MARK3* gene and the SNV rs22277458 in *GEMIN2* on hip and femoral neck BMD. The influence of these interactions on BMD is complex, concentrations of circulating factors related to calcium and phosphate metabolism might alter the effect of genetic risk factors and the subsequent loss of BMD. Studies considering the interaction of genes involved in BMD loss in conjunction with known factors involved in calcium and phosphorus metabolism will contribute to unravel this complex relationship. Furthermore, interactions between genetic and lifestyle factors have been suggested to play an important role on susceptibility to having low BMD and serum 25OHD levels. The risk caused by genetic variants may vary between populations due to exposition to different environmental factor and lifestyle habits. In this study, we found that the association of the rs22277458 in *GEMIN2* with serum 25OHD levels was strengthened in the presence of the rs6086746 *PCLB4*. However, the role of *GEMIN2* and *PCLB4* on vitamin D metabolism remains unknown. Also, we cannot exclude that variants in these genes may only indirectly affect 25 hydroxyvitamin D through pathways affecting both, exposure and outcome separately. Further, we cannot exclude the possibility that other mechanisms involving these genes may exist. Finally, the association of genetic variants in *GEMIN2* and *PCLB4* genes with serum 25OHD could represent a chance finding and, therefore, needs additional confirmation in an independent cohort.

This study has some strengths: first this analysis was conducted in a relatively large sample (n=1300) compared to other observational studies. Second, this is the first study focused on understanding the effect of genetic variants involved in vitamin D metabolism and bone mineral density in postmenopausal women. On the other hand, this study has some limitations. First, this work did not analyze GRS with serum calcium levels and bone fracture as reported in other studies. This could strengthen our hypothesis about the effect of SNVs of genes involved in vitamin D metabolism. Furthermore, since our study is cross-sectional, we cannot establish causality between SNVs, vitamin D levels, and BMD. In this work, it will be observed that vitamin D consumption is positively associated with BMD and is essential for efficient calcium absorption. However, a limitation of this study is that the relationship between serum calcium, ALP, and phosphate with BMD was not analyzed, these variables that have previously been reported for their association with bone growth and adequate osteoid mineralization. Furthermore, we acknowledge that the interaction observed between MARK3 and vitamin D levels may require replications in other independent populations, and functional studies are necessary to investigate whether the effect of

MARK3 on BMD is regulated by vitamin D levels. Another limitation is that our study represents the first report showing the association between the SNVs rs6086746 in PLCB4, and rs2277458 in GEMIN2 with vitamin D levels and BMD in a Mexican population, as these genes and their respective variants had not been previously related to bone metabolism, and there are no reports on their functional role. In addition to these limitations, show the need for future longitudinal research that can address these issues. Second, we did not adjust for multiple comparisons due to the effect size found, although in recent years it has been reported that adjustment by multiple testing controls overall type I error but significantly increases type II error (44).

5 Conclusions

Our study has provided independent replications of the associations reported for the *MARK3* (rs11623869), *PLCB4* (rs6086746), and *GEMIN2* (rs2277458) genetic variants with BMD and serum 25 hydroxy-vitamin D in a Mexican mestizo population. These results suggest that that genetic variants in these three genes may confer susceptibility for changes in BMD and serum 25 hydroxy vitamin D levels in Mexican-Mestizo, Chinese, and European-descent populations. Furthermore, we have found that SNVs rs22277458 in *GEMIN2*, rs11623869 in *MARK3* and rs6086746 in *PLCB4*, highlighting the complexity of genetic and environmental factors in determining bone health. These findings have important clinical and public health implications as they could help improve the prevention, diagnosis, and treatment of bone diseases such as osteoporosis in the Mexican population. However, further longitudinal research is required to fully understand the underlying mechanisms and clinical implications of these genetic associations.

Data availability statement

The original contributions presented in the study are included in the article/supplementary material, further inquiries can be directed to the corresponding author.

Ethics statement

The studies involving humans were approved by Ethics Committee from Mexican Social Security Institute (No. 12CEI 09 006 14), and the National Institute of Genomic Medicine (399–17/2016/I). The studies were conducted in accordance with the local legislation and institutional requirements. The participants provided their written informed consent to participate in this study.

Author contributions

DA-B: Writing – original draft, Writing – review & editing, Investigation, Visualization. RJ-O: Investigation, Visualization, Writing – original draft, Writing – review & editing. AB-C: Writing – review & editing, Methodology. AA-G: Writing – review & editing, Funding acquisition. VL-S: Writing – review & editing, Methodology. LC-A: Methodology, Writing – review & editing. JS: Funding acquisition, Writing – review & editing. AH-B: Funding acquisition, Writing – review & editing. BR-P: Data curation, Formal analysis, Writing – review & editing. RV-C: Conceptualization, Funding acquisition, Supervision, Writing – original draft, Writing – review & editing.

Funding

The author(s) declare financial support was received for the research, authorship, and/or publication of this article. This research was partially funded by the Instituto Nacional de Medicina Genómica, grant number 266-17/2016/I and 399-07/2019/I. RV-C received funding from CONACYT under grant: INFR-2016-01-270405. RJ-O is supported by a Postdoctoral Fellowship from the Consejo Nacional de Ciencia y Tecnología (Grant Ciencia de Frontera CF 2019-102962). AB-C is the recipient of a Postdoctoral Fellowship from the Consejo Nacional de Humanidades, Ciencia y Tecnología (CONAHCYT-Estancia Posdoctoral de Incidencia Inicial 2022 with CVU 508876).

Acknowledgments

The authors would like to thank the Health Workers Cohort Study participants and the staff of the Epidemiological Research Unit and Services of Health-IMSS, Cuernavaca, Morelos.

Conflict of interest

The authors declare that the research was conducted in the absence of any commercial or financial relationships that could be construed as a potential conflict of interest.

Publisher's note

Supplementary material

The Supplementary Material for this article can be found online at: https://www.frontiersin.org/articles/10.3389/fendo.2024.1392063/full#supplementary-material

References

1. Yong EL, Logan S. Menopausal osteoporosis: screening, prevention and treatment. *Singapore Med J*. (2021) 62:159–66. doi: 10.11622/smedj.2021036

2. Black DM, Rosen CJ. Clinical practice. Postmenopausal osteoporosis. *N Engl J Med*. (2016) 374:254–62. doi: 10.1056/NEJMcp1513724

3. Pisani P, Renna MD, Conversano F, Casciaro E, Di Paola M, Quarta E, et al. Major osteoporotic fragility fractures: Risk factor updates and societal impact. *World J Orthop*. (2016) 7:171–81. doi: 10.5312/wjo.v7.i3.171

4. Clark P, Ramírez-Pérez E, Reyes-López A. Umbrales de evaluación para la detección de casos en riesgo de OP (OP) y fracturas por fragilidad con FRAX en población mexicana para el primer nivel de salud. *Gaceta Médica México*. (2016) 152:22–31.

5. Mendoza N, Morón F, Santalla A. Genética de la osteoporosis posmenópausica: nuevos conocimientos y nuevos conceptos sobre su relación con los polimorfismos genéticos en la ruta estrogenica. *REEMO*. (2008) 17:106–11. doi: 10.1016/S1132-8460(08)72490-5

6. Ralston SH, Uitterlinden AG. Genetics of osteoporosis. *Endocr Rev*. (2010) 31:629–62. doi: 10.1210/er.2009-0044

7. Wu Q, Jung J. Genome-wide polygenic risk score for major osteoporotic fractures in postmenopausal women using associated single nucleotide polymorphisms. *J Transl Med*. (2023) 21:127. doi: 10.1186/s12967-023-03974-2

8. Özbaş H, Tutgun Onrat S, Özdamar K. Genetic and environmental factors in human osteoporosis. *Mol Biol Rep*. (2012) 39:11289–96. doi: 10.1007/s11033-012-2038-5

9. Machino H, Kaneko S, Komatsu M, Ikawa N, Asada K, Nakato K, et al. The metabolomic stress-activated checkpoint LKB1-MARK3 axis acts as a tumor suppressor in high-grade serous ovarian carcinoma. *Commun Biol*. (2022) 5:1–15. doi: 10.1038/s42003-021-02992-4

10. Calabrese GM, Mesner LD, Stains JP, Tommasini SM, Horowitz MC, Rosen CJ, et al. Integrating GWAS and co-expression network data identifies bone mineral density genes SPTBN1 and MARK3 and an osteoblast functional module. *Cell Syst*. (2017) 4:46–59.e4. doi: 10.1016/j.cels.2016.10.014

11. Li YM, Peng C, Zhang JG, Zhu W, Xu C, Lin Y, et al. Genetic risk factors identified in populations of European descent do not improve the prediction of osteoporotic fracture and bone mineral density in Chinese populations. *Sci Rep*. (2019) 9:6086. doi: 10.1038/s41598-019-42606-y

12. Greenblatt MB, Shim JH, Bok S, Kim JM. The extracellular signal-regulated kinase mitogen-activated protein kinase pathway in osteoblasts. *J Bone Metab*. (2022) 29:1–15. doi: 10.11005/jbm.2022.29.1.1

13. Tsai DJ, Fang WH, Wu LW, Tai MC, Kao CC, Huang SM, et al. The polymorphism at PLCB4 promoter (rs6086746) changes the binding affinity of RUNX2 and affects osteoporosis susceptibility: an analysis of bioinformatics-based case-control study and functional validation. *Front Endocrinol (Lausanne)*. (2021) 12:730686. doi: 10.3389/fendo.2021.730686

14. Liu TM, Lee EH. Transcriptional regulatory cascades in Runx2-dependent bone development. *Tissue Eng Part B Rev*. (2013) 19:254–63. doi: 10.1089/ten.TEB.2012.0527

15. Lee HJ, Koh JM, Hwang JY, Choi KY, Lee SH, Park EK, et al. Association of a RUNX2 promoter polymorphism with bone mineral density in postmenopausal Korean women. *Calcif Tissue Int*. (2009) 84:439–45. doi: 10.1007/s00223-009-9246-6

16. Auerkari EI, Suryandari DA, Umami SS, Kusdhany LS, Siregar TW, Rahardjo TB, et al. Gene promoter polymorphism of RUNX2 and risk of osteoporosis in postmenopausal Indonesian women. *SAGE Open Med*. (2014) 2:2050312114531571. doi: 10.1177/2050312114531571

17. Pineda B, Hermenegildo C, Laporta P, Tarín JJ, Cano A, García-Pérez MÁ. Common polymorphisms rather than rare genetic variants of the Runx2 gene are associated with femoral neck BMD in Spanish women. *J Bone Miner Metab*. (2010) 28:696–705. doi: 10.1007/s00774-010-0183-2

18. Ogawa C, Usui K, Aoki M, Ito F, Itoh M, Kai C, et al. Gemin2 plays an important role in stabilizing the survival of motor neuron complex. *J Biol Chem*. (2007) 282:11122–34. doi: 10.1074/jbc.M609297200

19. Schlaen RG, Mancini E, Sanchez SE, Perez-Santángelo S, Rugnone ML, Simpson CG, et al. The spliceosome assembly factor GEMIN2 attenuates the effects of temperature on alternative splicing and circadian rhythms. *Proc Natl Acad Sci U S A*. (2015) 112:9382–7. doi: 10.1073/pnas.1504541112

20. Çolak Y, Afzal S, Nordestgaard BG. 25-hydroxyvitamin D and risk of osteoporotic fractures: mendelian randomization analysis in 2 large population-based cohorts. *Clin Chem*. (2020) 66:676–85. doi: 10.1093/clinchem/hvaa049

21. Denova-Gutiérrez E, Flores YN, Gallegos-Carrillo K, Ramírez-Palacios P, Rivera-Paredez B, Muñoz-Aguirre P, et al. Health workers cohort study: methods and study design. *Salud Publica Mex*. (2016) 58:708–16. doi: 10.21149/spm.v58i6.8299

22. Xiao SM, Kung AW, Sham PC, Tan KC. Genetic analysis of recently identified osteoporosis susceptibility genes in southern Chinese. *J Clin Endocrinol Metab*. (2013) 98:E1827–34. doi: 10.1210/jc.2013-1055

23. Martínez-Zavala N, López-Sánchez GN, Vergara-Lopez A, Chávez-Tapia NC, Uribe M, Nuño-Lámbarri N. Vitamin D deficiency in Mexicans have a high prevalence: a cross-sectional analysis of the patients from the Centro Médico Nacional 20 de Noviembre. *Arch Osteoporos*. (2020) 15:88. doi: 10.1007/s11657-020-00765-w

24. Carrillo-Vega MF, García-Peña C, Gutiérrez-Robledo LM, Pérez-Zepeda MU. Vitamin D deficiency in older adults and its associated factors: a cross-sectional analysis of the Mexican Health and Aging Study. *Arch Osteoporos*. (2017) 12:8. doi: 10.1007/s11657-016-0297-9

25. Ramírez-Silva I, Rodríguez-Ramírez S, Barragán-Vázquez S, Castellanos-Gutiérrez A, Reyes-García A, Martínez-Piña A, et al. Prevalence of inadequate intake of vitamins and minerals in the Mexican population correcting by nutrient retention factors, Ensanut 2016. *Salud Publica Mex*. (2020) 62:521–31. doi: 10.21149/1109

26. von Mühlen DG, Greendale GA, Garland CF, Wan L, Barrett-Connor E. Vitamin D, parathyroid hormone levels and bone mineral density in community-dwelling older women: the Rancho Bernardo Study. *Osteoporos Int*. (2005) 16:1721–6. doi: 10.1007/s00198-005-1910-8

27. Shapiro R, Heaney RP. Co-dependence of calcium and phosphorus for growth and bone development under conditions of varying deficiency. *Bone*. (2003) 32:532–40. doi: 10.1016/s8756-3282(03)00060-7

28. Baqai U, Kurimchak AM, Trachtenberg IV, Purwin TJ, Haj JI, Han A, et al. Kinome profiling identifies MARK3 and STK10 as potential therapeutic targets in uveal melanoma. *J Biol Chem*. (2023) 299:105418. doi: 10.1016/j.jbc.2023.105418

29. Kato T, Reddy KR. Radiofrequency ablation for hepatocellular carcinoma: help or hazard? *Hepatology*. (2001) 33:1336–7. doi: 10.1053/jhep.2001.24738

30. Lund H, Gustafsson E, Svensson A, Nilsson M, Berg M, Sunnemark D, et al. MARK4 and MARK3 associate with early tau phosphorylation in Alzheimer's disease granulovacuolar degeneration bodies. *Acta Neuropathol Commun*. (2014) 2:22. doi: 10.1186/2051-5960-2-22

31. Styrkarsdottir U, Halldorsson BV, Gretarsdottir S, Gudbjartsson DF, Walters GB, Ingvarsson T, et al. New sequence variants associated with bone mineral density. *Nat Genet*. (2009) 41:15–7. doi: 10.1038/ng.284

32. Estrada K, Styrkarsdottir U, Evangelou E, Hsu YH, Duncan EL, Ntzani EE, et al. Genome-wide meta-analysis identifies 56 bone mineral density loci and reveals 14 loci associated with risk of fracture. *Nat Genet*. (2012) 44:491–501. doi: 10.1038/ng.2249

33. Zhang Q, Mesner LD, Calabrese GM, Dirckx N, Li Z, Verardo A, et al. Genomic variants within chromosome 14q32.32 regulate bone mass through MARK3 signaling in osteoblasts. *J Clin Invest*. (2021) 131:e142580. doi: 10.1172/JCI142580

34. de Rubio RG, Ransom RF, Malik S, Yule DI, Anantharam A, Smrcka AV. Phosphatidylinositol 4-phosphate is a major source of GPCR-stimulated phosphoinositide production. *Sci Signal*. (2018) 11:eaan1210. doi: 10.1126/scisignal.aan1210

35. Kanai SM, Heffner C, Cox TC, Cunningham ML, Perez FA, Bauer AM, et al. Auriculocondylar syndrome 2 results from the dominant-negative action of PLCB4 variants. *Dis Model Mech*. (2022) 15:dmm049320. doi: 10.1242/dmm.049320

36. Hidalgo-Bravo A, Hernández-Medrano C, Sevilla-Montoya R, Rivera-Paredez B, Ramirez-Salazar EG, Flores-Morales J, et al. Single-nucleotide polymorphism rs10036727 in the *SLIT3* gene is associated with osteoporosis at the femoral neck in older Mexican postmenopausal women. *Gynecol Endocrinol*. (2020) 36:1096–100. doi: 10.1080/09513590.2020.1804548

37. Kim YA, Yoon JW, Lee Y, Choi HJ, Yun JW, Bae E, et al. Unveiling genetic variants underlying vitamin D deficiency in multiple korean cohorts by a genome-wide association study. *Endocrinol Metab (Seoul)*. (2021) 36:1189–200. doi: 10.3803/EnM.2021.1241

38. Bhattarai HK, Shrestha S, Rokka K, Shakya R. Vitamin D, calcium, parathyroid hormone, and sex steroids in bone health and effects of aging. *J Osteoporos*. (2020) 2020:9324505. doi: 10.1155/2020/9324505

39. Takahashi N, Udagawa N, Suda T. Vitamin D endocrine system and osteoclasts. *Bonekey Rep*. (2014) 3:495. doi: 10.1038/bonekey.2013.229

40. Voulgaridou G, Papadopoulou SK, Detopoulou P, Tsoumana D, Giaginis C, Kondyli FS, et al. Vitamin D and calcium in osteoporosis, and the role of bone turnover markers: A narrative review of recent data from RCTs. *Diseases*. (2023) 11:29. doi: 10.3390/diseases11010029

41. Wang Q, Yu D, Wang J, Lin S. Association between vitamin D deficiency and fragility fractures in Chinese elderly patients: a cross-sectional study. *Ann Palliat Med*. (2020) 9:1660–5. doi: 10.21037/apm-19-610

42. Mithal A, Wahl DA, Bonjour JP, Burckhardt P, Dawson-Hughes B, Eisman JA, et al. IOF Committee of Scientific Advisors (CSA) Nutrition Working Group. Global vitamin D status and determinants of hypovitaminosis D. *Osteoporos Int*. (2009) 20:1807–20. doi: 10.1007/s00198-009-0954-6

43. Rivera-Paredez B, Quezada-Sánchez AD, Denova-Gutiérrez E, Torres-Ibarra L, Flores YN, Salmerón J, et al. Erratum to: Diet Modulates the Effects of Genetic Variants on the Vitamin D Metabolic Pathway and Bone Mineral Density in Mexican Postmenopausal Women; doi: 10.1093/jn/nxab067. *J Nutr*. (2021) 151:1675. doi: 10.1093/jn/nxab166

44. Sutton AL, MacDonald PN. Vitamin D: more than a "bone-a-fide" hormone. *Mol Endocrinol*. (2003) 17:777–91. doi: 10.1210/me.2002-0363

frontiers | Frontiers in Endocrinology

TYPE Original Research
PUBLISHED 10 May 2024
DOI 10.3389/fendo.2024.1326761

OPEN ACCESS

EDITED BY
Kok Yong Chin,
National University of Malaysia, Malaysia

REVIEWED BY
Carla Azevedo Piccinato,
University of Sao Paulo, Brazil
Rodrigo Paolo Flores Abuna,
University of Sao Paulo, Brazil

*CORRESPONDENCE
Shufen Li
lsf825825@126.com
Yongming Xi
xym700118@163.com
Zhiyu Zhou
zhouzhy23@mail.sysu.edu.cn

†These authors have contributed equally to this work and share first authorship

RECEIVED 23 October 2023
ACCEPTED 24 April 2024
PUBLISHED 10 May 2024

CITATION
Chen D, Zhou J, Lin C, Li J, Zhu Z, Rao X, Wang J, Li J, Chen H, Wang F, Li X, Gao M, Zhou Z, Xi Y and Li S (2024) A causal examination of the correlation between hormonal and reproductive factors and low back pain.
Front. Endocrinol. 15:1326761.
doi: 10.3389/fendo.2024.1326761

A causal examination of the correlation between hormonal and reproductive factors and low back pain

Dafu Chen[1†], Jiaxiang Zhou[2†], Chengkai Lin[3†], Junhong Li[3], Zhengya Zhu[3], Xuezhi Rao[4], Jianmin Wang[3], Jianfeng Li[3], Hongkun Chen[3], Fuan Wang[3], Xianlong Li[3], Manman Gao[3,5,6,7], Zhiyu Zhou[3,6*], Yongming Xi[2*] and Shufen Li[8*]

[1]Laboratory of Bone Tissue Engineering, Beijing Laboratory of Biomedical Materials, National Center for Orthopaedics, Beijing Research Institute of Traumatology and Orthopaedics, Beijing Jishuitan Hospital, Capital Medical University, Beijing, China, [2]Department of Spinal Surgery, The Affiliated Hospital of Qingdao University, Qingdao, China, [3]Innovation Platform of Regeneration and Repair of Spinal Cord and Nerve Injury, Department of Orthopaedic Surgery, The Seventh Affiliated Hospital of Sun Yat-sen University, Shenzhen, China, [4]Beijing University of Chinese Medicine, Beijing, China, [5]Department of Sport Medicine, Institute of Translational Medicine, The First Affiliated Hospital of Shenzhen University, Shenzhen Second People's Hospital, Shenzhen, China, [6]Guangdong Provincial Key Laboratory of Orthopedics and Traumatology, The First Affiliated Hospital of Sun Yat-sen University, Guangzho, China, [7]Shenzhen Key Laboratory of Anti-aging and Regenerative Medicine, Department of Medical Cell Biology and Genetics, Health Sciences Center, Shenzhen University, Shenzhen, China, [8]Changzhou Maternal and Child Health Care Hospital, Changzhou Medical Center, Nanjing Medical University, Changzhou, China

Background: The relationship between hormonal fluctuations in the reproductive system and the occurrence of low back pain (LBP) has been widely observed. However, the causal impact of specific variables that may be indicative of hormonal and reproductive factors, such as age at menopause (ANM), age at menarche (AAM), length of menstrual cycle (LMC), age at first birth (AFB), age at last live birth (ALB) and age first had sexual intercourse (AFS) on low back pain remains unclear.

Methods: This study employed Bidirectional Mendelian randomization (MR) using publicly available summary statistics from Genome Wide Association Studies (GWAS) and FinnGen Consortium to investigate the causal links between hormonal and reproductive factors on LBP. Various MR methodologies, including inverse-variance weighted (IVW), MR-Egger regression, and weighted median, were utilized. Sensitivity analysis was conducted to ensure the robustness and validity of the findings. Subsequently, Multivariate Mendelian randomization (MVMR) was employed to assess the direct causal impact of reproductive and hormone factors on the risk of LBP.

Results: After implementing the Bonferroni correction and conducting rigorous quality control, the results from MR indicated a noteworthy association between a decreased risk of LBP and AAM (OR=0.784, 95% CI: 0.689-0.891; p=3.53E-04), AFB (OR=0.558, 95% CI: 0.436-0.715; p=8.97E-06), ALB (OR=0.396, 95% CI: 0.226-0.692; p=0.002), and AFS (OR=0.602, 95% CI: 0.518-0.700; p=3.47E-10). Moreover, in the reverse MR analysis, we observed no significant causal effects of LBP on ANM, AAM, LMC and AFS. MVMR analysis demonstrated the continued significance of the causal effect of AFB on LBP after adjusting for BMI.

Conclusion: Our study explored the causal relationship between ANM, AAM, LMC, AFB, AFS, ALB and the prevalence of LBP. We found that early menarche, early age at first birth, early age at last live birth and early age first had sexual intercourse may decrease the risk of LBP. These insights enhance our understanding of LBP risk factors, offering valuable guidance for screening, prevention, and treatment strategies for at-risk women.

KEYWORDS

low back pain, reproductive factors, age at menarche, age at menopause, age at first birth, Mendelian randomization

Introduction

Low back pain (LBP) is a prevalent public health issue, affecting approximately 60-80% of individuals at various stages of their lives (1, 2). Intervertebral disc degeneration is a major contributing factor to LBP and a noticeable trend towards its occurrence at younger ages has been observed (3, 4). The prevalence of LBP is generally higher among women than men, which can be attributed to factors such as increased pain sensitivity, variations in the menstrual cycle, physiological responses to pregnancy and childbirth, and abdominal weight gain during the perimenopausal phase (5–11).

Some studies have found a higher propensity for LBP among postmenopausal women compared to men of equivalent age (12). There was also evidence of an increased likelihood of LBP in individuals undergoing postmenopausal hormone therapy (13, 14). However, conflicting perspectives exist, with some suggesting potential positive outcomes associated with hormone therapy (15–17). These divergent views highlighted the potential significance of hormonal and reproductive factors in the pathogenesis and progression of LBP.

A strong connection has been established between hormonal factors, such as age at menopause (ANM), age at menarche (AAM), length of menstrual cycle (LMC), and age at first birth (AFB), and the occurrence of LBP. Various studies have identified associations between these factors and the risk of developing LBP, although the causal relationship between these remains unclear (18–21).

Observational studies on this subject were prone to bias due to confounding factors and reverse causality. To overcome these limitations, researchers have proposed the use of Mendelian randomization (MR) analysis. MR is a genetic epidemiological approach that uses single nucleotide polymorphisms (SNPs) as instrumental variables (IVs) for risk factors, allowing for the assessment of potential causal effects of exposure on outcomes (22). This method is based on Mendel's second law (23), asserting that alleles are randomly allocated during meiosis and are typically unaffected by environmental influences (22, 24).

Prior to this investigation, MR analyses had not been used to explore the causal relationship between hormonal and reproductive factors and LBP. Therefore, we conducted the MR analysis focusing on four female hormonal and reproductive factors (ANM, AAM, LMC, AFB, AFS and ALB), examining their associations with LBP. Subsequently, Multivariate Mendelian randomization (MVMR) was employed to assess the direct causal impact of reproductive and hormone factors on the risk of LBP. These findings may enhance our understanding of the hormonal and reproductive mechanisms underlying LBP, guiding future research towards developing potential therapeutic or preventative strategies.

Abbreviations: ANM, Age at menopause; AAM, Age at menarche; AFB, Age at first birth; LMC, Length of menstrual cycle; ALB, Age at last live birth; AFS, Age first had sexual intercourse; BMI, Body mass index; LBP, Low back pain; IVDD, Intervertebral disc degeneration; MR, Mendelian randomization; GWAS, Genome-Wide Association Studies; IVW, Inverse-variance weighted; IVs, Instrumental variables; SNPs, Single nucleotide polymorphisms.

Materials and methods

Study design and data sources

We conducted a comprehensive analysis using publicly accessible Genome-Wide Association Studies (GWAS) database to explore the potential causal relationship between ANM, AAM, LMC, AFB, AFS and ALB, and the occurrence of LBP. A comprehensive overview of the proposed hypotheses was presented in (Figure 1). The current study adhered to the three fundamental assumptions essential for MR analyses (25): assumption 1, all chosen IVs exhibit a strong correlation with the exposure; assumption 2 the selected instrumental variables are independent of both exposure and outcome confounders; assumption 3, the selected instrumental variables impact the outcome solely through exposure. Previous MR studies have established BMI as a risk factor for LBP (26). And a reverse MR analysis was conducted to evaluate potential reverse causality. Consequently, we conducted MVMR to address this potential confounding factor. The exposure data were obtained from the GWAS database (https://gwas.mrcieu.ac.uk/). Data on LBP was sourced from the FinnGen Consortium (https://finngen.fi). The summary data for the GWAS of LBP from the FinnGen Consortium

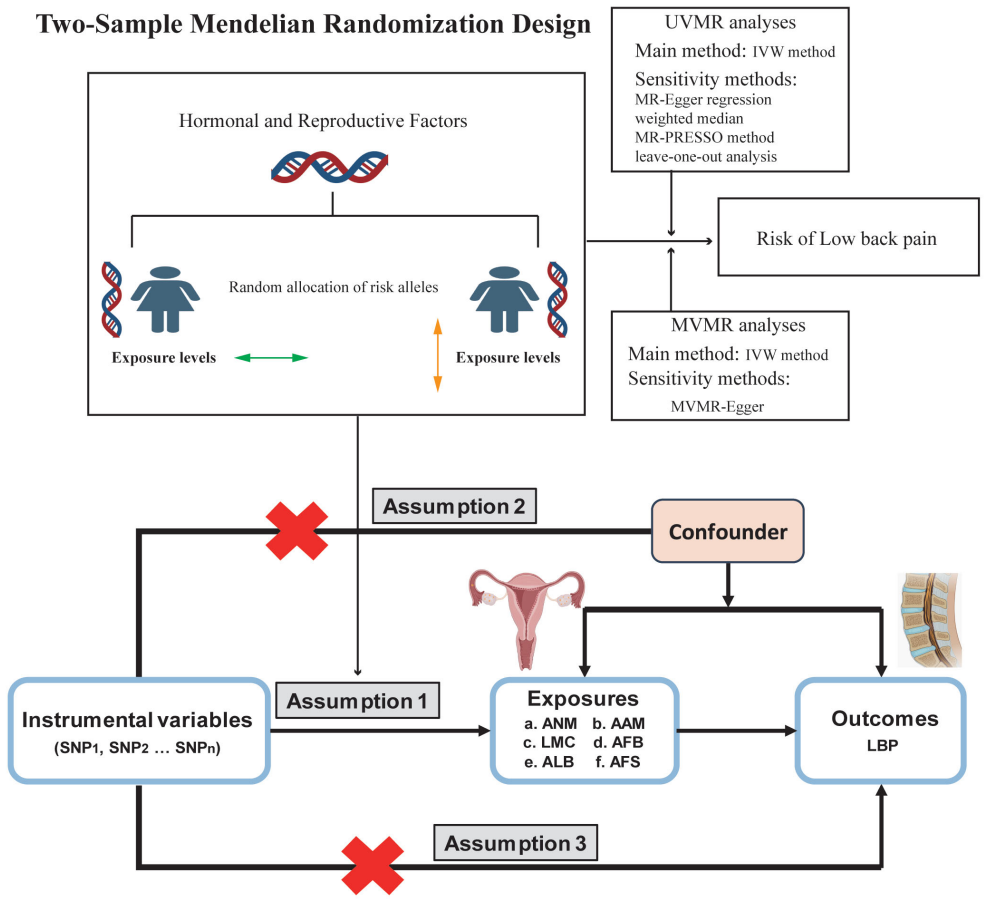

FIGURE 1
Scheme diagram of Mendelian randomization design.

comprises 177,860 participants of European ancestry (13,178 cases and 164,682 controls). Summary information for all datasets were presented in (Table 1) . All participants were of European origin, and informed consent was obtained from each. Since our data were derived from publicly accessible GWAS summary statistics, no ethical approval was necessary.

Selection of instrumental variables

Firstly, we carefully selected SNPs that demonstrated a strong association with exposure ($P < 5 \times 10^{-8}$) and excluded SNPs with F-values < 10, ensuring significance and mitigating weak instrumental variable bias (27). Secondly, we utilized specific parameters ($r^2 <$ 0.001, kb = 10,000 kb) to eliminate strong linkage disequilibrium, thus guaranteeing instrumental variable independence (28). Thirdly, we excluded SNPs associated with confounders and results using Phenoscanner V2. Additionally, palindromic SNPs with moderate allele frequencies were subsequently removed. Ultimately, we assessed the instrument strength through the F parameter, calculated using the formula $F = R^2 \times (n - 2)/(1 - R^2)$, where R^2 represents the proportion of variance in instruments. The formula for R^2 is given by $R^2 = 2 \times$ effect allele frequency $\times$ (1 - effect allele frequency) $\times$ (Beta/SD^2, with SD equaling 1), and n denotes the sample size. An F statistic exceeding 10 indicated a diminished likelihood of weak instrument bias.

Statistical analysis

In MR and MVMR analyses, the primary method employed was inverse variance weighting (IVW), complemented by MR-Egger, weighted median, simple mode, and weighted mode (29). In the absence of weak IVs, the primary outcome was determined using the IVW method, with the alternative methods considered as secondary outcomes. We employed MVMR as a statistical approach to incorporate SNP-phenotype associations into the analysis, facilitating the estimation of each phenotype's direct impact on the outcome. As indicated by previous studies (26), in MVMR, we adjusted for body mass index (BMI) to clarify the causal impact of hormonal and reproductive factors on LBP.

Heterogeneity and sensitivity test

Cochrane's Q-test was utilized to detect heterogeneity, while funnel plots indicated heterogeneity through symmetry (30). The MR-Egger intercept test and the MR polytomous residuals and outliers (MR-PRESSO) global test were employed to assess

10.3389/fendo.2024.1326761

TABLE 1 Summary of GWAS data for instrumental variables.

Analysis	Variable	ID	Sample size	Number of SNPs	Consortium	Population	Sex	Year
original analysis + validation analysis	ANM	ukb-b-17422	143,819	9,851,867	MRC-IEU	European	Males and Females	2018
	AAM	ukb-b-3768	243,944	9,851,867	MRC-IEU	European	Males and Females	2018
	LMC	ukb-a-351	30,245	10,894,596	Neale Lab	European	Males and Females	2017
	AFB	ukb-b-12405	170,498	9,851,867	MRC-IEU	European	Males and Females	2018
	ALB	ukb-b-8727	170,248	9,851,867	MRC-IEU	European	Males and Females	2018
	AFS	ukb-b-6591	406,457	9,851,867	MRC-IEU	European	Males and Females	2018
	BMI	ieu-b-40	681,275	2,336,260	GIANT	European	Males and Females	2018
original analysis	LBP	finn-b-M13_LOWBACKPAIN	13,178	16,380,287	NA	European	Males and Females	2021
validation analysis	LBP	ukb-d-M13_LOWBACKPAIN	361,194	12,184,069	NA	European	Males and Females	2018

ANM, age at menopause; AAM, age at menarche; LMC, length of menstrual cycle; AFB, age at first birth; ALB, Age at last live birth; AFS, Age first had sexual intercourse; BMI, Body mass index; LBP, low back pain.

pleiotropy (31). If significant pleiotropy was identified through the MR-PRESSO method, we will mitigate this concern by addressing outlier variability and subsequently reiterating the MR analysis. Lastly, the leave-one-out test was conducted to evaluate the sensitivity of the results. We utilized the TwoSample MR, MVMR, and MR-PRESSO packages in R software (version 4.3.1). Statistically significant associations were defined by results with a p-value < 0.05.

Results

Instrumental variables selection

After conducting a comprehensive quality assessment, we incorporated SNPs as reliable IVs for ANM, AAM, LMC, AFB, AFS, ALB and BMI. Detailed information regarding these IVs were provided in Supplementary Tables S1-S9. Notably, all the selected SNPs utilized as IVs possess F values exceeding 10, indicating their effectiveness as IVs.

MR analysis of each feature related to hormonal and reproductive factors on LBP

After implementing the Bonferroni correction, the results from MR indicated a noteworthy association between a decreased risk of LBP and AAM (OR=0.784, 95% CI: 0.689-0.891; p=3.53E-04), AFB (OR=0.558, 95% CI: 0.436-0.715; p=8.97E-06), ALB (OR=0.396, 95% CI: 0.226-0.692; p=0.002), and AFS (OR=0.602, 95% CI: 0.518-0.700; p=3.47E-10). Nevertheless, no significant association was observed between ANM (OR=0.988, 95% CI: 0.908-0.1.075; p=0.781) and LMC (OR=0.828, 95% CI: 0.687-0.999; p=0.056) with LBP. The causal association between genetically predicted reproductive and hormonal factors and the risk of LBP were presented in Figure 2. Scatter plots and funnel plots illustrating the association between reproductive and hormonal factors and LBP were presented in Supplementary Figures S1 and S2. Heterogeneity and pleiotropy are depicted in Table 2. The leave-one-out plot reinforces the robustness of our results, indicating that the influence of any individual SNP is unlikely to affect the causal estimate (Supplementary Figure S3).

In MVMR analysis adjusting for BMI, AFB (OR=0.522, 95% CI: 0.313-0.869; p=0.012) exhibited a significant association with LBP. The MR-Lasso test results remained unaffected by the removal of heterogeneous SNPs. Nevertheless, associations between AAM, ALB, and AFS with LBP did not persist after further adjustment for BMI. Detailed MVMR results are presented in Figure 3.

MR analysis of LBP on each feature related to hormonal and reproductive factors

In the reverse MR analysis, there is a causal negative relationship between LBP and AFB (OR=0.960, 95% CI: 0.931-0.989; p=0.030), as well as ALB (OR=0.968, 95% CI: 0.945-0.992; p=0.030). And no causal relationship was found between LBP and ANM (OR=1.003, 95% CI: 0.975-1.031; p=0.842), AAM (OR=0.984, 95% CI: 0.962-1.006; p=0.213), LMC (OR=1.036, 95% CI: 0.983-0.962; p=0.213) and AFS (OR=0.984, 95% CI: 0.964-1.005; p=0.213) (Figure 4). Information on pleiotropy and heterogeneity is referred to in Table 3. In addition, funnel plots, scatter plots and leave-one-out plots are shown in the Supplementary Figures S4-S6.

10.3389/fendo.2024.1326761

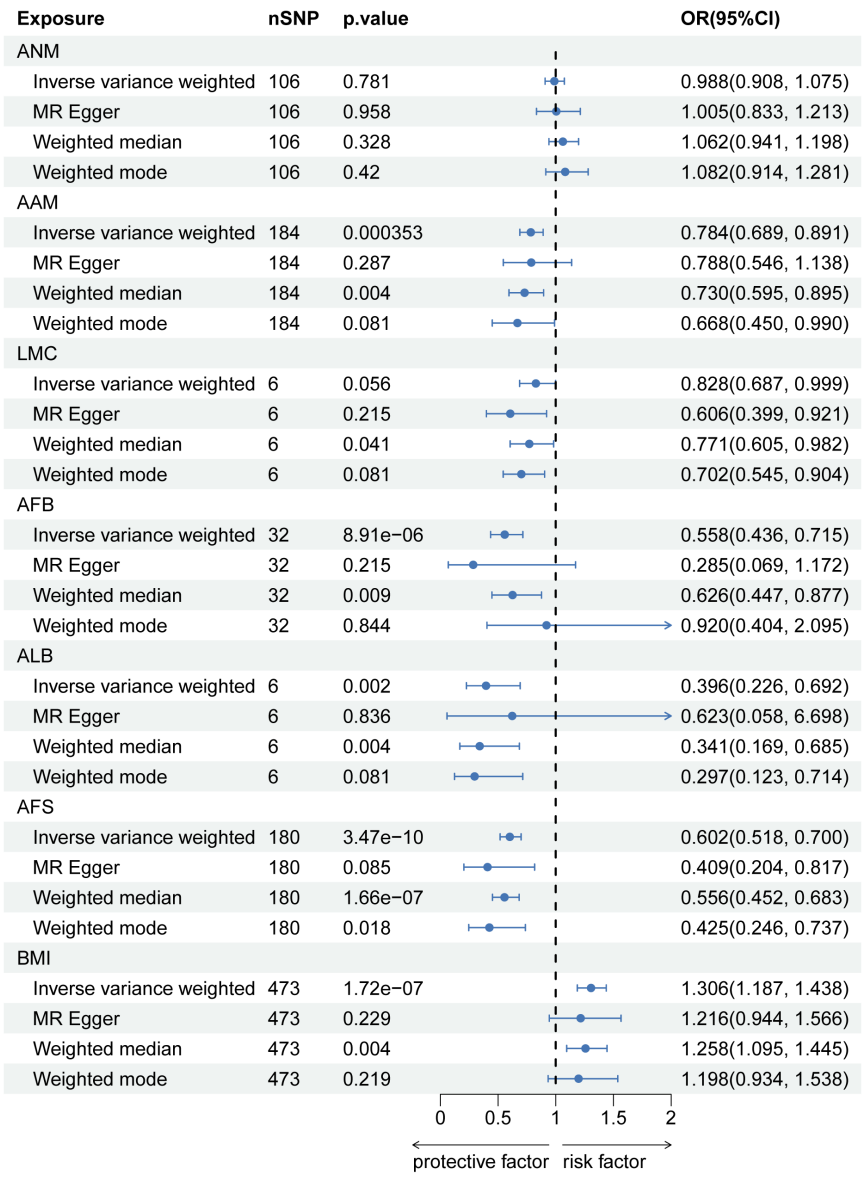

FIGURE 2
The causal relationship of genetically predicted Hormonal and Reproductive Factors and LBP.

TABLE 2 Sensitivity analysis of hormonal and reproductive factors causally linked to LBP.

Exposure	Outcome	Pleiotropy		Heterogeneity	
		Horizontal pleiotropy (Egger intercept)	Horizontal pleiotropy (*p*-value)	Heterogeneity (*Q*)	Heterogeneity (*p*-value)
ANM	LBP	-0.001	0.843	126.846	0.072
AAM		-1.13E-04	0.975	213.279	0.062
LMC		0.022	0.177	4.209	0.520
AFB		0.016	0.351	36.219	0.238
ALB		-0.011	0.719	3.011	0.698
AFS		0.007	0.262	215.809	0.031

ANM, age at menopause; AAM, age at menarche; LMC, length of menstrual cycle; AFB, age at first birth; ALB, Age at last live birth; AFS, Age first had sexual intercourse; BMI, Body mass index; LBP, low back pain.

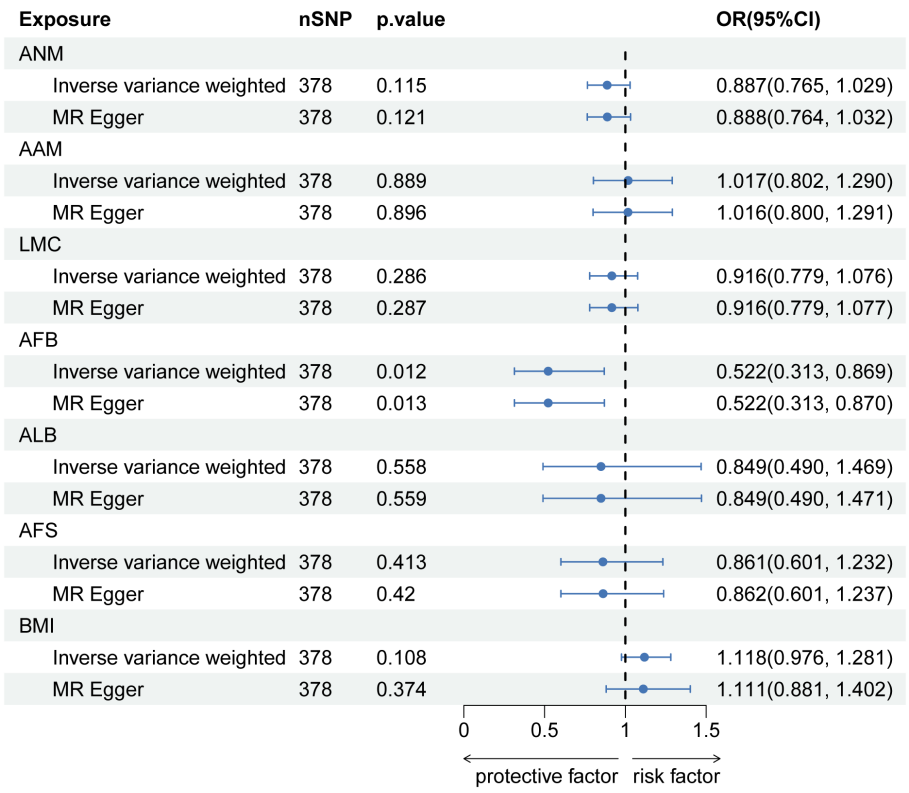

FIGURE 3
Causal estimates of Hormonal and Reproductive Factors on LBP in MVMR.

MR analysis of each feature related to hormonal and reproductive factors on LBP (validation analysis)

After implementing the Bonferroni correction, the results from MR indicated a noteworthy association between a decreased risk of LBP and AAM, AFB, ALB and AFS. Nevertheless, no significant association was observed between ANM and LMC with LBP (Figure 5). Scatter plots, funnel plots and leave-one-out plots illustrating the association between reproductive and hormonal factors and LBP were presented in Supplementary Figures S7-S9. Heterogeneity and pleiotropy are depicted in Table 4.

Discussion

Our study utilized a two-sample MR analysis to evaluate the potential causal effects of six hormonal and reproductive factors on the development of LBP. We uncovered novel insights regarding the influence of AAM, AFB, ALB and AFS on LBP. Through Bonferroni correction, we identified a negative causal relationship between these factors and the aforementioned spinal conditions. Specifically, early menarche, early age at first birth, early age at last live birth and early age first had sexual intercourse may elevate the risk of LBP. The verification results were consistent with the initial findings. After controlling for BMI, the association between AFB and LBP persisted, while the correlation between AAM, ALB, AFS and LBP did not endure. These insights underscore the importance of investigating hormonal and reproductive factors in spinal health, providing valuable directions for future research and clinical applications. We also recommend enhanced monitoring of women with these characteristics to proactively manage LBP.

Numerous observational studies have substantiated the connection between hormonal factors, reproductive factors and LBP. Nevertheless, there remains uncertainty regarding the potential influence of ANM, AAM, LMC, AFB, AFS and ALB on the development of LBP. The outcomes of the longitudinal cohort investigation aligned with our findings, affirming that an earlier AAM onset was associated with an increased likelihood of experiencing LBP (19). Other studies have also noted a positive association, with a cross-sectional study of more than 298,000 women discovering a positive link between early menarche and LBP ($p<0.001$) (32). Onset of menarche at age less than 11 years has been linked to a higher risk of experiencing LBP, as indicated by findings from both cross-sectional and cohort studies (18). However, it has also been shown that no association was found between ANM or AAM and risk of LBP (33). The existence of these contradictions could be attributed to potential bias in traditional epidemiological methods caused by confounding variables. Thus, employing MR methods could elucidate causality at the genetic level.

Many studies have shown that the prevalence of LBP in women was not significantly correlated with age, and the prevalence of LBP in the postmenopausal period was significantly different from that in the premenopausal period (34, 35). However, the Mexican study

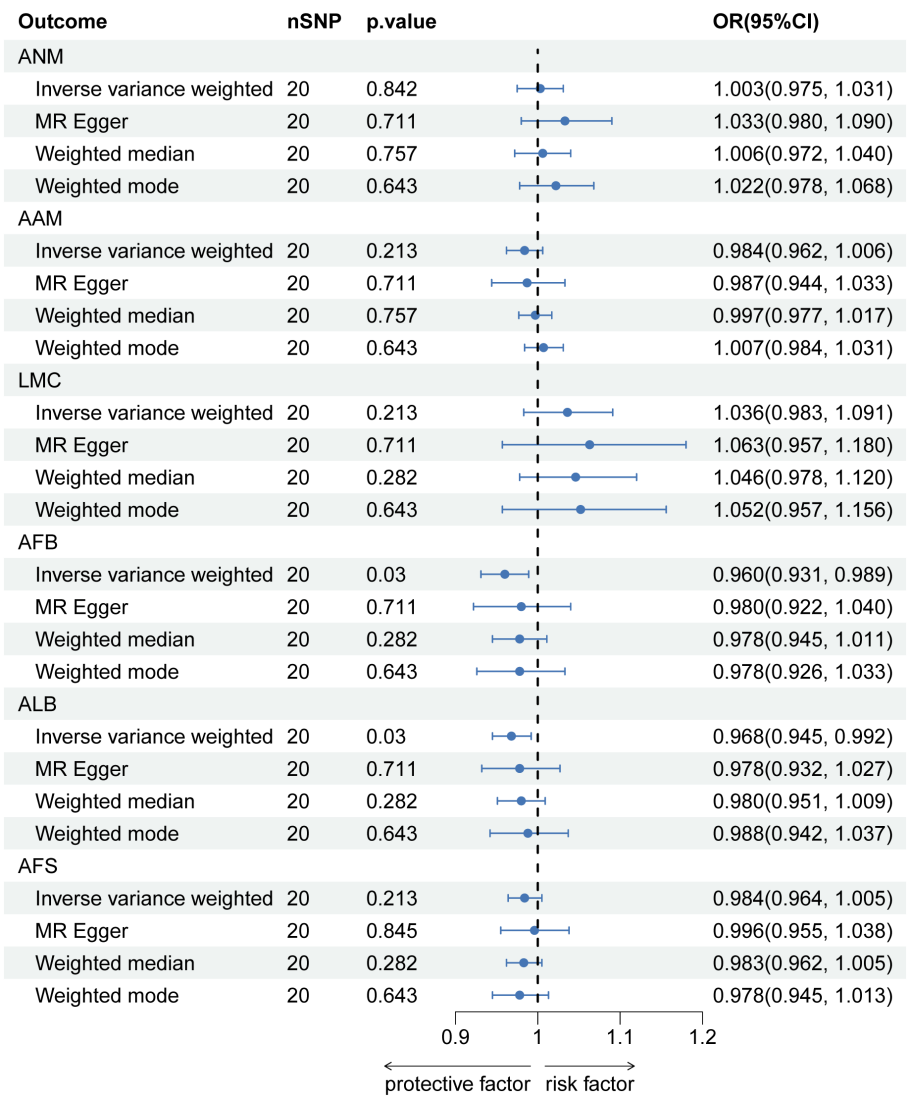

FIGURE 4
The causal relationship of genetically predicted LBP and Hormonal and Reproductive Factors.

TABLE 3 Sensitivity analysis of LBP causally linked to hormonal and reproductive factors.

Exposure	Outcome	Pleiotropy		Heterogeneity	
		Horizontal pleiotropy (Egger intercept)	Horizontal pleiotropy (*p*-value)	Heterogeneity (*Q*)	Heterogeneity (*p*-value)
LBP	ANM	-0.004	0.217	28.511	0.074
	AAM	-4.38E-04	0.855	59.342	4.92E-06
	LMC	-0.003	0.582	25.735	0.138
	AFB	-0.002	0.454	41.314	0.002
	ALB	-0.001	0.622	25.842	0.135
	AFS	-0.001	0.534	40.063	0.001

ANM, age at menopause; AAM, age at menarche; LMC, length of menstrual cycle; AFB, age at first birth; ALB, Age at last live birth; AFS, Age first had sexual intercourse; BMI, Body mass index; LBP, low back pain.

10.3389/fendo.2024.1326761

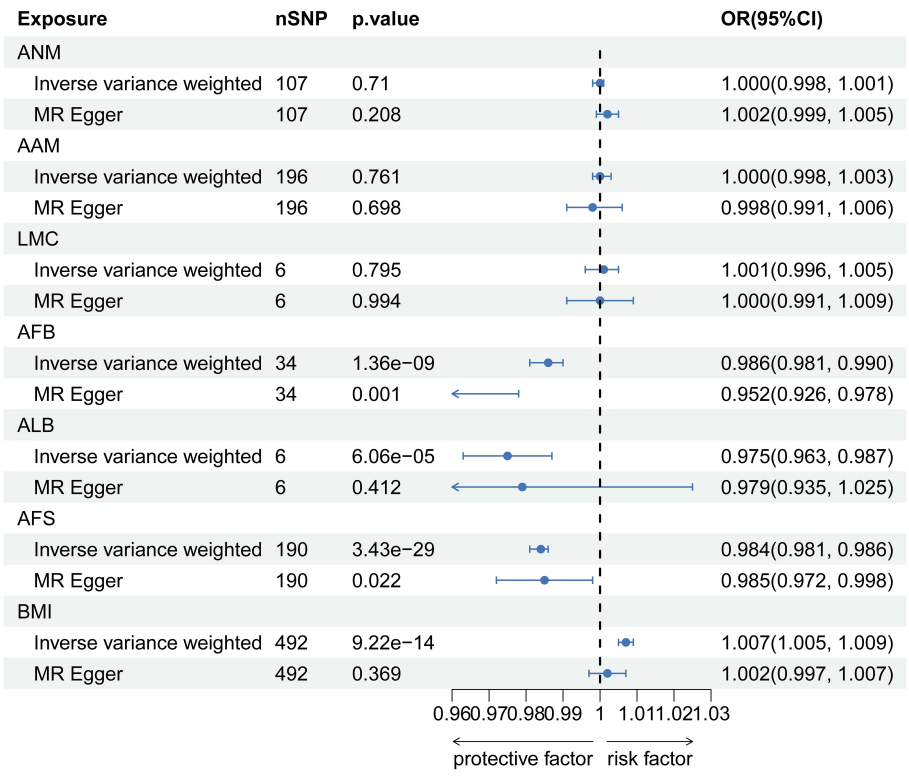

FIGURE 5
The causal relationship of genetically predicted Hormonal and Reproductive Factors and LBP (replication analysis).

revealed that women with back pain were more likely to be older (36). Adera et al. conducted a population-based cross-sectional study that elucidates a noteworthy correlation between premature menopause and an escalated susceptibility to LBP (37). Our findings at the genetic level provide evidence that ANM was not causally associated with LBP, corroborating prior studies. Instead, the occurrence of LBP and IVDD in menopausal women might be related to a rapid decrease in androgen levels. Scholarly investigations have predominantly utilized menarche as a parameter in delineating pubertal onset. However, pubertal development was a complex process that entails a spectrum of changes across various bodily systems (38). Furthermore, researchers concur that the commencement of menarche may not be the optimal indicator, as a substantial portion of growth and the emergence of secondary sexual characteristics precede its occurrence (39, 40). Prolonged and heightened exposure to estrogen over an extended period was postulated as an additional contributory factor to the increased susceptibility to LBP among women displaying early onset of menarche (18, 41).

A cross-sectional study showed that younger maternal age at the time of first birth (especially <20 years) was associated with chronic LBP, which was similar to our results (21). Meanwhile, in a prospective study, a statistically significant distinction was noted in the prevalence of LBP during pregnancy between younger and older women (42). Meanwhile, Heuch et al. have reported an association

TABLE 4 Sensitivity analysis of hormonal and reproductive factors causally linked to LBP (validation analysis).

Exposure	Outcome	Pleiotropy		Heterogeneity	
		Horizontal pleiotropy (Egger intercept)	Horizontal pleiotropy (*p*-value)	Heterogeneity (*Q*)	Heterogeneity (*p*-value)
ANM	LBP	-1.18E-04	0.097	112.910	0.305
AAM		4.10E-05	0.594	256.622	0.002
LMC		3.97E-05	0.899	3.281	0.657
AFB		0.001	0.015	26.194	0.794
ALB		-9.84E-05	0.873	6.580	0.254
AFS		-1.79E-05	0.873	201.169	0.259

ANM, age at menopause; AAM, age at menarche; LMC, length of menstrual cycle; AFB, age at first birth; ALB, Age at last live birth; AFS, Age first had sexual intercourse; BMI, Body mass index; LBP, low back pain.

between the incidence of lumbar discomfort and advancing age, as well as the cumulative instances of pregnancies (43). Our investigation revealed an observation wherein a heightened susceptibility to dorsal discomfort was discerned among youthful females. The MR method employed mitigates biases arising from various factors, including confounding, through genetic allelic assignment principles. This method corroborates, at the genetic level, the notion that an early AFB constitutes a risk factor for LBP. This phenomenon could stem from elevated hormone levels that impact the soft tissues supporting the spine, potentially leading to enduring laxity in joints and ligaments (43–46). This correlation aligns with an elevated risk of LBP observed in women undergoing hormone replacement therapy or using oral contraceptives (17, 20). Additionally, younger women demonstrate heightened sensitivity to hormonal variations in estrogen and relaxin, leading to more pronounced collagen relaxation (47, 48). This sensitivity may elucidate the increased risk of LBP among women giving birth at a younger age. Moreover, compression of the uterus on the developing spine during the first childbirth in younger girls may contribute to the onset of low back pain (43).

The prospective study by Brynhildsen et al. found that hormonal fluctuations during the menstrual cycle do not influence LBP (21). In contrast, Wijnhoven et al. identified a link between chronic LBP and irregular or prolonged menstrual cycles (20). Our study aligns with Brynhildsen et al.'s conclusion that shorter menstrual cycles are not associated with an increased risk of lower back pain LBP. This suggests that the menstrual cycle length is not a risk factor for LBP.

Several studies have documented the increasing severity of IVDD in women as they age (49–51), with a notably more rapid degeneration observed in females after the age of 60 compared to males (52). Epidemiological evidence supports the notion that disc degeneration correlates with age (53). This phenomenon was similarly observed by De Schepper et al. (54). The role of estrogen in IVD metabolism and its expression in annulus fibrosus and nucleus pulposus cells may explain these observations (55). IVD is the primary cause of LBP, with hormone levels playing a crucial role. Further investigation is needed to understand the specific mechanism of action.

Our study possesses several strengths. It marks the inaugural application of MR to investigate the causal relationship between hormonal and reproductive factors and LBP. Encompassing six distinct reproductive characteristics, our study offers a comprehensive understanding of the reproductive period. Utilizing data from a diverse range of cohorts enhances the reliability of our findings and minimizes overlap. Employing the principle of random allele assignment, we conducted a Bidirectional MR study to validate the robustness of these results. Furthermore, we corroborated the reliability of our conclusions through MVMR, with adjustments made for BMI.

However, the exclusive reliance on European GWAS data may limit the generalizability of our findings to other ethnic or geographic populations. Besides, the inclusion of both genders in the outcome data might also weaken the observed associations. The inclusion of both genders in the dataset introduced gender heterogeneity and potential bias. Ideally, the association between SNPs and outcome estimates should display gender heterogeneity. However, in the LBP GWAS database we used, with women comprising over 60%, it represents a predominantly female-led GWAS, thereby minimizing the likelihood of bias. Future MR studies should consider validating these results within female-only samples by appropriate stratification.

Conclusions

In conclusion, our study explored the causal relationship between ANM, AAM, LMC, AFB, AFS, ALB and the prevalence of LBP. We found that early menarche, early age at first birth, early age at last live birth and early age first had sexual intercourse may decrease the risk of LBP. These insights enhance our understanding of LBP risk factors, offering valuable guidance for screening, prevention, and treatment strategies for at-risk women.

Data availability statement

The original contributions presented in the study are included in the article/Supplementary Material. Further inquiries can be directed to the corresponding authors.

Ethics statement

Ethical approval was unnecessary due to the public nature of the GWAS data.

Author contributions

DC: Conceptualization, Funding acquisition, Investigation, Supervision, Visualization, Writing – original draft, Writing – review & editing. JZ: Conceptualization, Investigation, Methodology, Visualization, Writing – original draft, Writing – review & editing. JHL: Visualization, Writing – review & editing, Data curation. CL: Data curation, Visualization, Writing – review & editing. ZGZ: Formal analysis, Writing – review & editing. XR: Software, Writing – review & editing. JW: Formal analysis, Writing – review & editing. JFL: Formal analysis, Writing – review & editing. HC: Investigation, Writing – review & editing. FW: Investigation, Writing – review & editing. XL: Investigation, Writing – review & editing. MG: Methodology, Writing – review & editing. ZYZ: Conceptualization, Supervision, Writing – review & editing. YX: Conceptualization, Supervision, Writing – review & editing. SL: Conceptualization, Investigation, Supervision, Writing – original draft, Writing – review & editing.

Funding

The author(s) declare financial support was received for the research, authorship, and/or publication of this article. This work was financially supported by the National Natural Science Foundation of China (U22A20162, 31900583, 32071351, 81772400, 82102604, 81960395); Taishan Scholar Project of Shandong Province, China (No. ts20190985); Foundation of

Shenzhen Committee for Science and Technology Innovation (JCYJ20190809142211354), Sanming Project of Medicine in Shenzhen (SZSM201911002); Beijing Municipal Health Commission (BMHC-2021-6, BJRITO-RDP-2023); AO CMF CPP on Bone Regeneration (AOCMF-21-04S, supported by AO Foundation, AO CMF. AO CMF is a clinical division of the AO Foundation -an independent medically guided not-for-profit organization).

Acknowledgments

We express our gratitude for the utilization of the Genome-wide Association Study databases and FinnGen Consortium databases.

Conflict of interest

The authors declare that the research was conducted in the absence of any commercial or financial relationships that could be construed as a potential conflict of interest.

Publisher's note

Supplementary material

The Supplementary Material for this article can be found online at: https://www.frontiersin.org/articles/10.3389/fendo.2024.1326761/full#supplementary-material

SUPPLEMENTARY FIGURE S1
Scatter plot for LBP.

SUPPLEMENTARY FIGURE S2
Funnel plots for LBP.

SUPPLEMENTARY FIGURE S3
MR leave-one-out sensitivity analysis.

SUPPLEMENTARY FIGURE S4
Funnel plots for Hormonal and Reproductive Factors.

SUPPLEMENTARY FIGURE S5
reversed MR leave-one-out sensitivity analysis.

SUPPLEMENTARY FIGURE S6
Scatter plot for Hormonal and Reproductive Factors.

SUPPLEMENTARY FIGURE S7
Scatter plot for LBP (replication analysis).

SUPPLEMENTARY FIGURE S8
Funnel plots for LBP (replication analysis).

SUPPLEMENTARY FIGURE S9
MR leave-one-out sensitivity analysis (replication analysis).

SUPPLEMENTARY TABLE S1
SNPs of ANM for LBP in MR.

SUPPLEMENTARY TABLE S2
SNPs of AAM for LBP in MR.

SUPPLEMENTARY TABLE S3
SNPs of LMC for LBP in MR.

SUPPLEMENTARY TABLE S4
SNPs of AFB for LBP in MR.

SUPPLEMENTARY TABLE S5
SNPs of ALB for LBP in MR.

SUPPLEMENTARY TABLE S6
SNPs of AFS for LBP in MR.

SUPPLEMENTARY TABLE S7
SNPs of BMI for LBP in MR.

SUPPLEMENTARY TABLE S8
The SNPs selected for BMI factors in MVMR analysis.

SUPPLEMENTARY TABLE S9
SNPs of LBP for Hormonal and Reproductive Factors in MR.

References

1. Chen S, Chen M, Wu X, Lin S, Tao C, Cao H, et al. Xiao G: Global, regional and national burden of low back pain 1990-2019: A systematic analysis of the Global Burden of Disease study 2019. *J Orthopaedic Transl.* (2022) 32:49–58. doi: 10.1016/j.jot.2021.07.005

2. Urits I, Burshtein A, Sharma M, Testa L, Gold PA, Orhurhu V, et al. Low back pain, a comprehensive review: pathophysiology, diagnosis, and treatment. *Curr Pain Headache Rep.* (2019) 23:23. doi: 10.1007/s11916-019-0757-1

3. Adams MA, Roughley PJ. What is intervertebral disc degeneration, and what causes it? *Spine.* (2006) 31:2151–61. doi: 10.1097/01.brs.0000231761.73859.2c

4. Togo K, Ebata N, Yonemoto N, Abraham L. Safety risk associated with use of nonsteroidal anti-inflammatory drugs in Japanese elderly compared with younger patients with osteoarthritis and/or chronic low back pain: A retrospective database study. *Pain Pract: Off J World Institute Pain.* (2022) 22:200–9. doi: 10.1111/papr.13079

5. Leveille SG, Bean J, Ngo L, McMullen W, Guralnik JM. The pathway from musculoskeletal pain to mobility difficulty in older disabled women. *Pain.* (2007) 128:69–77. doi: 10.1016/j.pain.2006.08.031

6. Leveille SG, Ling S, Hochberg MC, Resnick HE, Bandeen-Roche KJ, Won A, et al. Widespread musculoskeletal pain and the progression of disability in older disabled women. *Ann Internal Med.* (2001) 135:1038–46. doi: 10.7326/0003-4819-135-12-200112180-00007

7. Eggermont LH, Leveille SG, Shi L, Kiely DK, Shmerling RH, Jones RN, et al. Pain characteristics associated with the onset of disability in older adults: the maintenance of balance, independent living, intellect, and zest in the Elderly Boston Study. *J Am Geriatr Soc.* (2014) 62:1007–16. doi: 10.1111/jgs.12848

8. Bailey A. Risk factors for low back pain in women: still more questions to be answered. *Menopause (New York NY).* (2009) 16:3–4. doi: 10.1097/gme.0b013e31818e10a7

9. Mohseni-Bandpei MA, Fakhri M, Ahmad-Shirvani M, Bagheri-Nessami M, Khalilian AR, Shayesteh-Azar M, et al. Low back pain in 1,100 Iranian pregnant women: prevalence and risk factors. *Spine J: Off J North Am Spine Soc.* (2009) 9:795–801. doi: 10.1016/j.spinee.2009.05.012

10. Bryndal A, Majchrzycki M, Grochulska A, Glowinski S, Seremak-Mrozikiewicz A. Risk factors associated with low back pain among A group of 1510 pregnant women. *J Pers Med.* (2020) 10(2):50. doi: 10.3390/jpm10020051

11. Bryndal A, Glowinski S, Majchrzycki M. Influence of pregnancy on the occurrence of lumbar spine pain in polish women: A retrospective study. *J Pers Med*. (2022) 12(3):357. doi: 10.3390/jpm12030357

12. Wáng YX, Wáng JQ, Káplár Z. Increased low back pain prevalence in females than in males after menopause age: evidences based on synthetic literature review. *Quant Imaging Med Surg*. (2016) 6:199–206. doi: 10.21037/qims

13. Baron YM, Brincat MP, Galea R, Calleja N. Intervertebral disc height in treated and untreated overweight post-menopausal women. *Hum Reprod (Oxford England)*. (2005) 20:3566–70. doi: 10.1093/humrep/dei251

14. Muscat Baron Y, Brincat MP, Galea R, Calleja N. Low intervertebral disc height in postmenopausal women with osteoporotic vertebral fractures compared to hormone-treated and untreated postmenopausal women and premenopausal women without fractures. *Climacteric: J Int Menopause Soc*. (2007) 10:314–9. doi: 10.1080/13697130701460640

15. Musgrave DS, Vogt MT, Nevitt MC, Cauley JA. Back problems among postmenopausal women taking estrogen replacement therapy: the study of osteoporotic fractures. *Spine*. (2001) 26:1606–12. doi: 10.1097/00007632-200107150-00023

16. Symmons DP, van Hemert AM, Vandenbroucke JP, Valkenburg HA. A longitudinal study of back pain and radiological changes in the lumbar spines of middle aged women. I. Clinical findings. *Ann Rheum Dis*. (1991) 50:158–61. doi: 10.1136/ard.50.3.158

17. Heuch I, Heuch I, Hagen K, Storheim K, Zwart JA. Menopausal hormone therapy, oral contraceptives and risk of chronic low back pain: the HUNT Study. *BMC Musculoskelet Disord*. (2023) 24:84. doi: 10.1186/s12891-023-06184-5

18. Heuch I, Heuch I, Hagen K, Storheim K, Zwart JA. Does the risk of chronic low back pain depend on age at menarche or menopause? A population-based cross-sectional and cohort study: the Trøndelag Health Study. *BMJ Open*. (2022) 12:e055118. doi: 10.1136/bmjopen-2021-055118

19. Innes S, Jacques A, Scott K, Walker B. Early age at menarche is associated with post-menarche back pain: An analysis of the Raine Study. *Eur J Pain (London England)*. (2021) 25:2155–65. doi: 10.1002/ejp.1828

20. Wijnhoven HA, de Vet HC, Smit HA, Picavet HS. Hormonal and reproductive factors are associated with chronic low back pain and chronic upper extremity pain in women–the MORGEN study. *Spine*. (2006) 31:1496–502. doi: 10.1097/01.brs.0000220706.96724.76

21. Brynhildsen JO, Hammar J, Hammar ML. Does the menstrual cycle and use of oral contraceptives influence the risk of low back pain? A prospective study among female soccer players. *Scand J Med Sci Sports*. (1997) 7:348–53. doi: 10.1111/j.1600-0838.1997.tb00165.x

22. Burgess S, Foley CN, Zuber V. Inferring causal relationships between risk factors and outcomes from genome-wide association study data. *Annu Rev Genomics Hum Genet*. (2018) 19:303–27. doi: 10.1146/annurev-genom-083117-021731

23. Smith GD, Ebrahim S. Mendelian randomization: prospects, potentials, and limitations. *Int J Epidemiol*. (2004) 33:30–42. doi: 10.1093/ije/dyh132

24. Burgess S, Davey Smith G, Davies NM, Dudbridge F, Gill D, Glymour MM, et al. Guidelines for performing Mendelian randomization investigations. *Wellcome Open Res*. (2019) 4:186. doi: 10.12688/wellcomeopenres

25. Davies NM, Holmes MV, Davey Smith G. Reading Mendelian randomisation studies: a guide, glossary, and checklist for clinicians. *BMJ (Clinical Res ed)*. (2018) 362:k601. doi: 10.1136/bmj.k601

26. Zhou J, Mi J, Peng Y, Han H, Liu Z. Causal associations of obesity with the intervertebral degeneration, low back pain, and sciatica: A two-sample mendelian randomization study. *Front Endocrinol*. (2021) 12:740200. doi: 10.3389/fendo.2021.740200

27. Burgess S, Thompson SG. Avoiding bias from weak instruments in Mendelian randomization studies. *Int J Epidemiol*. (2011) 40:755–64. doi: 10.1093/ije/dyr036

28. Hemani G, Zheng J, Elsworth B, Wade KH, Haberland V, Baird D, et al. The MR-Base platform supports systematic causal inference across the human phenome. *eLife*. (2018) 7:e34408. doi: 10.7554/eLife.34408

29. Hu J, Lu J, Lu Q, Weng W, Guan Z, Wang Z. Mendelian randomization and colocalization analyses reveal an association between short sleep duration or morning chronotype and altered leukocyte telomere length. *Commun Biol*. (2023) 6:1014. doi: 10.1038/s42003-023-05397-7

30. Greco MF, Minelli C, Sheehan NA, Thompson JR. Detecting pleiotropy in Mendelian randomisation studies with summary data and a continuous outcome. *Stat Med*. (2015) 34:2926–40. doi: 10.1002/sim.6522

31. Verbanck M, Chen CY, Neale B, Do R. Detection of widespread horizontal pleiotropy in causal relationships inferred from Mendelian randomization between complex traits and diseases. *Nat Genet*. (2018) 50:693–8. doi: 10.1038/s41588-018-0099-7

32. Lian Q, Li R, Elgar FJ, Su Q. Early physical maturation and subjective health complaints in adolescent girls: a pooled cross-sectional analysis. *J Epidemiol Community Health*. (2023) 77:108–14. doi: 10.1136/jech-2022-219547

33. Bergenudd H, Nilsson B, Udén A, Willner S. Bone mineral content, gender, body posture, and build in relation to back pain in middle age. *Spine*. (1989) 14:577–9. doi: 10.1097/00007632-198906000-00005

34. Tsuritani I, Honda R, Noborisaka Y, Ishida M, Ishizaki M, Yamada Y. Impact of obesity on musculoskeletal pain and difficulty of daily movements in Japanese middle-aged women. *Maturitas*. (2002) 42:23–30. doi: 10.1016/S0378-5122(02)00025-7

35. Gao HL, Lin SQ, Wei Y, Chen Y, Wu ZL. The effect of age and menopausal status on musculoskeletal symptoms in Chinese women aged 35-64 years. *Climacteric: J Int Menopause Soc*. (2013) 16:639–45. doi: 10.3109/13697137.2013.769095

36. Sievert LL, Goode-Null SK. Musculoskeletal pain among women of menopausal age in Puebla, Mexico. *J Cross-Cultural Gerontol*. (2005) 20:127–40. doi: 10.1007/s10823-005-9087-3

37. Adera T, Deyo RA , Donatelle RJ. Premature menopause and low back pain. A population-based study. *Ann Epidemiol*. (1994) 4:416–22. doi: 10.1016/1047-2797(94)90077-9

38. Moffitt TE, Caspi A, Belsky J, Silva PA. Childhood experience and the onset of menarche: a test of a sociobiological model. *Child Dev*. (1992) 63:47–58. doi: 10.1111/j.1467-8624.1992.tb03594.x

39. Rhee H. Relationships between physical symptoms and pubertal development. *J Pediatr Health Care*. (2005) 19:95–103. doi: 10.1016/j.pedhc.2004.10.004

40. Euling SY, Herman-Giddens ME, Lee PA, Selevan SG, Juul A, Sørensen TI, et al. Examination of US puberty-timing data from 1940 to 1994 for secular trends: panel findings. *Pediatrics*. (2008) 121 Suppl 3:S172–191. doi: 10.1542/peds.2007-1813D

41. Aldabe D, Ribeiro DC, Milosavljevic S, Dawn Bussey M. Pregnancy-related pelvic girdle pain and its relationship with relaxin levels during pregnancy: a systematic review. *Eur Spine J*. (2012) 21:1769–76. doi: 10.1007/s00586-012-2162-x

42. Turgut F, Turgut M, Cetinşahin M. A prospective study of persistent back pain after pregnancy. *Eur J Obstet Gynecol Reprod Biol*. (1998) 80:45–8. doi: 10.1016/S0301-2115(98)00080-3

43. Heuch I, Heuch I, Hagen K, Storheim K, Zwart JA. Associations between the number of children, age at childbirths and prevalence of chronic low back pain: the Nord-Trøndelag Health Study. *BMC Public Health*. (2020) 20:1556. doi: 10.1186/s12889-020-09480-0

44. Brynhildsen J, Hansson A, Persson A, Hammar M. Follow-up of patients with low back pain during pregnancy. *Obstet Gynecol*. (1998) 91:182–6. doi: 10.1016/S0029-7844(97)00630-3

45. Pang H, Chen S, Klyne DM, Harrich D, Ding W, Yang S, et al. Low back pain and osteoarthritis pain: a perspective of estrogen. *Bone Res*. (2023) 11:42. doi: 10.1038/s41413-023-00280-x

46. Mogren IM, Pohjanen AI. Low back pain and pelvic pain during pregnancy: prevalence and risk factors. *Spine*. (2005) 30:983–91. doi: 10.1097/01.brs.0000158957.42198.8e

47. Ostgaard HC, Andersson GB. Previous back pain and risk of developing back pain in a future pregnancy. *Spine*. (1991) 16:432–6. doi: 10.1097/00007632-199104000-00008

48. Kumle M, Weiderpass E, Alsaker E, Lund E. Use of hormonal contraceptives and occurrence of pregnancy-related pelvic pain: a prospective cohort study in Norway. *BMC Pregnancy Childbirth*. (2004) 4:11. doi: 10.1186/1471-2393-4-11

49. Lou C, Chen H, Mei L, Yu W, Zhu K, Liu F, et al. Association between menopause and lumbar disc degeneration: an MRI study of 1,566 women and 1,382 men. *Menopause (New York NY)*. (2017) 24:1136–44. doi: 10.1097/GME.0000000000000902

50. Takatalo J, Karppinen J, Niinimäki J, Taimela S, Näyhä S, Järvelin MR, et al. Prevalence of degenerative imaging findings in lumbar magnetic resonance imaging among young adults. *Spine*. (2009) 34:1716–21. doi: 10.1097/BRS.0b013e3181ac5fec

51. Teraguchi M, Hashizume H, Asai Y, Oka H, Nagata K, Ishimoto Y, et al. Association between modic changes, disc degeneration, and pelvic incidence-lumbar lordosis mismatch in a large population based cohort: the Wakayama spine study. *Eur Spine J*. (2023). doi: 10.1007/s00586-023-07702-8

52. Wang YX, Griffith JF, Ma HT, Kwok AW, Leung JC, Yeung DK, et al. Relationship between gender, bone mineral density, and disc degeneration in the lumbar spine: a study in elderly subjects using an eight-level MRI-based disc degeneration grading system. *Osteoporos Int*. (2011) 22:91–6. doi: 10.1007/s00198-010-1200-y

53. Wang YX, Griffith JF, Zeng XJ, Deng M, Kwok AW, Leung JC, et al. Prevalence and sex difference of lumbar disc space narrowing in elderly chinese men and women: osteoporotic fractures in men (Hong Kong) and osteoporotic fractures in women (Hong Kong) studies. *Arthritis Rheum*. (2013) 65:1004–10. doi: 10.1002/art.37857

54. de Schepper EI, Damen J, van Meurs JB, Ginai AZ, Popham M, Hofman A, et al. The association between lumbar disc degeneration and low back pain: the influence of age, gender, and individual radiographic features. *Spine*. (2010) 35:531–6. doi: 10.1097/BRS.0b013e3181aa5b33

55. Song XX, Yu YJ, Li XF, Liu ZD, Yu BW, Guo Z. Estrogen receptor expression in lumbar intervertebral disc of the elderly: gender- and degeneration degree-related variations. *Joint Bone Spine*. (2014) 81:250–3. doi: 10.1016/j.jbspin.2013.09.002

frontiers | Frontiers in Endocrinology

TYPE Original Research
PUBLISHED 21 May 2024
DOI 10.3389/fendo.2024.1363889

OPEN ACCESS

EDITED BY
Katherine A. Staines,
University of Brighton, United Kingdom

REVIEWED BY
Hiroya Ohta,
Hokkaido University of Science, Japan
Orazio Valerio Giannico,
Local Health Authority of Taranto, Italy

*CORRESPONDENCE
Zhiwen Zhang
zzwjjdd@163.com

†These authors have contributed equally to this work

RECEIVED 31 December 2023
ACCEPTED 01 May 2024
PUBLISHED 21 May 2024

CITATION
He Q, Chen B, Liang F and Zhang Z (2024) Association between the atherogenic index of plasma and bone mineral density among adult women: NHANES (2011–2018). *Front. Endocrinol.* 15:1363889. doi: 10.3389/fendo.2024.1363889

Association between the atherogenic index of plasma and bone mineral density among adult women: NHANES (2011–2018)

Qiwang He[1,2†], Bo Chen[3,4†], Fuchao Liang[5] and Zhiwen Zhang[2*]

[1]College of Acupuncture and Orthopedics, Hubei University of Chinese Medicine, Wuhan, China, [2]Department of Orthopedics, Hubei University Affiliated Hospital of Hubei University of Chinese Medicine, Wuhan, China, [3]Department of Endocrinology, Xiangyang Central Hospital, Affiliated Hospital of Hubei University of Arts and Science, Xiangyang, China, [4]Center for Clinical Evidence-Based and Translational Medicine, Xiangyang Central Hospital, Affiliated Hospital of Hubei University of Arts and Science, Xiangyang, China, [5]Department of Urology, Xiangyang Central Hospital, Affiliated Hospital of Hubei University of Arts and Science, Xiangyang, China

Background: Studies on the relationship between the atherogenic index of plasma (AIP) and bone mineral density (BMD) among adult women in the United States are limited. The purpose of this study was to explore this association using a sizable, nationally representative sample.

Methods: Data from the 2011 to 2018 National Health and Nutrition Examination Survey (NHANES) were used in this observational study. The AIP was computed as $\log_{10}$ (triglycerides/high-density lipoprotein cholesterol). Total BMD was measured via dual-energy X-ray densitometry. We constructed multiple linear regression models to evaluate the correlation between the AIP and BMD. The non-linear relationship was characterized by smooth curve fitting and generalized additive models. We also conducted subgroup and interaction analyses.

Results: In this study, we included 2,362 adult women with a mean age of 38.13 ± 12.42 years. The results of multiple linear regression analysis, the AIP and total BMD showed a negative association (β = −0.021, 95%CI: −0.037, −0.006). The curve fitting analysis and threshold effect analysis showed a non-linear relationship between the two variables, and the inflection point of the AIP was found to be -0.61. The total BMD decreased significantly when the AIP reached this value (β = −0.03, 95%CI: −0.04, −0.01). The results of the subgroup analysis showed that AIP and total BMD had a strong negative relationship in participants who were below 45 years old (β = -0.023; 95% CI: -0.041, -0.004), overweight (BMI ≥ 25 kg/m^2) (β = -0.022; 95% CI: -0.041, -0.002), had a higher education level (β = -0.025; 95% CI: -0.044, -0.006), and had no partners (β = -0.014; 95% CI: -0.06, -0.009).

Conclusions: We found a negative correlation between the AIP and total BMD. Clinicians should pay attention to patients with high AIP, which might indicate a low BMD and has reference significance in preventing osteoporosis.

KEYWORDS

atherogenic index of plasma, bone mineral density, NHANES, cross-sectional study, women

Introduction

As the global aging problem becomes more and more serious, osteoporosis (OP), the most prevalent metabolic bone disease, has become one of the major public health problems (1, 2). An estimated 1.5 million fractures are caused by OP each year in the United States (3, 4). The economic burden of treating osteoporotic fractures is expected to reach nearly $50 billion by 2040, putting tremendous strain on American society (5, 6). Currently, the gold standard for diagnosing OP is to assess a patient's bone mineral density (BMD) (7, 8). Therefore, it is important to identify modifiable risk factors associated with low BMD for the prevention of OP (9, 10).

Dobiásová and Frohlich introduced the atherogenic index of plasma (AIP) in 2001 as a novel lipid marker, indicating the nature and extent of aberrant lipid metabolism (11, 12). It is computed as the ratio of triglycerides (TG) with a logarithmic base of 10 to high-density lipoprotein cholesterol (HDL-C). TG, the most abundant lipid in human adipose tissue; HDL-C, contains hundreds of lipids and proteins, and a number of clinical studies have shown an association between TG and HDL-C and OP (13, 14). AIP, which combines TG and HDL-C levels, besides showing the ratio of TG to HDL-C, it also shows the particle size of lipoprotein, which is a more accurate indicator of the specificity and pathogenicity of dyslipidemia (15, 16). Several studies have shown that the AIP is a reliable indicator of cardiovascular events and death due to such events (17–19).

There is growing evidence that there is a biological link between lipid and bone metabolism, and that the disturbance of lipid metabolism can directly affect bone formation and absorption, thereby affecting the strength of bone (20, 21). Only a few epidemiological studies have investigated the relationship between AIP and BMD in the population, and these studies have found an inverse association (22–24). On the one hand, existing studies are limited to special postmenopausal population, and the association of the whole female population is not clear; on the other hand, the nonlinear association between AIP and BMD has not been deeply explored to find out the threshold of action, which is of great significance for clinical application. Meanwhile, here is a lack of studies on the association between AIP and BMD in adult women in the United States. It is estimated that approximately 40% of white women in the United States will experience at least one clinically significant osteoporotic fracture in their lifetime (25, 26). However, existing studies have focused on low and middle-income countries, and a multi-country cohort study found that among high-income countries, women in the United States had a higher risk of fracture than women in Australia, Canada, and Europe (27).

Therefore, in this study, we addressed these knowledge gaps by using the extensive National Health and Nutrition Examination Survey (NHANES) dataset and conducted an extensive cross-sectional investigation to assess the relationship between AIP and BMD among American adult women. We hypothesized that AIP and BMD are negatively correlated.

Materials and methods

Survey description

The multistage, cross-sectional NHANES is a nationally representative study designed to analyze the variables at risk related to health and nutrition in the American population. The NHANES started in 1999, it is performed every two years, with a new group of participants was included in each iteration of the survey. Mobile medical examination and in-home interviews are performed for the evaluation (28). The NHANES is authorized by the National Centre for Health Statistics study ethical review board, and written consent is provided by all participants (29).

Study population

Data collected for four two-year periods (2011–2012,2013–2014,2015–2016,2017–2018), in total, 39,156 people participated in the health examination survey. We used certain exclusion standards in our investigation to improve the reliability and validity of our conclusions. The exclusion criteria were as follows: (1) males, (2) younger than 18 years old, (3) missing AIP and total BMD data, (4) missing data for certain factors have missing data (SII, depression, blood pressure measured less than three times). In total, 2,362 individuals were included in the study (Figure 1).

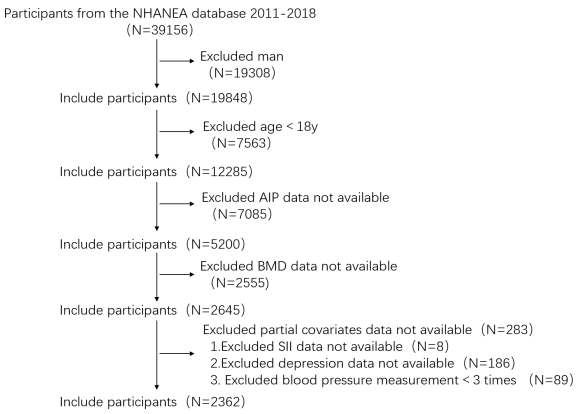

FIGURE 1
Flowchart of the sample selection process from the NHANES (2011–2018). (NHANES, National Health and Nutrition Examination Survey; AIP, atherogenic index of plasma; BMD, bone mineral density; SII, systemic immune-inflammation index).

Atherogenic index of plasma

The AIP was defined as $\log_{10}$ (triglyceride/high-density lipoprotein cholesterol) ratio (30). Based on the AIP quartiles, all individuals were divided into four groups: group Q1 (<-0.40), group Q2 (-0.40 to <-0.20), group Q3 (-0.20 to <0.03), and group Q4 (≥0.03).

Total bone mineral density

Previous studies have shown that the mean total BMD of non-Hispanic white women between the ages of 20 and 29 can be used as the reference value (31, 32). Any individual with BMD score of 2.5 standard deviations or more below the norm were considered osteoporosis, individuals with all BMD values of 1.0 standard deviations or more above the norm were considered normal BMD, and other cases were considered osteopenia. Finally, we collectively referred to subjects with osteoporosis or osteopenia as having a low BMD. Details are listed in Supplementary Table S1. Complete BMD was evaluated by DXA for all participants (included in the final analysis). The examination was performed by trained radiology technicians using Hologic QDR-4500A fan-beam densitometers (Hologic; Bedford, MA, USA). Details about the DXA exam were provided on the NHANES website (33).

Covariates

The selection of potential BMD confounders, such as age, ratio of family income to poverty (PIR), body mass index (BMI), systolic blood pressure, diastolic blood pressure, glycohemoglobin, low-density lipoprotein cholesterol (LDL-C), total cholesterol (TC), total protein intake, total calcium intake, serum 25-hydroxyvitamin D (25(OH)D), cotinine, systemic immune-inflammation index (SII), race, education level, marital status, smoking status, alcohol consumption, trouble sleeping, depressive symptoms, coronary heart disease, diabetes, kidney failure, gout and arthritis was based on previous studies.

Age (years), PIR, BMI (kg/m^2), systolic blood pressure (mmHg), diastolic blood pressure (mmHg), glycohemoglobin、LDL-C (mmol/L), TC (mmol/L), total protein intake (gm/d), total calcium intake (mg/d), serum 25(OH)D (nmol/L), cotinine (ng/mL), insulin (pmol/L), and SII were used as continuous variables. The average value of three measurements was recorded as the diastolic and systolic blood pressure. The SII was determined by evaluating the platelet count × neutrophil count/lymphocyte count, based on the findings of another study (34). Age (<45; ≥45 years) (35) and BMI (<25; ≥25 kg/m^2) (36) were divided into two groups for subsequent subgroup analysis. Detailed information on the categorical variables was as follows: the education level was divided into three categories: under high school, high school or equivalent, and above high school (37). Marital status was divided into two categories:having a partner (Married/Living with a partner) and having no partner (Divorced/Never married/Widowed/Separated) (38). Individuals were categorized as smokers or non-smokers based on their answers to the question, "Have you smoked at least 100 cigarettes in your life" (39). Alcohol consumption was categorized based on the answer to the question "On days of alcohol consumption in the past 12 months, how many drinks were consumed per day on average", and the individuals were categorized into two groups: ≥3 cups and < 3 cups per day (12). Trouble sleeping was classified as yes or no based on whether the patients told their doctor about sleeping difficulties. The instrument used to assess the symptoms of depression was the Patient Health Questionnaire (PHQ-9), scores ≥10 indicated the existence of clinically significant symptoms, and scores < 10 indicated no clinically relevant symptoms (40). Coronary heart disease, diabetes, kidney failure, gout, and arthritis were all classified as "yes" or "no" based on whether the individuals knew they had the disease.

Statistical analysis

The AIP was partitioned into quartiles, with the reference group being the lowest quartile (Q1). Continuous variables were presented as the mean (SD) or median (IQR), whereas, categorical variables were presented as frequencies and percentages. We compared categorical and continuous variables between groups using the Chi-square test or the Fisher's test and the one-way ANOVA test or the Kruskal-Wallis test, respectively. Multiple linear regression models were constructed to assess the link between the AIP and total BMD; smooth curve fitting and generalized additive models (GAM) were used to characterize the non-linear relationship between the AIP and total BMD. GAM is an extension of the Generalized Linear Model (GLM), which allows the modeling of nonlinear relations and non-parametric effects. The basic idea is to express the relationship between the dependent variable and multiple predictors as the sum of nonlinear functions, and to link the predictor to the response variable through the connection function, and the model parameters are estimated using

maximum likelihood estimation or other appropriate methods. In model 1, the covariates were not adjusted. In model 2, age, race and BMI were adjusted. In model 3, age, race, BMI, PIR, systolic blood pressure, diastolic blood pressure, glycohemoglobin, total protein intake, total calcium intake, serum 25(OH)D, insulin, SII, education level, marital status, smoking status, trouble sleeping, depression, coronary heart disease, diabetes, kidney failure, gout and arthritis were adjusted. A subgroup analysis was conducted with stratified factors, including age (<45; ≥45 years), BMI (<25; ≥25 kg/m^2), education level (less than high school, high school or more than high school) and marital status (having a partner or with no partner). Further, sensitivity analysis was carried out: 1. explore the relationship between BMD of femoral neck and AIP; 2. explore the relationship between OP and AIP; 3. explore the relationship between low BMD and AIP. The SPSS (version 27.0.1) software and the R programming language (version 4.3.2) were used to conduct all statistical analyses. A P-value less than 0.05 was considered to indicate statistical significance in all two-sided statistical tests.

Results

Baseline characteristics of the study population

In this study, 2,362 individuals (18 to 59 years old) were included. The average age of the population was 38.13 ± 12.42 years, and the mean total BMD was 1.08 ± 0.10 g/cm^2. The clinical characteristics of the individuals according to the AIP quartiles are shown in Table 1. No statistically significant associations were found between marital status, coronary heart disease, kidney failure, total protein intake, total calcium intake, serum 25(OH)D and the AIP (P>0.05). Individuals with AIP levels in the upper quartile were more likely to be non-Hispanic black (40.8%), have a high school education or above (54.5%), be overweight (BMI 32.43 ± 7.12), and have a lower family income-to-poverty ratio (2.20 ± 1.58). With the increase of AIP level, the proportion of smokers, patients with ≥3 cups of alcohol intake, patients with sleep

TABLE 1 Baseline characteristics of the study population based on the AIP quartiles.

Variable	Total	Q1 (<-0.40)	Q2 (-0.40 to <-0.20)	Q3 (-0.20 to <0.03)	Q4 (≥0.03)	*P*
Race (%)						<0.001
Mexican American	354 (15.0)	55 (9.3)	74 (12.5)	100 (16.9)	125 (21.2)	
Other Hispanic	254 (10.8)	51 (8.7)	57 (9.6)	74 (12.5)	72 (12.2)	
Non-Hispanic black	839 (35.5)	188 (31.9)	202 (34.1)	208 (35.2)	241 (40.8)	
Non-Hispanic white	519 (22.0)	179 (30.4)	158 (26.7)	120 (20.3)	62 (10.5)	
Other race	396 (16.8)	116 (19.7)	101 (17.1)	89 (15.1)	90 (15.3)	
Education level (%)						<0.001
Under high school	358 (16.4)	48 (9.2)	61 (11.1)	107 (19.7)	142 (24.8)	
High school or equivalent	419 (19.2)	69 (13.2)	104 (19.0)	127 (23.4)	119 (20.8)	
Above high school	1410 (64.5)	407 (77.7)	383 (69.9)	308 (56.8)	312 (54.5)	
Marital status (%)						0.140
Having a partner	1253 (57.3)	295 (56.3)	304 (55.5)	309 (57.0)	345 (60.2)	
No partner	934 (42.7)	229 (43.7)	244 (44.5)	233 (43.0)	228 (39.8)	
Smoking status (%)						<0.001
Yes	739 (31.8)	141 (24.4)	162 (27.7)	190 (33.2)	246 (41.8)	
No	1583 (68.2)	437 (75.6)	422 (72.3)	382 (66.8)	342 (58.2)	
Alcohol consumption (%)						0.019
≥3	492 (29.9)	109 (25.1)	132 (29.9)	130 (33.5)	121 (41.8)	
<3	1151 (70.1)	326 (74.9)	310 (70.1)	258 (66.5)	257 (68.0)	
Trouble sleeping (%)						<0.001
Yes	634 (26.8)	125 (21.2)	132 (22.3)	167 (28.3)	210 (35.6)	
No	1728 (73.2)	464 (78.8)	460 (77.7)	424 (71.7)	380 (64.4)	
Depressive symptoms (%)						<0.001

(Continued)

TABLE 1 Continued

Variable	Total	Q1 (<-0.40)	Q2 (-0.40 to <-0.20)	Q3 (-0.20 to <0.03)	Q4 (≥0.03)	*P*
Yes	233 (9.9)	36 (6.1)	45 (7.6)	57 (9.6)	95 (16.1)	
No	2129 (90.1)	553 (93.3)	547 (92.4)	534 (90.4)	495 (83.9)	
Coronary heart disease (%)						0.618
Yes	13 (0.6)	3 (0.6)	1 (0.2)	2 (0.4)	7 (1.2)	
No	2173 (99.4)	521 (99.4)	547 (99.8)	540 (99.6)	565 (98.8)	
Diabetes (%)						<0.001
Yes	175 (7.6)	10 (1.7)	21 (3.6)	37 (6.4)	107 (18.6)	
No	2138 (92.4)	569 (98.3)	557 (96.4)	545 (93.6)	467 (81.4)	
Kidney failure (%)						0.142
Yes	51 (2.3)	5 (1.0)	8 (1.5)	16 (3.0)	22 (3.8)	
No	2134 (97.7)	519 (99.0)	539 (98.5)	526 (97.0)	550 (96.2)	
Gout (%)						<0.001
Yes	34 (1.6)	3 (0.6)	7 (1.3)	4 (0.7)	20 (3.5)	
No	2153 (98.4)	521 (99.4)	541 (98.7)	538 (99.3)	553 (96.5)	
Arthritis (%)						<0.001
Yes	378 (17.3)	47 (9.0)	85 (15.5)	95 (17.6)	151 (26.5)	
No	1803 (82.7)	476 (91.0)	462 (84.5)	445 (82.4)	420 (73.5)	
Age (year)	38.13 ± 12.42	35.16 ± 12.11	37.10 ± 12.36	38.90 ± 12.76	41.37 ± 11.58	<0.001
PIR	2.41 ± 1.65	2.67 ± 1.69	2.52 ± 1.66	2.23 ± 1.64	2.20 ± 1.58	<0.001
BMI (kg/m^2)	29.19 ± 7.76	25.68 ± 6.78	28.15 ± 7.64	30.51 ± 7.76	32.43 ± 7.12	<0.001
Systolic blood pressure (mmHg)	116.01 ± 15.15	112.68 ± 14.55	114.53 ± 14.25	116.62 ± 15.60	120.21 ± 15.15	<0.001
Diastolic blood pressure (mmHg)	69.35 ± 10.42	67.64 ± 10.54	68.55 ± 9.86	69.28 ± 10.68	71.95 ± 10.09	<0.001
Glycohemoglobin (%)	5.59 ± 0.99	5.31 ± 0.51	5.45 ± 0.79	5.58 ± 0.93	6.02 ± 1.39	<0.001
LDL-C (mmol/L)	2.87 ± 0.88	2.49 ± 0.74	2.81 ± 0.79	3.00 ± 0.85	3.17 ± 0.99	<0.001
TC (mmol/L)	4.87 ± 1.02	4.58 ± 0.91	4.73 ± 0.94	4.90 ± 0.97	5.27 ± 1.11	<0.001
Total protein intake (gm/d)	67.18 (48.26,90.67)	68.11 (51.13,94.51)	69.82 (49.16,92.46)	64.78 (45.78,85.92)	66.41 (46.38,90.31)	0.059
Total calcium intake (mg/d)	736.00 (491.00,1073.00)	737.00 (492.00,1087.75)	768.00 (514.00,1083.00)	710.50 (482.00,1051.50)	739.00 (481.75,1061.50)	0.977
Serum 25(OH)D (nmol/L)	58.80 (43.10,77.40)	59.30 (41.75,78.35)	59.00 (42.50,75.95)	58.10 (43.30,77.90)	58.95 (44.05,77.93)	0.695
Cotinine (ng/mL)	0.03 (0.01,1.26)	0.03 (0.01,0.18)	0.03 (0.01,0.74)	0.04 (0.01,5.92)	0.04 (0.01,81.95)	<0.001
Insulin (pmol/L)	56.97 (36.17,90.56)	37.44 (25.20,53.97)	52.62 (36.06,76.38)	63.90 (40.86, 94.20)	90.90 (57.42,137.94)	<0.001
SII	452.06 (324.22,632.00)	399.64 (290.47,568.89)	426.56 (314.66,598.52)	488.84 (667.80,341.00)	504.57 (360.77,675.39)	<0.001
Total BMD (g/cm^2)	1.08 ± 0.10	1.09 ± 0.97	1.09 ± 0.10	1.08 ± 0.10	1.07 ± 0.10	<0.001

The mean (SD) or median (IQR) values of continuous variables, and the p-value was calculated by the one-way ANOVA test or the Kruskal–Wallis test. Percentage for categorical variables, the p-value was calculated by the Chi-square test or the Fisher's test. (AIP, atherogenic index of plasma; PIR, ratio of family income to poverty; BMI, body mass index; LDL-C, low-density lipoprotein cholesterol; TC, total cholesterol;25(OH)D, 25-hydroxyvitamin D;SII, systemic immune-inflammation index; BMD, bone mineral density).

difficulties, patients with depression, patients with diabetes, patients with gout and arthritis showed an increasing trend. Systolic blood pressure, diastolic blood pressure, glycohemoglobin, LDL-C, TC, cotinine, insulin, and SII were highest at Q4 levels compared to the low quartile of AIP.

Relationship between the AIP and BMD

Multiple linear regression analysis was performed to assess the relationship in three model between the AIP and total BMD in the three models. In model 1, no covariates were adjusted. In model 2, adjustments were made for age, race, and BMI. In model 3, further adjustments were made for PIR, systolic blood pressure, diastolic blood pressure, glycohemoglobin, total protein intake, total calcium intake, serum 25(OH)D, SII, education level, marital status, smoking status, trouble sleeping, depressive symptoms, coronary heart disease, diabetes, kidney failure, gout and arthritis (Table 2). The AIP and total BMD were found to have a negative relationship (β = -0.022; 95% CI: -0.034, -0.009). After adjusting for confounders, this negative correlation was found in model 2 (β = −0.018; 95%CI: −0.03, −0.005) and model 3 (β = −0.021; 95%CI: −0.037, −0.006) was still present. The AIP was converted into a categorical variable (quartile) from a continuous variable. The trend test was significant (P for trend < 0.001) in all three models. In Model 3, the total BMD of the highest quartile was 0.02g/cm² lower than that of the lowest quartile.

The non-linear relationship between the AIP and BMD

The non-linear relationship between the AIP and total BMD is shown in Figure 2. Using the two-segment piecewise linear regression model, we found that -0.61 was the AIP turning point. When the AIP was lower than -0.61, no difference was found in the total BMD with an increase in AIP, and the β value was 0.06 (95% CI: -0.07, 0.19). When the AIP was ≥ -0.61, it was negatively correlated with BMD, and the β value was -0.03 (95%CI: -0.04, -0.01), as shown in Table 3.

Subgroup analysis and interaction test

A subgroup analysis was performed to estimate the relationship between the AIP and total BMD (Table 4). A negative association between the AIP and total BMD was recorded in participants who were below 45 years old (β = -0.023; 95% CI: -0.041, -0.004), overweight (β = -0.022; 95% CI: -0.041, -0.002), with a higher education level (β = -0.025; 95% CI: -0.044, -0.006) and with no partners (β = -0.014; 95% CI: -0.06, -0.009) was more obvious. Strong interactions were found among BMI, education level and marital status.

Sensitivity analysis

The results of sensitivity analysis were consistent with those of main analysis. Details are listed in Supplementary Table S2.

Discussion

In this study, the results of multiple regression analysis revealed a negative correlation between the AIP and total BMD. Curve fitting and threshold effect analyses revealed a non-linear relationship between the two, and the inflection point was -0.61. When the AIP was ≥-0.61, the total BMD decreased with increasing AIP. The results of the subgroup analysis showed that this association was prominent in individuals who were < 45 years, with a BMI ≥25 (kg/m^2), a high education level, and without a partner.

Three studies were previously conducted on the AIP and BMD. Ersoy et al. found that the AIP negatively affected the BMD of postmenopausal women (22). Hernández et al. reported that the

TABLE 2 Associations between the AIP and total BMD.

	Model 1			Model 2			Model 3		
	β	95% CI	P	β	95% CI	P	β	95% CI	P
AIP	-0.022	-0.034, -0.009	<0.001	-0.018	-0.030, -0.005	<0.01	-0.021	-0.037, -0.006	<0.01
AIP(Quartile)									
Q1	Reference			Reference			Reference		
Q2	0	-0.011, 0.011	0.988	-0.002	-0.013, 0.008	0.679	0	-0.012, 0.012	0.994
Q3	-0.011	-0.022, 0.001	0.067	-0.013	-0.024, -0.002	<0.05	-0.008	-0.021, 0.004	0.188
Q4	-0.021	-0.033, -0.01	<0.001	-0.019	-0.031, -0.008	<0.001	-0.020	-0.034, -0.007	<0.01
P for trend	<0.001			<0.001			<0.001		

AIP: Q1 (<-0.40), Q2 (-0.40 to<-0.20), Q3 (-0.20 to <0.03), and Q4 (≥0.03); (AIP, atherogenic index of plasma; BMD, bone mineral density; BMI, body mass index; PIR, ratio of family income to poverty; 25(OH)D, 25-hydroxyvitamin D; SII, systemic immune-inflammation index; CI, confidence interval).
Model 1 no parameter was adjusted.
Model 2 continuous variables (age and BMI), categorical variables (race).
Model 3 continuous variables (age, BMI, PIR, systolic blood pressure, diastolic blood pressure, glycohemoglobin, total protein intake, total calcium intake, serum 25(OH)D, insulin, and SII), categorical variables (race, educational level, marital status, smoking status, trouble sleeping, depressive symptoms, coronary heart disease, diabetes, kidney failure, gout, and arthritis).

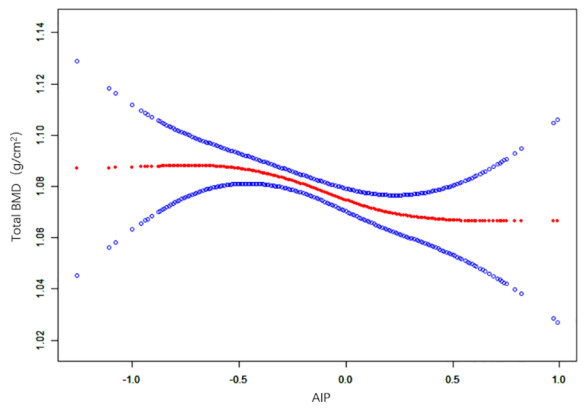

FIGURE 2
Non-linear relationship between the AIP and total BMD. (AIP, atherogenic index of plasma; BMD, bone mineral density).

AIP was significantly and independently associated with bone microstructure degradation in Spanish women, suggesting that when evaluating postmenopausal women's total bone metabolism, the AIP may be a helpful technique (23). In Sudanese women, Elmugadam et al. found that the AIP was positively associated with the risk of OP in postmenopausal women (24). Our findings were similar to those of previous studies. Using the NHANES database, we were the first study to show a negative relationship between the AIP and BMD among adult women in the United States. Based on these findings, the AIP is considered to be related to bone metabolism in women of different countries and ethnicities, and we hypothesize that the AIP could be used to manage and prevent OP effectively. Therefore, studies on the AIP and BMD or OP need to be performed in all populations with more participants to provide stronger evidence.

Although the common mechanism by which the AIP and bone loss develop is unclear, there are several explanations. First, adipokines such as lipocalin, leptin and chemotaxin promote the formation of atherosclerosis but they also participate in the remodeling of bones (41–44). For example, Varri et al. studied 290 postmenopausal women in Finland and found a connection between poor bone density, adipokines and vascular calcification (45). Second, systemic inflammation is also associated with levels of TG, HDL-C, and bone metabolism (46, 47). For example, Huang et al. found that HDL-C levels were lower and TG levels were higher in the group with systemic lupus erythematosus (SLE), compared to the healthy control group; Ruaro et al. found that BMD and trabecular scores were lower in SLE patients than in healthy matched controls (48, 49). Third, biological factors related to bone metabolism can also affect the levels of TG and HDL-C. For example, Sherief et al. found a positive correlation between serum osteoprotectin levels and TG; Fryes et al. found that the osteosclerosis protein had a positive correlation with TG and a negative correlated with HDL-C (50, 51). Since several clinical studies have shown that the AIP and bone metabolism are correlated, more basic studies are needed to answer the molecular mechanism of the two.

TABLE 3 Threshold effect analysis of the AIP and total BMD using the two-segment piecewise linear regression model.

Total BMD	Adjusted β (95% CI) P value
AIP	
Inflection point	-0.61
AIP < Inflection point	0.06 (-0.07, 0.19) 0.387
AIP > Inflection point	-0.03 (-0.04, -0.01) 0.003
Log-likelihood ratio	0.039

Age, race, BMI, PIR, systolic blood pressure, diastolic blood pressure, glycohemoglobin, total protein intake, total calcium intake, serum 25(OH)D, SII, education level, marital status, smoking status, trouble sleeping, depressive symptoms, coronary heart disease, diabetes, kidney failure, gout, and arthritis were adjusted. (AIP, atherogenic index of plasma; BMD, bone mineral density; CI, confidence interval).

The results of the subgroup analysis showed that the AIP could predict BMD in women below 45 years of age and BMI ≥25 (kg/m^2). Several studies have shown that age strongly influences the AIP and BMD (52, 53). Our results were inconsistent with those of previous studies that found a negative association between the AIP and BMD in postmenopausal women (22–24). Through comparison, we found that it might be caused by differences in the study design, ethnic characteristics, measurement sites, etc. Some relevant covariates such as estrogen levels were not included in this study. Second, in obese patients, the AIP was negatively correlated with BMD. Some studies have shown that, while obesity is closely related to an increase in the AIP, an increase in BMI may have adverse effects on the health of women (54–56). Although the exact process behind bone deterioration in obese individuals remains unclear, we speculated that inflammation and alterations in the hormone levels that regulate bone might influence the relationship between the AIP and BMD (57, 58).

Interestingly, we found a negative association between AIP and BMD in the higher education subgroup and no partner subgroup. Although little has been reported about this, through extensive literature review and clinical experience, we have identified several potential mechanisms to explain it. First, people with higher education levels may have higher disease awareness and take timely preventive measures and treatment (59). Second, people with higher levels of education have higher levels of income relative to those with lower levels of education. On the one hand, they have better nutrition and health during childhood and adolescence. On the other hand, they are more likely to have access to a healthy lifestyle, exercise opportunities and better health care (60, 61). For the single subgroup, first, the lifestyle of the single population (such as diet, physical activity patterns, etc.) may be relatively unhealthy compared with that of the partner population, and a single life may be more casual, and lack of care and supervision from others. Second, single people lack of sexual life, but appropriate sexual life has many benefits, such as improving sleep, reducing pain, soothing mood, etc., in the sexual process, women's pelvic congestion, accelerate local blood circulation, to a certain extent, can promote the blood supply of the uterus and ovaries, conducive to health (62).

As a rule, the ovarian function of postmenopausal women declines, the secretion of estrogen in the body is significantly reduced, and the lack of estrogen leads to more obvious upregulation of osteoclast activity than osteoblast activity, and

TABLE 4 Subgroup analysis for the association between the AIP and total BMD.

Subgroup analysis	β	95% CI	P-value	P for interaction
Age (year)				0.056
<45	-0.023	-0.041, -0.004	<0.05	
≥45	-0.022	-0.051, 0.006	0.127	
BMI (kg/m^2)				<0.05
<25	-0.013	-0.043, 0.016	0.378	
≥25	-0.022	-0.041, -0.002	<0.05	
Education level				<0.01
Less than high school	-0.009	-0.052, 0.034	0.685	
High school	-0.007	-0.045, 0.031	0.730	
More than high school	-0.025	-0.044, -0.006	<0.05	
Marital status				<0.01
Having a partner	-0.010	-0.030, 0.010	0.314	
No partner	-0.034	-0.060, -0.009	<0.01	

(AIP, atherogenic index of plasma; BMD, bone mineral density; BMI, body mass index; CI, confidence interval).

bone absorption accelerates and exceeds the rate of bone formation, resulting in rapid bone loss, thereby reducing BMD. On the other hand, estrogen levels also have an effect on triglyceride and HDL-C levels. Several studies have shown a negative correlation between estrogen and TG (63, 64). Some studies have found a positive correlation between estrogen and HDL-C (65, 66). In summary, covariable estrogen has a greater impact on the relationship between BMD and AIP. Therefore, the relationship between BMD and AIP in participants under 45 years old is less affected by estrogen fluctuations, which can better demonstrate the correlation between the two. Lipid metabolism is closely related to bone metabolism, and the disorder of lipid metabolism can directly affect the formation and absorption of bone, thus affecting BMD (21). A number of studies have found that cholesterol and TG are significantly correlated with BMD (67, 68). A high-cholesterol diet significantly reduced BMD and osteoblast activity, while increasing levels of bone resorption markers such as type I collagen pyridinoline cross-linked fragments (69, 70). Through experimental studies, it was found that high-cholesterol diet inhibited the proliferation and differentiation of osteoblast MC3T3-E, and after treatment, the expressions of bone morphogenetic protein (BMP2), dwarf-related transcription factor 2 (Runx2), alkaline phosphatase (ALP, ALPL), collagen type 1 (COL2A1) and other osteogenic genes were reduced. The normal expression of these genes is an important factor in the osteoblast process, suggesting that free cholesterol may inhibit the expression of Runx2, ALPL and COL2A1 in osteoblasts by inhibiting BMP2, thereby inhibiting the differentiation of osteoblasts. At the same time, a high-cholesterol diet may inhibit TGF-β/BMP2/Wnt signaling, which is essential for mammalian bone formation and is responsible for almost all osteoblast functions (71–73).

Compared to previous studies, our study had several advantages. First, previous studies on the AIP and BMD did not involve the U.S. population and were mostly limited to postmenopausal women, we were the first to investigate the connection between adult AIP and BMD in adult women from the USA. Second, we obtained data from the NHANES database, which has a relatively large sample size and excellent population representation. Third, the inflection point was found using the threshold effect analysis. However, our study has several limitations. First, this study had a cross-sectional design, which prevented us from determining the intricate causal link between the AIP and BMD. Second, as this was an observational study, we could not rule out any potential confounding factors that might have affected the outcomes. In order to improve the accuracy and authenticity of the results, we adjusted the relevant covariates available as far as possible. Third, Americans were included in this study, and thus, it is not known if the correlation between the AIP and BMD valid for people from other nations or ethnic backgrounds due to variations in genetic and environmental and other parameters. Fourth, self-report questionnaires were used to obtain information on some of the covariate data, which may not fully reflect the circumstances and may induce memory bias. Fifth, there are other methods to diagnose OP besides BMD, and more accurate studies will be conducted by combining multiple methods in the future. Therefore, given the limitations of this study, studies with a better design are needed to validate our findings.

Conclusions

To summarize, the results of this study showed a negative correlation between the AIP and total BMD. The AIP cut-off (-0.61) has a certain clinical application value, indicating that adult women in the United States might have a low BMD, which might contribute to the prevention of osteoporosis.

Data availability statement

Publicly available datasets were analyzed in this study. This data can be found here: Centers for Disease Control and Prevention (CDC), National Center for Health Statistics (NCHS), National Health and Nutrition Examination Survey (NHANES), https://wwwn.cdc.gov/nchs/nhanes/Default.aspx, NHANES 2011-2018.

Ethics statement

Ethical review and approval was not required for the study on human participants in accordance with the local legislation and institutional requirements. Written informed consent from the patients/participants or patients/participants' legal guardian/next of kin was not required to participate in this study in accordance with the national legislation and the institutional requirements.

Author contributions

QH: Conceptualization, Data curation, Formal analysis, Investigation, Methodology, Project administration, Software, Validation, Visualization, Writing – original draft, Writing – review & editing. BC: Conceptualization, Methodology, Software, Writing – review & editing. FL: Writing – review & editing. ZZ: Funding acquisition, Project administration, Supervision, Resources, Writing – review & editing.

Funding

The author(s) declare financial support was received for the research, authorship, and/or publication of this article. This work was supported by the Natural Science Foundation of Hubei Province of China (2022CFB406) and Wuhan Knowledge Innovation Special Project (2023020201010173).

Acknowledgments

The authors thank all the participants and staff of the National Health and Nutrition Examination Survey for their valuable contributions.

Conflict of interest

The authors declare that the research was conducted in the absence of any commercial or financial relationships that could be construed as a potential conflict of interest.

Publisher's note

Supplementary material

The Supplementary Material for this article can be found online at: https://www.frontiersin.org/articles/10.3389/fendo.2024.1363889/full#supplementary-material

References

1. Compston JE, McClung MR, Leslie WD. Osteoporosis. *Lancet*. (2019) 393:364–76. doi: 10.1016/s0140–6736(18)32112–3

2. Preventive Services Task Force US, Curry SJ, Krist AH, Owens DK, Barry MJ, Caughey AB, et al. Screening for osteoporosis to prevent fractures: US preventive services task force recommendation statement. *JAMA*. (2018) 319:2521–31. doi: 10.1001/jama.2018.7498

3. Black DM, Rosen CJ. Clinical practice. Postmenopausal osteoporosis. *N Engl J Med*. (2016) 374:254–62. doi: 10.1056/NEJMcp1513724

4. Aibar-Almazán A, Voltes-Martínez A, Castellote-Caballero Y, Afanador-Restrepo DF, Carcelén-Fraile MDC, López-Ruiz E. Current status of the diagnosis and management of osteoporosis. *Int J Mol Sci*. (2022) 23:9465. doi: 10.3390/ijms23169465

5. Miller PD. Management of osteoporosis. *Dis Mon*. (1999) 45:21–54. doi: 10.1016/S0011-5029(99)90010-X

6. Lin Y, Wang X, Wu R, Zhou J, Feng F. Association between segmental body composition and bone mineral density in US adults: results from the NHANES (2011–2018). *BMC Endocr Disord*. (2023) 23:246. doi: 10.1186/s12902-023-01506-z

7. Jiang Q, Gao H, Shi X, Wu Y, Ni W, Shang A. Total body bone mineral density and various spinal disorders: a Mendelian randomization study. *Front Endocrinol (Lausanne)*. (2023) 141285137:1285137. doi: 10.3389/fendo.2023.1285137

8. Yu J, Zhuang C, Guo W, Zhou X, Chen Y, Wang L, et al. Causal relationship between breakfast skipping and bone mineral density: a two-sample Mendelian randomized study. *Front Endocrinol (Lausanne)*. (2023), 141200892. doi: 10.3389/fendo.2023.1200892

9. Genant HK, Cooper C, Poor G, Reid I, Ehrlich G, Kanis J, et al. Interim report and recommendations of the World Health Organization Task-Force for Osteoporosis. *Osteoporos Int*. (1999) 10:259–64. doi: 10.1007/s001980050224

10. Lane NE. Epidemiology, etiology, and diagnosis of osteoporosis. *Am J Obstet Gynecol*. (2006) 194:S3–11. doi: 10.1016/j.ajog.2005.08.047

11. Dobiásová M, Frohlich J. The plasma parameter log (TG/HDL-C) as an atherogenic index: correlation with lipoprotein particle size and esterification rate in apoB-lipoprotein-depleted plasma (FER(HDL)). *Clin Biochem*. (2001) 34:583–8. doi: 10.1016/s0009–9120(01)00263–6

12. Shi Y, Wen M. Sex-specific differences in the effect of the atherogenic index of plasma on prediabetes and diabetes in the NHANES 2011–2018 population. *Cardiovasc Diabetol*. (2023) 22:19. doi: 10.1186/s12933–023-01740–8

13. Kim J, Ha J, Jeong C, Lee J, Lim Y, Jo K, et al. Bone mineral density and lipid profiles in older adults: a nationwide cross-sectional study. *Osteoporos Int*. (2023) 34:119–28. doi: 10.1007/s00198-022-06571-z

14. Zhao H, Li Y, Zhang M, Qi L, Tang Y. Blood lipid levels in patients with osteopenia and osteoporosis:a systematic review and meta-analysis. *J Bone Miner Metab*. (2021) 39:510–20. doi: 10.1007/s00774–020-01189–9

15. Fernández-Macías JC, Ochoa-Martínez AC, Varela-Silva JA, Pérez-Maldonado IN. Atherogenic index of plasma: novel predictive biomarker for cardiovascular illnesses. *Arch Med Res*. (2019) 50:285–94. doi: 10.1016/j.arcmed.2019.08.009

16. Alifu J, Xiang L, Zhang W, Qi P, Chen H, Liu L, et al. Association between the atherogenic index of plasma and adverse long-term prognosis in patients diagnosed with chronic coronary syndrome. *Cardiovasc Diabetol*. (2023) 22:255. doi: 10.1186/s12933-023-01989-z

17. Sadeghi M, Heshmat-Ghahdarijani K, Talaei M, Safaei A, Sarrafzadegan N, Roohafza H. The predictive value of atherogenic index of plasma in the prediction of cardiovascular events; a fifteen-year cohort study. *Adv Med Sci*. (2021) 66:418–23. doi: 10.1016/j.advms.2021.09.003

18. Kim SH, Cho YK, Kim YJ, Jung CH, Lee WJ, Park JY, et al. Association of the atherogenic index of plasma with cardiovascular risk beyond the traditional risk factors: a nationwide population-based cohort study. *Cardiovasc Diabetol*. (2022) 21:81. doi: 10.1186/s12933–022-01522–8

19. Huang Q, Liu Z, Wei M, Huang Q, Feng J, Liu Z, et al. The atherogenic index of plasma and carotid atherosclerosis in a community population: a population-based cohort study in China. *Cardiovasc Diabetol*. (2023) 22:125. doi: 10.1186/s12933-023-01977-3

20. Alekos NS, Moorer MC, Riddle RC. Dual effects of lipid metabolism on osteoblast function. *Front Endocrinol (Lausanne)*. (2020) 11578194:578194. doi: 10.3389/fendo.2020.578194

21. Kim H, Oh B, Park-Min KH. Regulation of osteoclast differentiation and activity by lipid metabolism. *Cells*. (2021) 10. doi: 10.3390/cells10010089

22. Ersoy GS, Simsek EE, Vatansever D, Kasikci HO, Keser B, Sakin O. Lipid profile and plasma atherogenic index in postmenopausal osteoporosis. *North Clin Istanb*. (2017) 4:237–41. doi: 10.14744/nci.2017.61587

23. Hernández JL, Olmos JM, Pariente E, Ramos C, Martínez J, Nan D. The atherogenic index of plasma is related to a degraded bone microarchitecture assessed by the trabecular bone score in postmenopausal women: The Camargo Cohort Study. *Maturitas*. (2021), 1481–6. doi: 10.1016/j.maturitas.2021.03.008

24. Elmugadam A, Elfadil GA, Hamad AI, El Shikieri AB, Aledrissy M, Altayb HN. Atherogenic index of plasma and anthropometric measurements among osteoporotic postmenopausal Sudanese women: possible risk for cardiovascular disease. *J Aging Res*. (2022), 20221545127. doi: 10.1155/2022/1545127

25. Melton LJ 3rd. How many women have osteoporosis now? *J Bone Miner Res*. (1995) 10:175–7. doi: 10.1002/jbmr.5650100202

26. Keen RW. Burden of osteoporosis and fractures. *Curr Osteoporos Rep*. (2003) 1:66–70. doi: 10.1007/s11914-003-0011-x

27. Tom SE, Adachi JD, Anderson FA Jr., Boonen S, Chapurlat RD, Compston JE, et al. Frailty and fracture, disability, and falls: a multiple country study from the global longitudinal study of osteoporosis in women. *J Am Geriatr Soc*. (2013) 61:327–34. doi: 10.1111/jgs.12146

28. Johnson CL, Dohrmann SM, Burt VL, Mohadjer LK. National health and nutrition examination survey: sample design, 2011–2014. *Vital Health Stat 2*. (2014) 162):1–33.

29. CDC. NCHS research ethics review board (ERB) approval (2022). Available online at: https://www.cdc.gov/nchs/nhanes/irba98.htm.

30. Onat A, Can G, Kaya H, Hergenç G. "Atherogenic index of plasma" (log10 triglyceride/high-density lipoprotein-cholesterol) predicts high blood pressure, diabetes, and vascular events. *J Clin Lipidol*. (2010) 4:89–98. doi: 10.1016/j.jacl.2010.02.005

31. Looker AC, Orwoll ES, Johnston CC Jr., Lindsay RL, Wahner HW, Dunn WL, et al. Prevalence of low femoral bone density in older U.S. adults from NHANES III. *J Bone Miner Res*. (1997) 12:1761–8. doi: 10.1359/jbmr.1997.12.11.1761

32. Tang Y, Wang S, Yi Q, Xia Y, Geng B. High-density lipoprotein cholesterol is negatively correlated with bone mineral density and has potential predictive value for bone loss. *Lipids Health Dis*. (2021) 20:75. doi: 10.1186/s12944–021-01497–7

33. CDC. Body composition procedures manual (2013). Available online at: https://www.cdc.gov/nchs/data/nhanes/nhanes_13_14/2013_Body_Composition_DXA.

34. Qin Z, Li H, Wang L, Geng J, Yang Q, Su B, et al. Systemic immune-inflammation index is associated with increased urinary albumin excretion: A population-based study. *Front Immunol*. (2022), 13863640. doi: 10.3389/fimmu.2022.863640

35. Peng P, Xiao F, Gao S, Fang W, Lin T, He W, et al. Association between serum ferritin and bone mineral density in US adults. *J Orthop Surg Res*. (2022) 17:494. doi: 10.1186/s13018–022-03357–1

36. Shin SH, Kwon SO, Kim V, Silverman EK, Kim TH, Kim DK, et al. Association of body mass index and COPD exacerbation among patients with chronic bronchitis. *Respir Res*. (2022) 23:52. doi: 10.1186/s12931–022-01957–3

37. Sun L, Ye Z, Ling Y, Cai S, Xu J, Fan C, et al. Relationship between polycyclic aromatic hydrocarbons and rheumatoid arthritis in US general population, NHANES 2003–2012. *Sci Total Environ*. (2020) 704135294. doi: 10.1016/j.scitotenv.2019.135294

38. Sun J, Guo G. Association between atherogenic index of plasma and periodontitis among U.S. adults. *BMC Oral Health*. (2023) 23:166. doi: 10.1186/s12903-023-02853-y

39. Xiao PL, Fuerwa C, Hsu CJ, Peng R, Cui AY, Jiang N, et al. Socioeconomic status influences on bone mineral density in American men: findings from NHANES 2011–2020. *Osteoporos Int*. (2022) 33:2347–55. doi: 10.1007/s00198–022-06498–5

40. Wu Z, Yue Q, Zhao Z, Wen J, Tang L, Zhong Z, et al. A cross-sectional study of smoking and depression among US adults: NHANES (2005–2018). *Front Public Health*. (2023) 111081706:1081706. doi: 10.3389/fpubh.2023.1081706

41. Kerekes G, Nurmohamed MT, González-Gay MA, Seres I, Paragh G, Kardos Z, et al. Rheumatoid arthritis and metabolic syndrome. *Nat Rev Rheumatol*. (2014) 10:691–6. doi: 10.1038/nrrheum.2014.121

42. Broni EK, Ogunmoroti O, Quispe R, Sweeney T, Varma B, Fashanu OE, et al. Adipokines and incident venous thromboembolism: The Multi-Ethnic Study of Atherosclerosis. *J Thromb Haemost*. (2023) 21:303–10. doi: 10.1016/j.jtha.2022.11.012

43. Neumann E, Junker S, Schett G, Frommer K, Müller-Ladner U. Adipokines in bone disease. *Nat Rev Rheumatol*. (2016) 12:296–302. doi: 10.1038/nrrheum.2016.49

44. Soh S, Han S, Ka HI, Mun SH, Kim W, Oh G, et al. Adiponectin affects the migration ability of bone marrow-derived mesenchymal stem cells via the regulation of hypoxia inducible factor 1α. *Cell Commun Signal*. (2023) 21:158. doi: 10.1186/s12964-023-01248-4

45. Värri M, Niskanen L, Tuomainen T, Honkanen R, Kröger H, Tuppurainen MT. Association of adipokines and estradiol with bone and carotid calcifications in postmenopausal women. *Climacteric*. (2016) 19:204–11. doi: 10.3109/13697137.2016.1139563

46. Xiao S, Wang X, Zhang G, Tong M, Chen J, Zhou Y, et al. Association of systemic immune inflammation index with estimated pulse wave velocity, atherogenic index of plasma, triglyceride-glucose index, and cardiovascular disease: A large cross-sectional study. *Mediators Inflammation*. (2023) 20231966680. doi: 10.1155/2023/1966680

47. Chen S, Sun X, Jin J, Zhou G, Li Z. Association between inflammatory markers and bone mineral density: a cross-sectional study from NHANES 2007–2010. *J Orthop Surg Res*. (2023) 18:305. doi: 10.1186/s13018–023-03795–5

48. Huang S, Zhang Z, Cui Y, Yao G, Ma X, Zhang H. Dyslipidemia is associated with inflammation and organ involvement in systemic lupus erythematosus. *Clin Rheumatol*. (2023) 42:1565–72. doi: 10.1007/s10067–023-06539–2

49. Ruaro B, Casabella A, Paolino S, Alessandri E, Patané M, Gotelli E, et al. Trabecular bone score and bone quality in systemic lupus erythematosus patients. *Front Med (Lausanne)*. (2020) 7574842:574842. doi: 10.3389/fmed.2020.574842

50. Sherief LM, Dawood O, Ali A, Sherbiny HS, Kamal NM, Elshanshory M, et al. Premature atherosclerosis in children with beta-thalassemia major: New diagnostic marker. *BMC Pediatr*. (2017) 17:69. doi: 10.1186/s12887–017-0820–1

51. Frysz M, Gergei I, Scharnagl H, Smith GD, Zheng J, Lawlor DA, et al. Circulating sclerostin levels are positively related to coronary artery disease severity and related risk factors. *J Bone Miner Res*. (2022) 37:273–84. doi: 10.1002/jbmr.4467

52. Płaczkowska S, Sołkiewicz K, Bednarz-Misa I, Kratz EM. Atherogenic plasma index or non-high-density lipoproteins as markers best reflecting age-related high concentrations of small dense low-density lipoproteins. *Int J Mol Sci*. (2022) 23. doi: 10.3390/ijms23095089

53. Eghbali P, Becce F, Goetti P, Vauclair F, Farron A, Büchler P, et al. Age- and sex-specific normative values of bone mineral density in the adult glenoid. *J Orthop Res*. (2023) 41:263–70. doi: 10.1002/jor.25379

54. Zhang JS, Yeh WC, Tsai YW, Chen JY. The relationship between atherogenic index of plasma and obesity among adults in Taiwan. *Int J Environ Res Public Health*. (2022) 19. doi: 10.3390/ijerph192214864

55. Dağ H, İncirkuş F, Dikker O. Atherogenic index of plasma (AIP) and its association with fatty liver in obese adolescents. *Children (Basel)*. (2023) 10. doi: 10.3390/children10040641

56. Li Y. Association between obesity and bone mineral density in middle-aged adults. *J Orthop Surg Res*. (2022) 17:268. doi: 10.1186/s13018-022-03161-x

57. Szekanecz Z, Raterman HG, Pethő Z, Lems WF. Common mechanisms and holistic care in atherosclerosis and osteoporosis. *Arthritis Res Ther*. (2019) 21:15. doi: 10.1186/s13075–018-1805–7

58. Shapses SA, Pop LC, Wang Y. Obesity is a concern for bone health with aging. *Nutr Res*. (2017), 391–13. doi: 10.1016/j.nutres.2016.12.010

59. Xu X, Liu L, Sharma M, Zhao Y. Smoking-related knowledge, attitudes, behaviors, smoking cessation idea and education level among young adult male smokers in Chongqing, China. *Int J Environ Res Public Health*. (2015) 12:2135–49. doi: 10.3390/ijerph120202135

60. Arabi A, Nabulsi M, Maalouf J, Choucair M, Khalifé H, Vieth R, et al. Bone mineral density by age, gender, pubertal stages, and socioeconomic status in healthy Lebanese children and adolescents. *Bone*. (2004) 35:1169–79. doi: 10.1016/j.bone.2004.06.015

61. Crandall CJ, Merkin SS, Seeman TE, Greendale GA, Binkley N, Karlamangla AS. Socioeconomic status over the life-course and adult bone mineral density: the Midlife in the U.S. Study. *Bone*. (2012) 51:107–13. doi: 10.1016/j.bone.2012.04.009

62. Arnot M, Mace R. Sexual frequency is associated with age of natural menopause: results from the Study of Women's Health Across the Nation. *R Soc Open Sci*. (2020) 7:191020. doi: 10.1098/rsos.191020

63. Pulchinelli AJr., Costa AM, de Carvalho CV, de Souza NC, Haidar MA, Andriolo A, et al. Positive association of the hepatic lipase gene polymorphism c.514C > T with estrogen replacement therapy response. *Lipids Health Dis*. (2011) 10197. doi: 10.1186/1476–511x-10–197

64. Han SI, Komatsu Y, Murayama A, Steffensen KR, Nakagawa Y, Nakajima Y, et al. Estrogen receptor ligands ameliorate fatty liver through a nonclassical estrogen

receptor/Liver X receptor pathway in mice. *Hepatology*. (2014) 59:1791–802. doi: 10.1002/hep.26951

65. Haffner SM, Valdez RA. Endogenous sex hormones: impact on lipids, lipoproteins, and insulin. *Am J Med*. (1995) 98:40s–7s. doi: 10.1016/s0002–9343(99)80058–8

66. Godsland IF. Effects of postmenopausal hormone replacement therapy on lipid, lipoprotein, and apolipoprotein (a) concentrations: analysis of studies published from 1974–2000. *Fertil Steril*. (2001) 75:898–915. doi: 10.1016/s0015–0282(01)01699–5

67. Wang P, Chen C, Song C, Jia J, Wang Y, Mu W. High cholesterol and low triglycerides are associated with total lumbar bone mineral density among adults aged 50 years and over: The NHANES 2017–2020. *Front Med (Lausanne)*. (2022), 9923730. doi: 10.3389/fmed.2022.923730

68. Kim D, Kim JH, Song TJ. Total cholesterol variability and the risk of osteoporotic fractures: A nationwide population-based cohort study. *J Pers Med*. (2023) 13. doi: 10.3390/jpm13030509

69. You L, Sheng ZY, Tang CL, Chen L, Pan L, Chen JY. High cholesterol diet increases osteoporosis risk via inhibiting bone formation in rats. *Acta Pharmacol Sin*. (2011) 32:1498–504. doi: 10.1038/aps.2011.135

70. Pelton K, Krieder J, Joiner D, Freeman MR, Goldstein SA, Solomon KR. Hypercholesterolemia promotes an osteoporotic phenotype. *Am J Pathol*. (2012) 181:928–36. doi: 10.1016/j.ajpath.2012.05.034

71. Hill TP, Später D, Taketo MM, Birchmeier W, Hartmann C. Canonical Wnt/beta-catenin signaling prevents osteoblasts from differentiating into chondrocytes. *Dev Cell*. (2005) 8:727–38. doi: 10.1016/j.devcel.2005.02.013

72. Glass DA 2nd, Bialek P, Ahn JD, Starbuck M, Patel MS, Clevers H, et al. Canonical Wnt signaling in differentiated osteoblasts controls osteoclast differentiation. *Dev Cell*. (2005) 8:751–64. doi: 10.1016/j.devcel.2005.02.017

73. Mo L, Ma C, Wang Z, Li J, He W, Niu W, et al. Integrated bioinformatic analysis of the shared molecular mechanisms between osteoporosis and atherosclerosis. *Front Endocrinol*. (2022), 13950030. doi: 10.3389/fendo.2022.950030

frontiers | Frontiers in Endocrinology

TYPE Original Research
PUBLISHED 18 July 2024
DOI 10.3389/fendo.2024.1342938

OPEN ACCESS

EDITED BY
Katherine A. Staines,
University of Brighton, United Kingdom

REVIEWED BY
Eleonora Palagano,
National Research Council (CNR), Italy
Jan Josef Stepan,
Charles University, Czechia

*CORRESPONDENCE
Tamara Alliston
tamara.alliston@ucsf.edu

RECEIVED 22 November 2023
ACCEPTED 26 June 2024
PUBLISHED 18 July 2024

CITATION
Yee CS, Meliadis C, Kaya S, Chang W and Alliston T (2024) The osteocytic actions of glucocorticoids on bone mass, mechanical properties, or perilacunar remodeling outcomes are not rescued by PTH(1-34). *Front. Endocrinol.* 15:1342938. doi: 10.3389/fendo.2024.1342938

The osteocytic actions of glucocorticoids on bone mass, mechanical properties, or perilacunar remodeling outcomes are not rescued by PTH(1-34)

Cristal S. Yee[1], Christoforos Meliadis[1], Serra Kaya[1], Wenhan Chang[2] and Tamara Alliston[1]*

[1]Department of Orthopaedic Surgery, University of California, San Francisco, San Francisco, CA, United States, [2]Endocrine Research Unit, San Francisco Veterans Affairs Medical Center, University of California, San Francisco, CA, United States

Glucocorticoids (GC) and parathyroid hormone (PTH) are widely used therapeutic endocrine hormones where their effects on bone and joint arise from actions on multiple skeletal cell types. In osteocytes, GC and PTH exert opposing effects on perilacunar canalicular remodeling (PLR). Suppressed PLR can impair bone quality and joint homeostasis, including in GC-induced osteonecrosis. However, combined effects of GC and PTH on PLR are unknown. Given the untapped potential to target osteocytes to improve skeletal health, this study sought to test the feasibility of therapeutically mitigating PLR suppression. Focusing on subchondral bone and joint homeostasis, we hypothesize that PTH(1-34), a PLR agonist, could rescue GC-suppressed PLR. The skeletal effects of GC and PTH(1-34), alone or combined, were examined in male and female mice by micro-computed tomography, mechanical testing, histology, and gene expression analysis. For each outcome, females were more responsive to GC and PTH(1-34) than males. GC and PTH(1-34) exerted regional differences, with GC increasing trabecular bone volume but reducing cortical bone thickness, stiffness, and ultimate force. Despite PTH(1-34)'s anabolic effects on trabecular bone, it did not rescue GC's catabolic effects on cortical bone. Likewise, cartilage integrity and subchondral bone apoptosis, tartrate-resistant acid phosphatase (TRAP) activity, and osteocyte lacunocanalicular networks showed no evidence that PTH(1-34) could offset GC-dependent effects. Rather, GC and PTH(1-34) each increased cortical bone gene expression implicated in bone resorption by osteoclasts and osteocytes, including *Acp5, Mmp13, Atp6v0d2, Ctsk*, differences maintained when GC and PTH(1-34) were combined. Since PTH(1-34) is insufficient to rescue GC's effects on young female mouse bone, future studies are needed to determine if osteocyte PLR suppression, due to GC, aging, or other factors, can be offset by a PLR agonist.

KEYWORDS

osteocyte, glucocorticoids, prednisolone, parathyroid hormone (PTH), PTH (1-34), perilacunar canalicular remodeling, osteocytic osteolysis, bone

1 Introduction

Common clinical therapies for immune suppression or osteoporosis include glucocorticoids and parathyroid hormone-based therapies, respectively. Therefore, understanding the effects of these common clinical therapies on skeletal health is important. Though the effects of these therapies alone or in combination on several aspects of bone health have been extensively studied in humans (1–3) and rodents (4–11), their combined effect on osteocyte-mediated perilacunar resorption, which is a target of both therapies independently, remains unclear.

Osteocytes are embedded in the bone matrix within the lacunar canalicular network (LCN). Osteocyte dendrites extend through canaliculi to communicate with other cells to regulate bone homeostasis, among other osteocytic functions. The LCN and bone quality are actively maintained by osteocytes through the homeostatic process of perilacunar canalicular remodeling (PLR), in which osteocytes resorb and then replace the local bone matrix (12–14). During this process, osteocytes acidify the local microenvironment and secrete factors such as matrix metalloproteases (MMPs) and cathepsin K to resorb local bone matrix, which can be visualized by enlargement and hypomineralization of the lacunae (12, 13, 15, 16), especially in response to lactation. Following weaning, the local bone matrix surrounding osteocytes is replenished.

Maintaining PLR homeostasis is critical as deviations compromise bone quality and increase bone fragility. For example, ablation of transforming growth factor, beta receptor II (*Tgfβr2*) in osteocytes impairs LCN integrity due to suppressed PLR-related gene expression (matrix metalloproteinase 13 (*Mmp13* mRNA), cathepsin K (*Ctsk* mRNA), tartrate resistant acid phosphatases (*Acp5* mRNA)) and increases bone fragility (17). Suppression of PLR not only impairs bone quality but also joint homeostasis. We and others reported signs of PLR suppression following glucocorticoid treatment in mice and in femoral heads from patients with glucocorticoid-induced osteonecrosis (6, 18). These signs include degeneration of the osteocyte LCN, down-regulation of PLR enzyme expression, collagen disorganization, and bone matrix hypermineralization (18). Furthermore, osteocyte-intrinsic ablation of the essential PLR enzyme MMP13 (19) or TGFβR2 (20) in mice suppresses PLR and causes subchondral bone sclerosis and canalicular degeneration. These osteocyte-dependent changes in subchondral bone are sufficient to exacerbate arthritic joint degeneration. Because subchondral bone changes due to PLR suppression may precede rather than follow cartilage degradation, osteocytes could be an ideal target to mitigate joint disease in post-traumatic osteoarthritis or osteonecrosis.

To oppose the effects of suppressed PLR in joint disease in osteoarthritis and osteonecrosis, a potential PLR agonist is parathyroid hormone (PTH). PTH-derived agents are used as bone anabolic therapies and importantly, these agents have proven effective in the treatment of glucocorticoid-induced osteoporosis (21, 22). Among the mechanisms by which PTH induces bone formation, PTH can act directly on osteocytes to suppress SOST expression (23). PTH is also a powerful agonist of osteocyte PLR, especially in lactation (12). This raises the question of whether PTH can rescue skeletal defects in glucocorticoid-treated bone by stimulating osteocytic PLR. We hypothesize that the PLR agonist (PTH(1-34)) can mitigate the effects of GC on the progression of bone and joint disease by restoring suppressed PLR to homeostasis.

To test the hypothesis that a PLR agonist, PTH(1-34), can oppose the suppression of PLR by glucocorticoids, we will evaluate *in vivo* PLR outcomes in a mouse model of glucocorticoid excess treated in the presence or absence of exogenous parathyroid hormone 1-34 (PTH(1-34)). Since suppressed PLR in the subchondral bone is associated with joint disease, the subchondral bone will be assessed using established qualitative and quantitative radiographic, histologic, and molecular approaches. This study aims to uncover the effects of GC and PTH(1-34) on the subchondral bone to guide our understanding of the combined effects of these therapies on the joint.

2 Materials and methods

2.1 Mouse studies

All animal experiments were approved by the Institutional Animal Care and Use Committee (IACUC) at the University of California, San Francisco. To facilitate comparison to prior work on the role of osteocytes in osteoarthritis, outcomes were analyzed in 16 week old mice (19, 20). Thirteen-week-old male and female FVB/NJ mice (The Jackson Laboratory, #001800, IMSR_JAX:001800) were acclimated to the University of California, San Francisco Laboratory Animal Resource Center (LARC) facility with 67°CF-74°CF, 30-70% humidity, a 12-hr light/dark cycle, and free access to water and irradiated standard chow (LabDiet 5058- PicoLab Rodent Diet 20) for a minimum of two weeks prior to experimental studies (19, 20, 24). At thirteen weeks, mice were randomly assigned for subcutaneous implantation with recommended placebo pellets (Innovative Research of America, cat# NG-111) or slow-releasing prednisolone (GC) pellets (2.1 mg/kg/d, 90-day release, cat# NG-151) for 21 days. Beginning the day after GC pellet implantation, mice received subcutaneous injections (5 days/week) of either vehicle (2% heat-inactivated FBS, 1mM HCl, 150mM NaCl) or rat parathyroid hormone 1-34 (PTH (1–34)) (80 μg/kg; Bachem Cat# H-5460), prior to euthanasia using an IACUC-approved standard procedure of carbon dioxide inhalation at 16 weeks of age.

2.2 Micro-computed tomography

Right femurs were dissected free of muscle, fixed in 10% neutral buffer formalin (NBF) for 3 days at 4°C, stored in 70% ethanol and scanned using a Scanco μCT50 scanner with x-ray potential of 55 kVP, current 109 μA, and 6W, at a voxel size (resolution) of 10μm, and 500ms integration time, as previously described (17, 25). Bone structural parameters were analyzed by manually contouring 100 slices of the trabecular (Tb) bone compartment (300μm proximal to epiphyseal plate) below the growth plate or cortical (Ct) compartment at mid-diaphysis using a Scanco analytic software.

Table 1 shows standard μCT parameters (26) for male (n=4-6/group) and female (n=6-7/group) mice.

2.3 Flexural strength tests/three-point bending test

Unfixed left femurs (n=4-8/group) were subjected to three-point bending at mid-shaft to assess mechanical properties using a Bose Electroforce 3200 (RRID: SCR_019752) test frame (27). Briefly, bones were hydrated in 1X phosphate-buffered saline (PBS) at room temperature and placed on 2 lower supporting jigs (8mm apart) with the anterior side facing down. The test probe was placed at the mid-point between the 2 supporting jigs to create bending with a displacement rate of 10 μm/s. Mechanical properties of stiffness, yield force, and ultimate force were calculated from load-displacement curves using a custom MATLAB (RRID: SCR_001622) script as previously described (27, 28). Material properties of elastic modulus, yield stress, ultimate stress was calculated from μCT measurements of left femurs from 16-week-old male (n=2-7/group) and female (n=5-6/group) mice using the femur cross-section diameter and moment of inertial (Imin/Cmin and Imin) and equations from Turner et al. and Jepsen et al. (28, 29).

2.4 Nanostring nCounter analysis

RNA was extracted from female humeri (n=4 mice/group) after removal of epiphysis and bone marrow to assess transcriptomic profiles of osteocyte-enriched cortical bone. Briefly, the dissected bones were flash frozen in liquid nitrogen and homogenized in QIAzol Lysis Reagent (Qiagen cat #79306), and total RNA was extracted using the RNeasy mini kit (Qiagen cat#74106) according to the manufacturer's instructions. Direct mRNA counts were determined using an automated Nanostring nCounter Mx system (RRID: SCR_021712) (30, 31) with a custom probe set for 94 mouse skeletal genes in the UCSF CCMBM Skeletal Biology and Biomechanics Core. Analysis of expression profiles was performed using the nSolver Analysis Software (RRID: SCR_003420) and nCounter Advanced Analysis Software and normalized with seven housekeeping genes (*Gapdh, Rpl19, Gilz* (*Tsc22d3*), bone sialoprotein (*Ibsp*), beta-2 microglobulin (*B2m*), beta actin (*Actb*), *Serpine2*). Highly significant gene expression fold

TABLE 1 Skeletal phenotyping of GC and PTH(1-34) treated male and female mouse bones.

Parameters	Male				Female			
	Control *(n=6)*	GC *(n=6)*	PTH(1-34) *(n=8)*	GC+PTH(1-34) *(n=4)*	Control *(n=7)*	GC *(n=7)*	PTH(1-34) *(n=6)*	GC+PTH(1-34) *(n=7)*
Distal Femur								
Tb. BV/TV	0.125 ± 0.030	0.140 ± 0.012	0.146 ± 0.024	0.145 ± 0.007	0.216 ± 0.037	0.378 ± 0.035[a,c]	0.351 ± 0.065[a,c]	0.452 ± 0.066[a]
Tb. N (1/mm)	4.747 ± 0.352	5.300 ± 0.435	4.806 ± 0.363	5.091 ± 0.359	5.770 ± 1.435	9.125 ± 0.964[a]	9.108 ± 1.256[a]	10.299 ± 1.002[a]
Tb. Th (mm)	0.042 ± 0.006	0.041 ± 0.003	0.047 ± 0.003	0.041 ± 0.003	0.056 ± 0.004	0.062 ± 0.007	0.066 ± 0.006[a]	0.068 ± 0.005[a]
Tb. Sp (mm)	0.213 ± 0.017	0.189 ± 0.014	0.210 ± 0.015	0.197 ± 0.017	0.185 ± 0.034	0.111 ± 0.012[a]	0.114 ± 0.017[a]	0.098 ± 0.011[a]
Tb. BMD (mg HA/cm^3)	197.150 ± 34.306	215.651 ±27.243	231.556 ± 36.914	206.775 ± 16.560	281.878 ± 25.99	315.579 ± 20.731[c]	309.501 ± 45.272[c]	369.269 ± 42.032[a]
Tb. TMD (mg HA/cm^3)	1097.840 ± 45.332	1109.404 ± 13.689	1111.047 ± 18.513	1091.108 ± 28.531	994.096 ± 64.466	835.282 ± 36.099[a]	849.375 ± 20.688[a]	827.451 ±37.303[a]
Midshaft Femur								
Ct. TA (mm^2)	1.876 ± 0.157	1.917 ± 0.111	1.929 ± 0.127	1.822 ± 0.085	1.754 ± 0.102	1.802 ± 0.128	1.837 ± 0.067	1.854 ± 0.104
Ct. BA (mm^2)	0.859 ± 0.055	0.840 ± 0.060	0.882 ± 0.117	0.779 ± 0.030	0.934 ± 0.061	0.893 ± 0.097	1.000 ± 0.063[b]	0.932 ± 0.020
Ct. BV/TV	0.458 ± 0.015	0.438 ± 0.018	0.456 ± 0.040	0.428 ± 0.014	0.532 ± 0.013	0.495 ± 0.020[a]	0.544 ± 0.021[b,c]	0.504 ± 0.025[a]
Ct. Th (mm)	0.193 ± 0.006	0.185 ± 0.010	0.183 ± 0.040	0.177 ± 0.005	0.219 ± 0.004	0.194 ± 0.016[a]	0.216 ± 0.011[b,c]	0.189 ± 0.013[a]
Ct. BMD (mg HA/cm^3)	698.210 ± 20.397	672.129 ± 45.756	704.795 ± 73.954	643.283 ± 19.773	722.743 ± 16.272	654.762 ± 30.918[a]	734.263 ± 25.539[b,c]	663.662 ± 37.091[a]
Ct. TMD (mg HA/cm^3)	1455.383 ± 30.407	1462.964 ± 37.229	1473.442 ± 28.144	1443.766 ± 28.680	1355.346 ± 14.940	1339.512 ± 10.523	1357.629 ± 6.483[c]	1326.397 ± 17.495[a]

Bone parameters on 16 week old male and female right femurs that were measured by μCT include trabecular (Tb.) and cortical (Ct.) parameters on the distal femoral and mid-shaft femur regions, respectively. Trabecular parameters were reported as: Trabecular bone volume fraction (Tb. BV/TV), Trabecular number (Tb. N), Trabecular thickness (Tb. Th), Trabecular separation (Tb. Sp), Trabecular bone mineral density (Tb. BMD), Trabecular tissue mineral density (Tb. TMD). Cortical parameters were reported as: Cortical total area (Ct. TA), Cortical bone area (Ct. BA), Cortical bone volume fraction (Ct. BV/TV), Cortical thickness (Ct. Th), Cortical bone mineral density (Ct. BMD), Cortical tissue mineral density (Ct. TMD). Data are presented as mean ± SD with [a]$p \le 0.05$ statistically different from Female Control group, [b]$p \le 0.05$ statistically different from Female GC group, [c]$p \le 0.05$ statistically different from Female GC+PTH(1-34) group. Statistical differences were determined with two-way ANOVA with post-hoc Holm Sidak.

changes were determined by unpaired t-tests between experimental groups.

2.5 Cell culture

Osteocyte-like MLO-Y4 cells (provided by L. Bonewald, RRID: CVCL_M098) were maintained in alpha-MEM supplemented with 2.5% fetal bovine serum, 2.5% bovine calf serum, and 1% penicillin-streptomycin and grown on rat tail collagen type 1 (0.16 mg/ml) coated plates. MLO-Y4 cells were treated with 0.1μM or 1μM dexamethasone with or without 50 nM rat parathyroid hormone 1-34 [PTH(1-34)] for 24 hours (n=3 biological replicates/group and 2 independent experiments). RNA was extracted for real-time quantitative PCR (qPCR), using iQ SYBR Green Supermix (BioRad) on a Biorad CFX96 Touch Real-Time PCR Detection System (RRID: SCR_018064). Gene expression levels were normalized to the housekeeping gene *Gapdh*. Additional details for primers are provided in the Supplementary Table 1. Fold change was determined using the delta-delta CT method (32). A one-way ANOVA was used for statistical analysis.

2.6 Histology

Female right femur/tibia joints were dissected free of muscle, fixed in 10% neutral buffered formalin (NBF), decalcified in 10% EDTA, dehydrated, and embedded with knee joints positioned at a 45 angle in paraffin as previously described (19, 20). Coronal sections (7μm) of the knee joints were obtained using a microtome (Leica Microsystems, Buffalo Grove, IL), followed by standard dewaxing and hydration protocols (19, 20) before various histological staining described below. All brightfield images were obtained on a Nikon Eclipse E800 microscope (RRID: SCR_020326).

2.7 Safranin O/fast green and OA scoring

Knee joints sections were stained with the Safranin O/Fast Green using the protocol adapted from University of Rochester (33) with the following modifications: Weigert's Iron Hematoxylin incubation for 3 mins, brief water rinse and differentiation in 1% acid-alcohol for 15 secs, stain with 0.02% Fast Green for 5 mins, differentiation with 1% acetic acid for 30 secs, rinse with water and incubation in 1% Safranin-O for 10 mins, prior to mounting with mounting media.

Osteoarthritis scoring of Safranin O/Fast Green-stained coronal sections (n=4/group) was performed by three blinded graders using the OARSI (34) and modified Mankin (35) scoring system. To maintain a consistent region of interest of the knee, sections with visible anterior cruciate ligament (ACL) and posterior cruciate ligament (PCL) were used for grading. Quantification of the whole knee joint was obtained using 10X and stitched 20X images to assess each quadrant of the knee joint (femur, tibia, lateral, medial). Mean scores across all blinded graders were obtained and the mean scores were averaged within each experimental group.

2.8 Tartrate-resistant acid phosphatase stain

Bone resorption activity in the knee joint was observed using the tartrate-resistant acid phosphatase (TRAP) Leukocyte Acid Phosphatase staining kit (Sigma cat# 387) following the manufacturer's instructions with slight modifications. Briefly, sections were post-fixed for 30 secs in Fixative Solution, rinsed in water, and incubated with a mixture of Fast Red Violet (Sigma cat#F3381) and Fast Garnet GBC Base Solution for 1 hour at 37°C in the dark. Slides were then rinsed in water and counterstained with 0.02% Fast Green (Sigma cat# F3381) and mounted. For quantification of bone resorption parameters, one image (20X) of the subchondral bone per quadrant of the knee joint (femur, tibia, medial, lateral) was evaluated. A total of 4 images per animal (n=4-5 mice/group) were analyzed by a blinded grader using the open source image analysis software TrapHisto (36) to measure the Osteoclast Surface per Bone Surface (Oc.S/BS %) and the Number of Osteoclasts per Tissue Volume (N.Oc/TV mm^{-2}). The mean of these parameters was averaged per quadrant of the knee for each animal and averaged within each experimental group to acquire mean total, medial and lateral joint values.

2.9 Ploton silver nitrate stain

The lacunocanalicular network of the subchondral bone in the knee was visualized by Ploton silver nitrate stain as previously described (17, 19, 20, 37). Briefly, right knee joint sections were stained in a fresh mixture of 50% silver nitrate and 1% formic acid in 2% gelatin with a 2:1 ratio for 55 mins in the dark and then counterstained with Cresyl Violet. For consistency, sections with visible ACL and PCL were chosen for staining. Four high-resolution images (100X) per knee joint subchondral bone quadrant (femur, tibia, medial, lateral) were used for quantitative analysis. ImageJ (RRID: SCR_003070) was used by a blinded grader to quantify lacunar number and lacunae size for a total of sixteen images per animal (n=4 mice group) by converting to a binary image, manually contouring each lacunae, and measuring with the Analyze Particles feature. Mean values were obtained per quadrant of the knee per animal and were then averaged within each experimental group.

2.10 Statistical analysis

All data are represented as mean ± standard deviation (SD) or standard error mean (SEM) as appropriate for each assay, as stated in the figure legends. For *in vivo* data, the number of samples per group is denoted as "n", while *in vitro* data, n indicates the number of independent experiments/biological replicates. GraphPad Prism (GraphPad Software version 10) was used for all statistical analysis and statistical significance required a p-value ¾ 0.05.

3 Results

3.1 Dimorphic effects of GC and PTH (1–34) on bone structure and mechanics

Micro-computed tomography (μCT) identified sex-dependent differences in the effect of GC, PTH(1-34), and combined GC +PTH(1-34) treatments on bone phenotypes (Figure 1; Table 1). At 16 weeks of age, male mice, regardless of treatment type, showed no significant changes in either trabecular (Tb) (Figures 1A–D) or cortical (Ct) (Figures 1E–H) bone parameters by the drug treatments versus vehicle controls, as visualized in the 3D-reconstructed images (Figure 1I) and their quantifications (Figures 1A–H). In contrast, female mice treated for 21 days with GC showed significant increases in Tb fraction (Tb.BV/TV) (Figure 1A) and number (Tb.N, Figure 1B), with a complementary decrease in spacing (Tb.Sp, Figure 1D). GC treatment caused loss of Ct bone in female mice (Figures 1E–H), similar to what we and others previously reported (6, 18, 38, 39), revealing the trabecular versus cortical region-specific effects of GC. In 16 week old female mice, intermittent PTH (1–34) treatment caused the anticipated anabolic response with significantly elevated Tb.BV/TV (Figure 1A), Tb.N (Figure 1B), and Tb.Th (Figure 1C), and reduced Tb.Sp (Figure 1D). Combined GC and PTH(1-34) treatment significantly increased Tb bone parameters relative to female controls (Figures 1A–D), with even greater increases in Tb.BV/TV than each treatment alone (Figure 1A). However, combined GC and PTH(1-34) did not mitigate GC-induced Ct bone loss (Figures 1E–H).

Mechanical testing by three-point bending showed that male femurs treated with PTH(1-34), relative to those treated with GC, have significantly increased yield force, but this effect is absent when GC and PTH(1-34) are combined (Figures 1J–L). Similar trends are present in females, with PTH-dependent increases in stiffness and ultimate force relative to bone from GC-treated mice (Figures 1J–L). As in males, PTH(1-34) does not overcome the effect of GC on mechanical properties in female bone (Table 2). Material properties of male or female bones were unaffected by GC or PTH(1-34) (Figure 1).

3.2 GC and PTH(1-34) regulation of genes implicated in bone resorption

We evaluated the effect of GC, PTH(1-34), and GC+PTH(1-34) treatment on gene expression from osteocyte-enriched humeri using Nanostring nCounter assay and a custom probe set of 96 mouse genes important in skeletal biology, including bone, cartilage, tendon, and muscle. By directly measuring mRNA, this assay provides increased sensitivity across a range of conditions (Supplementary Figures 2A–H). Volcano plots show regulation of several genes associated with bone remodeling in osteocyte-enriched bones across all treatment groups from female (Figures 2A–C) and, to a lesser extent, from male mice (Supplementary Figure 1). We previously reported that a 7-day GC treatment downregulates *Mmp2* (18), which is recapitulated with 21-day treatment of GC (Figure 2D). In addition, as anticipated based on prior reports (38, 40), GC reduced mRNA levels of osteocrin (*Ostn*), osteoprotegerin (*Tnfrsf11b*), gap junction alpha 1 protein (*Cx43*) (*Gja1*), while increasing mRNA levels for tartrate resistant acid phosphatase (*Acp5*) and cathepsin K (*Ctsk*) (Figure 2D), confirming the efficacy of GC in these conditions. We previously reported that a 7-day GC treatment suppressed bone remodeling genes implicated in PLR (18), however here we observe that a longer 21-day GC treatment significantly upregulates several PLR-related genes including *Acp5, Mmp13, Atp6v0d2, Ctsk* (Figure 2D).

As expected based on prior reports of PTH(1-34) induction of *Phex* (41, 42) and *Wnt4* (43), both genes are enriched in bone from the PTH (1–34) treated group (Figure 2E). Other PTH(1-34)-suppressed genes (*Sost*, *Dmp1, Osteocalcin*) (44–46) and PTH(1-34)-induced genes *(Tnfrsf11a* (*Rank), Tnfrsf11b (Opg)*) (43, 47) were not differentially expressed in these conditions. As we had hypothesized, PTH(1-34) also increased mRNA levels for several PLR-related genes (*Acp5, Ctsk, Atp6v0d2*), as well as *Tnfrsf11a (Rank)* (Figure 2E). The combined GC + PTH(1-34) treatment led to upregulation of *Tnfrsf11a* and the same PLR-related genes (*Acp5, Ctsk, Atp6v0d2*) as individual treatments (Figure 2F). Indeed, of the 21 genes in this panel that are significantly regulated by GC+PTH (1-34), relative to vehicle treated cells, all but 2 (*Foxo1* and *Igf1r*) are regulated in the same manner by GC or PTH(1-34) alone, with 7 regulated by both stimuli (Figures 2D–F, red bars). Overall, analysis of gene expression in these conditions suggests that GC and PTH(1-34), alone or combined, shift bone toward a more catabolic state.

3.3 Osteocyte-intrinsic suppression of MMP13 by GC is not rescued by PTH(1-34)

To determine the direct actions of GC and PTH(1-34) on osteocytic activities, we cultured osteocyte-like MLO-Y4 cells with dexamethasone (DEX) with or without PTH(1-34) for 24 hours prior to RNA isolation. Real-time qPCR analysis confirmed the dose-dependent (0.1μM and 1μM) effects of DEX on glucocorticoid-inducible *Atrogin1* and *Murf1* gene expression (Figures 3A, B). Consistent with the previously reported DEX-dependent decrease in *Mmp13* mRNA levels in cultured osteocytes (18), DEX suppresses *Mmp13* expression in an osteocyte-intrinsic manner (Figure 3C). This result suggests that other osteocyte-independent factors may counteract the direct actions of GC on osteocytes to increase *Mmp13* expression in osteocyte-enriched cortical bone *in vivo* (Figure 2). PTH(1-34) did not mitigate suppression of *Mmp13* expression by DEX (Figure 3C). These *in vitro* experiments along with the above *in vivo* studies highlight both cell-intrinsic and non-autonomous actions of GC and PTH(1-34) on osteocytes, and the inability of PTH(1-34) to rescue downregulated *Mmp13* expression of GC on osteocytes.

3.4 GC and PTH(1-34) regulation of articular cartilage and subchondral bone homeostasis

Given that several of the GC and PTH(1-34) regulated genes can participate in bone resorption executed by either osteoclasts or

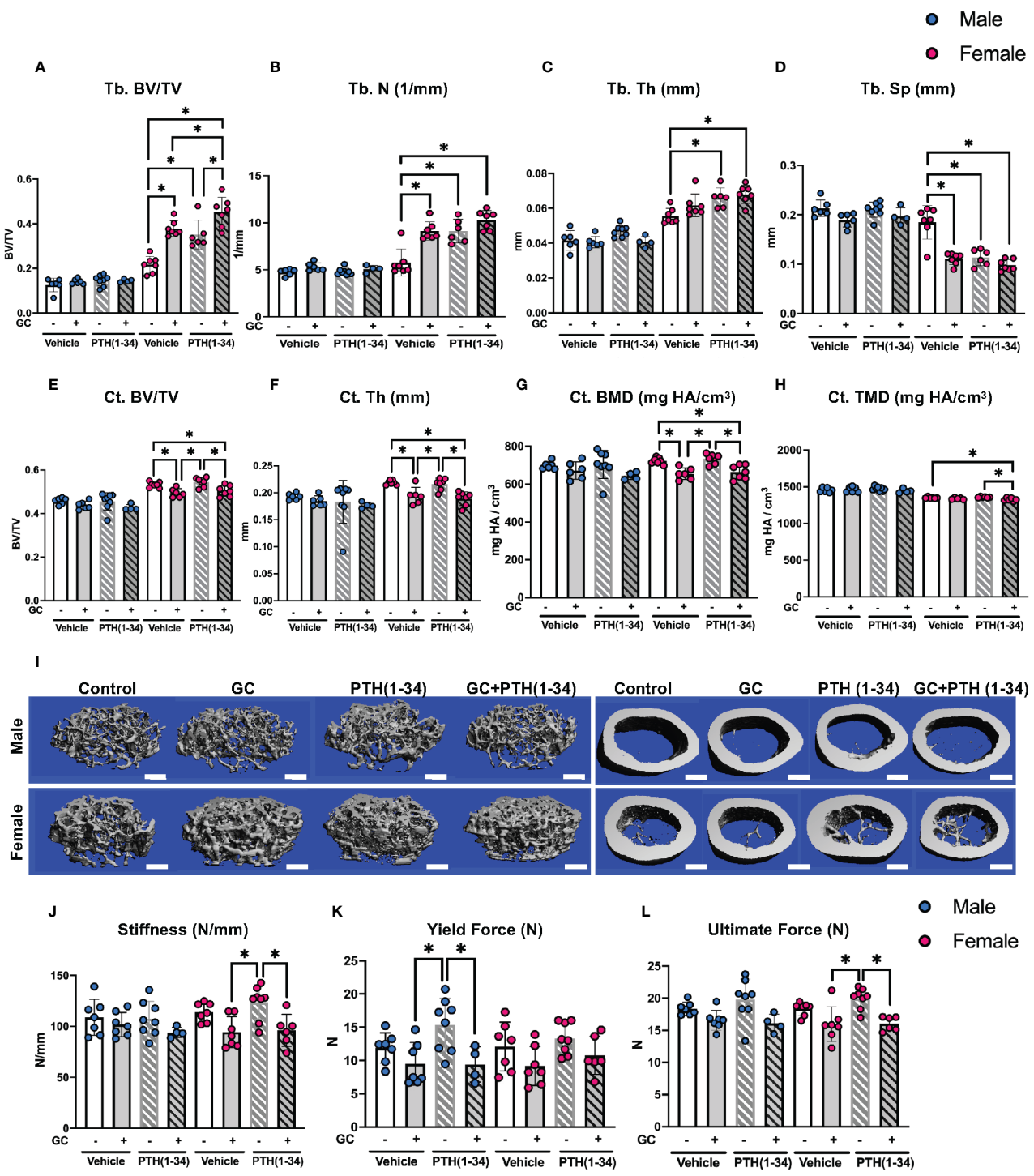

FIGURE 1
GC and PTH(1-34) effects on bone quantity and quality are sexually dimorphic. Femora of 16-week-old control and GC and/or PTH(1-34) treated male (n=4-8/group) and female (n=6-7/group) mice were analyzed using μCT for trabecular (Tb.) **(A–D)** and cortical (Ct.) parameters **(E–H)** on distal femur and mid-femur respectively. Results reveal trabecular bone/volume fraction (Tb. BV/TV, **A**), trabecular number (Tb. N, **B**), trabecular thickness (Tb. Th, **C**), trabecular separation (Tb. Sp, **D**), cortical bone volume fraction (Ct. BV/TV, **E**), cortical thickness (Ct. Th, **F**), cortical bone mineral density (Ct. BMD, **G**), and cortical tissue mineral density (Ct. TMD, **H**). Representative μCT reconstructions display sexual dimorphism (scale bar = 500μm) **(I)**. Three-point bending on male (n=4-8/group) and female (n=6-8/group) left femora show outcomes of flexural strength **(J–L)**. In each graph, male data is displayed as blue dots, with female data displayed as red dots. Data are presented as mean ± SD. Statistically significant differences (*p≤0.05) were determined by two-way ANOVA with *post-hoc* Holm Sidak within sex.

TABLE 2 Mechanical and Material properties of GC and PTH(1-34) treated male and female mice.

Flexural Strength Parameters	Male				Female			
	Control (n=7)	GC (n=7)	PTH(1-34) (n=8)	GC+PTH (1-34) (n=4)	Control (n=7)	GC (n=7)	PTH(1-34) (n=8)	GC+PTH (1-34) (n=6)
Stiffness (N/mm)	108.927 ± 17.683	101.823 ± 11.896	107.614 ± 17.106	94.115 ± 4.989	113.855 ± 9.294	94.414 ± 15.243	123.528 ± 16.690^{b,c}	96.115 ± 15.722
Yield Force (N)	11.887 ± 2.254	9.490 ± 3.205	15.358 ± 3.992$^{\#,\$}$	9.405 ± 2.637	12.089 ± 3.675	9.180 ± 2.943	13.311 ± 2.374	10.788 ± 2.860
Ultimate Force (N)	18.383 ± 0.996	16.581 ± 1.545	19.771 ± 3.214	16.075 ± 1.431	18.336 ± 1.040	15.960 ± 2.736	19.969 ± 1.599^{b,c}	16.038 ± 1.106
Material Property Parameters	**Male**				**Female**			
	Control (n=6)	GC (n=5)	PTH(1-34) (n=7)	GC+PTH (1-34) (n=2)	Control (n=6)	GC (n=5)	PTH(1-34) (n=6)	GC+PTH (1-34) (n=5)
Elastic Modulus (MPa)	117339.527 ± 87134.996	104138.674 ± 100265.754	122768.693 ± 93711.133	69529.000 ± 65118.411	111678.620 ± 81807.547	142092.636 ± 112922.939	945682.682 ± 67164.682	104878.108 ± 111369.976
Yield Stress (MPa)	590.547 ± 336.268	439.776 ± 501.112	717.127 ± 457.459	430.620 ± 414.944	608.432 ± 432.996	628.032 ± 537.062	551.870 ± 396.676	553.454 ± 666.289
Ultimate Stress (MPa)	925.777 ± 551.046	635.606 ± 517.754	974.986 ± 670.455	642.100 ± 466.959	896.548 ± 561.744	1129.804 ± 801.744	782.733 ± 466.431	728.002 ± 658.929

Flexural strength test of right femurs of 16 week old male and female mice were performed by three-point bending. Outcomes on femurs are reported as Stiffness (N/mm), Yield Force (N), and Ultimate Force (N). Material Properties are reported as Elastic Modulus (MPa), Yield Stress (MPa), and Ultimate Stress (MPa). Data are presented as mean ± SD with $^{\#}p \le 0.05$ statistically different from Male GC group, $^{\$}p \le 0.05$ statistically different from Male GC+PTH(1-34) group. $^{b}p \le 0.05$ statistically different from Female GC group, $^{c}p \le 0.05$ statistically different from Female GC+PTH(1-34) group. Statistical differences were determined with two-way ANOVA with post-hoc Holm Sidak.

osteocytes (12, 13, 48, 49), both of which can impact joint homeostasis (19, 50, 51), we sought to determine the effect of these treatments on articular cartilage and subchondral bone. Since microCT (μCT), mechanical testing, and gene expression analysis show greater sensitivity to GC and PTH(1-34) in females in these conditions, the remainder of this study focuses on female mice. The effect of GC and PTH(1-34) on the joint was evaluated in Safranin O/Fast green stained knee joint sections (Figure 4A) using standard OARSI (Figure 4B) (34) and modified Mankin Score (Figure 4C) grading systems (35). Across treatments, no signs of cartilage damage or early onset osteoarthritis were observed in 16-week-old female mice.

Among the catabolic genes induced by GC, PTH(1-34), and GC +PTH(1-34) is *Acp5 (Trap)*, which can be expressed by osteoclasts or by osteocytes engaged in PLR (12, 52). TRAP staining was used to distinguish the cell populations associated with differential *Acp5/Trap* expression in subchondral bone of the female mouse knee (Figure 5; Table 3). While abundant TRAP staining was detected on the surfaces of bony trabeculae, corresponding to osteoclasts (Figures 5B–D), relatively few TRAP-positive osteocytes were detected in any condition (Figure 5A). Quantitative analysis of the % osteoclast surface per bone surface (Oc.S/BS %) (Figure 5D) and number of osteoclast per tissue volume (N.Oc/TV mm^{-2}) (Figure 5G) revealed that GC significantly elevated TRAP activity in the medial subchondral bone, which contributed to the increase in total subchondral bone TRAP activity (Figures 5B, E). TRAP activity was unaltered by PTH(1-34) alone or in combination with GC (Figures B–G). The inability of PTH(1-34) to oppose GC-induced TRAP activity is consistent with their shared trabecular bone phenotype and *Acp5* expression profile.

Both GC and PTH(1-34) regulate osteocytic PLR (12, 18) and the expression of genes implicated in this process, including *Mmp13*, *Atp6v0d2*, and *Ctsk*, as shown previously (13, 18, 53) and in Figure 2. Disruption of the osteocyte lacunocanalicular network (LCN) is a hallmark of PLR suppression that results from GC treatment (18) or from osteocytic ablation of *Mmp13* or *Ctsk* (13, 19, 49). In addition, long-term GC exposure induces osteocyte apoptosis (54, 55). Therefore, to examine the effect of GC and PTH(1-34), alone or in combination, on subchondral bone, osteocyte apoptosis and the LCN were examined histologically using terminal deoxynucleotidyl transferase dUTP nick end labeling (TUNEL) and Ploton silver nitrate stain, respectively. Though some apoptotic marrow cells, osteoclasts, and osteocytes were detected in each condition, the number of TUNEL-positive osteocytes was low and unchanged by GC or PTH(1-34), alone or in combination (Supplementary Figure 3).

Silver staining permits qualitative analysis of canalicular organization (Figure 6A) and quantification of lacunar number (Figure 6B) and lacunae size (Figure 6C) were quantified in each subchondral bone quadrant of the knee. Unlike cortical bone, canalicular organization in trabecular bone is more variable, such that treatment-specific differences in canalicular integrity were not apparent. While GC-dependent differences in lacunar number or size were not observed, PTH(1-34) treatment showed the greatest effect on increased lacunar number in the femur medial compartment (Figure 6B) and decreased lacunar size in the tibia medial compartment (Figure 6C). The elevated number of lacunae and reduced average lacunar size observed with PTH(1-34) treatment is mitigated when combined with GC. This demonstrates that GC and PTH(1-34) effects on the osteocyte LCN in these conditions are mild, and that the modest effect of PTH(1-34) on lacunar size is blocked by exogenous GC.

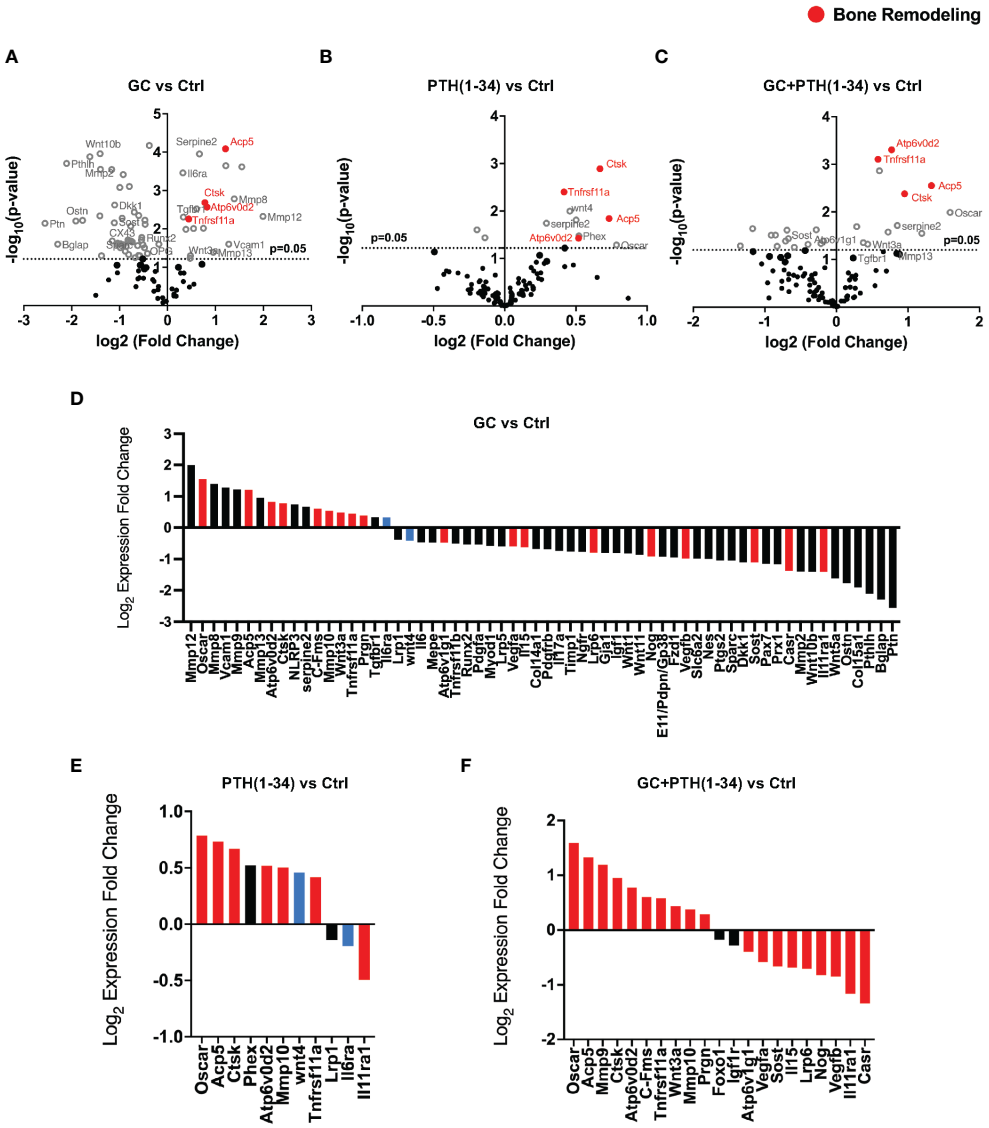

FIGURE 2
GC and PTH(1-34) effects on skeletal gene expression in female cortical bone. Volcano plots of 96 skeletal-associated mouse genes from Nanostring analysis shows significantly up- and down-regulated genes associated with bone remodeling (red dots) in treated (GC, PTH(1-34), and GC+PTH(1-34)) female mice (n=4) compared to controls **(A–C)**. Statistically expressed genes (gray dots) are above the horizontal p-value threshold (dotted gray line) and up-regulated or down-regulated genes fall to either to the right or left sides, respectively. Highly significantly gene expression fold changes was determined by unpaired t-test between experimental groups, normalized to 7 housekeeping genes (*Gapdh, Rpl19, Gilz* (*Tsc22d3*), bone sialoprotein (*Ibsp*), beta-2 microglobulin (*B2m*), beta actin (*Actb*), *Serpine2*). **(D–F)** show statistically up- or down-regulated genes in each condition, with red bars indicating genes that are regulated in the same manner as combined GC+PTH(1-34) treatment, and blue bars indicating genes that are opposingly regulated between GC and PTH(1-34) treatment.

4 Discussion

Given the central role of GC and PTH as powerful endocrine regulators, as well as their widespread therapeutic use, this study advances the field by examining their combined effects on clinically relevant markers of osteocyte function in the context of bone and joint health. GC is a well-established risk factor for osteonecrosis (56) that affects multiple cell types, including osteoblasts, osteoclasts, and osteocytes (6, 55, 57–62). We previously showed evidence of osteocyte PLR suppression in subchondral bone of humans and mice following glucocorticoid treatment (18). Since PTH can stimulate PLR (12, 23, 63), we sought to determine whether PTH(1-34) can oppose the suppression of osteocytic PLR by glucocorticoids in subchondral bone. We examined tissue, cellular, and molecular outcomes in bone from mice treated with or without glucocorticoid, in the presence or absence of parathyroid hormone 1-34. Although prior studies suggested that PTH might be sufficient to reverse some effects of GC on osteocyte PLR, we find that PTH(1-34) either has no effect or exacerbates the catabolic effects of GC on bone in these conditions.

The effects of PTH(1-34) and GC on the skeletal phenotype are sensitive to the treatment dose and timing, and to mouse age, sex, and strain. Here, PTH(1-34) was administered a day after GC pellet implantation, when these two treatments may be antagonizing each

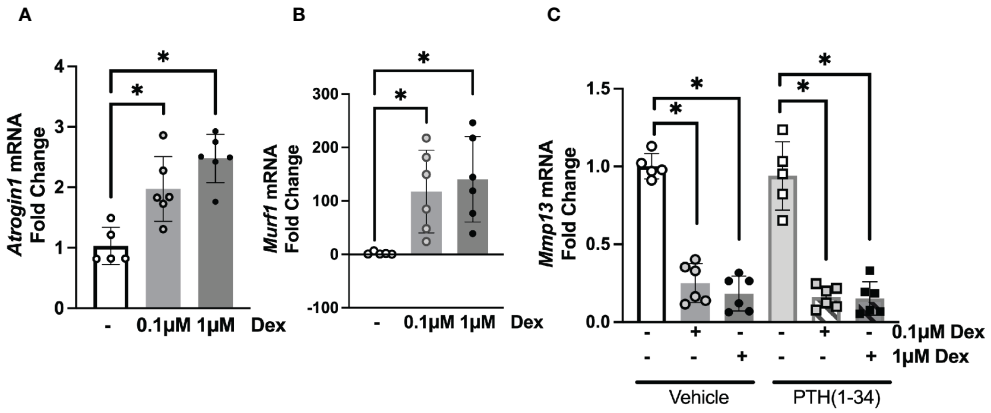

FIGURE 3
Osteocyte-intrinsic suppression of *Mmp13* by GC is not rescued by PTH(1-34). Real-time qPCR analysis on MLO-Y4 cells treated with low (0.1μM) or high (1μM) dose of Dexamethasone (DEX) causes induction of *Atrogin1* **(A)**, *Murf1* **(B)** and dose-dependent down-regulation of *Mmp13* **(C)** mRNA (n=3 replicates/group and 2 independent experiments) normalized to GAPDH. PTH(1-34) did not mitigate effects of GC treatment on *Mmp13* **(C)**. Data is displayed as mean ± SD and statistically significant differences (*p≤0.05) were determined using one-way ANOVA.

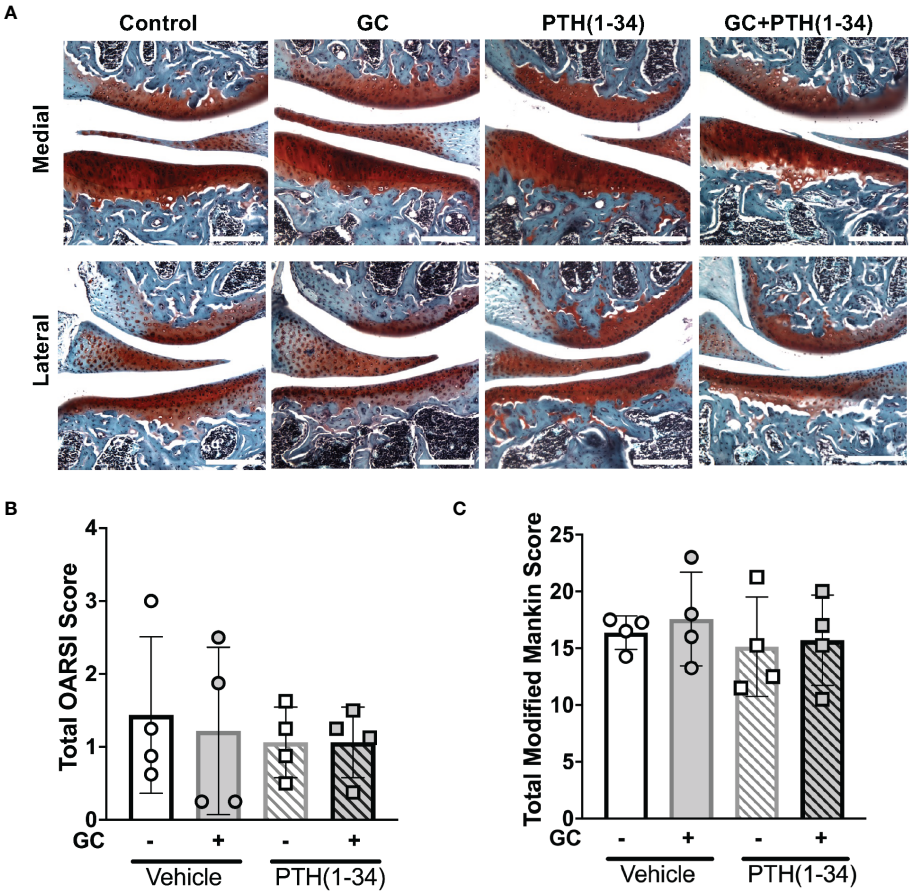

FIGURE 4
Joint and osteoarthritis assessment of GC and PTH(1-34) treated females. Safranin O/Fast Green stain of right knee joints from 16-week-old control and GC and/or PTH(1-34) treated females (n=4/group) show no changes in cartilage (red) and subchondral bone (counterstain blue/green) knee joint phenotypes in representative images (20X, scale bar = 200μm) **(A)**, supported by quantified total OARSI **(B)** and total Modified Mankin Score **(C)**. Data are presented as mean ± SEM and statistically significant differences were determined by two-way ANOVA with *post-hoc* Holm Sidak between experimental groups.

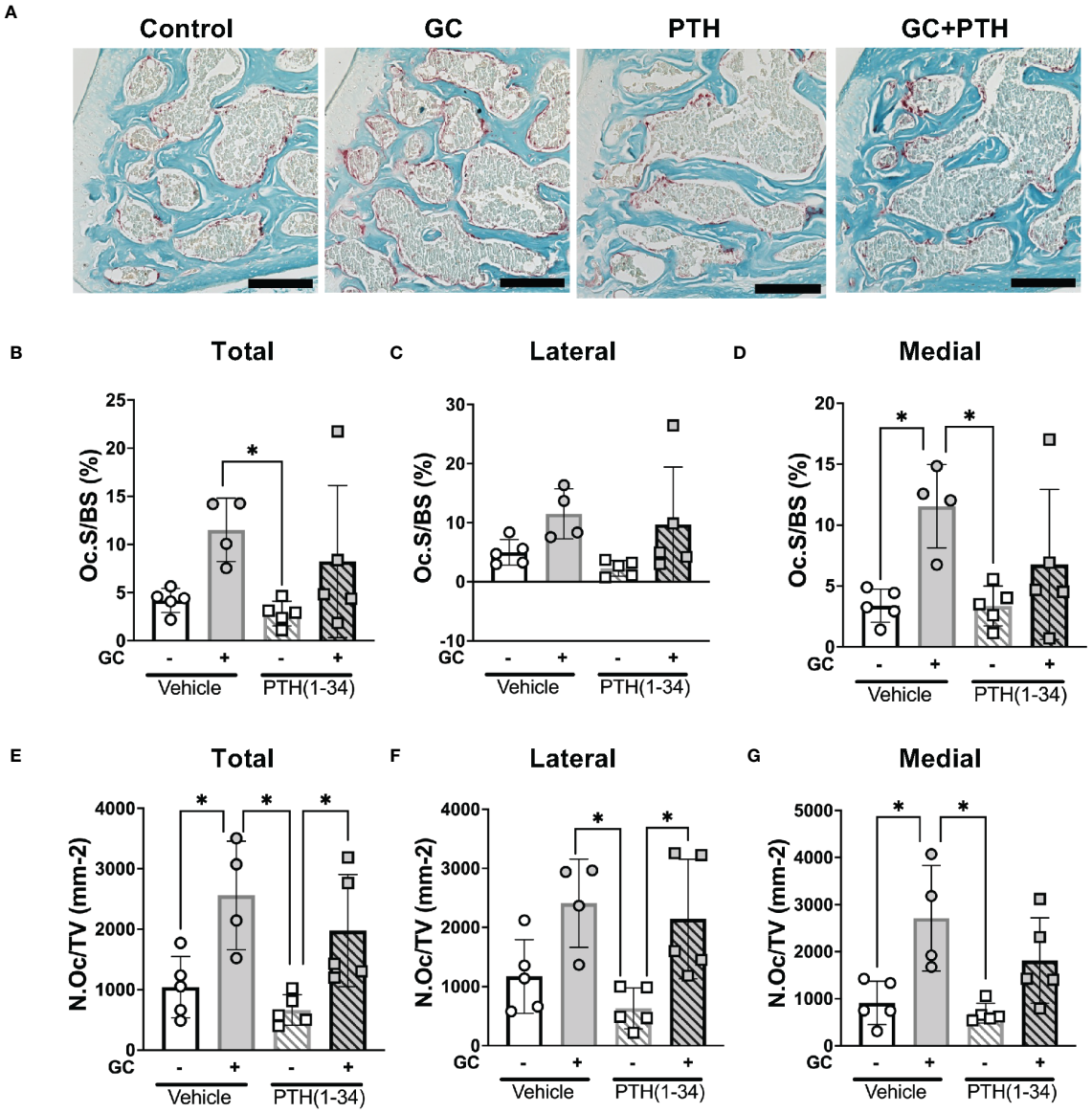

FIGURE 5
Effects of GC and PTH(1-34) on TRAP activity. TRAP staining on subchondral knee sections of control and treated (GC, PTH(1-34), or GC+PTH(1-34)) 16-week-old female mice (n=4-5/group). Representative images from each condition (**A** 20X, scalebar = 200 μm) provide visualization of TRAP+ stained cells (red), counterstained in methyl green. Quantification of Osteoclast Surface per Bone Surface (Oc.S/BS %) and Number of Osteoclasts per Tissue Volume (N.Oc/TV mm^{-2}) were analyzed in each joint compartment (femur, tibia, medial, lateral) and displayed as total **(B, E)**, lateral **(C, F)**, and medial **(D, G)**. Data are presented as mean ± SD and statistically significant differences (*$p \leq 0.05$) were determined by two-way ANOVA with *post-hoc* Tukey was performed between experimental groups.

other. Others have also observed attenuated anabolic effects of PTH (1-34) or abaloparatide, a parathyroid hormone-related peptide analog, in the presence of GC (24, 64, 65). PTH(1-34) may have shown a more robust effect if its administration after GC pellet implantation was delayed. For example, the loss of trabecular bone and decreased bone quality in GC-treated Swiss-Webster mice was restored by PTH(1-34) that was administered 28 days post-GC treatment (4). Optimal anabolic effects were reported in male mice treated with PTH of 30-60 μg/kd/day for 5-6 weeks beginning after 12 weeks of age (66). Treatments in this study commenced at 13 weeks of age and continued for 3 weeks with a higher dose of PTH (1-34) of 80 μg/kd/day. Greater anabolic effects of PTH(1-34) treatment may have been observed if treatment length was extended beyond 21 days and if PTH(1-34) treatment was delayed post-GC pellet implant.

Here we observe sexual dimorphism in the skeletal response to GC and PTH(1-34) treatment, where female mice are more sensitive to GC and PTH(1-34) compared to males. GC is known to have dimorphic effects, such that female mice are more sensitive to glucocorticoid-induced muscle atrophy (67), possibly due to differences in how GC is metabolized (68). In our study, GC induces more trabecular bone formation and cortical bone loss in female mice, highlighting GC's region-dependent effects on the bone phenotype. Similar sex-specific differences

TABLE 3 Bone resorption parameters of GC and PTH(1-34) treated female mice.

Bone Resorption Parameters	Female Control *(n=5)*	GC *(n=4)*	PTH(1-34) *(n=5)*	GC+PTH(1-34) *(n=5)*
Total				
Oc.S/BS (%)	4.180 ± 2.405	11.517 ± 4.091	2.827 ± 1.714[b]	8.235 ± 7.717
N.Oc/TV (mm^{-2})	1041.311 ± 617.545	2561.002 ± 1157.082[a]	661.324 ± 357.464[b,c]	1976.699 ± 927.426
Lateral				
Oc.S/BS (%)	5.068 ± 2.471	11.488 ± 4.577	2.013 ± 1.481	8.429 ± 9.293
N.Oc/TV (mm^{-2})	1120.549 ± 662.070	2409.868 ± 987.548	556.028 ± 379.503[b,c]	1900.331 ± 975.607
Medial				
Oc.S/BS (%)	3.382 ± 2.167	11.546 ± 3.862[a]	3.363 ± 1.835 [b]	6.769 ± 5.882
N.Oc/TV (mm^{-2})	911.490 ± 573.854	2712.136 ± 1357.012[a]	690.619 ± 351.894[b]	1810.291 ± 895.802

Tartrate-resistant acid phosphatase (TRAP) activity of the right knee subchondral bone regions of 16 week old female mice was detected by TRAP staining. Quantification on TRAP stains are reported as: Osteoclast Surface (Oc.S), Bone Surface (BS), Number of Osteoclasts (N.Oc) and Tissue Volume (TV). Data are presented as mean ± SD with [a]$p \leq 0.05$ statistically different from Control group, [b]$p \leq 0.05$ statistically different from GC group, [c]$p \leq 0.05$ statistically different from GC+PTH(1-34) group. Statistical differences were determined with two-way ANOVA with post-hoc Tukey.

were previously reported in C57BL/6 mice treated with prednisolone, with females more sensitive to glucocorticoid induced cortical bone loss and fragility than males (69). Although the increased trabecular bone may seem contrary to the well-defined GC-induced bone loss (70), the effects of GC on bone are sensitive to many factors, including the background strain of the mice (70–72), age, and dosing regimen. Other studies report elevated trabecular bone in female mice (73) and unaltered trabecular bone in the lumbar vertebrae of male rats (74). This study used FVB mice, which are the most susceptible strain to study GC-induced osteonecrosis, but at 13-weeks of age, they may be less sensitive to the catabolic action of GC on trabecular bone. Indeed, the effects of GC are age-dependent, such that others have shown that GC's effect on trabecular bone is unchanged (70, 72, 75, 76) or elevated (75) in younger mice. Another variable to consider is GC dosing effects, as shorter exposure to higher dose GC (77) or prolonged lower dose GC (40) treatment in younger mice can cause bone loss. As expected, PTH(1-34) effects on the skeletal phenotype also show sexual dimorphism (78, 79), where females are more sensitive to PTH(1-34) than males. The anabolic effects of PTH(1-34) on trabecular and cortical bone in females are blocked in the presence of GC. An increase in cortical porosity may contribute to the effect of PTH(1-34) on microCT (μCT) and mechanical outcomes observed here (80). Collectively, these studies highlight the critical role of biological variables in determining the effects of GC and PTH(1-34) on the skeleton, including age, sex, dose, and duration of the treatments.

Sexual dimorphic effects of glucocorticoid excess have also been observed in humans. For example, males with Cushing's syndrome, a condition with elevated glucocorticoid exposure, are more susceptible to osteoporosis, while females experience more metabolic symptoms such as hyperglycemia, obesity, and hyperlipidemia (68). On the other hand, female liver transplant patients on chronic glucocorticoid therapy have a higher risk of fracture than males (81). Other rodent studies show sexually dimorphic responses to glucocorticoids in metabolism (68, 82), inflammation (83, 84), skeletal muscle (85), stress responses (86), and liver, heart, and adipose tissues (68), all of which can exert primary or secondary effects on bone. The mechanisms by which glucocorticoids cause sexually dimorphic skeletal responses require further study.

Our prior studies supported the conclusion that GC suppressed PLR through osteocyte-intrinsic suppression of genes required for resorption of the peri-osteocytic bone matrix, such as *Mmp13* (18). Although the current study also shows GC-dependent repression of *Mmp13* mRNA levels in cultured osteocytes, prolonged treatment of GC increases mRNA levels for *Mmp13*. In addition, GC treatment of female mice for 21 days increased levels of many other catabolic genes in cortical bone, including *Ctsk, Acp5, Tnfrsf11a, Atp6v0d2*. Since these genes participate in bone resorption by both osteoclasts and osteocytes, it was unclear which cell type was the target of GC effects on gene expression. We observed significant changes in osteoclast TRAP activity, but the osteocyte-intrinsic effects of GC in this study are insufficient to explain the effect of GC on cortical bone gene expression, and may relate to acute vs. chronic effects of GC. Importantly, PTH(1-34), alone or in combination with GC, did not mitigate the induction of catabolic genes. Similar results were observed when GC blunted effects of the PTHrP analog, abaloparatide, on femoral bone mass and strength (24). These molecular findings support the tissue-level conclusions that PTH(1-34) does not oppose the effects of GC in osteocytes.

The recovery of bone following elevated glucocorticoid exposure has been examined in many clinical and preclinical studies. Following discontinuation of glucocorticoid use, patients have shown full (87) or partial recovery of bone mineral density bone (88) and decreased fracture risk (89, 90). Patients with Cushing's disease show recovery of bone mineralization after 6 months of disease remission, with fracture risk decreasing to baseline levels in controls after 9-15 months (91). Despite

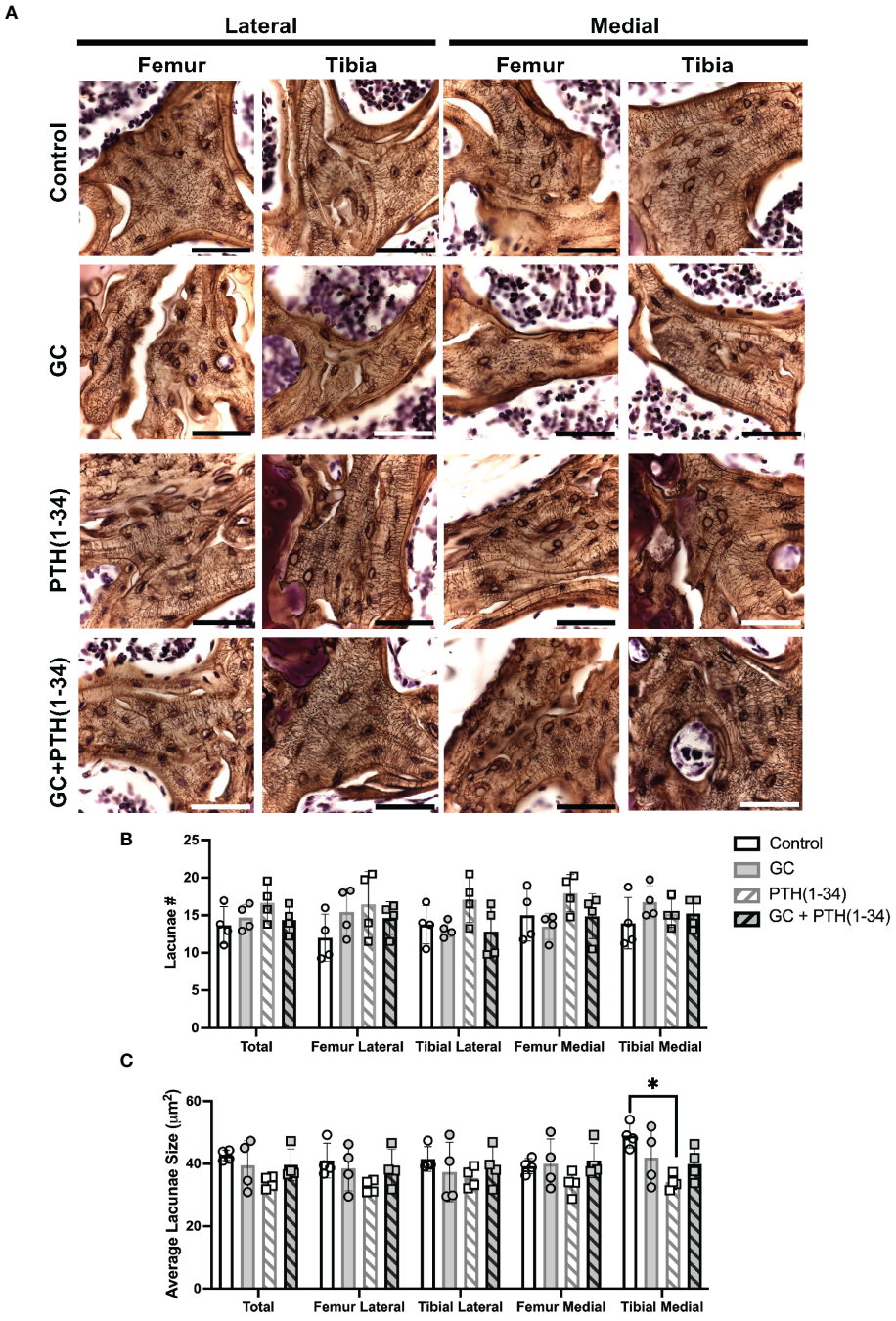

FIGURE 6
Subchondral bone assessment of GC and/or PTH(1-34) treated female mouse knees. Representative high-resolution images (100X, scale bar = 50 μm) of the right knee joints of control and treated (GC, PTH(1-34), or GC+PTH(1-34)) females at 16-week-old (n=4/group) stained with Ploton silver nitrate stain and counterstained with Cresyl Violet show the subchondral bone lacunocanalicular network (LCN) **(A)**. Quantitative analysis of the number (#) of lacunae **(B)** and average lacunae size **(C)** shows treatment effects on the LCN in each joint compartments (femur, tibia, medial, lateral). Data are presented as mean ± SD, and statistically significant differences (*p≤0.05) were determined by unpaired t-test between experimental groups.

recovery of bone density and fracture resistance, the effects of glucocorticoids on bone material properties remain (91). Supporting the persistent effects of glucocorticoids on bone, within 3 months after glucocorticoid withdrawal, rats showed partial recovery of bone loss but still have impaired bone quality (92). A better understanding of the reversibility of glucocorticoid effects on bone quality is especially relevant for glucocorticoid-induced osteonecrosis (18, 93, 94), and for post-menopausal women with long-term glucocorticoid use, whose risk of vertebral fractures is higher than expected based on their bone mineral density (58, 95).

Pathological changes in subchondral bone structure, mechanics, and vascularity are closely linked to the progression of post-traumatic osteoarthritis and osteonecrosis (93, 96, 97). Changes in PLR homeostasis can alter the subchondral bone and precede changes in joint homeostasis (18–20). When we examined the effect of GC and PTH(1-34) on articular cartilage histologically,

no differences in OARSI or Modified Mankin scores were observed. The lack of an effect on articular cartilage may result from biological variables that blunted the effect of GC, as previously mentioned. It is possible that GC and PTH(1-34)-dependent effects on the joint (98–102) would be more apparent with injury, since suppressed PLR exacerbated post-traumatic osteoarthritis in male mice with an osteocyte-intrinsic deletion of transforming growth factor, beta receptor II (*Tgfβr2*) (20).

This study has limitations, including the complexity of biological variables in the effects of GC and PTH(1-34) in the selected conditions, and the need to challenge the joint with injury, age, or diet in order to adequately assess the effect of GC and PTH (1-34) on joint homeostasis. As noted above, some of the effects of GC treatment, including on osteocyte lacunocanalicular outcomes, differed from our prior observations (18) and expectations. Our prior study examined PLR in an established model of GC-induced osteonecrosis (93), whereas the current study employed a less severe GC treatment model to test the ability of PTH(1-34) to recover GC-suppressed PLR. Contrary to the LCN degeneration we previously observed in a model of GC-induced osteonecrosis (18), the effects of GC on the osteocyte LCN were not apparent in the milder conditions chosen here. Though this limits our ability to test the hypothesis that PTH(1-34) mitigates the effects of GC on the LCN, results at the tissue, cellular, and molecular scale consistently show the inability of PTH(1-34) to overcome the effects of GC. Additional studies, such as ptychographic x-ray computed tomography (103), backscatter scanning electron microscopy (12), or confocal imaging of phalloidin/DiI stained bone (104) will be needed to identify strategies to rescue PLR suppression in osteocytes. If identified, PLR agonists may have potential to mitigate the loss of bone and joint homeostasis that occurs with glucocorticoid treatment, aging, or other conditions in which PLR is suppressed.

Data availability statement

The datasets generated for this study are included in the article/Supplementary Materials. Further inquiries can be directed to the corresponding author. The Nanostring data discussed in this publication have been deposited in the NCBI's Gene Expression Omnibus (Yee et al., 2025) and are accessible through GEO Series accession number GSE252085 (https://www.ncbi.nlm.nih.gov/geo/query/acc.cgi?acc=GSE252085).

Ethics statement

The animal study was approved by Institutional Animal Care and Use Committee (IACUC) at the University of California, San Francisco. The study was conducted in accordance with the local legislation and institutional requirements.

Author contributions

CY: Data curation, Formal analysis, Investigation, Methodology, Visualization, Writing – original draft. CM: Data curation, Formal analysis, Investigation, Writing – review & editing. SK: Data curation, Formal analysis, Investigation, Writing – review & editing. WC: Conceptualization, Data curation, Formal analysis, Funding acquisition, Methodology, Visualization, Writing – review & editing. TA: Conceptualization, Formal analysis, Funding acquisition, Methodology, Visualization, Writing – review & editing.

Funding

The author(s) declare financial support was received for the research, authorship, and/or publication of this article. This research was supported by U.S. Department of Defense (DOD) Congressionally Directed Medical Research Program (CDMRP) W81XWH-18-0155 and NIH R01DE019284-11A1 and P30AR075055-01 (to TA), U.S. NIH grants RF1AG075742 and Department of Veteran Affairs BLR&D I01BX005851 and IK6BX004835 (to WC).

Acknowledgments

The authors gratefully acknowledge Clarissa Aguirre Luna and Winston Zapet Bamac for assistance with histological analysis, Jennifer Salinas for *in vivo* technical assistance, Jihee Yoon for cell culture technical assistance, Stephanie Boula for mechanical testing assistance, and Reyna Villa for histological imaging. Research reported in this publication was supported by the National Institute of Arthritis and Musculoskeletal and Skin Disease of the National Institutes of Health under Award number P30AR075055. The content is solely the responsibility of the authors and does not necessarily represent the official views of the National Institutes of Health. The authors gratefully acknowledge the collaboration with our colleagues in the San Francisco Veteran's Administration Medical Center (SF-VAMC) Endocrine Unit.

Conflict of interest

The authors declare that the research was conducted in the absence of any commercial or financial relationships that could be construed as a potential conflict of interest.

Publisher's note

Supplementary material

The Supplementary Material for this article can be found online at: https://www.frontiersin.org/articles/10.3389/fendo.2024.1342938/full#supplementary-material

References

1. Saag KG, Shane E, Boonen S, Marin F, Donley DW, Taylor KA, et al. Teriparatide or alendronate in glucocorticoid-induced osteoporosis. *N Engl J Med*. (2007) 357:2028–39. doi: 10.1056/NEJMoa071408

2. Crandall C. Parathyroid hormone for treatment of osteoporosis. *Arch Intern Med*. (2002) 162:2297–309. doi: 10.1001/archinte.162.20.2297

3. Wiedmeier SE, Samlowski WE, Rasmussen CJ, Huang K, Daynes RA. Effect of ionizing radiation on thymic epithelial cell function. I. Radiation-spared thymic epithelial grafts expedite the recovery of T cell function in lethally irradiated and fetal liver reconstituted mice. *J Immunol*. (1988) 140:21–9. doi: 10.4049/jimmunol.140.1.21

4. Yao W, Cheng Z, Pham A, Busse C, Zimmermann EA, Ritchie RO, et al. Glucocorticoid-induced bone loss in mice can be reversed by the actions of parathyroid hormone and risedronate on different pathways for bone formation and mineralization. *Arthritis Rheum*. (2008) 58:3485–97. doi: 10.1002/art.23954

5. Skripitz R, Andreassen TT, Aspenberg P. Parathyroid hormone (1-34) increases the density of rat cancellous bone in a bone chamber. *A Dose-Response Study. J Bone Joint Surg Br*. (2000) 82:138–41. doi: 10.1302/0301-620X.82B1.9729

6. Lane NE, Yao W, Balooch M, Nalla RK, Balooch G, Habelitz S, et al. Glucocorticoid-treated mice have localized changes in trabecular bone material properties and osteocyte lacunar size that are not observed in placebo-treated or estrogen-deficient mice. *J Bone Miner Res*. (2006) 21:466–76. doi: 10.1359/JBMR.051103

7. Lane NE. Glucocorticoid-induced osteoporosis: new insights into the pathophysiology and treatments. *Curr Osteoporos Rep*. (2019) 17:1–7. doi: 10.1007/s11914-019-00498-x

8. Uda Y, Saini V, Petty CA, Alshehri M, Shi C, Spatz JM, et al. Parathyroid hormone signaling in mature osteoblasts/osteocytes protects mice from age-related bone loss. *Aging (Albany NY)*. (2021) 13:25607–42. doi: 10.18632/aging.v13i24

9. Saini V, Marengi DA, Barry KJ, Fulzele KS, Heiden E, Liu X, et al. Parathyroid hormone (Pth)/pth-related peptide type 1 receptor (Ppr) signaling in osteocytes regulates anabolic and catabolic skeletal responses to pth. *J Biol Chem*. (2013) 288:20122–34. doi: 10.1074/jbc.M112.441360

10. Bellido T, Saini V, Pajevic PD. Effects of pth on osteocyte function. *Bone*. (2013) 54:250–7. doi: 10.1016/j.bone.2012.09.016

11. Rhee Y, Allen MR, Condon K, Lezcano V, Ronda AC, Galli C, et al. Pth receptor signaling in osteocytes governs periosteal bone formation and intracortical remodeling. *J Bone Miner Res*. (2011) 26:1035–46. doi: 10.1002/jbmr.304

12. Qing H, Ardeshirpour L, Pajevic PD, Dusevich V, Jahn K, Kato S, et al. Demonstration of osteocytic perilacunar/canalicular remodeling in mice during lactation. *J Bone Miner Res*. (2012) 27:1018–29. doi: 10.1002/jbmr.1567

13. Tang SY, Herber RP, Ho SP, Alliston T. Matrix metalloproteinase-13 is required for osteocytic perilacunar remodeling and maintains bone fracture resistance. *J Bone Miner Res*. (2012) 27:1936–50. doi: 10.1002/jbmr.1646

14. Bonewald LF. The amazing osteocyte. *J Bone Miner Res*. (2011) 26:229–38. doi: 10.1002/jbmr.320

15. Liu L, Guo J, Chen X, Tong X, Xu J, Zou J. The role of irisin in exercise-mediated bone health. *Front Cell Dev Biol*. (2021) 9:668759. doi: 10.3389/fcell.2021.668759

16. Inoue K, Mikuni-Takagaki Y, Oikawa K, Itoh T, Inada M, Noguchi T, et al. A crucial role for matrix metalloproteinase 2 in osteocytic canalicular formation and bone metabolism. *J Biol Chem*. (2006) 281:33814–24. doi: 10.1074/jbc.M607290200

17. Dole NS, Mazur CM, Acevedo C, Lopez JP, Monteiro DA, Fowler TW, et al. Osteocyte-intrinsic tgf-beta signaling regulates bone quality through perilacunar/canalicular remodeling. *Cell Rep*. (2017) 21:2585–96. doi: 10.1016/j.celrep.2017.10.115

18. Fowler TW, Acevedo C, Mazur CM, Hall-Glenn F, Fields AJ, Bale HA, et al. Glucocorticoid suppression of osteocyte perilacunar remodeling is associated with subchondral bone degeneration in osteonecrosis. *Sci Rep*. (2017) 7:44618. doi: 10.1038/srep44618

19. Mazur CM, Woo JJ, Yee CS, Fields AJ, Acevedo C, Bailey KN, et al. Osteocyte dysfunction promotes osteoarthritis through mmp13-dependent suppression of subchondral bone homeostasis. *Bone Res*. (2019) 7:34. doi: 10.1038/s41413-019-0070-y

20. Bailey KN, Nguyen J, Yee CS, Dole NS, Dang A, Alliston T. Mechanosensitive control of articular cartilage and subchondral bone homeostasis in mice requires osteocytic transforming growth factor beta signaling. *Arthritis Rheumatol*. (2021) 73:414–25. doi: 10.1002/art.41548

21. Ponnapakkam T, Katikaneni R, Sakon J, Stratford R, Gensure RC. Treating osteoporosis by targeting parathyroid hormone to bone. *Drug Discov Today*. (2014) 19:204–8. doi: 10.1016/j.drudis.2013.07.015

22. Yuan C, Liang Y, Zhu K, Xie W. Clinical efficacy of denosumab, teriparatide, and oral bisphosphonates in the prevention of glucocorticoid-induced osteoporosis: A systematic review and meta-analysis. *J Orthop Surg Res*. (2023) 18:447. doi: 10.1186/s13018-023-03920-4

23. Wein MN. Parathyroid hormone signaling in osteocytes. *JBMR Plus*. (2018) 2:22–30. doi: 10.1002/jbm4.10021

24. Brent MB, Thomsen JS, Bruel A. Short-term glucocorticoid excess blunts abaloparatide-induced increase in femoral bone mass and strength in mice. *Sci Rep*. (2021) 11:12258. doi: 10.1038/s41598-021-91729-8

25. Zhou X, Lin MF, Wu LH, Huang LH, Xie HN. Enlarged cavum septi pellucidi Z-scores in fetuses with trisomy 18. *J Matern Fetal Neonatal Med*. (2022) 35:981–6. doi: 10.1080/14767058.2020.1742321

26. Bouxsein ML, Boyd SK, Christiansen BA, Guldberg RE, Jepsen KJ, Muller R. Guidelines for assessment of bone microstructure in rodents using micro-computed tomography. *J Bone Miner Res*. (2010) 25:1468–86. doi: 10.1002/jbmr.141

27. Yoon J, Kaya S, Matsumae G, Dole N, Alliston T. Mir181a/B-1 controls osteocyte metabolism and mechanical properties independently of bone morphology. *Bone*. (2023) 175:116836. doi: 10.1016/j.bone.2023.116836

28. Turner CH, Burr DB. Basic biomechanical measurements of bone: A tutorial. *Bone*. (1993) 14:595–608. doi: 10.1016/8756-3282(93)90081-K

29. Jepsen KJ, Silva MJ, Vashishth D, Guo XE, van der Meulen MC. Establishing biomechanical mechanisms in mouse models: practical guidelines for systematically evaluating phenotypic changes in the diaphyses of long bones. *J Bone Miner Res*. (2015) 30:951–66. doi: 10.1002/jbmr.2539

30. Veldman-Jones MH, Brant R, Rooney C, Geh C, Emery H, Harbron CG, et al. Evaluating robustness and sensitivity of the nanostring technologies ncounter platform to enable multiplexed gene expression analysis of clinical samples. *Cancer Res*. (2015) 75:2587–93. doi: 10.1158/0008-5472.CAN-15-0262

31. Geiss GK, Bumgarner RE, Birditt B, Dahl T, Dowidar N, Dunaway DL, et al. Direct multiplexed measurement of gene expression with color-coded probe pairs. *Nat Biotechnol*. (2008) 26:317–25. doi: 10.1038/nbt1385

32. Rao X, Huang X, Zhou Z, Lin X. An improvement of the 2^(-delta delta ct) method for quantitative real-time polymerase chain reaction data analysis. *Biostat Bioinforma Biomath*. (2013) 3:71–85.

33. *Safranin O/fast green stain for cartilage*. University of Rochester Center for Musculoskeletal Research (2017). Available at: https://www.urmc.rochester.edu/medialibraries/urmcmedia/musculoskeletal-research/core-services/histology/documents/SafraninOStainingProtocol.pdf.

34. Glasson SS, Chambers MG, Van Den Berg WB, Little CB. The oarsi histopathology initiative – recommendations for histological assessments of osteoarthritis in the mouse. *Osteoarthritis Cartilage*. (2010) 18:S17–23. doi: 10.1016/j.joca.2010.05.025

35. Furman F, Strand J, Chad W, Ward B, Farshud G, Olson S. Joint degeneration following closed intraarticular fracture in the mouse knee: A model of posttraumatic arthritis. *J Orthop Res*. (2007) 25:578–92. doi: 10.1002/jor.20331PMID-17266145

36. van 't Hof RJ, Rose L, Bassonga E, Daroszewska A. Open source software for semi-automated histomorphometry of bone resorption and formation parameters. *Bone*. (2017) 99:69–79. doi: 10.1016/j.bone.2017.03.051

37. Dole NS, Yee CS, Schurman CA, Dallas SL, Alliston T. Assessment of osteocytes: techniques for studying morphological and molecular changes associated with perilacunar/canalicular remodeling of the bone matrix. *Methods Mol Biol*. (2021) 2230:303–23. doi: 10.1007/978-1-0716-1028-2_17

38. Mazur CM, Castro Andrade CD, Tokavanich N, Sato T, Bruce M, Brooks DJ, et al. Partial prevention of glucocorticoid-induced osteocyte deterioration in young male mice with osteocrin gene therapy. *iScience*. (2022) 25:105019. doi: 10.1016/j.isci.2022.105019

39. Piemontese M, Xiong J, Fujiwara Y, Thostenson JD, O'Brien CA. Cortical bone loss caused by glucocorticoid excess requires rankl production by osteocytes and is associated with reduced opg expression in mice. *Am J Physiol Endocrinol Metab*. (2016) 311:E587–93. doi: 10.1152/ajpendo.00219.2016

40. Sato AY, Cregor M, Delgado-Calle J, Condon KW, Allen MR, Peacock M, et al. Protection from glucocorticoid-induced osteoporosis by anti-catabolic signaling in the absence of sost/sclerostin. *J Bone Miner Res*. (2016) 31:1791–802. doi: 10.1002/jbmr.2869

41. Newmann JP. Gender, life strains, and depression. *J Health Soc Behav*. (1986) 27:161–78. doi: 10.2307/2136314

42. von Stechow D, Zurakowski D, Pettit AR, Muller R, Gronowicz G, Chorev M, et al. Differential transcriptional effects of pth and estrogen during anabolic bone formation. *J Cell Biochem*. (2004) 93:476–90. doi: 10.1002/jcb.20174

43. Li X, Liu H, Qin L, Tamasi J, Bergenstock M, Shapses S, et al. Determination of dual effects of parathyroid hormone on skeletal gene expression in vivo by microarray and network analysis. *J Biol Chem*. (2007) 282:33086–97. doi: 10.1074/jbc.M705194200

44. Keller H, Kneissel M. Sost is a target gene for pth in bone. *Bone*. (2005) 37:148–58. doi: 10.1016/j.bone.2005.03.018

45. Bellido T, Ali AA, Gubrij I, Plotkin LI, Fu Q, O'Brien CA, et al. Chronic elevation of parathyroid hormone in mice reduces expression of sclerostin by osteocytes: A novel mechanism for hormonal control of osteoblastogenesis. *Endocrinology*. (2005) 146:4577–83. doi: 10.1210/en.2005-0239

46. Bellido T. Downregulation of sost/sclerostin by pth: A novel mechanism of hormonal control of bone formation mediated by osteocytes. *J Musculoskelet Neuronal Interact*. (2006) 6:358–9.

47. Lee M, Partridge NC. Parathyroid hormone signaling in bone and kidney. *Curr Opin Nephrol Hypertens*. (2009) 18:298–302. doi: 10.1097/MNH.0b013e32832c2264

48. Jähn K, Kelkar S, Zhao H, Xie Y, Tiede-Lewis LM, Dusevich V, et al. Osteocytes acidify their microenvironment in response to pthrp in vitro and in lactating mice in vivo. *J Bone Mineral Res*. (2017) 32:1761–72. doi: 10.1002/jbmr.3167

49. Lotinun S, Ishihara Y, Nagano K, Kiviranta R, Carpentier VT, Neff L, et al. Cathepsin K-deficient osteocytes prevent lactation-induced bone loss and parathyroid hormone suppression. *J Clin Invest*. (2019) 129:3058–71. doi: 10.1172/JCI122936

50. Park DR, Kim J, Kim GM, Lee H, Kim M, Hwang D, et al. Osteoclast-associated receptor blockade prevents articular cartilage destruction via chondrocyte apoptosis regulation. *Nat Commun*. (2020) 11:4343. doi: 10.1038/s41467-020-18208-y

51. Kozawa E, Nishida Y, Cheng XW, Urakawa H, Arai E, Futamura N, et al. Osteoarthritic change is delayed in a ctsk-knockout mouse model of osteoarthritis. *Arthritis Rheum*. (2012) 64:454–64. doi: 10.1002/art.33398

52. Burstone MS. Histochemical demonstration of acid phosphatase activity in osteoclasts. *J Histochem Cytochem*. (1959) 7:39–41. doi: 10.1177/7.1.39

53. Dole NS, Yee CS, Mazur CM, Acevedo C, Alliston T. Tgfbeta regulation of perilacunar/canalicular remodeling is sexually dimorphic. *J Bone Miner Res*. (2020) 35:1549–61. doi: 10.1002/jbmr.4023

54. O'Brien CA, Jia D, Plotkin LI, Bellido T, Powers CC, Stewart SA, et al. Glucocorticoids act directly on osteoblasts and osteocytes to induce their apoptosis and reduce bone formation and strength. *Endocrinology*. (2004) 145:1835–41. doi: 10.1210/en.2003-0990

55. Plotkin LI, Manolagas SC, Bellido T. Glucocorticoids induce osteocyte apoptosis by blocking focal adhesion kinase-mediated survival. *Evidence inside-out Signaling Leading to Anoikis. J Biol Chem*. (2007) 282:24120–30. doi: 10.1074/jbc.M611435200

56. Assouline-Dayan Y, Chang C, Greenspan A, Shoenfeld Y, Gershwin ME. Pathogenesis and natural history of osteonecrosis. *Semin Arthritis Rheum*. (2002) 32:94–124. doi: 10.1053/sarh.2002.33724b

57. Kerachian MA, Seguin C, Harvey EJ. Glucocorticoids in osteonecrosis of the femoral head: A new understanding of the mechanisms of action. *J Steroid Biochem Mol Biol*. (2009) 114:121–8. doi: 10.1016/j.jsbmb.2009.02.007

58. Weinstein RS. Glucocorticoid-induced osteoporosis and osteonecrosis. *Endocrinol Metab Clin North Am*. (2012) 41:595–611. doi: 10.1016/j.ecl.2012.04.004

59. Weinstein RS, Jilka RL, Parfitt AM, Manolagas SC. Inhibition of osteoblastogenesis and promotion of apoptosis of osteoblasts and osteocytes by glucocorticoids. *Potential Mech Their Deleterious Effects Bone J Clin Invest*. (1998) 102:274–82. doi: 10.1172/JCI2799

60. Gado M, Baschant U, Hofbauer LC, Henneicke H. Bad to the bone: the effects of therapeutic glucocorticoids on osteoblasts and osteocytes. *Front Endocrinol (Lausanne)*. (2022) 13:835720. doi: 10.3389/fendo.2022.835720

61. Hartmann K, Koenen M, Schauer S, Wittig-Blaich S, Ahmad M, Baschant U, et al. Molecular actions of glucocorticoids in cartilage and bone during health, disease, and steroid therapy. *Physiol Rev*. (2016) 96:409–47. doi: 10.1152/physrev.00011.2015

62. Sato AY, Peacock M, Bellido T. Glucocorticoid excess in bone and muscle. *Clin Rev Bone mineral Metab*. (2018) 16:33–47. doi: 10.1007/s12018-018-9242-3

63. Gardinier JD, Al-Omaishi S, Morris MD, Kohn DH. Pth signaling mediates perilacunar remodeling during exercise. *Matrix Biol*. (2016) 52-54:162–75. doi: 10.1016/j.matbio.2016.02.010

64. Oxlund H, Ortoft G, Thomsen JS, Danielsen CC, Ejersted C, Andreassen TT. The anabolic effect of pth on bone is attenuated by simultaneous glucocorticoid treatment. *Bone*. (2006) 39:244–52. doi: 10.1016/j.bone.2006.01.142

65. Postnov A, De Schutter T, Sijbers J, Karperien M, De Clerck N. Glucocorticoid-induced osteoporosis in growing mice is not prevented by simultaneous intermittent pth treatment. *Calcif Tissue Int*. (2009) 85:530–7. doi: 10.1007/s00223-009-9301-3

66. Zweifler LE, Koh AJ, Daignault-Newton S, McCauley LK. Anabolic actions of pth in murine models: two decades of insights. *J Bone Miner Res*. (2021) 36:1979–98. doi: 10.1002/jbmr.4389

67. Li S, Schonke M, Buurstede JC, Moll TJA, Gentenaar M, Schilperoort M, et al. Sexual dimorphism in transcriptional and functional glucocorticoid effects on mouse skeletal muscle. *Front Endocrinol (Lausanne)*. (2022) 13:907908. doi: 10.3389/fendo.2022.907908

68. Kroon J, Pereira AM, Meijer OC. Glucocorticoid sexual dimorphism in metabolism: dissecting the role of sex hormones. *Trends Endocrinol Metab*. (2020) 31:357–67. doi: 10.1016/j.tem.2020.01.010

69. Alam I, Oakes DK, Reilly AM, Billingsley C, Sbeta S, Gerard-O'Riley RL, et al. Overexpression of wnt16 does not prevent cortical bone loss due to glucocorticoid treatment in mice. *JBMR Plus*. (2019) 3:e10084. doi: 10.1002/jbm4.10084

70. Ersek A, Santo AI, Vattakuzhi Y, George S, Clark AR, Horwood NJ. Strain dependent differences in glucocorticoid-induced bone loss between C57bl/6j and cd-1 mice. *Sci Rep*. (2016) 6:36513. doi: 10.1038/srep36513

71. Shidara K, Mohan G, Evan Lay YA, Jepsen KJ, Yao W, Lane NE. Strain-specific differences in the development of bone loss and incidence of osteonecrosis following glucocorticoid treatment in two different mouse strains. *J Orthopaedic Translation*. (2019) 16:91–101. doi: 10.1016/j.jot.2018.07.001

72. Thiele S, Baschant U, Rauch A, Rauner M. Instructions for producing a mouse model of glucocorticoid-induced osteoporosis. *Bonekey Rep*. (2014) 3:552. doi: 10.1038/bonekey.2014.47

73. Grahnemo L, Jochems C, Andersson A, Engdahl C, Ohlsson C, Islander U, et al. Possible role of lymphocytes in glucocorticoid-induced increase in trabecular bone mineral density. *J Endocrinol*. (2015) 224:97–108. doi: 10.1530/JOE-14-0508

74. Briggs AM, Towler SC, Speerin R, March LM. Models of care for musculoskeletal health in Australia: now more than ever to drive evidence into health policy and practice. *Aust Health Rev*. (2014) 38:401–5. doi: 10.1071/AH14032

75. Schundeln MM, Hoppner J, Meyer FL, Schmuck W, Kauther MD, Hilken G, et al. Prednisone prevents particle induced bone loss in the calvaria mouse model. *Heliyon*. (2021) 7:e07828. doi: 10.1016/j.heliyon.2021.e07828

76. Dubrovsky AM, Nyman JS, Uppuganti S, Chmiel KJ, Kimmel DB, Lane NE. Bone strength/bone mass discrepancy in glucocorticoid-treated adult mice. *JBMR Plus*. (2021) 5:e10443. doi: 10.1002/jbm4.10443

77. Bergstrom I, Isaksson H, Koskela A, Tuukkanen J, Ohlsson C, Andersson G, et al. Prednisolone treatment reduces the osteogenic effects of loading in mice. *Bone*. (2018) 112:10–8. doi: 10.1016/j.bone.2018.04.002

78. Wang Y, Sakata T, Elalieh HZ, Munson SJ, Burghardt A, Majumdar S, et al. Gender differences in the response of cd-1 mouse bone to parathyroid hormone: potential role of igf-I. *J Endocrinol*. (2006) 189:279–87. doi: 10.1677/joe.1.06351

79. Babey M, Wang Y, Kubota T, Fong C, Menendez A, ElAlieh HZ, et al. Gender-specific differences in the skeletal response to continuous pth in mice lacking the igf1 receptor in mature osteoblasts. *J Bone Miner Res*. (2015) 30:1064–76. doi: 10.1002/jbmr.2433

80. Burr DB, Hirano T, Turner CH, Hotchkiss C, Brommage R, Hock JM. Intermittently administered human parathyroid hormone(1-34) treatment increases intracortical bone turnover and porosity without reducing bone strength in the humerus of ovariectomized cynomolgus monkeys. *J Bone Miner Res*. (2001) 16:157–65. doi: 10.1359/jbmr.2001.16.1.157

81. Shah SH, Johnston TD, Jeon H, Ranjan D. Effect of chronic glucocorticoid therapy and the gender difference on bone mineral density in liver transplant patients. *J Surg Res*. (2006) 135:238–41. doi: 10.1016/j.jss.2006.04.032

82. Stopa LRS, de Souza CF, Santos GF, Martins AB, Ferreira RN, de Andrade FG, et al. Sex differences in glucocorticoids-induced anabolic effects in rats. *Physiol Behav*. (2019) 209:112587. doi: 10.1016/j.physbeh.2019.112587

83. Duma D, Collins JB, Chou JW, Cidlowski JA. Sexually dimorphic actions of glucocorticoids provide a link to inflammatory diseases with gender differences in prevalence. *Sci Signal*. (2010) 3:ra74. doi: 10.1126/scisignal.2001077

84. Gasparini SJ, Swarbrick MM, Kim S, Thai LJ, Henneicke H, Cavanagh LL, et al. Androgens sensitise mice to glucocorticoid-induced insulin resistance and fat accumulation. *Diabetologia*. (2019) 62:1463–77. doi: 10.1007/s00125-019-4887-0

85. Salamone IM, Quattrocelli M, Barefield DY, Page PG, Tahtah I, Hadhazy M, et al. Intermittent glucocorticoid treatment enhances skeletal muscle performance through sexually dimorphic mechanisms. *J Clin Invest*. (2022) 132(6):e149828. doi: 10.1172/JCI149828

86. Moisan MP. Sexual dimorphism in glucocorticoid stress response. . *Int J Mol Sci*. (2021) 22(6):3139. doi: 10.3390/ijms22063139

87. Van Staa TP, Leufkens HG, Abenhaim L, Zhang B, Cooper C. Use of oral corticosteroids and risk of fractures. *J Bone Miner Res*. (2000) 15:993–1000. doi: 10.1359/jbmr.2000.15.6.993

88. Laan RF, van Riel PL, van de Putte LB, van Erning LJ, van't Hof MA, Lemmens JA. Low-dose prednisone induces rapid reversible axial bone loss in patients with rheumatoid arthritis. *A Randomized Controlled Study. Ann Intern Med*. (1993) 119:963–8. doi: 10.7326/0003-4819-119-10-199311150-00001

89. Balasubramanian A, Wade SW, Adler RA, Saag K, Pannacciulli N, Curtis JR. Glucocorticoid exposure and fracture risk in a cohort of us patients with selected conditions. *J Bone Miner Res*. (2018) 33:1881–8. doi: 10.1002/jbmr.3523

90. van Staa TP, Leufkens HG, Cooper C. The epidemiology of corticosteroid-induced osteoporosis: A meta-analysis. *Osteoporos Int*. (2002) 13:777–87. doi: 10.1007/s001980200108

91. Hayes KN, Baschant U, Hauser B, Burden AM, Winter EM. When to start and stop bone-protecting medication for preventing glucocorticoid-induced osteoporosis. *Front Endocrinol (Lausanne)*. (2021) 12:782118. doi: 10.3389/fendo.2021.782118

92. Shen G, Ren H, Qiu T, Liang D, Wei Q, Tang J, et al. Effect of glucocorticoid withdrawal on glucocorticoid inducing bone impairment. *Biochem Biophys Res Commun*. (2016) 477:1059–64. doi: 10.1016/j.bbrc.2016.07.036

93. Weinstein RS. Glucocorticoid-induced osteonecrosis. *Endocrine*. (2012) 41:183–90. doi: 10.1007/s12020-011-9580-0

94. Weinstein RS. Clinical practice. Glucocorticoid-induced bone disease. *N Engl J Med*. (2011) 365:62–70. doi: 10.1056/NEJMcp1012926

95. Angeli A, Guglielmi G, Dovio A, Capelli G, de Feo D, Giannini S, et al. High prevalence of asymptomatic vertebral fractures in post-menopausal women receiving chronic glucocorticoid therapy: A cross-sectional outpatient study. *Bone*. (2006) 39:253–9. doi: 10.1016/j.bone.2006.02.005

96. Bobinac D, Marinovic M, Bazdulj E, Cvijanovic O, Celic T, Maric I, et al. Microstructural alterations of femoral head articular cartilage and subchondral bone in osteoarthritis and osteoporosis. *Osteoarthritis Cartilage*. (2013) 21:1724–30. doi: 10.1016/j.joca.2013.06.030

97. Goldring MB, Goldring SR. Articular cartilage and subchondral bone in the pathogenesis of osteoarthritis. *Ann N Y Acad Sci*. (2010) 1192:230–7. doi: 10.1111/j.1749-6632.2009.05240.x

98. Macfarlane E, Cavanagh L, Fong-Yee C, Tuckermann J, Chen D, Little CB, et al. Deletion of the chondrocyte glucocorticoid receptor attenuates cartilage degradation through suppression of early synovial activation in murine posttraumatic osteoarthritis. *Osteoarthritis Cartilage*. (2023) 31:1189–201. doi: 10.1016/j.joca.2023.04.009

99. Madsen SH, Andreassen KV, Christensen ST, Karsdal MA, Sverdrup FM, Bay-Jensen AC, et al. Glucocorticoids exert context-dependent effects on cells of the joint in vitro. *Steroids*. (2011) 76:1474–82. doi: 10.1016/j.steroids.2011.07.018

100. Rusanen M, Gronblad M, Korkala O. Scanning electron microscopical study of the effects of crystalloid and water-soluble glucocorticoids on articular cartilage. *Scand J Rheumatol*. (1986) 15:47–51. doi: 10.3109/03009748609092668

101. Li G, Liu S, Xu H, Chen Y, Deng J, Xiong A, et al. Potential effects of teriparatide (Pth (1-34)) on osteoarthritis: A systematic review. *Arthritis Res Ther*. (2023) 25:3. doi: 10.1186/s13075-022-02981-w

102. Liang X, Li SR, Zhang XX, He SH, Li SS, Li TF. Teriparatide prevented synovial inflammation and cartilage destruction in mice with dmm. *Connect Tissue Res*. (2023) 64:274–84. doi: 10.1080/03008207.2022.2157723

103. Ciani A, Toumi H, Pallu S, Tsai EHR, Diaz A, Guizar-Sicairos M, et al. Ptychographic X-ray ct characterization of the osteocyte lacuno-canalicular network in a male rat's glucocorticoid induced osteoporosis model. *Bone Rep*. (2018) 9:122–31. doi: 10.1016/j.bonr.2018.07.005

104. Kamel-ElSayed SA, Tiede-Lewis LM, Lu Y, Veno PA, Dallas SL. Novel approaches for two and three dimensional multiplexed imaging of osteocytes. *Bone*. (2015) 76:129–40. doi: 10.1016/j.bone.2015.02.011

frontiers | Frontiers in Endocrinology

TYPE Original Research
PUBLISHED 02 August 2024
DOI 10.3389/fendo.2024.1359052

OPEN ACCESS

EDITED BY
J. Patrick O'Connor,
The State University of New Jersey, United States

REVIEWED BY
Melanie Haffner-Luntzer,
University of Ulm, Germany
Zhen Geng,
Shanghai University, China
Jun Zhang,
Shanghai Normal University, China
Jessica Cottrell,
Seton Hall University, United States

*CORRESPONDENCE
Sophie J. Gilbert
gilbertsj1@cardiff.ac.uk

RECEIVED 20 December 2023
ACCEPTED 17 July 2024
PUBLISHED 02 August 2024

CITATION
Gilbert SJ, Jones R, Egan BJ, Bonnet CS, Evans SL and Mason DJ (2024) Investigating mechanical and inflammatory pathological mechanisms in osteoarthritis using MSC-derived osteocyte-like cells in 3D.
Front. Endocrinol. 15:1359052.
doi: 10.3389/fendo.2024.1359052

Investigating mechanical and inflammatory pathological mechanisms in osteoarthritis using MSC-derived osteocyte-like cells in 3D

Sophie J. Gilbert[1]*, Ryan Jones[1], Ben J. Egan[1], Cleo Selina Bonnet[1], Sam L. Evans[1,2] and Deborah J. Mason[1]

[1]Biomechanics and Bioengineering Centre Versus Arthritis, School of Biosciences, Cardiff University, Cardiff, United Kingdom, [2]Biomechanics and Bioengineering Centre Versus Arthritis, School of Engineering, Cardiff University, Cardiff, United Kingdom

Introduction: Changes to bone physiology play a central role in the development of osteoarthritis with the mechanosensing osteocyte releasing factors that drive disease progression. This study developed a humanised *in vitro* model to detect osteocyte responses to either interleukin-6, a driver of degeneration and bone remodelling in animal and human joint injury, or mechanical loading, to mimic osteoarthritis stimuli in joints.

Methods: Human MSC cells (Y201) were differentiated in 3-dimensional type I collagen gels in osteogenic media and osteocyte phenotype assessed by RTqPCR and immunostaining. Gels were subjected to a single pathophysiological load or stimulated with interleukin-6 with unloaded or unstimulated cells as controls. RNA was extracted 1-hour post-load and assessed by RNAseq. Markers of pain, bone remodelling, and inflammation were quantified by RT-qPCR and ELISA.

Results: Y201 cells embedded within 3D collagen gels assumed dendritic morphology and expressed mature osteocytes markers. Mechanical loading of the osteocyte model regulated 7564 genes (Padj p<0.05, 3026 down, 4538 up). 93% of the osteocyte transcriptome signature was expressed in the model with 38% of these genes mechanically regulated. Mechanically loaded osteocytes regulated 26% of gene ontology pathways linked to OA pain, 40% reflecting bone remodelling and 27% representing inflammation. Load regulated genes associated with osteopetrosis, osteoporosis and osteoarthritis. 42% of effector genes in a genome-wide association study meta-analysis were mechanically regulated by osteocytes with 10 genes representing potential druggable targets. Interleukin-6 stimulation of osteocytes at concentrations reported in human synovial fluids from patients with OA or following knee injury, regulated similar readouts to mechanical loading including markers of pain, bone remodelling, and inflammation.

Discussion: We have developed a reproducible model of human osteocyte like cells that express >90% of the genes in the osteocyte transcriptome signature. Mechanical loading and inflammatory stimulation regulated genes and proteins

implicated in osteoarthritis symptoms of pain as well as inflammation and degeneration underlying disease progression. Nearly half of the genes classified as 'effectors' in GWAS were mechanically regulated in this model. This model will be useful in identifying new mechanisms underlying bone and joint pathologies and testing drugs targeting those mechanisms.

KEYWORDS

osteocyte, mechanical load, osteoarthritis, inflammation, 3D model, RNAseq analysis

1 Introduction

Abnormal joint loading through skeletal malalignment, age and obesity are key risk factors for osteoarthritis (OA) (1). At least 12% of the OA population are younger, with post-traumatic OA (PTOA) arising from prior joint injury (2), and although progression rate varies, injury can cause debilitating chronic pain and reduced mobility within 10 years. Changes to bone physiology play a central role in the development of OA (3) manifesting clinically as disruption of the tidemark, subchondral bone sclerosis and osteophyte formation alongside articular cartilage destruction. These changes are mediated by bone resorbing osteoclasts, bone forming osteoblasts, and osteocytes whose primary role is to maintain the integrity and function of bone (4) in response to its metabolic, mechanical and inflammatory environment, by regulating gene and protein expression. The osteocytes, which comprise 90–95% of all bone cells, release a variety of factors in response to mechanical load including nitric oxide (NO), prostaglandin E2 (PGE2), and receptor activator of nuclear factor kappa-B ligand (RANKL) to regulate osteoclast and osteoblast function as well as acting in an endocrine manner, releasing factors that target distant cells in other tissues (5–8). The extensive osteocytic network embedded within a lacuno-canalicular system throughout the bone, with cell-cell and cell-matrix connections that extend to the bone surface (9, 10) is ideally suited to the role of osteocytes as principal regulators of bone mechanosensation and mechanotransduction [reviewed in (11)].

In knee OA, mechanical loading causes pain, but the mechanism underlying the link between load and pain is unknown; bone is highly innervated and is one of the only tissues in the joint where structural changes correlate to pain in OA (12). Glutamate, the major excitatory neurotransmitter in the nervous system, also signals in peripheral and non-neuronal tissue. Both the regulation of glutamate release and the ability to respond to glutamate by expression of glutamate receptors (GluRs) has been reported in a range of joint cells including osteocytes (13–15). Glutamate signalling in bone is regulated by mechanical load (16) and linked to joint pain in humans (17). Increases in synovial fluid glutamate concentrations occur in both rheumatoid arthritis (RA) and OA patients (18) and correlate with an increase in inflammatory mediators in RA (19). In addition, synovial fluid glutamate levels in patients following anterior cruciate ligament (ACL) rupture and meniscal damage are comparable to that of OA patient synovial fluid levels and decrease with time post injury (13). Glutamate induces knee inflammation (20) and contributes to arthritic pain and swelling in an inflammatory arthritis model (21). Glutamate receptor antagonists within the joint alleviate symptoms of OA including pain, inflammation, and bone and cartilage pathology (13, 22). Inhibition of AMPA/KA GluRs with NBQX at the time of onset, improves pain related behaviour in rat inflammatory arthritis (antigen induced) and mouse PTOA model (ACL rupture) and reduces swelling and inflammation (13, 22). This protection is partly explained by NBQX inhibiting AMPA/KA GluR release of interleukin-6 (IL-6), an early driver of inflammation in both models of arthritis (15, 22, 23). IL-6 acts as a mechano-sensitive cytokine playing a key role in the biochemical control of bone remodelling (24, 25). Mechanical loading of osteocytes increases NO and IL-6 release and increases IL-6, osteoprotegerin (OPG), RANKL, and tumour necrosis factor-alpha (TNF-α) gene expression (26). Chronic IL-6 overexpression increases bone remodelling causing a net loss of bone by activating RANKL-induced bone resorption (27–29). Both pro-inflammatory and anti-inflammatory cytokines have been implicated in the pathogenesis of OA (30) with IL-6 among the most prominently elevated cytokine involved in the OA inflammatory response (31, 32). Increased circulating IL-6, as well as increased body mass index, predicts development of radiographic knee OA (33) and single nucleotide polymorphisms in the IL-6 gene are associated with radiographic hand OA (34). In addition, serum IL-6 levels are strongly associated with the incidence of age-related OA (35) and a predictive marker for the risk of OA progression (36). The role of IL-6 in OA pathophysiology has been studied in OA animal models showing that IL-6 is largely destructive (37) affecting both cartilage and subchondral bone (38).

Although mechanical load is the major driver of human OA, humanised *in vitro* osteocyte models investigating mechanics and its interactions with inflammation are very limited and have not been validated against *in vivo* models or human clinical data (39, 40). We have used our humanised *in vitro* model of osteocytes to detect early responses to either IL-6, a driver of degeneration and

bone remodelling in animal (22, 37) and human (33, 34) joint injury, or mechanical loading, to mimic early OA stimuli in joints. Our osteocyte model (adapted from Vazquez et al. (41)) is derived from human Y201 stem cells differentiated into osteocytes in 3D type I collagen gels and mechanical strain applied using our custom loading device (adapted from Vazquez et al. (41)). The aim of this current study was to assess the effect of pathological mechanical load on the osteocyte signature and determine the influence of IL-6 on readouts that have been reported in OA. This will help identify mechanical and inflammatory mechanisms that cause pain or alter bone tissue structure *in vitro* and provide new mechanistic insight into disease progression.

2 Materials and methods

Chemicals were from Sigma (Poole, UK) and tissue culture and molecular biology reagents from Thermo Fisher Scientific (Invitrogen, Paisley, UK) unless otherwise stated and were of analytical grade or above. sIL6r and IL6 were from Peprotech, UK.

2.1 Cell culture

Y201 hTERT-MSCs, gifted from Prof Paul Genever (University of York), were used as a model human MSC line (42). These cells can rapidly differentiate in 3D to osteocytes in a manner similar to bone marrow MSCs in spheroid cultures (43) and maintain mechanoresponsive behaviour (44). Cells were cultured in basal medium [Dulbecco's modified Eagle's medium (DMEM), high glucose, pyruvate, GlutaMAX™, supplemented with 5% fetal bovine serum (FBS), 100 U/mL penicillin and 100 µg/mL streptomycin] at 37°C in a humidified atmosphere of 5% CO_2, 95% air. At 80–85% confluency cells were sub-cultured by treating with TrypLE™. Y201 cells were incorporated into type I collagen gels at a concentration previously determined (41). Briefly, lyophilised rat tail tendon type I collagen was dissolved in 7mM glacial acetic acid and mixed 4:1 with 10X MEM containing 11g/L sodium bicarbonate on ice and neutralized [1M tris (hydroxymethyl)aminomethane (Tris) base, pH 11.5] to give 2mg/mL type I collagen gels. Y201 cells (0.125 x 10^6 cells/gel or 0.05 x 10^6 cells/gel for RNAseq) diluted in αMEM (<10% of total gel volume) were added to the collagen on ice and 250µL distributed into 48-well plastic (phenotype studies and IL-6 studies) or silicone (loading studies (41)) plates (Supplementary Methods 1), for polymerization at 37°C. After 1 hour, 800µL basal medium supplemented with osteogenic differentiation factors (50µg/mL ascorbate-2-phosphate, 5mM β-glycerophosphate, 1nM dexamethasone) was added onto the surface of the gels and cells cultured at 37°C with media changes every 3–4 days for the indicated periods.

2.1.1 Assessment of cell viability

Cultures grown in plastic plates for 7 days were rinsed with phosphate buffered saline, pH 7.3 (PBS), incubated with 1µL hoescht (1mg/mL) and 4µL propidium iodide (100µg/mL) in serum free medium for 2 hours at 4°C and then for a further 2.5 hours at 37°C before washing overnight at 37°C in normal culture medium with gentle agitation. Cells were fixed in 1% (wt/vol) paraformaldehyde for 30 minutes at 4°C, washed in PBS prior to overnight infiltration with 50% OCT compound (Tissue Tek) in PBS at 4°C. Gels were frozen in fresh OCT compound onto cryostat stubs using dry ice and cryosections cut at 20µm using a Bright OTF5000 cryostat and collected on polysine slides (VWR, Lutterworth, UK). Slides containing sections were mounted in VECTASHIELD® Mounting Medium containing DAPI (1.5 µg/mL) to counterstain DNA (Vector Laboratories, Peterborough, UK) and viewed using a light microscope (BX61, Olympus).

2.1.2 Assessment of cell phenotype

2.1.2.1 Cell shape and immunolocalization of osteocyte markers

Cultures grown in plastic plates for 7 days were rinsed with PBS, and gels fixed in 1% (wt/vol) paraformaldehyde, frozen and sectioned as outlined above. Sections were stained with phalloidin to assess cell morphology or processed for immunocytochemistry. Phalloidin-iFluor conjugate staining was carried out according to manufacturer's protocol (Abcam). Slides were removed from -20°C, allowed to equilibrate to room temperature and hydrated with 2mL of PBS per section. PBS was aspirated off, sections permeabilised with 0.1% Triton X-100 in PBS for 5 minutes and washed 3x with PBS prior to treatment with 100µL of 1X phalloidin conjugate (1µL per 1mL of PBS + 1% BSA) per section. Sections were left to stain for 60 minutes at room temperature whilst protected from light and washed 3x with an excess volume of PBS prior to mounting in VECTASHIELD® Mounting Medium containing DAPI (1.5 µg/mL). Stained sections were visualised using fluorescent imaging (BX61, Olympus). For immunocytochemistry, each step was performed at room temperature unless stated otherwise and between each incubation step, sections were washed 3x 5 min in 0.01 M PBS containing 0.001% Tween 20 (wash buffer). All antibodies were diluted in wash buffer. Cells were washed before blocking in 2% (v/v) normal goat serum (Dako UK, Ely, UK) for 1 hour. After overnight incubation at 4°C with a rabbit polyclonal primary antibody to Sclerostin (Abcam; ab75914) diluted 1:100, cells were washed before incubating for 1 hour with goat anti-rabbit Alexa 488 conjugated secondary antibody (4 µg/mL; Molecular probes, Invitrogen). Finally, after washing, cells were mounted in VECTASHIELD® Mounting Medium containing DAPI (1.5 µg/mL). Representative cells from multiple fields of view were imaged by confocal microscopy (Leica TCSSP2, Germany) using a 63x oil immersion objective lens and appropriate settings for AlexaFluor 488 (green) and DAPI (blue). Negative controls where the primary antibody was omitted or replaced with rabbit IgG were devoid of fluorescent signal (data not shown).

2.1.2.2 RT-PCR analysis of osteocyte markers

RNA was extracted from cells grown in gels from duplicate cultures at day 7 and analysed for the expression of osteocyte markers by RT-qPCR. Briefly, gels were placed into 600µl buffer

RLT Plus (RNeasy Plus kit, Qiagen) and 6µl β-mercaptoethanol added prior to loading onto a QIAshredder spin column to disrupt the gels. Samples were centrifuged for 2 minutes at full speed and the lysate added to gDNA Eliminator spin columns to digest genomic DNA. Samples were processed according to manufacturer's instructions (Qiagen) and RNA eluted in 30µl RNAse/DNAse free water. RNA quality and concentration were assessed by TapeStation Analysis (Agilent Technologies, UK). cDNA was generated in a 20 µL reaction from 500 ng RNA using 50 ng random hexamers (0.5 mg/mL; Promega) RNasin® RNase Inhibitor (40U), 5mM DTT, 0.5mM each dNTP, and Superscript IV reverse transcriptase (200 units). Gene expression was measured by SYBR green RT-PCR using the Platinum™ SYBR™ Green qPCR mix and the AriaMX qPCR system according to manufacturer's instructions (Agilent Technologies UK) with 200 nM forward and reverse primers (Supplementary Table 1A) and the following cycle conditions: 1 cycle of 95°C, 3 minutes; 40 cycles of 95°C, 15 seconds and 60°C, 30 seconds; 1 melt cycle of 95°C, 1 minute, 65°C 30 seconds, 95°C 1 minute.

2.2 Mechanical loading of collagen gels

2.2.1 Strain validation in collagen gels

Force strain relationships were validated in collagen gels within the custom-built Cardiff loading device which comprises a deformable silicone multiwell plate within a 3D printed loading device (Supplementary Figures 1A, B). Defined vertical displacements applied with a Bose Electroforce 3200 machine (TE Instruments) extend the levers outwards and caused the plate to stretch. Collagen gels (2mg/mL) containing 500µL of blue- and violet-coloured microspheres (10µm, Polysciences, Park Scientific Ltd, UK) subjected to vertical displacements of 0- 2.1mm at 0.35mm intervals were imaged by light microscopy and a tracking code, written in Matlab calculated the strain/displacements relationships (Supplementary Figures 1C–E). There was a linear relationship between displacement and strain up to displacements of 0.7mm. A displacement of 0.7mm represented a pathophysiological load of 4300µε (± 103) and was used for all experiments.

2.2.2 Mechanical loading

For loading, 3D Y201 cultures were prepared and cultured in the silicone plate in 800µL of basal medium containing osteogenic differentiation factors and incubated at 37°C in 5% CO2/95% air atmosphere for 5-days. After this time, the media were replenished and left for 24 hours. One hour prior to loading, media were removed and 800µL osteogenic media added. An hour later, silicone plates were loaded using a BOSE ElectroForce® 3200 loading instrument (TE Instruments, UK) to stretch the plate causing cyclic compression in all wells (pathophysiological load 4300µε induced by 0.7mm displacement, 10Hz, 3000 cycles (41, 45, 46). The loading regime was chosen to recapitulate *in vivo* models where validated high physiological strains induced osteogenesis (45, 47, 48). This high (pathophysiological) strain down regulated sclerostin (Supplementary Figure 1F) a known osteocyte derived mechanoresponsive molecule that is a potent regulator of bone formation (46) as well as inflammatory mediators relevant to osteoarthritis (41). In addition, osteocytes respond to mechanical load within seconds, revealing gene expression changes within 1 hour (49) and protein changes 24–72 hours later (41). Control gels in the silicone plate were placed into the loading device but received no load. Loading was controlled using WinTest® Software 4.1 with TuneIQ control optimization (BOSE). Media was collected after 1hr and 24hrs, aliquoted and frozen (-20°C) for analysis of released factors. Gels, 1hr post load, were placed into 600µL buffer RLT Plus (RNeasy Plus kit, Qiagen) and stored at -80°C prior to RNA extraction.

2.2.3 Confirmation of the osteocyte response to load

RNA was extracted 1 hour post load using RNeasy Plus kits, RNA eluted in 30µl RNAse/DNAse free water, cDNA synthesised and RTqPCR performed as described above (section 2.1.2.1). Reference genes, 36B4, YWHAZ, RPL13A, 18S, β-actin, GAPDH were tested across experimental conditions. The geometric mean of YWHAZ and 18S (stability value 0.292), were identified by RefFinder (50) as the most stable and used to calculate fold change relative to untreated cells using the ΔΔCT method (51). All primers (Supplementary Table 1A) were purchased from MWG and validated using a standard curve of five serial cDNA dilutions with primer efficiencies between 90–110% (52).

2.2.4 RNAseq analysis: generation of the osteocyte 'mechanosome'

RNA was extracted from loaded samples 1 hour post load (n=6) and unloaded controls (n=5) using RNeasy Plus kits as described above (section 2.1.2.2). RNA was eluted in 30µl RNAse/DNAse free water and RNA quality, and concentration assessed by TapeStation Analysis (Agilent). An RNA sequencing library was prepared for the mechanically loaded and control samples, using the New England Biolabs Ultra II directional RNA library prep kit (Wales Gene Park). cDNA was synthesized using this RNA which, after undergoing fragmentation, had adaptors ligated to the ends. The MiSeq Nano system (Illumina) was used to complete a sequencing library quality control after which sequencing was performed using the NovaSeq 6000 system (Illumina) running a 2 x 100bp paired-end reads run on a NovaSeq S1 flow cell. Trimming to remove adapter sequencer and poor-quality ends of reads was performed by Trim Galore using default parameters in paired-end mode. Trimmed paired-end reads were aligned to the GRCh38 no_alt_plus_hs38d1 analysis set reference using STAR (v2.5.1b), an ultrafast universal RNAseq aligner, following the 2-pass method (53). QC metrics were generated using FastQC (v0.11.2), and summary statistics were generated using Samtools (v0.1.19) flagstat. Raw counts were calculated for all samples for both (i) exons and (ii) genes using Subread featureCounts Version 1.5.1. Counts were generated for paired end read fragments summarized at exon level and then aggregated at transcript level. Ambiguity between the labels on sample C1 and L1 and the suspicion that these

2 samples had been inadvertently switched led to an additional PCA analysis which showed C1 to cluster with loaded samples (Supplementary Figure 2); because of this C1 and L1 were excluded from further analysis leaving n=4 controls and n=5 loaded samples. Differentially expressed genes were identified using an DEseq2 analysis (54) on normalised count data. The resultant p-values were corrected for multiple testing and false discovery issues using the FDR method (55). RNAseq data are available from Mendeley Data (DOI: 10.17632/5md5rnybcs.1).

2.2.5 Human osteoprotegerin and glutamate ELISAs

Media collected 1 hour, and 24 hours post-load were analysed for the release of Glutamate (KA1909, Bio-Techne) and OPG (AB100617, Abcam) using commercial kits following manufacturer's instructions.

2.2.6 Cytokine analysis

Frozen media samples were thawed on ice and centrifuged for 5 minutes at 3000 rpm, and 23 cytokines profiled (Supplementary Table 1B) in each sample by Luminex bead based multiplex assay using a Merck Milliplex® MAP human cytokine/chemokine magnetic bead panel kit (2923824 HCYTOMAG-60K-23) following the manufacturer's instructions.

2.3 sIL6r/IL6 treatment of Y201 cells in 3D gels

Y201 cells were embedded in 3D type I collagen gels as described above at a density of 0.125 x 10^6 cells/gel and grown in 48-well plastic plates for 24 hours in basal media at 37°C, 5% CO2. Media was replaced with 800µL osteogenic media and cells cultured for 7 days with media changes every 3 days. At day 7, the media was replaced with 800µL osteogenic media containing IL-6 (5ng/mL) and sIL-6r (40ng/mL) in all but the control wells (26, 31, 32). At 24 and 72 hours, media was removed and stored at -20°C for cytokine analysis. TRIzol™ reagent (500µL) was added to each gel at 24 hours and pipetted repeatedly to dissolve the gels and lyse the cells, prior to storage at -80°C.

2.3.1 RNA extraction and RT-qPCR analysis of gene expression

Total RNA was extracted from gels using TRIzol™ reagent according to the manufacturer's protocol. RNA was DNase treated to remove genomic DNA (Ambion; Applied Biosystems, UK) and re-suspended in 50 µL RNase-free water. RNA integrity and concentration were assessed by Nanodrop™. cDNA was generated in a 20 µL reaction from 150 ng RNA as described above (section 2.1.2.2). RT-qPCR was carried out as described above using the geometric mean of EEF and RPL13A (RefFinder stability value 0.375) for normalisation.

2.3.2 Cytokine analysis

Aliquoted media samples were centrifuged to remove cells and supernatants vortexed briefly prior to use. A multiplex electrochemiluminescence (ECL) kit (Supplementary Table 1C; U-Plex Proinflam Combo 1 Human K15049; Meso Scale Discovery, USA) and single-plex ELISAs (Glutamate KA 1909 Abnova, OPG RDR-OPG-Hu 2bScientific) were utilised to measure levels of released molecules according to manufacturer's instructions. Multiplex ECLs were carried out in the Central Biotechnological Services (Cardiff University) utilising a Mesoscale discovery (MSD) plate reader to determine chemiluminescence measurements.

2.4 Statistics and data analysis

Results are presented as mean ± SEM. Graphs show individual data points, box and whisker plots of minimum and maximum values, 25th and 75th quartiles and median. Data were tested for normality and equal variances prior to transformations where necessary and appropriate statistical testing as indicated in the figure legends (Minitab 20). Differences were considered significant at $p=0.05$. For all statistics, unless stated otherwise, treatments were compared to untreated controls. Functional gene enrichment and pathway enrichment analysis were performed on up and down DEG sets using gProfiler (56) and Enrichr databases (57–59), respectively. RNAseq data was compared to the osteocyte signature (60) as well as a list of gene ontology terms (GO terms), compiled using AmiGO (61–63) and the search terms 'bone', 'pain', 'inflammation', and 'mechanical load'. For phenotype studies, data is collected from 4 independent studies (N=4). For IL-6 effects on bone remodelling, OPG gene data is representative of 3 independent studies (N=3).

3 Results

3.1 Osteocyte–like cell viability and phenotype

Y201 cells produced dendritic processes within one hour of embedding in 3D collagen gels and formed interconnected networks by day 7, remaining viable (data not shown) and osteocyte-like (Figures 1A–E). After 7 days in 3D collagen gels, phalloidin staining revealed a dendritic morphology (Figures 1E, F; Supplementary Video 1) and immunolocalization confirmed sclerostin protein expression (Figures 1G, H). Cells did not proliferate between days 5 and 7 (data not shown). RTqPCR analysis confirmed cells expressed osteocyte markers sclerostin (SOST) and podoplanin (PDPN) and expressed osteocalcin (BGLAP), osteoprotegerin (TNFRSF11B), and type I collagen (COL1A1) (Supplementary Figure 3A).

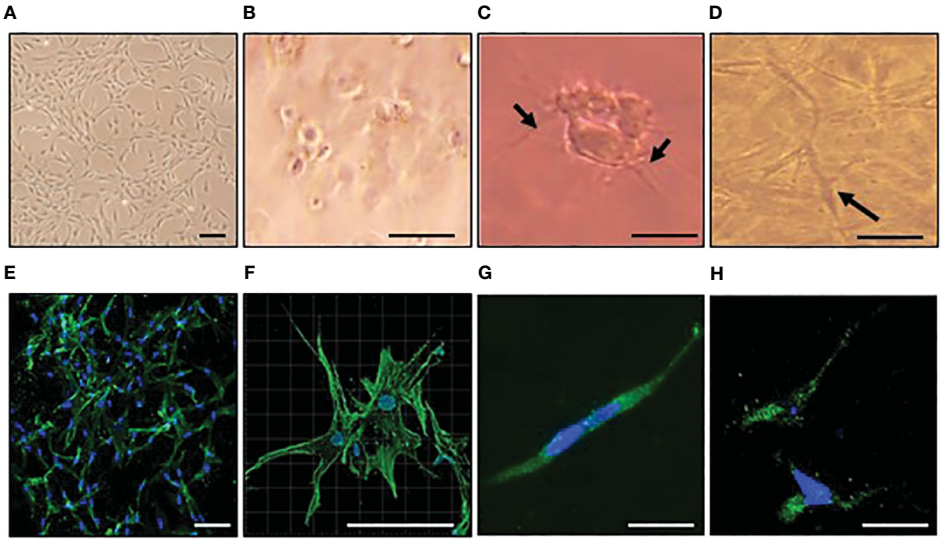

FIGURE 1
Osteocyte–like cells differentiated from Y201 mesenchymal stem cells are viable with an appropriate phenotype. Y201 mesenchymal stem cells were expanded in culture **(A)** prior to embedding in type I collagen gels **(B-D)**. Within 1 hour of culture **(B)**, cells were beginning to send out dendritic processes which were evident by 4 hours **(C)**. A 3D network of interconnecting cells was clearly evident by day 7 **(D)**. Phalloidin staining of cells revealed dendritic processes **(E, F)**; green) and sclerostin expression **(G, H)**; green) at day 7 of culture. DAPI nucleus = blue. Images were captured using a x4 **(A)**, x10 **(E)**, x20 **(B-D, G, H)**, and x40 **(F)** objective. Scale bar = 20μm B-D, G,H; 100 μm **(A, E, F)**.

3.2 Differentially expressed genes, model reproducibility and the osteocyte signature

RNA extracted from cells differentiated in silicone plates 1 hour post load was of high quality (RIN scores >9; Supplementary Figures 3B). RT-qPCR analysis revealed SOST expression was decreased by loading thereby confirming that the model cells were responding appropriately to load (Supplementary Figure 1F). RNA was processed for RNAseq and the dataset generated analysed for the presence of genes involved in the development and maturation of osteocytes and the mineralisation process (Figure 2A). Our data was compared to publicly available data generated from IDGSW3 cells at day 3, 14 and 35 of differentiation (Figure 2B) (57), and osteocyte-isolated samples from the Osteocyte Enrichment cohort (Figure 2C) (65) and the relative temporal expression of various osteogenic markers during the transition from osteoblast to osteocyte summarized [Figure 2D; adapted from (10)].

Hierarchical clustering of the sample set grouped replicates and separated biological conditions (Supplementary Figure 2C). Principal component analysis (PCA) characterised further the experimental variability revealing loaded samples L2 and L3 to be different to L4-L6 (Supplementary Figures 2D, E).

In total 7564 genes were differentially regulated (Padj $p<0.05$): 3026 down and 4538 up regulated by mechanical load (Supplementary Table 2A). Of these, 3824 genes were up regulated and 532 down regulated fold change (FC) >2. A volcano plot representing the log of the adjusted P value as a function of the log ratio of differential expression shows differentially regulated genes as red dots or triangles, the latter corresponding to genes where log2 FC is too low/high to be displayed on the plot (Supplementary Figure 2F). We compared our *in vitro* osteocyte 'mechanosome' data to the 1004 protein encoding genes from the published osteocyte signature representing human genes enriched in osteocytes relative to bone marrow and other osteoblast lineage cells (60). This revealed that 937/1004 osteocyte signature genes were expressed (Supplementary Table 2B) and 67 were not expressed in our dataset (Supplementary Table 2C). Of these, 379 were regulated by mechanical load (248 UP, 131 DOWN; Padj<0.05; Supplementary Table 2D). Functional gene enrichment analysis of the DEGs using gProfiler revealed alterations in genes involved in several biological processes, molecular function, cell compartments, and the reactome (Supplementary Table 3A). Analysis of the up regulated gene set revealed enrichment of genes including those involved in metabolic processes, cell response to stress, and cell component organization as well as genes involved in post-translational modification and toll-like receptor signalling (Supplementary Table 3A GEA.UP). Down regulated genes were enriched in RNA processes, and cilium processes (Supplementary Table 3A GEA.DOWN). Additional gene ontology searches were performed for terms related to mechanical load including 'response to mechanical signalling', 'mechanically gated ion channels', 'mechanosensory behaviour', 'cell response to mechanical stimulus', and 'detection of mechanical stimulus' revealing several regulated genes (Supplementary Table 3B). Of the 166 genes listed across these terms, 46 genes were upregulated and 24 downregulated by mechanical load (padj <0.05).

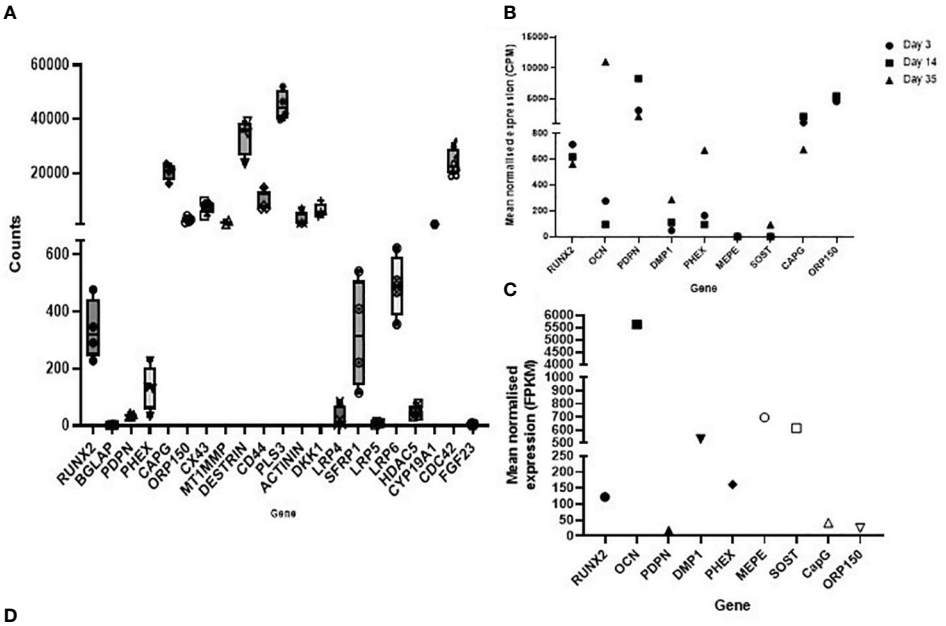

D

Gene	1	2	3	4	5	6	Y201 derived osteocytes
Runx2	+	+	-	-	-	-	+1
OCN (BGLAP)	-	+	+	+	+	-	+1,2
PDPN	-	-	+	+	+	-	+1,2
DMP1	-	-	+	+	+	+	-
PHEX	-	-	+	+	+	+	+1
MEPE	-	-	-	+	+	+	-
SOST	-	-	-	-	-	+	+2,3
CAPG	-	-	+	+	+	+	+1
ORP150	-	-	-	-	-	+	+1

FIGURE 2
Osteocyte–like cells differentiated from Y201 mesenchymal stem cells express phenotypic markers of osteocyte development and maturation. RNAseq data quantifying gene expression associated with the development and maturation of osteocytes and the mineralisation process in **(A)** the Y201 osteocyte model used to generate the mechanosome. Data is compared to **(B)** IDGSW3 cells at day 3, 14 and 35 of differentiation (60), and **(C)** osteocyte-isolated samples from the Osteocyte Enrichment cohort (64). B and C were plotted using data publicly available (60, 64), respectively. **(D)** table [adapted from (10)] showing the relative temporal expression of various osteogenic markers during the transition from osteoblast to osteocyte where 1 = preosteoblast; 2 = osteoblast; 3 = embedding osteoblast; 4 = osteoid osteocyte; 5 = mineralizing osteocyte; 6 = mature osteocytes compared to expression of these markers in the Y201 derived osteocytes (1 = mechanosome RNAseq data, 2 = RTqPCR data, 3 = immunohistochemistry, detected = +, not detected = -).

3.3 Mechanical load of osteocytes regulates readouts of osteoarthritis

Gene ontology searches were performed for terms related to readouts of OA including pain (Supplementary Table 3C), bone remodelling (Supplementary Table 3D) and inflammation (Supplementary Table 3E).

3.3.1 Pain and the glutamate signalling pathway

Pathophysiological loading of osteocytes in our 3D model regulated genes known to be involved in gene ontology pathways linked to OA pain including genes related to sensory perception of pain and neuropathic pain and members of the glutamate signalling pathway (Supplementary Table 3C). Of the 253 genes listed across these terms, 43 genes were up regulated, and 22 genes downregulated by mechanical load (Padj < 0.05, Supplementary Table 2A). GRIK1, GRIA4, GRIN2B, GRIN2C, GRIN2D, GRIN3A, SLC1A2, SLC1A3, GRID2 were expressed but not regulated by load (data not shown). In addition, COL12A1 and COL16A1, present in bone marrow lesions (BMLs) (66) which correlate to OA pain (67), were upregulated 4- (padj=0.000) and 1.7-fold (padj= 0.049) by load, respectively (data not shown).

Glutamate release was measured by ELISA (Figure 3A). Over the 24-hrs of culture, cells increased release of glutamate into the media; loading dampened this response (control 1-hr vs 24-hr 7-fold, p<0.001; loaded 2.7-fold, p=0.003).

3.3.2 Bone remodelling

Pathophysiological loading of osteocytes in our 3D model regulated genes known to be involved in gene ontology pathways linked to bone remodelling including ossification, bone resorption,

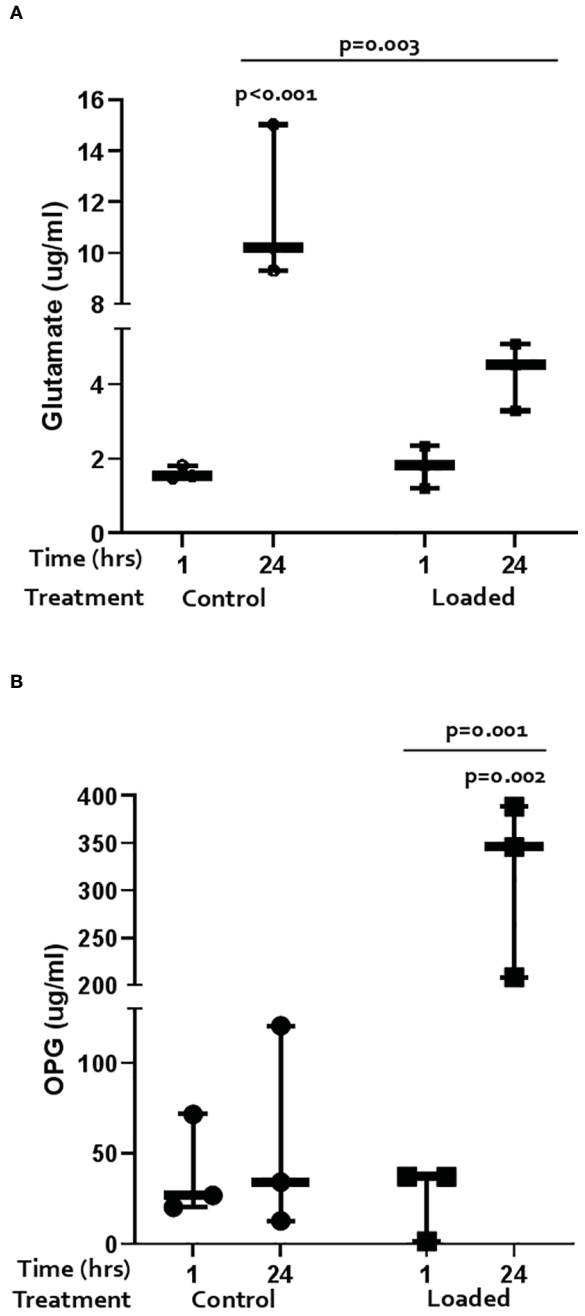

FIGURE 3
Regulation of markers of pain and bone remodelling markers in the 3D osteocyte model. The amount of **(A)** glutamate and **(B)** OPG released into the media from loaded osteocytes at 1 hour and 24 hours post-load (n=3/treatment, GLM ANOVA and Tukey's post-hoc tests).

and bone mineralisation (Supplementary Table 3D). Of the 217 genes listed across these terms, 49 genes were upregulated and 31 downregulated by mechanical load (Padj < 0.05). In addition, RANKL (TNFSF11) and OPG (TNFRSF11B) were expressed but not regulated by mechanical load; SOST was not detected by RNAseq (data not shown). Pathway enrichment analysis of mechanically regulated genes using Enrichr (57–59) revealed associations with the bone remodelling/RANKL pathway (Biocarta 2016: 10/16 p = 7.20E-04 and Bioplanet 2019: 18/54 p = 0.048, respectively; Supplementary Table 4). The Elsevier pathway database showed that mechanically regulated genes were associated with aberant bone cell function in several diseases inlcuding 'osteoclasts function in Osteopetrosis' (10/19 p = 0.004), 'osteoclast activation in Rheumatoid Arthritis' (20/57 p = 0.022), 'osteoclast activation in postmenopause' (16/42 p = 0.017), 'WNT signaling dysregulation in osteoblasts' (7/15 p = 0.035), 'osteoclast activation in Psoriatic Arthritis' (16/47 p = 0.049), and 'TNF and IL1B induce metalloproteinase synthesis in Osteoarthritis' (14/38 p = 0.034) (Supplementary Table 4).

OPG and RANKL release was measured by ELISA. OPG release did not change over time in control cultures but was significantly increased by load at 24 hours (Figure 3B; 5.6-fold p=0.003; load at 24 hours vs load at 1 hour p=0.001). RANKL was below the level of detection in all cultures (data not shown).

3.3.3 Inflammation

Pathophysiological loading of osteocytes in our 3D model regulated genes known to be involved in pathways linked to inflammation including genes associated with an acute and chronic inflammatory response (Supplementary Table 3E). Of the 371 genes listed in these terms, 69 genes were upregulated, and 32 genes downregulated by mechanical load (Padj <0.05). Many of these genes also belonged to GO terms related to NFkB signalling including 'regulation of IkBk/NFkB signalling' (GO:0043122; 70/224 Padj 0.002), 'IkBk/NFkB signalling' (GO:0007249; 23/62 Padj 0.007), 'positive regulation of IkBk/NFkB signalling' (GO:0043123; 51/171 Padj 0.018), and 'NFkB binding' (GO:0051959; 11/25 Padj 0.014) (Supplementary Table 3). Enrichr database analysis also revealed association with the NFkB pathway (Biocarta 2016: 12/21 p = 6.59E-04) (Supplementary Table 4).

Several cytokines were detected in the control media from the osteocyte model (Figure 4) including GM-CSF, MCP-1, IL-6, IL-8, IP-10, RANTES, IL-10, IL-12p70, IL-5, and MIP1a. Levels of GM-CSF (1.8-fold vs 1-hr; p=0.005), MCP-1 (2.4-fold; p<0.001), IL-6 (2.7-fold; p=0.038), IL-8 (3.9-fold; p=0.018), IP-10 (2.3-fold; p=0.016), and RANTES (3.2-fold; p=0.001) increased over the 24-hrs in culture (Figure 4). Loading reduced the release of some cytokines after 1-hr and abolished the increase observed with time in culture (Figure 4). These included GM-CSF (1-hr vs control 1-hr: 3-fold, p<0.001; 24-hr vs control 24-hr: 3.9-fold, p<0.001), MCP-1 (1-hr 3.7-fold, p=0.006; 24-hr 3.2-fold, p<0.001), IL-6 (1-hr 6.3-fold, p=0.001; 24-hr 7.6-fold, p=0.001), IL-8 (1-hr 9.6-fold, p<0.001; 24-hr 11.3-fold, p<0.001), IP-10 (1-hr 3.5-fold, p=0.004; 24-hr 2.8-fold, p=0.011), and RANTES (1-hr 16.7-fold, p<0.001; 24-hr 5.8-fold, p<0.001). IL-10, IL-12p70, IL-5, and MIP1a were expressed but levels not elevated with time in culture or affected by load (data not shown).

3.4 IL-6 stimulation of osteocytes regulates readouts of osteoarthritis

Since IL-6 has been reported to be elevated in OA (31) and after knee injury significantly contributing to baseline KOOS and

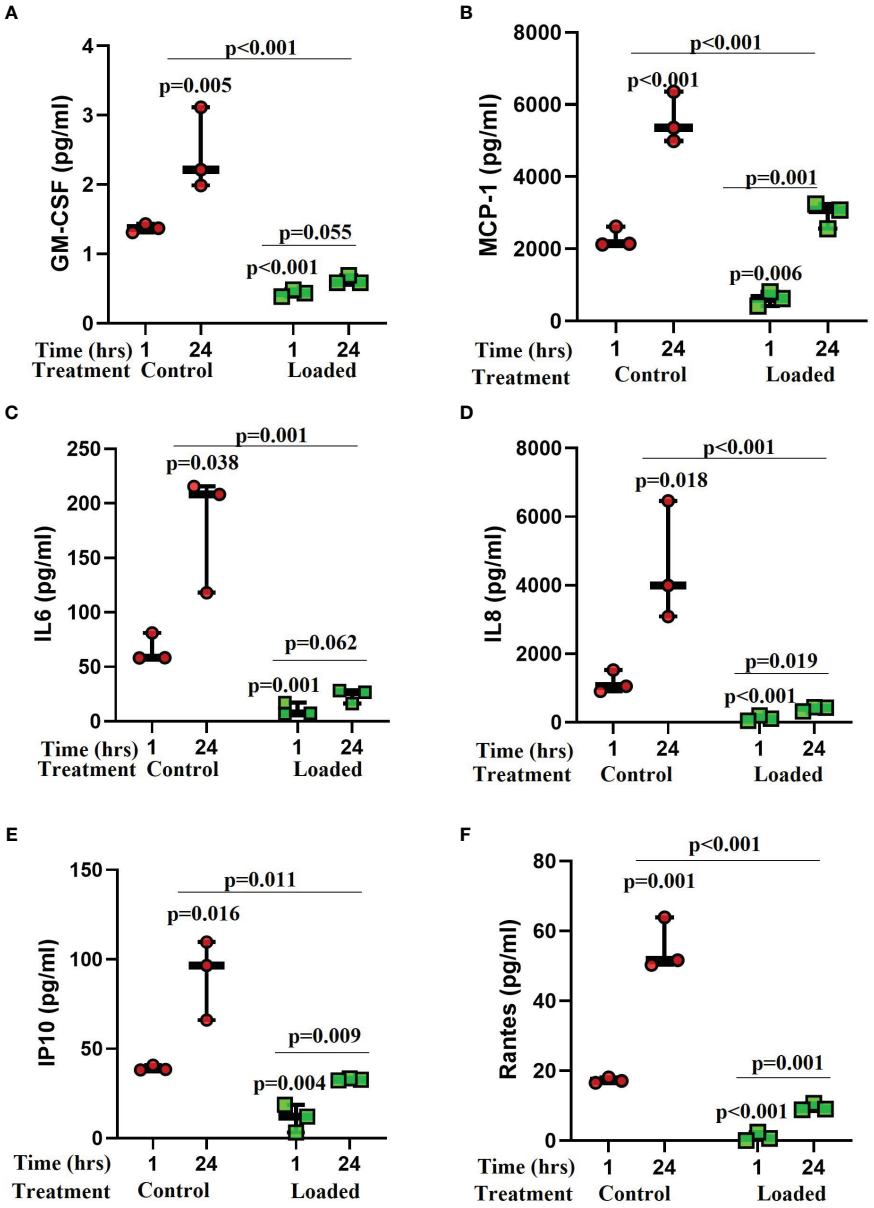

FIGURE 4
The effect of mechanical load on cytokine release from osteocytes grown in 3D collagen gels. Media was analysed for the release of cytokines 1 and 24 hours post load using a Luminex bead based multiplex assay (Merck Milliplex® MAP human cytokine/chemokine magnetic bead panel kit). Samples were compared to control at 1 hour unless stated otherwise (n=3/treatment; GLM ANOVA with Tukey *post hoc* tests; IL-6 and GM-CSF logged data; IP-10 and RANTES 2-sample t-tests).

change in KOOS over 3 months (32), we stimulated our model with concentrations of IL-6 and its soluble receptor reported in synovial fluid from patients with OA (31) or following injury (32).

3.4.1 Pain and the glutamate signalling pathway

IL-6/sIL-6r treatment downregulated GRIA1 (3-fold, p=0.007) mRNA expression (Figure 5A). SLClA1 and SLC1A3 were expressed but levels did not change with IL-6 treatment (data not shown). Glutamate release into the media increased with time in culture in control (p=0.005) and IL-6/sIL-6r (p=0.006) treated cultures but there was no effect of IL-6/sIL-6r treatment on glutamate release (Supplementary Figure 4).

3.4.2 Bone remodelling

IL-6/sIL-6r treatment downregulated ALPL (2-fold; p=0.003), BGLAP (1.6-fold; p=0.042), TNFRSF11B (2-fold; p=0.029) mRNA expression (Figure 5B). Levels of Col1A1 did not change (data not shown). OPG release into the media increased with time in culture in control (p<0.001) and IL6/sIL6r (p<0.001) treated cultures but there was no effect of IL-6/sIL-6r treatment on OPG release (Supplementary Figure 4).

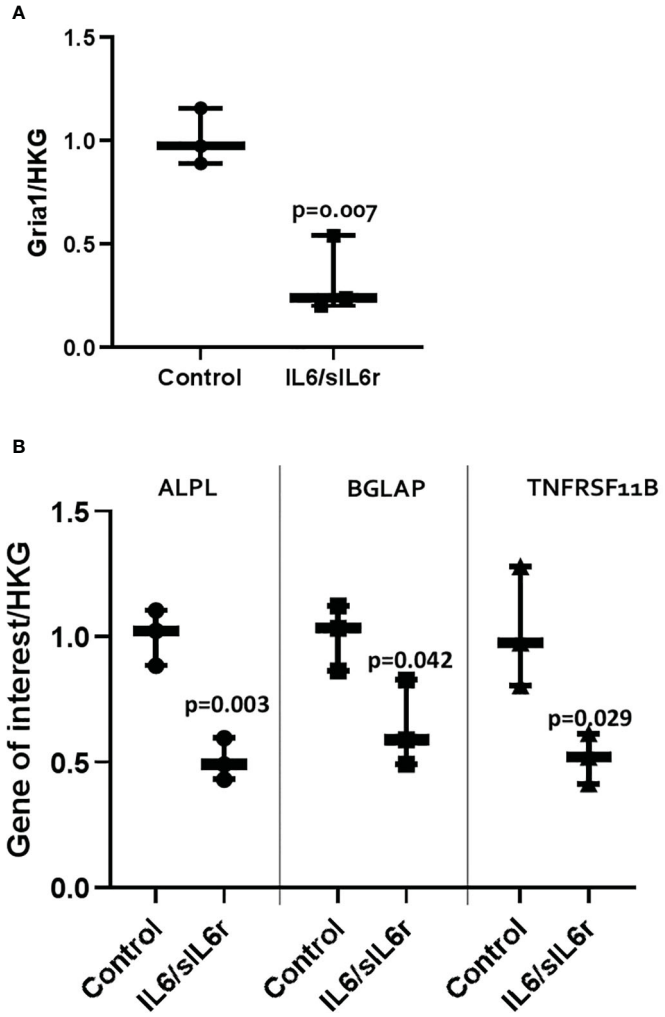

FIGURE 5
The effect of IL-6/sIL-6r on the expression of markers of **(A)** pain and **(B)** bone in osteocytes grown in 3D collagen gels. Gene expression was assessed at 24 hours post IL-6 (5ng/ml) and sIL-6r (40ng/ml) treatment and normalised to the geomean of two housekeeping genes (HKG), EEF and RPL13A. Samples were compared to control at 24 hours (One way ANOVA with Tukey *post hoc* tests; n=3).

3.4.3 Treatment of osteocytes with IL6/sIL6r increases the release of inflammatory mediators

Several cytokines detected in control media increased over the 72 hours of culture including IL-12p70 (5-fold; p=0.003; Figure 6A), IL-4 (2.2-fold; p<0.001; Figure 6B), TNF-α (3-fold; p=0.005; Figure 6C), IL-2 (4.5-fold; p=0.001; Figure 6D), IFN-g (not expressed at 24-hrs but present at 72 hours; Supplementary Figure 5A), IL-10 (3-fold; p<0.001; Supplementary Figure 5B), IL-13 (2.2-fold; p=0.002; Supplementary Figure 5C), IL-1β (2-fold; p=0.055; Supplementary Figure 5D), and IL-8 (1.9-fold; p=0.017; Supplementary Figure 5E). Treatment of cells with IL-6/sIL-6r increased the amount of IL-12p70 (24-hrs 11.3-fold, p<0.001; 72-hrs 3-fold; p=0.012), IL-4 (24-hrs 12-fold, p<0.001; 72-hrs 4.6-fold, p<0.001), TNF-α (72-hr 1.6-fold p=0.01), IL-2 (24-hrs 2.3-fold, p=0.131), and IFN-g (72-hrs 2.4-fold, p=0.044) released into the media compared to untreated controls. IL-10, IL-13, IL-1β, and IL-8 levels were not changed by IL-6 treatment (Supplementary Figures 5B–E).

4 Discussion

4.1 A 3D model of human osteocyte like cells

Y201 cells embedded in 3D collagen gels for 7 days displayed appropriated dendritic morphology (68), and expressed the mediator of osteocyte mechano-responses, sclerostin (69). SOST is not expressed in the early stages of differentiation of the osteoblast lineage, but levels increase as the osteocyte matures and become surrounded by mineralized bone (70). In addition, several genes were expressed that have been identified as being involved in the development and maturation of osteocytes [reviewed in (71–73)]. These included PDPN and CD44, markers of early osteocyte differentiation and required by osteocytes to initiate proper dendrite formation (74, 75), and a number of cytoskeletal proteins involved in actin dynamics such as PLS3, which encodes for an actin bundling protein required for osteocyte cytoskeleton

organization (76), destrin, CAPG, and CDC42 (77). GJA1 (CX43) which is required for osteocyte communication (78), and MMP14, which is involved in canaliculi formation (72, 79) were also expressed along with DKK1, PHEX and FGF23 which play important roles in osteocyte development (72). BGLAP, COL1A1, TNFRSF11B, TNFSF11, PHOSPHO1, HDAC5, CYP19A1, RUNX2, DLX5, ATF4 and AP1 were also present representing genes that encode for proteins involved in osteocyte maturation and the mineralisation process [reviewed in (71)] (80). The genes involved in osteocyte development and maturation (5, 10, 70, 72, 74–79, 81–84) and found to be present in our dataset are summarized in Figure 7. Of the 1004 known human protein coding genes reported to reflect the *in vivo* osteocyte transcriptome signature (60), 93% were expressed in our model indicating that the cell phenotype and differentiation status is a good representation of osteocyte-like cells. The 7% of osteocyte signature genes not expressed in our RNAseq dataset included genes associated with the nervous system, the skeleton, angiogenesis, and cell function (Supplementary Table 2C). However, these may have been below the limit of detection since SOST was detected by RT-qPCR suggesting a reduced sensitivity in the RNAseq technology.

4.2 Mechanical loading regulates readouts of osteoarthritis in our 3D model of osteocytes

Mechanical loading decreased SOST expression in all 3D osteocyte cultures consistent with its regulation *in vivo* (46, 85) and regulated 70 genes linked to known mechanical responses by GO term enrichment confirming the model's expected response to mechanical load. In total, mechanical loading of osteocytes down regulated 3026 genes and upregulated 4538 genes. Functional enrichment analysis using gProfiler revealed these were involved in many important cellular processes. Of note was the down regulation of processes involved in the primary cilia, an important key player in osteocyte mechanosensing (86) and bone formation in response to mechanical forces [reviewed in (87, 88)]. Thirty eight percent of the previously reported osteocyte signature genes (60) were regulated by mechanical load in our 3D model consistent with the dogma that osteocytes are highly responsive to mechanical load (60). Load regulated several genes associated with skeletal diseases such as osteopetrosis, osteoporosis and osteoarthritis in keeping with the human orthologs associated with osteoarthritis and osteoporosis reported in the *in vivo* mouse

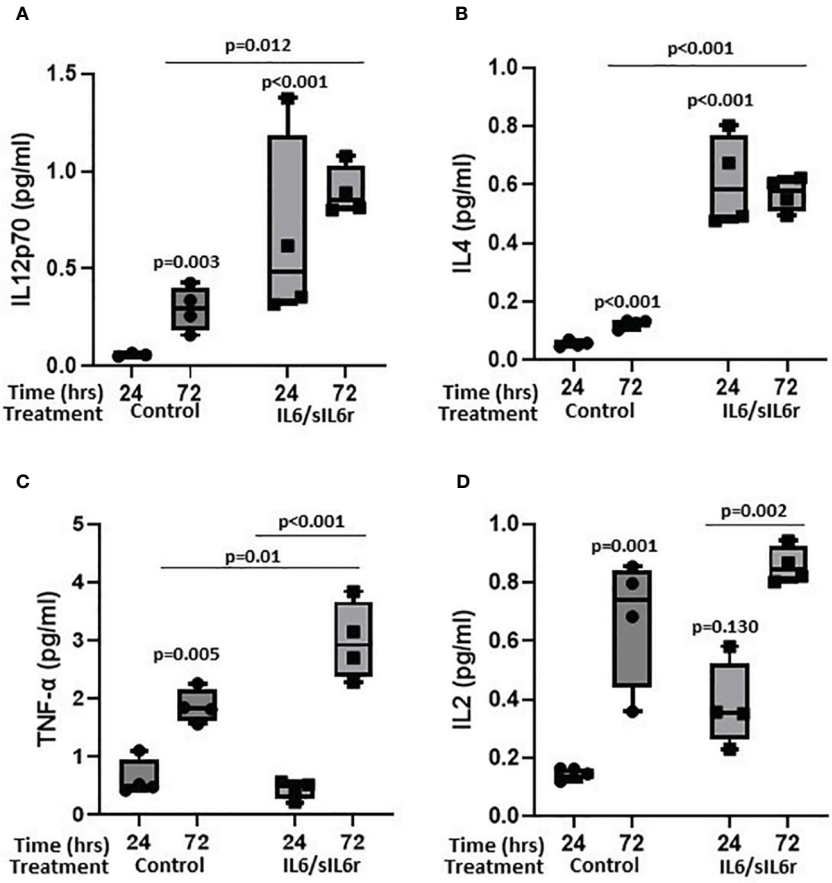

FIGURE 6
The effect of sIL-6r/IL-6 treatment on cytokine release from osteocytes grown in 3D collagen gels. Media was analysed for the release of **(A)** IL12p70, **(B)** IL4, **(C)** TNF-alpha, and **(D)** IL2 24 and 72 hours post treatment with IL-6 (5ng/ml) and sIL-6r (40ng/ml) using a multiplex ECL kit (Meso Scale Discovery). Samples were compared to control at 24 hour unless stated otherwise (n=3–4/treatment; GLM ANOVA with Tukey *post hoc* tests).

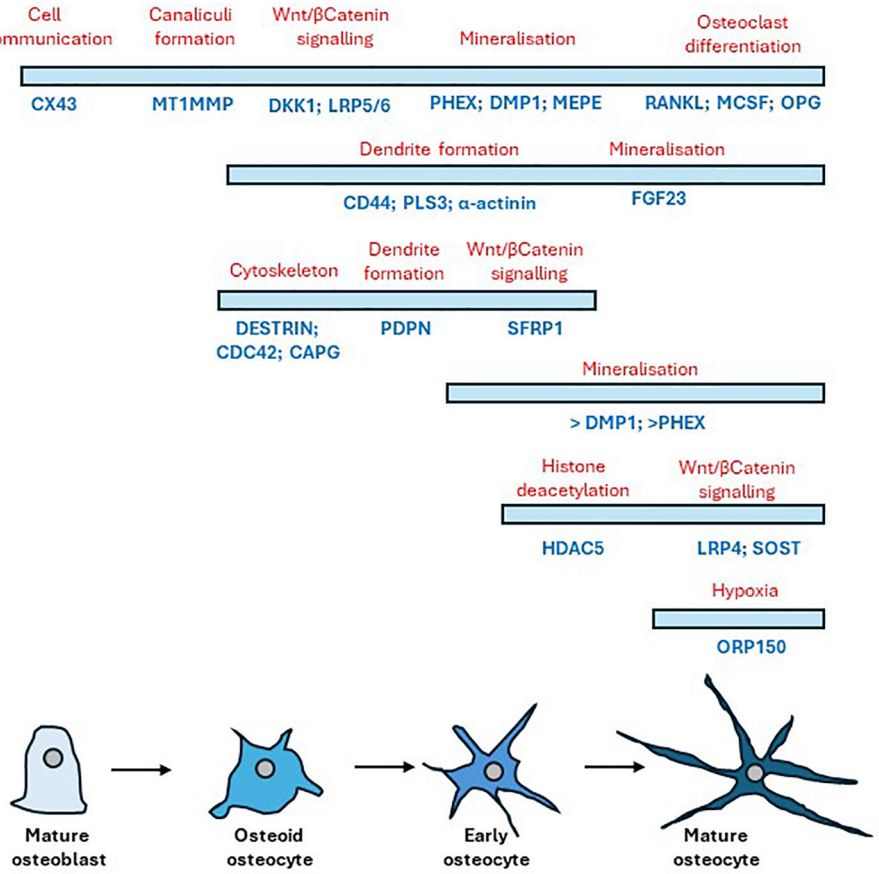

FIGURE 7
Timeline of gene expression changes that occur following the differentiation of mature osteoblasts to mature osteocytes. Bars indicate cell stage (blue) showing the relative temporal expression of various osteogenic markers underneath (dark blue) during the transition from osteoblast to osteocyte with their respective protein role above (red). Adapted from (72) and (10).

osteocyte transcriptome (60). Of the 25 genes of the osteocyte transcriptome signature associated with a skeletal phenotype (60), 15 were expressed but not regulated in our model, 3 were upregulated (CADM1, KAZN, STARD13) and 3 downregulated (CC2D2A, LTBP1, PLS3) by mechanical load (Supplementary Table 5A). Interestingly, mutation in PLS3 which encodes for plastin-3 an actin bundling protein required for organisation of the cytoskeleton in osteocytes (76) results in X-linked osteoporosis (89). In addition, of the 211 genes enriched within the signature that are associated with a skeletal phenotype in the Mouse Genome Informatics database (MGI) (60), our model expressed 108 genes that were not regulated by load, 50 that were upregulated, and 37 that were downregulated (Supplementary Table 5B). Bone marrow lesions (BMLs) occur in areas of bone remodelling and are associated with subchondral bone microdamage and correlate with pain in OA (67, 90, 91). Their presence and location are associated with altered joint loading as occurs in joint malalignment and absence/regression of BMLs occurs following reduction of focal contact stress across the joint (92). Joint pain resolution is associated with diminished BMLs. Comparison of our mechanosome data to the 78 DEGS identified as BML hub (93) revealed 56 genes to be expressed in our dataset, with 8 down regulated and 24 upregulated by load (Supplementary Table 5C). Additional components of BMLs such as COL12A1 (4-fold) and COL16A1 (1.7-fold), present in BMLs (66) which correlate to OA pain (67), were upregulated by load.

To determine whether mechanical load activated readouts classically associated with the structural and symptomatic changes in osteoarthritis, we performed gene ontology searches for pain, bone remodelling and inflammation and pathway enrichment analysis using Enrichr.

4.2.1 Pain

Mechanical loading of osteocytes in our 3D model regulated 26% of the 253 genes known to be involved in gene ontology pathways linked to OA pain (Supplementary Table 3C). However, an important mediator of pain in human and animal osteoarthritis, Nerve Growth Factor (NGF), although expressed in all our osteocyte cultures, was not regulated by load (Padj = 0.067). Expression of NGF has previously been reported to be upregulated in osteoblasts by physiological mechanical forces although it was not detected in osteocytes (94). In addition, several of the proposed mediators of OA pain such as neuropeptide Y (NPY), and substance P were not expressed in our model. However, Neuropeptide Y 1 receptor (NPY1R) was expressed and mechanically downregulated in our osteocyte model,

consistent with the mouse osteocyte transcriptome (60) but we did not detect NPY itself, also reported in osteocyte transcriptome. NPY is released by osteocytes, is important in balancing adipocyte and osteoblast differentiation and mediates its effects via receptors, NPY1R and NPY2R which localise to pain centres in the nervous system (95). NPY influences nociceptive signalling in neuropathic and inflammatory pain (96). It is an important regulator of bone homeostasis and its expression is increased in osteoarthritic synovium and the concentration in synovial fluid from osteoarthritic patients positively correlates with pain scores, and is increased in late stages of OA (97). Since osteocyte NPY acts through NPY1R to suppress osteogenesis and promote adipogenesis of bone marrow stem cells, the effect of the mechanically induced 70% reduction in NPY1R expression that we observed requires further study. We and others have previously shown that glutamate receptors are involved in neural responses to inflammatory pain and that glutamate receptor antagonists alleviate pain and degeneration in animal models (13, 22). AMPA (GRIA1/3/4), kainate (GRIK1/2/4/5) and NMDA (GRIN2A-D and 3A) ionotropic glutamate receptor subunits mRNAs were expressed in our osteocyte model. Of these GRIN2D and GRIK2 were identified in the osteocyte signature and involved with IDSWG3 maturation and GRIA3, GRIK5, GRIN2A and 3A in the osteocyte transcriptome (60). Kainate (GRIK2, 2-fold) and AMPA (GRIA3, 0.4-fold; GRIA4 20-fold) receptor subunits were mechanically regulated in osteocytes. This, along with reports of *in vivo* osteocyte expression of glutamate receptor proteins (AMPAR2 (13, 22); GRIN1, GRIA1/4 (14)), indicates a potential for mechanically-regulated glutamatergic signalling in osteocytes. Glutamate transporters (SLC1A1–3/EAAT1–3) were expressed by osteocytes consistent with previous reports *in vivo* (EAATs 1 and 2; SLC1A1 and 3 (60). Mechanical loading upregulated osteocyte SLC1A1/EAAT3 mRNA expression 3-fold but the mechanically-induced down regulation of SLC1A3/EAAT1 observed in osteocytes *in vivo* (16) was not recapitulated in this model. Upregulation of EAAT3 may explain why osteocytic glutamate release over 24 hours was reduced by mechanical loading. Increased concentrations of glutamate present in joint fluids in osteoarthritis, after joint injury, and at onset of joint inflammation (13, 22), are associated with pain and joint pathology (reviewed in (98)). The mechanically induced control of extracellular glutamate concentrations and regulation of glutamate receptor and transporter expression implicates osteocytes in the regulation of osteoarthritic pain and pathology although the effect of glutamate receptor activation in osteocytes is unknown.

4.2.2 Bone remodelling

Mechanical loading of osteocytes in our 3D model regulated 40% (23% upregulated; 16% downregulated) of the 217 genes known to be involved in gene ontology pathways linked to bone remodelling (Supplementary Table 3C).

The nearly 6-fold increase in OPG protein release after loading, without detectable changes in RANKL protein expression reveals a potential mechanically-induced inhibition of osteoclastogenesis and bone resorption consistent with the role of osteocytes in regulating bone remodelling in response to their mechanical environment (99). Mechanically regulated genes reflected pathways associated with RANKL signalling and abnormal bone cell function in a range of skeletal diseases, involving osteoclast activation and dysregulation of WNT signalling in osteoblasts. Interestingly similar pathways were identified as those that differed in the osteocyte transcriptome with age and sex (60).

4.2.3 Inflammation

Pathophysiological loading of osteocytes in our 3D model expressed 371 genes involved in acute and chronic inflammation with 27% of these genes being mechanically regulated (19% upregulated, 8% downregulated) (Supplementary Table 3D). NFkB signalling was particularly activated by mechanical load consistent with osteocytic loading playing a role in activating important proinflammatory and apoptotic pathways. In addition to the gene changes, several cytokine proteins were released by our osteocyte model, with mechanical loading reducing expression of both pro-resorptive (GM-CSF, IL-6, and RANTES) as well as anti-inflammatory (MCP-1, IL-8, IP-10) proteins. This indicates that osteocytes can directly link mechanical loading to inflammation potentially mediating pathological processes in mechanically driven diseases such as osteoarthritis.

4.3 IL-6 regulate readouts of osteoarthritis in our 3D model of osteocytes

IL-6 and its soluble receptor were used at concentrations reported in human synovial fluids from patients with OA (32) or following knee injury (31) to stimulate inflammation in our 3D osteocyte model. Although IL6/sIL6r downregulated the AMPA glutamate receptor mRNA, GRIA1, treatment with IL-6 had limited effects on the glutamate signalling pathway and did not regulate expression of either glutamate transporters or glutamate release. Conversely, IL-6 treatment did affect markers of bone remodelling, halving OPG expression and reducing indicators of bone formation (BGLAP) and mineralisation (ALPL) indicative of increased resorption and reduced osteogenesis. Treatment with IL-6/sIL-6r resulted in the release of both pro- and anti-inflammatory cytokines causing a >10-fold increase in IL-12p70 and IL-4 and approximately doubling TNF-α and IFN-γ protein release by osteocytes in our model all of which have been implicated in OA [reviewed in (100)] (30, 32),]. IL-4 and IL12 have been shown to be anti-osteoclastogenic and exert anti-resorptive effects on bone (101, 102). These data show that osteocytes in our 3D model respond to an inflammatory stimulus to modulate readouts of OA including markers of pain, bone remodelling and inflammation.

4.4 Links to human OA

We analysed our mechanosome dataset to determine whether genes that have been specifically identified as effector genes in OA patients were differentially expressed. A genome-wide association study (GWAS) meta-analysis across 13 international cohorts

(826,690 individuals, 177,517 with osteoarthritis) identified 77 putative effector genes by analysis of functional genomics, fine-mapping, eQTL, and associations with animal and human musculoskeletal and neuronal phenotypes (65). Of the 77 genes with strong evidence as effector genes (score3+), 83% were expressed in our osteocyte model with nearly half mechanically regulated (17 upregulated; 15 downregulated) (Supplementary Table 6A). The druggable genome database (reference (103) in (65)), revealed that twenty tier 1 (approved/clinical-phase drugs), five tier 2 (binding partners to approved drug targets) and twenty tier 3 (druggable pathways) were associated with these 77 putative causal genes. Of the 32 mechanically regulated genes in our model, identified as 'effector genes', 10 represented potential druggable targets (tier 1: TGFB1, TNC, CTSK, NOS3; tier 3A: GDF5, LTBP3, SERPINF1, NOG, LTBP1; tier 3B: MGP). A GWAS study by Tachmazidou et al. found 9 genes underlying monogenic forms of bone development diseases and ten likely early OA effector genes (104). Six genes underlying monogenic diseases were expressed in our dataset (2 upregulated by load) and 7/10 OA effector genes were present (2 upregulated and 2 down regulated by load) (Supplementary Table 6B). In addition, a search of the OMIM® database (https://omim.org/) using the terms 'osteoarthritis AND bone revealed 97 gene entries with a phenotype related to OA; 26 of the associated genes were regulated by load in our dataset, 16 up regulated and 10 down regulated and another further 38 genes were present but not regulated (Supplementary Table 6C). A recent study by Zhou et al. (105) also reported links between OA and mechanical responsive osteocyte genes including POSTN, NID2, and ASPN; all regulated by load in our dataset. Collectively, this data shows that mechanical loading of osteocytes in our model regulates the expression of several genes shown to be important in human osteoarthritis susceptibility and potential treatment.

4.5 Limitations

There are several limitations to our model. The type I collagen gel is not mineralised or organised as it would be *in vivo* and represents newly formed osteoid; with time this may become change and future studies could examine this. This means it does not exhibit the physical and chemical properties of bone and whilst the osteocyte-like cells appear to have good molecular and morphological phenotypes, these will not be completely the same as those *in vivo*. We have applied compressive strain based on measurements of the gel under loading, and mimicked strains observed in rodent bones (45). The mechanical environment experienced by the cells is not the same as it would be in a mineralised bone since the osteocytes are not located within lacunae with fluid flowing through them under load and the strain on the cell and the way the strain changes over the culture period is not defined. The cells are subjected to compressive, tensile stretch and fluid low all of which will influence the cell's responses; further work, beyond the scope of the current study, could perform finite element modelling to help clarify this. Finally, the load was a single load of 3000 cycles that occurred over approximately 5 minutes. This could reflect joint trauma, or high strains caused by an episode of abnormal loading through the joint. The intention is to identify osteocyte derived mechanoresponsive signals that could contribute to disease processes in osteoarthritis, not to model the chronic disease and all joint tissues. We only used osteocytes in the current study; future work could co-culture osteoblasts and/or osteoclasts to mimic more closely the bone environment or other cell types to investigate tissue interactions. PCA analysis revealed a potential variation in differentiation status across cultures, with the gene expression profile of sample C2 varying somewhat from C3–5 and the L2 and L3 response to load varying from L4–6. This variation is likely due to subtle differences in cell density or distribution when embedding within the type I collagen, leading to a delay in cell-cell interactions, network connectivity and inhibition of cell division (10). Despite this, we have shown that our cells express an osteocyte phenotype using several approaches including RT-qPCR expression of osteocyte markers, high homology to the osteocyte signature, which are genes enriched in osteocytes relative to bone marrow and other osteoblast lineage cells (60), and protein expression of the mechanosensing osteocyte protein, sclerostin; the cells would not express high levels of sclerostin. A timeline of gene expression changes that occur following the differentiation of mature osteoblasts to mature osteocytes is shown in Figure 7 [adapted from (10, 72)].

5 Conclusion

We have developed a reproducible model of human osteocyte like cells that express >90% of the genes in the osteocyte transcriptome signature. Mechanical loading and inflammatory stimulation regulated many genes and proteins implicated in osteoarthritis symptoms of pain as well as inflammation and degeneration underlying disease progression. Nearly half of the genes classified as 'effectors' in GWAS were mechanically regulated in this model. This model reveals that osteocyte mechanobiology plays an important role in osteoarthritic pathology. The model will be useful in identifying new mechanisms underlying bone and joint pathologies and testing drugs targeting those mechanisms.

Data availability statement

The data presented in this study are deposited in the Mendeley Data repository, DOI: 10.17632/5md5rnybcs.1.

Author contributions

SG: Writing – review & editing, Writing – original draft, Visualization, Validation, Supervision, Resources, Project administration, Methodology, Investigation, Funding acquisition, Formal Analysis, Data curation, Conceptualization. BE: Writing – review & editing, Validation, Methodology, Investigation. CB: Writing – review & editing, Validation, Methodology,

Investigation, Funding acquisition. RJ: Writing – review & editing, Validation, Software, Methodology, Investigation, Data curation. SE: Writing – review & editing, Validation, Software, Methodology, Investigation, Formal Analysis, Data curation. DM: Writing – review & editing, Writing – original draft, Validation, Supervision, Resources, Project administration, Methodology, Funding acquisition, Formal Analysis, Conceptualization.

Funding

The author(s) declare financial support was received for the research, authorship, and/or publication of this article. This work was funded by the NC3Rs CRACK IT Challenge 22: Osteo-chip, NC3Rs Project grant (NC/Y000951/1), Wellcome Trust Collaborative Award (209233/Z/17/Z), and the Biomechanics and Bioengineering Research Centre Versus Arthritis (EC/20781).

Acknowledgments

The author's wish to thank Peter Giles (Wales Gene Park) for the RNA sequencing and analysis, Professor Paul Genever (University of York) who kindly provided the Y201 cell line and associated methods, and Alexander Dufour, Pauline Nicole, Justine Cailleau and Bethany Keenan for their help with the strain calculations.

Conflict of interest

DM and CB hold patents for the use of glutamate receptor antagonists to prevent osteoarthritis.

The remaining authors declare that the research was conducted in the absence of any commercial or

financial relationships that could be constructed as a potential conflict of interest.

The author(s) declared that they were an editorial board member of Frontiers, at the time of submission.

Publisher's note

Supplementary material

The Supplementary Material for this article can be found online at: https://www.frontiersin.org/articles/10.3389/fendo.2024.1359052/full#supplementary-material

References

1. Guilak F. Biomechanical factors in osteoarthritis. *Best Pract Res Clin Rheumatol.* (2011) 25:815–23. doi: 10.1016/j.berh.2011.11.013

2. Watt FE, Corp N, Kingsbury SR, Frobell R, Englund M, Felson DT, et al. Towards prevention of post-traumatic osteoarthritis: report from an international expert working group on considerations for the design and conduct of interventional studies following acute knee injury. *Osteoarthritis Cartilage.* (2019) 27:23–33. doi: 10.1016/j.joca.2018.08.001

3. Kim JR, Yoo JJ, Kim HA. Therapeutics in osteoarthritis based on an understanding of its molecular pathogenesis. *Int J Mol Sci.* (2018) 19:674. doi: 10.3390/ijms19030674

4. Findlay DM, Atkins GJ. Osteoblast-chondrocyte interactions in osteoarthritis. *Curr Osteoporos Rep.* (2014) 12:127–34. doi: 10.1007/s11914-014-0192-5

5. Bonewald LF. The amazing osteocyte. *J Bone Miner Res.* (2011) 26:229–38. doi: 10.1002/jbmr.320

6. Asada N, Katayama Y, Sato M, Minagawa K, Wakahashi K, Kawano H, et al. Matrix-embedded osteocytes regulate mobilization of hematopoietic stem/progenitor cells. *Cell Stem Cell.* (2013) 12:737–47. doi: 10.1016/j.stem.2013.05.001

7. Bergwitz C, Juppner H. Regulation of phosphate homeostasis by PTH, vitamin D, and FGF23. *Annu Rev Med.* (2010) 61:91–104. doi: 10.1146/annurev.med.051308.111339

8. Sato M, Asada N, Kawano Y, Wakahashi K, Minagawa K, Kawano H, et al. Osteocytes regulate primary lymphoid organs and fat metabolism. *Cell Metab.* (2013) 18:749–58. doi: 10.1016/j.cmet.2013.09.014

9. Repp F, Kollmannsberger P, Roschger A, Kerschnitzki M, Berzlanovich A, Gruber GM, et al. Spatial heterogeneity in the canalicular density of the osteocyte network in human osteons. *Bone Rep.* (2017) 6:101–8. doi: 10.1016/j.bonr.2017.03.001

10. Dallas SL, Prideaux M, Bonewald LF. The osteocyte: an endocrine cell more. *Endocr Rev.* (2013) 34:658–90. doi: 10.1210/er.2012-1026

11. Qin L, Liu W, Cao H, Xiao G. Molecular mechanosensors in osteocytes. *Bone Res.* (2020) 8:23. doi: 10.1038/s41413-020-0099-y

12. Hunter DJ, Guermazi A, Roemer F, Zhang Y, Neogi T. Structural correlates of pain in joints with osteoarthritis. *Osteoarthritis Cartilage.* (2013) 21:1170–8. doi: 10.1016/j.joca.2013.05.017

13. Bonnet CS, Gilbert SJ, Blain EJ, Williams AS, Mason DJ. AMPA/kainate glutamate receptor antagonists prevent posttraumatic osteoarthritis. *JCI Insight.* (2020) 5:e134055. doi: 10.1172/jci.insight.134055

14. Chenu C, Serre CM, Raynal C, Burt-Pichat B, Delmas PD. Glutamate receptors are expressed by bone cells and are involved in bone resorption. *Bone.* (1998) 22:295–9. doi: 10.1016/S8756-3282(97)00295-0

15. Flood S, Parri R, Williams A, Duance V, Mason D. Modulation of interleukin-6 and matrix metalloproteinase 2 expression in human fibroblast-like synoviocytes by functional ionotropic glutamate receptors. *Arthritis Rheumatol.* (2007) 56:2523–34. doi: 10.1002/art.22829

16. Mason DJ, Suva LJ, Genever PG, Patton AJ, Steuckle S, Hillam RA, et al. Mechanically regulated expression of a neural glutamate transporter in bone: a role for excitatory amino acids as osteotropic agents? *Bone.* (1997) 20:199–205. doi: 10.1016/S8756-3282(96)00386-9

17. Alstergren P, Ernberg M, Nilsson M, Hajati AK, Sessle BJ, Kopp S. Glutamate-induced temporomandibular joint pain in healthy individuals is partially mediated by peripheral NMDA receptors. *J Orofac Pain.* (2010) 24:172–80. doi: 10.11607/jofph.24.2.05

18. McNearney T, Speegle D, Lawand N, Lisse J, Westlund KN. Excitatory amino acid profiles of synovial fluid from patients with arthritis. *J Rheumatol.* (2000) 27:739–45.

19. McNearney T, Baethge BA, Cao S, Alam R, Lisse JR, Westlund KN. Excitatory amino acids, TNF-alpha, and chemokine levels in synovial fluids of patients with active arthropathies. *Clin Exp Immunol.* (2004) 137:621–7. doi: 10.1111/j.1365-2249.2004.02563.x

20. Lawand NB, McNearney T, Westlund KN. Amino acid release into the knee joint: key role in nociception and inflammation. *Pain.* (2000) 86:69–74. doi: 10.1016/S0304-3959(99)00311-5

21. Lam FF, Ng ES. Substance P and glutamate receptor antagonists improve the anti-arthritic actions of dexamethasone in rats. *Br J Pharmacol.* (2010) 159:958–69. doi: 10.1111/j.1476-5381.2009.00586.x

22. Bonnet CS, Williams AS, Gilbert SJ, Harvey AK, Evans BA, Mason DJ. AMPA/kainate glutamate receptors contribute to inflammation, degeneration and pain related

behaviour in inflammatory stages of arthritis. *Ann Rheum Dis*. (2015) 74:242–51. doi: 10.1136/annrheumdis-2013-203670

23. Gilbert SJ, Bonnet CS, Stadnik P, Duance VC, Mason DJ, Blain EJ. Inflammatory and degenerative phases resulting from anterior cruciate rupture in a non-invasive murine model of post-traumatic osteoarthritis. *J Orthop Res*. (2018) 36(8):2118–27. doi: 10.1002/jor.23872

24. Chen W, Ma Y, Ye H, He Y, Li X, Li J, et al. ERK1/2 is involved in cyclic compressive force-induced IL-6 secretion in MLO-Y4 cells. *Biochem Biophys Res Commun*. (2010) 401:339–43. doi: 10.1016/j.bbrc.2010.09.044

25. Sanchez C, Gabay O, Salvat C, Henrotin YE, Berenbaum F. Mechanical loading highly increases IL-6 production and decreases OPG expression by osteoblasts. *Osteoarthritis Cartilage*. (2009) 17:473–81. doi: 10.1016/j.joca.2008.09.007

26. Bakker AD, Kulkarni RN, Klein-Nulend J, Lems WF. IL-6 alters osteocyte signaling toward osteoblasts but not osteoclasts. *J Dent Res*. (2014) 93:394–9. doi: 10.1177/0022034514522485

27. De Benedetti F, Rucci N, Del Fattore A, Peruzzi B, Paro R, Longo M, et al. Impaired skeletal development in interleukin-6-transgenic mice: a model for the impact of chronic inflammation on the growing skeletal system. *Arthritis Rheumatol*. (2006) 54:3551–63. doi: 10.1002/art.22175

28. Rufo A, Del Fattore A, Capulli M, Carvello F, De Pasquale L, Ferrari S, et al. Mechanisms inducing low bone density in Duchenne muscular dystrophy in mice and humans. *J Bone Miner Res*. (2011) 26:1891–903. doi: 10.1002/jbmr.410

29. Feng W, Liu H, Luo T, Liu D, Du J, Sun J, et al. Combination of IL-6 and sIL-6R differentially regulate varying levels of RANKL-induced osteoclastogenesis through NF-kappaB, ERK and JNK signaling pathways. *Sci Rep*. (2017) 7:41411. doi: 10.1038/srep41411

30. Nees TA, Rosshirt N, Zhang JA, Reiner T, Sorbi R, Tripel E, et al. Synovial cytokines significantly correlate with osteoarthritis-related knee pain and disability: inflammatory mediators of potential clinical relevance. *J Clin Med*. (2019) 8:1343. doi: 10.3390/jcm8091343

31. Kotake S, Sato K, Kim KJ, Takahashi N, Udagawa N, Nakamura I, et al. Interleukin-6 and soluble interleukin-6 receptors in the synovial fluids from rheumatoid arthritis patients are responsible for osteoclast-like cell formation. *J Bone Miner Res*. (1996) 11:88–95. doi: 10.1002/jbmr.5650110113

32. Watt FE, Paterson E, Freidin A, Kenny M, Judge A, Saklatvala J, et al. Acute molecular changes in synovial fluid following human knee injury: association with early clinical outcomes. *Arthritis Rheumatol*. (2016) 68:2129–40. doi: 10.1002/art.39677

33. Livshits G, Zhai G, Hart DJ, Kato BS, Wang H, Williams FM, et al. Interleukin-6 is a significant predictor of radiographic knee osteoarthritis: The Chingford Study. *Arthritis Rheumatol*. (2009) 60:2037–45. doi: 10.1002/art.24598

34. Blumenfeld O, Williams FM, Valdes A, Hart DJ, Malkin I, Spector TD, et al. Association of interleukin-6 gene polymorphisms with hand osteoarthritis and hand osteoporosis. *Cytokine*. (2014) 69:94–101. doi: 10.1016/j.cyto.2014.05.012

35. Singh T, Newman AB. Inflammatory markers in population studies of aging. *Ageing Res Rev*. (2011) 10:319–29. doi: 10.1016/j.arr.2010.11.002

36. Spector TD, Hart DJ, Nandra D, Doyle DV, Mackillop N, Gallimore JR, et al. Low-level increases in serum C-reactive protein are present in early osteoarthritis of the knee and predict progressive disease. *Arthritis Rheumatol*. (1997) 40:723–7. doi: 10.1002/art.1780400419

37. Ryu JH, Yang S, Shin Y, Rhee J, Chun CH, Chun JS. Interleukin-6 plays an essential role in hypoxia-inducible factor 2alpha-induced experimental osteoarthritic cartilage destruction in mice. *Arthritis Rheumatol*. (2011) 63:2732–43. doi: 10.1002/art.30451

38. Wu X, Cao L, Li F, Ma C, Liu G, Wang Q. Interleukin-6 from subchondral bone mesenchymal stem cells contributes to the pathological phenotypes of experimental osteoarthritis. *Am J Transl Res*. (2018) 10:1143–54.

39. Johnson CI, Argyle DJ, Clements DN. *In vitro* models for the study of osteoarthritis. *Vet J*. (2016) 209:40–9. doi: 10.1016/j.tvjl.2015.07.011

40. Samvelyan HJ, Hughes D, Stevens C, Staines KA. Models of osteoarthritis: relevance and new insights. *Calcif Tissue Int*. (2021) 109:243–56. doi: 10.1007/s00223-020-00670-x

41. Vazquez M, Evans BA, Riccardi D, Evans SL, Ralphs JR, Dillingham CM, et al. A new method to investigate how mechanical loading of osteocytes controls osteoblasts. *Front endocrinology*. (2014) 5:208.doi: 10.3389/fendo.2014.00208

42. James S, Fox J, Afsari F, Lee J, Clough S, Knight C, et al. Multiparameter analysis of human bone marrow stromal cells identifies distinct immunomodulatory and differentiation-competent subtypes. *Stem Cell Rep*. (2015) 4:1004–15. doi: 10.1016/j.stemcr.2015.05.005

43. Kim J, Adachi T. Cell-fate decision of mesenchymal stem cells toward osteocyte differentiation is committed by spheroid culture. *Sci Rep*. (2021) 11:13204. doi: 10.1038/s41598-021-92607-z

44. Galarza Torre A, Shaw JE, Wood A, Gilbert HTJ, Dobre O, Genever P, et al. An immortalised mesenchymal stem cell line maintains mechano-responsive behaviour and can be used as a reporter of substrate stiffness. *Sci Rep*. (2018) 8:8981. doi: 10.1038/s41598-018-27346-9

45. Hillam RA, Skerry TM. Inhibition of bone resorption and stimulation of formation by mechanical loading of the modeling rat ulna in vivo. *J Bone Miner Res*. (1995) 10:683–9. doi: 10.1002/jbmr.5650100503

46. Robling AG, Niziolek PJ, Baldridge LA, Condon KW, Allen MR, Alam I, et al. Mechanical stimulation of bone in *vivo* reduces osteocyte expression of Sost/sclerostin. *J Biol Chem*. (2008) 283:5866–75. doi: 10.1074/jbc.M705092200

47. Mason DJ, Hillam RA, Skerry TM. Constitutive in *vivo* mRNA expression by osteocytes of beta-actin, osteocalcin, connexin-43, IGF-I, c-fos and c-jun, but not TNF-alpha nor tartrate-resistant acid phosphatase. *J Bone Miner Res*. (1996) 11:350–7. doi: 10.1002/jbmr.5650110308

48. Rubin C, Turner AS, Bain S, Mallinckrodt C, McLeod K. Anabolism. Low mechanical signals strengthen long bones. *Nature*. (2001) 412:603–4. doi: 10.1038/35088122

49. Robling AG, Turner CH. Mechanical signaling for bone modeling and remodeling. *Crit Rev eukaryotic Gene expression*. (2009) 19:319–38. doi: 10.1615/CritRevEukarGeneExpr.v19.i4

50. Xie F, Xiao P, Chen D, Xu L, Zhang B. miRDeepFinder: a miRNA analysis tool for deep sequencing of plant small RNAs. *Plant Mol Biol*. (2012) 5. doi: 10.1007/s11103-012-9885-2

51. Livak KJ, Schmittgen TD. Analysis of relative gene expression data using real-time quantitative PCR and the 2(-Delta Delta C(T)) Method. *Methods*. (2001) 25:402–8. doi: 10.1006/meth.2001.1262

52. Taylor S, Wakem M, Dijkman G, Alsarraj M, Nguyen M. A practical approach to RT-qPCR-Publishing data that conform to the MIQE guidelines. *Methods*. (2010) 50: S1–5. doi: 10.1016/j.ymeth.2010.01.005

53. Dobin A, Gingeras TR. Mapping RNA-seq reads with STAR. *Curr Protoc Bioinf*. (2015) 51:11.14.1–19. doi: 10.1002/0471250953.bi1114s51

54. Love MI, Huber W, Anders S. Moderated estimation of fold change and dispersion for RNA-seq data with DESeq2. *Genome Biol*. (2014) 15:550. doi: 10.1186/s13059-014-0550-8

55. Benjamini Y, Drai D, Elmer G, Kafkafi N, Golani I. Controlling the false discovery rate in behavior genetics research. *Behav Brain Res*. (2001) 125:279–84. doi: 10.1016/S0166-4328(01)00297-2

56. Reimand J, Kull M, Peterson H, Hansen J, Vilo J. g:Profiler–a web-based toolset for functional profiling of gene lists from large-scale experiments. *Nucleic Acids Res*. (2007) 35:W193–200. doi: 10.1093/nar/gkm226

57. Chen EY, Tan CM, Kou Y, Duan Q, Wang Z, Meirelles GV, et al. Enrichr: interactive and collaborative HTML5 gene list enrichment analysis tool. *BMC Bioinf*. (2013) 14:128. doi: 10.1186/1471-2105-14-128

58. Xie Z, Bailey A, Kuleshov MV, Clarke DJB, Evangelista JE, Jenkins SL, et al. Gene set knowledge discovery with enrichr. *Curr Protoc*. (2021) 1:e90. doi: 10.1002/cpz1.90

59. Kuleshov MV, Jones MR, Rouillard AD, Fernandez NF, Duan Q, Wang Z, et al. Enrichr: a comprehensive gene set enrichment analysis web server 2016 update. *Nucleic Acids Res*. (2016) 44:W90–7. doi: 10.1093/nar/gkw377

60. Youlten SE, Kemp JP, Logan JG, Ghirardello EJ, Sergio CM, Dack MRG, et al. Osteocyte transcriptome mapping identifies a molecular landscape controlling skeletal homeostasis and susceptibility to skeletal disease. *Nat Commun*. (2021) 12:2444. doi: 10.1038/s41467-021-22517-1

61. Carbon S, Ireland A, Mungall CJ, Shu S, Marshall B, Lewis S, et al. AmiGO: online access to ontology and annotation data. *Bioinformatics*. (2009) 25:288–9. doi: 10.1093/bioinformatics/btn615

62. Ashburner M, Ball CA, Blake JA, Botstein D, Butler H, Cherry JM, et al. Gene ontology: tool for the unification of biology. *Gene Ontology Consortium. Nat Genet*. (2000) 25:25–9. doi: 10.1038/75556

63. Gene Ontology C, Aleksander SA, Balhoff J, Carbon S, Cherry JM, Drabkin HJ, et al. The gene ontology knowledgebase in 2023. *Genetics*. (2023) 224:25–9. doi: 10.1038/75556

64. St John HC, Bishop KA, Meyer MB, Benkusky NA, Leng N, Kendziorski C, et al. The osteoblast to osteocyte transition: epigenetic changes and response to the vitamin D3 hormone. *Mol Endocrinol*. (2014) 28:1150–65.

65. Boer CG, Hatzikotoulas K, Southam L, Stefansdottir L, Zhang Y, Coutinho de Almeida R, et al. Deciphering osteoarthritis genetics across 826,690 individuals from 9 populations. *Cell*. (2021) 184:4784–818 e17. doi: 10.1136/annrheumdis-2017-211396

66. Kuttapitiya A, Assi L, Laing K, Hing C, Mitchell P, Whitley G, et al. Microarray analysis of bone marrow lesions in osteoarthritis demonstrates upregulation of genes implicated in osteochondral turnover, neurogenesis and inflammation. *Ann Rheum Dis*. (2017) 76:1764–73. doi: 10.1136/annrheumdis-2017-211396

67. Felson DT, Chaisson CE, Hill CL, Totterman SM, Gale ME, Skinner KM, et al. The association of bone marrow lesions with pain in knee osteoarthritis. *Ann Intern Med*. (2001) 134:541–9. doi: 10.7326/0003-4819-134-7-200104030-00007

68. Palumbo C, Palazzini S, Zaffe D, Marotti G. Osteocyte differentiation in the tibia of newborn rabbit: an ultrastructural study of the formation of cytoplasmic processes. *Acta Anat (Basel)*. (1990) 137:350–8. doi: 10.1159/000146907

69. Tu X, Rhee Y, Condon KW, Bivi N, Allen MR, Dwyer D, et al. Sost downregulation and local Wnt signaling are required for the osteogenic response to mechanical loading. *Bone*. (2012) 50:209–17. doi: 10.1016/j.bone.2011.10.025

70. Dallas SL, Bonewald LF. Dynamics of the transition from osteoblast to osteocyte. *Ann New York Acad Sci*. (2010) 1192:437–43. doi: 10.1111/j.1749-6632.2009.05246.x

71. Delgado-Calle J, Bellido T. The osteocyte as a signaling cell. *Physiol Rev*. (2022) 102:379–410. doi: 10.1152/physrev.00043.2020

72. Plotkin LI, Bellido T. Osteocytic signalling pathways as therapeutic targets for bone fragility. *Nat Rev Endocrinol*. (2016) 12:593–605. doi: 10.1038/nrendo.2016.71

73. Dallas SL, Prideaux M, Bonewald LF. The osteocyte: an endocrine cell … and more. *Endocrine Rev*. (2013) 34:658–90. doi: 10.1210/er.2012-1026

74. Zhang K, Barragan-Adjemian C, Ye L, Kotha S, Dallas M, Lu Y, et al. E11/gp38 selective expression in osteocytes: regulation by mechanical strain and role in dendrite elongation. *Mol Cell Biol*. (2006) 26:4539–52. doi: 10.1128/MCB.02120-05

75. Hughes DE, Salter DM, Simpson R. CD44 expression in human bone: a novel marker of osteocytic differentiation. *J Bone Miner Res*. (1994) 9:39–44. doi: 10.1002/jbmr.5650090106

76. Kamioka H, Sugawara Y, Honjo T, Yamashiro T, Takano-Yamamoto T. Terminal differentiation of osteoblasts to osteocytes is accompanied by dramatic changes in the distribution of actin-binding proteins. *J Bone Miner Res*. (2004) 19:471–8. doi: 10.1359/JBMR.040128

77. Guo D, Keightley A, Guthrie J, Veno PA, Harris SE, Bonewald LF. Identification of osteocyte-selective proteins. *Proteomics*. (2010) 10:3688–98. doi: 10.1002/pmic.201000306

78. Plotkin LI, Bellido T. Beyond gap junctions: Connexin43 and bone cell signaling. *Bone*. (2013) 52:157–66. doi: 10.1016/j.bone.2012.09.030

79. Plotkin LI. Connexin 43 and bone: not just a gap junction protein. *Actualizaciones En Osteologia*. (2011) 7:79–90. doi: 10.1016/j.bone.2015.07.035

80. Javaheri B, Carriero A, Staines KA, Chang YM, Houston DA, Oldknow KJ, et al. Phospho1 deficiency transiently modifies bone architecture yet produces consistent modification in osteocyte differentiation and vascular porosity with ageing. *Bone*. (2015) 81:277–91. doi: 10.1016/j.bone.2015.07.035

81. Paic F, Igwe JC, Nori R, Kronenberg MS, Franceschetti T, Harrington P, et al. Identification of differentially expressed genes between osteoblasts and osteocytes. *Bone*. (2009) 45:682–92. doi: 10.1016/j.bone.2009.06.010

82. Sato T, Verma S, Andrade CDC, Omeara M, Campbell N, Wang JS, et al. A FAK/HDAC5 signaling axis controls osteocyte mechanotransduction. *Nat Commun*. (2020) 11:3282. doi: 10.1038/s41467-020-17099-3

83. Bernhardt A, Weiser E, Wolf S, Vater C, Gelinsky M. Primary human osteocyte networks in pure and modified collagen gels. *Tissue Eng Part A*. (2019) 25:1347–55. doi: 10.1089/ten.tea.2018.0338

84. Boukhechba F, Balaguer T, Michiels JF, Ackermann K, Quincey D, Bouler JM, et al. Human primary osteocyte differentiation in a 3D culture system. *J Bone Miner Res*. (2009) 24:1927–35. doi: 10.1359/jbmr.090517

85. Holguin N, Brodt MD, Silva MJ. Activation of wnt signaling by mechanical loading is impaired in the bone of old mice. *J Bone Miner Res*. (2016) 31:2215–26. doi: 10.1002/jbmr.2900

86. Temiyasathit S, Jacobs CR. Osteocyte primary cilium and its role in bone mechanotransduction. *Ann N Y Acad Sci*. (2010) 1192:422–8. doi: 10.1111/j.1749-6632.2009.05243.x

87. Chinipardaz Z, Liu M, Graves DT, Yang S. Role of primary cilia in bone and cartilage. *J Dent Res*. (2022) 101:253–60. doi: 10.1177/00220345211046606

88. Yuan X, Yang S. Primary cilia and intraflagellar transport proteins in bone and cartilage. *J Dent Res*. (2016) 95:1341–9. doi: 10.1177/0022034516652383

89. Makitie O, Zillikens MC. Early-onset osteoporosis. *Calcif Tissue Int*. (2022) 110:546–61. doi: 10.1007/s00223-021-00885-6

90. Laslett LL, Dore DA, Quinn SJ, Boon P, Ryan E, Winzenberg TM, et al. Zoledronic acid reduces knee pain and bone marrow lesions over 1 year: a randomised controlled trial. *Ann Rheum Dis*. (2012) 71:1322–8. doi: 10.1136/annrheumdis-2011-200970

91. Hunter DJ, Guermazi A, Lo GH, Grainger AJ, Conaghan PG, Boudreau RM, et al. Evolution of semi-quantitative whole joint assessment of knee OA: MOAKS (MRI Osteoarthritis Knee Score). *Osteoarthritis Cartilage*. (2011) 19:990–1002. doi: 10.1016/j.joca.2011.05.004

92. Callaghan MJ, Parkes MJ, Hutchinson CE, Gait AD, Forsythe LM, Marjanovic EJ, et al. A randomised trial of a brace for patellofemoral osteoarthritis targeting knee pain and bone marrow lesions. *Ann Rheum Dis*. (2015) 74:1164–70. doi: 10.1136/annrheumdis-2014-206376

93. Zeng MH, Wang XS, Chen TY, Ruan GF, Li J, Xue S, et al. Comprehensive analysis on subchondral bone marrow lesions of human osteoarthritis by integrating bulk and single-cell transcriptomes. *BMC musculoskeletal Disord*. (2023) 24:e3632–41. doi: 10.1186/s12891-023-06676-4

94. Tomlinson RE, Li Z, Li Z, Minichiello L, Riddle RC, Venkatesan A, et al. NGF-TrkA signaling in sensory nerves is required for skeletal adaptation to mechanical loads in mice. *Proc Natl Acad Sci U S A*. (2017) 114:E3632–E41. doi: 10.1073/pnas.1701054114

95. Lin ST, Li YZ, Sun XQ, Chen QQ, Huang SF, Lin S, et al. Update on the role of neuropeptide Y and other related factors in breast cancer and osteoporosis. *Front endocrinology*. (2021) 12:705499.doi: 10.3389/fendo.2021.705499

96. Tan CMJ, Green P, Tapoulal N, Lewandowski AJ, Leeson P, Herring N. The role of neuropeptide Y in cardiovascular health and disease. *Front Physiol*. (2018) 9:1281.doi: 10.3389/fphys.2018.01281

97. Wang L, Zhang L, Pan H, Peng S, Lv M, Lu WW. Levels of neuropeptide Y in synovial fluid relate to pain in patients with knee osteoarthritis. *BMC Musculoskelet Disord*. (2014) 15:319. doi: 10.1186/1471-2474-15-319

98. Wen ZH, Chang YC, Jean YH. Excitatory amino acid glutamate: role in peripheral nociceptive transduction and inflammation in experimental and clinical osteoarthritis. *Osteoarthritis Cartilage*. (2015) 23:2009–16. doi: 10.1016/j.joca.2015.03.017

99. Robling AG, Bonewald LF. The osteocyte: new insights. *Annu Rev Physiol*. (2020) 82:485–506. doi: 10.1146/annurev-physiol-021119-034332

100. Li J, Zhang H, Han Y, Hu Y, Geng Z, Su J. Targeted and responsive biomaterials in osteoarthritis. *Theranostics*. (2023) 13:931–54. doi: 10.7150/thno.78639

101. Cheng J, Liu J, Shi Z, Xu D, Luo S, Siegal GP, et al. Interleukin-4 inhibits RANKL-induced NFATc1 expression via STAT6: a novel mechanism mediating its blockade of osteoclastogenesis. *J Cell Biochem*. (2011) 112:3385–92. doi: 10.1002/jcb.23269

102. Horwood NJ, Elliott J, Martin TJ, Gillespie MT. IL-12 alone and in synergy with IL-18 inhibits osteoclast formation in vitro. *J Immunol*. (2001) 166:4915–21. doi: 10.4049/jimmunol.166.8.4915

103. Finan C, Gaulton A, Kruger FA, Lumbers RT, Shah T, Engmann J, et al. The druggable genome and support for target identification and validation in drug development. *Sci Transl Med*. (2017) 9:eaag1166. doi: 10.1126/scitranslmed.aag1166

104. Tachmazidou I, Hatzikotoulas K, Southam L, Esparza-Gordillo J, Haberland V, Zheng J, et al. Identification of new therapeutic targets for osteoarthritis through genome-wide analyses of UK Biobank data. *Nat Genet*. (2019) 51:230–+. doi: 10.1038/s41588-018-0327-1

105. Zhou J, He Z, Cui J, Liao X, Cao H, Shibata Y, et al. Identification of mechanics-responsive osteocyte signature in osteoarthritis subchondral bone. *Bone Joint Res*. (2022) 11:362–70. doi: 10.1302/2046-3758.116.BJR-2021-0436.R1

frontiers | Frontiers in Endocrinology

TYPE Hypothesis and Theory
PUBLISHED 07 November 2024
DOI 10.3389/fendo.2024.1480274

OPEN ACCESS

EDITED BY
Katherine A. Staines,
University of Brighton, United Kingdom

REVIEWED BY
Karan Mehul Shah,
The University of Sheffield, United Kingdom
Zhen Geng,
Shanghai University, China

*CORRESPONDENCE
Deborah J. Mason
masondj@cardiff.ac.uk

RECEIVED 13 August 2024
ACCEPTED 16 October 2024
PUBLISHED 07 November 2024

CITATION
Jones R, Gilbert SJ, Christofides SR and Mason DJ (2024) Osteocytes contribute to sex-specific differences in osteoarthritic pain. *Front. Endocrinol.* 15:1480274. doi: 10.3389/fendo.2024.1480274

Osteocytes contribute to sex-specific differences in osteoarthritic pain

Ryan Jones, Sophie J. Gilbert, Sarah R. Christofides and Deborah J. Mason*

Biomechanics and Bioengineering Research Centre Versus Arthritis, School of Biosciences, Cardiff University, Cardiff, United Kingdom

Osteoarthritic (OA) pain affects 18% of females and 9.6% of males aged over 60 worldwide, with 62% of all OA patients being women. The molecular drivers of sex-based differences in OA are unknown. Bone is intricately coupled with the sensory nervous system and one of the only joint tissues known to show changes that correlate with patient pain in OA. There are fundamental sex differences in pain sensation and bone biology which may be intrinsic to OA disease progression, however these differences are vastly under researched. We have utilised three data sets to investigate the hypothesis that potential mediators responsible for sex dependent pain mechanisms displayed in OA are derived from mechanically stimulated osteocytes. Our published dataset of the *in vitro* human osteocyte mechanosome was independently compared with published data from, sex-based gene expression differences in human long bone, the sex-based gene expression differences during the skeletal maturation of the mouse osteocyte transcriptome and sex specific OA risk factors and effector genes in a large human GWAS. 80 of the 377 sex-specific genes identified in the mouse osteocyte transcriptome were mechanically regulated in osteocytes with enrichment associated with neural crest migration and axon extension, and DISEASES analysis enrichment for the rheumatoid arthritis pathway. 3861 mechanically regulated osteocytic genes displayed sex-specific differences in human long bone with enrichment for genes associated with the synapse, sensory perception of pain, axon guidance, immune responses, distal peripheral sensory neuropathy, sensory neuropathy, and poor wound healing. 32 of 77 effector genes and 1 of 3 female specific OA risk factor genes identified in the human GWAS were differentially expressed in the osteocyte mechanosome and male and female bone. This analysis lends support to the hypothesis that mechanically regulated genes in osteocytes could influence sex specific differences in osteoarthritic pain and highlights pain pathways with approved drugs that could potentially treat elevated pain susceptibility in females with OA.

KEYWORDS

osteoarthritis, pain, osteocyte, sex differences, menopause

1 Introduction

Chronic pain in osteoarthritis (OA) is a severe and debilitating condition affecting an estimated 530 million sufferers worldwide, limiting patient mobility, ability to perform daily activities and live independently (1). Sex-based differences in the clinical presentation and prevalence of OA has been described for decades but are widely under-researched (2). Women over the age of 55 have a higher prevalence of knee OA than men of the same age (3) and a higher prevalence of hand OA (4). Women with OA also suffer more debilitating pain (3), more annual articular cartilage loss (5) and have a more severe radiographic OA when compared to equivalent male patients. Female sex hormones, such as oestrogen, are known to act directly on nociceptors to mitigate pain (6) and exert protective roles in articular cartilage and subchondral bone (5, 7) and more than half of post-menopausal women suffer with OA pain (8). Therefore, it has been assumed that the differences in male and female OA pain and progression are due to withdrawal of the protective effects of oestrogen (9) but research results are controversial. In a large cohort study, Cirillo et al. found that oestrogen treatment alone lowered the prevalence of hip replacement but not knee replacement (10) whereas another study of post-menopausal woman with both symptomatic and radiographic OA receiving hormone therapy, reported a lower prevalence of knee OA (11).

Bone is sexually dimorphic, displaying different gene expression profiles, sex hormone sensitivities and mechanical responses between males and females. Subchondral bone is also one of the only tissues to show structural changes that correlate to pain in OA patients (12). The inhibition of bone resorption to prevent OA disease progression in animal models and OA patients is also an emerging research area (reviewed in 13). There are intimate associations between nerves and bone. Skeletal sensory nerve sprouting, invasion and sensitisation are associated with bone pathologies, demonstrated in rodent and human OA joints, and intrinsic to pain responses in animal models of OA (14), and humans with OA (15). Densely innervated subchondral bone channels have been shown to accompany sclerotic subchondral bone remodelling in the tibial plateaux and femoral condyles of end-stage OA knees in animal models (16). Areas of OA structural damage, necrosis and remodelling in the subchondral bone known as bone marrow lesions (BML) are characterised by sensory nerve invasion and correlate with pain (17). Enlargement of BMLs is associated with worsening joint degeneration and increased pain, whereas reduced BML severity relieves pain (18). The formation of BMLs is known to be modulated by mechanical loading. Abnormal joint loading through obesity, malalignment, trauma, or joint instability are key risk factors for OA (19). BML presence and location are associated with joint malalignment (20); medial BMLs occur mostly in varus knee, lateral in valgus (20). Absence/regression of BMLs occurs following mechanical (bracing) (21) or bone sparing pharmaceutical (Zoledronic acid) interventions (22). Osteocytes, the mechanosensing cells in bone, orchestrate bone remodelling in response to mechanical load, inflammation, and hormones (23). In a previous study, we developed a human 3D model of osteocytes differentiated from Y201 Mesenchymal Stem Cells in Type I collagen (24). This model shows dendritic morphology, and expresses osteocyte markers BGLAP SOST, PDPN, OPG, GJA1, C44, FGF23, PHEX and PHOSPHO1 (24). Pathophysiological (4300 microstrain) (25) loads applied to this osteocyte model under osteogenic conditions regulated proteins reflecting bone remodelling and inflammation. RNAseq analysis on pathophysiologically loaded versus unloaded osteocytes in this 3D model revealed 7564 differentially expressed genes (DEGs), which we have called the osteocyte mechanosome (24). The osteocyte mechanosome included genes involved in inflammation, matrix organisation, ageing, ossification, bone morphogenesis, cartilage development, and bone mineralisation (24) as well as > 200 genes directly involved in nociception, neuropathic pain, nociceptor sensitisation, neuronal axonal guidance, and neuro-sensitivity (24). We have previously used this model to investigate mechanical and inflammatory mechanisms underlying osteoarthritic pathology (24). In the current hypothesis and theory paper, we have compared published data with the osteocyte mechanosome to test the notion that genes that are mechanically regulated in osteocytes and differentially expressed in males and females could explain sex-specific susceptibility to pain.

We hypothesise that differences between male and female susceptibility to osteoarthritic pain is influenced by sex-specific responses of osteocytes to mechanical stimulation. To test this, we have performed a meta-analysis of published RNAseq data to determine whether regulated genes in the osteocyte mechanosome are differentially expressed in male and female bone. The resulting sex-specific mechanically regulated genes were compared with OA risk loci from human Genome Wide Association Studies (GWAS) to highlight mediators linked to sex differences in OA. We then investigate whether these sex specific genes in the osteocyte mechanosome are associated with pathways linked to the generation of pain and represent new druggable targets that could treat female heightened susceptibility to osteoarthritic pain.

2 Methods and results

Three independent analyses were used to interrogate the above hypothesis; these were then combined to investigate the potential mediators responsible for the osteocyte-derived sex dependent pain mechanisms displayed in OA (Figure 1). All analysis was performed using R 4.3.1 (31) in RStudio 2023.12.0 (32). Our published dataset (24) of *in vitro* human osteocyte responses to pathophysiological mechanical loading ('osteocyte mechanosome') was independently compared with published data from, sex-based gene expression differences during the skeletal maturation of the mouse osteocyte transcriptome (Analysis 1) (26), the sex-based gene expression differences in human long bone explant-derived osteoblasts (Analysis 2) from 4 healthy children (a reanalysis of a subset of published dataset in Sex-Associated Gene Database repository number 00129 (27, 33) and sex specific OA risk factors and effector genes in a large human GWAS of 826,690 individuals from 9 populations (Analysis 3) (28). The osteocyte transcriptome and SAGD datasets were selected as they represent the only available RNA sequencing datasets detailing sex-

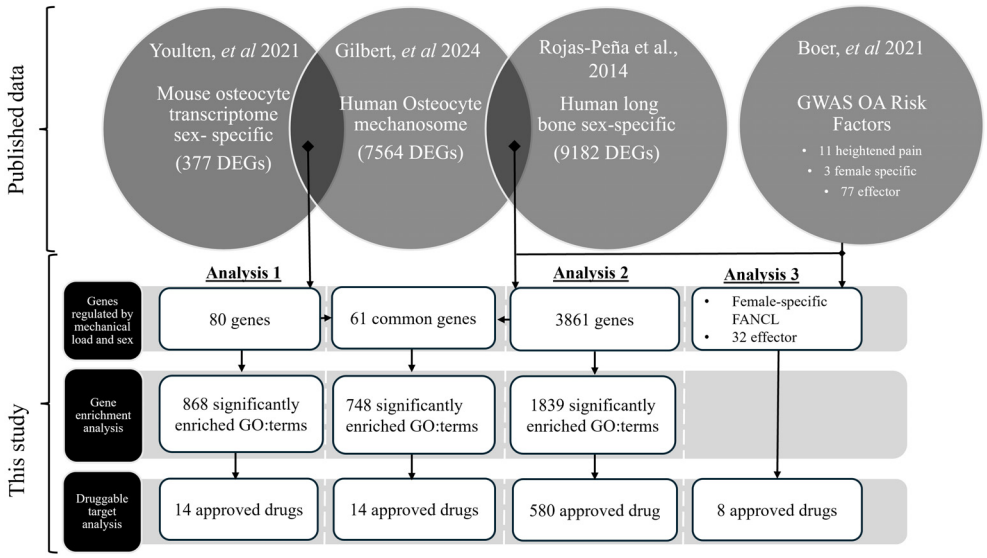

FIGURE 1
RNA sequencing data from mechanically regulated osteocytes ('the osteocyte mechanosome') (24) were independently compared with sex specific differences identified in the mouse osteocyte transcriptome (26) (Analysis 1) and sex-specific human long bone derived osteoblasts (27) (Analysis 2), and genes that showed co-regulation taken forward for further analysis. Mechanically regulated genes in the osteocyte mechanosome that also displayed sex regulation in the human long bone derived osteoblasts (Analysis 2) were combined with human GWAS loci associated with increased risk of OA in females and heightened OA pain (28) (Analysis 3). Sex specific mechanically regulated genes in osteocytes were searched for functional and disease pathway enrichment (29) and druggable targets (30).

regulated gene expression within bone. The GWAS data was selected as the largest OA GWAS currently available worldwide. Log2 fold changes (log2FC) were standardised so that females were always the numerator and males the denominator (*i.e.*, a positive log2FC would correspond to higher expression in females, and a negative log2FC to a higher expression in males. Positive log2FC within the osteocyte mechanosome indicates genes upregulated by mechanical load, whereas negative log2FC indicates downregulation in response to loading.

Protein encoding genes that displayed significant regulation by mechanical loading in the osteocyte mechanosome and by sex in published datasets (Analyses 1 and 2) were used to identify potential mediators of sex-based differences in OA pain (Figure 1). GWAS loci associated with heightened OA pain, female specific risk factors and OA effector genes (28) was combined with the sex-specific mechanically regulated genes identified from Analysis 2 to reveal sex specific OA risk factors in the osteocyte mechanosome (Analysis 3) (Figure 1).

The resulting genes from each analysis that displayed significant co-regulation were annotated with GO terms from Ensembl. Over-representation analysis was performed using clusterProfiler (29) and GO.db (34), using all genes represented in the osteocyte mechanosome as the enrichment background. Computational prediction of protein-protein network interactions of significantly regulated genes was performed using String.db (35). The top 1000 protein-protein interactions were generated in R (31) then uploaded to the string online interface (string-db.org) for STRING network analysis. Gene Ontology, KEGG pathway, human phenotype (Monarch) Disease-gene association (DISEASES) and annotated keyword (UniProt) functional enrichment analyses of the generated network were also performed using this online interface. GO:terms known to be affiliated with the generation of pain responses or joint pathology that were enriched within the dataset were extracted and used to highlight mediator genes in biplot graphs and tables. Within individual biplots, all genes beyond a set Log2-fold change threshold (Supplementary Table 1) were labelled to ensure graph clarity and specific genes of interest outside this range italicised. Sex specific genes in the osteocyte mechanosome were searched for druggable targets (30) (https://www.dgidb.org).

2.1 Analysis 2 - the osteocyte mechanosome and sex specific differences in human long bone derived osteoblasts

In Analysis 1 (Figure 1), our osteocyte mechanosome was combined with a published dataset from within the osteocyte transcriptome reflecting DEGs in mouse male and female osteocytes (26). Differentially expressed osteocyte enriched genes were identified from bones of skeletally mature (16 weeks) and aged (26 weeks) male and female mice. The data from Youlten et al. (26) was downloaded from the associated GitHub repository (26) and their analysis recapitulated using their code to regenerate a list of genes associated with the osteocyte transcriptome. In brief, differential expression between male and female mice in their dataset was calculated just for osteocyte-associated genes using *edgeR* (36) and *limma* (37). Sex comparisons were carried out separately for 16-week-old and 26-week-old mice.

In total, 80 DEGs in the osteocyte mechanosome were also differentially expressed in mouse osteocytes from males and females at either 16 (Figure 2, Supplementary Table 2) or 26 (Figure 3, Supplementary Table 3) weeks of age. In 16-week-old

10.3389/fendo.2024.1480274

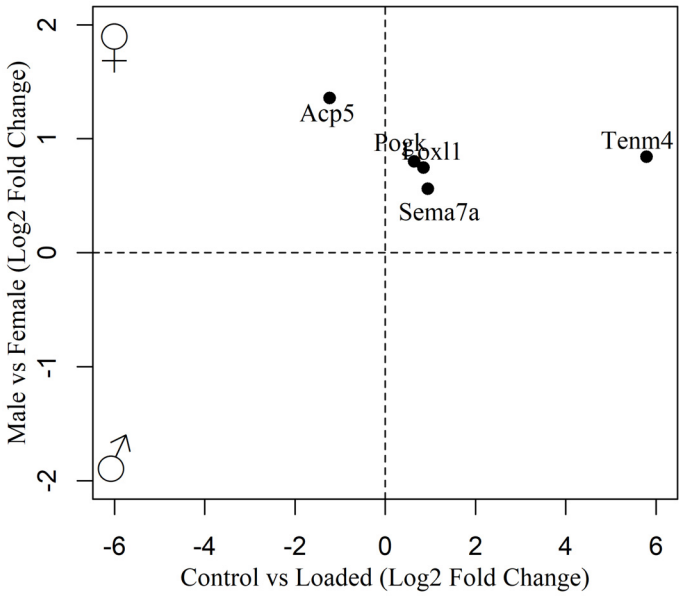

FIGURE 2
Biplot of genes regulated in the osteocyte mechanosome and differentially expressed in osteocytes from male and female 16-week-old skeletally mature mice.

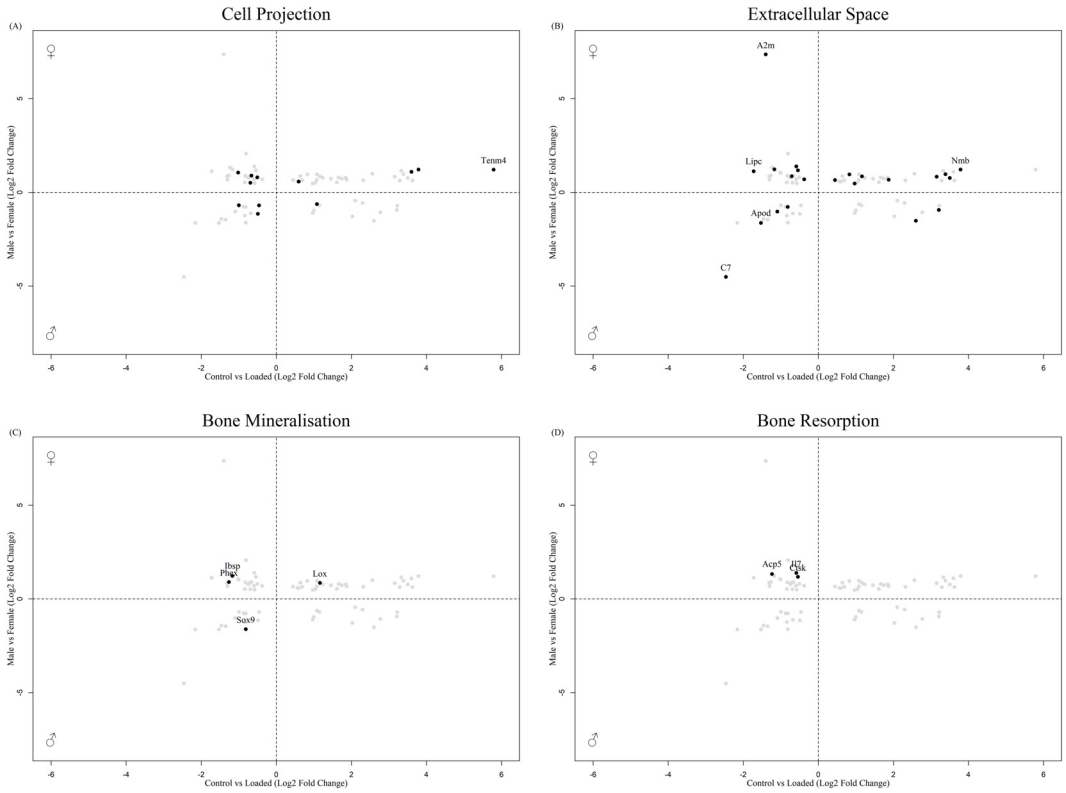

FIGURE 3
Biplot of genes regulated in the osteocyte mechanosome and differentially expressed in osteocytes from male and female 26-week-old mice. Points highlighted by GO Enrichment analysis. **(A)** Cell projection, **(B)** Extracellular space, **(C)** Bone mineralisation, **(D)** Bone resorption.

mice, 5 osteocyte mechanosome DEGs also displayed differential expression between males and females: TENM4, SEMA7A, LOXL1, POGK and ACP5 (Figure 2). GO term enrichment of these genes was associated with collagen-containing extracellular matrix and bone morphogenesis and resorption, neural crest migration, and positive regulation of axon extension (Supplementary Figure 1). In contrast, in aged, 26-week-old mice, 77 DEGs in the osteocyte mechanosome showed significant differences between male and female osteocytes (Figure 3). Of note, these included TENM4, LOX and CTSK all of which displayed higher expression in females and mechanical regulation (Figure 3, Table 1).

GO:term enrichment revealed that DEGs in the osteocyte mechanosome and regulated by sex in aged mice bones were predominantly associated with cell projection, extracellular space, bone mineralisation and bone resorption (Supplementary Figure 2). No genes associated with the nerve growth factor signalling pathway GO terms were significantly regulated in the dataset.

STRING analysis of all protein interactions that were significantly sex regulated in osteocyte signature and in the osteocyte mechanosome produced a protein interaction network with 25 predicted functional associations compared to the number of expected interactions of 11 (Supplementary Figure 3). Functional enrichment analysis of the network showed a protein-protein interaction enrichment P value of < 0.001 and pathways relevant to pain in OA. KEGG pathway analysis revealed the rheumatoid arthritis pathway (count 4 of 83, strength 1.23, fdr 0.0195) and osteoclast differentiation pathway (count 4 of 120, strength 1.07, fdr 0.0280) were enriched in this protein interaction network.

2.2 Analysis 2 - the osteocyte mechanosome and sex specific differences in human long bones

In Analysis 2 (Figure 1), our osteocyte mechanosome was compared with a published dataset containing 9182 DEGs between human male and female long bone explant-derived osteoblasts downloaded from the sex-associated gene database (repository number 00129; SAGD http://bioinfo.life.hust.edu.cn/SAGD, (27, 33).

3861 of those sex-regulated genes were affected by mechanical load in the osteocyte mechanosome (Supplementary Table 4). GO: term enrichment showed that these co-regulated genes are associated with numerous biological processes including those relevant to mechanical loading of bone and pain, such as collagen containing extracellular matrix (ECM), signal transduction, synapse, neural projection, angiogenesis and integrin, cadherin, and calcium ion binding (Supplementary Figure 3, Supplementary Table 5). The co-regulated genes included 86 associated with neural projection including TENM4 (Figure 4A), 155 associated with the synapse (Figure 4B) 4 genes associated with the sensory perception of pain including PTGES, EDNRB and 8 members of the MAPK

TABLE 1 Pathways significantly enriched in the top 1000 protein-protein interactions in the genes regulated in the osteocyte mechanosome and by sex in human long bone derived osteoblasts.

Group	Analysis	Pathway	Count	Strength	fdr
Top 1000 protein-protein interactions in genes significantly regulated in Analysis 1	**KEGG**	rheumatoid arthritis	13 of 83	0.49	0.0129
		TGF-β signalling	14 of 91	0.48	0.0108
		complement and coagulation cascades	14 of 82	0.53	0.0056
	DISEASES	bone disease	54 of 540	0.29	0.0066
		neurodegenerative disease	47 of 481	0.28	0.024
		musculoskeletal disease	106 of 1154	0.26	<0.0001
		nervous system disease	161 of 2275	0.14	0.0145
	Monarch	severe generalised osteoporosis	6 of 11	1.03	0.0034
		distal peripheral sensory neuropathy	5 of 12	0.91	0.0207
		sensory neuropathy	14 of 85	0.51	0.0078
		osteolysis of the upper limb	7 of 19	0.86	0.0053
		osteolysis	12 of 73	0.51	0.0078
		poor wound healing	7 of 20	0.84	0.0064
	Annotated Keywords (Uniprot)	osteogenesis imperfecta	8 of 83	0.26	0.0022
		Charcot-Marie-Tooth	10 of 55	0.55	0.0159
		neuropathy	17 of 108	0.49	0.0027
		angiogenesis	20 of 131	0.48	0.0013
Largest cluster of protein interactions	**DISEASES**	degenerative disc disease	3 of 13	1.83	0.0081
	TISSUES	rheumatoid arthritis synovial tissues	3 of 9	1.98	0.00056

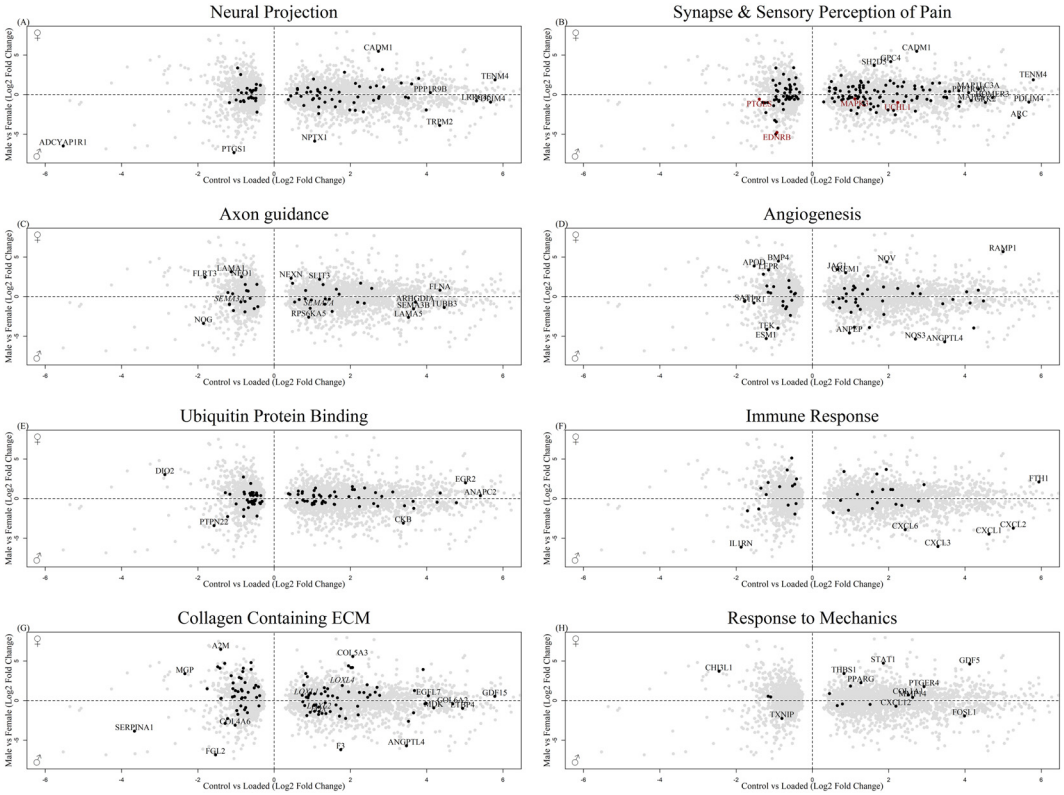

FIGURE 4
Biplot of genes regulated in the osteocyte mechanosome and differentially expressed in male and female human long bone derived osteoblasts. Points highlighted by GO: Term. **(A)** Neural Projection, **(B)** Black = Synapse, Red = Sensory perception of pain **(C)**. Axon guidance, **(D)** Angiogenesis, **(E)** Ubiquitin protein binding **(F)** Immune response, **(G)** Collagen-containing extracellular matrix **(H)** Response to mechanical stimulus.

signalling pathway (Figure 4B, red), and 44 genes associated with axon guidance including, SEMA3A and SEMA7A (Figure 4C). In addition, co-regulated genes included 88 genes associated with angiogenesis including NOS3 (Figure 4D), 93 genes associated with ubiquitin protein ligase binding (Figure 4E), 39 genes associated with immune responses (Figure 4F) and 108 genes associated with collagen containing ECM (Figure 4G). Out of the 11 GO terms for mechanical regulation, the GO term 'response to mechanical stimulus' identified 17 DEGs in the osteocyte mechanosome that were also differentially regulated in male and female long bones (Figure 4H).

STRING analysis was performed on the top 1000 protein interactions that were significantly sex regulated in human long bone derived osteoblasts and in the osteocyte mechanosome. This produced a protein interaction network with 8786 predicted functional associations (Supplementary Figure 2). Functional enrichment analysis of the network showed significant protein-protein interaction enrichment ($P < 0.001$) and numerous pathways relevant to pain in OA (Table 1). Biological process Gene Ontology enrichment showed a very large number of overrepresented pathways: the highest enrichment was for angiogenesis and blood vessel related genes, including retinal blood vessel morphogenesis, data not shown. The most enriched KEGG pathways were associated with the cell cycle, metabolism, and ECM interactions. Interestingly, the rheumatoid arthritis pathway (Figure 5A), transforming growth factor-β (TGF-β) signalling (Figure 5B) and complement and coagulation cascades all showed enrichment. Disease-gene associations (DISEASES) pathway analysis of co-regulated genes identified bone disease (Figure 5C), neurodegenerative disease (Figure 5D), musculoskeletal disease (Figure 5E), and nervous system disease. Human phenotype (Monarch) analysis of the protein interactions within this dataset revealed enrichment of severe generalised osteoporosis, distal peripheral sensory neuropathy (Figure 5F, Black), sensory neuropathy (Figure 5F, Red), osteolysis of the upper limb, osteolysis, and poor wound healing. Analysis of the Annotated Keywords (Uniprot) of the protein interaction network revealed enrichment in pathways of osteogenesis imperfecta, Charcot-Marie-Tooth, Neuropathy, and angiogenesis. MCL clustering of the protein interaction network produced 292 clusters, 29 of which included more than 5 genes. The largest cluster was compiled of 68 genes including CXCL12, CTSK and MMP1-3. and was predominantly associated with degenerative disc disease in disease -gene associations (DISEASES) enrichment and included rheumatoid arthritis disease specific synovial tissues in Tissue expression (TISSUES) analysis (Table 1).

Analysis 2 revealed numerous genes associated with cell projection (Figure 6A), extracellular space (Figure 6B) and bone biology (Figures 6C, D), including ASPN and CTSK, that were regulated by mechanical load in the osteocyte mechanosome and by sex. Members of the LOX pathway showed upregulation by

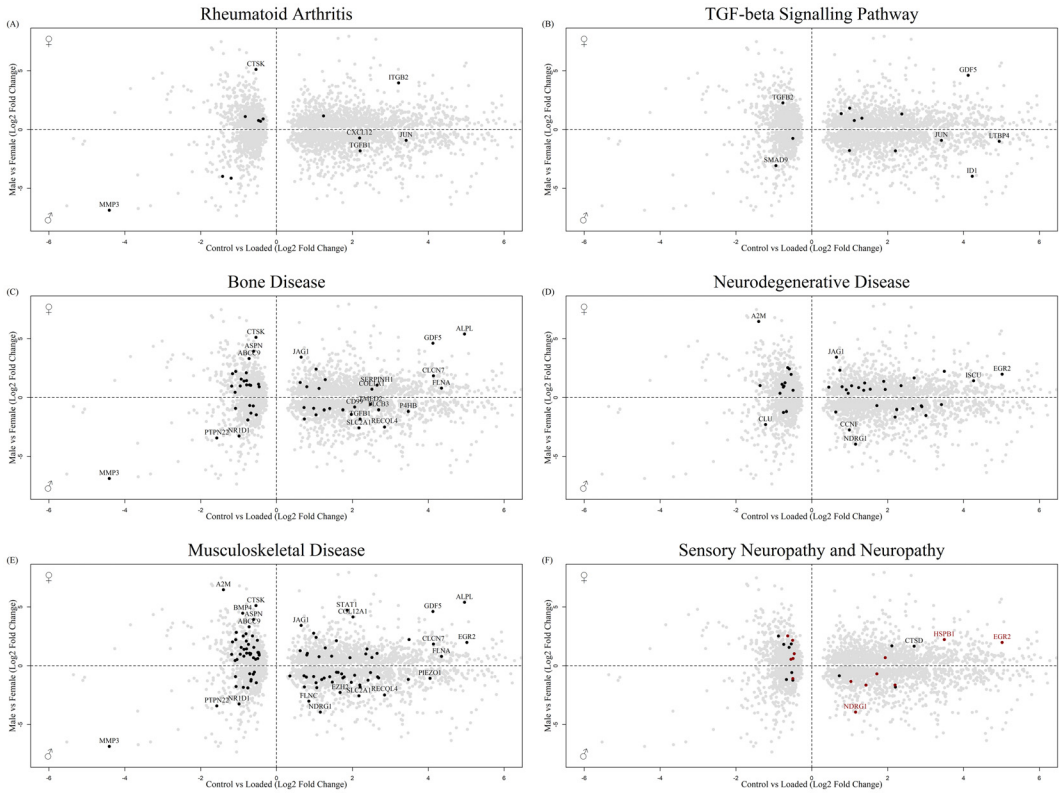

FIGURE 5
Biplot of genes regulated in the osteocyte mechanosome and differentially expressed in male and female human long bone derived osteoblasts. Points highlighted by STRING Enrichment analysis. **(A)** Rheumatoid arthritis, **(B)** TGF-beta signalling pathway, **(C)** Bone disease, **(D)** Neurodegenerative disease, **(E)** Musculoskeletal disease, **(F)** Black = Sensory neuropathy & Red = neuropathy.

mechanical loading in the osteocyte mechanosome and regulation by sex in human long bones. LOX and LOXL2 were increased in males. LOXL1 and LOXL4 conversely were increased in females. No genes associated with the nerve growth factor signalling pathway GO:terms were significantly regulated in the combined dataset. The fold changes and p values of individual genes of interest selected from these GO:term analyses can be found in Table 2.

2.3 The osteocyte mechanosome and sex specific differences in both human long bone derived osteoblasts and the mouse osteocyte transcriptome signature

Comparisons of the osteocyte mechanosome (24), with differentially expressed in males and females in the osteocyte transcriptome (26) (Analysis 1) and genes differentially regulated in males and females in human long bone (27) (Analysis 2) revealed several genes in common across datasets. Of the five genes regulated in the mouse transcriptome at 16-weeks (Section 2.1, Figure 2), three (TENM4, LOXL1, and SEMA7A) were also regulated by sex in the human long bone derived osteoblasts (Section 2.1, Figure 4) (Supplementary Table 6). Furthermore, 58 genes were regulated in the mouse osteocyte transcriptome at 26-weeks (Section 2.1) and by sex in the human long bone dataset (Supplementary Table 7). Of note, the collagen cross-linking enzyme lysyl oxidase (LOX) and its paralogs, LOX-like-1, 2, and -4 were regulated in the osteocyte mechanosome and either Analysis 1 or 2 (Figures 4–6). TENM4 was the only regulated gene in the osteocyte mechanosome that was also sex regulated across all datasets (Tables 2, 3).

2.4 Analysis 3 - the osteocyte mechanosome and sex specific OA risk factors

Analysis 3 (Figure 1), compared genes regulated in the osteocyte mechanosome and by sex in human long bone (Analysis 2) with OA risk loci associated with sex-specific OA and OA pain identified by a GWAS meta-analysis across 826,690 individuals, including 177,517 with OA (28). This study identified 3 sex-specific OA risk loci using a sex-differentiated test of association and a test of heterogeneity in allelic effects, and 11 genes associated with total joint replacement (TJR) surgery which the authors proposed were candidate genes associated with heightened OA pain [Supplementary Table 5, (28)].

Of the 3 female specific OA risk loci shown by Boer et al. (28), FANCL, C8orf34, UBAP2 (28), only one gene (FANCL) showed significant down regulation by mechanical loading (P(adj)=0.00087, -0.519-log2FC) in the osteocyte mechanosome. FANCL also showed a significant regulation by sex in the human male and female long bones

10.3389/fendo.2024.1480274

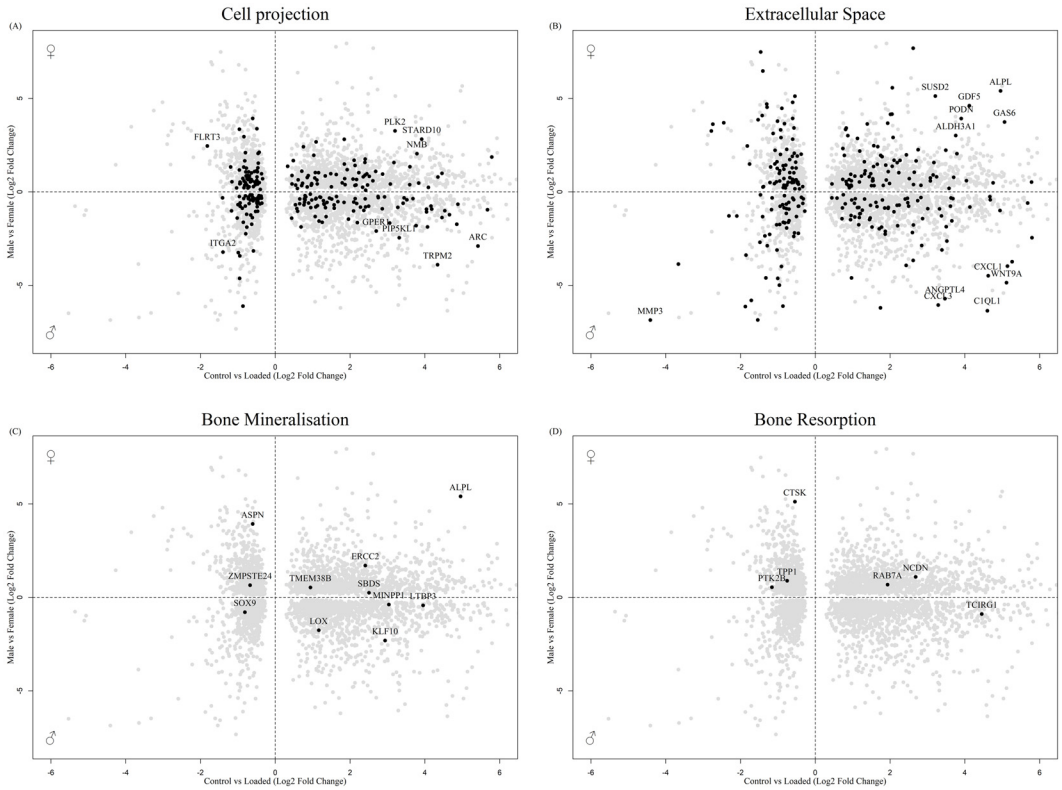

FIGURE 6
Biplot of genes regulated in the osteocyte mechanosome and differentially expressed in male and female human long bone derived osteoblasts. Points highlighted by GO Enrichment analysis. **(A)** Cell projection, **(B)** Extracellular space, **(C)** Bone mineralisation, **(D)** Bone resorption.

TABLE 2 Genes regulated in the osteocyte mechanosome and by sex in human long bone derived osteoblasts identified as potential mediators linked to pain generation in OA pathology.

	Mechanosome		Human long bone	
Gene	log2FC	P(adj)	log2FC	P(adj)
TENM4	5.79	0.001	1.22	0.0144
PTGES	-1.39	0.006	-0.99	<0.0001
EDNRB	-0.929	0.045	-4.73	<0.0001
UCHL1	2.24	0.0308	-1	<0.0001
SEMA3A	-1.17	<0.0001	-0.949	<0.0001
SEMA7A	0.945	0.002	-1.48	<0.0001
NOS3	2.7	0.0007	-5.36	0.0034
ASPN	-0.605	0.196	3.93	<0.0001
CTSK	-0.542	0.001	5.12	<0.0001
RUNX2	-0.84	0.005	0.924	<0.0001
LOX	1.16	0.0125	-1.76	<0.0001
LOXL1	0.844	0.0124	0.417	<0.0001
LOXL2	1.79	<0.0001	-1.37	<0.0001
LOXL4	1.18	0.0212	1.88	<0.0001

dataset [SAGD_00129, (27)]. Female long bones showed significantly lower FANCL expression compared with males (P(adj)=0.005, -0.701 - log2FC). Of the 11 genes associated with TJR surgery reflecting heightened OA pain, both PTCH1 (P(adj)=0.02, 1.927 - log2FC), and SERPINA1 (P(adj) 0.007, -3.66 - log2FC) were DEGs in the osteocyte mechanosome, but none showed sex regulation in either the human long bone or mouse osteocyte transcriptome datasets.

Analysis of the 77 OA effector genes published in this GWAS dataset [Supplementary Table 10, (28)] revealed 32 effector genes that are mechanically regulated in the osteocyte mechanosome and sex regulated in human long bones (Supplementary Table 8). These genes included: CTSK, RUNX2, NOS3 and members of the TGF-β pathway TGFB1, LTBP1 and LTBP3. No GWAS derived effector genes were significantly regulated by sex in the mouse osteocyte transcriptome.

2.5 Druggable targets

The genes in the osteocyte mechanosome shown to be sex specific in either GWAS, human long bones or the mouse osteocyte transcriptome were searched on the Drug-Gene Interaction Database to identify potential druggable targets [https://www.dgidb.org, (30)].

In Analysis 1, none of the 5 genes identified in 16-week-old mice were druggable. In 26-week-old mice, 14 of the 58 genes in

TABLE 3 Genes regulated in the osteocyte mechanosome and differentially expressed by sex in mouse osteocyte transcriptome selected for discussion within text as mediators linked to pain generation in OA pathology.

	Mechanosome		16- week Mouse osteocyte		26- week Mouse osteocyte	
Gene	log2FC	P(adj)	log2FC	P(adj)	log2FC	P(adj)
TENM4	5.79	0.001	5.7	>0.0001	1.21	0.014
SEMA7A	0.945	0.002	0.945	0.002		
LOXL1	0.844	0.0124	0.844	0.012		
POGK	0.64	0.01	0.64	0.01		
ACP5	-1.23	>0.0001	1.23	>0.0001		
LOX	1.16	0.0125			0.859	0.0257
CTSK	-0.542	0.001			1.18	>0.0001

common represented druggable targets with 9 of these genes having at least one approved drug (Supplementary Table 9).

793 of the 3861 genes regulated by mechanical loading in the osteocyte mechanosome and by sex in the human long bone dataset (Analysis 2) represent druggable targets with 580 of these having at least one approved drug (Supplementary Table 10). In total this represents 4332 approved drugs due to gene target redundancy. GO term analysis of these druggable targets revealed enrichment for genes associated with the extracellular space and protein phosphorylation and kinase activity. Druggable targets included 107 of the 275 ECM associated genes (442 drugs), 39 of the 93 genes associated with ubiquitin ligase (218 drugs), 18 of the 39 genes associated with immune responses (76 drugs), 54 of the 155 synapse genes (321 drugs), and 2 of the 44 axon guidance genes (1 drug).

In Analysis 3, FANCL, the female specific risk variant for OA (28) that was mechanically downregulated in osteocytes and differentially expressed in male and female human long bones, is also a druggable target with the approved drug Olaparib. Of the 26 GWAS effector genes shown to be significantly regulated by mechanical load in the osteocyte mechanosome and by sex in the human long bone dataset 10 genes had associated drugs with 7 of these being approved.

3 Discussion

Combining our transcriptome data of the *in vitro* 3D osteocyte response to pathophysiological mechanical load (24), with published datasets, of osteocyte specific sex-based transcriptome differences (Analysis 1) (26), human long bone explant-derived osteoblast sex-based transcriptome differences (Analysis 2) [repository number 00129 from (33)], and patient sex-specific OA risk factors (Analysis 3) (28), revealed a wide array of sex-regulated genes that are also significantly regulated by pathophysiological loading in osteocytes. Oestrogen deficiency in menopause is thought to contribute to the higher burden of pain experienced by female patients (38). This may involve both the chondroprotective signalling effect of oestrogen (39) as well as its well-established role in protecting bone mass.(14) Despite the high association of oestrogen deficiency predisposing to musculoskeletal pain, a causal link is lacking (8). The disparity between cartilage degradation and pain, and new revelations displaying nociceptor plasticity and invasion of subchondral bone [reviewed in (16)], and the association of BMLs with pain (12), suggests a role for bone in explaining sex differences in OA pain sensation.

LOXL1, SEMA7A and TENM4 were the only differentially expressed genes in the osteocyte mechanosome that were also sex regulated genes common across the 16-week-old mouse transcriptome and the human long bone dataset. TENM4 was the only regulated gene present across all datasets. TENM4 was upregulated by mechanical loading in the osteocyte mechanosome and increased in females in all analyses. TENM4 encodes for Teneurin transmembrane protein 4, a protein important in establishing proper neuronal connectivity during development (40) which has been linked to changes in pain sensitivity (41). Tenm4 mutant mice (Tenm4$^{em1(IMPC)Tcp}$ allele) exhibit sex-specific increased bone mineral content in older female mice [(42); www.mousephenotype.org]. LOX was upregulated by mechanical load in the osteocyte mechanosome, and in the female mouse osteocyte transcriptome at 26 weeks but decreased in female long bones. LOX was not detected in the mouse osteocyte transcriptome at 16 weeks. In addition, LOXL1 was upregulated in the mechanosome, female mouse osteocytes and female long bones. LOXL1 was not detected in mouse osteocyte transcriptome at 26 weeks. LOX and LOXL1 were also highlighted in the STRING protein interaction network analysis of the osteocyte mechanosome combined with sex differences in both human long bones and the osteocyte transcriptome. These enzymes are critical for elastin biogenesis and collagen cross-link formation and play roles in matrix remodelling in normal and disease states (43). Knockouts of LOXL1 have also been shown to induce deterioration of trabecular bone structure in long bones and vertebrae in female mice but not in males (44). Proteolytic activation of LOX is enhanced by the interaction of periostin and BMP1 (45). The sex-specific mechano-regulation of the LOX pathway we have reported links to the findings of Zhou et al. who found POSTN, the gene encoding periostin, to be mechanoresponsive and co-regulated in OA and the osteocyte signature (46). SEMA7A, encoding the neuroimmune axon guidance factor Semaphorin7A was upregulated by load in the osteocyte mechanosome and regulated

by sex in our analysis. SEMA7A was down regulated in human female long bones but up regulated in 16-week-old female mouse osteocytes. Semaphorin7A is a signalling ligand that promotes neuron axon elongation and invasion in the developing embryo (47) and is essential in establishing innervation of the dentin-pulp complex (48). CTSK, encoding the lysosomal cysteine protease Cathepsin K a marker of osteoclast bone resorption, was down regulated by mechanical loading in the osteocyte mechanosome but up regulated in both the female human long bone dataset and the female mouse osteocyte transcriptome at 26 weeks. CTSK has been implicated in the pathogenesis of osteoporosis and OA [reviewed in (49)] with inhibition of Cathepsin K delaying OA progression in animal models (50). CTSK was also found to be an OA effector gene (28).

Pathophysiological mechanical loading of osteocytes down regulated the expression of FANCL a ubiquitin ligase previously shown to be associated with female specific risk of hip OA (28). The down regulation of FANCL is associated with cytogenetic instability, hypersensitivity to DNA crosslinking agents, increased chromosomal breakage, and defective DNA repair (51). Both human genetic studies and mouse gene knockouts (52) indicate that loss of function mutations in FANCL, cause premature ovary insufficiency, a condition that leads to early menopause (53). This is of interest as menopausal and post-menopausal females are two times more likely to suffer from joint pain than pre-menopausal females (54, 55). Our data implicates osteocyte response to mechanical loading as a potential mechanism underlying the heightened susceptibility of females with FANCL mutations to OA.

Interestingly, mechanical loading of osteocytes (24) regulated numerous genes associated with bone responses which show differential expression by sex. Bone disease and musculoskeletal disease were enriched in disease gene associated analysis of the protein interactions of the osteocyte mechanosome when combined with the sex regulated genes in human long bones. GO:term enrichment showed that both in the mouse osteocyte data and in human long bone data the mechanosome revealed regulated genes associated with bone mineralisation and bone resorption that were differentially expressed by sex. The osteocyte mechanosome and human long bone sex differences dataset also showed regulation of RUNX2 an essential transcription factor in osteoblast differentiation and an OA effector gene in GWAS analysis (28). Mechanical load down regulated RUNX2, whereas RUNX2 was upregulated in females. This data suggests that the regulation of bone formation and resorption by osteocytes in response to mechanical loading is different in males and females.

39 genes associated with immune responses showed co-regulation by mechanical load in the osteocyte mechanosome and by sex in the human long bone dataset. Differential expression of genes in females also showed enrichment for the rheumatoid arthritis pathway. These data show that pathophysiological loading of osteocytes causes immune factor expression that is significantly differentially expressed in females. Interestingly, NOS3 was identified by Boer et al. as an OA effector gene (28) and is upregulated by mechanical load and in male human long bones. This endothelium isoform of nitric oxide synthase is the predominant constitutive isoform of NOS within bone (56), mechanically regulated in osteocytes (57) and expressed in human osteocytes *in vivo* (58). It is an important mediator of inflammatory signalling (59), and plays a role in mediating oestrogen-induced bone formation in female mice (58). These data suggest that differences in inflammatory and immune signalling in the mechanical responses of females may drive differential immune signalling leading to higher nociceptive signalling in females.

The TGF-β signalling pathway was also shown to be differentially expressed in STRING pathway enrichment analysis of the osteocyte mechanosome and human long bone sex differences combined datasets. Members of this pathway were identified by Boer et al. as effector genes in a large GWAS analysis (28). TGF-β is a pleiotropic cytokine that is only active in the healthy joint after mechanical loading. In the OA joint, TGF-β signalling is greatly enhanced (60). Sexual dimorphism in TGF-β responses was demonstrated in mice, where osteocyte specific knockout of the TGF-β receptor II increased subchondral bone thickening in male but not female mice and was associated with cartilage degeneration (61). The sex-regulation of the TGF-β pathway shown in this analysis reinforces the evidence that differential inflammatory and immune signalling in females may drive differences in OA progression and pain. Asporin acts as a negative regulator of chondrogenesis by inhibiting TGF-β function (62). Recently, ASPN has been shown to be a disease-relevant gene, contributing to subchondral bone remodelling in OA (46). ASPORIN (ASPN) is a small leucine-rich repeat proteoglycan (SLRP) with polymorphisms that are strongly associated with OA (63). It directly binds TGF-β1 and subsequently collagen, playing a role in collagen fibrillogenesis and metabolism (64, 65). ASPN more highly expressed in female human long bones compared to equivalent male samples but was not significantly regulated in the mouse osteocyte transcriptome by sex.

Comparison of the mechanosome with genes differentially expressed in human male and female long bones highlighted pathways involved in neuronal activity, ECM, immune response, and identified associations with many painful musculoskeletal diseases involving bone and neuropathies. 93 genes associated with ubiquitin protein ligase binding were significantly regulated by sex in the human long bone dataset and significantly regulated in our osteocyte mechanical loading dataset. No genes associated with ubiquitin function were differentially expressed between males and females in the sex specific osteocyte transcriptome when combined the osteocyte mechanosome. Ubiquitin disfunction in OA is an emerging pathway in driving pathology especially in regulating the apoptosis and hypertrophic differentiation of chondrocytes (66). It is also likely that changes in ubiquitin function contribute to bone changes in OA as it plays an important role in regulating bone remodelling as well as osteocyte apoptosis (67) with proteosome inhibitors effectively reducing bone turnover and increasing osteocyte viability in multiple myeloma (68).

155 genes associated with the synapse, 4 genes associated with the sensory perception of pain and 44 genes associated with axon guidance and cell projection were significantly regulated by osteocyte mechanical loading and by sex in the human long bone dataset. The regulation of this number of neuronally associated genes in both datasets provides evidence that the nociceptor bone interface, and the response of osteocytes to pathological load differs in female

OA patients compared to that of males. TENM4 and SEMA7A in both the sex differential human long bone and mouse derived osteocyte signature dataset shows that in both mouse models and in human patients, differential axon guidance signalling in males and females may result in differing levels of nociceptor plasticity and sensitivity in females. All the semaphorin signalling ligands displayed higher differential expression in males in human long bones. Axon guidance signalling factors have been shown to regulate sensory nerve sprouting and invasion in mouse models (69) and to regulate the membrane potential of sensory neurons (70), with signalling cascades that integrate to the signalling of NGF (71). The axon guidance signalling pathway has also recently been reported by Zhou et al. to be a significantly enriched pathway in the 223 main contributory genes between the medial OA subchondral bone and lateral plateau in mice OA models (46). In contrast we saw no differences in NGF signalling in our analyses.

Significantly more DEGs were detected in ageing 26-week-old male and female mouse osteocytes and the osteocyte mechanosome compared with 16-week-old mice. Hyperalgesia lasts longer and is more pronounced in older rats, with aged females exhibiting the most impaired responses (72). Age also impacts OA pain in humans with clinical studies revealing older woman to have more chronic pain (73, 74). (75) hypothesised that brain changes observed in the early stages of monosodium iodoacetate-induced OA in rats may account for the increased risk for ageing females to develop chronic pain. This is supported by our String analysis which revealed the significant enrichment of neurodegenerative diseases in females. GO term analysis revealed regulation of DEGS involved in the immune response in both the mechanosome and osteocytes of aging mice. Studies have linked higher pain scores and lower pain thresholds in woman to enhanced inflammatory responses (76–78). In addition, sex differences exist in the relationship between individual systemic markers of inflammation and pain in knee osteoarthritis (79, 80).

4 Limitations and conclusions

The greatly reduced number of sex-regulated genes in the mouse osteocyte transcriptome data raises questions as to the similarities between bone-nerve interactions in mouse models compared to patients. It is established that female and male bone display many differences in physiology and intricate associations with the nervous system. Recent research has shown that there are large differences between the peripheral sensory nervous systems in mice and humans (81). Sensory nerve gene expression, molecular fingerprint, and sensory nerve sub populations have been shown to be different between mouse models and human patients. This analysis therefore raises the possibility that the differential expression of factors that influence sensory nerve changes in animal models limit their effectiveness in studying nociceptor changes in OA. Since the human sex specific long bone data was based on bone explant derived osteoblasts rather than osteocytes *in vivo*, it is also possible that sex specific differences from the human data set are not osteocyte specific.

This analysis has shown a wide array of factors regulated in osteocytes by mechanical loading that are differentially expressed by sex and influence innervation, neural activity and bone remodelling associated with OA pain. It remains to be determined whether these sex specific differences in responses would differentially effect nociceptor populations in males and females. To test this, sex-specific differences in receptor complexes or susceptibility to the differences in osteocyte derived neural signalling would need to be investigated.

Our comparison of the osteocyte mechanosome to published data reflecting sex specific gene expression and susceptibility to OA pain has highlighted pain related pathways potentially responsible for elevated pain susceptibility in females with osteoarthritis. The large number of approved drugs available to target these pathways reveals a great opportunity to modulate mechanically driven osteoarthritic pain particularly in susceptible females.

Data availability statement

The original contributions presented in the study are included in the article/Supplementary Material. Further inquiries can be directed to the corresponding author.

Author contributions

RJ: Conceptualization, Data curation, Formal analysis, Funding acquisition, Investigation, Methodology, Project administration, Resources, Software, Supervision, Validation, Visualization, Writing – original draft, Writing – review & editing. SG: Data curation, Methodology, Writing – original draft, Writing – review & editing, Conceptualization, Formal analysis, Funding acquisition, Investigation, Project administration, Supervision, Visualization. SC: Data curation, Methodology, Writing – original draft, Writing – review & editing, Formal analysis, Investigation, Project administration, Supervision, Validation, Visualization. DM: Conceptualization, Data curation, Formal analysis, Funding acquisition, Investigation, Methodology, Project administration, Resources, Software, Supervision, Validation, Visualization, Writing – original draft, Writing – review & editing.

Funding

The author(s) declare that financial support was received for the research, authorship, and/or publication of this article. This work was funded by NC3Rs CRACK IT Challenge 22: Osteo-chip, NC3Rs Project grant (NC/Y000951/1), Biomechanics and Bioengineering Research Centre Versus Arthritis (EC/20781), Wellcome Trust Collaborative Award (209233/Z/17/Z).

Acknowledgments

We would like to thank Cleo Bonnet for her contribution to the osteocyte model, Sam Evans for his contribution to the loading

device design, Peter Giles (Wales Gene Park) for the RNA sequencing and analysis, and Professor Paul Genever (University of York) who kindly provided the Y201 cell line and associated methods.

Conflict of interest

DM holds patents for the use of glutamate receptor antagonists to prevent osteoarthritis.

The remaining authors declare that the research was conducted in the absence of any commercial or financial relationships that could be construed as a potential conflict of interest.

The author(s) declared that they were an editorial board member of Frontiers, at the time of submission. This had no impact on the peer review process and the final decision.

Publisher's note

Supplementary material

The Supplementary Material for this article can be found online at: https://www.frontiersin.org/articles/10.3389/fendo.2024.1480274/full#supplementary-material

SUPPLEMENTARY FIGURE 1
Bar plot of the significantly enriched GO: Terms produced by GO:term enrichment of genes differentially expressed in both the osteocyte mechanosome and by sex in osteocytes from 16-week-old skeletally mature mice. Bar colour is representative of adjusted p value. Bar length represents the number of genes associated with each GO:term within the dataset.

SUPPLEMENTARY FIGURE 2
Bar plot of the significantly enriched GO: Terms produced by GO:term enrichment of genes differentially expressed in both the osteocyte mechanosome and by sex in osteocytes from 26-week-old skeletally mature mice. Bar colour is representative of adjusted p value. Bar length represents the number of genes associated with each GO:term within the dataset.

SUPPLEMENTARY FIGURE 3
Protein-protein interactions with high confidence interaction score within significantly regulated osteocyte mechanosome and sex differences within mouse osteocyte transcriptome dataset. Coloured nodes represent genes within the dataset within the first shell of interactions. Node content represents predicted protein 3D structure. Connecting lines represent the established protein-protein associations. Line thickness represents the confidence score of these interactions.

SUPPLEMENTARY FIGURE 4
Bar plot of the significantly enriched GO: Terms produced by GO:term enrichment of genes regulated by sex in human long bone derived osteoblasts and mechanical loading in osteocytes. **(A)** All enriched GO: Terms, **(B)** Enriched biological process GO: Terms, **(C)** Enriched Cellular compartment GO: Terms, **(D)** Enriched molecular function GO: Terms. Bar colour is representative of adjusted p value. Bar length represents the number of genes associated with each GO:term within the dataset.

SUPPLEMENTARY FIGURE 5
Protein-protein interactions with high confidence interaction score within significantly regulated osteocyte mechanosome and sex differences within human long bone derived osteoblast dataset. Coloured nodes represent genes within the dataset within the first shell of interactions. Node content represents predicted protein 3D structure. Connecting lines represent the established protein-protein associations. Line thickness represents the confidence score of these interactions.

References

1. Long H, Liu Q, Yin H, Wang K, Diao N, Zhang Y, et al. Prevalence trends of site-specific osteoarthritis from 1990 to 2019: findings from the global burden of disease study 2019. *Arthritis Rheumatol.* (2022) 74:1172–83. doi: 10.1002/art.42089

2. O'Connor MI. Sex differences in osteoarthritis of the hip and knee. *J Am Acad Orthop Surg.* (2007) 15 Suppl 1:S22–25. doi: 10.5435/00124635-200700001-00007

3. Srikanth VK, Fryer JL, Zhai G, Winzenberg TM, Hosmer D, Jones G. A meta-analysis of sex differences prevalence, incidence and severity of osteoarthritis. *Osteoarthritis Cartilage.* (2005) 13:769–81. doi: 10.1016/j.joca.2005.04.014

4. Gazeley DJ, Yeturi S, Patel PJ, Rosenthal AK. Erosive osteoarthritis: A systematic analysis of definitions used in the literature. *Semin Arthritis Rheum.* (2017) 46:395–403. doi: 10.1016/j.semarthrit.2016.08.013

5. Tschon M, Contartese D, Pagani S, Borsari V, Fini M. Gender and sex are key determinants in osteoarthritis not only confounding variables. A systematic review of clinical data. *J Clin Med.* (2021) 10:3178. doi: 10.3390/jcm10143178

6. Dawson-Basoa ME, Gintzler AR. Estrogen and progesterone activate spinal kappa-opiate receptor analgesic mechanisms. *Pain.* (1996) 64:169–77. doi: 10.1016/0304-3959(95)00092-5

7. Ziemian SN, Ayobami OO, Rooney AM, Kelly NH, Holyoak DT, Ross FP, et al. Low bone mass resulting from impaired estrogen signaling in bone increases severity of load-induced osteoarthritis in female mice. *Bone.* (2021) 152:116071. doi: 10.1016/j.bone.2021.116071

8. Watt FE. Musculoskeletal pain and menopause. *Post Reprod Health.* (2018) 24:34–43. doi: 10.1177/2053369118757537

9. Xu J, Yan Z, Wu G, Zheng Y, Liao X, Zou F. Identification of key genes and pathways associated with sex difference in osteoarthritis based on bioinformatics analysis. *J Musculoskelet Neuronal Interact.* (2022) 22:393–400.

10. Cirillo DJ, Wallace RB, Wu L, Yood RA. Effect of hormone therapy on risk of hip and knee joint replacement in the Women's Health Initiative. *Arthritis Rheum.* (2006) 54:3194–204. doi: 10.1002/art.22138

11. Jung JH, Bang CH, Song GG, Kim C, Kim J-H, Choi SJ. Knee osteoarthritis and menopausal hormone therapy in postmenopausal women: a nationwide cross-sectional study. *Menopause.* (2018) 26:598–602. doi: 10.1097/GME.0000000000001280

12. Hunter DJ, Guermazi A, Roemer F, Zhang Y, Neogi T. Structural correlates of pain in joints with osteoarthritis. *Osteoarthritis Cartilage Pain Osteoarthritis.* (2013) 21:1170–8. doi: 10.1016/j.joca.2013.05.017

13. Zhu X, Chan YT, Yung PSH, Tuan RS, Jiang Y. Subchondral bone remodeling: A therapeutic target for osteoarthritis. *Front Cell Dev Biol.* (2021) 8:607764. doi: 10.3389/fcell.2020.607764

14. Aso K, Shahtaheri SM, Hill R, Wilson D, McWilliams DF, Nwosu LN, et al. Contribution of nerves within osteochondral channels to osteoarthritis knee pain in humans and rats. *Osteoarthritis Cartilage.* (2020) 28:1245–54. doi: 10.1016/j.joca.2020.05.010

15. Mitchell SAT, Majuta LA, Mantyh PW. New insights in understanding and treating bone fracture pain. *Curr Osteoporos Rep.* (2018) 16:325–32. doi: 10.1007/s11914-018-0446-8

16. Malfait A-M, Miller RE, Miller RJ. Basic mechanisms of pain in osteoarthritis: experimental observations and new perspectives. *Rheum Dis Clin North Am.* (2021) 47:165–80. doi: 10.1016/j.rdc.2020.12.002

17. Kuttapitiya A, Assi L, Laing K, Hing C, Mitchell P, Whitley G, et al. Microarray analysis of bone marrow lesions in osteoarthritis demonstrates upregulation of genes implicated in osteochondral turnover, neurogenesis and inflammation. *Ann Rheum Dis.* (2017) 76:1764–73. doi: 10.1136/annrheumdis-2017-211396

18. Perry TA, Parkes MJ, Hodgson RJ, Felson DT, Arden NK, O'Neill TW. Association between Bone marrow lesions & synovitis and symptoms in symptomatic knee osteoarthritis. *Osteoarthritis Cartilage*. (2020) 28:316–23. doi: 10.1016/j.joca.2019.12.002

19. Guilak F. Biomechanical factors in osteoarthritis. *Best Pract Res Clin Rheumatol*. (2011) 25:815–23. doi: 10.1016/j.berh.2011.11.013

20. Felson DT, McLaughlin S, Goggins J, LaValley MP, Gale ME, Totterman S, et al. Bone marrow edema and its relation to progression of knee osteoarthritis. *Ann Intern Med*. (2003) 139:330–6. doi: 10.7326/0003-4819-139-5_part_1-200309020-00008

21. Callaghan MJ, Parkes MJ, Hutchinson CE, Gait AD, Forsythe LM, Marjanovic EJ, et al. A randomised trial of a brace for patellofemoral osteoarthritis targeting knee pain and bone marrow lesions. *Ann Rheum Dis*. (2015) 74:1164–70. doi: 10.1136/annrheumdis-2014-206376

22. Laslett LL, Doré DA, Quinn SJ, Boon P, Ryan E, Winzenberg TM, et al. Zoledronic acid reduces knee pain and bone marrow lesions over 1 year: a randomised controlled trial. *Ann Rheum Dis*. (2012) 71:1322–8. doi: 10.1136/annrheumdis-2011-200970

23. Delgado-Calle J, Bellido T. The osteocyte as a signaling cell. *Physiol Rev*. (2022) 102:379–410. doi: 10.1152/physrev.00043.2020

24. Gilbert SJ, Jones R, Egan BJ, Bonnet CS, Evans SL, Mason DJ. Investigating mechanical and inflammatory pathological mechanisms in osteoarthritis using MSC-derived osteocyte-like cells in 3D. *Front Endocrinol*. (2024) 15:1359052. doi: 10.3389/fendo.2024.1359052

25. Mason DJ, Suva LJ, Genever PG, Patton AJ, Steuckle S, Hillam RA, et al. Mechanically regulated expression of a neural glutamate transporter in bone: A role for excitatory amino acids as osteotropic agents? *Bone*. (1997) 20:199–205. doi: 10.1016/S8756-3282(96)00386-9

26. Youlten SE, Kemp JP, Logan JG, Ghirardello EJ, Sergio CM, Dack MRG, et al. Osteocyte transcriptome mapping identifies a molecular landscape controlling skeletal homeostasis and susceptibility to skeletal disease. *Nat Commun*. (2021) 12:2444. doi: 10.1038/s41467-021-22517-1

27. Rojas-Peña ML, Olivares-Navarrete R, Hyzy S, Arafat D, Schwartz Z, Boyan BD, et al. Characterization of distinct classes of differential gene expression in osteoblast cultures from non-syndromic craniosynostosis bone. *J Genomics*. (2014) 2:121–30. doi: 10.7150/jgen.8833

28. Boer CG, Hatzikotoulas K, Southam L, Stefánsdóttir L, Zhang Y, Coutinho de Almeida R, et al. Deciphering osteoarthritis genetics across 826,690 individuals from 9 populations. *Cell*. (2021) 184:4784–4818.e17. doi: 10.1016/j.cell.2021.07.038

29. Wu T, Hu E, Xu S, Chen M, Guo P, Dai Z, et al. clusterProfiler 4.0: A universal enrichment tool for interpreting omics data. *Innovation (Camb)*. (2021) 2:100141. doi: 10.1016/j.xinn.2021.100141

30. Freshour SL, Kiwala S, Cotto KC, Coffman AC, McMichael JF, Song JJ, et al. Integration of the Drug-Gene Interaction Database (DGIdb 4.0) with open crowdsource efforts. *Nucleic Acids Res*. (2021) 49:D1144–51. doi: 10.1093/nar/gkaa1084

31. R Core Team (2019). _R: A Language and Environment for Statistical Computing_. R Foundation for Statistical Computing, Vienna, Austria.

32. RStudio Team (2020). RStudio: Integrated Development for R. RStudio, PBC: Boston, MA Available at: https://www.rstudio.com/.

33. Shi M-W, Zhang N-A, Shi C-P, Liu C-J, Luo Z-H, Wang D-Y, et al. SAGD: a comprehensive sex-associated gene database from transcriptomes. *Nucleic Acids Res*. (2019) 47:D835–40. doi: 10.1093/nar/gky1040

34. Carlson M (2019). GO.db: A set of annotation maps describing the entire Gene Ontology. *R package version 3.8.2*.

35. Szklarczyk D, Gable AL, Lyon D, Junge A, Wyder S, Huerta-Cepas J, et al. STRING v11: protein–protein association networks with increased coverage, supporting functional discovery in genome-wide experimental datasets. *Nucleic Acids Res*. (2019) 47:D607–13. doi: 10.1093/nar/gky1131

36. Robinson MD, McCarthy DJ, Smyth GK. edgeR: a Bioconductor package for differential expression analysis of digital gene expression data. *Bioinformatics*. (2010) 26:139–40. doi: 10.1093/bioinformatics/btp616

37. Ritchie ME, Phipson B, Wu D, Hu Y, Law CW, Shi W, et al. limma powers differential expression analyses for RNA-sequencing and microarray studies. *Nucleic Acids Res*. (2015) 43:e47. doi: 10.1093/nar/gkv007

38. Chlebowski RT, Cirillo DJ, Eaton CB, Stefanick ML, Pettinger M, Carbone LD, et al. Estrogen alone and joint symptoms in the Women's Health Initiative randomized trial. *Menopause*. (2013) 20:600–8. doi: 10.1097/GME.0b013e31828392c4

39. Ge Y, Zhou S, Li Y, Wang Z, Chen S, Xia T, et al. Estrogen prevents articular cartilage destruction in a mouse model of AMPK deficiency via ERK-mTOR pathway. *Ann Transl Med*. (2019) 7:336. doi: 10.21037/atm.2019.06.77

40. Peppino G, Ruiu R, Arigoni M, Riccardo F, Iacoviello A, Barutello G, et al. Teneurins: role in cancer and potential role as diagnostic biomarkers and targets for therapy. *Int J Mol Sci*. (2021) 22:2321. doi: 10.3390/ijms22052321

41. Fontanillas P, Kless A, Bothmer J, Tung JY. Genome-wide association study of pain sensitivity assessed by questionnaire and the cold pressor test. *Pain*. (2022) 163:1763–76. doi: 10.1097/j.pain.0000000000002568

42. Groza T, Gomez FL, Mashhadi HH, Muñoz-Fuentes V, Gunes O, Wilson R, et al. The International Mouse Phenotyping Consortium: comprehensive knockout phenotyping underpinning the study of human disease. *Nucleic Acids Res*. (2023) 51:D1038–45. doi: 10.1093/nar/gkac972

43. Ma H-Y, Li Q, Wong WR, N'Diaye E-N, Caplazi P, Bender H, et al. LOXL4, but not LOXL2, is the critical determinant of pathological collagen cross-linking and fibrosis in the lung. *Sci Adv*. (2023) 9:eadf0133. doi: 10.1126/sciadv.adf0133

44. Alsofi L, Daley E, Hornstra I, Morgan EF, Mason ZD, Acevedo JF, et al. Sex-linked skeletal phenotype of lysyl oxidase like-1 mutant mice. *Calcif Tissue Int*. (2016) 98:172–85. doi: 10.1007/s00223-015-0076-4

45. Maruhashi T, Kii I, Saito M, Kudo A. Interaction between periostin and BMP-1 promotes proteolytic activation of lysyl oxidase. *J Biol Chem*. (2010) 285:13294–303. doi: 10.1074/jbc.M109.088864

46. Zhou J, He Z, Cui J, Liao X, Cao H, Shibata Y, et al. Identification of mechanics-responsive osteocyte signature in osteoarthritis subchondral bone. *Bone Joint Res*. (2022) 11:362–70. doi: 10.1302/2046-3758.116.BJR-2021-0436.R1

47. Liu H, Juo ZS, Shim AH-R, Focia PJ, Chen X, Garcia KC, et al. Structural basis of semaphorin-plexin recognition and viral mimicry from sema7A and A39R complexes with plexinC1. *Cell*. (2010) 142:749–61. doi: 10.1016/j.cell.2010.07.040

48. Koh J-M, Oh B, Lee JY, Lee J-K, Kimm K, Kim GS, et al. Association study of semaphorin 7a (sem^7) polymorphisms with bone mineral density and fracture risk in postmenopausal Korean women. *J Hum Genet*. (2006) 51:112–7. doi: 10.1007/s10038-005-0331-z

49. Dai R, Wu Z, Chu HY, Lu J, Lyu A, Liu J, et al. Cathepsin K: the action in and beyond bone. *Front Cell Dev Biol*. (2020) 8:433. doi: 10.3389/fcell.2020.00433

50. Soki FN, Yoshida R, Paglia DN, Duong LT, Hansen MF, Drissi H. Articular cartilage protection in Ctsk-/- mice is associated with cellular and molecular changes in subchondral bone and cartilage matrix. *J Cell Physiol*. (2018) 233:8666–76. doi: 10.1002/jcp.26745

51. Helbling-Leclerc A, Garcin C, Rosselli F. Beyond DNA repair and chromosome instability—Fanconi anaemia as a cellular senescence-associated syndrome. *Cell Death Differ*. (2021) 28:1159–73. doi: 10.1038/s41418-021-00764-5

52. Cen C, Chen J, Lin L, Chen M, Dong F, Shen Z, et al. Fancb deficiency causes premature ovarian insufficiency in mice†. *Biol Reprod*. (2022) 107:790–9. doi: 10.1093/biolre/ioac103

53. Yang Y, Guo T, Liu R, Ke H, Xu W, Zhao S, et al. FANCL gene mutations in premature ovarian insufficiency. *Hum Mutat*. (2020) 41:1033–41. doi: 10.1002/humu.23997

54. Prieto-Alhambra D, Judge A, Javaid MK, Cooper C, Diez-Perez A, Arden NK. Incidence and risk factors for clinically diagnosed knee, hip and hand osteoarthritis: influences of age, gender and osteoarthritis affecting other joints. *Ann Rheum Dis*. (2014) 73:1659–64. doi: 10.1136/annrheumdis-2013-203355

55. Szoeke CE, Cicuttini FM, Guthrie JR, Dennerstein L. The relationship of reports of aches and joint pains to the menopausal transition: a longitudinal study. *Climacteric*. (2008) 11:55–62. doi: 10.1080/13697130701746006

56. Cho K, Demissie S, Dupuis J, Cupples LA, Kathiresan S, Beck TJ, et al. Polymorphisms in the endothelial nitric oxide synthase gene and bone density/ultrasound and geometry in humans. *Bone*. (2008) 42:53–60. doi: 10.1016/j.bone.2007.09.051

57. Zaman G, Pitsillides AA, Rawlinson SC, Suswillo RF, Mosley JR, Cheng MZ, et al. Mechanical strain stimulates nitric oxide production by rapid activation of endothelial nitric oxide synthase in osteocytes. *J Bone Miner Res*. (1999) 14:1123–31. doi: 10.1359/jbmr.1999.14.7.1123

58. Samuels A, Perry MJ, Gibson RL, Colley S, Tobias JH. Role of endothelial nitric oxide synthase in estrogen-induced osteogenesis. *Bone*. (2001) 29:24–9. doi: 10.1016/s8756-3282(01)00471-9

59. Sharma JN, Al-Omran A, Parvathy SS. Role of nitric oxide in inflammatory diseases. *Inflammopharmacology*. (2007) 15:252–9. doi: 10.1007/s10787-007-0013-x

60. van der Kraan PM. Differential role of transforming growth factor-beta in an osteoarthritic or a healthy joint. *J Bone Metab*. (2018) 25:65–72. doi: 10.11005/jbm.2018.25.2.65

61. Bailey KN, Nguyen J, Yee CS, Dole NS, Dang A, Alliston T. Mechanosensitive control of articular cartilage and subchondral bone homeostasis in mice requires osteocytic transforming growth factor β Signaling. *Arthritis Rheumatol*. (2021) 73:414–25. doi: 10.1002/art.41548

62. Önnerfjord P, Khabut A, Reinholt FP, Svensson O, Heinegård D. Quantitative proteomic analysis of eight cartilaginous tissues reveals characteristic differences as well as similarities between subgroups. *J Biol Chem*. (2012) 287:18913–24. doi: 10.1074/jbc.M111.298968

63. Loughlin J. Polymorphism in signal transduction is a major route through which osteoarthritis susceptibility is acting. *Curr Opin Rheumatol*. (2005) 17:629–33. doi: 10.1097/01.bor.0000176687.85198.49

64. Kalamajski S, Oldberg A. The role of small leucine-rich proteoglycans in collagen fibrillogenesis. *Matrix Biol*. (2010) 29:248–53. doi: 10.1016/j.matbio.2010.01.001

65. Lorenzo P, Aspberg A, Onnerfjord P, Bayliss MT, Neame PJ, Heinegard D. Identification and characterization of asporin. a novel member of the leucine-rich repeat protein family closely related to decorin and biglycan. *J Biol Chem*. (2001) 276:12201–11. doi: 10.1074/jbc.M010932200

66. Zheng C, Chen J, Wu Y, Wang X, Lin Y, Shu L, et al. Elucidating the role of ubiquitination and deubiquitination in osteoarthritis progression. *Front Immunol*. (2023) 14:1217466. doi: 10.3389/fimmu.2023.1217466

67. Teramachi J, Miki H, Nakamura S, Hiasa M, Harada T, Abe M. Myeloma bone disease: pathogenesis and management in the era of new anti-myeloma agents. *J Bone Miner Metab*. (2023) 41:388–403. doi: 10.1007/s00774-023-01403-4

68. Toscani D, Palumbo C, Dalla Palma B, Ferretti M, Bolzoni M, Marchica V, et al. The proteasome inhibitor bortezomib maintains osteocyte viability in multiple myeloma patients by reducing both apoptosis and autophagy: A new function for proteasome inhibitors. *J Bone Miner Res*. (2016) 31:815–27. doi: 10.1002/jbmr.2741

69. Jurcak NR, Rucki AA, Muth S, Thompson E, Sharma R, Ding D, et al. Axon guidance molecules promote perineural invasion and metastasis of orthotopic pancreatic tumors in mice. *Gastroenterology*. (2019) 157:838–850.e6. doi: 10.1053/j.gastro.2019.05.065

70. Wong VSC, Meadows M, Goldberg D, Willis DE. Semaphorin 3A induces acute changes in membrane excitability in spiral ganglion neurons *in vitro*. *Eur J Neurosci*. (2019) 50:1741–58. doi: 10.1111/ejn.14360

71. Dontchev VD, Letourneau PC. Nerve growth factor and semaphorin 3A signaling pathways interact in regulating sensory neuronal growth cone motility. *J Neurosci*. (2002) 22:6659–69. doi: 10.1523/JNEUROSCI.22-15-06659.2002

72. Ro JY, Zhang Y, Tricou C, Yang D, da Silva JT, Zhang R. Age and sex differences in acute and osteoarthritis-like pain responses in rats. *J Gerontol A Biol Sci Med Sci*. (2020) 75:1465–72. doi: 10.1093/gerona/glz186

73. Felson DT, Naimark A, Anderson J, Kazis L, Castelli W, Meenan RF. The prevalence of knee osteoarthritis in the elderly. The Framingham Osteoarthritis Study. *Arthritis Rheum*. (1987) 30:914–8. doi: 10.1002/art.1780300811

74. Shane Anderson A, Loeser RF. Why is osteoarthritis an age-related disease? *Best Pract Res Clin Rheumatol*. (2010) 24:15–26. doi: 10.1016/j.berh.2009.08.006

75. Da Silva JT, Tricou C, Zhang Y, Tofighbakhsh A, Seminowicz DA, Ro JY. Pain modulatory network is influenced by sex and age in a healthy state and during osteoarthritis progression in rats. *Aging Cell*. (2021) 20(2):e13292. doi: 10.1111/acel.132929

76. Glass N, Segal NA, Sluka KA, Torner JC, Nevitt MC, Felson DT, et al. Examining sex differences in knee pain: the multicenter osteoarthritis study. *Osteoarthritis Cartilage*. (2014) 22:1100–6. doi: 10.1016/j.joca.2014.06.030

77. Pan J, Zhou X, Li W, Novotny JE, Doty SB, Wang L. *In situ* measurement of transport between subchondral bone and articular cartilage. *J Orthop Res*. (2009) 27:1347–52. doi: 10.1002/jor.20883

78. Solheim N, Östlund S, Gordh T, Rosseland LA. Women report higher pain intensity at a lower level of inflammation after knee surgery compared with men. *Pain Rep*. (2017) 2:e595. doi: 10.1097/PR9.0000000000000595

79. Kosek E, Finn A, Ultenius C, Hugo A, Svensson C, Ahmed AS. Differences in neuroimmune signalling between male and female patients suffering from knee osteoarthritis. *J Neuroimmunology*. (2018) 321:49–60. doi: 10.1016/j.jneuroim.2018.05.009

80. Perruccio AV, Badley EM, Power JD, Canizares M, Kapoor M, Rockel J, et al. Sex differences in the relationship between individual systemic markers of inflammation and pain in knee osteoarthritis. *Osteoarthr Cartil Open*. (2019) 1:100004. doi: 10.1016/j.ocarto.2019.100004

81. Rostock C, Schrenk-Siemens K, Pohle J, Siemens J. Human vs. Mouse nociceptors – similarities and differences. *Neuroscience*. (2018) 387:13–27. doi: 10.1016/j.neuroscience.2017.11.047

Frontiers in Endocrinology

Explores the endocrine system to find new therapies for key health issues

The second most-cited endocrinology and metabolism journal, which advances our understanding of the endocrine system. It uncovers new therapies for prevalent health issues such as obesity, diabetes, reproduction, and aging.

Discover the latest Research Topics

See more →

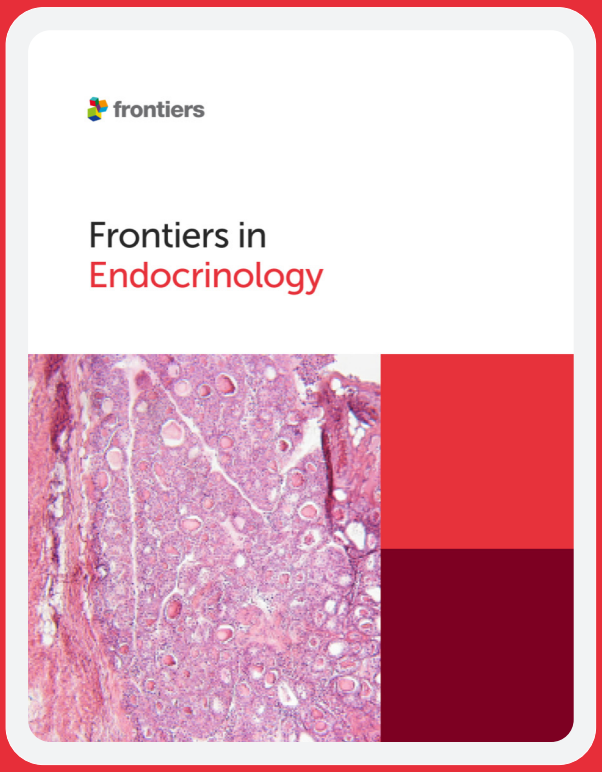

Frontiers

Avenue du Tribunal-Fédéral 34
1005 Lausanne, Switzerland
frontiersin.org

Contact us

+41 (0)21 510 17 00
frontiersin.org/about/contact